
# 24th INTERNATIONAL MULTIDISCIPLINARY SCIENTIFIC GEOCONFERENCE - SGEM 2024

**01 – 07 July 2024 - Albena, Bulgaria**

## CONFERENCE PROCEEDINGS OF SELECTED PAPERS in

## INFORMATICS, GEOINFORMATICS AND REMOTE SENSING

## ISSUE 2.1

**DISCLAIMER**

The **International Multidisciplinary Scientific GeoConference SGEM (Survey, Geology, Ecology, and Management)** serves as a global platform for pioneering research and scientific dialogue across the diverse fields of geosciences. It is dedicated to advancing interdisciplinary solutions for the most pressing environmental challenges of our time — **Global Warming, Climate Change, $CO_2$ Reduction, Biodiversity Conservation, and the Development of Green Technologies**. By fostering a collaborative exchange of knowledge and **aligning its objectives** with the **United Nations Sustainable Development Goals (SDGs), SGEM aims to inspire scientific excellence and drive sustainable practices toward a greener, more resilient future for our planet.**

Authors are responsible for the content and accuracy of the written papers. Opinions expressed are not meant to represent or reflect the position of the SGEM International Scientific Committee members.


Haidingergasse 1, C / 1113, Vienna 1030, Austria
Published by STEF92 Technology
Total print: 5000

E-mail: **sgem@sgem.org** | URL: **www.sgem.org**

**ISBN 978-619-7603-69-9**

**ISSN 1314-2704**

**DOI: 10.5593/sgem2024/2.1**

## FOREWORD

**Dear Readers,**
It is with great pleasure that we introduce the second issue of the **24th volume SGEM GeoConference 2024 Conference Proceedings**, dedicated to advancements in **Informatics, Geoinformatics, Geodesy and Mine Surveying, Photogrammetry and Remote Sensing, and Cartography and GIS**. These fields represent the cutting edge of digital and spatial sciences, offering tools and methods that are crucial for understanding and addressing some of the most complex challenges facing our world today.

This conference proceedings underscores the importance of multidisciplinarity within the geosciences. By integrating the latest innovations in informatics, geoinformatics, and GIS, researchers are able to analyze and interpret data with unprecedented precision. This has direct applications in **tackling global challenges such as climate change, urbanization, and sustainable resource management.**

The research compiled here also aligns with several UN Sustainable **Development Goals (SDGs), including sustainable cities and communities (SDG 11), climate action (SDG 13), and industry, innovation, and infrastructure (SDG 9).** Through the application of cutting-edge technologies like remote sensing, machine learning, and cyber-physical systems, the studies presented in this book offer actionable insights that drive innovation and sustainability.

**Highlights of this issue:**

- Informatics explores the **impact of digitization on various industries**, from optimizing production processes to developing cyber-physical systems for enhanced safety and efficiency.
- **Geoinformatics** showcases the **power of automated classification and mapping**, with applications ranging from landform analysis to urban environment monitoring.
- **Geodesy and Mine Surveying** focus on improving the precision and cost-efficiency of surveying methods, which are essential for infrastructure development and natural disaster prevention.
- **Photogrammetry and Remote Sensing** provide critical insights into land degradation, coastal preservation, and the integration of deep learning for spatial intelligence.
- **Cartography and GIS** emphasize the importance of mapping technologies in understanding phenomena such as the urban heat island effect and improving forest management.

The diversity of topics and methodologies in this collection of selected papers **highlights the interconnectedness of geosciences and the vital role of technological innovation in solving real-world problems.**

**Commitment to Excellence**
This publication represents the culmination of a rigorous **peer review process**, ensuring that each paper **meets the highest standards of scientific excellence**. We extend our gratitude to the authors, reviewers, and editorial team for their dedication and

contributions, which have made this proceedings a **valuable resource for researchers, practitioners, and policymakers alike.**

As you delve into the research presented here, we encourage you to reflect on the profound impact of these studies and their potential to drive meaningful change in our society. Together, we advance the frontiers of **science and work toward a more sustainable and resilient future.**

**Sincerely yours,**

**Prof. Dr. hab. oec. Baiba Rivza**
Editor-in-Chief of XXIV SGEM GeoConference Proceedings
*Member of the Presidium of the Latvian Academy of Sciences, LATVIA*
*President of the Latvian Academy of Agricultural and Forestry Sciences*
*Vice-chair of the Latvian Council of Higher education*
*President of Latvian universities professors' association*
*Expert from the European Academy of Sciences Academic Advisory Board (EASAC)*

**Prof. DSc. Oleksandr Trofymchuk**
Editor-in-Chief of XXIV SGEM GeoConference Proceedings
*National Academy of Sciences of Ukraine, UKRAINE*

# CONFERENCE PROCEEDINGS CONTENTS

## INFORMATICS

## GEOINFORMATICS



## GEODESY AND MINE SURVEYING

# SECTION INFORMATICS

# A MULTIDISCIPLINARY APPROACH TO TELEGRAM DATA ANALYSIS

**Velizar Varbanov**[1]

**Kalin Kopanov**[1]

**Prof. Dr. Tatiana Atanasova**[1]

[1] Institute of Information and Communication Technologies - Bulgarian Academy of Sciences, **Bulgaria**

## ABSTRACT

This paper presents a multidisciplinary approach to analyzing data from Telegram for early warning information regarding cyber threats. With the proliferation of hacktivist groups utilizing Telegram to disseminate information regarding future cyberattacks or to boast about successful ones, the need for effective data analysis methods is paramount. The primary challenge lies in the vast number of channels and the overwhelming volume of data, necessitating advanced techniques for discerning pertinent risks amidst the noise. To address this challenge, we employ a combination of neural network architectures and traditional machine learning algorithms. These methods are utilized to classify and identify potential cyber threats within the Telegram data. Additionally, sentiment analysis and entity recognition techniques are incorporated to provide deeper insights into the nature and context of the communicated information.

The study evaluates the effectiveness of each method in detecting and categorizing cyber threats, comparing their performance and identifying areas for improvement. By leveraging these diverse analytical tools, we aim to enhance early warning systems for cyber threats, enabling more proactive responses to potential security breaches. This research contributes to the ongoing efforts to bolster cybersecurity measures in an increasingly interconnected digital landscape.

**Keywords:** Machine Learning, FNN, LSTM, SVM, Cyber Security

## INTRODUCTION

In the wake of recent geopolitical conflicts such as the Ukraine-Russia conflict and the Israel-Palestine tensions, the digital landscape has become increasingly fraught with cybersecurity risks [1, 2]. Hacktivist groups have leveraged platforms like Telegram to disseminate information regarding their intentions for cyberattacks or to celebrate successful exploits. However, with the vast data space in Telegram channels, distinguishing relevant cyber threat information from other data is a huge challenge.

To address this challenge, this study adopts a multidisciplinary approach, harnessing the power of advanced data analysis techniques to extract actionable insights from Telegram data. Our investigation focuses on channels associated with hacktivist groups. Notably, we observed two prominent topics dominating these channels: discussions about political events and cyber threats [3].



https://doi.org/10.5593/sgem2024/2.1/s07.01

Motivated by the need for effective data triage, we utilized two distinct datasets, each comprising approximately 4000 statements. These datasets were meticulously curated to facilitate the training of machine learning algorithms [3] and neural network architectures. By segregating the data according to thematic relevance – cyber threats and political discourse – we aimed to provide cybersecurity analysts with focused datasets tailored to their expertise.

The study evaluates the efficacy of three primary methodologies: Feedforward Neural Network (FNN), Long Short-Term Memory (LSTM), and Support Vector Machine (SVM). Through rigorous testing and comparative analysis, we seek to elucidate the strengths and weaknesses of each approach in identifying and categorizing cyber threats within the Telegram data streams. Furthermore, to augment the discernment of valuable intelligence, we integrate entity recognition and sentiment analysis techniques [4, 5] into our analytical framework. By discerning key entities and gauging sentiment, we aim to provide nuanced contextual understanding, enabling more informed decision-making by cybersecurity experts and policymakers.

This research endeavour represents a concerted effort to fortify early warning systems against cyber threats in an increasingly volatile digital environment [6]. By leveraging interdisciplinary methodologies and innovative analytical techniques, we endeavour to empower stakeholders with actionable insights, thereby enhancing proactive cybersecurity measures and safeguarding digital infrastructures.

## MATERIALS AND METHODS

We progressed through various phases during the execution of our experiments:

**Data Collection** - It was gathered data from Telegram channels affiliated with hacktivist groups supporting various geopolitical causes, including Ukraine, Russia, Palestine, and Israel. This diverse selection of groups provided a comprehensive dataset reflecting a spectrum of political ideologies and cyber activities. Utilizing Python libraries, we implemented web scraping techniques to extract textual data from these Telegram channels.

**Data Scraping Process** - Python libraries such as “requests” and “BeautifulSoup” were instrumental in scraping data from Telegram channels. By sending HTTP requests to the Telegram web interface and parsing the HTML content, we retrieved textual data from targeted channels. Moreover, we employed the *telethon l*ibrary, a Python wrapper for the Telegram API, to access channel content programmatically. This facilitated the extraction of data in a structured format, ensuring consistency across datasets.

**Data Pre-processing** - To accomplish this goal, we implemented a system where each dataset includes a “class” column. Here, a value of “0” denotes data related to politics, while “1” signifies data relevant to cybersecurity. This binary classification framework is essential for aiding machine learning (ML) and neural network (NN) algorithms in understanding the content of the data during training.

Our approach involves a data preprocessing pipeline to streamline model training and evaluation. This pipeline consists of two primary stages: data splitting and TF-IDF vectorization.

Initially, we segment our dataset into training and testing subsets using the train_test_split function from the sklearn.model_selection module. This step randomly

divides our dataset into two parts: one for training, comprising 75% of the data, and another for testing, encompassing 25% of the data. By maintaining a consistent random state (random_state = 42), we ensure reproducibility across experiments.

Subsequently, we employ TF-IDF (Term Frequency-Inverse Document Frequency) vectorization to convert textual data into numerical representations. This is accomplished through the TfidfVectorizer from the sklearn.feature_extraction.text module. Initially, the vectorizer is fitted to the training data (x_train), which involves learning the vocabulary and computing the TF-IDF weights. Afterwards, both the training and testing textual data (x_train and x_test, respectively) are transformed into TF-IDF numerical vectors. This transformation ensures that our model can effectively interpret textual data, thereby facilitating subsequent machine learning tasks.

**Dataset Creation -** Upon scraping the data, we organized it into two distinct datasets, each featuring columns for content, date, and the name of the group. This segregation facilitated the subsequent training and evaluation of machine learning models. The division into two datasets, one focusing on cyber threats and the other on political discourse, allowed for targeted analysis by domain experts.

**Model Training and Evaluation** - For model training, we employed libraries such as TensorFlow and scikit-learn, leveraging their rich ecosystem of algorithms.

We used Feedforward Neural Network (FNN), designed for a binary classification task. The model architecture is specified using the Sequential API, consisting of three fully connected layers (Dense). The first layer has 128 neurons and an input shape corresponding to the number of features in the training dataset, using the ReLU activation function. To mitigate overfitting, a Dropout layer with a rate of 0.5 is added after the first and second dense layers. The second dense layer has 64 neurons, also using ReLU activation. The final layer consists of a single neuron with a sigmoid activation function to output a probability score for the binary classification.

The model is compiled with the Adam optimizer, binary cross-entropy loss function, and accuracy as a metric to evaluate performance. Training is conducted over 10 epochs with a batch size of 32, and the performance is validated using the test set (xv_test, y_test).

Next, we used Long Short-Term Memory (LSTM) model from the Keras library, designed for a binary classification task. The model architecture is specified using the Sequential API. The first layer is an LSTM layer with 128 units, configured to process input data with a shape of (1, xv_train.shape[1]), where the input shape indicates sequences of length 1 with a number of features equal to xv_train.shape[1]. Following the LSTM layer, a Dropout layer with a rate of 0.5 is added to reduce overfitting by randomly setting half of the input units to 0 at each update during training. The next layer is a fully connected Dense layer with 64 neurons and ReLU activation function, followed by another Dropout layer with a rate of 0.5. The final layer is with a single neuron and a sigmoid activation function to output a probability score for the binary classification.

The model is compiled with the Adam optimizer, binary cross-entropy loss function, and accuracy as a metric to evaluate performance. Training is conducted over 10 epochs with a batch size of 32, using reshaped training data (xv_train_reshaped) and validated on reshaped test data (xv_test_reshaped).



https://doi.org/10.5593/sgem2024/2.1/s07.01

Next we explore the application of a Support Vector Machine (SVM) for our task. An SVM classifier (`SVC` from `sklearn`) is then employed for the classification task. The model is trained on the vectors derived from the training datasets. Predictions are generated, and a classification report is produced to provide detailed metrics, including precision, recall, and F1-score for each class.

To further assess the model's performance, several error metrics are computed. These include the Root Mean Squared Error (RMSE), Mean Absolute Error (MAE), Residual Sum of Squares (RSE), and the $R^2$ Score (Coefficient of Determination). The results indicate the effectiveness of using SVM in text classification, providing a comprehensive evaluation through both classification metrics and regression error measures.

The goal of our experiments is to successfully analyse hacktivists behaviour patterns by following the outlined steps.

## RESULTS

The results of our experiments showing the performance scores of different classification algorithms are in Table 1: FNN (0.90), LSTM (0.89) and SVM (0.88). Despite the proximity of results, FNN stands out slightly superior. Notably, we conducted 10 tests for each algorithm and selected the highest score attained in each case.

**Table 1** – Tests results

| | **Feedforward NN** | **LSTM** | **SVM** |
|---|---|---|---|
| **Score** | 0.90 | 0.89 | 0.88 |
| **Root Mean Squared Error (RMSE)** | 0.30 | 0.32 | 0.34 |
| **Relative Absolute Error (RAE)** | 0.22 | 0.10 | 0.11 |
| **Relative Squared Error (RSE)** | 0.37 | 0.43 | 0.47 |
| **Coefficient of Determination** | 0.63 | 0.56 | 0.52 |

We proceeded with our investigations using Telegram data that hadn't been included in the two datasets used to train our algorithms. Utilizing the VADER (Valence Aware Dictionary and sEntiment Reasoner), we conducted sentiment analysis. The outcomes are encouraging, showing that sentiment analysis is yielding satisfactory results (Figure 1).

```
Message 1: Sentiment Score: -0.8464, Text: I Killmilk, represented by the organizer of the hacker group Killnet, of
ficially take full responsibility for causing particularly serious damage to the network infrastructure of the Bulg
arian corrupt government. And I declare this officially! Chief Prosecutor of the Republic of Bulgaria Ivan Geshev F
uck you!
Message 2: Sentiment Score: 0.7003, Text: South Africa was a victim of apartheid for decades. We don't want any nat
ions experience it again. This time Israel is committing genocide against Palestinians. We are doing our best to st
op Israel and Free Palestine. We tried to sue against Israel in International court, and now be keep on our try in
cyber court…Long live the South Africa, long live the Palestine
```

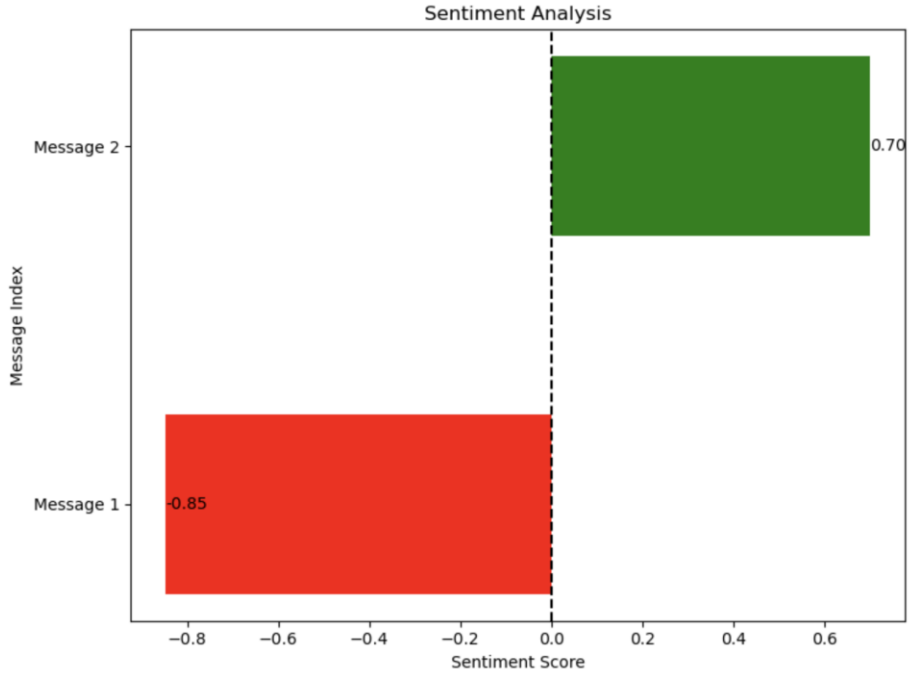


**Figure 1:** Results of Sentiment Analysis

Additionally, entity recognition is carried out using spaCy's named entity recognition (NER) module. For each message, entities such as persons, organizations, and geopolitical entities are extracted and stored in a structured format.

```
Entities:
Message 1:
  Person: Killmilk, Killnet
  Norp: Bulgarian
  Gpe: the Republic of, Bulgaria
Message 2:
  Gpe: South Africa, Israel, Israel, Israel, South Africa
  Date: decades
  Norp: Palestinians
```

**Figure 2:** Results of Entity Recognition

While we did encounter some false positive results, overall, we find the outcomes satisfactory. These results should provide analysts with enough information to discern potential vectors of attack, objectives, and relevant topics.

## DISCUSSION

The experimental findings endorse the initial inquiry regarding the application of NLP, neural networks, and machine learning for early warning detection, consistent with prior



https://doi.org/10.5593/sgem2024/2.1/s07.01

research conducted by other investigators [7, 8, 9]. Notably, our study revealed the efficacy of sentiment analysis, even in cases where negative statements contained positive words or positive statements featured numerous negative words. Despite some inaccuracies in entity recognition, particularly in identifying nouns as names, the overall test outcomes are satisfactory and will aid analysts in filtering out irrelevant data.

## CONCLUSION

The research findings highlight the promising performance of FNN, LSTM, and SVM models in analyzing data from Telegram channels for early threat detection. Neural networks, in particular, produce superior results but require more computational resources and time. The effectiveness of these models is significantly influenced by the quality of the datasets, underscoring the importance of robust dataset creation for training. Sentiment analysis and entity recognition are valuable for identifying threats and helping analysts filter out non-threatening data. The results suggest that neural networks have the potential to significantly aid cybersecurity experts in identifying threats more efficiently, leading to considerable time savings.

Interpreting these findings reveals that although neural networks perform better, the trade-off in computational resources might not always be justified, especially given the efficiency of other machine learning algorithms like SVM. This highlights the need for a balanced approach, considering both performance and resource constraints when selecting models.

Future research should focus on expanding datasets from hacktivist groups and analyzing these larger datasets with a broader range of algorithms and models beyond those used in this study. Additionally, exploring advanced techniques such as reinforcement learning or ensemble methods could further enhance threat detection capabilities. These research directions will contribute to the development of more robust and efficient threat detection systems.

## ACKNOWLEDGEMENTS

This work was partly supported by the National Science Program “Security and Defense”, which has received funding from the Ministry of Education and Science of the Republic of Bulgaria under the grant agreement No. Д01-74/19.05.2022.

## REFERENCES

[1] Newman, L. H., Burgess M., Activist Hackers Are Racing Into the Israel-Hamas War — for Both Sides, Wired, https://www.wired.com/story/israel-hamas-war-hacktivism/, 2023.

[2] Vu, A., Thomas, D., Collier, B., Hutchings, A., Clayton, R., & Anderson, R., Getting Bored of Cyberwar: Exploring the Role of Low-level Cybercrime Actors in the Russia-Ukraine Conflict. WWW '24: The ACM Web Conference 2024.

[3] Banerjee, S., Swearingen, T., Shillair, R., Bauer, J. M., Holt, T., & Ross, A. Using Machine Learning to Examine Cyberattack Motivations on Web Defacement Data. Social Science Computer Review, 40(4), pp 914-932. https://doi.org/10.1177/0894439321994234, 2022.

[4] Taghandiki K., Ehsan R. E., Types of Approaches, Applications and Challenges in the Development of Sentiment Analysis Systems, arXiv:2303.11176, 2023.

[5] B. Liu, Sentiment analysis and opinion mining. Synthesis lectures on human language technologies, 5 (1), 1-167, 2012.

[6] Bidollahkhani M., Kunkel J. M., Revolutionizing System Reliability: The Role of AI in Predictive Maintenance Strategies, CLOUD COMPUTING 2024: The Fifteenth International Conference on Cloud Computing, GRIDs, and Virtualization, ISBN: 978-1-68558-156-5, pp 49-57, 2024.

[7] Kopanov, K. Comparative Performance of Advanced NLP Models and LLMs in Multilingual Geo-Entity Detection. Cognitive Models and Artificial Intelligence Conference (AICCONF '24), Istanbul, Turkey, ACM. https://doi.org/10.1145/3660853.3660878, 2024.

[8] P. Evangelatos, C. Iliou, T. Mavropoulos, K. Apostolou, T. Tsikrika, S. Vrochidis, and I. Kompatsiaris, Named entity recognition in cyber threat intelligence using transformer-based models, in 2021 IEEE International Conference on Cyber Security and Resilience (CSR). IEEE, 2021, pp. 348–353.

[9] E. Rabieinejad, A. Yazdinejad, and R. M. Parizi, A deep learning model for threat hunting in ethereum blockchain, in 2021 IEEE 20th International Conference on Trust, Security and Privacy in Computing and Communications (TrustCom). IEEE, 2021, pp 1185–1190.



https://doi.org/10.5593/sgem2024/2.1/s07.01

# ADDRESSING HYDROGEN SAFETY INSIGHTS AND CHALLENGES BY MEANS OF SOFTWARE TOOLS

**Dr. Vlad Mihai Pasculescu** [1]

**Dr. Marius Cornel Suvar** [1]

**Dr. Marius Simion Morar** [1]

**Eng. Laurentiu Munteanu** [1]

**Eng. Zoltan Vass** [1]

[1] National Institute for Research and Development in Mine Safety and Protection to Explosion – INSEMEX Petroșani, **Romania**

## ABSTRACT

Hydrogen is gaining popularity as a fuel source for more and more fields around the globe. The use of hydrogen for transport represents one of the important applications of this chemical substance, in this sense the development of infrastructures, but especially the safety of hydrogen filling stations representing an important element. Using hydrogen to power transportation can reduce harmful ozone-depleting emissions while improving air quality. Hydrogen fuel cell vehicles can help improve air quality and solve climate challenges. After all, the only substance that escapes through the tailpipe of a fuel cell vehicle is water. One of the major disadvantages of using hydrogen to fuel vehicles is the high risk of explosion (between 4 and 75% hydrogen mixed with air). Both technical and organizational measures must be taken to prevent and protect against explosions. Technological progress and the development of knowledge in the field of explosion protection have made it possible to develop software tools, open-source and commercial, that can analyze the hazards and adverse consequences that explosion-type events can have. This study presents the applicability of such a software tool, for modeling the hypothetical discharges of untimely hydrogen discharges within a vehicle fueling station, as well as the consequence modelling of such an undesired event.

**Keywords:** explosion, hydrogen, safety, software

## INTRODUCTION

Hydrogen has emerged as a key player in the global quest for sustainable energy solutions, especially within the transportation sector. The establishment of hydrogen refueling stations is becoming more common worldwide as countries aim to lower carbon emissions and shift towards cleaner energy sources [9, 10]. However, the widespread adoption of hydrogen as an energy carrier requires a comprehensive understanding of the potential risks and safety concerns associated with its storage, handling, and distribution [7, 12].



https://doi.org/10.5593/sgem2024/2.1/s07.02

Accidents at hydrogen refueling stations are a significant concern due to hydrogen's unique properties, such as its high reactivity and flammability. These incidents not only threaten infrastructure integrity but also raise serious safety concerns for personnel and the surrounding environment. Consequently, there is an increasing demand for effective risk assessment methodologies to mitigate the impact of these accidents and ensure the safe operation of hydrogen refueling facilities [1, 2, 3].

Numerical modeling, especially using advanced software like PHAST (Process Hazard Analysis Software Tool), provides a robust method for simulating and analyzing the dynamics of accidents at hydrogen refueling stations [8, 11]. By utilizing sophisticated computational tools and simulation techniques, researchers can obtain valuable insights into potential scenarios and outcomes of hydrogen-related incidents. PHAST software, known for its precision and versatility in hazard analysis, allows for the evaluation of various factors, including hydrogen dispersion, ignition, and the resulting consequences.

## MATERIALS AND METHODS

### H2 Refueling stations

Looking ahead, the future of hydrogen refueling stations promises significant advancements and transformative potential for the transportation and energy sectors. As the demand for hydrogen-powered vehicles grows, the need for an expanded network of refueling stations will also increase. This expansion will not only involve adding more stations but also improving their accessibility and coverage to ensure seamless travel for hydrogen vehicles across regions.

Technological innovations will continue to shape the future of hydrogen refueling stations, aiming to enhance efficiency, safety, and convenience [4, 5, 6]. These advancements could include improvements in hydrogen production, storage, and dispensing technologies, as well as the integration of renewable energy sources like solar and wind to power the refueling stations.

With a growing emphasis on green hydrogen production, future refueling stations may adopt electrolysis-based hydrogen production methods utilizing renewable energy sources. This shift towards green hydrogen will further boost the environmental sustainability of hydrogen-powered transportation.

Future hydrogen refueling stations are likely to be integrated into smart grid systems, allowing for dynamic monitoring and optimization of hydrogen production, distribution, and consumption. This integration will enhance efficiency, reliability, and grid stability while facilitating the incorporation of renewable energy sources into the hydrogen supply chain.

The development of hydrogen refueling stations will be closely linked with the broader hydrogen mobility ecosystem, including hydrogen production facilities, distribution networks, and various applications beyond transportation, such as industrial and residential uses.

### Application of specialized software

PHAST (Process Hazard Analysis Software Tool) is a widely used software application developed by DNV GL for conducting process hazard analyses across various industries, including oil and gas, chemical processing, and pharmaceuticals. PHAST

provides a comprehensive set of capabilities and specific functionalities essential for assessing the safety of hydrogen refueling stations.

- **Hydrogen Dispersion Modeling**: PHAST can simulate the spread of hydrogen within and around refueling stations, taking into consideration factors such as wind speed, atmospheric conditions, and the facility's layout. This capability is crucial for evaluating the potential for hydrogen accumulation and the risks of creating hazardous scenarios.
- **Ignition Source Analysis**: PHAST enables users to identify and analyze potential ignition sources within hydrogen refueling stations, such as electrical equipment, static electricity, and hot surfaces. This analysis is essential for pinpointing ignition risks and assessing the likelihood of fires or explosions.
- **Consequence Analysis**: PHAST allows for detailed predictions of the outcomes of hydrogen-related incidents, including fires, explosions, and toxic releases. This includes calculating blast overpressures, thermal radiation levels, and toxic gas concentrations, which are vital for assessing the potential impact on personnel, equipment, and the surrounding environment.
- **Mitigation Measures Evaluation**: PHAST aids in evaluating the effectiveness of various mitigation strategies and safety systems designed to reduce the impact of hydrogen-related incidents. This encompasses assessing the performance of safety equipment, emergency response protocols, and containment measures to ensure their adequacy in managing potential hazards.
- **Regulatory Compliance**: PHAST supports ensuring adherence to relevant safety regulations, standards, and guidelines for the design and operation of hydrogen refueling stations. This includes assessing compliance with codes such as the NFPA 2: Hydrogen Technologies Code and local regulatory requirements, thereby facilitating safe and lawful operations.

Overall, PHAST offers a robust suite of capabilities for thoroughly assessing the safety of hydrogen refueling stations. This includes comprehensive hazard identification, risk assessment, scenario analysis, safety barrier evaluation, and ensuring regulatory compliance. Its specialized features for handling hydrogen-related hazards make it an invaluable tool for the safe design, operation, and maintenance of hydrogen refueling infrastructure.

**Accident simulation**

The majority of hydrogen refueling stations operate at two specific pressure levels: 35 MPa (350 Bar) for buses and trucks, and 70 MPa (700 Bar) for cars. This paper examines the equipment used in hydrogen refueling and storage, with a particular focus on potential leaks in stations operating at these pressures. Previous risk assessments by researchers have highlighted pipeline leaks and valve damage due to structural flaws as major contributors to accidents, especially those caused by failures in opening and closing mechanisms. In the performed simulations, leak diameters of 15 mm and 30 mm are considered, using pressure tanks filled with 2000 kg of hydrogen at either 350 or 700 bar. The study is conducted under typical environmental conditions, with a wind speed of 1 m/s and neutral atmospheric stability (category D). Upon hydrogen leakage, the immediate probability of ignition is relatively low. As the leakage continues, hydrogen disperses into the atmosphere, triggering alarms from combustible gas detectors. This prompts the activation of emergency shut-off valves to stop the leak. The



https://doi.org/10.5593/sgem2024/2.1/s07.02

entire process, from the onset of the leak to its cessation, takes 18.75 seconds. Therefore, the paper investigates the dispersion of combustible gas clouds 18.75 seconds after the initiation of the leak

## RESULTS AND DISCUSSION

### Dispersion

Hydrogen has low density, large diffusion coefficient, and wide explosion limit and fast flame speed. Under standard atmospheric pressure, the explosion limit of hydrogen is between 4.0% and 75.6%. For performing the simulations in Phast software, the following input parameters have been set for the weather conditions: wind speed - 2 m/s, Pasquil stability: D – neutral – little sun and high wind or overcast/windy night; atmospheric temperature 20 degC; Relative humidity 50%; Solar radiation flux 0.5 kW/m$^2$. The source term considered is "Leak": a hole in the tank results in the release of Hydrogen to the atmosphere. The discharge calculations are carried out in Phast using "leak" model, which calculates release rate and state of the gas after its expansion to the atmospheric pressure. Relevant input parameters corresponding to the 4 accident scenarios considered are presented in Table 1 below. The dispersion charts are shown in Figure 1 a, b, c, d, e.

**Table 1.** Input parameters

| | **Case 1** | **Case 2** | **Case 3** | **Case 4** |
|---|---|---|---|---|
| Material | Hydrogen | | | |
| Mass inventory | 2000 kg | | | |
| State | Vapour | | | |
| Temperature | -25 degC | | | |
| Pressure | 350 bar | 700 bar | 350 bar | 700 bar |
| Scenario | Leak | | | |
| Orifice diameter | 15 mm | 15 mm | 30 mm | 30 mm |
| Phase to be released | Vapour | | | |
| Concentration of interest | 4% (40000 ppm) | | | |

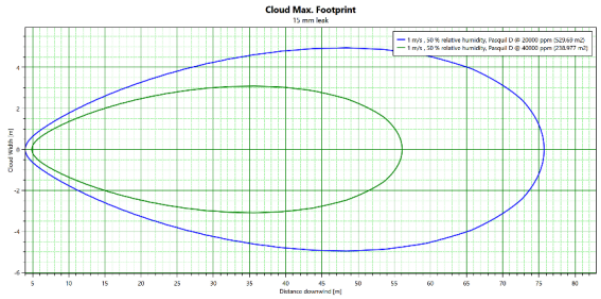


**a)** Case 1

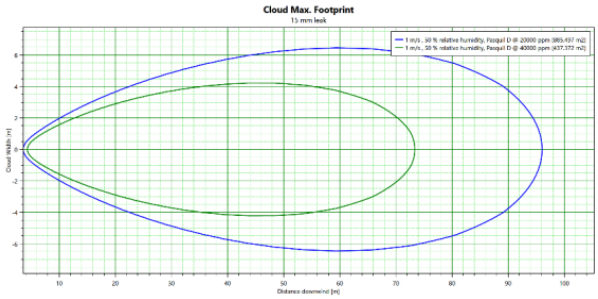


**b)** Case 2

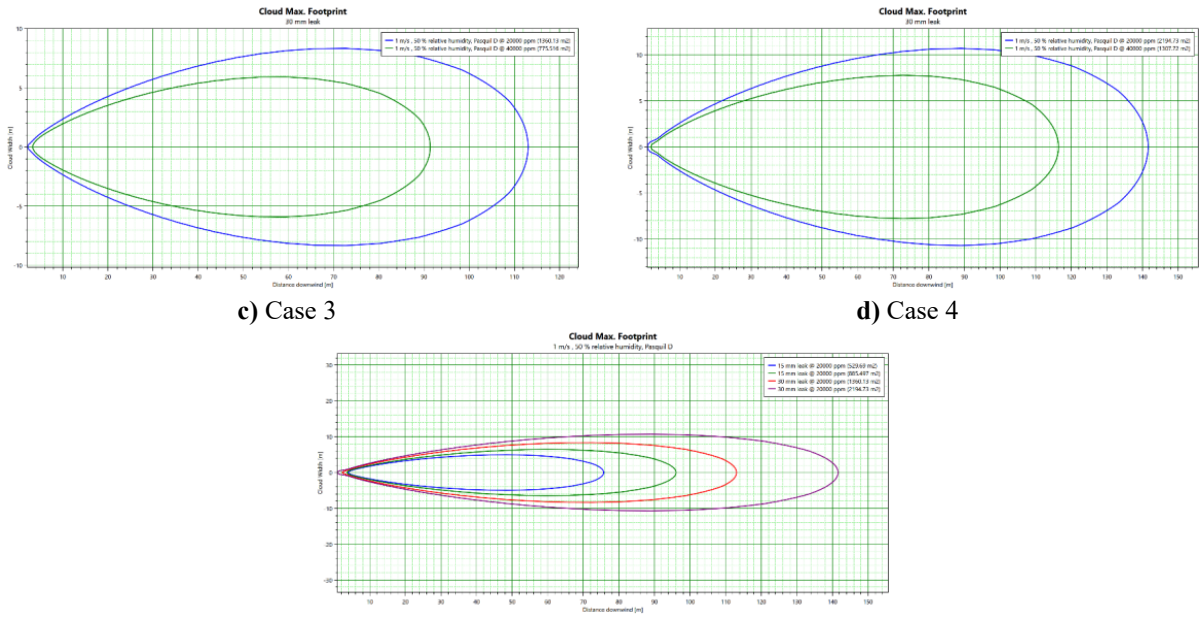


**c)** Case 3 **d)** Case 4

**e)** combined view

**Fig. 1** Cloud maximum footprint

## Radiation – Jet fire

When hydrogen refuelling station leaks, if safety devices such as combustible gas detectors or emergency shut-off valves fail, hydrogen will continue to leak, and a jet fire will occur immediately after ignition. The simulation results are shown in Figure 2 a, b, c, d, e - for the four cases taken into account.

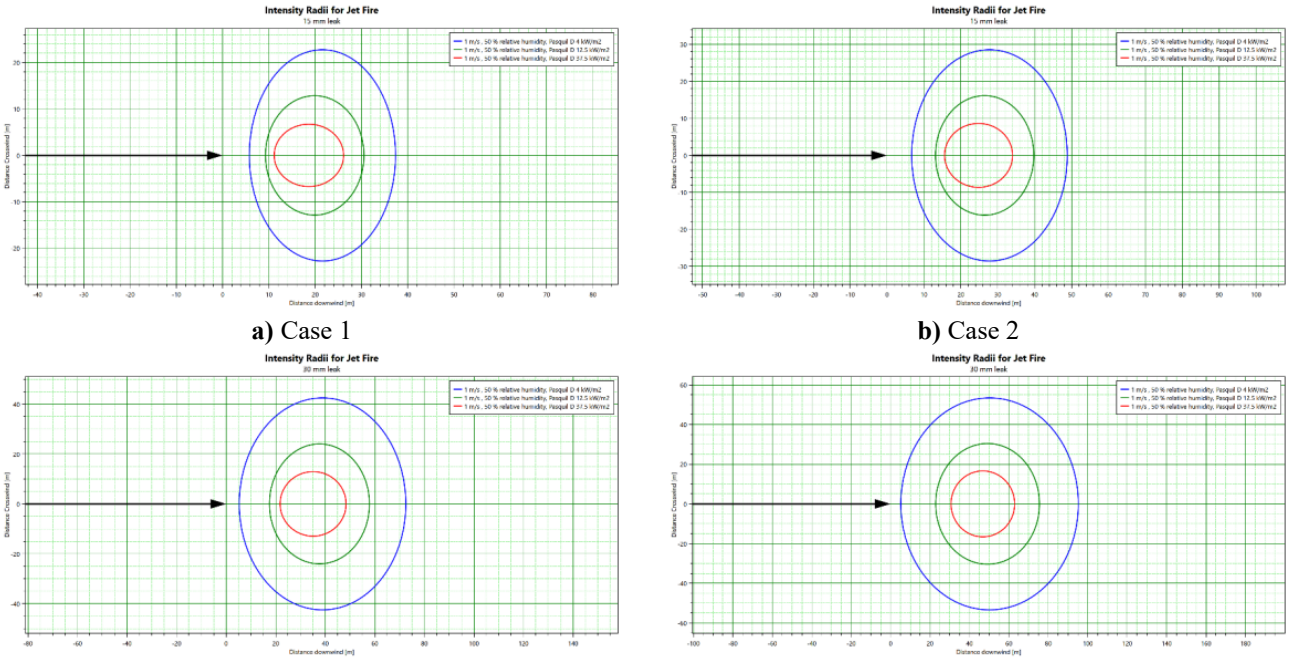


**a)** Case 1 **b)** Case 2

**c)** Case 3 **d)** Case 4



https://doi.org/10.5593/sgem2024/2.1/s07.02

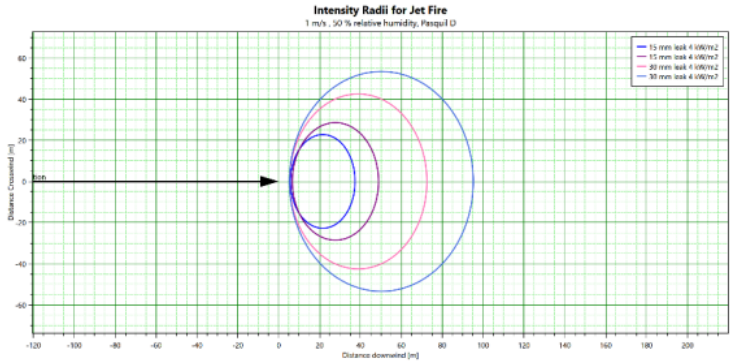


**e)** combined view of the four cases

**Fig. 2** Intensity radii for jet fire

From Figure 2 there may be easily read the areas affected by jet fire in the four cases, with regard to the three radiation values of:

- 4 kW/m$^2$,
- 12.5 kW/m$^2$
- 37.5 kW/m$^2$.

**Explosion**

Figure 3 a, b, c, d, e unveils the detailed graphic outcomes of explosion scenarios generated by PHAST software. Through precise simulations, we've analysed blast dynamics fact which can provide critical insights into risk assessment and safety protocols.

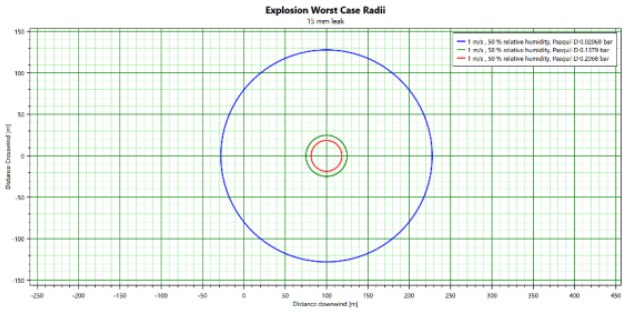


**a)** Case 1

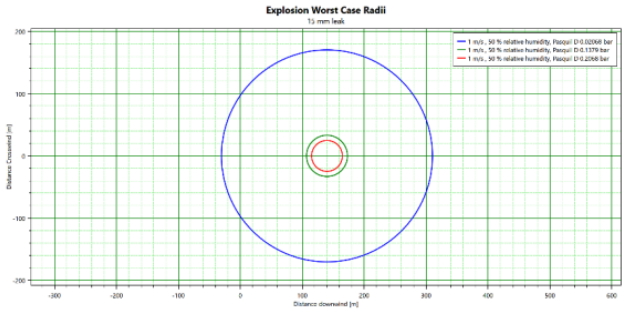


**b)** Case 2

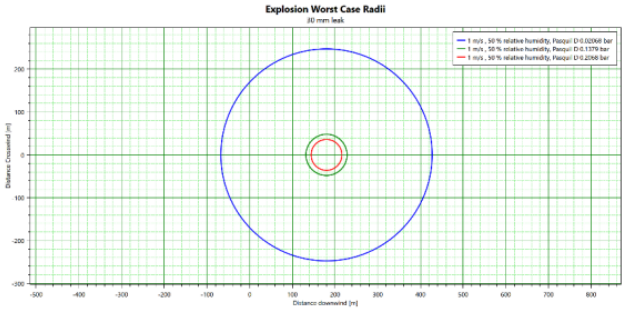


**c)** Case 3

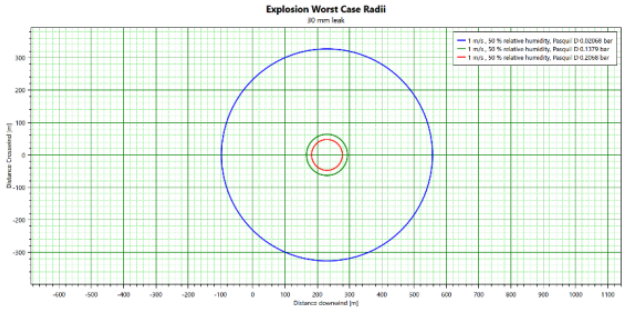


**d)** Case 4

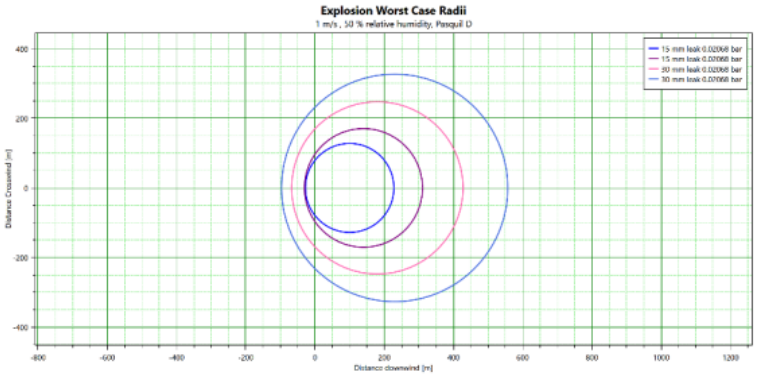


**e)** combined view of the four cases
**Fig. 3** Explosion worst case radii

## CONCLUSIONS

Through advanced computational simulations, hazardous scenarios such as hydrogen leaks, dispersion, jet fires, and explosions can be identified and thoroughly analyzed. This detailed analysis allows for a comprehensive assessment of potential risks to personnel, infrastructure, and the surrounding environment, enabling the development of proactive risk management and mitigation strategies. PHAST simulations facilitate the evaluation of existing safety measures and mitigation strategies in hydrogen refueling stations.

By examining the effectiveness of safety equipment, emergency response protocols, and containment measures, stakeholders can pinpoint areas for improvement and optimize safety practices to minimize the impact of potential accidents. Analyzing the results of PHAST simulations provides valuable lessons that can be incorporated into the design and operation of hydrogen refueling stations. Identifying weaknesses in current systems and understanding the conditions that lead to failures allows stakeholders to make informed decisions on design modifications and operational changes.

Continuous feedback from simulation results can be integrated into safety practices, leading to the iterative improvement of safety protocols and technologies. This process promotes the sustainable growth of hydrogen infrastructure by ensuring that safety measures evolve in response to new insights and technological advancements. By leveraging the capabilities of PHAST simulations, stakeholders can significantly enhance the safety performance of hydrogen refueling stations, mitigate risks effectively, and support the sustainable expansion of hydrogen as a clean energy source.

## ACKNOWLEDGEMENTS

This work was carried out through the ”Nucleu” Program within the National Plan for Research, Development and Innovation 2022-2027, with the support of the Romanian Ministry of Research, Innovation and Digitalisation, project no. 23 32 02 02, title: Numerical modelling on the ignition and propagation of explosions generated by air-hydrogen mixtures – H2Model.



https://doi.org/10.5593/sgem2024/2.1/s07.02

## REFERENCES

[1] Ganci F.; Carpignano A.; Mattei N.; Carcassi M.N., Hydrogen release and atmospheric dispersion: Experimental studies and comparison with parametric simulations, International Journal of Hydrogen Energy, Vol. 36, Issue 3, ISSN 0360-3199, 2011

[2] Hansen O.R.; Hansen E.S., CFD-modelling of large-scale LH2 release and explosion experiments, Process Safety and Environmental Protection, Vol. 174, ISSN 0957-5820, 2023

[3] Hansen O.R., Middha P., CFD-based risk assessment for hydrogen applications, Process Safety Progress, Vol. 27, Issue 1, ISSN 1066-8527, 2008

[4] Hasslberger J., Kim H.K., Kim B.J., Ryu I.C., Sattelmayer T., Three-dimensional CFD analysis of hydrogen-air-steam explosions in APR1400 containment, Nuclear Engineering and Design, Vol. 320, ISSN 0029-5493, 2017

[5] Jang C.B., Jung S., "Numerical computation of a large-scale jet fire of high-pressure hydrogen in process plant". Energy Science and Engineering 4, 406-417, 2016

[6] Li Y.C., Bi, MS, Zhou, YH; Jiang, HP; Huang, L; Zhang, K; Gao, W, Experimental and theoretical evaluation of hydrogen cloud explosion with built-in obstacles, International Journal of Hydrogen Energy, Vol. 45, Issue 51, ISSN 0360-3199, 2020

[7] Mohammadfam I., Zarei E., Safety risk modeling and major accidents analysis of hydrogen and natural gas releases: A comprehensive risk analysis framework, International Journal of Hydrogen Energy, Vol. 40, Issue 39, ISSN 0360-3199, 2015

[8] Niculescu T, Pasculescu D., „Use of numerical simulation to study capacitive loads which is connecting to an AC power source", In15th International Multidisciplinary Scientific Geoconference SGEM 2015 2015 (pp. 391-398).

[9] Niculescu T, Pasculescu D, Pasculescu VM, Stoica IO., „Evaluation of electrical parameters of intrinsic safety barriers of the electrical equipment intended to be used in atmospheres with explosion hazard", International Multidisciplinary Scientific GeoConference Surveying Geology and Mining Ecology Management. 2014; 1(2):169-76.

[10] Pana L, Grabara J, Pasculescu D, Pasculescu VM, Moraru RI., „Optimal quality management algorithm for assessing the usage capacity level of mining transformers", Polish Journal of Management Studies. 2018;18(2):233-44.

[11] Pasculescu V.M., Vlasin N.I., Ghicioi E., Florea G.D., Suvar M.C., New tools for estimating the extent of hazardous areas generated by gas leak explosions, Environmental Engineering and Management Journal, vol. 18/issue 4, pp. 889-900, 2019.

[12] Vlasin N.I., Pasculescu V.M., Florea G.D., Suvar M.C., Computational study of scenarios regarding explosion risk mitigation, World Multidisciplinary Earth Sciences Symposium (WMESS 2016), Pts 1-4, Vol. 44 ISSN 1755-1307, 2016

# ARCHITECTURAL ABSTRACTIONS IN THE DESIGN OF DISTRIBUTED EMBEDDED SYSTEMS PLATFORMS

**Postgrad. Stud. Maxim Kolchurin**[1]
**Prof. Dr. Alexey Platunov**[1]
**Postgrad. Stud. Asminkin Fedor**[1]
**Assoc. Prof. Ph.D. Vasiliy Pinkevich**[1]
[1] ITMO University, **Russia**

## ABSTRACT

The work is dedicated to formalizing the process of designing embedded systems with distributed heterogeneous organization. The original model of representing a computational system as a set of computational platforms interconnected both hierarchically and within the same level is taken as the basis. The abstraction of a 'design platform' is interpreted as a design solution that is fixed for reuse and provides an application interface for building an "upward" hierarchy of abstractions alongside specifications for creating implementations "downward".

Today, the stages of system design still suffer from a lack of essential design abstractions, which is evident both in the level of information presentation in technical documentation and in the capabilities of the design tools. The focus has shifted from discussing conceptual solutions toward final implementations. The authors demonstrate a system of architectural and microarchitectural abstractions aimed at developing methods and tools for conceptual-level design. This enhances the rationale behind design decisions by representing embedded systems as compositions of abstractions with a wide range of engineering-relevant parameters and characteristics.

The authors develop an aspect-oriented approach to designing embedded computational systems, proposing a method for formalizing engineering-relevant attributes for diverse design abstractions such as network interfaces, protocols, controllers, drivers, operating systems, their components, programming languages, their translators, and virtual machines.

**Keywords:** distributed embedded system, computational platform, computer architecture, industrial network, architectural abstraction

## INTRODUCTION

Building distributed embedded systems (ES) has become the de facto standard in the field of industrial and infrastructure automation. These systems are based on universal or specialized programmable logic controllers, which provide flexibility, simple program logic, hardware reliability, and interaction with various sensors and actuators. Often, such systems are complex constructs that combine heterogeneous systems and networks. In solving real-world problems, developers still encounter technical and organizational-financial constraints.



https://doi.org/10.5593/sgem2024/2.1/s07.03

Approaches to design (methodologies) and the actual design routes depend on various factors [1, 2, 3, 4]. However, in practice, solutions based on system templates prevail or (if no suitable template exists) are developed 'from the microprocessor' [5, 6]. In doing so, efficiency and quality may suffer.

It is proposed to consider the design route of a computational system (CS) as a unified complex of activities for organizing the computational process. In this context, it is convenient to assume that the role of functionally complete computing devices is performed not only by physical equipment (processors and peripheral devices) but also by software platforms (operating systems, drivers, communication subsystems, virtual machines, etc). The computational process can include a whole range of actions performed at the design stages.

The work explores the design of platforms for distributed ES with a focus on the phases of project space exploration and microarchitectural design. The authors propose an approach of representing both known and original architectural and microarchitectural abstractions (mechanisms), enhancing the design formalization by presenting ES as compositions of abstractions equipped with an engineering-significant set of parameters and characteristics.

## ABSTRACTIONS IN EMBEDDED SYSTEMS DESIGN

Abstractions of different levels and purposes serve as models that assist developers in understanding, designing, and evaluating complex systems by highlighting essential characteristics and disregarding non-essential details. In the field of distributed ES, we categorize abstractions into the following groups:

1. Design Process: ES design, project infrastructure, project space, aspect space.
2. Basic Elements of CS: Computational mechanism, computational platform, architectural aggregate.
3. System Level: Architecture, architectural platform, architectural model, microarchitecture, design aspect.
4. Concepts and Metrics for Evaluating Design Decisions: Computational process, virtual machine, Model of Computation (MoC).

Let's examine the system of abstractions we use in design.

**The project and aspect space of a system.** We will refer to the project space of a system as the aggregate of activities and artifacts during the design phase in the system's life cycle.

Let us define an aspect as a segment of the project space and/or the system's life cycle associated with a specific problem or group of requirements. Aspects can be conceptual (relevant throughout the entire lifecycle) or local, identified at various stages. Their combination defines the project's aspect space. Organizational aspects give rise to new requirements in behavioral aspects and constrain the design solution space.

In our High-Level Design methodology [7], an aspect is a specific design problem within the context of creating an ES. Figure 1[8, 9], illustrates examples of representing the project and aspect spaces of embedded systems.

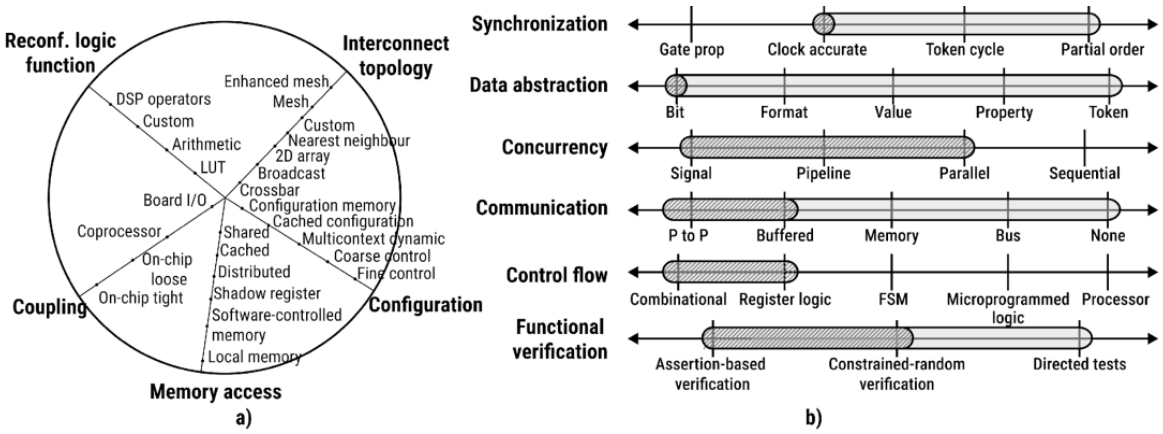


**Figure 1** - Examples of representing design and aspect spaces a) microcontroller b) programming system

**Platforms.** For us, the most crucial property of a computational platform is its ability to abstract away from specific implementations within specified bounds, while being fixed for reuse. The computational platform is considered as a unity of "external" and "internal" representations of a functionally-complete and functionally-significant object within the CS. The platform serves as a technical solution documented in the project for reuse and acts as the primary tool for reuse at the architectural level.
In today's practice, design often relies on existing computational platforms (hardware, software, instrumental, structural, etc.), which are unfortunately chosen based on secondary criteria. There is a need to enhance and refine the selection or creation of a comprehensive set of project computing platforms.
**Architectural Platform.** The architectural platform is considered as a tool for reusing the following conceptual solutions: a list of design aspects, computational models (or model), external logic of aspect interactions (design criteria), and a set of established reuse patterns.

Identifying individual functionally complete mechanisms within the project space plays a crucial role in ensuring effective reuse of abstractions and components during system development. We will refer to such mechanisms as project platforms. They provide an application interface for constructing an upward hierarchy of abstractions and specifications for creating downward implementations. In the context of software architecture, reusable architectural platforms are documented as architectural patterns.

**Computational Models, Computational Mechanisms, and Virtual Machines.** A MoC is a mathematical model that demonstrates the computational capabilities and rules for using a computational subject. The computational mechanism captures principles and technical solutions. Virtualization represents an abstract (model-based) representation of computational resources in a computing platform, and a virtual computing machine is a technical solution that implements the semantics of the MoC.

Levels of complexity in Computational Mechanisms:

1. Atomic (Standard) computational functional elements (SN74, language operators, etc.);
2. Composite computational functional elements (composed of multiple basic elements);



https://doi.org/10.5593/sgem2024/2.1/s07.03

3. Subsystems for organizing computational processes (interrupt handling, caching, and queues);
4. Complex computational processes;
5. Virtual computing machines exhibit significant computational functionality and are self-sufficient for solving complete computational tasks.

Considering abstract mechanisms and virtual machines invariantly with respect to hardware and/or software implementation is beneficial. Architectural mechanisms allow us to describe a system at a high level of abstraction, but certain parts of the system require detailed consideration at intermediate (microarchitectural) levels.

The microarchitecture level is the internal structure of functionally complete blocks of a computer system, such as communication controllers, memory blocks of various purposes, virtual machines, computing platforms. It can be said that architecture is general principles, and microarchitecture is private principles of computer organization. The main tasks of microarchitectural design are [8]: formation, visualization and documentation of the design solution space; generation of design solutions and exploration of the design solution space; verification and selection of design solutions.

**Organization of computational processes and aspect-oriented design.** As noted, the process of designing ES as an object that solves the final task is proposed to be considered as the organization of computational processes in space and time within specified constraints. This allows formulating the principle of computational process actualization as a set of transformations from the initial representation of the target algorithm to its final form and supplementing the concept of 'solving the target task at Run-time' with a set of 'computational' preparatory operations during the 'Design-time' phase.

The aspect-oriented model complements the view of organizing computational processes. Examples of aspects include functional, instrumental, reliability, energy-related, synchronization, real time issues, reconfigurability, and an open list, which is determined by the developer.

**Reconfigurable Systems.** With today's technological advancements, the architectural characteristic of reconfigurability in ES is gaining increasing importance [10]. It significantly influences the organization of computational processes. However, a precise interpretation of this property remains elusive. Specialists include architectures ranging from homogeneous computational environments with varying granularity of elements (such as FPGAs) to computational networks of different scales (both spatially distributed configurations and on-chip networks).

The presented system of architectural abstractions allows considering reconfigurability in ES as the ability to adapt for the current execution stage of the MoC, overcoming rigid opposition in implementation (hardware or software), elevating the level of abstraction, and unifying design solutions. Figure 2 shows a generalized diagram of the reconfiguration process.

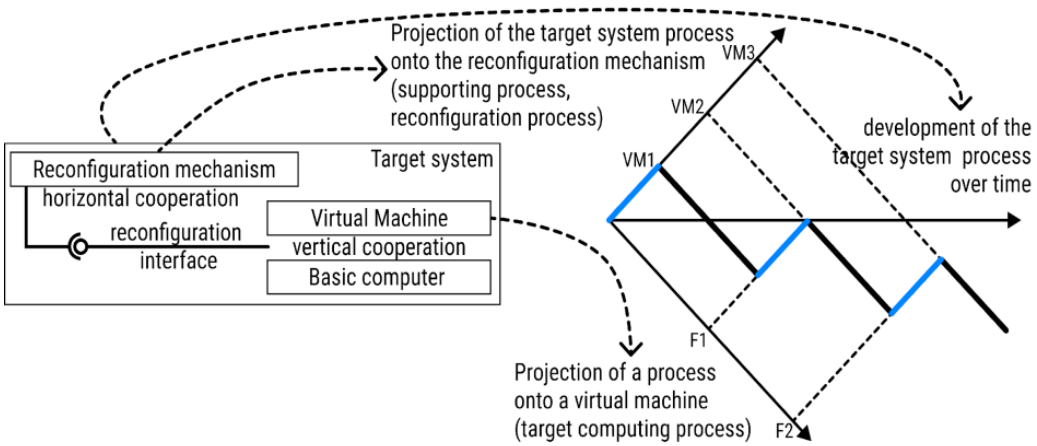


**Figure 2** - Generalized diagram of the reconfiguration process.

## APPLICATION OF ABSTRACTION SYSTEM WHILE CREATING DISTRIBUTED EMBEDDED SYSTEMS

Development of distributed heterogeneous ES platforms demands joint usage of various architectural templates. Developers are forced to merge diverse devices on communication protocols and internal working logic. Processes in nodes are parallel, which significantly complicates the task of developing and debugging. We will comment on key aspects that represent the most difficulties in designing platforms for distributed ES.

**Heterogenous networks.** The differences of the hardware blocks and software implementations of protocol stacks demands complex unification systems for providing effective communication between net devices. A balanced solution to such a task can be done only with deep analysis of common and private mechanisms, platforms and technologies.

**Levels and domains of programming.** The runtime environment, representing abstractions and various approaches to programming, can be based on a virtual machine, interpreter, compiler or explicitly machine code [11]. Using a language virtual machine provides a domain-specific sandbox and hides the internal structure of the platform from the programmer. Configuration plays an important role, requiring the development of specialized algorithms or individual customization to meet customer requirements.

**Engineering-significant properties and attributes.** In technical documentation, there is a lack of essential engineering-significant attributes of design abstractions, which obstructs to make an informed choice at the conceptual level of mechanisms, technologies and technical solutions. Examples of such technical characteristics, metrics, attributes are: application functionality, system mechanisms and processes, basic computing architecture, communication blocks and protocols supported by them, low-level technical parameters, design, reliability set of issues, information security solutions, tools, configuration, software updates, security and quality of documentation, etc. Organizational aspects such as command structure, decision-making processes and work coordination are also important.

Let's consider examples using the proposed abstraction system.



https://doi.org/10.5593/sgem2024/2.1/s07.03

**Evaluating the performance of various programming stacks.** Programmable Logic Controller systems simplify for engineers without requiring extensive programming knowledge. The IEC 61131-3 standard offers a logical model for such a controller [12], in addition, they can support general-purpose programming languages (C/C++, Python, Java etc.). A virtual machine can be the execution environment for systems, for example, WebAssembly Micro Runtime (WAMR), is a lightweight and high-performance runtime for WebAssembly that supports fast interpretation, JIT and AOT compilation, XIP, multithreading and native platform function calls [13]. It supports various platforms including Windows, Mac, Linux and various real-time operating systems (RTOS) such as Zephyr, ESP-IDF, Riot, NuttX, rt-thread etc. However, due to differences in interface implementations between the virtual machine runtime and the system platform, not all programming languages and performance testing tools (Dhrystone, Coremark, Jetstream etc.) can be run on supported platforms. Coremark tests showed differences in performance across various platforms. On the Apple M1, performance dropped by about 10% in AOT mode, while on the Cortex-M7 in Zephyr it decreased by more than 15 times (Table 1).

**Table 1.** Result of running Coremark 1.0 (4000 iterations, Clang 17.0.6)

| CPU | Target | Op/sec |
|---|---|---|
| Apple M1 | Native | 33076.31 |
| Apple M1 | WAMR AOT | 30389.74 |
| Apple M1 | WAMR classic interpreter | 1577.6 |
| Cortex M7 | Native (based on STM32H743 datasheet) | 2424 |
| Cortex M7 | WAMR AOT | 156.42 |
| Cortex M7 | WAMR classic interpreter | 5.2 |

**Data transfer protocols** offer various application models of interaction, which is manifested in addressing, the amount of data transferred, time restrictions, and data representation models. To unify such solutions, the developer can create a level of abstraction and unification. This will allow different protocols to be used together on one platform. The effectiveness of such unification is impossible without understanding the associated protocols at the microarchitectural level. Figure 3 shows a possible arrangement of such protocols for joint use within a single platform.

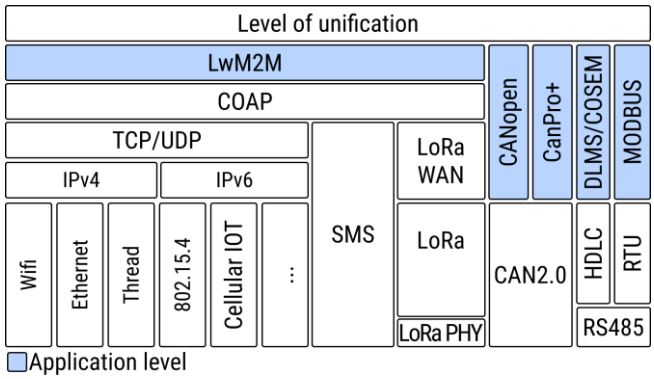


**Figure 3** - Possible arrangement of wired/wireless stacks within one platform

**The choice of a microcontroller** for a ES with a graphical HMI and CAN, RS485, GPIO interfaces must take into account that displaying graphic information from external RAM requires an analysis of the characteristics of the peripheral RAM unit, the time delays of the memory chip, the width of the data bus and the available pins of the microcontroller. An overview of the microcontroller's properties presented in the basic documentation, allows us only to roughly estimate its suitability for a specific task.

## DISCUSSION

To qualitatively assess the situation and prospects for the development of high-level embedded systems design methods, we will try to answer a number of questions.

Why is there a shortage of high-quality technical documentation, which presents not only "implementation level" material, but also information at the conceptual, microarchitectural level? We see the reason in the insufficient number of specialists capable of describing the essence of solutions and technologies from such perspectives.

What ways are there to increase the number of such "advanced" specialists? This is due to the market need for them and the ability of the educational environment to prepare them in sufficient quantities. Today we answer the question like this. In general, the demand for such specialists in the industry is a unique situation. For the academy, graduating such specialists is "piece production." The initiative should rather come from the industry.

The situation with the tools: they are actually being developed through the efforts of individual specialists and groups who create high-level design methods [3, 14, 15]. The industry is inert in terms of their implementation. The goal of the academy for such design methods is to lower the "barrier to entry".

## CONCLUSION

One of the possible approaches to designing distributed heterogeneous computing systems is based on representing the computational system through a system of abstractions. The elements of this approach should be considered as a methodological direction called High-Level Design (HLD), the formalization of which occurs during its formation. Nevertheless, in practice, the community applies this view to computer technology and continues to work towards formalizing its individual parts. A number of complex projects have been successfully completed, and their results have been integrated into serial production.

As we see it, the view demonstrated in the work has many advantages, primarily in the field of embedded distributed systems, where there is a high proportion of custom design. As part of scientific activity, work is underway to formalize this methodology and bring it to the level of technology or a set of technologies.

## REFERENCES

[1] Sangiovanni-Vincentelli A., Martin G. Platform-based design and software design methodology for embedded systems, IEEE Design and Test of Computers, 2001, vol. 18, no.6, pp.23–33, doi: 10.1109/54.970421;



https://doi.org/10.5593/sgem2024/2.1/s07.03

[2] J. Sifakis, "A framework for component-based construction," Third IEEE International Conference on SEFM, Germany, 2005, pp. 293-299, doi: 10.1109/SEFM.2005.3;

[3] Sangiovanni-Vincentelli A., Damm W., Passerone R., Taming Dr. Frankenstein: Contract-Based Design for Cyber-Physical Systems, Eur. J. Control. 2012. Vol. 18. P. 217-238, doi: 10.3166/ejc.18.217-238.

[4] Teich J. Hardware/software codesign: the past, the present, and predicting the future. Proceedings of the IEEE, 2012, vol. 100, pp. 1411–1430, doi: 10.1109/JPROC.2011.2182009;

[5] Sehr M.A., Lohstroh M., Weber. M, Ugalde I., Witte M., Neidig J., Hoeme S., Niknami M., Lee E.A., Programmable Logic Controllers in the Context of Industry 4.0, in IEEE Transactions on Industrial Informatics, vol. 17, no. 5, pp. 3523-3533, May 2021, doi: 10.1109/TII.2020.3007764;

[6] Embedded Systems Engineering Roadmap, Dec 23, 2023, url: https://github.com/m3y54m/Embedded-Engineering-Roadmap?tab=readme-ov-file;

[7] Kolchurin M.V., Pinkevich V.Yu., Platunov A.E. Strengthening the role of microarchitectural stages of embedded systems design. Scientific and Technical Journal of Information Technologies, Mechanics and Optics, 2022, vol. 22, no. 4, pp. 716–724 (in Russian). doi: 10.17586/2226-1494-2022-22-4-716-724;

[8] Pinkevich V., Platunov A. Using architectural abstractions in embedded system design, Proceedings of the 4th Mediterranean Conference on Embedded Computing (MECO 2015), Works in Progress in Embedded Computing, 2015, Vol.1, No.1, pp. 3-6;

[9] Chattopadhyay A., Ingredients of Adaptability: A Survey of Reconfigurable Processors, VLSI Design. 2013. doi: 10.1155/2013/683615;

[10] Lech J., Nadia N., Modern Architectures for Embedded Reconfigurable Systems - a Survey., Journal of Circuits, Systems, and Computers, April 2009, 18. p209-254. 10.1142/S0218126609005034;

[11] Panagopoulos, G. Papakonstantinou, N. Alexandridis, and T. ElGhazawi, “A comparative evaluation of models and specification languages for Embedded System design”, LCTES-03, San Diego, Ca., June 11-13, 2003;

[12] Catalão, T., Sousa, M.D, IEC 61131-3 Front-End for the LLVM Compiler Family, ETFA, pp. 1191-1194, 2020 doi: 10.1109/ETFA46521.2020.9211921;

[13] Xu J., He L., Wang X., Huang W., Wang N., A fast WebAssembly Interpreter design in WASM-Micro-Runtime, 07.10.2021, url: https://www.intel.com/content/www/us/en/developer/articles/technical/webassembly-interpreter-design-wasm-micro-runtime.html;

[14] D. Densmore, R. Passerone, A. Sangiovanni-Vincentelli, "A Platform-Based Taxonomy for ESL Design," in IEEE Design & Test of Computers, vol. 23, no. 5, pp. 359-374, May 2006, doi: 10.1109/MDT.2006.112;

[15] Menard C., Lohstroh M., Bateni S., Chorlian M., Deng A., Donovan P., Fournier C., Lin S., Suchert F., Tanneberger T., Kim H., Castrillon J., and Lee E.A., High-performance Deterministic Concurrency Using Lingua Franca. ACM Trans. Archit. Code Optim. 20, 4, Article 48 (December 2023), doi: 10.1145/3617687.

# ARTIFICIAL NEURAL NETWORK VS. LINEAR REGRESSION FOR MODELING REACTOR OF THE CATALYTIC CRACKING PROCESS

**Asist. Prof. Dr. Bogdan Doicin**[1]

**Asist. Prof. Dr. Mădălina Cărbureanu**[1]

**Assoc. Prof. Dr. Cristina Roxana Popa**[1]

[1] Petroleum Gas University of Ploiesti, **Romania**

## ABSTRACT

The paper presents the research and results obtained by authors concerning the reactor modeling of the catalytic cracking process using two methods: artificial neural network (ANN) and multiple linear regression (MLR). This study is structured in four parts. The first part presents the process description, and the existing models in the literature. The second part presents the multiple linear regression method, the reactor model obtained with this method, and the comparison between the output experimental data of the reactor and output variables predicted with the MLR method. The experimental data were taken from a Romanian refinery. The next section describes the steps involved to build the neural network developed by authors for modeling the reactor, and the result of the comparison between the output experimental data of the reactor and output variables predicted with the ANN. The result shows that the neural model developed for the reactor is superior to the statistical model obtained with multiple linear regression.

**Keywords:** catalytic cracking, artificial neural network, regression

## INTRODUCTION

The catalytic cracking plant is one of the most important units in a refinery. The final products of the catalytic cracking process are gasoline, diesel, gas from lower feedstock resulting as byproducts from other plants such as vacuum distillation. This process is, at the same time, a supplier of heat from the regenerator of spent catalyst. The performance increase of the catalytic cracking plant is influenced by how the process is designed and modelled, and by control structure design. In this paper, the authors focused on reactor modelling, one of the main process components which influence the reactor performance [1].

The catalytic cracking process consists of two components, respectively the reactor and the regenerator. The reactor can be decomposed into several sub-processes, namely [2]:

- interfusion node sub-process, located at the reactor base. Here, the feed stock is mixed with the regenerated catalyst.
- riser sub-process, where the chemical reactions take place. The result is in the form of the reaction products.
- stripper sub-process, located at the reactor upper zone, where the reaction products are separated from catalyst.

https://doi.org/10.5593/sgem2024/2.1/s07.04

The regenerator is a complex system, resembling with a perfect mixing reactor, in which the regeneration of the catalyst takes place by partial combustion of the coke deposited on the catalyst.

Due to the complexities and uncertainties of this process, in recent years, most papers in the literature deal with modelling using artificial intelligence techniques. Papers [3, 4] are describing the steady-state behavior of the reactor, using artificial neural networks. Papers [5, 6] are using machine learning models based on regression to develop the model to control the yield of the output variable of the catalytic cracking process. A hybrid model for the catalytic cracking based on regression method and artificial neural network was presented in papers [7, 8].

This work presents the results obtained by modeling the reactor of catalytic cracking process using artificial neural networks and machine learning based on multiple linear regression. Industrial data from a Romanian petroleum refinery waere used to develop, train, and validate the obtained models. This work is focused on determining the output variables of the reactor interfusion nod e temperature $T_{nod}$, reactor temperature $T_r$, yield gasoline and octane number research. The input variables are feedstock temperature - $T_{mp}$, regenerated catalyst temperature -$T_{reg}$, feedstock flow – $Q_{mp}$, and regenerated catalyst flow -$Q_{cat.}$.

## MULTIPLE LINEAR REGRESION

Multiple linear regression (MLR) is a supervised ML algorithm used to determine the analyzed process model based on the relationship between the process output (dependent variable or response variable) and input variables (independent variables or predictor variables) [9, 10, 11]. It is probably the simplest and most popular way to measure the relationship between a continuous predictor and a response variable.
The MLR equation is given by the following formula [33, 34]:

$$Y = \beta_0 + \beta_1 \times X_1 + \beta_2 \times X_2 + \cdots + \beta_n \times X_n \quad (1)$$

In equation (1), Y represents the dependent variable (response variable), $X_1$ to $X_n$ represent the independent variables (continuous predictor) while $\beta_0$ to $\beta_n$ represent the equation parameters.

Figs. 1- 4 present the comparison between the output experimental data of the reactor (experimental data of the interfusion nod-$T_{nod\_exp}$, experimental data of the reactor temperature – $T_{react\_exp}$, experimental data of the gasoline yield- $Q_{gasoline\_exp.}$, experimental data of the COR- $COR_{exp}$) and the output variables predicted with the MLR method (predict data of the interfusion nod-$T_{nod\_pred}$, predict data of the reactor temperature – $T_{react\_pred}$, predict data of the gasoline yield- $Q_{gasoline\_pred}$, predict data of the COR - $COR_{pred}$). In this aspect, it uses the Linear Regression class from the Scikit-Learn Python library.

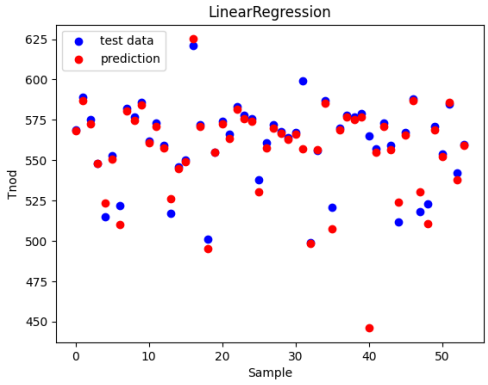


**Figure 1.** Comparison between $T_{nod\_exp}$ and $T_{nod\_pred}$ using MLR.

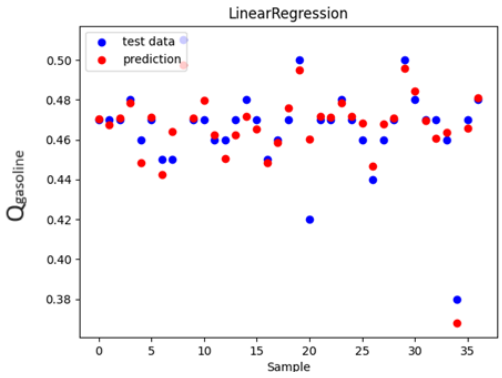


**Figure 3.** Comparison between $Q_{gasoline\_exp}$ and $Q_{gasoline\_pred}$ using MLR.

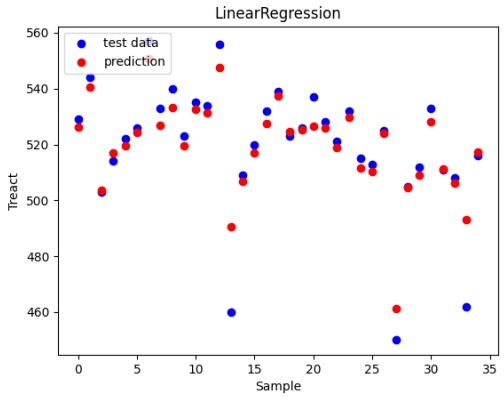


**Figure 2.** Comparison between $T_{react\_exp}$ and $T_{react\_pred}$ using MLR.

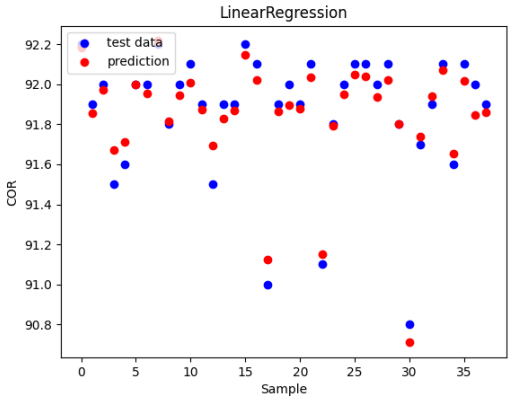


**Figure 4.** Comparison between $COR_{\_exp}$ and $COR_{pred}$ using MLR.

Table 1 presents the obtained model's evaluation metrics (using Linear Regression class from Scikit-Learn Python library) for MLR algorithm, such as: explained variance score (the errors dispersion degree), $R^2$ score (the coefficient of determination), mean absolute error (the average of the individual predictions errors absolute values), mean absolute percentage error (the average of the absolute percentage value of the individual predictions error) and median absolute error (the average distance between the data set values and their average) [12].

**Table 1.** The model evaluation metrics for the MLR algorithm.

| **Performance criteria / Output variable** | **Explained variance score** | **$R^2$ score** | **Mean absolute error** | **Mean absolute percentage error (MAPE)** | **Median absolute error** |
|---|---|---|---|---|---|
| *Tnod* | 0.741 | 0.50 | *7.87* | *0.02* | 6.511 |
| *Tr* | 0.865 | 0.865 | *1.15* | *0.01* | 5.114 |
| $Q_{gasoline}$ | 0.815 | 0.815 | *0.47* | *1* | 0.114 |
| *COR* | 0.947 | 0.944 | *6.51* | *0.01* | 0.133 |

https://doi.org/10.5593/sgem2024/2.1/s07.04

## ARTIFICIAL NEURAL NETWORKS

Artificial neural networks (ANNs) are an AI method, inspired by the structure and function of the human brain [13]. They are represented as a collection of nodes, known as artificial neurons, connected in a specific way. The developed model using ANNs is a black box described by mathematical equations that calculate the output variables depending on the input variables [13]. ANNs are trained, validated, and tested using different data sets. In this study, the Keras Python library was used for developing an ANN model for the reactor.

The training of the ANN, the output, and the input experimental data were split randomly into training, validation, and testing data, such as 66% training data, 17% validation data, and 17% testing data.

The ANN development involved the following steps: data preprocessing, the determination of the ANN structure, the establishing the best network parameters, evaluating the ANN's estimation precision using the testing data.

Data preprocessing involves the use of the Min-Max Scale algorithm to resize or normalize the input variable sizes of the raw data [14]. Normalizing the input variables is supposed to bring the value of the input variables into a specific interval, usually between 0 and 1 or 1 and -1. This is a common practice in neural network training, being useful in the efficient training and setting of the input sizes values, the fact that facilitates the rapid convergence and stability of the model [14]. The Min-Max Scale algorithm is based on the following relations [14]:

$$X_{std} = \frac{X - X_{min}}{X_{max} - X_{min}} \quad (3)$$

$$X_{scaled} = X_{std} * (Xmax - Xmin) + min \quad (4)$$

In equations (3) and (4), x is the original value, $min$ - the lower bound of the scaling range, max the upper bound of the scaling range, X min – the minimum value of the dataset's inputs, $X_{max}$ – the maximum value of the dataset's inputs, $X_{std}$ – the standard deviation of the dataset.
Another problem that is encountered before the construction of the ANN is the identification of the relationships between the input variables of the reactor, to evaluate the data collinearity or redundancy problems. This relationship between input variables is represented by a correlation matrix, which is a square matrix in which each element represents the correlation coefficient between two variables.

The analysis of the correlation matrix can help in the identification of variables that are highly correlated with each other. The highly correlated input variables can be considered redundant and as a result, can be removed from the dataset to reduce the neural network model size and complexity [15]. The visualization of these correlations is illustrated through the heatmap graph, depicted in figure 5. From figure 5, it can be noticed that the regenerated catalyst flow and the feedstock flow are highly correlated, with a correlation coefficient of 0.87. This can mean that the regenerated catalyst flow can be redundant, thus it can be removed.

The main structure of ANN is shown in figure 6. There is an input layer, a hidden layer, and an output layer. The input layer consists of four neurons (the number of neurons equal

to the input variables of the model) and the output layer consists of four neurons. The neuron number of the hidden layer and the activation function were determined using the Grid Search algorithm from the Python Keras library. The number of hidden layer neurons is two hundred and ten and the activation function is the exponential linear (in Python represented by "elu" function). For the output layer, the activation function is rectified liner (in Python represented by "relu" function). The Backpropagation algorithm was used to train the ANN.

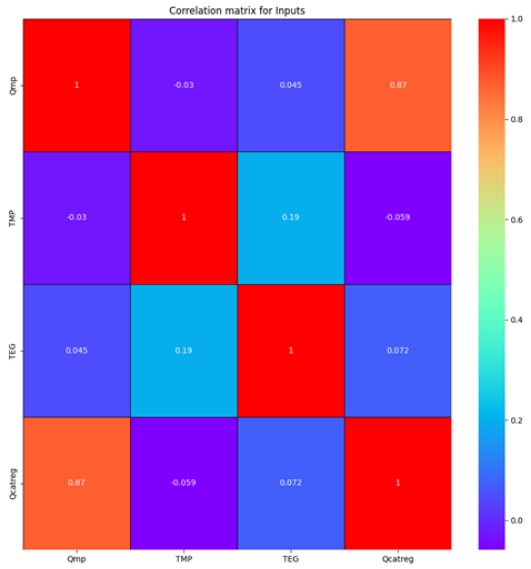


**Figure 5.** Input variables heatmap graph.

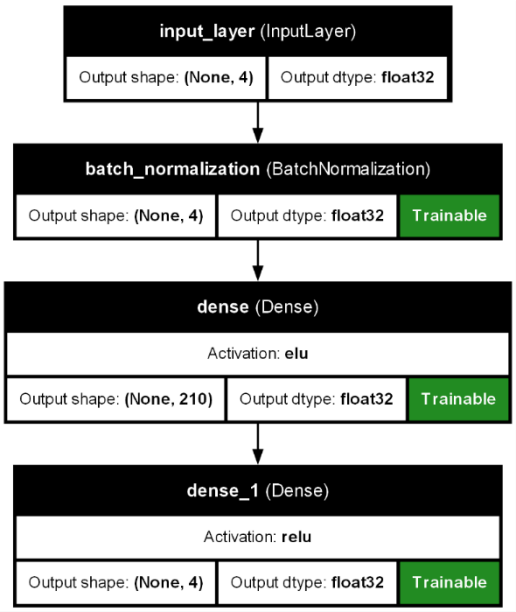


**Figure 6.** The structure of the ANN.

Figures. 7-10 present the comparison between the output experimental data of the reactor (experimental data of the interfusion nod-$T_{nod\_exp}$, experimental data of the reactor temperature – $T_{react\_exp}$, experimental data of the gasoline yield- $Q_{gasoline\_exp}$, experimental data of the RON- $COR_{exp}$) and output variables predicted using ANN(predict data of the interfusion nod-$T_{nod\_pred}$, predict data of the reactor temperature – $T_{react\_pred}$, predict data of the gasoline yield- $Q_{gasoline\_pred}$, predict data of the RON - $COR_{pred}$). Table 2 presents the model's performance developed with ANN.

**Table 2.** The evolution metrics for ANN.

| Performance criteria / Output variable | Explained variance score | $R_2$Score | Mean absolute error | Mean absolute percentage error (MAPE) | Median absolute error |
|---|---|---|---|---|---|
| Tnod | 0.455 | 0.535 | 6.0 | 0.0107 | 2.04 |
| Treact | 0.812 | 0.763 | 4.90 | 0.009 | 2.77 |
| $Q_{gasoline}$ | 0.717 | 0.631 | 0.005 | 0.013 | 0.004 |
| COR | 0.711 | 0.767 | 0.060 | 0.0006 | 0.051 |

https://doi.org/10.5593/sgem2024/2.1/s07.04

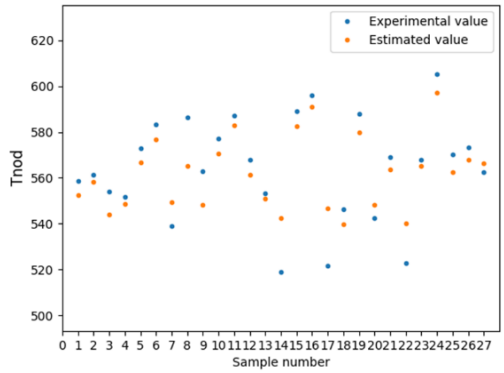


**Figure 7.** Comparison between $T_{nod\_exp}$ and $T_{nod\_pred}$ using ANN.

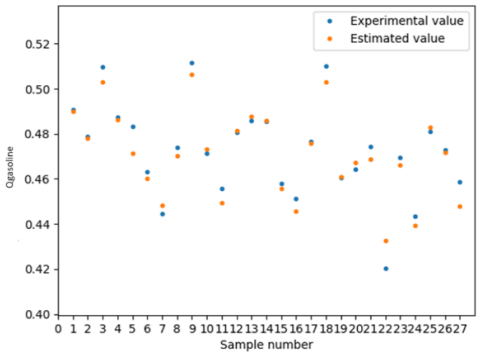


**Figure 9.** Comparison between $Q_{gasoline\_exp}$ and $Q_{gasoline\_pred}$ using ANN.

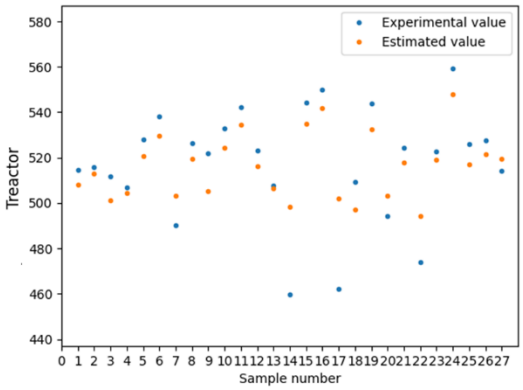


**Figure 8.** Comparison between $T_{react\_exp}$ and $T_{react\_pred}$ using ANN.

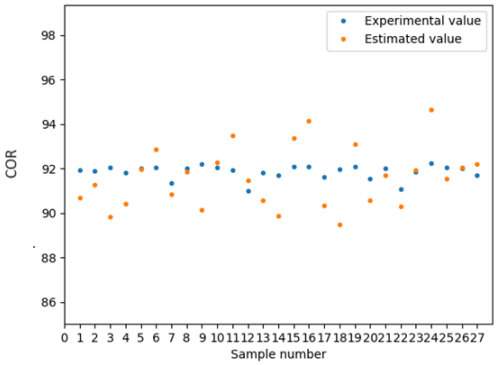


**Figure 10.** Comparison between $RON_{\_exp}$ and $RON_{pred}$ using ANN.

## RESULTS AND DISCUSSION

A comparison of gasoline yield and RON with two methods is lustrated in figures 11 and 12. As it can be observed, the artificial neural network is more suitable for estimating the yield of gasoline and RON.

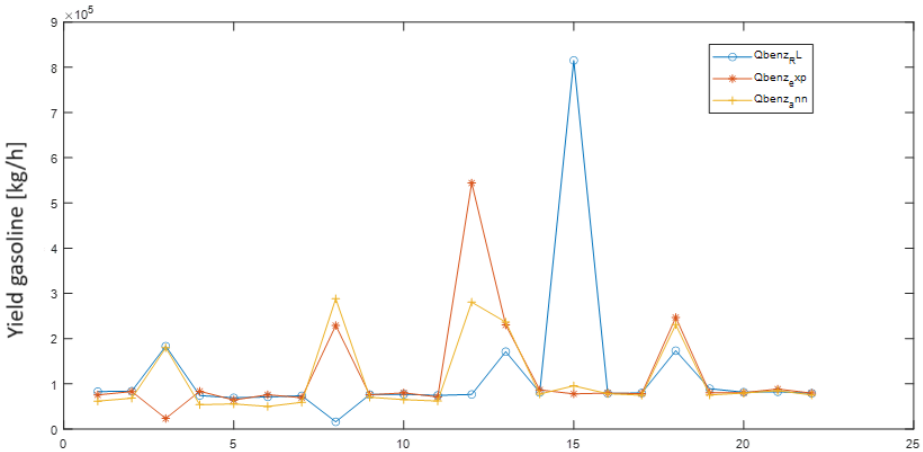


**Figure 11.** Comparison between yield gasoline experimental date - $Q_{benz\_exp}$, yield gasoline estimate data with ANN- $Q_{benz\_ann}$ and yield gasoline estimate data with MLR- $Q_{benz\_RL}$.

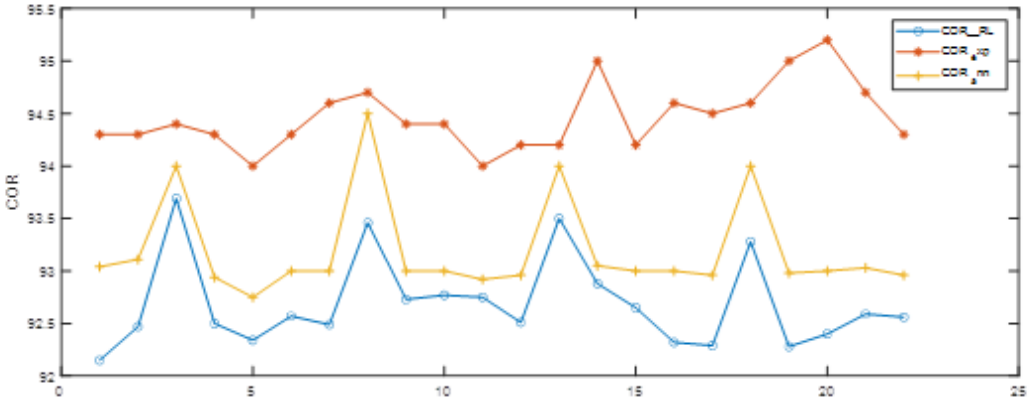


**Figure 12.** Comparison between RON experimental date - $COR_{exp}$, RON estimate data with ANN - $COR_{\_ann}$ and RON estimate data with MLR- $COR_{\_RL}$.

## CONCLUSION

This paper is focused on developing two models of the steady-state behavior of the catalytic cracking reactor: artificial neural networks and multiple linear regression. The models were developed on measured data from an industrial catalytic cracking process.

The linear regression model is based on a polynomial equation. The ANN model is based on three layers, the first layer has four neurons representing the input variable of the reactor, the second layer has 201 neurons, the output layer has four neurons representing the output variables of the reactor. The used learning algorithm is backpropagation and the activation functions that were used were exponential linear unit and rectified linear.

A comparison of the data obtained with the two methods, showed that the artificial neural network method (ANN) is more suitable to estimate de yield of gasoline and COR, because the mean absolute percentage error is much lower (0.013, respectively 0.001) in this case compared with mean absolute percentage error calculated for multiple linear regression (1 respectively 0.0006).

The artificial intelligence techniques (in this case the artificial neural networks and the machine learning method based on multiple linear regression) can be successfully used in modelling the catalytic cracking process, because it has a highly nonlinear behavior.

## REFERENCES

[1] Popa C., Pătrășcioiu C., Approach in Modelling, Simulation and Hierarchical Control of the Fluid Catalytic Cracking Process I - Process Modeling, vol. 61, 2010, pp. 419-426.

[2] Reza S., Fluid Catalytic Cracking Handbook Design, Operating and Troubleshooting of FCC Facilities, Gulf Publishing Company, Houston Texas, 2000.

[3] Michalopouls J., Papapdokonstadakis S. AramPatzis G., Lygeros A., Modelling an industrial fluid catalytic cracking unit using neural networks, Tans I Chem E., vol 79 Part A, 2001, pp. 137-143.

[4] Mustapha K, K, Mujahed A. D., Othman T., Artificial intelligence perspectives: A systematic literature review on modeling, control and optimization of fluid catalytic cracking, Alexandria Engineering Journal, vol. 80, 2023, pp 295-314.

[5] Al- Enezi G., Fawzi N., Elkamel A., Development of regression models to control product yields and properties of fluid catalytic cracking process, Petroleum Scinec technology, vol. 17, 1999, pp. 535-552.

[6] Yang F., Zhaiu M., Dai C. N., Cao J., Construction, and analysis of gasoline yield prediction model for FCCC unit based on artificial intelligence algorithm, Acta Petrolei Sinica, vol. 35, 2019, pp 807-817.

[7] Bollas G.M., Papapdokinstadakis S., Mivhalopoulos J., Arampatiz G., Lygeros A., Using hybrid neural networks in scaling an FCC model from pilot plant to an industrial unit, Chemical Engineering Process, vol 42, 2003, pp. 697-713.

[8] Yang F., Dai C., Tang J., Jin X., Cao J., A hybrid deep learning and mechanistic kinetics model for a prediction of fluid catalytic cracking performance, Chemical Engineering Research and Desing, vol. 15, 2020, pp 202-220.

[9] Maulud D. H., Abdulazeez A. M, A Review on Linear Regression Comprehensive in Machine Learning, Journal of Applied Science and Technology Trends, vol. 1, 2010, pp. 140 –147.

[10] Mechelli A, Vieira S., Machine Learning: Methods and Applications to Brain Disorders, Elsevier, 2019.

[11] Tosun E., Aydin K, Bilgili M., Comparison of linear regression and artificial neural network model of a diesel engine fueled with biodiesel-alcohol mixtures, Alexandria Engineering Journal, vol. 55, 2016, pp. 3081-3089.

[12] Cărbureanu M., Mihalache S. F., Zamfir F., Machine Learning Methods Applied for Wastewater pH Neutralization Process Modeling, 2022 14th International Conference on Electronics, Computers and Artificial Intelligence (ECAI), Ploiesti, Romania, 2022, pp. 1-6.

[13] Haykin S., Neural Networks: A Comprehensive Foundation, Pentice Hall, Ontario, 1999.

[14] Sinsomboonthon S., Performance Comparison of New Adjusted Min-Max with Decimal Scaling and Statistical Column Normalization Methods for Artificial Neural Network Classification, International Journal of Mathematics and Mathematical Sciences, vol. 6, 2022, pp. 2-11.

[15] Reza R. R, Mohammadreza B., Sajadi S.M, Pirmoradian M., Renani M.M., Baghaei Sh., Salahshour S., Prediction of the thermal behavior of multi-walled carbon nanotubes-CuO-CeO2 (20-40-40)/water hybrid nanofluid using different types of regressors and evolutionary algorithms for designing the best artificial neural network modeling, Alexandria Engineering Journal, vol . 84, 2000, pp. 184–203.

# CONTROL SYSTEM FOR GREENHOUSES USING INDUSTRIAL NETWORKED DEVICES

**Assoc. Prof. Dr. Alexandru Dumitrascu**
National University of Science and Technology Politehnica Bucharest, **Romania**

## ABSTRACT

The modern monitoring and control systems that are currently used in most fields are based on intelligent algorithms, distributed management systems, and a new generation of communication buses. For the monitoring and control of the processes inside a greenhouse, the use of sophisticated algorithms or complex devices is not required. However, to make the activity more efficient and increase the production of a greenhouse, a proposed solution is to use data management and control system such as PLC and HMI devices, which are interconnected using industrial bus and communication protocol – Profinet and ModbusTCP. The data acquired from the greenhouse are retrieved by means of sensors connected to nodes with wireless transmission. The wireless communication variant proved to be the most efficient, in the greenhouse environment being an increased humidity due to the irrigation process of the plants. Also, the need for space for the plants requires giving up the wires drawn through the greenhouse.

**Keywords**: control system, PLC, HMI, wireless sensors, greenhouse

## INTRODUCTION

The main objective of this paper is to develop an automatic monitoring and control system for ecological areas in closed spaces, with greenhouse application. The proposed solution has both a hardware and a software part, which involves a wireless communication of the parameters measured by the sensors in the greenhouse environment, so that this space can be managed to the maximum.

The distributed control system is based on a dedicated hardware architecture and an appropriate software package, which includes steps such as data acquisition and data processing, communication methods and data transmissions, automatic control modules and, finally, the appropriate actuators elements from the process level of the greenhouse environment - in this case, the irrigation process. Knowing the fact that, for investments in agriculture, the interest is on the rise, in the case of the ecological system of the greenhouse farm type, timely irrigation of crops is the key operation in obtaining superior productions, in terms of volume and quality [1]. Due to its versatility, the system can be implemented on a smaller scale to be studied as a teaching platform.

The monitoring and control architecture are used as parameters of interest both the internal and the external parameters of the greenhouse environment. Thus, the internal parameters of the greenhouse environment are soil humidity and soil temperature, which are used to carry out the irrigation process. The external parameters of the greenhouse environment are obtained from a micro-weather station, which is mounted near the greenhouse. These external parameters are amount of precipitation, barometric pressure,



https://doi.org/10.5593/sgem2024/2.1/s07.05

wind direction, wind speed, solar radiation, dew point, temperature, and humidity of the environment. By monitoring all these internal and external parameters of the greenhouse, optimal decisions can be made for the automatic control of the irrigation process of the plants and obtaining a favorable climate for them [2].

The configuration stages of the experimental system for monitoring and control the greenhouse environment consist of the following: 1) design and configuration of the wireless sensor network; 2) testing the PLC and HMI equipment used to control the irrigation process; 3) implementation of dedicated software packages, for monitoring and control, at the level of PLC and HMI type equipment; 4) implementation of a communication protocol, which makes possible the transfer of data between the data acquisition system and the data processing system, with a role in decision-making and the control of actuators.

The equipment used for data processing and automatic control are represented by S7-1200 PLCs and LOGO! 0BA8, and two touch operator panels were used for local monitoring: Simatic KTP600 and ēlo Touchsystems. The TIA Portal software platform was used to program these devices. For the acquisition of the data received from the sensors, a PC-type server was configured, on which a Linux Debian distribution runs. Also, the server runs a software application that can store the purchased data for a long time, thanks to the very large capacity hard disk. At the same time, this software application offers the possibility to graphically display, over a certain period, a history of the data values provided by the sensors. At the same time, this graphical interface can also be accessed remotely, for monitoring the values of environmental parameters or possible data exports. Also, a Modbus-TCP communication protocol was implemented to make possible the data transfer between the server that manages the database and the automatic control system, represented by PLC and HMI equipment, so that, initially, they could not communicate with each other.

## DATA ACQUISITION AND MONITORING SYSTEM

The data acquisition and monitoring system of the irrigation process in the micro-greenhouse refers to a network of sensors with wireless transmission, which measure the humidity and temperature values in the soil. The values of the measured parameters can be managed in databases and monitored via a user interface. The hardware components of the acquisition subsystem are sensors, wireless nodes, radio base and server. The sensors used inside the greenhouse are: ES1101 – soil humidity and temperature sensor, ES1110 – soil water quantity sensor and ES1201 – ambient humidity and temperature sensor. The sensors are connected via wires to the wireless nodes. Each node has 4 connection ports available. The power supply of the nodes is dual, using both rechargeable batteries and solar batteries, which is why the operating time extends over a long period of time. From the nodes, the values of the measured parameters are transmitted wirelessly to the radio base, which manages the 7 nodes of the acquisition system. Of these, 6 nodes are placed inside, and one is outside, for the micro-weather station, presented in Figure 1, which takes data from the external environment of the greenhouse, providing values for the following parameters: temperature, humidity and air dew point, wind direction and speed, amount of precipitation, solar radiation and barometric pressure [3].


**Fig. 1.** The micro-weather station, the radio-base and a wireless node.

The central component of the data acquisition and monitoring system is the server, a PC-type device running a Linux-Debian distribution. On this server, the acquisition and storage of the data received from the sensors is carried out, having integrated several software packages, two of which are the main ones:

- a web application through which the network of ground-air sensors is configured and managed, the result being the acquisition and local or remote monitoring of all the values of the parameters measured by the sensors.
- a software package based on the ModbusTCP communication protocol, implemented to establish the connection, on the Profinet bus, between the data server and the central device of the control system, represented by the S7-1200 PLC, LOGO! PLC, and KTP600 touch-panel.

All data is stored in SQLite database, carrying out separate data sampling, with the possibility of displaying at intervals of a day, a week, a month, 6 months, or a year. Thus, it is possible to monitor the current values of the parameters for each individual node, obtain graphs with their histories over the mentioned periods or set warning alerts when the values of some parameters exceed a preset threshold, as can be seen in Figure 2. At the same time, this interface also provides data on the status of the network of wireless nodes, as well as the possibility of exporting the data in ".csv" type files.

**Fig. 2.** The Web-interface of data acquisition application.

Starting from the values taken from the field by the sensors and up to the commands provided by the network of programmable PLCs, the entire data flow fulfills the task of monitoring the parameters in the greenhouse space (soil and air) and outside it (air), in order to maintains through irrigation, within the limits imposed by the user, the water requirement for a series of plants inside the greenhouse [4,5].



https://doi.org/10.5593/sgem2024/2.1/s07.05

## THE CONTROL SYSTEM

Modern PLC and HMI equipment were used for the control system. The central component of the automation equipment, with the role of Master, is represented by a Siemens Simatic S7-1200 PLC, with a 1214C processor. In its default configuration, it has the Profinet communication interface, 14 digital inputs, two analog inputs and 10 digital outputs. Connected to the Profinet network with the S7-1200 Master is another PLC from the Simatic range, respectively LOGO! 0BA8, with the role of Slave, which has 12 digital inputs, 8 digital outputs and 4 analog inputs. Through the outputs of LOGO!, 4 actuators of the irrigation system are ordered: a pump and 3 electro-valves. For user-interface with the process, the Simatic KTP600 touch panel, with color screen, is used in the automatic control system. Thus, all parameter values from the 7 wireless nodes that connect the sensors in the field can be monitored locally, at the process level, as can be seen in figure 3.

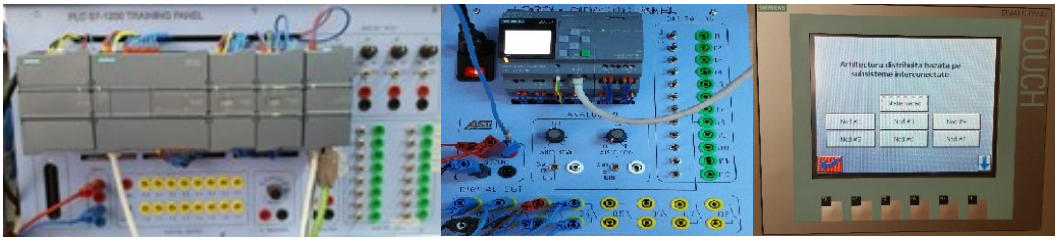


**Fig. 3.** The S7-1200 PLC – Master, LOGO! 0BA8 PLC – Slave, and KTP600 HMI equipment.

The PLC and HMI devices communicate each other on the Profinet bus through a CSM 1277 industrial switch, with 4 RJ45 ports. The 4th RJ45 port is used to connect the control system with the Server of the wireless sensor network for the transmission of the acquired data. To program the Master PLC, the TIA Portal package was used, using the method based on the Ladder Diagram. The programming of the KTP600 touch panel was done using the graphic module of TIA Portal, and the Slave PLC was programmed using the LOGO! SoftComfort v8.1 software. The control application is implemented in the Master S7-1200 equipment using simple numerical control rules. Here, the complexity is not represented by the control algorithm, which does not even have to be an elaborate one, but the part of achieving communication between equipment that, initially, did not have a common "language". Thus, a communication protocol based on ModbusTCP was implemented to transfer data from the data acquisition server to the S7-1200 Master in the irrigation control system.

## THE IRRIGTION SYSTEM

The connection between the control system and the irrigation system is made through the LOGO! PLC, which has inputs directly connected to the level sensors of the irrigation tank and outputs connected to the 4 actuators used. Both the level sensors and the actuators are ON/OFF type devices. The irrigation tank is fed directly from the general water supply network. The water tank has 3 float-type level sensors inside for maximum, middle, and minimum level, a float-type closing element to stop the water supply, and a submersible pump. The pump is powered by 12V DC voltage and has a maximum water flow of 18 l/min. The pump is connected to output Q4 of the LOGO! PLC.

The 3 electro-valves, presented in Figure 4, used in the irrigation system are:

- two NC (normal closed) electro-valves type, EV_2 and EV_3 in the Figure 5, with a 24V DC coil. These electro-valves are used to feed two separate irrigation channels. These actuators are connected to the first two outputs Q1 and Q2 of the LOGO! PLC, from which they also receive the supply voltage.
- one NO (normally open) electro-valve type, EV_1 in Figure 5, with a 220V AC coil. It is characterized by the fact that the electric valve closes only when the coil is supplied with energy. In the irrigation system, the NO electro-valve is used to turn off the general water supply to the water tank. This actuator is connected to the last output, Q4, of LOGO! PLC.

**Fig. 4.** The NC and NO electro-valves.

By coupling the data acquisition and monitoring system from inside and outside the greenhouse with the control system based on PLCs and the irrigation system, a distributed management architecture was obtained, which is presented in Figure 5.

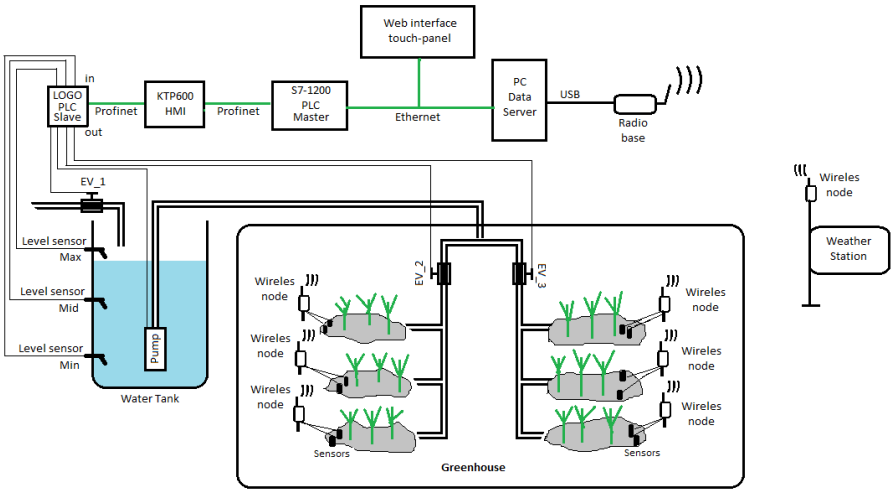


**Fig. 5.** The monitoring and control distributed architecture.

Another application made within the distributed irrigation system is represented by a software package implemented in C# and installed on a PC, which is connected to an information touchscreen. This touchscreen has an interface role for monitoring the data acquired by the server from the micro-weather station, as can be seen in Figure 6.



https://doi.org/10.5593/sgem2024/2.1/s07.05


**Fig. 6.** The Web interface of information touch-panel.

The data taken from the micro-weather station and displayed in the information touch-panel interface are wind speed, wind direction, rain accumulation, barometric pressure, air temperature, air humidity, solar radiation, and dew point. Thus, it is possible to remotely monitor both the values of the parameters of the environment inside the greenhouse, as well as the values of the parameters of the environment outside the greenhouse.

## CONCLUSIONS

The architecture of the proposed system is intended to be one of the successful solutions in the design and experimentation of an automatic system for monitoring and control the irrigation process in greenhouses, which uses modern equipment and communication bus, through which a series of tasks such as the acquisition and processing of process data, as well as the monitoring and control of greenhouse environment parameters, and through generalization the idea of implementing an "intelligent" greenhouse farm can be developed.

Moreover, in the current conditions there is more and more talk about ecological methods to produce the necessary food for people, this example of the proposed system lends itself very well to satisfying all the strict conditions imposed by a "green" economy, in which the effort and costs are minimal, and the production is at least satisfactory.

Thus, the microsystem described in this paper can be exported to larger areas, to represent an integrated system of data acquisition and processing, as well as automatic decision and control.

## REFERENCES

[1] C. Negru, G. Musat, M. Colezea, C. Anghel, A. Dumitrascu, F. Pop, C. De Maio, A. Castiglione, “Dependable workflow management system for smart farms”, Connection Science Journal, Volume 34, Issue1, Page1833-1854, DOI: 10.1080/09540091.2022.2083078, ISSN0954-0091, eISSN1360-0494, Publisher Taylor & Francis LTD, 2022.

[2] R.G. Alves, R.F. Maia, F. Lima, “Discrete-event simulation of an irrigation system using Internet of Things”, Journal IEEE Latin America Transactions, Volume 20, Issue 6, Page 941-947, DOI: 10.1109/TLA.2022.9757736, 2022.
[3] J. Zewei, Y. Shihong, L. Zhenyang, et all, “Coupling machine learning and weather forecast to predict farmland flood disaster: A case study in Yangtze River basin”, Journal Environmental Modelling & Software, Volume 155, Article Number 105436, DOI 10.1016/j.envsoft.2022.105436, 2022.
[4] F. da Silveira, F.H. Lermen, F.G. Amaral, “An overview of agriculture 4.0 development: Systematic review of descriptions, technologies, barriers, advantages, and disadvantages”, Journal of Computers And Electronics In Agriculture, Volume 189, Article Number 106405, DOI 10.1016/j.compag.2021.106405, 2021.
[5] R.F. Maia, C.B. Lurbe, J. Hornbuckle, “IRRISENS: An IoT Platform Based on Microservices Applied in Commercial-Scale Crops Working in a Multi-Cloud Environment”, SENSORS Journal, Volume 20, Issue 24, Article Number 7163, DOI 10.3390/s20247163, 2020.


https://doi.org/10.5593/sgem2024/2.1/s07.05

# IMPACT OF DIGITIZATION ON KEY PERFORMANCE INDICATORS OF THE PRODUCTION PROCESS ON THE EXAMPLE OF THE AGH LEANLINE PROJECT

**Eng. Szymon Ziaja**
University of Science and Technology in Krakow, **Poland**

## ABSTRACT

Digitalization and the concepts of Industry 4.0 undoubtedly contribute to companies' competitive advantage, which can be achieved, among other things, by improving the efficiency and stability of the production process through their implementation. The main purpose of the article is to demonstrate the impact of digitization on the most important indicators of production efficiency using the example of a student project of a production line simulation system, implemented by the Student Scientific Circle of Management. The project concerns the construction of a comprehensive system for teaching Lean Manufacturing methods and tools. The article presents plans for the digitization and autonomization of this project, including the implementation of technologies implementing the concept of Industry 4.0 in the simulation of the production process. It was shown that by digitizing production it is possible to raise the component levels of the OEE process efficiency index and process stability. It was decided to relate the impact of digitization to the real future advantages of implementing new technologies into the project methodology, doing so both numerically and descriptively. The implementation of the new technology, according to the author, will allow to ultimately increase the level of process efficiency (increase the level of the Overall Equipment Effectiveness index) and increase the stability of the production process.

**Keywords:** OEE, efficiency, Industry 4.0, optimalization, digitalization.

## INTRODUCTION

The “AGH LeanLine 4.0” project is a continuation of the extension with new organisational solutions and technologies of the Internet of Things (IoT) of a novel production line simulation system designed and developed by Paweł Bogacz, Prof. of AGH, together with the AGH Student Scientific Circle Management at the Laboratory of Production Engineering and Quality Engineering at AGH, called “LeanLab”, as presented in Figure 1. AGH LeanLine is a comprehensive environment for teaching lean manufacturing methods and tools. It enables advanced simulations of the production process, on the basis of which it is possible to gain practical knowledge in the areas of process management and lean management, among others. The primary objective of the project is therefore to enable the practical presentation and dissemination of knowledge about lean manufacturing, as well as the new digital technologies of automation and autonomisation that support it. Simulations of the production process are conducted using a chair made of LEGO bricks. With each simulation round, further attempts are made to improve the production process. Figure 2 shows a diagram of the structure and flow of the product in the production process.



https://doi.org/10.5593/sgem2024/2.1/s07.06

**Fig. 1** AGH LeanLine project group meeting with Paweł Bogacz, Prof. AGH, at the AGH Production Engineering and Quality Laboratory

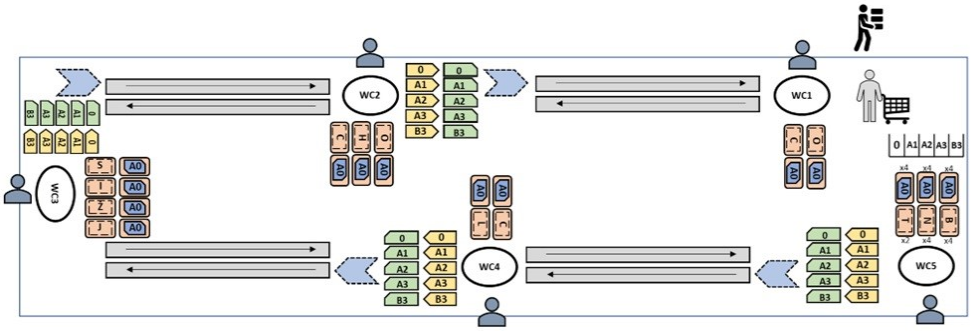


**Fig. 2** Product flow with Kanban system at AGH LeanLine

The above-mentioned assumed and implemented project plans concern three main areas that are complementary:

- automation, robotisation and autonomisation,
- organisational optimisation at workplaces,
- training and education using the created line design.

In this article, the author focused on the first of the cited areas with the intention of demonstrating the impact of digitisation on the key performance indicators of the production process using the AGH LeanLine system. It was decided to relate the impact of digitisation to the actual future benefits of implementing new technologies into the project methodology both numerically and descriptively. Most of the conclusions formulated were related to the practical context, so the author cited a compilation of selected research results on current trends in the approach of manufacturing companies to the implementation of tools implementing the Industry 4.0 concept.

## PRODUCTION PROCESS EFFICIENCY INDICATORS

Continuous control and evaluation of the results achieved should be carried out in various areas of a production company that is oriented towards process management. This is made possible, among other things, by key performance indicators, or so-called KPIe (key performance indicators). These measures are divided into two main groups:

result indicators and performance indicators, which are mostly non-financial in nature [1]. Common characteristics of these indicators are: timeliness, supervisability, simplicity, significant impact on the success of the organisation [1]. Methods and tools to assess the efficiency of the production process should be geared primarily towards the achievement of the set objectives. Some of the most relevant objectives for improving production efficiency include: increasing productivity, increasing the quality of manufactured products, reduction of the amount of work in progress, reduction of production cycle times, reduction in the time or number of changeovers [2]. The most important and most frequently used indicator in terms of monitoring production efficiency is the OEE (overall equipment effectiveness) index [2]. It is a measure of the overall effectiveness of a workplace in operational terms. This indicator can define the percentage of achievable efficiency for a machine, a set of machines, but also for a workstation or the entire production line. It is the basis for taking measures to optimise capacity utilisation. Flexibility, standardisation of processes and the correct interpretation of the efficiency index are essential factors needed to eliminate waste and continuously improve the organisation [3]. Mathematically speaking, OEE is the product of these three components (availability, performance and quality). The world OEE level, according to an international standard, oscillates around 85% and is achieved by leading manufacturing companies. The average level of OEE is considered to be around 60%, while enterprises beginning to monitor production efficiency often report an initial indicator value of no more than 40% [2]. On the basis of the above indications, in each of the simulations of the production process carried out in the AGH LeanLine environment, the level of the OEE indicator is calculated. Within the observed levels of the OEE indicator, a number of types of losses are caught that affect its individual components. The underestimation of availability will be influenced primarily by unplanned downtime, while process efficiency will be most affected by all losses related to inadequate, excessively low production rates. Product defects, on the other hand, are crucial for the third component of the indicator, quality. In addition to the measure of workplace efficiency in operational terms, the levels of costs associated with production should also be counted. At the beginning of each AGH LeanLine simulation round, initial parameters are set, which, in combination with data from the NFC readings (the times at which successive pieces of products come off the workstations), allows the financial result to be determined, i.e. the level of profit or loss generated.

## DIGITZLISATION AS MEANS OF INCREASING PRODUCTION EFFICIENCY

The term Industry 4.0 was coined in 2011 and is primarily identified with cyber-physical systems, the internet of things, sensor networks, advanced automation, cloud computing, big data, digital twins or machine learning and others. The definitions of Industry 4.0 are generally consistent with each other and address both technological and process aspects. The fourth industrial revolution, with which the term Industry 4.0 is often identified, is defined as a concept for a process of transformation, both technological and organisational, of the enterprise, linking together the value chain as well as new business models and digitalisation [4]. It is worth asking therefore what is in favour of digital transformation in manufacturing companies. The answer is provided by a survey conducted on a representative group of 197 companies from the automotive sector, the percentage results of which are shown in Figure 3. What is important about it is that the answers with an indication greater or equal to 40% relate directly or indirectly



https://doi.org/10.5593/sgem2024/2.1/s07.06

to the OEE indicator. Indeed, increasing OEE is a decisive factor in the implementation of such solutions. At the top of the responses, entrepreneurs also indicate increasing production and quality, and this also relates to quality and productivity, which are components of OEE. Drawing conclusions from some of the financial performance indicators, it should be considered that cost minimisation (declared by 43% of the respondents) should be an indispensable activity preceding the counting of the performance indicator.

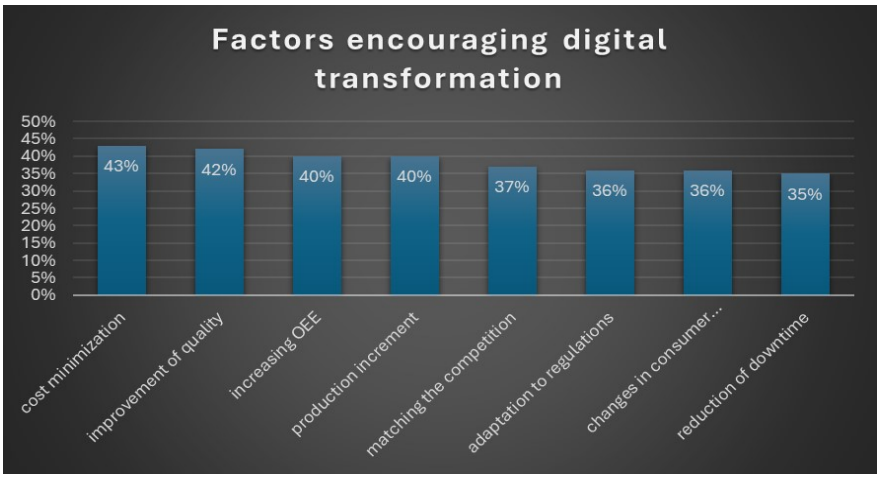


**Fig. 3** Factors favouring digital transformation in automotive companies
Source: own elaboration based on [5]

In the cited study, it was also decided to ask about the main reasons inhibiting digital transformation in manufacturing companies. A picture of the results obtained is summarised in Figure 4. The factors determining the non-implementation of digitalisation of production, which received the highest percentage of answers, are: insufficient knowledge of new technologies, lack of skills to manage them, or reluctance of employees to change.

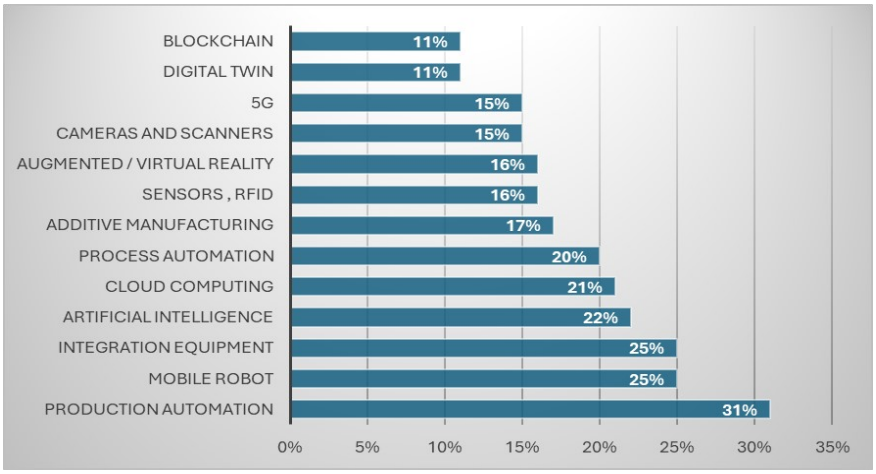


**Fig. 4** Factors inhibiting digital transformation in automotive companies
Source: own elaboration based on [5]

The third part of the presented study concerned the identification of technologies implementing Industry 4.0 concepts that provide the highest return on investment. The results in the form of percentage indications for the individual technologies used are shown in Figure 10. In their context, it is important to note that some of the companies' indications, such as the Internet of Things, machine integration, cloud, sensors, RFID, cameras, 5G network, are technologies implemented in the AGH Production Engineering and Quality Laboratory, i.e. in the LeanLab, or planned to be implemented there in the near future.

## THE CURRENT AND PLANNED LEVEL OF DIGITALISATION AND AUTONOMISATION OF THE AGH LEANLINE PROJECT

In its initial phase, in 2019, the AGH LeanLine project was based on constructions made from LEGO Mindstorms EV3 programmable bricks. Currently, the AGH LeanLine also uses elements of wooden transport ramps, a system of integrated NFC readers, a communication system compatible with the Vorne 800XL board, and a high-tech system for autonomous visual inspection of final quality control features in the form of Balluff's SmartCamera. It was specially designed and manufactured by a student working group from the Student Management Scientific Circle, with the help of Dr Paweł Bogacz, prof. AGH. All of the above were implemented in 2020. In 2021, Amister created a solution specifically for the AGH LeanLine project that collects, almost in real time, information from the current status of the simulated production process [4]. Thanks to the software prepared in this way, it is possible to present the collected data on a diagram, record the history of readings and, consequently, perform dynamic calculations of the efficiency and effectiveness indicators of the production process [4]. The above-described installation of equipment using near-field communication technology and the construction of an appropriate analytical system on this basis allowed the automatic collection of data from each simulation run. Plans for expansion in 2024 of the AGH LeanLine project in the area of automation, robotics and autonomisation primarily concern the replacement of the current Lego Mindstorms EV3 with the more responsive, powerful and compatible M5 Stack IoT developer modules, which have been an industrial-scale technology for about two years. M5 Stack is a multi-dimensional manufacturing analytics system that enables the creation of high-quality sensory prototypes at an industrial level [6]. An example of what the M5 Stack module looks like, along with some of its accessories, is shown in Figure 5.



https://doi.org/10.5593/sgem2024/2.1/s07.06

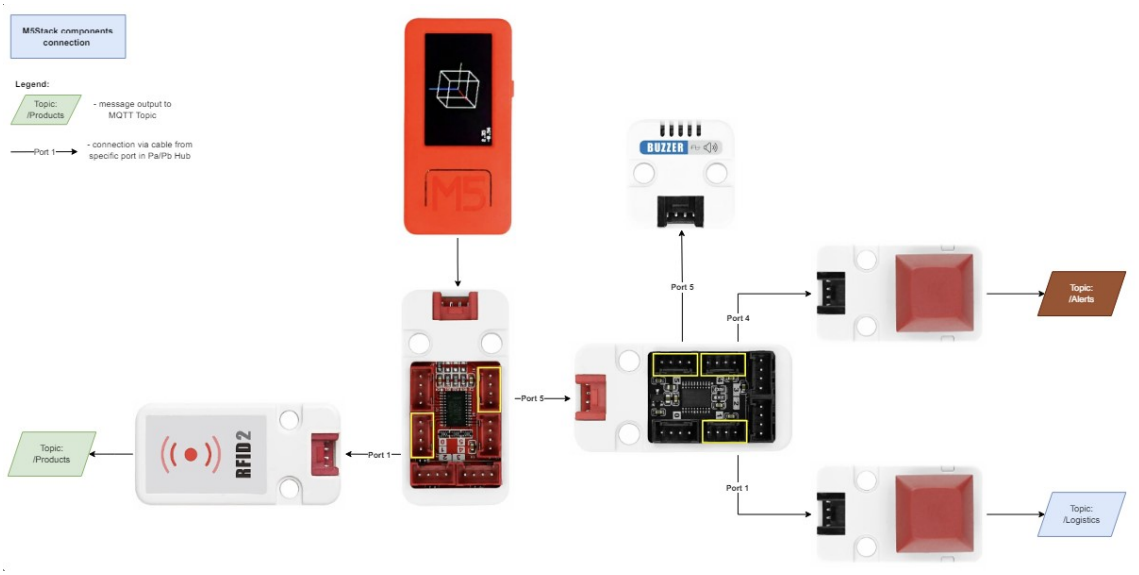


**Fig. 5** IoT developer module - M5 Stack with RFID reader and button in "LeanLab"

Key functional advantages of the M5 Stack developer modules include [6]: ease of programming, simplicity in use, small size of the modules, wide selection of peripherals - sensors, possibility to build devices communicating via wi-fi and Bluetooth, fast sensor data transfer time, availability of many different forms of microcontrollers depending on the application need, different data transfer standards, ability to integrate modules with each other and with other systems, industrial-scale application. In addition to this, it is also worth noting the great potential of IoT developer modules in terms of the use of a wide variety of sensors in the systems created from them. For this reason, it is possible to connect sensors to the M5 Stack multidimensional data analytics system, recording, for example, various properties of the products being manufactured or the movements of operators. A network of sensors is not to be missed in manufacturing companies betting on Industry 4.0 technologies. Among the most commonly used sensors in machines or workstations are proximity, capacitive, temperature, optical, ultrasonic, pressure and strain gauge sensors [7]. he above solution proposed by M5 Stack therefore addresses these issues. Preliminary tests of the M5 Stack technology have been carried out at the Laboratory of Production Engineering and Quality Engineering at the AGH University of Science and Technology, which allowed comparison of selected times reported during simulation (operational and changeover) before and after initial implementation of the new modules. The comparative results in seconds are shown in Table 1. The achieved benefits in terms of time after the application of the new apparatus are given in Table 1 on a percentage scale. As can be observed, the inter-operational times, which are associated with the transition of the product from one workstation to the next, were reduced by 40% with the implementation of the new solution, while the total system adjustment time for simulation was reduced by more than 91%. The reduction in these times has had a direct impact on the OEE component, which is productivity

**Table 1.** Summary of times achieved before and after digitalization [s]

| Characteristics | BEFORE DIFITALIZATION | AFTER DIGITALIZATION |
|---|---|---|
| Average product transition time from one station to the next | 5 | 3 |
| Total inter-operation times | 25 | 15 |
| Total profit (interoperation times) | 10 (**40%**) | |
| Changeover time (preparing the system for simulation) | 3600 | 300 |
| Total profit (time to adapt the system to the simulation) | 3300 (**91,6%**) | |

Source: own elaboration

The reduction in set-up time - preparing the environment for simulation - will also translate into an increased availability rate, as workstations will be able to be set up and ready to start 'production' in a much shorter time, especially in advanced simulation rounds, where inter-operational times are reported from NFC readers. In summary, it should be noted that the implementation of the new technology will, in the author's opinion, allow for a targeted increase in process efficiency levels, involving:
 a reduction in operating times - the significant differences between the times required for very accurate NFC reader proximity (as is currently the case) and those after the introduction of the M5 Stack, recorded product transition times between stations will be reduced as a result of moving readers from station to station using the more accurate and precise apparatus of this technology;
 an increase in process stability due to the introduction of more accurate sensors recording the descent of successive manufactured products from workstations;
 a reduction in the time needed to prepare the system for production simulation (changeover time) by about 92% (from several dozen to several minutes);
 the possibility to actually assess the efficiency of the production process and, on this basis, to introduce solutions increasing the values of the components of the OEE index.

## SUMMARY

There is a lot of uncertainty in the global economy, but the trend regarding digital transformation is certain, and it is indeed gaining ground mainly in terms of the use of data and software and autonomisation in production processes. This article presents a technology that follows/ incorporates the concept of Industry 4.0, which will be implemented in the methodological framework of the AGH LeanLine project. It was shown that the M5 Stack development modules described therein can have optimisation applications in this project. This was confirmed by the results of the tests carried out, from which conclusions could be drawn about the possibility of reducing inter-operational times by 40% and changeover times by up to 92%. The realisation of this objective was made possible by first characterising the concepts of production efficiency monitoring, or terms relating to Industry 4.0, as well as relating the context of the article to recent research in the field of companies' approaches to undertaking



https://doi.org/10.5593/sgem2024/2.1/s07.06

implementation activities in the areas of digitalisation and autonomisation. Several specific conclusions are formulated:

 With the digitisation of production, it is possible to raise the component levels of the OEE process efficiency index and, consequently, the value of the index itself.
 Digitisation of production processes primarily increases the speed of information flow, which directly improves production efficiency.
 Digitisation of production processes increases the level of production flexibility, process stability, availability of workstations and has a positive impact on the value of resource utilisation and the level of reduction of production losses.
 The pace of development of the Industry 4.0 concept is largely dictated by the dynamic development and availability on the market of smart sensors equipped with communication modules, enabling connection and digital networks.

## REFERENCES

[1] Parmenter D., *Kluczowe wskaźniki efektywności (KPI): tworzenie, wdrażanie i stosowanie*, Wydawnictwo Onepress, Gliwice, Poland, 2016, ISBN: 978-83-283-8523-8.

[2] Koliński A., *Przegląd metod i technik oceny efektywności procesu produkcyjnego*, Logistyka, nr 5, 2011, Poland, pp. 1083–1091, ISSN 1231-5478.

[3] Murdzek M., Richert M., Hubicki R., *Wskaźnik efektywności OEE w systemie produkcji gniazdowej*, [w:] Dudek M. (red.), *Nowoczesne metody i narzędzia w inżynierii produkcji i zarządzaniu*, Wydawnictwa AGH, Kraków 2021, Poland, pp. 19–128, ISBN 978-83-66727-19-9.

[4] Baranowski M., Kordowska M., Pisarek J., Ziemacki Z., Hetmańczyk M., Pollak A., *Przemysł 4.0: identyfikacja trendów technologicznych*, Narodowe Centrum Badań i Rozwoju, Warszawa, Poland, 2023, ISBN : 9788396783240.

[5] Rockwell Automation, *8th Annual State of Smart Manufacturing Report*, https://www.rockwellautomation.com/en-us/capabilities/digital-transformation/state-of-smart-manufacturing.html [access to the website: 11.12.2023].

[6] M5Stack, https://m5stack.com/, [access to the website: 15.02.2024].

[7] Poreda R., *5 elementów rewolucji IoT w przemyśle 4.0*, Biznes i Produkcja, 18.06.2020,https://www.astor.com.pl/biznes-i-produkcja/5-elementow-rewolucji-iot-w-przemysle-4-0/ , Poland, [access to the website: 15.02.2024].

# KNOWLEDGE SHARING IN DISTRIBUTED TEAMS - THE IMPACT OF VIRTUAL COLLABORATION TOOLS

**Zuzanna Piwowarczyk**[1]

[1] AGH University of Krakow, **Poland**

## ABSTRACT

This study analyzes the impact of virtual collaboration tools on knowledge sharing in distributed and virtual teams, operating at the intersection of technology, human behavior, and organizational processes. It aims to unravel the complexities of knowledge sharing in modern workplaces by examining the role of these tools in facilitating knowledge exchange, identifying factors for effective practices, and exploring the impact of organizational culture and industry dynamics. Through empirical research, including a self-completed online questionnaire and secondary data sources, the study addresses key research objectives and hypotheses, seeking to maintain elevated levels of knowledge sharing with increasing virtual collaboration.

Building on previous research on IT management models and knowledge exchange, the study finds that virtual collaboration tools positively influence knowledge sharing, with specific tools and functions such as speed of access and file storage contributing significantly. However, challenges remain in transparency of information structure and integration with organizational tools. Despite limitations in sample size, the research offers valuable insights and practical strategies for organizations navigating today's dynamic work landscape, supporting best practices in environments user planning and IT tool design, and deepening the understanding of knowledge sharing in virtual.

**Keywords:** Virtual collaboration tools, Knowledge sharing, Distributed teams, Organizational processes, Technology

## INTRODUCTION

Distributed teams are often created to meet the need for groups of specialists operating in various locations, providing additional flexibility at both the formation and operation stages. Analysis of the advantages and disadvantages of virtual teams has gained popularity, especially due to the remote work surge caused by the COVID-19 pandemic [1]. However, earlier attempts to characterize this type of collaboration had already identified many significant advantages. Among the most notable for organizations are increased speed of response to change due to flexibility, connecting remote workers from different locations with varied experiences to improve performance and productivity [2], the ability to complete tasks on a 24-hour cycle by hiring employees from different time zones [3], the option for flexible working hours, and saving time and money as team members do not need to commute to the company's headquarters. Additionally, cross-cultural dispersed teams benefit from diversity, leading to innovation [4].

Distributed teams rely heavily on computer-mediated communication (CMC) to function effectively. To maximize the benefits of virtual collaboration and mitigate its



https://doi.org/10.5593/sgem2024/2.1/s07.07

drawbacks, selecting the appropriate tools for remote collaboration is crucial [5]. These tools play a significant role in knowledge sharing and knowledge management. Information systems provide platforms and electronic storage solutions that simplify access and encourage the reuse of knowledge within the organization. They facilitate the transfer of knowledge into explicit structural formats, making information storage, sharing, and retrieval easier.

This leads to the first hypothesis:

**Hypothesis 1:** The use of virtual collaboration tools positively influences knowledge sharing in distributed teams.

The use of collaborative technologies in virtual teams is intended to promote knowledge sharing and integration activities, which are the core activities of these teams [6]. IT systems act as electronic repositories of information, offering centralized and easily accessible storage, simplifying the process of archiving, retrieving, and disseminating knowledge assets. However, the usability of these knowledge bases is affected by factors such as how information is added, search capabilities and the ability to structure resources.

Collaboration tools also enable individuals to locate each other within the organization and provide various forms of communication, facilitating real-time interactions, discussions, and joint efforts, promoting a culture of open communication and exchange of ideas. The creation and sharing of organizational knowledge in a distributed system can vary depending on the virtual collaboration tools used and the functions required by the team.

**Hypothesis 2:** Specific virtual collaboration tools play a key role in the effectiveness of knowledge sharing within distributed teams.

**Hypothesis 3:** Identified features of virtual collaboration tools contribute to the overall effectiveness of knowledge sharing in distributed teams.

Despite the many benefits, distributed teams face numerous challenges and obstacles to collaboration. Communication challenges in a virtual environment can lead to misinterpretation of tasks and requirements, duplication of efforts and obstacles to achieving goals [7]. Reduced face-to-face interaction due to the virtualization of collaboration often results in less effective communication, as team members lack non-verbal cues and informal interactions, leading to increased formality and potential misunderstandings. This calls for proper communication management in virtual teams to increase consistency and efficiency. Flexibility in working hours and the presence of employees in different time zones make work asynchronous. Teams with significant dispersion using text-based communication technologies, such as chats and emails, often encounter delays in responses. Additionally, using a foreign language to communicate can create a language barrier, even if both parties are fluent in the language used [8]. Despite these difficulties, research indicates that team deployment does not significantly affect performance, with virtual and traditional teams reporting similar levels of task-related conflict and interpersonal problems [9].

A survey of 141 respondents from twenty-four teams from five companies also found no significant differences in levels of conflict between distributed and traditional teams, nor in the use of communications technology [10]. These results suggest that distributed teams, aware of the unique challenges they face, are developing effective patterns of

collaboration. To illustrate the study's theory, a conceptual model was prepared (Figure 1), visualizing key elements and broader factors such as tool type, frequency of use, user familiarity and comfort, and general considerations of knowledge sharing, including improved team dynamics, task performance and knowledge transfer. Factors specific to distributed teams, such as level of distribution, cultural homogeneity, team size, management style and form of collaboration were also considered.

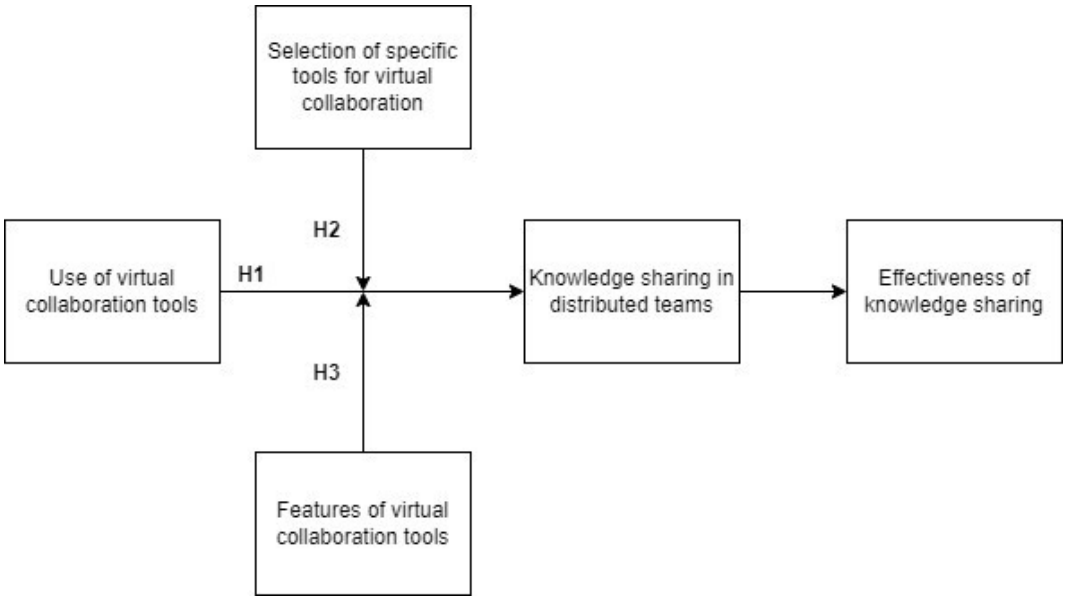


**Figure 1** Conceptual model.

Turning to a detailed description of these categories, Rudawska [11] identified specific factors that negatively affect knowledge sharing in organizations. Technology-related issues include incompatibility between different information systems and processes, lack of infrastructure to support knowledge-sharing practices, and inadequate technical solutions to meet employees' needs. Organizational factors include a lack of training in IT solutions, employees not being informed about the benefits of new communication solutions, a lack of space for informal knowledge sharing, and being locked into individual corners. Individual factors include employee reluctance to use IT solutions due to inexperience and unfamiliarity.

## MATERIALS AND METHODS

The study used a deductive approach to verify hypotheses about the impact of virtual collaboration tools on knowledge sharing in distributed teams. This approach allowed for a structured study of the relationships between variables, providing a systematic framework for hypothesis verification. The primary method of data collection was a self-administered online questionnaire, ensuring standardization of data collection among different participants and enabling efficient data processing. This method was particularly effective in collecting data from geographically dispersed respondents, allowing precise targeting of the survey group and collection of a significant amount of data.

A diverse sample of dispersed teams from different industries and countries was selected to increase the generalizability of the results. To increase response rates, the



https://doi.org/10.5593/sgem2024/2.1/s07.07

survey was conducted in two languages: Polish for Polish-speaking participants and English for non-Polish speakers. This linguistic inclusion was intended to reach a larger and more representative survey group. The target group included individuals working in distributed, fully remote and hybrid teams. Follow-up questions were included in the questionnaire to ensure that respondents were indeed working in distributed teams.

The questionnaire included the following sections:

1. Use of virtual collaboration tools
2. Knowledge sharing practices using collaboration tools
3. Organizational culture
4. Team distribution level and demographic information

To collect the research group, a snowball method was used. Industry forums, professional networking platforms, social networks, and personal contacts with representatives of both Polish and foreign companies were used. Prior to the main survey, pilot studies were conducted with five people from different industries over two days. Feedback from the pilot study helped refine the questionnaire for clarity and relevance, ensuring linguistic accuracy in both the Polish and English versions. This process ensured clarity, relevance, and efficiency in capturing the required information.

Participants were informed about the study's purpose, consented before participation, and remained anonymous. Data was collected and stored according to ethical guidelines to protect confidentiality.

The conducted research collected a sample of just sixty-two respondents for questionnaires in both languages. The research sample was too small to fully evaluate the hypotheses, which limited the use of inferential statistics. However, data elements were used to address the research hypotheses through behavioral and opinion analysis. Quantitative survey data on the use of virtual collaboration tools and knowledge sharing behaviors were examined for patterns, frequency, and specific functions. Opinion analysis dove into respondents' attitudes, perceptions, and beliefs, integrating quantitative behavioral patterns with qualitative opinions for a comprehensive analysis. This integrated approach aimed to advance understanding of the relationship between tool use, knowledge sharing and its perceived impact on distributed teams. Potential discrepancies between observed behaviors and expressed opinions were addressed to ensure consistency and reliability. Relying on self-reported data posed a risk of response error, potentially skewing generalized results. To mitigate this, demographic questions were included in the questionnaire to provide context for interpreting the results.

## RESULTS

The analysis begins with a quantitative examination of respondents' behavior related to the use of virtual collaboration tools. The indicators of frequency of tool use show that the respondents use tools to communicate or collaborate with their team members and most use them daily (83,3%) or several times a week (11.6%). This indicates that all respondents are continuous users of these types of tools. Therefore, they constitute a representative group to analyze the features and impact of these tools on knowledge sharing.

The types of tools used most are email (95.5%), instant messaging (95.5%), video conferencing tools (86.4%), document sharing platforms (81.8%), synchronous document editing platform (77.3%). Turning to specific tools, among video messaging, MS Teams dominates, but for chat messaging, Teams' share falls in favor of Slack. In other tool categories, such as document editing and storage platforms, there are no dominant tools. All respondents agree that the tools fulfill the basic functions of performing job duties effectively. Accessibility and intuitiveness of the tools were also rated as at least good by 90.9% of respondents.

Most respondents, however, experienced problems using these tools. Work is hampered by long waits for answers or information from other team members, frequent tool crashes or technical problems that make it difficult to work smoothly, and difficult access to necessary tools or files online. All the above factors, however, have minor impact on work efficiency and knowledge sharing.

A basic analysis indicates that most respondents believe that the use of virtual collaboration increases the likelihood of knowledge sharing. Moreover, in most cases (79%), team members exchange information, ideas, and experiences through virtual collaboration tools. Subsequent analysis of opinions related to the effectiveness of specific tools indicates that it is at least sufficient for 84% of respondents. The vast majority of respondents also agreed with the statement that if it were not for IT solutions, knowledge sharing would be much more difficult.

Turning to the analysis of the types of tools and their role in the knowledge sharing process, the first conclusions can already be drawn from the combined chart showing opinions on the effectiveness of specific tools in the process (Figure 2).

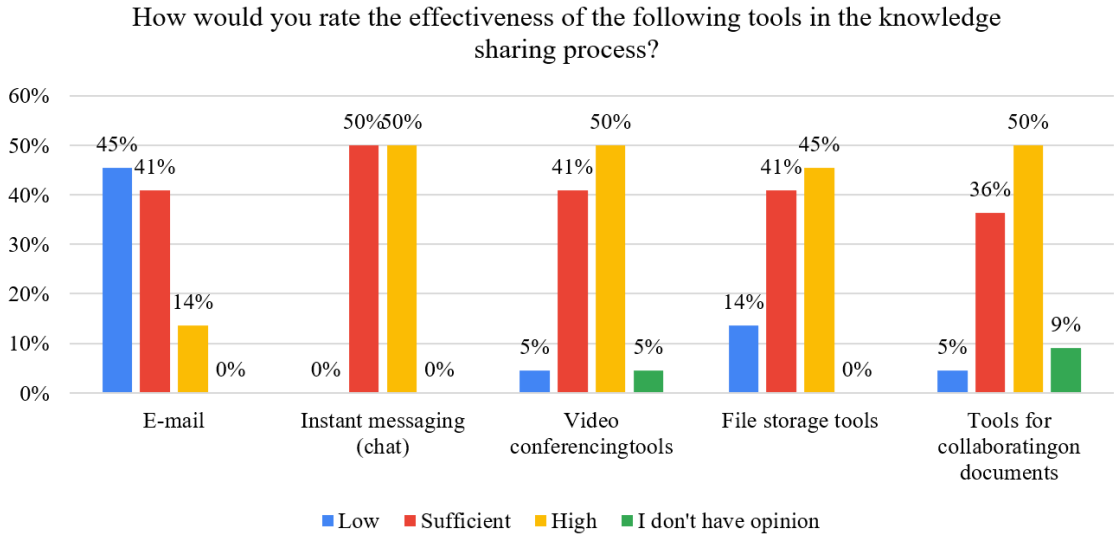


**Figure 2 Effectiveness of specific tools in the knowledge sharing process.**

The primary communication channel, such as email, is insufficient in knowledge sharing processes. The others proposed are characterized as more than sufficient for the vast majority. The best of the process for respondents are instant massaging tools. This shows how virtual collaboration and knowledge transfer have changed and improved with the development of IT tools. Teams that would be completely devoid of



https://doi.org/10.5593/sgem2024/2.1/s07.07

communication channels via text and video messages are characterized by a deteriorated knowledge sharing process.

Turning to in-depth opinions on virtual collaboration tools, there were a few specific sentences to test opinion on some knowledge sharing activities. The highest average (based on the codification of responses to numerical values) was the opinion that the ability to store and share files significantly supports the exchange of information within the respondents' team. In the case of facilitating real-time information sharing through remote collaboration tools used in the organization and finding needed information and knowledge through the presence of IT infrastructure, the average response has a positive value. Both this value and the median response show that the entire surveyed group tended to agree with the suggested positive impact of the tools.

When it comes to specific additional features provided by certain tools, respondents appreciated that one tool allows me to do both video conferencing and chatting (63.6%). Most also indicated that the ability to video conference results in a much better understanding of work-related messages.

Although respondents indicated that their work was particularly hampered by long waits for answers or information from other team members, they unanimously agreed that speed of access to information was considered the greatest support for knowledge sharing. Not surprisingly, they also emphasized support for file storage and sharing, as well as the ability to rate and comment on content. The latter helps build understanding and context for information.

In terms of specific additional features provided by certain tools, respondents appreciated the fact that one tool allows me to both video conference and chat (63.6%). Most also indicated that the ability to videoconference results in a much better understanding of work-related messages.

Although respondents indicated that their work was particularly hampered by long waits for answers or information from other team members, they unanimously agreed that speed of access to information was considered the greatest support for knowledge sharing. Not surprisingly, they also emphasized support for file storage and sharing, as well as the ability to rate and comment on content. The latter helps build understanding and context for the information.

## DISCUSSION

The data collected from the survey supports the hypotheses to varying extents.

**Hypothesis 1:** The Use of Virtual Collaboration Tools Positively Influences Knowledge Sharing

The first hypothesis is strongly supported. The high frequency of tool usage and the positive feedback on their effectiveness in facilitating knowledge sharing indicate that virtual collaboration tools play a crucial role in this process. Despite some technical challenges, the respondents overwhelmingly believe that knowledge sharing would be significantly more difficult without these tools.

**Hypothesis 2:** Specific Virtual Collaboration Tools Play an Important Role in the Effectiveness of Knowledge Sharing

The second hypothesis is confirmed, particularly highlighting instant messaging as the most effective tool for knowledge sharing. Email, while widely used, is considered insufficient for this purpose. The effectiveness of tools like video conferencing and document sharing platforms further supports this hypothesis.

**Hypothesis 3:** Identified Features of Virtual Collaboration Tools Contribute to the Overall Effectiveness of Knowledge Sharing

The third hypothesis is partially confirmed. Features such as speed of access, file storage, and the ability to comment on content are recognized as beneficial. However, other features like transparency of information structure and integration with organizational tools received mixed responses. The lack of appreciation for certain features may indicate either their limited presence in the tools used or a perception of their lesser relevance to knowledge sharing.

The findings align with existing literature, which emphasizes the importance of virtual collaboration tools in enhancing communication and knowledge sharing within distributed teams. The positive impact of instant messaging and the challenges associated with email are consistent with previous research. However, the mixed responses regarding certain features suggest a need for further investigation into the specific functionalities that best support knowledge sharing.

## CONCLUSION

The widespread use of IT tools has positively influenced knowledge sharing in distributed teams, with instant messaging proving to be particularly effective. However, despite the overall effectiveness of virtual collaboration tools, technical challenges were reported, emphasizing the need for continuous improvement and enhancement of IT infrastructure to support seamless collaboration. The study highlighted the critical link between information technology and organizational culture, stressing the importance of adapting information systems to the unique needs and dynamics of distributed teams. By integrating IT solutions that promote transparency, accessibility, and ease of use, organizations can enhance knowledge-sharing practices and foster a culture of innovation and collaboration.

The novelty of this research lies in its comprehensive analysis of the specific features of virtual collaboration tools that contribute to knowledge sharing, providing valuable insights into optimizing these tools for distributed teams. The contribution of the authors is evident in their identification of instant messaging as the most effective tool for knowledge sharing, as well as their detailed examination of the benefits and challenges associated with other tools like video conferencing and document sharing platforms.

Future research should further explore the intricate relationship between IT tools, organizational culture, and knowledge sharing dynamics within distributed teams. Additionally, efforts to expand the sample size and conduct more comprehensive analyses will provide deeper insights into optimizing virtual collaboration practices in diverse organizational settings.

In conclusion, this study underscores the transformative impact of IT on distributed teamwork, highlighting the key role of IT tools in improving communication, collaboration, and knowledge sharing among geographically dispersed team members.



https://doi.org/10.5593/sgem2024/2.1/s07.07

By harnessing the power of IT, organizations can create more productive and innovative distributed teams capable of thriving in today's increasingly digital workplace.

## REFERENCES

[1] Garro-Abarca, V., Palos-Sanchez, P., Aguayo-Camacho, M., Virtual teams in times of pandemic: Factors that influence performance, Frontiers in Psychology, vol. 12, 2021, DOI:10.3389/fpsyg.2021.624637.

[2] Alaiad, A., Alnsour, Y., & Alsharo, M., Virtual Teams: Thematic Taxonomy, Constructs Model, and Future Research Directions, IEEE Transactions on Professional Communication, vol, 62/issue 3, pp 211-238, 2019, DOI:10.1109/TPC.2019.2929370.

[3] Stroińska E., Zarządzanie zespołami wirtualnymi–wybrane aspekty, Przedsiębiorczość i Zarządzanie, Poland, vol. 17/issue 11.1, pp. 39-56, 2016.

[4] Krawczyk-Bryłka B., Budowanie zespołu wirtualnego: zasady i wyzwania, Studia Informatica Pomerania, Poland, vol. 2/issue 40, pp 99-111, 2016, DOI:10.18276/si.2016.40-09.

[5] Shachaf P., Cultural diversity and information and communication technology impacts on global virtual teams: An exploratory study, Information & Management, vol.45/issue 2, pp 131-142, 2008, DOI:10.1016/j.im.2007.12.003.

[6] Samarah, I., Paul, S., Tadisina, S., Collaboration Technology Support for Knowledge Conversion in Virtual Teams: A Theoretical Perspective, 2007 40th Annual Hawaii International Conference on System Sciences, USA, pp 37-37, 2007, DOI:10.1109/HICSS.2007.129.

[7] Alsharo M., Knowledge sharing in virtual teams: The impact on trust, collaboration, and team effectiveness, Doctoral dissertation, University of Colorado Denver, USA, 2013, ISBN: 978-1-3031-0340-7.

[8] Hunsaker, P. L., Hunsaker, J. S, Virtual teams: a leader's guide, Team Performance Management: An International Journal, vol.14/issue 1/2, 2008, pp 86-10, DOI:10.1108/13527590810860221.

[9] Griffith, T. L., Mannix, E. A., Neale, M. A., Conflict in virtual teams, Virtual teams that work: Creating conditions for virtual team effectiveness, pp 335-352, 2003.

[10] Mortensen, M., Hinds, P. J., Conflict and shared identity in geographically distributed teams, International Journal of Conflict Management, vol.12/issue 3, pp 212-238, 2001, DOI:10.1108/eb022856.

[11] Rudawska A., Dzielenie się wiedzą w organizacjach–istota, bariery i efekty, Organization and Management, Poland, vol. 157, pp 89-103, 2013, ISSN: 0137-5466.

# MODEL OF ASSOCIATIVE MEMORY IN A BIG DATA PROCESSING ENVIRONMENT

**Assist. Prof. I. V. Kalinin**[1]

**V. A. Sevostyanov**[1]

[1] Saint Petersburg State University of Telecommunications (SPbSUT University), **Russia**

## ABSTRACT

In the modern world, neural networks are becoming an integral part of human life. In particular, neural networks began to be used for the task of constructing information security tools; in connection with this, the need gradually began to arise to strengthen and improve the mechanisms of artificial intelligence itself, including when using big data technology.

Let's consider the basic concepts of working with Big Data technology, in particular the processing of assimilation memory to build a general visual picture of the current situation of the presence of user agents and software. The assimilative memory model is an important component that evaluates the state of the system, remembers events, produces correlation indicators, and accumulates information for a potential intellectual intrusion detection system.

The constructed associative memory can be used to build, for example, efficient structures of on-board geoinformation databases, especially when used in autonomous vehicles (for example, UAVs). The use of an intrusion detection system to protect on-board geoinformation databases in vehicles can improve the security and integrity of data.

**Keywords:** intrusion detection system, neural networks, artificial intelligence, computer appliance, information system, multilayer neural network

## INTRODUCTION

The use of an intrusion detection system (IDS - Intrusion Detection System) in vehicles with on-board geoinformation databases will help ensure the security and integrity of this data in mobile environments. A banal attack was carried out. Using the NetDiscover script, the attacker finds the IP addresses of the victim’s devices; knowing the required IP addresses, it is possible to temporarily disrupt the operation of the network router with these devices, forcing the victim to check the settings in the administration panel.

After entering account information on the authorization page, the script will send the user to the original site, and the attacker will be presented with the login and password entered by the victim. Subsequently, having access to the Apache Ranger administration panel, the attacker will be able to change access policies and account roles, as a result of which it becomes possible to penetrate further and gain a foothold in the corporate network of the enterprise. The vulnerability map gives an attacker the ability to know where a potential vulnerability is located that can be exploited in the future. After analyzing all

the data obtained from the data flow diagram and vulnerability diagram, the attacker begins to create his own exploit.

## MAIN SECTION

Associative memory in an intrusion detection system can be used as a mechanism for remembering and recognizing attack patterns. It allows the system to quickly identify previously unknown attacks based on their similarity to already known attacks [1]. Associative memory works by matching input data to existing attack patterns. If a match is found, the system may issue a warning about a possible intrusion. This process may be automated or may require human intervention for confirmation. Additionally, the associative memory in YaVi was tuned to define software and user agents in the RIS through additional clustering and aggregation of parameters "on the fly" with the collection of information about protected objects [2].

One of the advantages of using associative memory in IDS is its ability to process large amounts of data and quickly respond to new attacks. However, like any IDS, it can also experience false positives and errors due to the difficulty of accurately identifying all possible attacks.

This course of processes originates from replication in Big Data RIS, where the element of the computational moment for the intelligent IDS is laid [3]. Then the influence scheme is applied to the associative memory component, after which normalization of the transferred processes and data for the neural network(NN) is achieved for each cluster.

In this case, NNs often look like this when estimating system parameters (Fig. 1). This takes into account the diversity of the number of nodes and correlation indicators that arise in the event of external unauthorized influence (attacks or intrusions) [4].

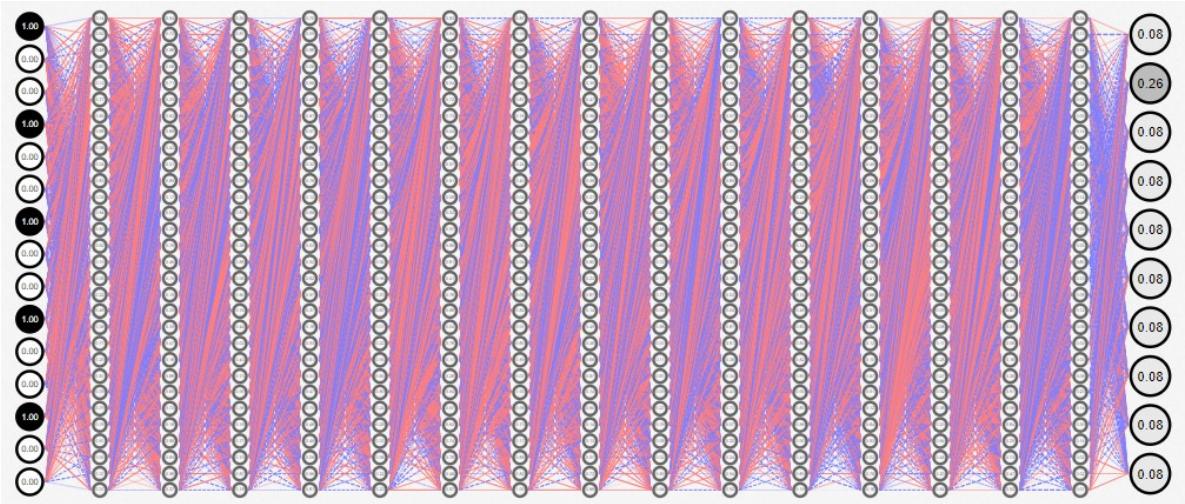


Figure 1. Multilayer multi-level NN for search algorithm operations in order to find optimal data for solving the problem of preserving the combinatorial functions of an intelligent IDS.

More often, a multi-level multilayer NN is taken, where random parameters are introduced. Figure 2 shows that one of the nodes will have a higher output processing ratio. The NS in the YaVi concept will try to bypass it.

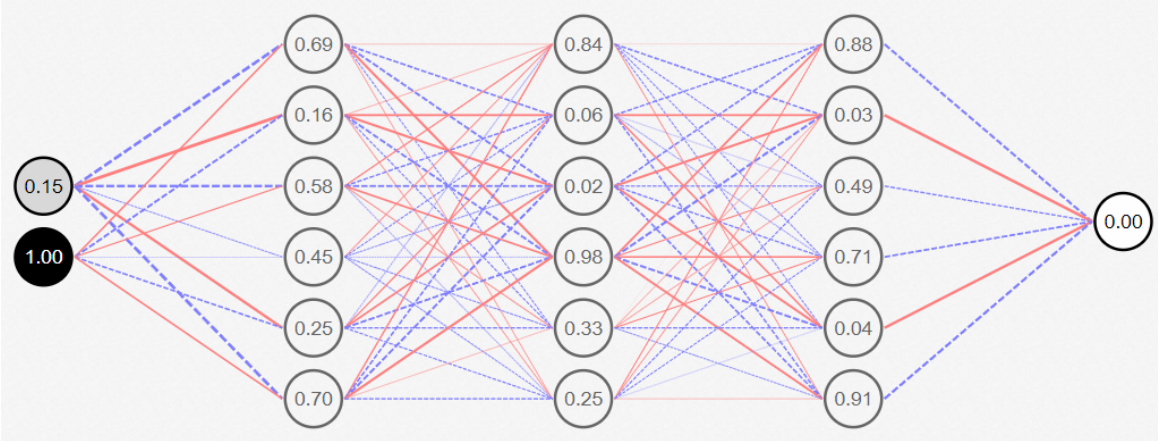


Figure 2. Reduction of different output parameters to obtain 100% data processing result

According to the Heaviside function (Fig. 3), a process of correlation changes is still observed. Here the neural network will still have errors, even for 7644 operations in total. The maximum error error in this case is 0.17325846492581165 distorted data, for an arbitrary 6015 operations.

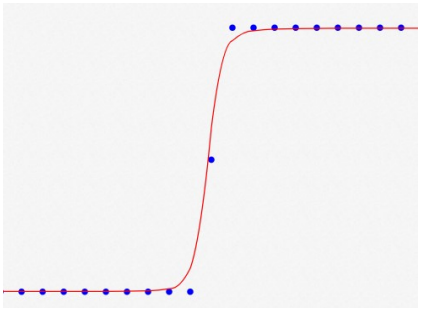

Figure 3. The resulting Heaviside function as a result of combining different output parameters of data processing

In its general implementation, the Kitovras PA module, having standard generative learning, produces the following data on retraining, having, for example, out of 3, only one that is not corrupted (with a value of 0.00) (see Fig. 4).

Here, the calculation error rate dropped to 0.19953693773445622 after 497256 data processing steps, but the output still produced a corrupted data item. Those. Mokosh's associative memory did not remember everything. Those. RIS self-study data is 94% accurate. The dependency of connections in Mokosh can be visualized and the criteria for filling each Kvasura PA block can be seen (see Fig. 4).

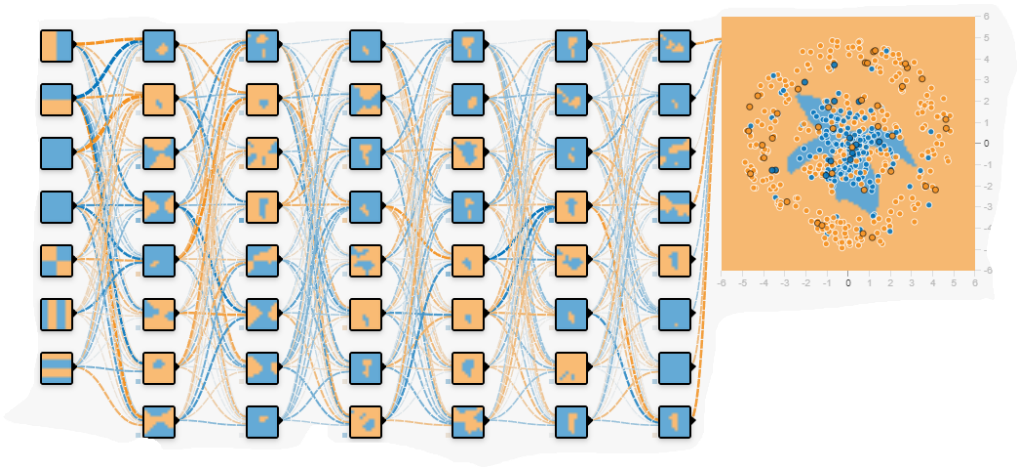

Figure 4. Visualization of data processing information in the Kvasura PA module.

An assumption is made about the accumulation of calculated information using the associative memory of an intellectual SOV. For example, when affecting integrity (installing or unzipping YaVI modules), the entire AI behaves as follows:

1. Orange dots – knowledge about the saved software (the larger it is, the more data the software contains).

2. Blue dots - knowledge about the saved PA (the larger the dots, the more data the PA contains).

3. Orange areas – unexplored but possibly occupied software area in FIG.

Blue areas are unexplored but possibly occupied PA areas in FIG.

However, over time, the picture of the study of associative memory changes, namely, the blue area becomes larger (Fig. 5). About 15 seconds passed, Po remained in place, but the orange area began to decrease, which indicates the potential influence and spread of individual PAs in the RIS.

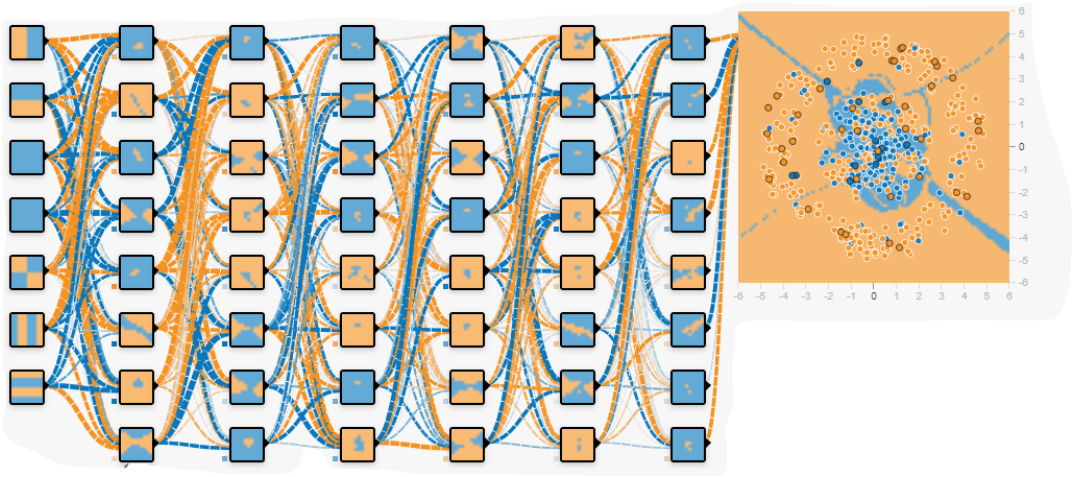

Figure 5. Visualization of data processing information in the Kvasura PA module (after 15 seconds).

## CONCLUSION

This analysis is key in building further interaction of intelligent IDS in RIS. A key designation can be made that the model of associative memory in the Big Data processing environment takes into account new factors of storing and processing information, clearly distinguishing what is software and what is PA in RIS.

This result is useful because for the NN as a whole it becomes possible to accumulate information and prepare potential AI for further self-defense in the RIS. It is possible to obtain estimates of information security indicators after an attack on RIS resources, where it is clear how associative memory determined the structures of software and user agents, clearly dividing them. The error in the model was 6%.

This chapter focuses on the mutually beneficial use of parameters not only IDS, but also SIEM, which has a beneficial effect on the accumulation of information about roses and the accumulation of experience for associative memory. It cannot be said that the technique acts as an addition to the associative memory processing model, but it can be argued that a self-organizing map is capable of giving the YaVi system a complete picture of intrusions and ensuring the integrity and centralization of its entire architecture.

## REFERENCES

[1] Shterenberg, S. I. design of the architecture of an intrusion detection system with deep and machine learning based on the quasi-biological paradigm / S. I. Shterenberg, O. I. Shelukhin, A. D. Lebedeva // Bulletin of the St. Petersburg State University of Technology and Design. Series 1: Natural and technical sciences. – 2023. – No. 1. – P. 86-91.

[2] Shterenberg S.I. Development of a methodology for protecting artificial intelligence systems in distributed information systems. // Bulletin of SibGUTI. 2023;17(3): pp. 78-86.

[3] Krasov A.V., Shterenberg S.I., Goluzina D.R. Methods for visualizing big data in information security systems for generating vulnerability reports // Electrosvyaz. 2019. No. 11. pp. 39-47.

[4] Shterenberg S.I. Methodology for managing systems for processing and collecting big data with monitoring support by built-in software agents // Bulletin of the St. Petersburg State University of Technology and Design. Series 1: Natural and technical sciences. 2020. No. 4. pp. 26-35.

# ORGANIZATION OF MIXED-CRITICAL COMPUTING SYSTEMS FOR CONTROL OF MULTI-OPERATIONAL TECHNOLOGICAL SYSTEMS

**Assoc. Prof. Ph.D. Vasiliy Pinkevich**[1]
**Assoc. Prof. Ph.D. Arkady Kluchev**[1]
**Prof. Dr. Alexey Platunov**[1]
**Postgrad. Stud. Vladislav Kluchev**[1]
[1] ITMO University, **Russia**

## ABSTRACT

Automation of complex technological and laboratory systems requires the creation of specialized mixed-critical computing systems. They must control the technological process at several levels (control subsystem) and maintain the user interface with technological data management (information subsystem). So, they execute tasks with significantly different criticality.

Also, it is assumed that the development of physical components, the implementation and configuration of the control subsystem at different stages of the life cycle is carried out by applied specialists (industrial engineers, servicemen, end-users), not professional computer and software engineers.

In this article we propose and justify the architecture of the automation platform and computing systems for such technological and laboratory systems.

For efficient control of customized technological process, it is necessary to partition it to several levels from primitive operations to batch execution of hundreds and thousands of tasks, each including thousands of primitive operations. The methods of partitioning are proposed with an emphasis on finding a balance between flexibility and difficulty of configuration.

The ways of further expanding of the platform are proposed through the introduction of alternative and more advanced algorithms for solving non-trivial technological process control issues, for example, dynamic process planning.

Solutions of instrumental issues related to the creation and support of specialized programming/configuration languages, compilers, and virtual machines throughout the entire life cycle of the platform are proposed.

**Keywords:** mixed-critical system, computing platform, computer architecture, cyber-physical system, automated control system

## INTRODUCTION

With the reduction in cost and the growth of computing capabilities, the sphere where automation of technological installations becomes economically justified continues to expand. There is a growing demand for appropriate computing systems, methods and their design tools.

Modern complex laboratory and technological installations designed for automated execution of experiments include several units performing different operations in parallel. They are designed for continuous streaming execution of many similar sequences of operations on workpieces or test materials. For this purpose, the possibility of continuous supply of necessary raw materials, workpieces and technological consumables is provided.

Let us call such installations multi-operational technological installations (MOTI). They are used for conducting physical, chemical and biological studies, performing medical analyses, in assembly plants, etc.

MOTI computing systems (CS) combine the functions of multi-level process control, maintenance of a powerful information system with databases, user interface, engineering tools, and communication with external information systems. At the same time, the ability to configure and program control algorithms at different levels for application users who are not computer experts should be supported.

A MOTI CS computing process feature is the need to simultaneously perform computational tasks with different types of real-time constraints and different requirements for the strictness of compliance with these constraints. A relatively new trend is to consider complex computing systems operating in real time within a single hardware platform as systems with mixed criticality [1]. When combining heterogeneous types of tasks in one system without special design methods, there are high risks of negative interference of different parts of the computing system.

MOTI is a vivid example of modern sophisticated cyber-physical systems (CPS). There are semantic gaps between the groups of competencies of the specialists involved in working with them, which make communication and collaboration on the project difficult, cause delays and make it more expensive.

This article discusses the features of the computing process in the computing system of MOTI with mixed criticality and suggests methods for organizing their computational processes. These methods are aimed at increasing the transparency and manageability of the design process, reducing the negative mutual influence of computational tasks with different levels of criticality, increasing the degree of reuse of technical solutions when creating computing systems of this class.

## RELATED WORKS

In fact, the MOTI CS should include a complete automation pyramid – from low-level I/O to resource planning. But for such computing system, the classic programmable logic controller (PLC) based on the IEC 61131-3 standard is not applicable “as is”. The limited set of methods for the computing process organization makes it problematic to describe parallel computing and implement mixed criticality. Our team has a fairly rich experience in creating and using tools for PLC, and we agree with the conclusions of the article [2]. The solutions recommended there to increase the flexibility and reliability of the PLC are currently not standardized and must be implemented manually.

Also, other products traditionally used at higher levels of the industrial automation pyramid stack cannot be used directly. This technology stack is very cumbersome, inflexible and too expensive for this class of systems.

The creation of the MOTI CS requires the development of custom components for a significant share of the computer technology stack levels and in fact requires to employ the entire set of tools that are used to create modern CPS [3, 4]. At the same time, the existing specialized design models intended for CPS design cover only narrow subsets of design tasks [4-7]. At the same time, they are still far from being implemented into end-to-end methodologies and tools that would allow the creation of custom CPS and especially CPS platforms to be available for use by applied specialists who are not computer experts. Such computing system development still requires a research stage in order to choose a way to decompose the computing system into levels and platforms [8, 9], which will allow you to fulfil performance limitations, reaction time, configuration capabilities, computing resources requirements and cost.

The team of authors develops the own approach to the high–level design of complex specialized computing systems – the HLD methodology of embedded systems design [10], focused on the use of architectural abstractions at early design stages for the analysis and selection of design alternatives. This article demonstrates a practical approach to the implementation of a system with mixed criticality based on a custom computing platform developed within the framework of the HLD methodology.

## MOTI CS REQUIREMENTS

From the point of process control view, the computing system must ensure the scheduling of the installation's operation unit work, taking into account:

- increasing the throughput of the MOTI;
- real-time constraints for each technological task performed and its individual steps (these requirements often are quite strict and do not allow deviations in either direction);
- priorities of technological tasks – from tasks that need to be completed even at the cost of damaging the installation, to optional ones performed during idle mode;
- periodic automatic maintenance of the installation to ensure its continuous operation;
- periodic stops for human service;
- restarting tasks that failed;
- performing recovery operations after errors of different criticality.

From the platform configuration point of view, the following configuration data and programs should be provided:

- description of I/O controllers, sensor types and actuators;
- algorithms for performing technological tasks and auxiliary operations with up to individual sensors and actuators manipulation;
- rules for organizing the operation of the installation in continuous mode: performing maintenance operations, reloading of materials and consumables;
- sets of rules for planning the execution of technological tasks and operations, taking into account the above requirements.

## MOTI CS PLATFORM

Let us allocate several levels of the applied computing process in the platform and create a chain of translators (specialized virtual machines) that will solve the tasks of each level. This allows to introduce intermediate levels of abstraction between physical endpoints and application tasks.

The following levels are allocated (Fig. 1, 2):

1) command level is the execution of the minimum possible indivisible actions with sensors and actuators;
2) operations level is the execution of chains of commands scheduled as a whole;
3) the level of steps of applied tasks is the execution of chains of operations designed to perform one stage of material processing;
4) the level of applied tasks is the execution of logically completed algorithms providing for obtaining the result from workpieces using consumables.

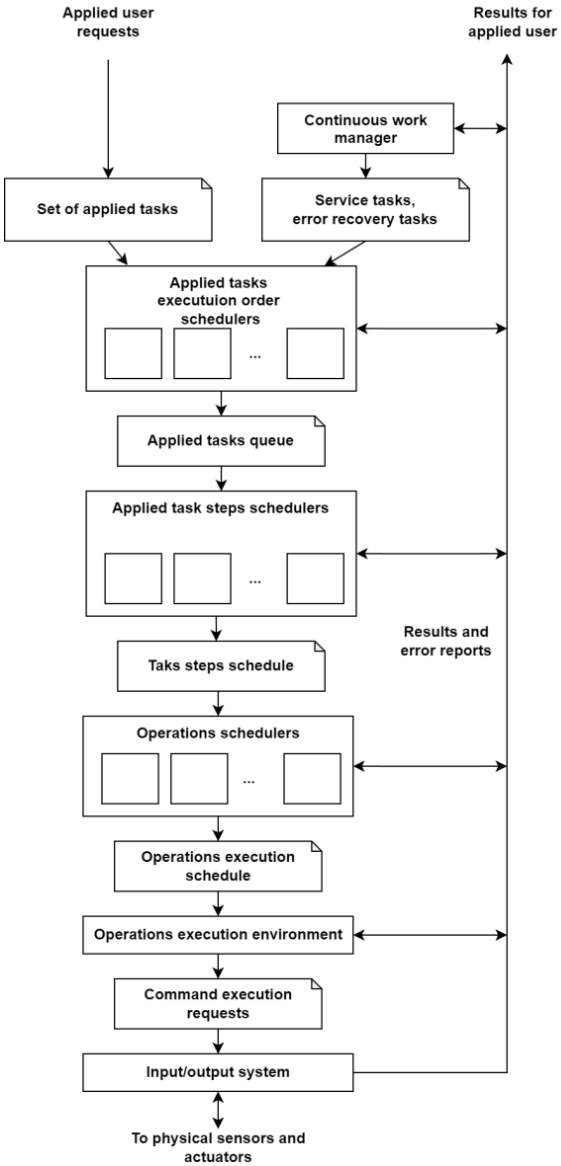


**Figure 1.** Generalized scheme of the MOTI CS control platform

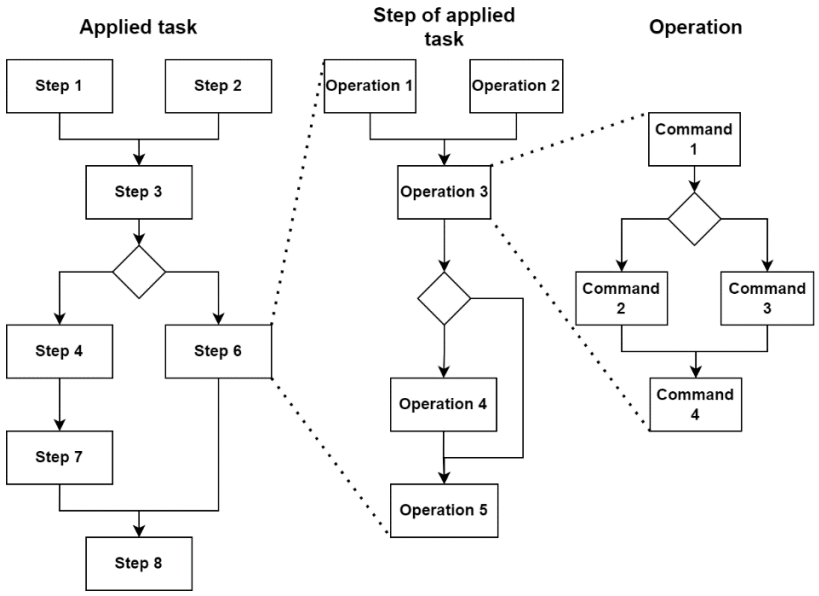


**Figure 2.** Nesting of elements of the applied computing process

The I/O subsystem is responsible for executing commands, including the peripheral controller drivers and the controllers themselves, to which sensors and actuators are connected. Commands, operations and steps of applied tasks are control synchronized using the same principles of structural programming and interprocess communication. Operations, task steps, and tasks have real-time constraints that can set the maximum, minimum, and typical average execution time. The operations and task steps are time synchronized with schedulers and executing dispatchers. They use time constraints to create a schedule and then to verify them during execution. The top-level scheduler handles the set of tasks submitted for execution and optimizes the order in which tasks are started according to the set of steps each task requires.

The scheduler of each level performs the following functions:

- assigning time slots for actions taking into account real-time constraints;
- monitoring the execution of tasks, including an assessment of the states of various processes;
- tracking errors that occur during execution and correcting work at its own level, as well as transmitting error information to higher levels of schedulers.

The implementation of different levels of criticality usually requires the creation of scheduling algorithms with fundamentally different and even incompatible requirements. For example, some of the applied tasks can be performed in hard real time according to a static schedule, and the other part in soft real time with dynamic scheduling to optimize throughput. Separate virtual machines must be provided for them. At this level, a coordinator is required who can suspend/restart task virtual machines (VMs) with a lower level of criticality, as well as ensure consistent operation.

The proposed approach is a generalization of the method of isolating tasks with different real-time requirements widely used in embedded systems. The low-level I/O is implemented on a processor core running a real–time operating system or even on “bare metal”, and the network interaction and user interface are implemented on a processor core running Linux. Failure in the tasks of the second group is much more likely due to bugs in the implementation of protocols and in third-party components due to their high

complexity. But they are less dangerous for the functional safety of the target system than a failure in low-level management of physical devices. The advantage of this approach is not only the logical isolation of tasks within the framework of different scheduling models, but also physical isolation from interference in processor core utilization and failures.

In the proposed approach, it is also possible to physically isolate virtual machines of different levels and different criticality within the same level. If they are separated only logically, one should make sure that they do not have a negative mutual impact on performance, and that the platform on where virtual machines are running has the necessary isolation mechanisms of application: memory protection; limitation of system resources used (processor time, RAM, network traffic, access to external media); individual restart of applications.

These mechanisms are natural in physical applications isolation on different processor cores, and they are also available within general-purpose operating systems such as Linux. Real-time operating systems are usually much simpler and do not always provide the necessary isolation mechanisms.

The disadvantage of physical isolation is the redundancy of computing resources, so it is not always achievable and justified. It is necessary to group components with a similar level of criticality within nodes with lower software mechanisms of mutual isolation, as well as check the availability of necessary isolation mechanisms and implement the missing ones.

## MOTI CS IMPLEMENTATION EXAMPLE

Using the proposed approach, the authors developed the MOTI CS platform for automating a family of laboratory research installations. Let's take a closer look at examples of requirements and technical solutions that complement the principles described above.

Applied tasks must be performed with strict real-time constraints, observing time limits for each task step. At the same time, optimal utilization of the installation is achieved by pipelining tasks with parallel execution of different steps for different tasks.

Application tasks include from 3 to 10 steps, each step consisted of 2-20 operations, each operation requires execution of 10 to 100 commands. The typical execution time of one operation is from 1 to 5 seconds, one step – from 10 seconds to 10 minutes, one task – up to 20 minutes. The large variation in the step duration is explained by the fact that same steps of different tasks can be performed simultaneously on a set of workpieces due to several positions in the processing unit.

The principle of static planning has been adopted at all levels, since the priority is to perform applied tasks in hard real time. The scheduler is started at any change in the conditions under which planning took place: a set of application tasks change; abnormal situations requiring non-scheduled processing; user intervention occurs (the request to suspend operation). The queue of application tasks is scheduled based on their priorities and the availability of consumables, as well as the ability to launch new tasks with minimal pauses. There is also a separate scheduler for running service tasks related to installation maintenance. Task step scheduling is mainly related to resource planning: linking installation units and consumables to the specific task steps. It is necessary to decide which of the same type of elements to assign to complete the task step, and

whether there is enough stock of consumables to complete the tasks. The scheduling of operations is carried out using a static cyclic schedule, which is developed manually. This schedule is natural for a specific type of installation, as it is developed together with the processing units and their mutual arrangement for the most efficient processing of workpieces. Also, time slots are provided in the cycle schedule for the safe execution of installation maintenance operations.

Only I/O controllers that implement low-level protocols are physically isolated. The remaining applied virtual machines of the control hierarchy and information system components are implemented using standard Kotlin programming tools and are located on the same computer with a powerful multi-core processor running Linux, since such an organization allows to meet the required time constraints. Within each virtual machine with configuration capabilities, local error handling tools are provided to reduce the impact of failures on the overall behaviour of the system, as well as the ability to recover from failures. If the work can be continued after the restoration and the time limits of the task are not violated, the operation is repeated. If it is impossible to complete the task in a regular manner, measures are taken to safely eliminate the consequences and the rest of the tasks are continued. The task affected by the failure can be started again.

To configure different levels of the control system, a relatively simple specialized cLabScript language has been developed, which is available for mastering by entry- and intermediate-level specialists. The language is multi-paradigm and can support different computing models, as well as declarative and imperative coding styles. Developing own language and tools, despite the complexity, gives the advantage of optimizing the language for the needs of the project without creating add-ons over standard languages, as well as isolating applied users from system software. The language allows to describe algorithms for performing operations and applied tasks using standard structural programming primitives and supports parallelism. The language is extensible, it adds support for different computing models for working with entities such as an operation and a task step, which differ significantly in their semantics from the command. cLabScript programs are executed by VMs within the runtime environment, which provides loading of executable code into a VM, means of inter-VM communication, VM management, management of actors of different computing models (for example, within the Kahn Process Network [11], the actor is a process, and the actor is state in the Finite State Machine).

The components of the MOTI CS platform have built-in tools for collecting statistics on the execution of elements of applied tasks. Based on this information, it is possible to analyze the accuracy of compliance with time limits, processing units idling, degradation of actuators, which manifests itself in a change in command execution time. Then you can use these findings to compile reports on the quality of the system, calibration, manual or automated correction of settings and applied algorithms, and performance optimization through dynamic planning.

## CONCLUSION

The creation of custom computing systems for the automation of complex technological installations is one of the most difficult problems in the embedded computing systems design. As part of such a project, it is required to develop specialized analogues of components of almost the entire automation pyramid, and at the same time meet

relatively limited computing resources, as well as a development budget. At the same time, such systems have a mixed criticality of computational tasks, which further complicates the design problem.

In this article, the principles of creating embedded computing systems of multi-operational technological installations are proposed based on the multilevel partition of the applied computing process. Also, an example of applying these principles to automate a real installation is presented.

The authors plan to develop the proposed solutions in the direction of further detailing the principles of organizing custom-made computing systems with mixed criticality and the necessary design abstractions.

**REFERENCES**

[1] Alan Burns and Robert I. Davis, Mixed Criticality Systems - A Review (13th Edition, February 2022), 97pp, Department of Computer Science, University of York, York, UK

[2] Martin A. Sehr, Marten Lohstroh, Matthew Weber, Ines Ugalde, Martin Witte, Joerg Neidig, Stephan Hoeme , Mehrdad Niknami, and Edward A. Lee: “Programmable Logic Controllers in the Context of Industry 4.0”. IEEE transactions on industrial informatics, vol. 17, no. 5, may 2021

[3] Marwedel P., Embedded System Design. Embedded Systems Foundations of Cyber-Physical Systems, 2nd ed. Springer, 2011.

[4] Lee E. A. and Seshia S. A., Introduction to Embedded Systems - A Cyber-Physical Systems Approach, Second Edition, MIT Press, 2017.

[5] Sangiovanni-Vincentelli A., Damm W., Passerone R., Taming Dr. Frankenstein: Contract-Based Design for Cyber-Physical Systems, Eur. J. Control. 2012. Vol. 18. P. 217-238.

[6] M. Barabanov. Introducing RTLinux (Report). Linux Journal. URL: https://www.linuxjournal.com/article/232

[7] M. Cashmore, M. Fox, D. Long, D. Magazzeni, B. Ridder, A. Carrera, N. Palomeras, N. Hurtos, M. Carreras. ROSPlan: Planning in the Robot Operating System. Proceedings International Conference on Automated Planning and Scheduling, ICAPS. 2015. 333-341. 10.1609/icaps.v25i1.13699.

[8] Lee E. A., Neuendorffer S., Wirthlin M. J., Actor-Oriented Design of Embedded Hardware and Software Systems, J. Circuits, Syst. Comput. 2003. V. 12, p. 231-260.

[9] Sangiovanni-Vincentelli A., Martin G., Platform-based design and software design methodology for embedded systems, IEEE Des. Test Comput., 2001., vol. 18, no. 6, pp. 23-33.

[10] Platunov, A., Kluchev, A., Penskoi, A. Expanding design space for complex embedded systems with HLD-methodology, International Congress on Ultra Modern Telecommunications and Control Systems and Workshops, 2015-January, pp. 157-164.

[11] Kahn, G. (1974). Rosenfeld, Jack L. (ed.). The semantics of a simple language for parallel programming

# THE SECURITY REQUIREMENTS FOR CYBER-PHYSICAL SYSTEMS

**PhD Akmaral Imanbayeva**[1]

**Rabiga Syzdykova** [2]

[1] Al Farabi Kazakh National University, **Kazakhstan**
[2] Almaty University of Power Engineering and Telecommunications, **Kazakhstan**

## ABSTRACT

Cyber-physical physical systems find their place in all spheres of modern life and are in a stage of rapid development. The prospects for the development of cyber-physical systems affect the interests of society as a whole, so they should be considered not only in a technical, but also in a broader socio-cultural aspect. The scope of application of cyber-physical systems extends to industrial systems, energy, transport and military systems, as well as all types of life support systems. Researchers repeatedly consider issues related to ensuring the reliability and security of cyber-physical systems. It is very important to solve the proposed problem, firstly, a cyber-physical system is a complex system with a large number of structural elements that require coordinated and continuous operation of the elements for their operation. Secondly, the cyber-physical system is a fully automated system, and the reliability and security issues of automated systems have not yet been resolved. An important aspect of the development of cyber-physical systems is the requirement of security. Therefore, security requirements engineering has developed rapidly in recent years, and more and more security techniques have been proposed in the research community. To date, there are several studies available in the literature that have focused on examining security requirements engineering from different perspectives. In paper, information was obtained about the considered solutions for developing security requirements and tools for their implementation. The results showed that there is a growing trend of interest in security requirements engineering, especially in cyber-physical systems research. Research helps to better understand the methods used to ensure safety.

**Keywords:** cyber-physical systems, control management, security requirements, analysis of security methods.

## INTRODUCTION

The term cyber-physical systems (CPS) refers to the creation of systems with integrated computing and physical capabilities. These systems can interact with other systems in a variety of ways. Interconnected systems create a large-scale network that represents multidisciplinary and physically aware engineering systems [1-4]. Such a network contains components with advanced capabilities: recognition, data collection, data transmission and mechanical actuation. Physical and software components are deeply intertwined in cyber-physical systems. The CPS concept is closely related to the 4th Industrial Revolution. Preference is given to high production flexibility, simple and accessible participation of all involved business process subjects in this new industrial concept [5]. In this regard, strategic imperatives have driven vendors to build advanced functionality into the core of enterprise systems to support industry strategy in the quest

for a smart factory for responsive, flexible, holonic and elastic manufacturing. These functions can leverage and manage change and development. Each component of both physical assets and cyber devices requires a certain level of security compliance. A scalable and distributed level of coordination is required to ensure its stability [6-9]. Trillions of devices are included in Industry 4.0 CPS, and therefore communication between devices must be highly scalable. Despite the high relevance of scientific research in the field of theoretical research on the development of cyber-physical systems, many problems of creating CPS remain unresolved. Thus, the theoretical justification for the principles of constructing cyber-physical systems is insufficient. Issues of functional completeness and synergistic effect from combining various components into a system, tasks for managing target objects, and others remain undeveloped. This is only a small part of the problems facing the creation, development and implementation of cyber-physical systems.

An important issue that requires an early solution for cyber-physical systems is the formalization of flows and the formation of parallel algorithms in the structure of a cyber-physical system to optimize control. Controlled cyber-physical systems must be supported by intelligent nodes, which is a new concept for communication and control systems, including organizational and technical systems. Cyber-physical systems emerged as a result of the evolution and development of technical and technological tools.

Artificial intelligence, robots, new data processing methods, transport, virtual world, Internet of Things (IoT), information security areas, rapidly developing cyber-physical physical systems. From a technical point of view, implemented cyber-physical systems based on the Internet of Things, Industrial Internet, Machine-to-Machine, Fog and Cloud Computing have much in common with grid structures. High-quality and secure communications are necessary to protect such systems, and account management and access control systems are also needed. So, the purpose of this work is to reveal the features of the use of cyber-physical systems in management and in determining the goals of security management. To achieve this goal, the tasks of a classification of information on various technical solutions according to security requirements and methods of their implementation proposed by various researchers has been carried out.

Thus, there are currently many different approaches to developing security requirements, including multi-faceted (SQUARE), UML-based (UMLsec), goal-oriented (KAOS/Tropos) and common criteria-based (SREP) approaches [10,11]. Multilateral approaches are more relevant than unilateral approaches because they take into account and try to reach a compromise between the views of various stakeholders, which is an important and integral part of the process. There are a number of proposals that address security issues early in the control lifecycle that are not specific to CPS. To date, many security requirements methodologies have been developed.

## METHODS

A systematic review analysis of the safety criteria was conducted using the relevant guidelines for systematic reviews in software engineering proposed in [12]. The guidelines cover the three stages of a systematic literature review: planning the review, conducting the review, and reporting the review. The search for methods and safety requirements, designed to obtain a maximum of articles corresponding to the field and scope of research, was carried out using well-known databases of scientific literature. The

search strategy allowed us to assess the completeness of the search. This methodology reduces the potential for bias in findings in the literature, although it does not protect against publication bias in primary studies. This systematic literature review requires significantly more effort than traditional literature reviews. This made it possible to identify as much relevant literature as possible. This systematic review requires clear inclusion and exclusion criteria to evaluate each potential primary study.

The review questions guide the entire systematic review methodology:

- the search will identify primary studies that address security models in cyber-physical systems;
- the data extraction process will highlight the data elements needed to answer the questions;
- during the data analysis process, the data will be summarized in such a way that the questions posed can be answered.

The development of a standard specification (information structure or schema) is important when designing cyber-physical systems. Structural modeling methods, based on the use of graphical representations of models of complex systems, are widely used in system design.

## RESULTS

Distinctive features of cyber-physical systems include such aspects as digital integration, digital distributed communication, allowed parallelism of processes, the presence of lower, upper flows and control flows, a combination of synchronous and asynchronous control, etc. There is a need to use fundamentally new approaches in the case of an increase in the complexity of systems, in the case of an increase in the scale of distributed systems that require management.

Since the main goal of this paper is to identify security management goals that are especially important for cyber-physical systems, we present our main results here. Initially, the work was carried out to adjust the methodology of control questions, using the data presented in Tables 1 and 2.

**Table 1.** Quality assessment process

| Phase | Method | Assessment Criteria |
|---|---|---|
| 1st Phase | Identify articles using search string | Keywords/ Query string execution |
| 2nd Phase | Remove duplicate articles | Duplicate removal |
| 3rd Phase | Exclude articles based on titles | Search strings in titles “Accepted” or “Rejected” |
| 4th Phase | Exclude articles based on abstracts | Search strings in abstracts “Accepted” or “Rejected” |
| 5th Phase | Obtain selected articles that pertain to the goals of the study | Papers, addressing security requirement cyber-physical systems “Accepted” or “Rejected” |

A special analysis protocol was used to conduct such a study. The first step is to find research papers. Available articles were found in four literature databases. Since many articles in these databases are paid, we found them on other free sites, on the personal

Internet pages of scientists and on the social network Researchgate.net. IEEE Xplore, Spinger, Elsevier and ACM DL are the main literature databases. Many methods are fully discussed in [13], so some data is taken from there. This algorithm is presented in Figure 1. As a result, 205 scientific papers were received (Table 2).

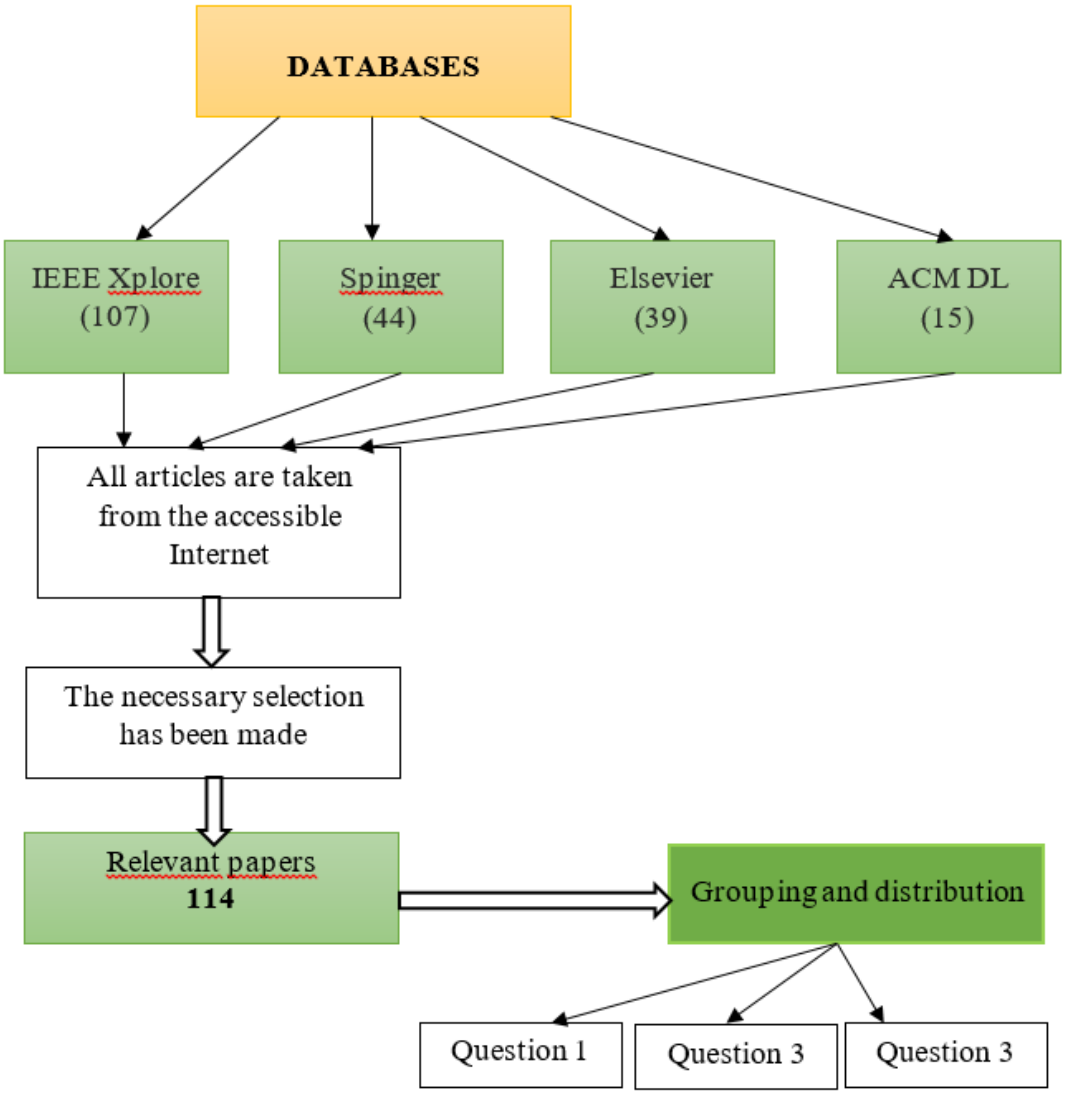


**Figure 1.** Research algorithm

**Table 2.** Quality assessment process

| Databases | Selected papers | Relevant papers |
|---|---|---|
| IEEE | 107 | 68 |
| Springer | 44 | 22 |
| Elsevier | 39 | 18 |
| ACM DL | 15 | 6 |
| Total | 205 | 114 |

The second stage is to systematize the literature, that is, study only the necessary articles according to the purpose, group the security methods presented in them, methods and means that can only be used when managing cyber-physical systems. As a result, 114 scientific papers were selected.

The third stage is the regulation of methods in 32 works on the following issues:

- Question 1: What solutions exist in the literature for developing security requirements for cyber-physical systems?
- Question 2: What security goals are considered particularly important for such systems?
- Question 3: What experimental methods are used to evaluate proposed security requirements engineering solutions?

## DISCUSSION

The algorithm we have considered establishes the criteria that will guide the study. The three research questions formulated in the process and the characteristics identified are shown in Table 3 along with their descriptions.

**Table 3.** Solutions presented in the papers

| Contribution | Name | Implementation tool |
|---|---|---|
| Framework | STS-ml extension | STS tool |
| | Secure Tropos | ST-tool |
| | Parmenides | NFL |
| | UML based business process framework | UML |
| | CORAS | XML Tool |
| Approach | AUTOFOCUS | AUTOFOCUS Tool |
| | Secure Tropos | Off-the-Shelf LPG-td Planner |
| | Scenario Driven | Conceptual Model |
| | SURE | ASSURE |
| | Trust Assumptions | Using trust assumptions built into the solution |
| Method | MOQARE | Misuse Tree |
| | Conceptual Framework | Reference Implementation |
| | SQUARE | CASE Tool |
| | UMLsec | UMLsec |

To address the third issue, we identified experimentally evaluated articles. 45% of the articles were assessed theoretically. Researchers used case study as the most frequently used method in articles 27% for experimental evaluation, followed by controlled experiment 9%, survey 7%, 2% are prototype study, 5% are mixed experiment. The full results are presented as a chart (Figure 2).

The study provided valuable information about the solutions proposed by researchers for developing security requirements and the means of implementing them.

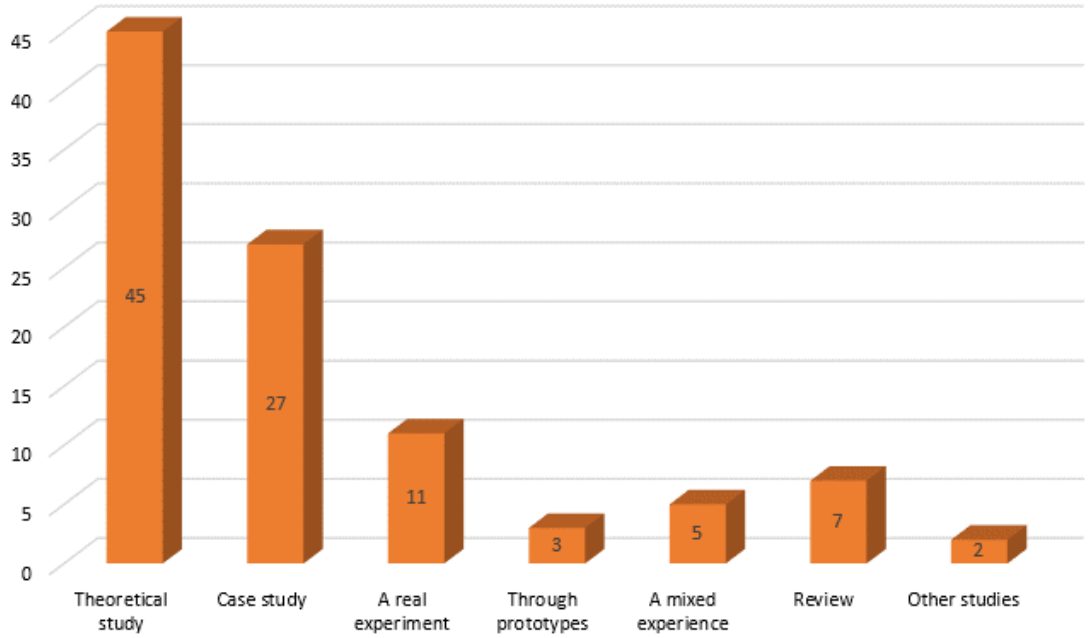


**Figure 2.** Distribution of research methods

In addition, the results presented in the study showed that there is a growing trend of interest in developing security requirements, especially in the research of cyber-physical systems. The research helps to better understand the methods used to ensure security.

## CONCLUSION

Thus, cyber-physical systems are distinguished from complex systems by the use of modern methods and algorithms for communication between computational and physical elements, security, reliability and performance. The heterogeneous structure and close connection of components within the system, intelligent mobility and autonomy and automation of processes, the use of big data technologies are also distinctive characteristics. Each component operates at different spatial and temporal scales, exhibits many different behaviors, and interacts with each other in a variety of ways that vary depending on the context. Cyber-physical systems have additional security requirements compared to classical systems. This is the result of the inclusion of sensor networks and actuators, also called the perception layer.

Valuable information about the solutions proposed by researchers for the development of security requirements and the means for their implementation was obtained during the study. In addition, the results presented in the study showed that there is a growing trend of interest in security requirements engineering, especially in cyber-physical systems research. Research helps to better understand the methods used to ensure safety.

## REFERENCES

[1] Gunes V., Peter S., Givargis T., Vahid F., A Survey on Concepts, Applications, and Challenges in Cyber-Physical Systems, KSII Trans. Internet Inf. Syst., vol. 8, no. 12, pp. 4242-4268, 2014. DOI: 10.3837/tiis.2014.12.001;

[2] Dokhanchi A., et al, Formal requirement debugging for testing and verification of cyber-physical systems, ACM TECS, vol. 17(2), pp.34, 2018. DOI: 10.1145/3147451;

[3] Son H.S., Kim W.Y., et al, Metamodel Design for Model Transformation from Simulink to ECML in Cyber Physical Systems, Computer Applications for Graphics, Grid Computing, and Industrial Environment, Springer, pp. 56-60, 2012. DOI: 10.1007/978-3-642-35600-1_8;

[4] Jiang Y., Chen C.L.P. & Duan J., A new practice-driven approach to develop software in a cyber-physical system environment, EIS, vol.10:2, pp.211-227, 2016. DOI: 10.1080/17517575.2014.939107;

[5] Li Da Xu & Lian Duan, Big data for cyber physical systems in industry 4.0: a survey, Enterprise Information Systems, vol.13, pp.148-169, 2019. DOI: 10.1080/17517575.2018.1442934;

[6] Yar-Mukhamedova G.S., A mathematical model of formation of the structure of composite films by the cut-off method, Materials Science, vol.36(4), pp.598–601, 2000. DOI: 10.1023/A:1011382609756;

[7] Xu Q., Ren P., et al. Security-Aware Waveforms for Enhancing Wireless Communications Privacy in Cyber-Physical Systems via Multipath Receptions, IEEE Internet of Things Journal, vol.4, iss.6, pp.1924-1933, 2017. DOI: 10.1109/JIOT.2017.2684221;

[8] Yar-Mukhamedova G., Muradov A., Mukashev K., et.al. Mathematical model of composite materials formation, Internat. Multidisciplinary Sci. GeoConf. SGEM2017, vol.17(61), pp. 201–208, 2017. DOI: 10.5593/sgem2017/61/S24.027;

[9] Imanbayeva A., et al. Evaluating the effectiveness of information security based on the calculation of information entropy, Journal of Physics: Conference Series, vol.1783(1), pp.012042, 2021. DOI: 10.1088/1742-6596/1783/1/012042;

[10] Anwar M.N. Mohammad, Nazir M. & Mustafa K. A Systematic Review and Analytical Evaluation of Security Requirements Engineering Approaches, Arabian J for Sci and Engineering, vol.44, pp.8963-8987, 2019. DOI: 10.1007/s13369-019-04067-3;

[11] Amangeldina A.K., Khayrosheva K.B. Confidentiality of wireless network data based on an information-theoretical approach, Recent Contributions to Physics, vol. 73 No.2, pp.82-88, 2020 (in Russ.). DOI: doi.org/10.26577/RCPh.2020.v73.i2.09;

[12] Kitchenham B., Charters S.M. Guidelines for performing Systematic Literature Reviews in Software Engineering, Version 2.3, EBSE Technical Report, 65 p., 2007. https://legacyfileshare.elsevier.com/promis_misc/525444systematicreviewsguide.pdf;

[13] Keshk M., Sitnikova E. et.al. An Integrated Framework for Privacy-Preserving Based Anomaly Detection for Cyber-Physical Systems, IEEE Transactions on Sustainable Computing, vol.6, Iss.1, pp.66-79, 2021. DOI: 10.1109/TSUSC.2019.2906657.

# TRANSACTION-LEVEL DESIGNING OF NEUROMORPHIC PROCESSORS MICROARCHITECTURE

**Ivan Lukashov**[1]

**Assoc. Prof. PhD Alexander Antonov** [1]

[1] ITMO University, **Russia**

## ABSTRACT

Spiking neural networks (SNNs) is a promising research direction to their ability to imitate certain functions of brain. Hardware acceleration of SNN can offer orders of magnitude increase in performance and power efficiency. However, traditional hardware description languages have a barrier for rapid development and prototyping of custom internal hardware mechanisms that affect hardware construction throughout the entire processor structure. Mainstream high-level design methods also have disadvantages, e.g. poor focus on transaction streams management description in dynamically scheduled pipelined structures. To accelerate development of custom neuromorphic processors, we propose Neuromorphix software library, which implements a flexible, reconfigurable microarchitectural template enabling selection of a set of transactions specific to neuromorphic processors. Neuromorphix is based on the previously developed ActiveCore open-source framework, which provides a hardware-oriented intermediate representation for generation of hardware data types, operations and behavioral logic. Development process is accelerated by automatic generation of hardware structures typical for neuromorphic processors using transaction-level approach. At the same time, Neuromorphix supports the option to integrate user-defined hardware blocks and also enables reuse of high-level hardware mechanisms which allows to achieve fold decrease of entry barrier for a wide range of neuromorphic processors developers.

**Keywords:** neuromorphic processor, transaction-level designing, spiking neural network, HLS

## INTRODUCTION

With the advancement of neural network algorithms, there is growing interest in spiking neural networks (SNNs) due to their energy efficiency and computational features such as resistance to catastrophic interference and efficient temporal pattern analysis, making them superior compared to mainstream second-generation neural networks [1]. Energy efficiency of SNNs is achieved through their sparse computation, which significantly reduces power consumption. These advantages make SNNs a promising direction in the field of intelligent data processing.

To achieve high performance and energy efficiency, SNNs require hardware acceleration in the form of specialized neuromorphic processors. Such processors can be implemented in Application-Specific Integrated Circuit (ASIC) or Field Programmable Gate Arrays (FPGA). Like in software design domain, efficient design methods,

languages, and tools become a cornerstone to enable rapid design, optimization, and prototyping of these processors.

## PROBLEM STATEMENT

Hardware developers often spend a lot of time modifying descriptions and matching design components, which slows down design space exploration. Furthermore, when designing accelerators at system level, system developers are faced with the need to flexibly change the microarchitectural design as part of hardware and software co-design. Traditional design flow based on commonly used hardware description languages (HDL) offers lower level of abstraction, focusing on the modeling of combinational logic blocks and memory circuits. Therefore, there is a need for new design methods that accelerate development and facilitate integration of ideas in construction of custom microarchitectures on high level of abstraction. These ideas can be design-wide and span configuration of subsystems throughout the entire hardware structure of the processor.

## RELATED WORKS

There are several major high-level design approaches that have both advantages and disadvantages in the context of complex hardware design. High-level synthesis (HLS) methods reduce development time and cost by enabling behavioral-level descriptions of hardware pipelines. However, HLS is limited to synchronous structures with a fixed schedule for operation timing, where data is guaranteed to be ready for any branch of the algorithm's execution by the allocated hardware resources [2]. This approach is not always suitable for complex neuromorphic architectures. At the microarchitectural level, operation of a neuromorphic processor can be effectively described as multiple concurrent transaction streams circulating within the accelerator's structure.

Currently, three main directions in the "transactional" approach can be highlighted:

- System bus transactions (SystemC/TLM);
- Data packet transactions circulating in computational pipelines (TL-Verilog [3], ActiveCore [4]);
- Atomic transitions of multiple registers to new states (Bluespec).

SystemC/TLM transactions primarily relate to read/write operations of System-on-Chip (SoC) interconnects and are not suitable for flexible and detailed exploration of the microarchitecture of particular blocks. Atomic transactions in Bluespec provide structured, detailed control over state transitions in multiple registers of the synthesized block, but do not automate transaction pipelining and other high-level computational process management mechanisms.

In this work, we present an approach to constructing microarchitecture of spiking neural network accelerators based on transactions decoupled from specific computations. We propose to make them "high-level" by annotating them with additional high-level information that describes how these transactions behave within the certain computational process management scheme, which enables rapid re-design, optimization, and flexible design adaptation to custom and changing project needs.

## SYNTHESIZED NEUROMORPHIC PROCESSORS MICROARCHITECTURE

The primary components of neuromorphic processors include hardware blocks that model the behavior of spiking neurons, store dynamic and static parameters, manage communication between computational resources, and manage the data flow. This article focuses on the design methods of digital synchronous accelerators for SNNs based on the Leaky Integrate-and-Fire (LIF) model.

Computational process in a neuromorphic processor begins with the reception of incoming spikes, which are typically messages containing address of the target or the source neuron. The neuron's selector controller then reads the necessary dynamic and static parameters of the neurons from memory. Depending on the modeled neuron, the controller performs operations by neuron processing unit to update dynamic parameters (e.g. membrane potential or adaptive threshold). The controller employs time-multiplexing to sequentially manage hardware resources for processing neurons.

For common LIF neuron models, computational process consists of time slots divided into ticks. During each tick, incoming spikes are processed for each neuron. At the end of the tick, a leakage function is performed, and the resulting dynamic potential is compared with the neuron's potential threshold. If the accumulated potential exceeds the threshold, the neuron fires a spike and resets its accumulated potential.

This computational process is supported by various structural blocks (Fig. 1) in neuromorphic architectures that implement the necessary set of microarchitectural mechanisms. Buffer-schedulers are employed to manage the incoming queue of spikes, storing them for target neurons within the current time slot. Memory banks are used for storing static and dynamic parameters. The word width in the synaptic weight memory can vary, for example, when support for on-chip learning or includes additional synaptic tags, such as synaptic delay or the type of synapse [5]. The depth of memory bank for neuron membrane potentials is corresponds to the number of neurons processed. Additionally, there is I/O interface for external communications [6-8].

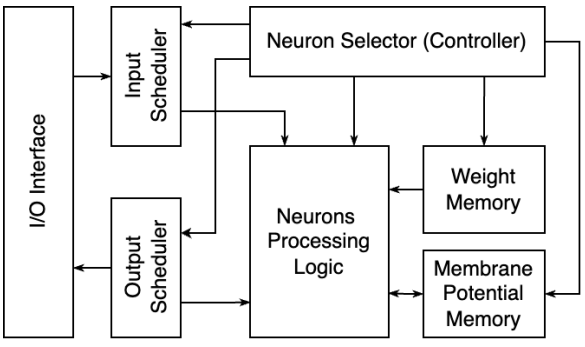


**Fig. 1.** Structure blocks of synthesized neuromorphic processors

Thus, a specific microarchitectural level of neuromorphic processors can be distinguished, formalizing the computational process of such accelerators. This allows decoupling the microarchitectural mechanisms intended for organizing communication and managing data flows from the mechanisms implementing spiking neurons processing. Synthesis of communication subsystem and the transaction flow control subsystem is automated, while the logic for processing neuron models remains flexibly programmable by the developer.

## NEUROMORPHIX PROCESSOR DESCRIPTION LANGUAGE

The above-mentioned separation of microarchitectural mechanisms is implemented based on ActiveCore open-source framework. ActiveCore supports definition of a set of reusable transactions, events, synchronization primitives, and other synthesizable microarchitectural mechanisms for a specific class of microarchitectures. To describe user-defined functionality, ActiveCore framework includes the Hwast module, which implements a hardware-oriented abstract syntax tree (AST). This module simplifies implementation of various hardware data types, operations, and behavioral logic. Thus, it is possible to clearly decouple automatically generated design of supporting microarchitectural mechanisms (communication and flow control) from the user-defined logic. The hwast package provides a base class for creating a list of containers containing procedures, on the basis of which the AST is built for subsequent translation into Register Transfer Level (RTL).

The developed Neuromorphix package adds methods for describing neuromorphic architectures, providing the developer with the ability to use abstractions for the formal description of designs specific to neuromorphic processor microarchitectures.

1. Transactions

To implement transaction-level design, it is necessary to define the possible types of variables. The ActiveCore framework includes a base class for hardware variables (*hw_var*), which provides the ability to inherit the basic properties of hardware data types. In Neuromorphix, three types of variables are defined for designing customized accelerator architectures.

The first type of variables is defined by the class of local variables (*neuro_local*) and is used to describe transactions whose lifetime is limited by the clock signal. Essentially, these are combinational signals. These variables represent signals that implement data and control flows for communication exchange between the hardware resources. This class is essential for defining transactions that describe, for example, intermediate data flows within the neuron processing block. The second type of transactions is epochal transactions (*neuro_epochal*) that preserve their state within a time slot between ticks. These transactions are used to describe data flows that are processed once during the time slot. The third type consists of global transactions (*neuro_global*), which describe transactions that remain unchanged during the entire operation period. These variables have different constructors to automate the definition of variable types for the target design.

2. Memory banks

As discussed in the “Structure of Neuromorphic Processors” section, typical architectures of neuromorphic processors contain two main memory blocks: memory for storing synaptic weight coefficients and memory for storing the membrane potentials of neurons. The structure and size of these memory banks depend on the target architectures of the SNNs. To implement the specified properties, Neuromorphix accepts parameters for word format and buffer depth, allowing them to be used for describing design-specific logic for executing neuron models.

3. Schedulers

The scheduler depth is parameterized based on the model being executed. The scheduler is automatically generated and connected to the accelerator’s input-output interface. The

template includes two similar schedulers: an input scheduler and an output scheduler. The flow control for the schedulers, as well as for the input and output interfaces, is automatically generated upon invoking by the translate method.

## PROCESSOR SYNTHESIS ALGORITHM

The Cyclix module, which is part of ActiveCore, is used to generate RTL code. This module allows creating an intermediate representation of a computational hardware procedure at the register transfer level. In Neuromorphix, the Translate method is implemented for this purpose, which accepts the AST from the list of procedures resulting from the user design.

The Translate method (Fig. 2) ensures the translation of Neuromorphix data types into Cyclix data types, which are compiled into a synthesizable digital logic block. Cyclix has local data types (combinational signal) and global data types (combinational signal with a register for storing values between clock cycles). To perform the translation, it is necessary to map the local and global data types of the modules.

```
fun translate(debug_lvl : DEBUG_LEVEL) : cyclix.Generic {
    var cyclix_gen = cyclix.Generic("Neuromorphix_design")
    var TranslateInfo = __TranslateInfo(this) // Context that consist of
                                              variables, neuron handlers, counters
    /* lists of variables (locals, globals) for associating */
    /* global variables for schedulers, static and dynamic memory */
    var input_spike = cyclix_gen.local(("input_spike" ), "0")
    /* other variable for neuron selector */
    // Generating resources for variables
    for (global in globals) { /* associating global variables */ }
    for (local in locals) { /* associating local variables */ }
    var tick = cyclix_gen.local("tick_sig", "0")
    // Generate resources for neurons processing handler
    for (CUR_HANDLER_INDEX in 0 until TranslateInfo.NeuronHandlersList.size) {
        var curStage = TranslateInfo.NeuronHandlersList[CUR_HANDLER_INDEX]
        /* lists of hw_vars for epochal transactions within processing handler */
        // Generating resources for epochal transaction
        var epoch_timeoff = local("epoch_timeoff", "0")
        for (epochal in epoochals){
            cyclix_gen.begif(not(tick))
            run { cyclix_gen.assign(epoch_timeoff, hw_imm("0"))}
            /* associating epochal variable */ } }
    // Generate resources for counting of neurons
    var presyn_neurons_count = cyclix_gen.global("presyn_neurons_count",  "0")
    /* others variables for counter */
    cyclix_gen.begif(not(tick))
    /* neurons counting */
    // Binding memories resources
    input_spike.assign(scheduler.indexed(presyn_neurons_count)) // Assign spike
    static_param.assign(static_mem.indexed(input_spike))  // Assign weight coefficient
    /* Assign other memories resources */
    return cyclix_gen
}
```

**Fig. 2.** Part of translate method for reconstruction user-defined design with automatic generation logic

Mapping the epochal data type in Neuromorphix has a specific feature: it adds additional logic for managing Cyclix global variables based on ticks. Thus, when the tick signal is low, the values of the global variable associated with epochal are reset.

The method automatically generates input and output schedulers, which are connected to the I/O interface declared by the user. Schedulers represent buffers, with the word width equal to log2(n), where n is the number of postsynaptic neurons. The depth of the input scheduler is equal to the number of presynaptic neurons multiplied by the number

of postsynaptic neurons, while the depth of the output scheduler equals the number of postsynaptic neurons. The input scheduler stores all spikes received during a tick slot.

To generate the control logic, the translate method accepts global variables for the number of presynaptic and postsynaptic neurons. The values of these variables are set by a parameter defined by the user when declaring an object of the Neuromorphix class. A local variable is used to count the processed presynaptic and postsynaptic neurons. The flow control logic is based on the sequential processing of each neuron. Spikes are extracted from the scheduler by clocks. Then the operations described by the user are performed on them.

This generated logic enables automatic generation of microarchitectural mechanisms typical for neuromorphic architectures. Based on this method, input and output schedulers are added to the user logic, and control logic implementing time-multiplexing within tick slots is generated. This enables the development of custom designs for neuromorphic accelerators based on transactions entering the input interface and subsequently circulating through the hardware resources specified by the developer, which are generated into a time-multiplexing design.

Thus, Neuromorphix represents a template with typical microarchitectural mechanisms of neuromorphic processors, such as time-multiplexing neuron selection for processing. The generated neuron's selector block has a neuron counter for processing and ensures sequential access to memory banks storing static (weight coefficients) and dynamic (membrane potential) parameters of the computed neurons. The structural and behavioral view of the template is presented in the Fig. 3.

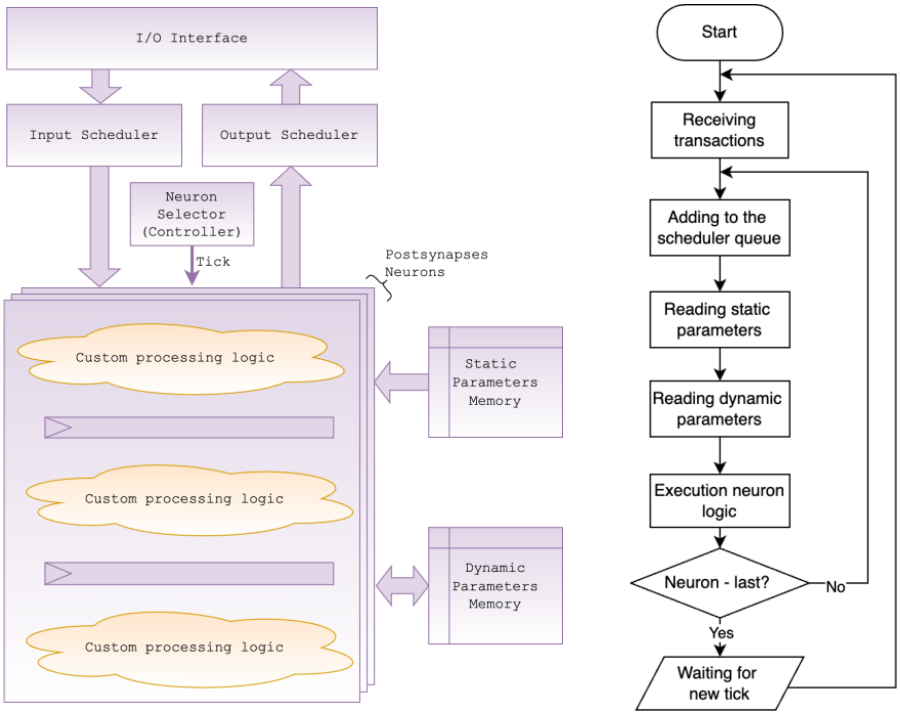


**Fig. 3.** Microarchitectural template and its behavioral representation in Neuromorphix

## EXAMPLE OF A NEUROMORPHIC PROCESSOR DESIGN

A neuromorphic processor design supporting LIF neuron computation was developed (Fig.4), exemplified by the implementation of a fully connected spiking neural network.

The design is implemented in the form of *LIF_accelerator* class, defining variables and user logic for computing the spiking neural network model. The accelerator implements sequential processing of postsynaptic neurons based on incoming spikes from presynaptic neurons.

```
class LIF_accelerator() : Neuromorph("LIF_accelerator", NEURAL_NETWORK_TYPE.SFNN, 5000) {
    var input_if = io_if("input_if", hw_type(DATA_TYPE.BV_UNSIGNED, hw_dim_static(7, 0)))
    var output_if = io_if("output_if", hw_type(DATA_TYPE.BV_UNSIGNED, hw_dim_static(7, 0)))
    var LIF = neuron_handler("LIF", 256, 256)
    var input_spike = neuro_local("input_spike",  8, 0, "0")
    var output_spike = neuro_local("output_spike",  8, 0, "0")
    var updated_membr_potential = neuro_epochal("membrane_potential", 5, 0, "0")
    /* other variables */
    LIF.begin()
    run{
        input_spike.assign(input_if.data_in)
        updated_membr_potential.assign(input_spike.plus(updated_membr_potential))
        /* other LIF-realizing logic */
        output_spike.assign(output_if.data_out)
    }; end_proc()
}
```

**Fig. 4.** User-defined design of spiking neural network accelerator based on LIF neuron

The given processor description has been sent to Neuromorphix library as configuration for the processor generation. Neuromorphix constructed the processor according to this configuration and internal template using Cyclix library. In its turn, the generated Cyclix-based design has been synthesized to hardware in SystemVerilog HDL through rtl hardware generation library available in ActiveCore framework. This design has been checked for synthesizability and available online at: https://github.com/ivlukashov/activecore/.

## RESULTS

For the given design example implemented as LIF_accelerator class, by leveraging the transaction-level approach and ActiveCore infrastructure, we estimate a 35% reduction in code size compared to traditional Hardware Description Language (HDL) methods for the given example. The framework's flexibility allowed for rapid modifications to the design, significantly shortening iteration cycles. By utilizing Nuromorphix, we have reduced the need for manual changes to the hardware description when developing and debugging the neuron processing accelerator. According to our evaluations, the number of places for change in code has been reduced to 30%. This has led to a substantial decrease in overall development effort and complexity in prototype creation.

## CONCLUSION

Implementation of the Neuromorphix framework has demonstrated significant advantages in automating the design and development of neuromorphic processors. The automated design structure provided by Neuromorphix has streamlined the development process, leading to faster design iterations and reduced verification overhead. In our experiments, we successfully created a deeply variable design twice as fast compared to the mainstream workflow.

The hardware design example implemented as LIF_accelerator class, demonstrates practical application of Neuromorphix in creating a fully connected spiking neural network. This accelerator implements sequential processing of postsynaptic neurons based on incoming spikes from presynaptic neurons. The design supports LIF neuron

computation and demonstrates capability of Neuromorphix to handle complex neuromorphic architectures efficiently.

Furthermore, RTL code generated by Neuromorphix is fully synthesizable and compatible with FPGA configuration. The design quality remains on par with manually developed designs. Neuromorphix, as a zero-cost abstraction solution, provides a cycle-accurate representation of the execution process, enabling developers to maintain precise control over the design.

Overall, Neuromorphix framework has proven to be an effective tool for developing custom neuromorphic processor designs, providing a robust and flexible platform for developers and researchers in the field of intelligent data processing by SNNs.

## ACKNOWLEDGEMENTS

The work has been done in Software Engineering and Computers Systems Faculty of ITMO University, Saint-Petersburg, Russian Federation, and has been supported by Russian Science Foundation, grant № 22-11-00145.

## REFERENCES

[1] Vaila R., Chiasson J., Saxena V., Deep Convolutional Spiking Neural Networks for Image Classification, 2019, Available at: https://doi.org/10.48550/arXiv.1903.12272 (accessed 1 June 2024).

[2] Coussy P., Gajski D., Meredith M., Takach A., An Introduction to High-Level Synthesis, IEEE Design & Test of Computers, 2009.

[3] Hoover S., Salman A., Top-Down Transaction-Level Design with TL-Verilog, 2018, Available at: https://doi.org/10.48550/arXiv.1811.01780 (accessed 1 June 2024).

[4] Antonov A., Structured Design of Complex Hardware Microarchitectures Based on Explicit Generic Implementations of Custom Microarchitectural Mechanisms, Electronics 2022, Vol. 11, Issue 7, article 1055, 2022.

[5] Davies M., Srinivasa N., Lin T.H., Chinya G., Cao Y., Choday S.H., Dimou G., Joshi P., Imam N., Jain S. and Liao Y., Loihi: A neuromorphic manycore processor with on-chip learning. Ieee Micro, 38(1), pp.82-99, 2018.

[6] Frenkel C., Lefebvre M., Legat J. D., and Bol D., A 0.086-mm² 12.7-pJ/SOP 64k-Synapse 256-Neuron Online-Learning Digital Spiking Neuromorphic Processor in 28-nm CMOS, IEEE Transactions on Biomedical Circuits and Systems, vol. 13, no. 1, pp. 145-158, 2019.

[7] Modaresi F., Guthaus M., Eshraghian J.K., Openspike: An openram snn accelerator, IEEE International Symposium on Circuits and Systems (ISCAS) 2023 May 21 (pp. 1-5), 2023.

[8] Ye W., Chen Y., Liu Y., The implementation and optimization of neuromorphic hardware for supporting spiking neural networks with MLP and CNN topologies, IEEE Transactions on Computer-Aided Design of Integrated Circuits and Systems. 2022 May 30;42(2):448-61, 2022.

# UTILIZING ALGORITHMS FOR IMAGING MEDICAL RESULTS FROM CT, MRI, AND PET INTO VIRTUAL REALITY

**PhD Piotr Kardasz** [1]

**Krzysztof Kolebski** [2]

**Assoc. Prof. Piotr Jednaszewski** [3]

[1] Fundacja BRI, **Poland**

[2] Developer Team Sp. zo.o., **Poland**

[3] St Mary`s Institute Limited, Ireland, **United Kingdom**

## ABSTRACT

Utilizing algorithms for imaging medical results from CT, MRI, and PET into Virtual Reality. There is a growing interest in the field of medical imaging in understanding the impact of algorithm parameters on the quality and interpretability of the obtained images. In the developed software VRMed3D aimed at educating students using medical images in virtual reality technology, Gaussian noise was utilized to identify the most effective edge detection algorithms. The search was for an algorithm that provided the most optimal quality of generated images while maintaining the shortest possible waiting time.
The aim of this study is to present the results of tests on the impact of changing input parameters of algorithms on the outcome. The article discusses the current state of research, then describes the conducted analysis of algorithms: Gaussian noise, grouping neighboring illumination values, noise removal, and edge detection. Finally, the effects of algorithm configurations on the final outcome are discussed.

**Keywords:** CT, MRI, PET, VR, algorithms

## INTRODUCTION

There is a growing interest in the field of medical imaging in understanding the impact of algorithm parameters on the quality and interpretability of the obtained images. In the developed software VRMed3D aimed at educating students using medical images in virtual reality technology, Gaussian noise was utilized to identify the most effective edge detection algorithms. The search was for an algorithm that provided the most optimal quality of generated images while maintaining the shortest possible waiting time.

The aim of this study is to present the results of tests on the impact of changing input parameters of algorithms on the outcome. The article discusses the current state of research, then describes the conducted analysis of algorithms: Gaussian noise, grouping neighboring illumination values, noise removal, and edge detection. Finally, the effects of algorithm configurations on the final outcome are discussed.

## 1. Research Status

Edge detection has been extensively described in the literature. Biswas and Hazra [1] proposed an edge detection method based on a modified Moore's neighborhood algorithm. This algorithm works in two steps, namely the modified Moore's neighborhood algorithm, followed by range filtering to detect edges. Unfortunately, edge computations take a lot of time. Meng [2] proposed an edge detection method based on the local adaptive Canny method. It has more advantages compared to global thresholding. Researchers [3] also used the Canny algorithm along with gradient, length, and direction change of edges to detect edges in noisy images. Zhang [4] developed an improved Sobel edge detection algorithm. This algorithm increases the edge detection angle and has more accurate gradient calculations, which enhances the detection accuracy and detects more edges in the image. Romani [5] introduced an edge detection method based on RBF interpolation which relies on the compact C2 Wendland function. They applied this method to X-ray and standard images, but the accuracy and computation time did not improve significantly. Shubhangi [6] conducted a comparative study of femur edge detection in X-ray images. Comparing images obtained from different edge detection operators, it was concluded that the Laplace operator is the best. However, standard parameters were not considered.

Jianfang [7] implemented an image edge detection algorithm based on the Otsu-Canny operator on the Hadoop platform. The Otsu algorithm is used to optimize the dual threshold of the Canny operator, which improves edge detection efficiency. The proposed approach requires less execution time compared to Canny, parallel Canny, and Otsu-Canny algorithms. According to article [8], the Canny operator is commonly used for edge detection in images. However, as the size of the image dataset increases, the performance of the Canny edge detection operator decreases, and its operation time becomes excessive. Gaurav and Ghanekar [9] proposed an innovative steganography algorithm based on local edge detection with a reference pattern and an exclusive OR property (XOR). This algorithm exhibits higher embedding capacity (bpp) compared to existing steganographic techniques, while maintaining PSNR and SSIM values.

Mathur et al. [10] proposed an innovative approach to brain tumor detection in MRI images using k-means clustering, fuzzy Mamdani inference system, and Sobel edge detector. This method provides accurate tumor localization based on appropriate threshold selection. However, it requires establishing fuzzy rules to achieve high accuracy.

As indicated by the above examples, the topic of edge detection in various digital images is being explored by researchers at multiple levels.

## 2. Algorithm Analysis

### 2.1 Gaussian Noise Algorithm

In the analysis of medical images, Gaussian noise is used to model natural fluctuations in pixel intensities in medical images such as computed tomography or magnetic resonance imaging. This allows for improving the quality of images by simulating instabilities and imperfections in the image acquisition process.

In the developed program, tests were conducted to extract the most effective Gaussian algorithm, which would provide the best quality of generated images while maintaining the most optimal generation time. The starting point was the original algorithm, with a predetermined blur strength of 1. During the generation of images using the standard algorithm, the execution time of the noise application operation for the loaded illumination file was 127 s, and for the ultra-fast algorithm, it was 4.86 s.

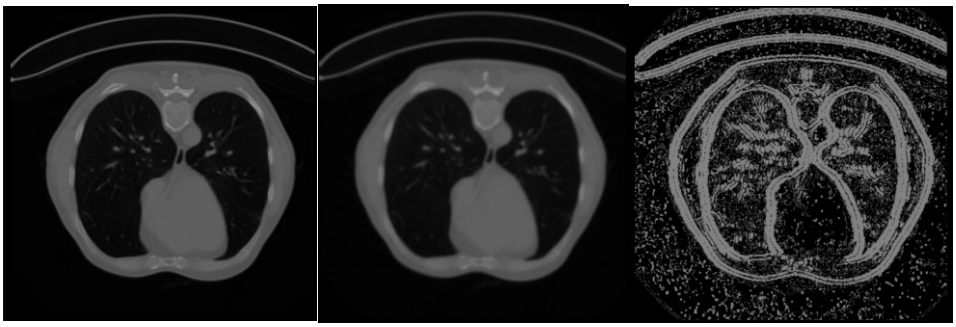

Fig. 1. Test Results in Graphical Form from left: visualization of the standard algorithm, visualization of the ultra-fast algorithm, overlay of the results of both algorithms. The color of pixels illustrates the scale of differences between the images – the brighter the pixel, the greater the difference in the generated images at that location.

Regardless of the strength used, the final effect for both the original and ultra-fast methods is very similar. The algorithm works best and produces the best results when using strength 1 or 2. Ultimately, the tests proved that the improved algorithm with significantly shortened waiting time for result generation works drastically faster than the original. Waiting for just under 5 seconds compared to 127 seconds for the standard algorithm constitutes a satisfactory improvement in quality. In the case of the ultra-fast algorithm, when using noise at each of the tested strengths, it produces almost identical results to the standard algorithm, and the differences between the algorithm results do not negatively affect the expected outcome. Using the highest strength allows, at the expense of detail, to obtain images with the most pronounced edges without using an algorithm and can therefore be used for analyses requiring images with significant edge delineation.

The conducted tests also allowed for examining the impact of different strengths used during image generation on the final outcome of the entire edge detection process. It was noticed that at higher values, the algorithm focuses more on finding larger objects, removing smaller details. This results in greater transparency of the interior of the illuminated object unless user requirements are different, in which case adjusting the parameter to the required material preparation needs is recommended.

## 2.2 Grouping Adjacent Illumination Values and Noise Removal Algorithm

The next step in the analysis was to determine the impact of parameters of the grouping and noise removal algorithm on its operation. Changes in the algorithm's operation were analyzed based on the following variables: the blur strength of the Gaussian algorithm used (r), the range of neighboring pixels used (range), the method of calculating the pixel based on neighbors (Method: mean, median, q3), and the range of jump to the next processed pixel (Step: one, half range, range).


Fig. 2 Comparative Analysis for Variables (r=1), range=2, Method=mean, Step= one and (r=5), range=2, Method=mean, Step= one. The last image depicts the overlay of the previous images.

Fig. 2 illustrates the results of one of the comparative analysis attempts for the assigned variables. In the case of changing the noise strength and the range parameter, creating the largest possible discrepancy, it can be observed that despite this, the state of the image obtained for the weakest strength and the smallest range, and the strongest strength and the largest range, remains practically unchanged. The quality of the obtained images and their level of detail remains within acceptable parameters, which in turn proves that using a faster computational method for the created algorithms allows saving user time without significantly negatively impacting the perception of the content generated by the algorithm.

### 2.3 Edge Detection Algorithm - Differences

Three popular edge detection methods were used in the developed program. The Sobel algorithm uses two masks to calculate gradients, which are then summed to obtain the total result, indicating the presence of edges in the image. It is highly sensitive to noise. Roberts is another algorithm that was used in edge detection research. It uses masks that are applied to pixels in the image, which in turn detect edges in different directions. It is one of the simpler but less accurate algorithms.

The third algorithm used was Prewitt, similar to Sobel and using two masks to calculate gradients for horizontal and vertical directions, which are then summed to obtain the total gradient indicating the presence of edges. Its significant advantage is its lower sensitivity to noise compared to the fairly similar Sobel algorithm in other respects.

Next, on the same image, the capabilities of the individual algorithms were compared against each other. The Prewitt and Sobel algorithms significantly better mark the edges of the image with a wider processing range, but Roberts allows for a fuller picture in terms of the displayed amount of detail.

Using all algorithms with different ranges as well as adding Gaussian noise strength to the variables, hundreds of results were obtained - most of them did not meet the criteria, but within the experiments, several combinations were selected, which together provide satisfactory or interesting results from the project's perspective. The most detailed images, simultaneously possessing clearly defined edges, are created from a combination of Sobel and Prewitt algorithms.

## 3. Effects of Algorithm Configurations on the Final Outcome

Taking into account all the variables mentioned above, as well as the types of edge detection algorithms that can be used, their strengths and weaknesses, and the impact of the level of Gaussian noise on the clarity of the conveyed image, final tests were conducted using alternately all of the above, particularly focusing on those that yielded the most promising results in the previous section.

The conclusions indicated that to obtain the best images, a relatively low value of Gaussian noise is needed, while simultaneously utilizing algorithms of greater complexity, such as Sobel or Prewitt. Additionally, the edge detection methods themselves using quartiles or the entire range do not significantly affect the appearance of the image. However, when combined with an expanded range, these two parameters can lead to a mosaic effect on the image. The effect will be more noticeable, the stronger the noise was initially applied by the Gaussian algorithm.

## CONCLUSIONS

All predicted dependencies between the level of noise and edge detection algorithms, as well as other variables affecting the generation of images, were verified in the research. All three edge detection algorithms were tested using all variables across their entire range of values. The analysis conducted allowed for the determination of the most optimal solutions and combinations contributing to the creation of the most transparent versions of the image.

Additionally, Gaussian noise and its impact on image quality were examined. Higher levels of noise generate images with fewer details but sharper delineated edges of the image. Furthermore, the assumption that it is possible to use a faster algorithm than the standard one to create images of the same or very similar quality for the end user was tested. This assumption proved to be true, as the conducted tests demonstrated that using an ultra-fast algorithm with a processing time of under 5 s produces images indistinguishable in quality from those generated using the standard method, which takes about 140 s. This allowed for the utilization of a faster algorithm version in the product.

## REFERENCES

[1] S. Biswas, R. Hazra - Robust edge detection based on Modified Moore-Neighbor', Optik, Int. J. Light Electron Opt., 168 (2018), pp. 931-943

[2] Y. Menga, Z. Zhang, H. Yin - Automatic detection of particle size distribution by image analysis based on local adaptive canny edge detection and modified circular Hough transform, Micron, 106 (2018), pp. 34-41

[3] H.O. Lawend, A.M. Muad, A. Hussain, Robust edge detection based on canny algorithm for noisy images, J. Theor. Appl. Inf. Technol., 95 (19) (2017), pp. 5104-5114

[4] K. Zhang, Y. Zhang, P. Wang, An improved sobel edge algorithm and FPGA implementation, Procedia Comput. Sci., 131 (2018), pp. 243-248

[5] L. Romani, M. Rossini, D. Schenone, Edge detection methods based on RBF interpolation, J. Comput. Appl. Math., 349 (2018), pp. 532-547

[6] D.C. Shubhangi, S.C. Raghavendra, P.S. Hiremath, Edge detection of Femur bones in X-ray images – a comparative study of edge detectors, Int. J. Comput. Appl., 42 (2) (2012), pp. 13-16

[7]C. Jianfang, C. Lichao, M. Wang, Implementing a parallel image edge detection algorithm based on the otsu-canny operator on the Hadoop platform, Comput. Intell. Neurosci., 3 (2018), pp. 1-12

[8] K. Gaurav, U. Ghanekar, Image steganography based on Canny edge detection, dilation operator and hybrid coding, J. Inf. Secur. Appl., 41 (2018), pp. 41-51

[9] S . Yuan, D. Xiang, X. Liu Edge detection based on computational ghost imaging with structured illuminations, Opt. Commun., 410 (2018), pp. 350-355

[10] N. Mathur, S. Mathur, D. Mathur, A novel approach to improve sobel edge detector, Procedia Comput. Sci., 93 (2016), pp. 431-438

# SECTION GEOINFORMATICS

# AN EXPERIMENT OF AUTOMATIC CLASSIFICATION AND MAPPING OF THE LANDFORMS OF THE YAMAL PENINSULA

**Lead Researcher Dr. Sergey Kharchenko**[1,2]
[1] Lomonosov Moscow State University, **Russia**
[2] Institute of Geography, RAS, **Russia**

## ABSTRACT

This study investigates the potential of automated geomorphological mapping using geomorphometric analysis and machine learning on the Yamal Peninsula, Russia. The research aims to classify landforms based solely on geomorphometric characteristics, bypassing traditional manual interpretation of aerial imagery and digital elevation models (DEMs). The study utilized a DEM of the Yamal Peninsula and a reference geomorphological map, including 10 distinct landform types. A total of 119 geomorphometric variables, including spectral characteristics of the terrain, were calculated and used for training a Random Forest classifier. The results demonstrate that the model achieved a 65.4% overall accuracy, significantly exceeding the baseline accuracy of 10%. While some landforms, like the first river terrace, were accurately classified with 98% precision, others, such as floodplains, showed lower accuracy. The study identified key geomorphometric variables contributing to the classification, highlighting the importance of "focal" characteristics reflecting the texture and pattern of topographic dissection. The findings suggest that automated classification based on geomorphometric analysis holds promise for geomorphological mapping. It can be used to expedite the creation of geomorphological maps and assist in identifying areas of uncertainty for further investigation. However, future research is necessary to improve the accuracy of specific landform classifications, particularly those with high spatial variability.

**Keywords:** geomorphological map, supervised classification, medium scale, digital elevation model, geomorphometric analysis.

## INTRODUCTION

The field of geomorphological mapping has witnessed a surge in recent years, driven by advancements in remote sensing technologies and the increasing availability of high-resolution digital elevation models (DEMs). This progress has paved the way for semi-automated and fully automated methods to delineate geomorphological boundaries at various hierarchical levels, including genetic types of landforms, individual forms, and their components [11]. However, the feasibility of recognizing not only morphological, but also genetic and age-related boundaries through satellite imagery and DEMs remains a subject of debate. This raises the question of whether the potential for extracting information about the genesis and age of landforms from morphological features has been fully exploited.

Several studies have demonstrated the potential for both typological (e.g., drumlin identification) and general geomorphological mapping (in a chrono-morpho-genetic legend) using remote sensing data [2], [5]. However, the success of such efforts is

constrained by several factors: 1) the chosen legend, determining the types of features being sought, 2) the morphological characteristics employed for boundary recognition, and 3) the selected method of classification or segmentation of the elevation data.

This paper seeks to address the classic challenge of landform classification [4] using an unconventional approach – relying solely on morphometric analysis and supervised machine learning. We apply this method to the Yamal Peninsula, a region with a diverse and challenging landscape.

## MATERIALS AND METHODS

This study utilizes a digital elevation model (DEM) of the Yamal Peninsula, specifically the GMTED 2010 7.5" dataset [3]. For the application of supervised classification, a training dataset is crucial. This dataset consists of a collection of points within the study area, each associated with a known landform type. To achieve this, we utilized the R-40-42 sheet of the 1:1,000,000 scale geomorphological map [12], created with a chrono-morpho-genetic legend.

The optimal set of morphometric characteristics and the ideal level of detail for examining landform morphology are not pre-determined. Therefore, we initially calculated 119 morphometric characteristics, divided into two categories: local and focal. Local characteristics are calculated at individual points (e.g., absolute elevation, slope, aspect) while focal characteristics are calculated for the surrounding neighborhood of each point, providing information on the pattern of topographic dissection. Focal characteristics are often parametrized, with their values depending on the chosen radius of analysis, as exemplified by the Topographic Position Index (TPI) [14].

In addition to traditional morphometric characteristics, spectral characteristics of the terran were derived by decomposing the two-dimensional elevation field into individual oscillating components (harmonics) with varying direction, frequency, and amplitude [8].

The chosen supervised classification method is the Random Forest algorithm, a commonly used technique for spatial data analysis [10]. This method offers the advantage of identifying the most informative variables for distinguishing between the different landform classes.

The Yamal Peninsula is entirely located within the northern province of the West Siberian Plain [13], specifically in the Yamal geomorphological region, characterized by a low (0–90 m) terraced plain (Fig. 1). The summit surfaces of the peninsula were formed during the Pliocene and Early-Middle Pleistocene transgressions of the World Ocean, represented by small fragments of erosional and accumulative, subhorizontal sections.

The remaining territory exhibits a Late Pleistocene and Holocene age. The upper three marine terraces (from the second to the fourth, as identified in the topography) are predominantly bedrock-based, while the lowermost, first marine terrace, is characterized by an accumulative layer of Late Pleistocene marine sediments. These terraces occupy the majority of the peninsula. At lower elevation levels, located in the estuarine sections of relatively large river valleys, coastal-estuarine deltaic plains can be observed. Further down, layd (a type of low-lying land) and beaches are present, often on the surfaces of

sand spits. Around large thermokarst lakes, both existing and drained (alas), lake terraces are distinguishable. River valley floors exhibit two levels: floodplains and the first terrace above the floodplain. The surfaces of high terraces have been significantly altered by thermokarst and cryogenic processes, resulting in a dense network of lake basins.

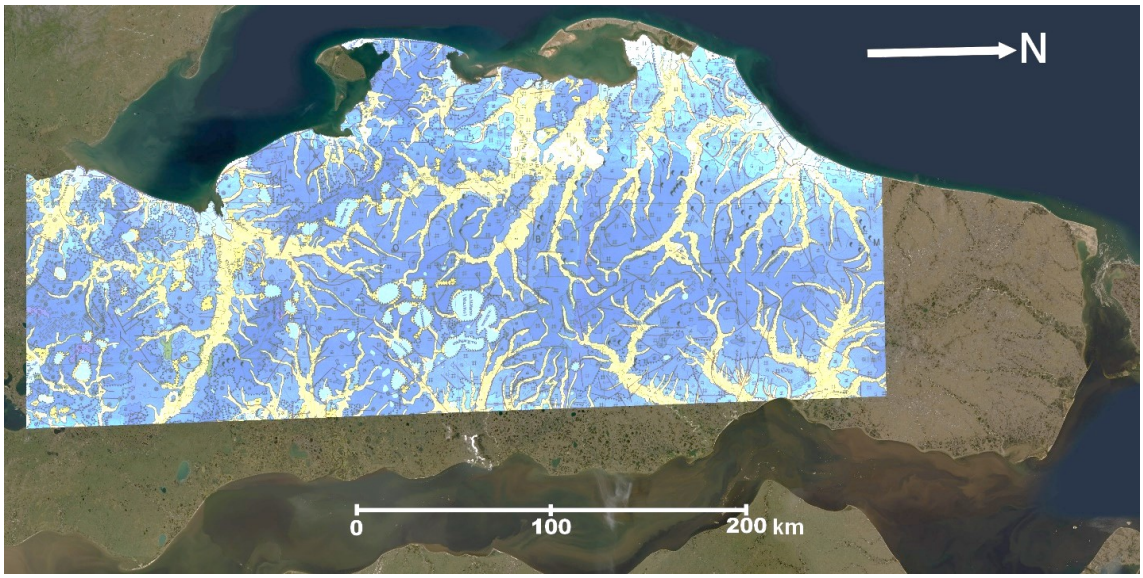


Fig.1. Geomorphologic scheme of a part of the Yamal Peninsula (within the limits of sheet R-40-42 of the topographic map at the scale 1:1000000). Blue shades - surfaces of marine origin, yellow-green shades – surfaces of fluvial and lake origin.

The diversity of landforms on the peninsula, considering the scale of analysis, is relatively limited. The reference map contains only 10 landform types, yet these types share similar morphologies and are close in elevation, potentially posing a challenge for automated classification.

Table 1. Lists the landform types present on the Yamal Peninsula within the boundaries of the R-40-42 sheet of the Gosgeolkarta [12].

| ***No.*** | ***Origin*** | ***Age*** | ***Description*** | ***% of the area*** |
|---|---|---|---|---|
| 1 | Fluvial accumulation | Q IV | Floodplains | 16.9 |
| 2 | Fluvial accumulation | Q $III_4$-$IV_1$ | The first river terrace* | 3.4 |
| 3 | Lacusturine accumulation | Q III-IV | Lake terraces | 6.2 |
| 4 | Seashore accumulation | Q IV | Laida / layd (0-7 m a.s.l.) | 7.7 |
| 5 | Seashore accumulation | Q III-IV | Coastal-estuarine deltaic plain (0-15 m a.s.l.) | 6.6 |
| 6 | Seashore accumulation | Q $III_4$-$IV_1$ | The first sea terrace (10-15 m a.s.l.) | 14.2 |
| 7 | Seashore denudation | Q $III_3$ | The second sea terrace (18-25 m a.s.l.) | 14.5 |
| 8 | Seashore denudation | Q $III_{1-2}$ | The third sea terrace (30-50 m a.s.l.) | 13.5 |
| 9 | Seashore denudation | Q $III_1$ | The forth sea terrace (55-85 m a.s.l.) | 11.6 |
| 10 | Seashore accumulation and denudation | N2 – Q II | Summit surface. Secondary marine erosional and accumulative plains | 5.4 |

## RESULTS

For the entire study area, 119 morphometric variables were calculated. Of these, 81 represent spectral characteristics of the terrain derived using a moving window analysis at nine different scales (2 km, 3 km, …, 10 km). The remaining 38 variables consist of "classic" morphometric characteristics such as absolute elevation, its first and second derivatives (slope, aspect, various types of curvature), relative heights and depths of dissection within elementary basins, the Topographic Position Index (TPI), multiresolution indices characterizing the microrelief of the lower (valley bottoms) and upper (summit surfaces of interfluves) subhorizontal tiers of the relief, and others.

A classification model was created based on a training sample comprising 500 points for each landform class, as defined on the original map. It is worth noting that instead of a pre-existing map, expert interpretation of satellite imagery and DEMs could also be used to generate this training data. Considering the total area covered by the original data on landform affiliation - 109,000 $km^2$ - the five thousand individual sample observations cover only 50 $km^2$ or 0.04% of the total area.

The application of Random Forest for supervised classification offers an advantage over several competing methods as it allows for evaluating the most representative variables for distinguishing the landform classes. Among the top twenty most informative characteristics, almost all (apart from absolute elevation) turned out to be "focal" morphometric variables, reflecting the textural features of the topography and its dissection pattern. The highest level of informativeness is attributed to the "multiresolution index of valley bottoms flatness" and "multiresolution index of roof tops flatness" [6], in conjunction with the absolute elevation parameter. A significant amount of information for reliable classification is provided by relative heights within elementary basins ("normalized height" [1]), the Topographic Wetness Index [1], and the "terrain texture" parameter by Pike and Iwahashi [7]. Additionally, spectral characteristics of the terrain, particularly the measure of deviation of the topography dissection character from strictly fractal (when small-scale landforms are superimposed on similar, but larger-scale forms), as well as the amplitude of heights corresponding to the main rhythm of surface dissection (the most significant harmonic when decomposing the surface into individual wave components) contribute to the model's accuracy. The essence of spectral characteristics of the terrain is presented, for example, in [9].

Some landform classes exhibit significant overlap in their morphometric characteristics. This means that for a randomly selected pair of landform types, a specific morphometric variable (e.g., absolute elevation, see Fig. 2, columns 1, 5, 6 - floodplains and low marine terraces) might be insufficient to differentiate them. The same may hold true for any other morphometric characteristic. However, by considering a multitude of variables, the selected pair of landforms can be effectively separated.

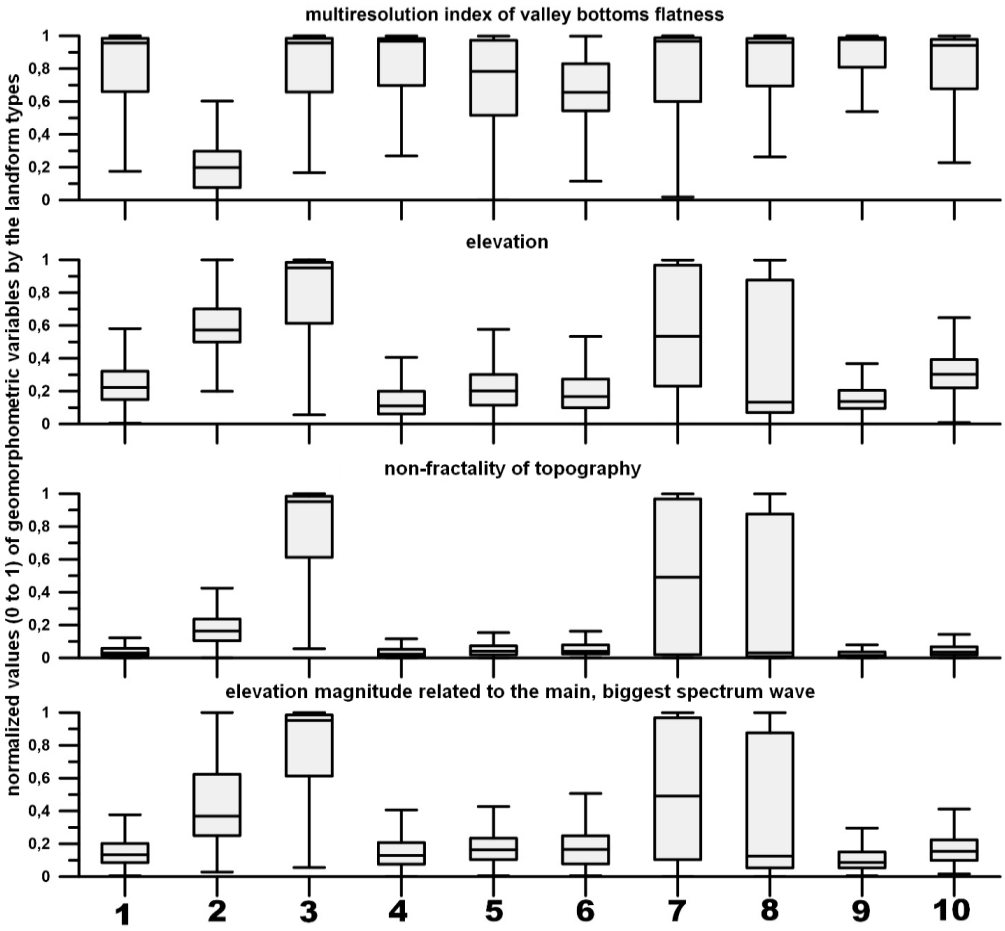


Fig.2. The distribution of the normalized values of some geomorphometric variables by ten different landforms (the indices are matched with the table 1)

The accuracy of the "null model" (a reference value for classification accuracy when the model is no more effective than random guessing) when identifying 10 different landform classes is 10%. In our case, the overall accuracy reached 65.4%, exceeding the reference value by several folds. However, individual accuracies for different landform types ranged from 98% to only 21%.

Figure 3 shows the result of the automated landform classification for the same area covered by the geomorphological schema in Fig. 1, using the same color scheme. A high degree of contour matching between the two schemes is evident, while classification errors are also significant. The floodplain level (class 1), particularly in the lower reaches of rivers, was often classified as layd (which is unlikely an error) and beaches (class 4). The areas of summit surfaces of interfluves (class 10), representing a heavily reworked ancient marine plain, partially accumulative, partially corresponding to the highest erosional level for this territory formed during the high Pliocene transgressions of the ocean, were often overestimated. In some cases, slightly lower and younger marine bedrock terraces were misidentified as this landform type.

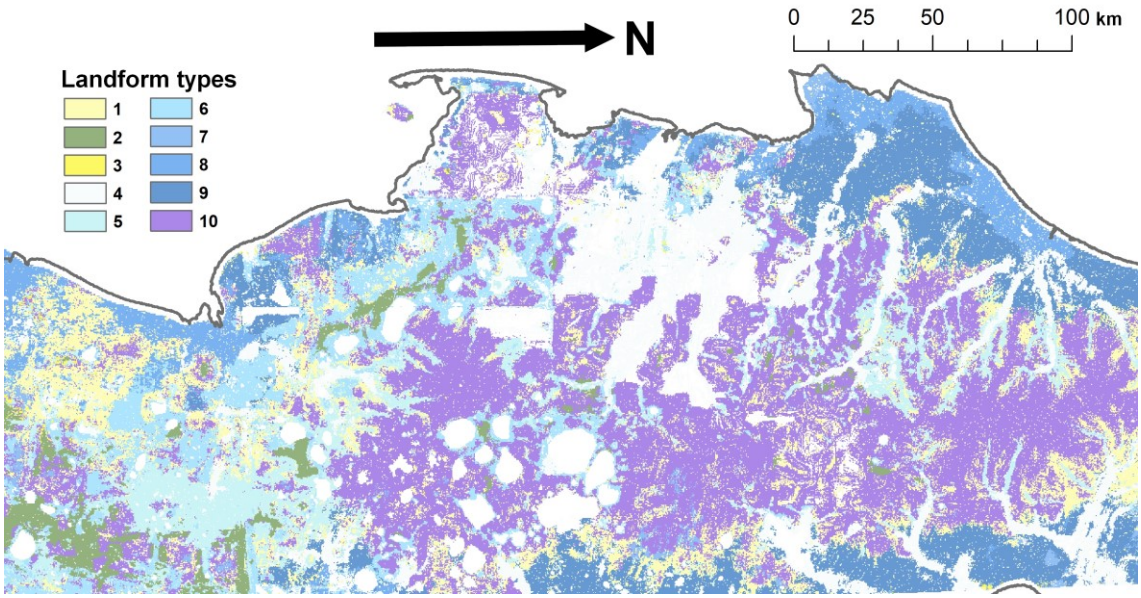


Figure 3. Geomorphologic scheme of the territory constructed by applying the classification model with morphometric data for the whole area. Landforms designations are correlated with Table 1

The achieved model accuracy, despite utilizing such a small training sample, suggests significant potential for partially automating the creation of geomorphological maps through formalizing and extrapolating expert rules for delineating boundaries between different landform types. Furthermore, a promising direction is the use of automated classification results to identify areas with uncertain or debatable affiliation to a specific landform or genetic type of the surface (at least based on morphological indicators) for subsequent detailed study. Current classification errors require further analysis and possibly the development of specific morphometric characteristics to enhance the predictive power of models for particular landform types, such as floodplains in our case.

## DISCUSSION

The high model accuracy is achieved through formalizing and extrapolating expert rules for delineating boundaries between different landform types. Furthermore, the results suggest a promising direction for future research: using automated classification to identify areas with uncertain or debatable affiliation to a specific landform or genetic type of the surface. These areas can then be targeted for more detailed and focused study.

Current classification errors require further analysis, and improvement may involve the development of specific morphometric characteristics to enhance the predictive power of models for particular landform types. For example, in this case, further work is needed to accurately delineate floodplains. The successful classification of the first river terrace, identified as a terrace-like surface below valley edges but significantly higher than the thalweg and floodplain elevations, with a high accuracy of 98% demonstrates the potential of this approach. However, the unsatisfactory classification of floodplains, likely due to their high variability in elevation along the river course and the lack of

adjacent subhorizontal areas below them (unlike terraces), highlights areas for improvement. Adding a morphometric variable like "height above the nearest watercourse" to the model might allow for more reliable delineation of floodplains. Overall, the model's accuracy surpasses the null model by 6.5 times when predicting 10 distinct landform classes. This result was achieved primarily by utilizing focal morphometric characteristics that capture the various textural patterns of topographic dissection. Importantly, this was achieved using a training dataset that represents only 0.04% of the total area, emphasizing the efficiency of this approach.

## CONCLUSION

This study, focusing on landform classification on a portion of the Yamal Peninsula using exclusively morphometric and statistical methods, demonstrates the promise of this approach for partially automating geomorphological mapping. By relying on "expert" data, be it a previously created geomorphological map or the results of manual interpretation and classification of representative points, we can create reliable landform classifications.

This study achieved a model accuracy 6.5 times higher than the null model, correctly predicting 10 different landform classes. This success was primarily attributed to the utilization of focal morphometric characteristics, which effectively capture the various textures and patterns of topographic dissection. Notably, this level of accuracy was attained using a training dataset representing a mere 0.04% of the total area.

While some classes, like the first river terrace, were recognized with high accuracy (98%), others, particularly floodplains, exhibited lower accuracy. This discrepancy underscores the need for refining the model, potentially by incorporating additional morphometric variables that account for the unique characteristics of specific landforms. Future research should focus on addressing these misclassification errors and improving the predictive power of the model for challenging landform types.

The findings highlight the potential of automated classification based solely on morphometric data for assisting in the creation of geomorphological maps, particularly when combined with expert knowledge. Furthermore, this approach can be instrumental in identifying areas of uncertainty or ambiguity in landform classification for further, targeted investigation.

## ACKNOWLEDGEMENTS

This work was supported by the Russian Science Foundation, project No. 19-77-10036.

## REFERENCES

[1] Boehner J., Selige T., Spatial Prediction of Soil Attributes using Terrain Analysis and Climate Regionalization, SAGA – Analysis and Modelling Applications, Goettinger Geographische Abhandlungen, Goettingen, Germany, pp. 13–28, 2006.

[2] Clark C.D., Hughes A.L., Greenwood S.L., Spagnolo M., Ng F.S., Size and Shape Characteristics of Drumlins, Derived from a Large Sample, and Associated Scaling Laws, Quaternary Science Reviews, vol. 28, no. 7-8, pp. 677–692, 2009.

[3] Danielson J.J., Gesch D.B., Global Multi-resolution Terrain Elevation Data 2010 (GMTED2010): U.S. Geological Survey Open-File Report 2011–1073, U.S. Geological Survey, 2011, 26 p.

[4] Deng Y., Wilson J., Sheng J., Effects of Variable Attribute Weights on Landform Classification, Earth Surface Processes and Landforms, no. 31, pp. 1452–1462, 2006.

[5] d'Oleire-Oltmanns S., Eisank C., Drăgut L., Blaschke T., An Object-based Workflow to Extract Landforms at Multiple Scales from Two Distinct Data Types, IEEE Geoscience and Remote Sensing Letters, vol. 10, no. 4, pp. 947–951, 2013.

[6] Gallant J.C., Dowling T.I., A Multiresolution Index of Valley Bottom Flatness for Mapping Depositional Areas, Water Resources Research, no. 39(12), pp. 1347–1360, 2003.

[7] Iwahashi J., Pike R.J., Automated Classifications of Topography from DEMs by an Unsupervised Nested-Means Algorithm and a Three-Part Geometric Signature, Geomorphology, vol. 86, pp. 409–440, 2007.

[8] Kharchenko S.V., Application of Harmonic Analysis for the Quantitative Description of Earth Surface Topography, Geomorfologiya, Russia, vol. 2, pp. 14-24, 2017. (in Russian).

[9] Kharchenko S.V., Bolysov S.I., Using of the Spectral Geomorphometric Characteristics for Automatized Classification of Landforms (On the Example of Australia), 18th International Multidisciplinary Scientific GeoConference SGEM, Albena, Bulgaria, pp. 719–724, 2018.

[10] Khatib A., Malinnikov V.A., Automated Classification of the Vegetation Cover of Mediterranean Landscape using Spectral-Textural and Topographic Features of High Spatial Resolution Satellite Imagery, Sovremennye Problemy Distantsionnogo Zondirovaniya Zemli Iz Kosmosa, Russia, vol. 18, no. 2, pp. 51-63, 2021.

[11] MacMillan R.A., Martin T.C., Earle T.J., McNabb D.H., Automated Analysis and Classification of Landforms using High-resolution Digital Elevation Data: Applications and Issues, Canadian Journal of Remote Sensing, no. 29(5), pp. 592–606, 2003.

[12] State Geological Map of the Russian Federation (New Series). Scale 1:1,000,000. Geomorphological Map. Sheet R-40-42, 2000. (in Russian).

[13] Voskresenskiy S.S., Anan'ev G.S., Andreeva T.S., Varushchenko S.I., Leont'ev O.K., Luk'yanova S.A., Spasskaya I.I., Spiridonov A.I., Ul'yanova N.S., Geomorphological Zoning of the USSR and Adjacent Seas, Vysshaya Shkola, Moscow, Russia, 1980, 343 p. (in Russian).

[14] Weiss A., Topographic Position and Landforms Analysis, ESRI User Conference, San Diego, CA, USA, 2001.

# IMPORTANCE OF GEOMORPHOMETRIC AND GEOLOGIC VARIABLES FOR AUTOMATED DELINEATION OF GEOMORPHOLOGICAL UNITS (ON THE EXAMPLE OF YAMAL PENINSULA)

**Lead Researcher Dr. Sergey Kharchenko**[1,2]
[1] Lomonosov Moscow State University, **Russia**
[2] Institute of Geography, RAS, **Russia**

## ABSTRACT
This study assesses the efficiency of various geomorphometric terrain characteristics and a number of categorical geological parameters in training statistical models to create geomorphological maps. The study area is the central sector of the western coast of Yamal Peninsula (S = 10 400 km$^2$). The terrain is exceptionally flat and morphologically similar, but the genesis and age of the surfaces are diverse. The background surface type is marine terraces of various (Middle Pleistocene to Holocene) ages, subsequently reworked by fluvial, cryogenic, and other exogenous processes. The classification method used is random forest. For representativeness assessment, we used 211 raster images reflecting the spatial distribution over the area of quantitative characteristics of the earth's surface morphology, as well as substrate parameters (the age of different sediment packs, basement structures), geophysical anomalies, etc. It has been established that using sample data covering fractions of the area percent (0.04–1%) allows for the automatic construction of a geomorphological map for the rest of the area with an accuracy of 78–79%, which is more than 7 times higher than the accuracy of random guessing. The most representative parameters are elevation, various metrics of relative heights/depths, supplemented by texture characteristics of topographic dissection: "non-fractality" and "harmony" of the terrain, etc.
**Keywords:** geomorphological mapping, predictive modeling, supervised classification, terrain geomorphometric analysis, spectral terrain variables.

## INTRODUCTION

The development of technologies for automating chrono-morpho-genetic mapping of landforms [5] presents researchers with the challenge of selecting a representative set of input predictor variables that correlate spatially with different landforms or entire genetic complexes of related forms. While exclusively morphological mapping of terrain based on its digital elevation models (DEMs) is a well-developed problem [7], the question of extracting genetic and age-related geomorphological boundaries from these models remains a subject of debate [5], including the fundamental possibility of doing so. At the same time, notable successes in this area can be found even in publications from 50–60 years ago [12].
This paper describes an attempt to perform automated classification of terrain in a part of the Yamal Peninsula using a training sample of varying sizes with the "random forest" method [1] and assess the representativeness of various natural characteristics, potential predictors for surfaces of different genesis. These predictors can be both real factors shaping a specific landform here and the consequence of its presence (for example, ongoing exogenous processes in a particular place can be a consequence of its location on a particular landform; however, knowledge of local exomorphogenesis can

allow us to judge the landform, i.e., to solve the inverse problem). Assigning a particular point on the Earth's solid surface to a particular landform is referred to as classification in this paper.
The assessment of the significance of individual variables when using random forest for classification is done automatically: the predictive potential of individual "decision trees" is calculated, and then we see how the variables were distributed across effective and ineffective individual trees. This assessment is formalized as a specific statistical indicator called "Gini impurity" (mean decrease Gini [10]). The higher this impurity, the more useful, on average, that particular predictor is in the model.
The study area covers the central sector of the western coast of the Yamal Peninsula and the coastal zone, an area representing a vast strip of land where landforms of marine genesis (marine terraces) have been preserved at higher levels of the World Ocean's water level. These surfaces were then modified by fluvial, cryogenic, slope, and modern marine processes, creating a complex configuration of boundaries of landforms of different genesis. The width of the coastal strip here, under conditions of low terrain, reaches 100 km or more. The boundaries of the area are: southern – 70° N, eastern – 69° E, northern – 71.33° N, western – 66° E (Fig. 1).

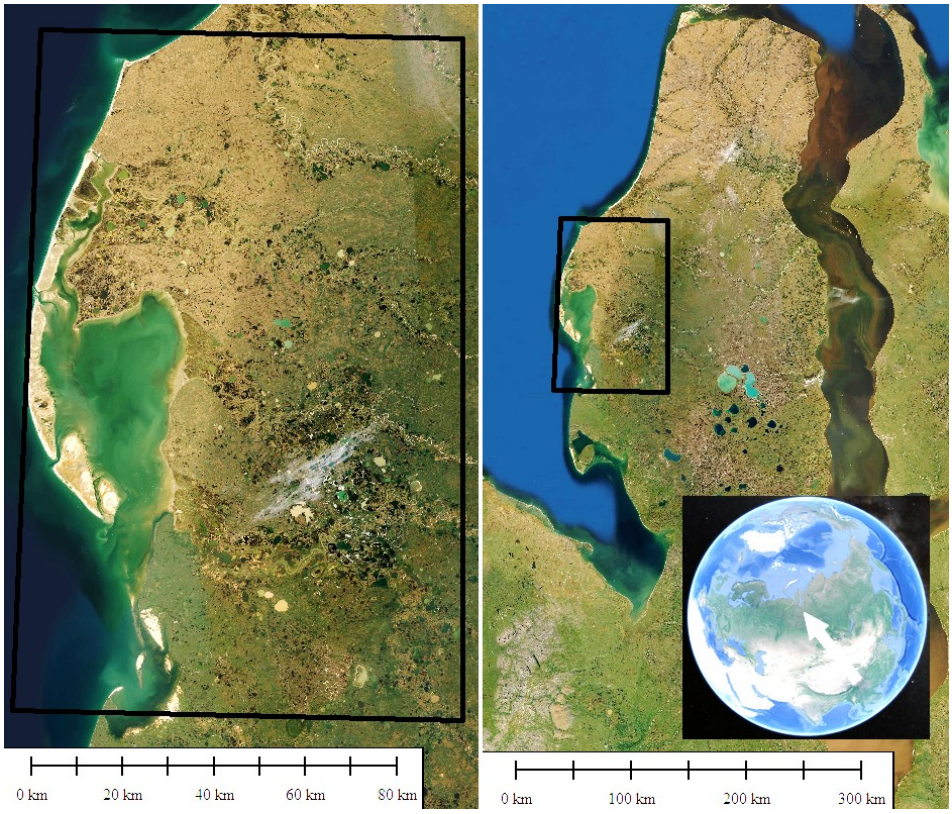


Fig.1. Study area – west side of the Yamal Peninsula

## MATERIALS AND METHODS

The work is based on the use of the Alos World 3D global digital elevation model [11] with a spatial resolution of 30 m within the boundaries of six sheets of the topographic map R-42-7,8,9,13,14,15 at a scale of 1:200 000. The elevation model was used to calculate various morphometric terrain variables, which the statistical model relied upon for automated classification.

In addition, the following characteristics were extracted from sheets of the State Geological Map of Russia at a scale of 1:200 000 [6] as source materials: tectonic zoning of the territory (boundaries of first-order tectonic structures), age and petrographic composition of Precambrian and Paleozoic rocks of the basement, characteristics of pre-Quaternary and Quaternary geological formations of the sedimentary cover, hydrogeological zoning (based on the upper water-bearing horizon, excluding perched water), engineering-geological zoning based on the activity of modern exogenous processes, as well as two parameters characterizing geophysical fields, but available only in the form of an isoline map, not a digital field model: gravity anomalies and Earth magnetic field anomalies expressed on an interval scale (the first in mGal, the second in nTl).

Following geological data, the second group of data used was geomorphometric terrain characteristics, specifically, calculated using the standard GIS tools of SAGA. Classic local values (hereafter referred to as basic morphometric characteristics – BMC) were calculated, for which the value can be determined at a point—absolute height and its first and second derivatives, as well as their modifications (slope, aspect, and its orthogonal components – "northness" and "eastness", curvatures, etc.). It is traditionally considered ([8] and others) that, for example, slope is one of the most representative variables for terrain classification. Indeed, at first approximation, plains, low-, medium-, and high-mountain ranges will be very clearly differentiated by this parameter. Except for the gentle bottoms of mountain valleys and some other exceptions. However, our work shows [4] that with more refined terrain classification, where classes are close to each other in terms of this parameter (a canonical example is erosional-denudational extraglacial and moraine glacial plains), using slope and other local morphometric characteristics is ineffective.

In addition to local BMCs, we calculated BMCs corresponding to various features of the topographic position (its index or TPI), the nature of the terrain of valley bottoms and interfluves (multiresolution index of valley bottom flatness and multiresolution index of ridge tops flatness), parameters of relative heights within elementary basins, topographic roughness within a given radius, topographic texture, etc. All these parameters are calculated for each point of the source elevation model, but they characterize the terrain in a given neighborhood of a varying radius for that point. Thus, they can describe a particular "pattern" of the earth's surface with one number; in this article, they are called "focal" because this quantitative characteristic of each pattern is assigned to a single focus point by the calculation algorithm.

The third group of parameters used was spectral terrain characteristics (hereafter referred to as STC) [2], [4], which are essentially focal morphometric characteristics but not yet classical in the quantitative description of the Earth's surface. These characteristics are obtained by decomposing the DEM over a sliding window into a two-dimensional Fourier series, from which individual oscillatory components—harmonics—are then extracted and numerically described. The harmonic with the largest amplitude corresponds to the main rhythm of terrain dissection, its spatial frequency, or, conversely, its wavelength (the distance between the main divides/thalwegs of the largest valleys), its direction (if clearly expressed), and its height amplitude. We can probably say that the main harmonic plays the most significant role in terrain formation, i.e., we are not talking so much about the genesis of the surface as about the contribution to its final morphology. The main oscillations are superimposed by oscillations of smaller scales (but sometimes also of lower frequency—for example,

wave-like oscillations of the surface related to lateral compression in the Earth's crust, insignificant in height but with very long wavelengths). These oscillations provide secondary, complicating surface features. In an ideal case, when the terrain has a fractal character (and the use of its fractal analysis for description is generally not new [9]), oscillations with increasing spatial frequency/decreasing wavelength will decrease in amplitude. However, in reality, this dependence strongly deviates from the standard [4] hyperbolic dependence, which in a generalized form can be represented as A = A0/f, where A is the amplitude of the oscillations, A0 is the amplitude of the "zero harmonic" (approximately corresponds to the potentially maximum depth of the largest valleys to the global erosion base and, thus, degenerates to the average/background height of the area), and f is the frequency of the waves.

Flat or gently sloping planar surfaces of various genesis are used as the object of prediction: Holocene accumulative (floodplains; deltas; sea beaches, layd, and partially flooded islands; flat surfaces of thermokarst bogs and lake terraces), Pleistocene-Holocene accumulative-denudational (gently sloping, heavily swamped plain of the Late Pleistocene-Holocene first alluvial-marine terrace; flat, slightly dissected, swamped in places surface of the second marine terrace; weakly undulating surface of the third marine terrace), and Holocene colluvial-solifluction slopes. The genesis of several surfaces is debatable; in this work, we rely on the geomorphological diagram [6] (Fig. 2 and Table 1).

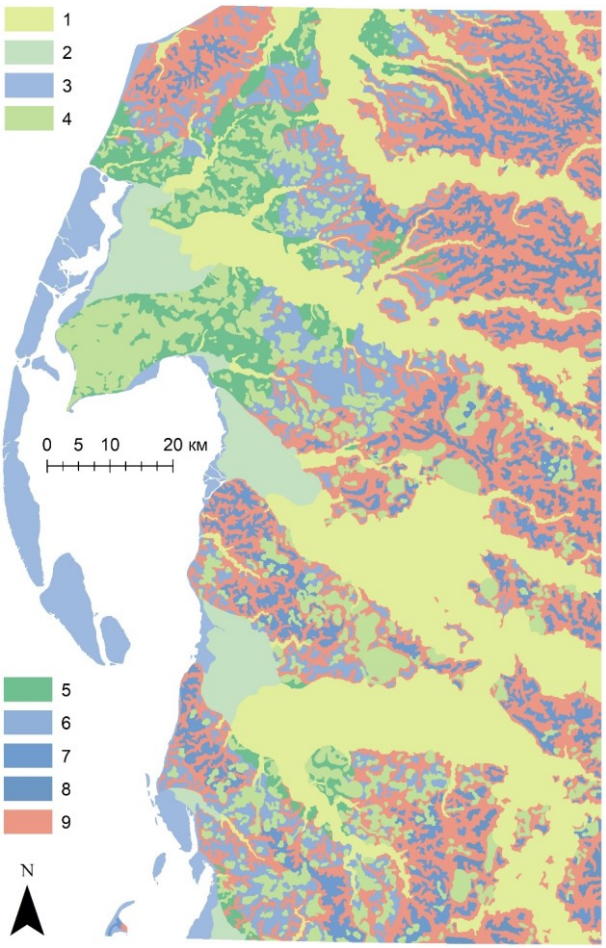


Fig.2. Geomorphological scheme of the area (for legend see Table 1), adapted by the author based on [6]

Table 1. Landforms of study areas

| No | Landforms | Age |
|---|---|---|
| Accumulative | | |
| 1 | Floodplains | QH |
| 2 | Deltas | QH |
| 3 | Sea beaches, layd, and partially flooded islands | QH |
| 4 | Flat surfaces of thermokarst bogs and lake terraces | QH |
| Accumulative-denudational | | |
| 5 | Gently sloping, heavily swamped plain of the first alluvial-marine terrace | QIII-H |
| 6 | Flat, slightly dissected, swamped in places surface of the second marine terr ace | QIII |
| 7 | Weakly undulating surface of the third marine terrace | QIII |
| 8 | Flat or weakly convex residual surfaces of the Quaternary marine terrace | QIII |
| Denudational | | |
| 9 | Colluvial-solifluction slopes | QH |

**RESULTS AND DISCUSSION**

In this work, the author's primary interest is in assessing the representativeness and significance of various terrain and geological substrate characteristics for predicting surfaces of different genesis and age in the central sector of the western coast of the Yamal Peninsula.

211 raster models of morphometric terrain characteristics and 8 vector datasets about the geological features of the territory were used as source data. Terrain classification was performed at 500 068 regularly scattered points across the entire area using four different variants of sets of variables. This allowed for the reconstruction of a raster image from them. A sample of 4941 points was used for training (549 objects for each landform). Considering the cell size of the source DEM, 30×30 m, a direct 4.45 $km^2$ out of 10 400 $km^2$ (0.04%) of the total area was involved in the training. However, indirectly, focal morphometric characteristics made it possible to take into account the geomorphological context of each point. Another estimate of the areas involved in training and validation of the model—for each point used in training, there were slightly more than 100 points with predicted morphogenetic surface characteristics (i.e., 1% is the upper estimate).

Naturally, the best result was achieved with complete freedom for the classifier to choose the most successful variables from different groups. The classifier's own accuracy across all variables was 78.7%, which, in the task of recognizing 9 different types of planar surfaces, is 7 times higher than the accuracy of the "null model". The latter is considered to be a random assignment of classes, in which case the accuracy would be 100% / 9 = 11.1%. At the same time, the classifier's own accuracy is assessed in relation to the same data on which the random forest was trained. When this model (based on the complete set of variables) was applied to the entire area, the accuracy dropped to 66.6%, which is still 6 times higher than the null accuracy. However, this indicates an overfitting effect, where the random forest learns to well recognize the indicators (morphometric, geological) of various types of plains at the points of the

source sample, to the detriment of recognizing these indicators across the more diverse entire area. This first, most effective, model will be discussed in more detail below, after comparing four private models. The results of testing different sets of variables are summarized in Table 2.

Table 2. Comparison of classification results based on different sets of variables

| No | Variable sets | Training accuracy, % | Validation accuracy, % |
|---|---|---|---|
| 1 | All | 78,7 | 66,6 |
| 2 | Geological | 57,3 | 47 |
| 3 | Spectral terrain characteristics + elevation | 75,6 | 61,9 |
| 4 | Spectral terrain characteristics | 70,2 | 53 |
| 5 | Base terrain characteristics | 70,9 | 64 |
| 6 | Base terrain characteristics + elevation | 66,6 | 60,1 |
| 7 | Base terrain characteristics + Spectral terrain characteristics | 76,2 | 65,4 |

A comparative analysis of the significance of variables (based on the Gini impurity criterion) shows that for the tiered terrain of marine terraces on the western coast of the Yamal Peninsula, the most powerful indicator of recognizing geomorphological boundaries is absolute height, surpassing the closest competing parameter by almost 2 times. Normalized height adds predictive power to the created model, which is the relative value of heights within local catchments of varying hierarchical levels. Perhaps, for inclined, homogeneous surfaces (which is more characteristic of river terraces with a gradual decrease in elevation from the headwaters to the mouth, not marine levels), it is the relative heights in different sections of the thalweg network that can be significant, as opposed to absolute heights, the values of which can "intersect" at different levels in the terrain. The valley depth parameter is calculated as the depth at each point from the summit surface passing through the ridge lines. The linear correlation coefficient of normalized height and valley depth is -0.57; both parameters, characterizing relative height differences in different ways, complement each other in the random forest model.

The hydrogeological zoning map of the territory correlates spatially with geomorphological boundaries (spatial correlation using the method [3] is 0.43). These relationships are quite natural. Cryogenic-talik aquifers correspond to floodplains, the surfaces of thermokarst bogs, and lake terraces, where the waterbearing capacity of the upper aquifer is related to the warming effect of water bodies on permafrost. The average-age cryogenic interpermafrost Pliocene-Quaternary aquifer is distributed over the area (according to geomorphological units) relatively evenly, while the most ancient Paleocene-Quaternary aquifer is primarily confined to high marine terraces. Obviously, this may be related not to its selective distribution over the study area, but to the fact that in some areas (at lower levels), this aquifer, as the upper aquifer, was replaced by younger ones.

The multiresolution index of valley bottom flatness, based on combined analysis of relative topographic position at different scales of consideration and surface slope, showed high efficiency in recognizing floodplains and thermokarst bogs. Surface convexity is a parameter reflecting the proportion of DEM cells with positive total curvature (convex) within a given radius of consideration. This parameter allows us to

distinguish low beach and layd surfaces (where it tends to zero for the studied area) from other low surfaces—floodplains, deltas, etc. Height above the base surface reflects the relative position of points on the terrain above the surface interpolated from the elevation levels of valley bottoms.

Unfortunately, it is not possible to consider all representative parameters in this paper. However, it is worth noting that in the list of the top forty indicators, twenty-four are spectral terrain characteristics. At the same time, some parameters, such as the wavelength of the prevailing oscillations in the elevation field, the general direction, and the prominence of any direction, were absolutely insignificant. At the same time, two other parameters show high efficiency. The first is "non-fractality" of the terrain, the deviation (residuals of regression approximation) of the distribution of frequencies and amplitudes of individual harmonics from the hyperbolic law. For example, in the case of the terrain of erosional plains, this deviation is small. In the case where smaller complicating forms (for example, for Yamal, thermokarst lake basins) create even greater height differences at the chosen scale of consideration than large segments of gentle forms (marine terraces), these deviations will be significant. This indicator allows for the automatic differentiation of such situations of hierarchical "inversion" of landforms, when small forms are more pronounced in the elevation field than large ones, and vice versa. The second significant parameter is the "harmony" of the terrain, the proportion of the variance of the elevation field described by a small number (depending on the window size) of the most important harmonics.

## CONCLUSION

Morphometric variables, when applied to classification methods with training, can be an effective tool for automated terrain mapping based on selective spatial data. Their use, together with geological data obtained both through aerial surveys and from fieldwork, allowed us to achieve an accuracy of automated classification that is 6–7 times higher than random guessing (79% during training and 67% during validation). However, as shown, substrate characteristics, geological structures, and geophysical fields increase accuracy by only 1–2.5 pp. relative to the use of only morphometric variables, calculated completely automatically from the freely distributed global digital elevation model, Alos World 3D. This result was achieved for a "complex" territory, the leveled, almost flat western coast of the Yamal Peninsula, with elevation differences of less than 100 m over an area of 10 thousand $km_2$, where surfaces of different genesis (marine, alluvial, complex) and age are very close to each other morphologically. This is a strong testament to the possibilities of automated geomorphological mapping (including in a chrono-genetic context) based on readily available quantitative, exclusively geometric parameters of the Earth's surface.

## ACKNOWLEDGEMENTS

This work was supported by the Russian Science Foundation, project No. 19-77-10036.

## REFERENCES

[1] Breiman L. Random forests. Machine learning. 2001, vol. 45, no. 1, pp. 5–32. DOI:10.1023/A:1010950718922.

[2] Bugnicourt P., Guitet S., Santos V. F., Blanc L., Sotta E. D., Barbier N., Couteron P. Using textural analysis for regional landform and landscape mapping, Eastern Guiana Shield. Geomorphology, 2018, vol. 317, pp. 23–44. DOI:10.1016/j.geomorph.2018.03.017.

[3] Hargrove W. W., Hoffman F. M., Hessburg P. F. Mapcurves: a quantitative method for comparing categorical maps. Journal of Geographical Systems, 2006, vol. 8, no. 2, pp. 187–208. DOI:10.1007/s10109-006-0025-x.

[4] Kharchenko S.V. Automatic recognition of the landforms origin in the Kola Peninsula based on morphometric variables, Geodesy and Cartography, 2022, vol. 83, no. 2, pp. 12–25. DOI: 10.22389/0016-7126-2022-980-2-12-25. (In Russian) DOI: 10.22389/0016-7126-2022-980-2-12-25.

[5] Kharchenko S.V. New Challenges of Geomorphometry and Automatic Morphological Classifications in Geomorphology. Geomorfologiya, 2020, no. 1, pp. 3–21. (In Russian) DOI: 10.31857/S043542812001006X.

[6] Kozlov E. P., Cherdantsev S. G., Sokolovsky A. P., Novoseltseva R. G., Nikitin Yu. N., Voronov V. N., Suslov S. L. State Geological Map of the Russian Federation. Scale 1: 200,000. West Siberian series. Subseries Tyumen-Salekhardskaya. Sheets R-42-VII-IX, XIII-XV. Explanatory note. Moscow, MF VSEGEI (Publ.), 2015. 103 p. (In Russian)

[7] Maxwell A. E., Shobe C. M. Land-surface parameters for spatial predictive mapping and modeling. Earth-Science Reviews, 2022, vol. 226, pp. 103944. DOI: 10.1016/j.earscirev.2022.103944.

[8] McDermid G. J., Franklin S. E. Spectral, spatial, and geomorphometric variables for the remote sensing of slope processes. Remote Sensing of Environment, 1994, vol. 49, no. 1, pp. 57–71. (In Russian) DOI:10.1016/0034-4257(94)90059-0.

[9] Mel'nik M.A., Pozdnyakov A.V. Fractals in the erosion dissection and self-oscillations in geomorphosystems' dynamics. Geomorfologiya, 2008, no. 3, pp. 86–95. (In Russian). DOI: 10.15356/0435-4281-2008-3-86-95.

[10] Ng V. W., Breiman L. Bivariate variable selection for classification problem. Technical report. Berkeley: Department of Statistics, University of California-Berkeley, 2005. 22 p.

[11] Open Topography – ALOS World 3d – 30 m. – 2021. – URL: https://portal.opentopography.org/raster?opentopoID=OTALOS.112016.4326.2. Available at 01.01.2022.

[12] Serebryanny L.R., Chuklenkova I.N. Density of lakes as an age indicator of glacigenetic morphosculpture: an application of morphometric analysis in the northwestern areas of the Russian Plain. Geomorfologiya, 1973 no. 4, pp. 79–85. (In Russian) DOI: 10.15356/0435-4281-1973-4-.

# HOW TO FIND THE BEST ROUTE? A COMPARISON OF ROUTE SEARCHING SERVICES

**Ing. Ondrej Kolodziej** [1]

**prof. Ing. Jiří Horák, Dr.** [2]

**Ing. Pavel Kukuliač, Ph.D.** [3]

[1] VSB – Technical University of Ostrava, **Czech Republic**

[2] VSB – Technical University of Ostrava, **Czech Republic**

[3] VSB – Technical University of Ostrava, **Czech Republic**

## ABSTRACT

Route search engines are essential tools in online applications that address a wide range of user needs. However, the distribution of such applications and simple search engines presents a diverse landscape with different outputs for the same routing tasks. Although they rely on well-established algorithms, the use of different datasets often leads to different results. This paper aims to compare selected route search engines, investigate the differences in their outputs, and provide useful recommendations to users. Prague and Adelaide were chosen as test environments due to their different characteristics. The performance, route characteristics, and recommended routes of major search engines such as Bing Maps, Google Directions, TomTom, Open Source Routing Machine (OSRM), and OpenRouteService were evaluated and compared with Google Directions serving as the baseline for statistical analysis and comparison due to its extensive community use. This research highlights the key role of real-time traffic data in route discovery, particularly in large cities. Notably, the testing was conducted during peak and off-peak hours, revealing significant differences not only in response times for individual services, where Bing Maps and TomTom exhibited the highest disparities in response times, up to 76 %, but also when comparing individual routes during the different hours resulting in up to a 16% decrease in travel times. In contrast, OSRM and OpenRouteService were unable to accommodate real-time traffic data. In addition, statistical analysis revealed interesting patterns of significance correlated with specific locations within the tested cities. While TomTom continues to be recommended for online services due to its reliable data sources and consistent outputs, OSRM emerges as the preferred choice in response times, offering optimal results. By shedding light on these nuances, this paper increases transparency in the understanding of route finders and allows users to make informed decisions, determining whether or not the choice of route finders is important. It highlights how crucial it is to select a preferred service based on effectiveness and comprehensive support for different modes of transport.

**Keywords:** GIS, route, traffic, analysis, navigation

## INTRODUCTION

Nowadays, navigation systems are an important component of intelligent transportation systems. They have become a standard feature in vehicles as well as in mobile devices, such as smartphones and tablets. Many web-based mapping services also provide navigation tools. The availability and variability of services in recent years indicates a significant increase in usage. Despite being a standard pre-installed app on Android smartphones, Google Maps alone has reached 25.5 million downloads in the United States, followed by Waze with 13.4 million downloads in 2021 [1].

Path planning, a core component of various navigation applications, involves identification of the shortest path for any given O-D pair in a directed graph in which a non-negative weight is applied to the length or travel time for road segments. The Dijkstra algorithm [2] and label correcting (LC) algorithm [3] are two classical methods used to solve the shortest path problem [4], lately superseded by A* algorithm [5]. These standard algorithms are then modified with some unpublished improvements which then result in major differences throughout the calculated results for each service.

Conventional path-planning algorithms often ignore real-time traffic and road characteristics [4], however most web services have integrated them [6]. Estimated Time of Arrivals (ETAs) [7] consider factors such as speed limits and real-time traffic. City logistics planning needs data on urban traffic, especially travel times affected by recurrent congestion [8] particularly during rush hours. Traffic congestion increases inefficiency of a transport system and environmental load (air pollution, noise, etc.). Navigation systems like Google, Bing, and Waze offer real-time traffic data, but routes may quickly become outdated [9]. Open-source solutions like OSRM, ORS, and OSM offer route planning for different modes, ensuring result reproducibility. However, online OSRM services suffer from processing delays, prompting a preference for local server setups. Manual testing of Routing Services APIs is cumbersome and error-prone, driving the shift towards efficient and accurate automated testing resulting in the usage of an automatized code execution.

The aim of the paper is to shed light on the critical features of main search engines, offering a set of fundamental recommendations for deployment of navigation services with a focus on optimizing vehicle paths for drivers. Offering insights into the current state of the transportation network may be helpful to researchers, transport planners, and logistics experts.

## MATERIALS AND METHODS

A set of services was selected for comparison, including remote service providers such as TomTom, Google Directions and Bing Maps, as well as locally installed services such as OSRM and ORS, representing open-source options. To ensure meaningful evaluation, a virtual private server (VPS) was set up to host local services, strategically located in the Netherlands to minimise any possible distortions when addressing various distant web search engines. Two case studies focused on Prague and Adelaide, cities with different road network layouts and population densities.

Prague, the capital of the Czech Republic, has a rich history and cultural significance and a well-developed public transport system including a metro, trams, buses, and ferries. The city faces traffic problems, particularly in the historic centre, where more than 1.25 million vehicles contribute to recurring traffic congestion. Despite the

fluctuations, traffic volumes remain relatively stable, with a decrease in traffic in certain areas.

Adelaide, the capital of South Australia, is characterised by its Mediterranean climate and well-planned network layout in the central business district. The city's road network is well maintained, but traffic is a concern that has caused a continuous drop in commute speed over the last ten years. Despite its size, Adelaide experiences abnormal traffic congestion compared to other Australian cities and ranks as the second most congested city in the country.

The study focuses on testing response time and path quality of selected route search engines, assuming established 24/7 availability and capacity of leading global services. This process involved several steps to ensure accuracy and consistency across services and scenarios. First, 50 random points of interest (POIs) were selected to form pairs as an initial set of origin and destination points (2450 trips in each city) (fig. 1). OpenStreetMap (OSM) data was used to ensure that the selected points were located close to the road network to minimize connectivity issues.

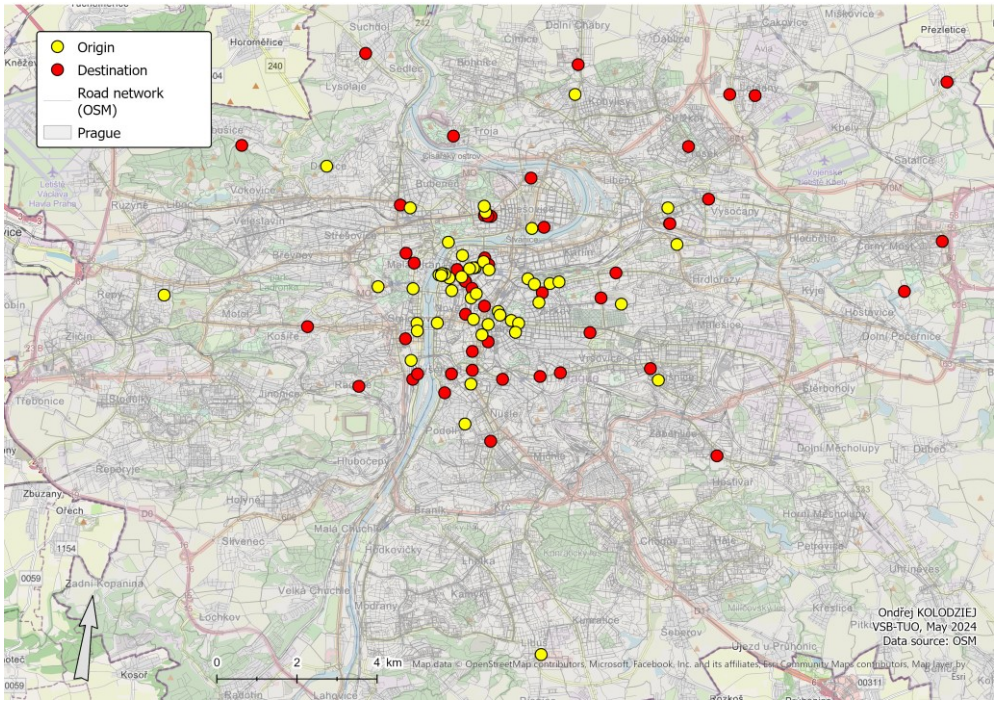


**Fig. 1.** Selected origins and destinations for trip searching in the centre of Prague

The prepared data was then utilized within each API to calculate a distance matrix. The Postman program was used for this task, equipped with a set of tools allowing the execution of scripts. Simple Python scripts were written to send instructions to all APIs simultaneously, mitigating any timing differences that could affect the comparison. After calculating the distance matrices, the outputs from each API, provided in JSON format, were converted into tables. The necessary calculations and comparisons were made for each service, including travel distance, travel time, and response time. Statistical analysis was performed in SPSS. The Google Directions result was used as a baseline due to its popularity among users.

Several indicators can be used for performance assessment, and when combined, they provide a comprehensive view of the case of study:

- Response time – average time interval between the initiation of a request and its completion (ms).
- Average path distance – average length of a travel path between sources and origins (m).
- Average path duration - average travel time between sources and origins (s).

Using this methodology, the study provided a systematic and robust evaluation of route finders and allowed for the identification of performance gaps and critical areas within the tested cities. Temporal variability was analysed during peak and off hours in which the time slots were chosen based on local traffic patterns and pricing structures [10-11]: for Prague in Peak at 8:00 and Off hours at 18:00; for Adelaide in Peak at 9:00 and Off hours at 19:00 (testing date 10.3.2024). The total number of cases is 19,600.

## RESULTS

Results indicate that performance depends on the observed city (fig. 2) which may be related to the size of the road network. As expected, dedicated services such as OSRM or ORS are fastest with only small differences between them (60-80 ms). The most significant differences were observed for TomTom, whose response time is nearly doubled in Adelaide compared to Prague. Similarly, Google had slower response times in Adelaide while Bing showed better performance. On average, Bing was approximately 18-33 ms (20-25%) slower than the dedicated services, followed by Google, which was 50-96 ms (60-75%) slower, and then TomTom, which was slower by 43-121 ms (50-150%). Despite these variations, all average response times remained below 0.2 seconds, ensuring efficient performance across both cities.

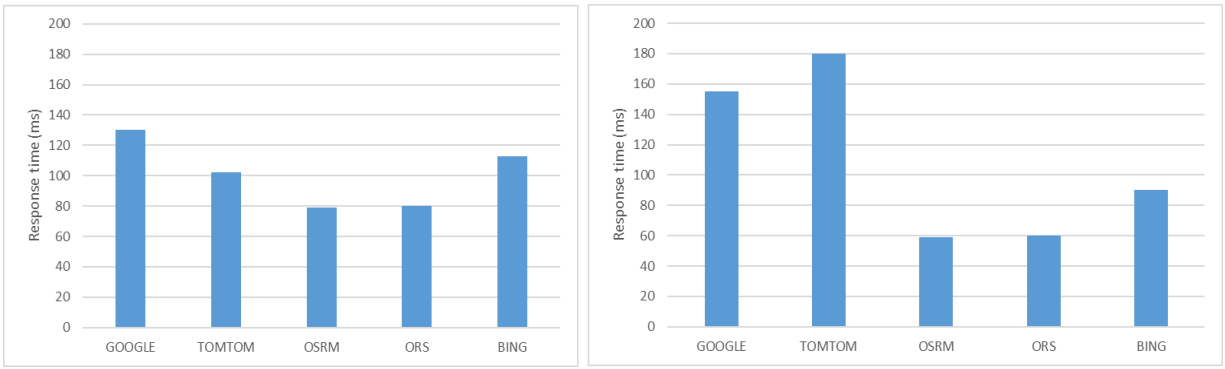


**Fig. 2.** Average response times of search engines for Prague (left) and Adelaide (right)

The average trip duration and distances show significant differences between the two cities (table 1 and 2). Prague's trips are much shorter than Adelaide's (approx. 7 km and 20 km, resp.) which is reflected also by shorter duration (900 s and 1600 s, resp.). Services for Adelaide reflect about 3 times longer distances due to the size of the city compared to Prague (3260 km² vs 496 km²). More interesting are differences in the behaviour of search engines. Average durations of trips in Prague during the peak hours are almost the same and there are no significant differences between services. We can see significant disparities in Adelaide: TomTom offers the quickest journeys, followed

by Bing and Google with a very little difference. For dedicated services, there is a larger step having roughly 100 seconds longer duration.

For off-peak time in Prague, average trip duration dropped by 12% for all non-dedicated services. The order of performance for services in Adelaide is the same as for peak time (TomTom, Bing, Google, ORS, OSRM). No differences for OSRM and OSM between different time slots exist due to missing traffic data. It is also worth noting the probable existing differences in the speed applied by various services. It seems OSRM and OSM use quite a slow average speed for duration calculation compared to Google and other services.

The comparison of average distances shows a slightly different pattern. Open-source services, OSRM and ORS, provide the shortest distances (except of Adelaide off-time). For other services, Google, TomTom, and Bing follow with the specific order varying by location and time. Google is usually the best one (the shortest distance for all combinations except for Prague off time). TomTom usually provides the second shortest distances among non-dedicated services (except for Adelaide peak time). But if you compare individual paths, no clear preference can be seen (see fig. 3b with approximately equal distribution on both sides of the equity line).

While duration shortening between peak and off-peak times are practically the same for all three non-dedicated services (all -12 % for Prague and -16 % for Adelaide), large variability can be seen for distances. Great distance shortening can be seen in Prague for TomTom and Bing, but in Adelaide it is Google which provides larger distance shortening.

**Table 1 –** Average trip duration

| | Peak time | | Peak-off time | | Difference | |
|---|---|---|---|---|---|---|
| | Prague | Adelaide | Prague | Adelaide | Prague | Adelaide |
| Google | 907 | 1 621 | 797 | 1 370 | - 12 % | -15,5 % |
| TomTom | 906 | 1 590 | 797 | 1 325 | - 12 % | -16 % |
| OSRM | 907 | 1 705 | 907 | 1 705 | 0 % | 0 % |
| ORS | 906 | 1 700 | 906 | 1 700 | 0 % | 0 % |
| BING | 906 | 1 606 | 798 | 1 355 | - 12 % | -16 % |

**Table 2 –** Average trip distance

| | Peak time | | Peak-off time | | Difference | |
|---|---|---|---|---|---|---|
| | Prague | Adelaide | Prague | Adelaide | Prague | Adelaide |
| Google | 7 061 | 21 176 | 6 640 | 19 047 | - 6 % | - 10 % |
| TomTom | 7 064 | 21 303 | 6 225 | 19 811 | - 12 % | - 7 % |
| OSRM | 6 675 | 20 527 | 6 675 | 20 527 | 0 % | 0 % |
| ORS | 6 674 | 20 525 | 6 674 | 20 525 | 0 % | 0 % |
| BING | 7 069 | 21 198 | 6 222 | 20 188 | - 12 % | - 5 % |

Further, a comparison of services and Euclidean distances were calculated, with the primary goal being to identify any outliers which may significantly influence results. No problematic outliers affecting the results were found.

Differences between services can be seen on graphs for selected interval of distances (fig. 3). TomTom and Google show almost even distribution along the equilibrium line indicating there are no significant differences of path distances for this interval between the given search engines. Contrarily, OSRM provides significantly shorter distances than Google (for this distance interval). We assume the OSM network used by OSRM is more generalized which results in shorter trips. Another factor could be the border effect due to the data cut off at the boundaries of both cities, leading to incomplete and potentially skewed results at the city's borders.

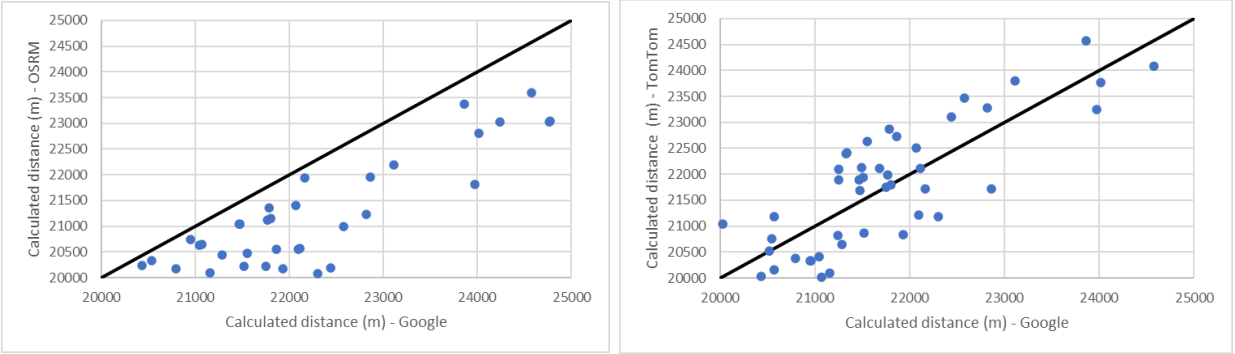


**Fig. 3.** Paths' distances of OSRM (left) and TomTom (right) against Google (Prague, peak time)

Significant differences (p=0.05) between TomTom and Google (fig. 6) were found only in 14 % of cases in the Prague center. Such places could be the differentiators in the analysis up to the base differences in distances and times in both cities. We find that significant differences appear to be positively associated with road network, notably the main roads, despite no obvious preference for any of the services in the spatial distribution of the significant points in Prague and Adelaide.

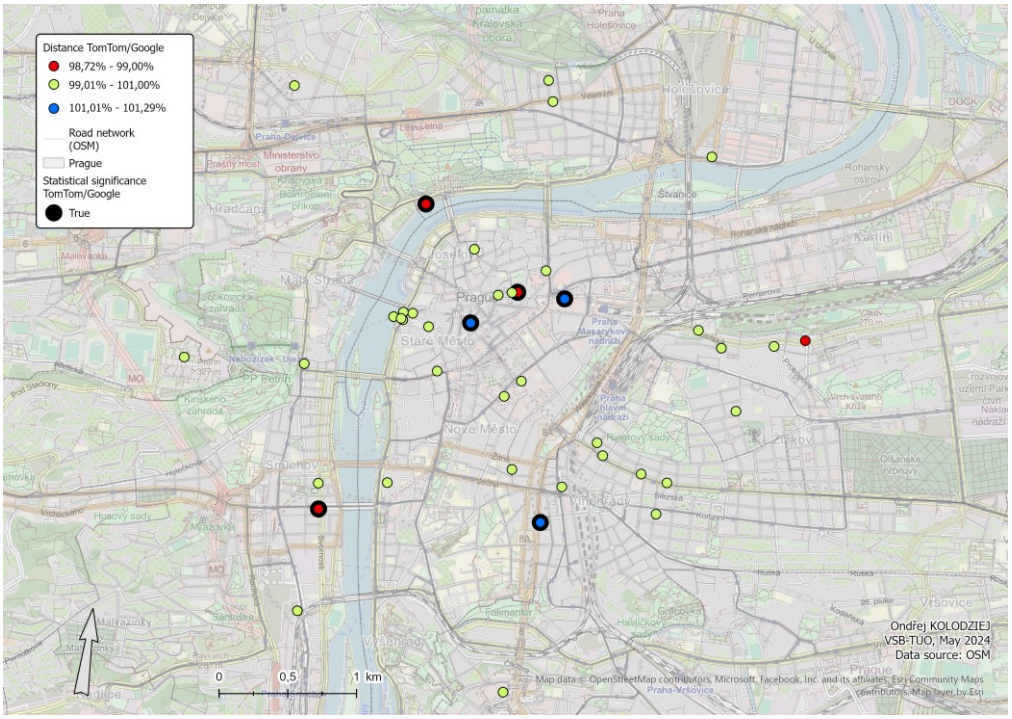


**Fig. 4.** Difference between TomTom and Google paths' distances in Prague's centre

## DISCUSSION

The results revealed that OSRM and ORS achieved the best results in terms of response time. However, it is important to consider the network's size because a smaller network would likely result in faster calculation times.

Another factor is that it is impossible to ensure that the actual user load occurring at any one time during the computation is reflected, even with the use of distant and guaranteed VPS for OSRM and ORS. This could probably be simulated independently if long-term measurements were made throughout the day.

Neis [12] compared several OSM routing engine APIs and the Google Maps API. He found that OSRM provided the fastest response times and also the shortest trips among the tested routing engines. These results may be outdated (2011) but later studies also confirm good results, namely processing speed, for OSRM [13]. However, a good knowledge of the software structure is needed to make use of all the functions.

Another aspect that should be considered when comparing search engines is the real-time traffic data availability. While some commercial solutions, such as TomTom and Google Directions, do not offer modification settings for traffic modes other than car navigation, Huber [14], for example, describes the possibility of modifying OSRM by including other traffic modes if the necessary data is available. The analysis would benefit from optional turn on/off real-time traffic statistics.

Concerning the spatial distribution of significant differences between services, some of them seem to be located by, and may be related to, important traffic veins in the city centre such as Husitska Street in Prague and R1 in Adelaide. Probably each of these services approaches these locations with a different priority during the calculation process, i.e., some choose other, alternative routes, while for some it is the conventional,

congestion laden route. Long-term monitoring might help us understand the causes of these differences.

## CONCLUSION

This study compared routing in Prague and Adelaide and analysed the temporal variability of traffic. Locally installed ORS and OSRM showed the fastest response times, while TomTom lagged behind with an average time of 22 milliseconds. Adelaide generally had higher response times than Prague, with greater variability. Regional factors such as server location and network infrastructure likely influenced these differences. It was also found that the decrease in travel time and travel distance was up to 12 % in Prague and 16 % in Adelaide. This suggests the potential for significant improvements in both cities in terms of travel efficiency and distance optimisation.

To summarize, the following recommendations can be delivered:

- Users modelling routes under different conditions (e.g., changes of road network or different transport modes) should prefer OSRM and ORS.
- Users integrating current car routing services into their application should implement Google, TomTom or Bing services according to their license and technical implementation preferences. The difference in provided results in terms of response time, path distances and path duration are dependent on local conditions, and generally, the average values do not indicate preferred solutions.

Future research should include updated comparisons with broader metrics and features with more time periods to be tested and calculated, allowing for a comprehensive understanding of routing service performance across time periods. The integration of different modes and the creation of a user guide for service recommendations would be beneficial.

## ACKNOWLEDGEMENTS

The authors gratefully acknowledge the support of VSB – Technical University of Ostrava in a grant SP2024/076 - Accessibility, transport conditions and mobility in the urban environment. We also acknowledge the use of data from the presented route providers and the ability to use API in our research.

## REFERENCES

[1] Ceci L., Leading mapping apps in the United States in 2021, by downloads, Statista, 2022; Retrieved from: https://www.statista.com/statistics/865413/most-popular-us-mapping-apps-ranked-by-audience/

[2] Dijkstra E. W., A note on two problems in connexion with graphs, Numer Math (Heidelb), Germany, 1959, pp. 269-271; DOI: https://doi.org/10.1007/BF01386390.

[3] Bellman R., On a routing problem, Q Appl Math, USA, 1958, pp. 87-90; DOI: 10.1090/qam/102435.

[4] Li Q., Zeng Z., Zhang T., Li J., Wu Z., Path-finding through flexible hierarchical road networks: An experiential approach using taxi trajectory data, Int. J. Appl. Earth Obs. Geoinf., 2011, pp. 110-119; DOI: 10.1016/j.jag.2010.07.003.

[5] Hart P., Nilsson N., Raphael B., A Formal Basis for the Heuristic Determination of Minimum Cost Paths, IEEE Transactions on Systems Science and Cybernetics, USA, 1968, pp. 100-107; DOI: 10.1109/TSSC.1968.300136.

[6] Chen Y., Gong J., Wu C., Design and Application of Optimal Path Service System on Multi-level Road Network, Computational Science and Its Applications – ICCSA 2007, Germany, 2007, pp. 1152-1164; DOI: 10.1007/978-3-540-74484-9_101.

[7] Cameron M., Brown A., Intelligent transportation system Mayday becomes a reality, Proceedings of the IEEE 1995 National Aerospace and Electronics Conference. NAECON 1995, USA, 1995, pp. 340-347; DOI: 10.1109/NAECON.1995.521962.

[8] Geotab, Traffic Congestion: Causes and Solutions, Retrieved from: https://www.geotab.com/blog/traffic-congestion/.

[9] Aldwyish A., Xie H., Tanin E., Karunasekera S., Ramamohanarao K., Using a Traffic Simulator for Navigation Service, Proceedings of the 25th ACM SIGSPATIAL Int. Conf. on Adv. in GIS, USA, 2017, pp. 1-4; DOI: 10.1145/3139958.3139998.

[10] Somenahalli S., Sleep C., Primerano F., Wadduwage R., Mayer C., Public Transport Usage in Adelaide, Procedia Soc Behav Sci, Australia, 2013, pp. 855-864; DOI: 10.1016/j.sbspro.2013.11.180.

[11] Truong L. T., Somenahalli S., Exploring mobility of older people: a case study of Adelaide, Australia, 2011.

[12] Neis P., Comparison of (OSM) routing-engines, Retrieved from: http://neis-one.org/2011/07/comparison-reloaded/.

[13] Dornhofer M., Bischof W., Krainz E., Comparison of Open Source routing services with OpenStreetMap Data for blind pedestrians, Presented at FOSS4G-Europe 2014, Germany, 2014; Retrieved from: https://europe.foss4g.org/2014/sites/default/files/04-Dornhofer_0.pdf.

[14] Huber S., Rust C., Calculate Travel Time and Distance with Openstreetmap Data Using the Open Source Routing Machine (OSRM), The Stata Journal: Promoting Communications on Statistics and Stata, USA, 2016, pp. 416-423; DOI: 10.1177/1536867X1601600209.

# INTEGRATING GEODETIC UNDERGROUND UTILITY DATASETS WITH BIM: IFC 4.3 FOR IMPROVED STRUCTURAL DESIGN IN POLAND

**Mikołaj Kowalski Eng.**[1]

**Łukasz Ortyl PhD** [2]

[1] AGH University of Krakow, Mayor of Engineering and Industrial Surveying, **Poland**
[2] AGH University of Krakow, Department of Engineering Surveying and Civil Engineering, **Poland**

## ABSTRACT

Numerous studies have examined the potential integration of Building Information Modeling (BIM) with Geographic Information Systems (GIS), typically focusing on simplifying complex BIM data for presentation within a GIS environment. However, there is a unique circumstance with extensive geodetic databases that remain untapped in construction processes in Poland. The emergence of the more applicable IFC format version 4.3, particularly relevant to surveying, presents an opportunity. The article proposes leveraging geodetic datasets, specifically underground utilities, to enhance BIM-based structural design. A Python-based converter was developed to translate data between the prevalent GML format for geodetic data collection and the IFC schema. The challenges include GML's surveyor-centric design and varying file structures, requiring the conversion tool to be adaptable and robust. Additionally, transforming 2D linear data with height and diameter attributes into 3D spatial representations poses geometry challenges. Presented program's version can convert GML file to pandas.DataFrame, but some errors are seen in IFC 3D representation. Despite these obstacles, the developed converting tool paves the way for integrating GIS and BIM for underground utilities in Poland, and holds promise for broader application in the future, such as enabling the use of 3D models of underground utilities for infrastructure projects.

**Keywords:** BIM and GIS, IFC, GML, Data conversion, Underground utilities

## INTRODUCTION

Digitisation of Polish geodetic data has been carried out through compliance with the INSPIRE. To avoid the mistakes made in the early stages of the directive's implementation, significant changes have been made to the digitization process over the last decade. After the introduction of the new law in 2021, each surveyor's job needs to be added to land administration databases, which are divided into BDOT (Topographic Objects Database), EGiB (Parcels and Buildings Register), and GESUT (Geodetic Register of Land Development Systems) [1]. Moreover, the input file for the mentioned databases must have a universal format, Geographical Markup Language (GML) [2], [3]. That was caused by the increasing influence of informatisation and understanding the possibilities of using a Geographical Information System (GIS). Worldwide trends have demonstrated that more data can be extracted and analyzed effectively. In this paper, analysis of underground utilities, which are gathered in the GESUT database [4], was a basic goal. The underground environment from the GESUT is everything connected to waterworks, sewerage, electricity grid, telecommu-nications, and gas networks.



https://doi.org/10.5593/sgem2024/2.1/s08.16

It is evident that the building industry is undergoing changes, with employees moving from paper documentation to digital one. Each complex and expensive project should be designed in BIM technology, which is dominated by high-end software. The foremost reason why we develop digitization is the density increasing in the urban area around the world [5], [6]. No building can exist without utilities. This is why the universal schema of building modeling is increasingly used for optimization of smart cities. The construction evolution changed to an infrastructure revolution when Industry Foundation Classes (IFC) 4.3 came [7]. Fundamentally, IFC is an open standard that focuses on BIM interoperability. The new version not only opens up new opportunities for the Architecture, Engineering, and Construction (AEC) and Facility Management (FM) sectors as in the past, but also for an infrastructure industry connected with roads, bridges, railways, and more [8].
Many papers arose on the BIM and GIS theoretical and practical integration. We can divide the topics into conversion GIS to BIM [9], [10], [11], BIM to GIS [5], [12], and integration of both environments inside external systems [13]. Researchers mostly focused on the acquisition of more detailed data from BIM and represented it in less extensive GIS. They note the advantages of BIM, such as information representation and management, while pointing out the advantage of GIS, which is the ease of performing geospatial analysis. Researchers analyzed possibilities for introducing existing underground spatial data to BIM by IFC. On the other hand, if there are papers about the conversion of GIS into BIM, researchers usually decide to use CityGML as an intermediate format before the IFC creation. An exception to that rule was presented by Maier's prototype converter [9].
The whole world is turning to 3D visualization. The megacities need to have their models created, due to future infrastructure projects, and to avoid possible accidents in facilities, which can be costly for public funds and health [5]. Moreover, 3D visualization can enhance the execution of below-surface facilities in land administration [14]. Authors want to follow these trends, so the decision has been made to create a conversion tool that can create a BIM model from available data gathered by the government.

## MATERIALS AND METHODS

The converter uses Python because of diverse libraries and a widespread understanding of the language globally. After the experiment, authors are planning to prepare a library to decrease the programming toughness presented topic.

### Processing a GML file

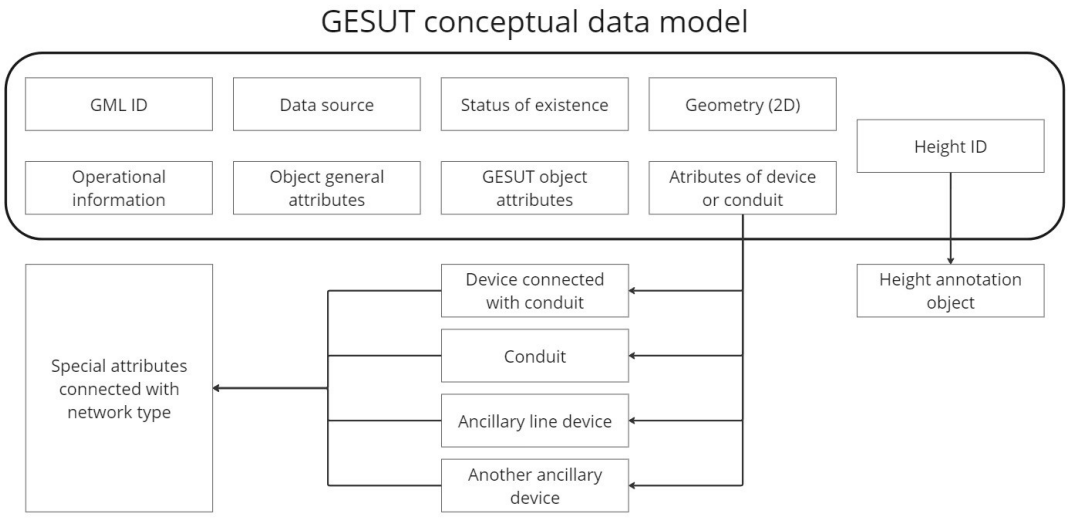


**Figure 1.** GESUT conceptual data model

A goal of this part is to import the data to the program as “pandas.DataFrame”. The GESUT GML file structure is precisely described in Polish law [4]. Moreover, it is compatible with GML 3.2.1 schema [2]. Each file in that format consists of FeatureCollection, where many FetureMembers might be found. The dependency is comparable to the analogy between folders and files on computers. For a better understanding of what is covered inside each FeatureMember of GESUT, a general object representation schema was prepared. (Figure ***1***). To obtain information from the GESUT database, an “xml2dict” library is used, which can read a GML file as a dictionary. From that variable type, there is a straight way to achieve a data frame. The next problem was an extraction of spatial information from the ”ges:geometry” column because of an extensive hierarchy in GML files objects. This issue was a reason why some cells were imported as a dictionary. An algorithm needs to be prepared that can differentiate between geometry types and access information about horizontal coordinates. The geometry schema is presented in Figure 2.

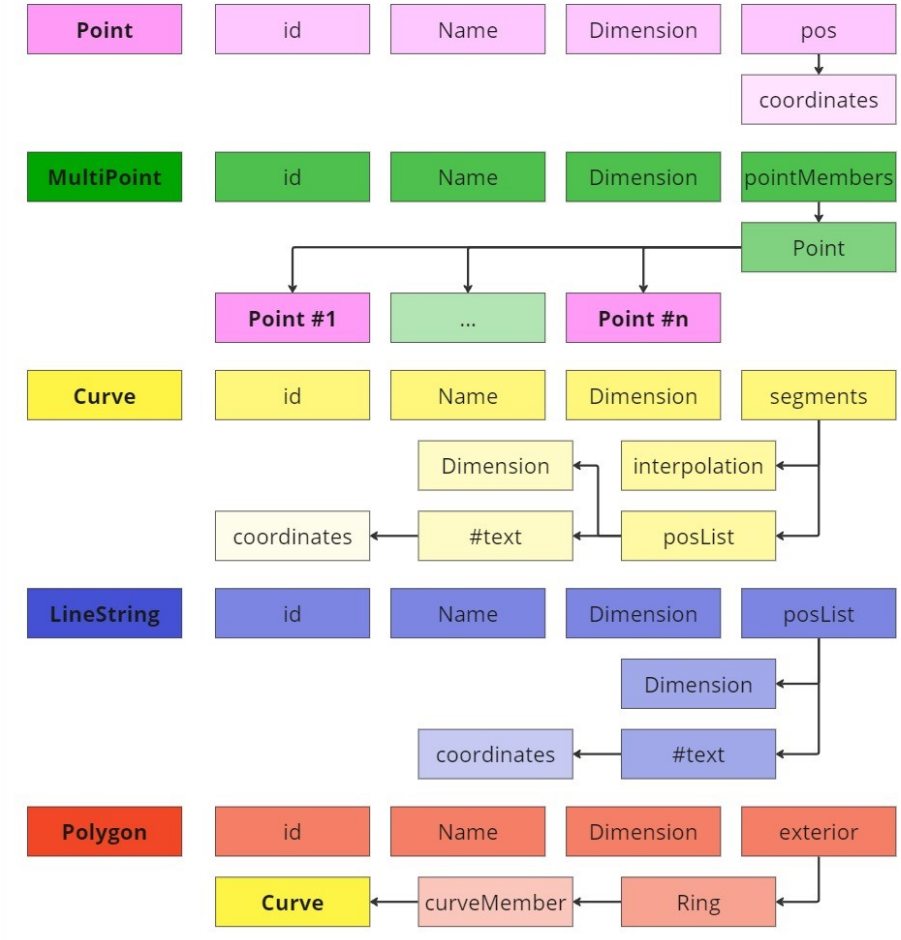


**Figure 2.** GML 3.2.1 geometry types schema

To achieve more flexibility, 2 classes are designed. A RawImporter is created, which has already been described. Then, a ComplexImporter is prepared, which specializes better in the GESUT database, because it can analyze height annotations objects and credit themselves as utility attributes. Connection is carried out by GML ID value. It is an example of GML surveyor-centric design, because height is only an annotation of 2D data in maps. The authors did not anticipate using this in 3D.


https://doi.org/10.5593/sgem2024/2.1/s08.16

**Structural design in IFC**

The IFC file is divided into a header and a body. "IfcOpenShell" library has an in-build function that automatically creates a header. The header structure is composed of 3 elements: FileName, FileDescription, and FileSchema. But from authors' point of view, a schema parameter can only be defined as "4.3". The body part must contain only one IfcProject object, which gathers crucial information about units and representation context. IfcProject has a similar role to FeatureCollection. Furthermore, it is connected with IfcSite, which is a base for each element. IfcSite is divided on IfcElementAssemblys. It is a general object that is used for sorting and gathering. Conduit types are defined and linked to assembled segments. The relations and more detailed schema are presented in Figure 3 [15], [16]. Schema without conduits on the bottom shows what can be done using ProjectDefinition class from ifc part of the library.

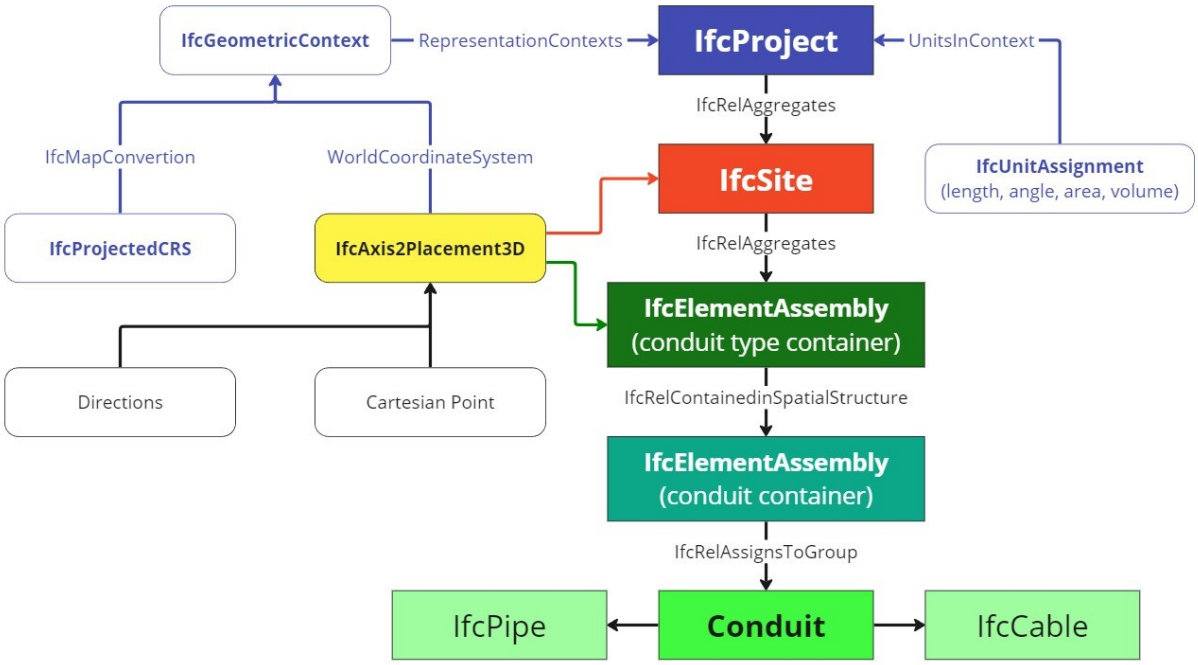


**Figure 3.** IFC structure schema

Because the IFC file base structure is prepared, it is possible to move to utilities creation. IFC anticipates the use of 2 conduits: IfcPipe and IfcCable. Inside a distribution system, cables are created for electricity, telecommunication, optical fiber systems, etc. On the other hand, pipes focus on fluid and gas transmission. Examples include: sewages, waterworks, and gas pipelines. This may seem obvious, but various conduits have different parameters in Polish databases. Even if they have the same description names, they have different values. In addition, not all of them need to be finished, thus leaving many crucial parameters empty. A group of IfcProperty-SingleValue was prepared, which was gathered in IfcPropertySet. It was

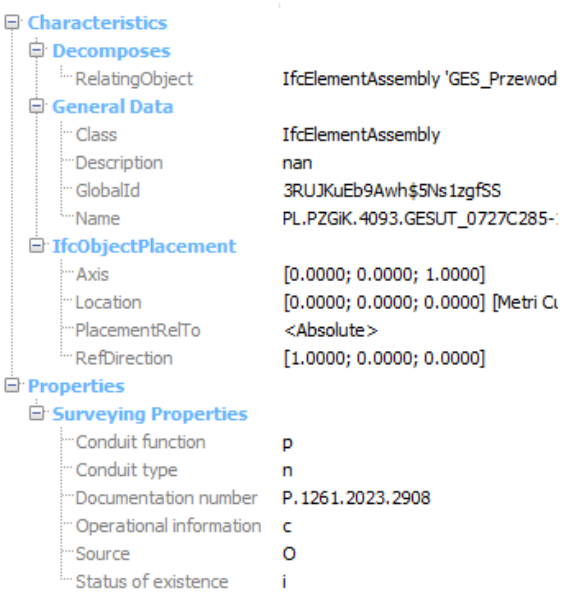


**Figure 4.** Conduit container properties with additional property sets

named surveying properties (Figure 4). The sewage and telecommunications systems have an additional set, accordingly sewerage type and bundle. Finally, future users can rewrite every important parameter from the data frame. Body representation was based on local placements, where a conduit's perimeter is defined at radius or horizontal and vertical measures, so there is a possibility to have elliptic and circular shapes. Then, those 2D shapes are extruded for segment length in direction calculated from given points. If the radius was not known, the program automatically used a value equal to 5 cm. From a geometrical point of view, the biggest problem was with elbows and other conduit connectors representation. It was managed by creating complex and simple type class. SimplePipe and SimpleCable are designed for conduits that contain only 2 points, so there is no need to create junctions. For this case, ComplexPipe and ComplexCable exist. Complex bends, junctions, etc. were excluded from this project. The graphical view for projected body representation is shown in Figure 5 on an example of IfcPipeSegment, where bright orange represents in-build functions and gray color shows "IfcOpenShell" classes. The relations between objects are presented in Figure 3. Additionally, IfcPropertySet was linked by IfcRelDefinesByProperties.

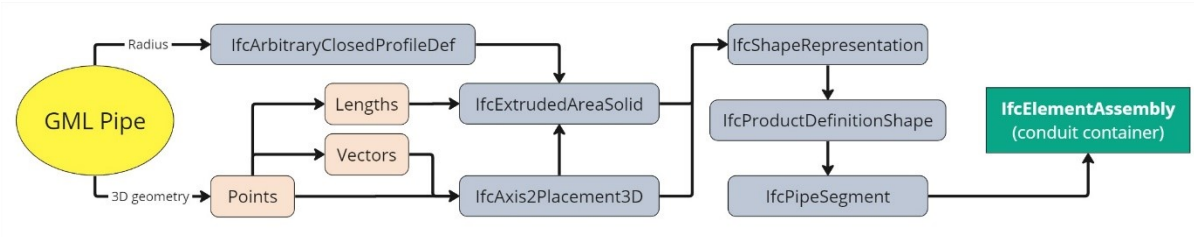


**Figure 5.** Geometry representation creation (IfcPipeSegment)

## Dataset

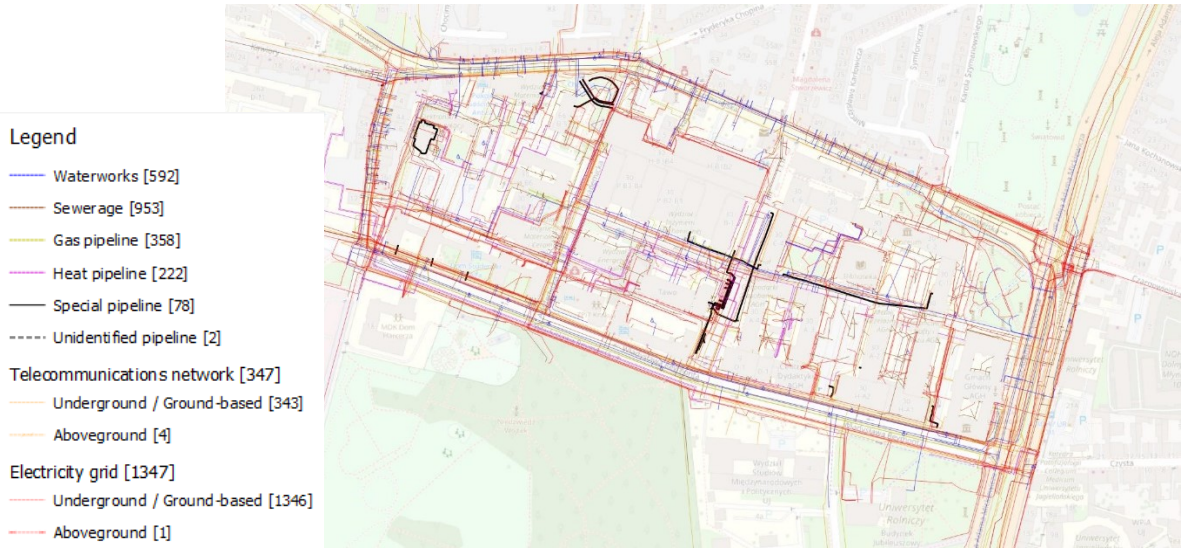


**Figure 6.** Sketch of pipelines in dataset

Map presents a dataset visualization, which is a part of GESUT database at AGH University of Krakow Campus and some surroundings. Dataset combined 8677 objects, where there were 112 polygons, 3 multipoints, 4127 curves, 18 linestrings, and 4417 points. We checked the file using a validator, which is available as QGIS plugin, and a creator of the plugin is Polish Head Office of Land Surveying and Cartography. Report showed us 1 error


https://doi.org/10.5593/sgem2024/2.1/s08.16

caused by empty source value. For our case, we can have avoided it. Some people might ask, why are there so many features? Because GML files include height as separate objects. Moreover, we decided to focus only on conduits and cables, so we finally had 3899 by using the ComplexImporter function, which combined height with utilities.

## RESULTS

The GESUT dataset was processed with conduits, where each of them was properly imported into "pandas.DataFrame". Then, it was converted to an IFC file, with a size of 41 MB. It is 4 times bigger than the GML file. After comparing the structure to Autodesk Revit's exported IFC file, it turns out the work authors' file is smaller. It was proved that it is possible to create a 3D model from Polish surveyor's databases. Information about height had only 1778 objects. Not every pipeline had a radius or horizontal and vertical measures. But for non-spatial properties, the same problem of data shortage was noticed. The bigger issue is geometric representation. In general view, pipeline networks look like those presented in Figure 6, but each conduit is assessed individually. 3 error types are found (Figure 7): clashes (1), topological mistakes (2), and depth differences (3).

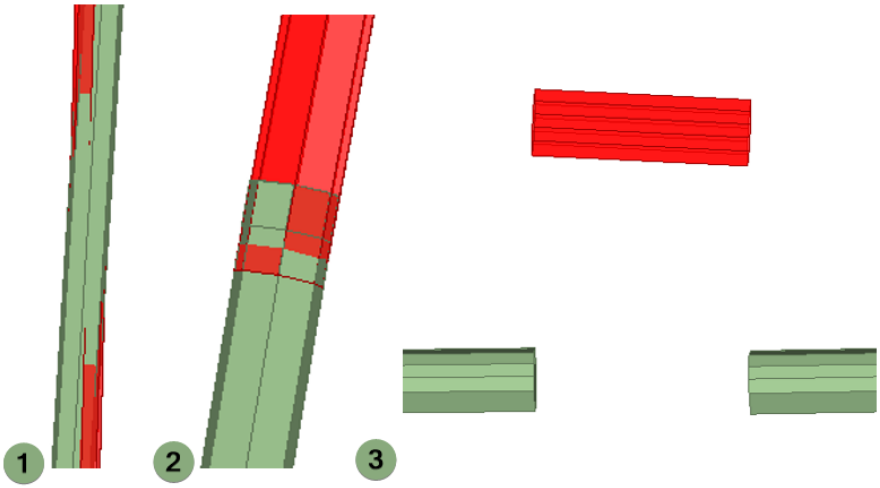


**Figure 7.** Error examples (1. clashes, 2. topological mistakes, 3. depth differences)

## DISCUSSION

Firstly, the converter can easily transform a GML file into a Python-based data frame. Even if it is a large amount of objects, as it was presented in the experiment. Secondly, the program can transfer attributes into new IFC objects. The next step of attribute import will be to recode abbreviations into names, accordant with Polish law (Figure 4. Conduit container properties with additional property sets – Surveying properties). The most interesting things are connected to geometrical representation. Clashes and depth differences likely have similar causes, and there is a shortage of pipe height values. Topological error is not straightforward. For instance, geometrical mistakes during conduit creation can cause this, but it is also known that sometimes the GML validator accepts files with misconceptions. The proposed solution is to add topological rules during pipe and cable creation. Figure 7 demonstrates the expectations of geometrical dependencies presented by Krijnen et al. [16] were not met, and using this model for complex analysis is not viable. The presumed solution can be preparing a more flexible program that can avoid emptiness in data. Though, we can reach a close future level of details, which our converter will be used by excavators on site to prevent

accidents. Furthermore, it is necessary to upgrade surveyors' mindset from 2D to 3D. The simplicity of the converter shows that there is no way to transform data for future smart city needs without additional measurements using indirect techniques like Ground Penetration Radar (GPR) [6], [17].

## CONCLUSION

To summarize, there exists a field and precise directions to develop a demonstrated tool. It will be hard to proceed without more detailed data. Furthermore, authors find future 2D to 3D maps transformation challenging. The difficulty lies in complex geometry shapes and a lack of ready solutions. During the experiment, numerous problems with IFC viewers were met. Some of them can display the data, but without creating schema or vice versa. Nevertheless, the authors maintain a positive attitude due to the new ISO standard coming into effect in April 2024. Consequently, there is a chance that companies need more time to adapt themselves. Even in one case, IfcOpenShell was not ready for the 4.3 version, because it did not accept “FiberTube” or “FiberSegment” as cable type, which limited the diversity of the telecommunication network. There is also an issue within the surveying sector. Presented workflow can transform geometrical features and attributes from existing surveying databases, but it is not enough for future needs of detailed 3D models. It should be emphasized that the introduction of IFC 4.3 in infrastructure will play a pivotal role, because it is impossible to think about road or railway design without analyzing the route and localization of underground utilities. Ready-to-use converters will decrease costs and speed up infrastructure project design.

## REFERENCES

[1] “Ustawa z dnia 17 maja 1989 r. Prawo geodezyjne i kartograficzne,” 2023.

[2] C. Portele, “OpenGIS® Geography Markup Language (GML) Encoding Standard,” 2007. [Online]. Available: http://www.opengeospatial.org/legal/.

[3] Polish Minister of Development, “Rozporządzenie w sprawie standardów technicznych wykonywania geodezyjnych pomiarów sytuacyjnych i wysokościowych oraz opracowywania i przekazywania wyników tych pomiarów do państwowego zasobu geodezyjnego i kartograficznego,” 2020.

[4] Polish Minister for Development Labour and Technology, “Rozporządzenie w sprawie geodezyjnej ewidencji sieci uzbrojenia terenu,” Warsaw, 2021. Accessed: Mar. 11, 2024. [Online]. Available: https://isap.sejm.gov.pl/isap.nsf/download.xsp/WDU20210001374/O/D20211374.pdf

[5] M. Wang, Y. Deng, J. Won, and J. C. P. Cheng, “An integrated underground utility management and decision support based on BIM and GIS,” *Autom Constr*, vol. 107, Nov. 2019, doi: 10.1016/j.autcon.2019.102931.

[6] J. Yan, S. W. Jaw, R. Van Son, K. H. Soon, and G. Schrotter, “Three-dimensional data modeling for underground utility network mapping,” in *International Archives of the Photogrammetry, Remote Sensing and Spatial Information Sciences - ISPRS Archives*, International Society for Photogrammetry and Remote Sensing, Sep. 2018, pp. 87–92. doi: 10.5194/isprs-archives-XLII-4-711-2018.

[7] buildingSMART, “IFC 4.3 Standards Documentation.” Accessed: May 05, 2024. [Online]. Available: https://ifc43-docs.standards.buildingsmart.org/

[8] M. Pszczolka, “The Key Changes in IFC Schema Shaping OpenBIM for Infrastructure.” Accessed: May 05, 2024. [Online]. Available:



https://doi.org/10.5593/sgem2024/2.1/s08.16

https://bimcorner.com/key-changes-in-ifc-schema-shaping-openbim-for-infrastructure/
[9] J. Maier, "Prototype of an open GIS-to-BIM Converter," 2023.
[10] O. Moryc, "GESUT 3D in the area of BIM, automation and optimization in the design of utilities networks," Cracow, 2023.
[11] N. Salheb, K. Arroyo Ohori, and J. Stoter, "AUTOMATIC CONVERSION of CITYGML to IFC," in *International Archives of the Photogrammetry, Remote Sensing and Spatial Information Sciences - ISPRS Archives*, International Society for Photogrammetry and Remote Sensing, Sep. 2020, pp. 127–134. doi: 10.5194/isprs-archives-XLIV-4-W1-2020-127-2020.
[12] H. Tauscher, "Towards a generic mapping for ifc-citygml data integration," in *International Archives of the Photogrammetry, Remote Sensing and Spatial Information Sciences - ISPRS Archives*, International Society for Photogrammetry and Remote Sensing, 2020, pp. 151–158. doi: 10.5194/isprs-archives-XLIV-4-W1-2020-151-2020.
[13] A. Sharafat, M. S. Khan, K. Latif, W. A. Tanoli, W. Park, and J. Seo, "Bim-gis-based integrated framework for underground utility management system for earthwork operations," *Applied Sciences (Switzerland)*, vol. 11, no. 12, Jun. 2021, doi: 10.3390/app11125721.
[14] R. Ramlakhan, E. Kalogianni, P. van Oosterom, and B. Atazadeh, "Modelling the legal spaces of 3D underground objects in 3D land administration systems," *Land use policy*, vol. 127, Apr. 2023, doi: 10.1016/j.landusepol.2023.106537.
[15] M. Pszczolka, "Relations I used to create IFC 4.3 for infrastructure." Accessed: May 05, 2024. [Online]. Available: https://bimcorner.com/ifcrelationship-in-infrastructure-ifc-4-3/
[16] T. Krijnen, F. Noardo, K. A. Ohori, H. Ledoux, and J. Stoter, "Validation and Inference of Geometrical Relationships in IFC," Eduardo Toledo Santos and Sergio Scheer, Aug. 2020, pp. 98–111. doi: 10.46421/2706-6568.37.2020.paper008.
[17] R. Becker, S. Dörr, Y. Fahlenbock, L. Kahlert, H. Vassilev, and J. Blankenbach, "Detection and Digital Modeling of Subsurface Pipe Structures from Ground Penetration Radargrams," 2023. [Online]. Available: https://www.ogc.org/standard/citygml/

# LAND USE-COVER CHANGE TRAJECTORY AND IMPLICATION ON THE AGRICULTURAL AREAS OF SÃO PAULO CITY: A GEOINFORMATICS APPROACH

**Dr. Chukwudi Nwaogu[1,2]*, Mr. Babatunde Alabi[3], Mr. Nasir A. Umar[2], Dr. Bridget E. Diagi[2], Dr. Victor A. Agidi[2], Mrs. Chinwe G. Onwuagba[2], Mrs. Iheoma E. Mbuka-Nwosu[2], Mrs. Chidinma A. Acholonu[2], Mrs. Chinonye V. Ekweogu[2], Mr. Chukwuemeka O. Ulor[2], Engr. Chidi P. Ugochukwu[2], Dr. Joseph I. Nwachukwu[2], Dr. Susan I. Ajiere[4], Dr. Simon I. Okweche[5], Mr. Pius Agaji Oko[5], Prof. Mauricio R. Cherubin[1,6]**

[1]Department of Soil Science "Luiz de Queiroz", College of Agriculture, University of São Paulo, **Brazil**
[2]Department of Environmental Management, Federal University of Technology, **Nigeria**
[3]Department of Surveying & Geoinformatics, Federal University of Technology, **Nigeria**
[4]Dep. of Geography and Environmental Management, University of Port-Harcourt, **Nigeria**
[5]Department of Forestry and Wildlife Resources Management, University of Calabar, **Nigeria**
[6]Center for Carbon Research in Tropical Agriculture (CCARBON), University of São Paulo, Piracicaba, SP 13418-900, **Brazil**

## ABSTRACT

Agricultural productivity and environmental changes can be greatly affected by agricultural and other land use. Mapping of vegetation and land cover is a fundamental way of managing the natural resources on the earth surface. To determine or study the crop productivities of any geographical location, agricultural land use is one of the crucial clues for reliable information. We aimed to investigate the effects of urbanization on agricultural lands in São Paulo city. A 30-year multi-temporal satellite imagery dataset from four distinct years were mapped: 1992 (Landsat TM), 2002 (Landsat ETM+), 2012 (Landsat ETM+), and 2022 (Sentinel) were collected and analyzed using geospatial tools. Identified land use were waterbody, settlement, agricultural land, wetland, and forest. Change detection analysis was performed using Erdas imagine software and future prediction was achieved by applying Idrisi selva 15 software. The result indicated between 1992 and 2022 settlement and wetland increased in areas while agricultural land, forest and waterbody decreased. These observed changes in the spatial pattern of LULC could be attributed to the encroachment and converted to other uses such as settlement and urban agriculture. The overall changes depicted in the evolution matrix and map demonstrated that, because of speculation practices, urbanization has primarily affected agricultural land use. Application of geospatial technologies (remote sensing and GIS) has proved effective in monitoring LULC changes and providing vital information for policy making in São Paulo City's food (in)security and urban sustainable development.

**Keywords:** Urbanization, land use change, agricultural systems, GIS, São Paulo-Brazil.

## INTRODUCTION

The concepts of land use (LU) and land cover (LC) are common terminologies used to define the robust interactions prevailing between humans and their environment. Land use denotes the anthropogenic change in the land cover, while land cover signifies the actual features of the Earth's landscapes. Rapid urbanization due to population growth has prompted various anthropogenic activities (e.g., deforestation, mining, environmental degradation, etc) and consequently substantial land use changes in most urban centres and cities. Studies have revealed that over the past 6 decades, approximately 32% of global LULC has changed [1].

Changes in LULC have caused critical attention globally as they create significant impacts in the global socioeconomic and environmental systems [2,3]. LULC changes are induced by two common processes namely, conversion and transition. Urbanization is one of the major causes of land use transition [4], while agriculture is a key driver of land use conversion [2,5]. These have various degrees of effects of planetary health through climate change, loss of biodiversity, impediments of ecosystem services and food insecurity. Considering the change dynamics of various land uses, and their indispensable roles in human and environmental health, there is a crucial need for the adoption of spatiotemporal analytical tools such as RS and GIS for effective monitoring and assessment of LULC changes.

Remote sensing (RS) and Geographical information system (GIS) have been applied in many studies especially in the urban centres to map and model changes in LULC, understand the drivers of the changes, predict future changes, and proffer targeted recommendations applicable for policymaking on sustainable land use management [6,7]. Urban centres and cities tend to be the most targets because many LULC changes are predominant in the rapidly growing area including São Paulo. São Paulo is a megacity that has been growing rapidly [8]. The city is characterized by a mix of modern skyscrapers and historic buildings, and diverse transport networks proving its rich architectural heritage. Famous landmarks include the São Paulo Cathedral, Copan Building, and Municipal Theatre. The city also has many prestigious universities and research institutions (e.g., FAPESP), making it also a hub for higher education and scientific research in Brazil. These socioeconomic and physical landscapes contributed significantly to the huge LULC changes in the area which impacted on the agricultural landscape. Though the impact of urbanization is crucial in the agricultural land use and sector, it is rare to find studies that focused on the implications of the rapid urban growth on the agriculture and forest areas. The growing population needs food as much as the infrastructural facilities and a study that appraised the status of the agricultural landscape amid the urban built-up is necessary. Therefore, the study aimed to investigate the effects of urbanization on agricultural lands in São Paulo city by applying the tools of geoinformatics. Findings from the study could provide vital information for policy making in the areas of food security and sustainable development of the city.

## MATERIALS AND METHODS

### Study area

São Paulo is a megacity in Brazil found in São Paulo state (a province in the southeast region of Brazil), and it was established in 1554 by the Jesuits [9]. In the 20th Century, São Paulo became the most famous economic and commercial hub center of Brazil with more than 11 million people currently [8-10]. Geographically, São Paulo is located between latitude and longitude 47°0′ W to 46°20′ W and 23°15′ S to 23°60′ S, respectively, and covering an area of 5025 km2, the city has a diverse and robust economy that includes finance, commerce, services, and manufacturing industries [8]. It occupies parts of the Atlantic Forest and Cerrado biomes with severe changes in land use-land cover due to changes in settlement and agriculture. Main soil types are Oxisols, Ultisols, and Alfisols.

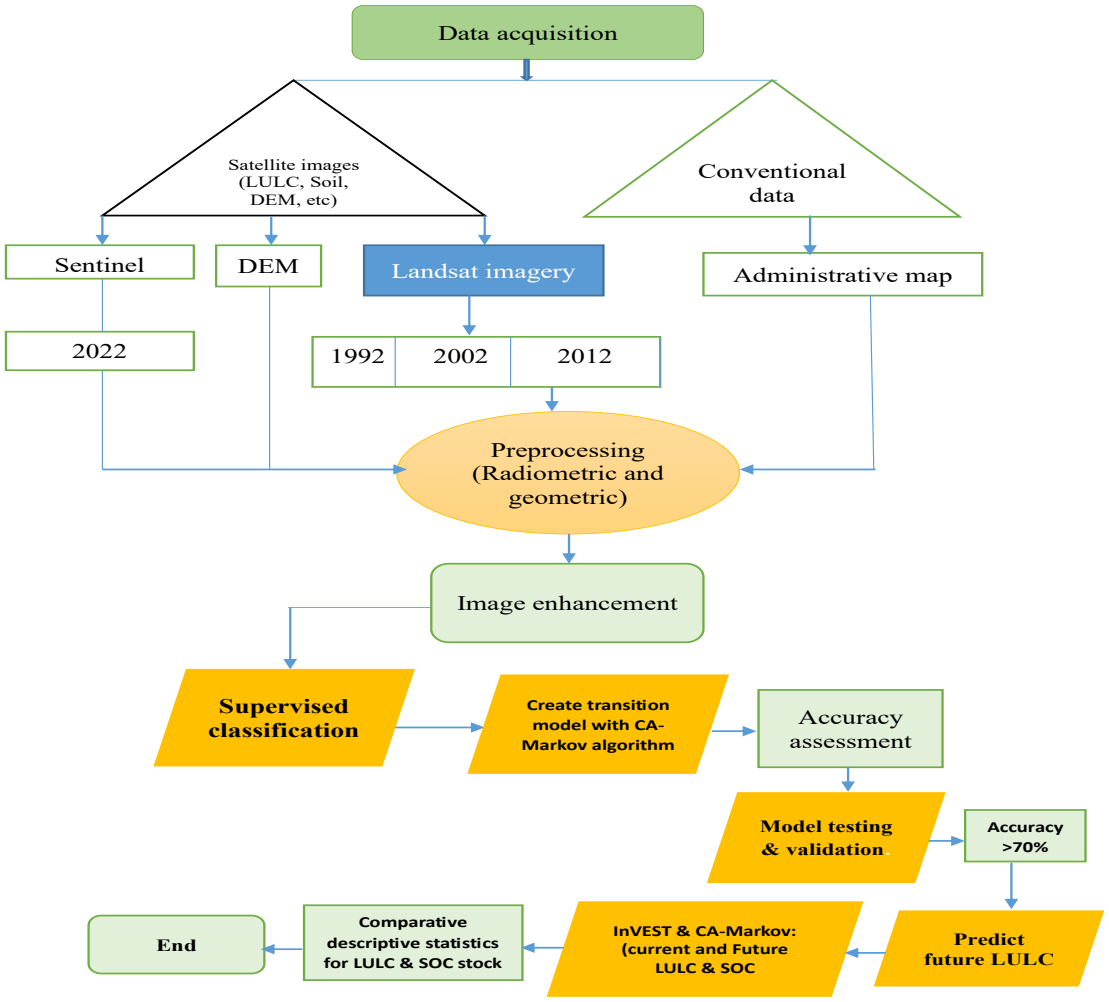


**Figure 1**. Flowchart of the research methodology

## Data collection and analysis

The flowchart of the research methodology is shown in Figure 1. The study made used of both primary and secondary sources data which includes a sentinel image, Landsat TM, ETM+ satellite image and administrative map of Brazil from December 1992. Landsat pictures of the review region for 1992, 2002, 2012 and sentinel of 2022 were gained from USGS. High resolution satellite imagery was acquired which served as the basis for the ground-truth information that was required for the classification and estimation of the accuracy of the classified TM and ETM+ images. Partial field survey was carried out to gather the ground-truth information necessary for the classification and accuracy evaluation of the Landsat images. QGIS 3.3 software was used for radiometric correction of the Landsat images before it was exported to ArcGIS 10.5 for further processing and analysis. The data were preprocessed, georeferenced, and classified using the supervised Maximum Likelihood Classification approach to determined land use classes and the area covered per each of the land use. This was done in ERDAS Imagine using the Accuracy Assessment tool. Accuracy assessment of processed images was done in two ways: the overall accuracy and the Kappa Statistics.

## RESULTS

Five LULC classes including water body, settlement, agricultural land, wetland, and forest were determined. Accuracy assessment revealed 95% for overall accuracy, and 94.4% for the Kappa coefficient (Table 1).

**Table 1**. LULC area, %, and change % between 1992 -2022

| **LULC Class** | **1992** | | **2002** | | **1992-2002** | **2012** | | **2002-2012** | **2022** | | **2012-2022** | **1992-2022** |
|---|---|---|---|---|---|---|---|---|---|---|---|---|
| | **Area (ha)** | **Area (%)** | **Area (ha)** | **Area (%)** | **% of change** | **Area (ha)** | **Area (%)** | **% of change** | **Area (ha)** | **Area (%)** | **% of change** | **% of change** |
| Waterbody | 5772 | 3.79 | 6724 | 4.41 | **0.63** | 6942 | 4.56 | **0.14** | 5683 | 3.73 | 0.82 | 0.06 |
| Settlement | 76318 | 50.07 | 81015 | 53.16 | **3.09** | 56556 | 37.11 | 16.05 | 85851 | 56.32 | **19.21** | **6.25** |
| Agric. land | 22058 | 14.47 | 27790 | 18.23 | **3.76** | 41871 | 27.47 | **6.24** | 21366 | 14.02 | 13.46 | 0.46 |
| Wetland | 9087 | 5.96 | 24070 | 15.79 | **9.83** | 25622 | 16.81 | **1.02** | 12001 | 7.87 | 8.94 | **1.91** |
| Forest | 39184 | 25.71 | 12802 | 8.40 | 17.31 | 21406 | 14.05 | **5.65** | 27519 | 18.06 | **4.01** | 7.65 |
| Total | 152422 | 100 | 152422 | 100 | | 152422 | 100 | | 152422 | 100 | | |
| Overall accuracy | 95% | | | | | | | | | | | |
| Kappa coefficient | 94.4% | | | | | | | | | | | |

Settlement and wetland increased in areas between 1992 and 2022, while agricultural land, forest and waterbody decreased (Table 1, Figure 2). Agricultural land increased between 1992 and 2002, and between 2002 and 2012 but decreased between 2012 and 2022. Forest on the other hand decreased in 2002 but increased in the subsequent years. On the other hand, settlement and wetland increased in 2002 by 3.09% and 9.83%, and between 1992-2022 by 6.25% and 1.91% respectively. Meanwhile, settlement recorded the highest percentage increase between 2012 and 2022 by 19.21%.

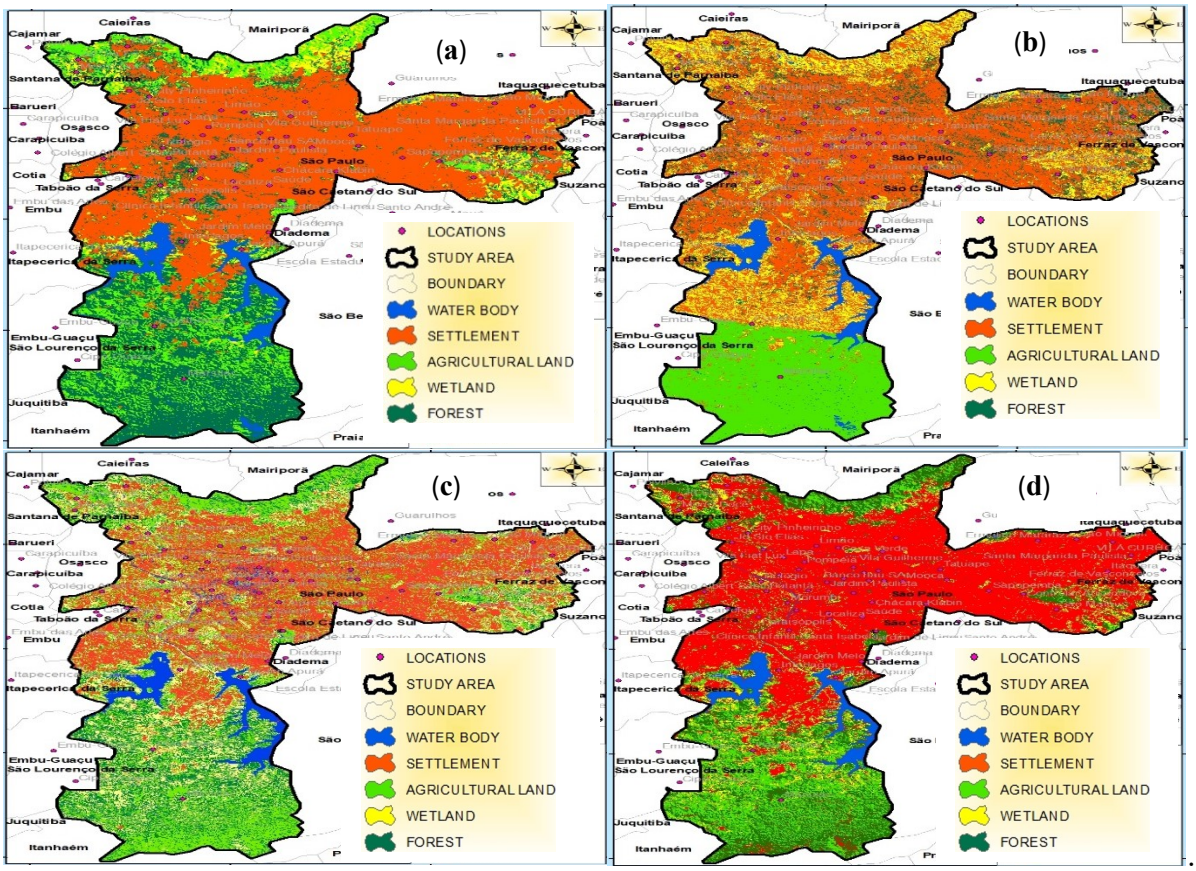


**Figure 2**. LULC of São Paulo city for (a) 1992 (b) 2002 (c) 2012 and (d) 2022

## DISCUSSION

The accuracy assessment of 95% for overall accuracy and with no LULC class is below 80%. Similarly, the Kappa coefficient was 94.4%. These results were valid and acceptable values based on the findings from previous studies [11-13]. For example, it has been recommended that overall accuracy of 85% with no class less than 70% and a Kappa coefficient of at least 60% is accurate and acceptable in a LULC classification [14].

Settlement increased during the study periods, and this might be attributed to rapid population growth which has been a major global issue threatening most countries especially in the developing countries in Africa, Asia, and Latin America including Brazil [15,16]. Several studies have held rapid population growth as a responsible factor for significant LULC change in Sao Paulo, the mega city of Brazil [15,16]. This is because the increase in human population increases the need for land for farming, settlement, and infrastructural developments, thereby impacting significantly on the LULC [2,4,5]. The growth in the demographic indices is to a larger extent responsible to the decrease in forest and agricultural land use between 1992 and 2022. This is because the forest and agricultural lands were converted to artificially built environmental structures such as houses, roads, and other infrastructural facilities [17].

## CONCLUSION

The hybridization of RS and GIS tools and techniques was effective in monitoring LULC changes in São Paulo City. Agricultural land, water body, settlement, wetland, and forest were the main LULC classes identified in the study. The Kappa coefficient overall accuracy met the acceptable values and all the LULC had more than 80% accuracy rate. Settlement increased during the study periods, a situation that might be described by rapid population growth which has been a major concern in Brazil, and most developing countries. The rapid population growth is a prime driver LULC change in São Paulo city because the need for infrastructures caused the decline in forest and agricultural areas as they were converted to urban artificial built-up structures. Meanwhile, further study is needed to predict the LULC scenario in future (maybe in 2050 and beyond) by elucidating the rate of future urbanization and impacts on agricultural land use in São Paulo City. Findings from the study might provide vital information for decision makers on how to improve food security and sustainable development São Paulo City.

## ACKNOWLEDGEMENTS

The study was funded by São Paulo Research Foundation (FAPESP) [process numbers: 2021/11757-1; 2023/05122-9, and 2021/10573-4]. Chukwudi Nwaogu is grateful to the FAPESP for the funding (2021/11757-1 and 2023/05122-9), and Cherubin M.R. thanks CNPq for his Research Productivity Fellowship (311787/2021-5). We also give thanks to the Center for Carbon Research in Tropical Agriculture (CCARBON) sponsored by FAPESP (2021/10573-4).

## REFERENCES

[1] Juez C., Garijo N., Nadal-Romero E., Vicente-Serrano S. M. Wavelet analysis of hydro-climatic time-series and vegetation trends of the Upper Aragón catchment (Central Spanish Pyrenees). Journal of Hydrology, 614, 128584, 2022.

[2] Nyirarwasa A., Han F., Yang Z., Mperejekumana P., Dufatanye Umwali E., Nsengiyumva J.N., Habibulloev S. Evaluating the Impact of Environmental Performance and Socioeconomic and Demographic Factors on Land Use and Land Cover Changes in Kibira National Park, Burundi. Sustainability, 16(2), 473, 2024. https://doi.org/10.3390/su16020473

[3] Bhattarai H., Tai A.P., Martin M.V., Yung D.H. Impacts of changes in climate, land use, and emissions on global ozone air quality by mid-21st century following selected Shared Socioeconomic Pathways. Science of The Total Environment, 906, 167759, 2024. https://doi.org/10.1016/j.scitotenv.2023.167759

[4] Yang S., Yang X., Zhang J., Gao X., Zhou J., Wu X. Assessing the impacts of rural depopulation and urbanization on vegetation cover: Based on land use and nighttime light data in China, 2000–2020. Ecological Indicators, 159, 111639, 2024.

[5] Miah M.T., Fariha J.N., Kafy A.A., Islam R., Biswas N., Duti B.M., Fattah M.A., Alsulamy S., Khedher K.M., Salem M.A. Exploring the nexus between land cover change dynamics and spatial heterogeneity of demographic trajectories in rapidly growing ecosystems of south Asian cities. Ecological Indicators, 158, 111299. 2024.

[6] Peeling J.A., Chen C., Judge J., Singh A., Achidago S., Eide A., Tarrio K., Olofsson P. Applications of Remote Sensing for Land Use Planning Scenarios with Suitability Analysis. IEEE Journal of Selected Topics in Applied Earth Observations and Remote Sensing, 17, 6366-6378, 2024. doi: 10.1109/JSTARS.2024.3370379

[7] Aslam R.W., Shu H., Tariq A., Naz I., Ahmad M.N., Quddoos A., Javid K., Mustafa F., Aeman H. Monitoring landuse change in Uchhali and Khabeki wetland lakes, Pakistan using remote sensing data. Gondwana Research, 129, 252-267, 2024.

[8] Venkatraman S., Kandasamy V., Rajalakshmi J., Begum S., Sujatha M. Assessment of urban heat island using remote sensing and geospatial application: A case study in Sao Paulo city, Brazil, South America. Journal of South American Earth Sciences, 134, 104763, 2024. https://doi.org/10.1016/j.jsames.2023.10476

[9] Britannica São Paulo. Available online: https://www.britannica.com/place/Sao-Paulo-Brazil (accessed on 15 March 2024).

[10] IBGE 2022. Available online: https://cidades.ibge.gov.br/brasil/sp/sao-paulo/panorama (accessed on 15 March 2024).

[11] Kerbo A.A., Degaga D.T., Beyene A.D. Eucalyptus tree expansion and land use and land cover dynamics in Ethiopia-empirical evidence from Gurage Zone, Ethiopia. Land Use Policy, 141, 107149, 2024.

[12] Chowdhury M.S. Comparison of accuracy and reliability of random forest, support vector machine, artificial neural network and maximum likelihood method in land use/cover classification of urban setting. Environmental Challenges, 14, 100800, 2024.

[13] Gowri L., Manjula K.R. Detection of land cover usage from optimized learnable parameter artificial neural network (OLPANN) using multispectral images. Multimedia Tools and Applications, pp.1-31, 2024.

[14] Pham Q.B., Ali S.A., Parvin F., Van On V., Sidek L.M., Đurin B., Cetl V., Šamanović S., Minh N.N. Multi-spectral remote sensing and GIS-based analysis for decadal land use land cover changes and future prediction using random forest tree and artificial neural network. Advances in space research, 2024. https://doi.org/10.1016/j.asr.2024.03.027

[15] Côrtes J.C., de Oliveira D'Antona Á., Perz S. Extended families and demographic explanations for land use-cover change in the Brazilian Amazon. Population and Environment, 46(1), 1-20, 2024.

[16] de Souza J.C., Mendes T.S.G., Bignotto R.B., de Alcântara E.H., Massi K.G. Land use dynamics in a tropical protected area buffer zone: is the management plan helping?. Journal of Environmental Studies and Sciences, 1-11, 2024.

[17] Abebe M.G. Impacts of urbanization on food security in Ethiopia. A review with empirical evidence. Journal of Agriculture and Food Research, 15,100997, 2024. https://doi.org/10.1016/j.jafr.2024.100997

# ONLINE SERVICES FOR URBAN ENVIRONMENT MONITORING

**Assoc. Prof. Dr. Alexander Ivanov**[1]

**Maria Ivanova**[2]

[1] Nizhny Novgorod State University of Architecture and Civil Engineering, **Russia**
[2] Nizhny Novgorod State University of Architecture and Civil Engineering, **Russia**

## ABSTRACT

Urban meteorological parameters and traffic emissions are characterized by microterritorial variability. Online weather and traffic information is the basis for creating online services to provide users with information about the toxicological risk, noise effects and thermal stress risk. The purpose of this work is to assess the possibilities of online environmental modeling. The methodology includes special field studies to select model parameters, developing models for online calculations of noise levels, concentrations of pollutants from traffic flows and microterritorial changes in temperature and wind speed, as well as tools for providing processing and storage of information. As a result, it was found that the concentration of nitrogen and carbon oxides in the roadside zone reaches maximum permissible values, which corresponds to the modeling results. The noise level exceeds 70 dBA and also corresponds to the simulation results. The effective temperature mitigation inside closed-canopy green areas compared to open space is several Celsius degrees and provides protection from thermal stress in accordance with the proposed model. The result of the work is the development of a test version of three services, including calculation of the concentration of pollutants during traffic congestion; calculation of the noise level produced by intensive traffic flow and calculation of the effective temperature during thermal stress for the hottest summertime. It is during thickening of traffic flows that the highest concentrations of pollutants are observed and at this time the risks of toxicological and noise effects are significant. The research conditions correspond in time and space to the highest level of local environmental risk. To perform online calculations, in addition to the parameters obtained during field studies, real-time information about the weather and traffic flow speed is required. The online services can be used both for users to make immediate decisions and for city policies to reduce emissions risks and to create urban green islands of thermal safety with a closed canopy that protects during extreme heat.

**Keywords:** online services, urban environment monitoring, climate change, thermal stress

## INTRODUCTION

In the last decade, among real-time Internet resources, a significant role is played by resources that provide the user with information about the state of the environment in cities in real time. These are systems that monitor the concentration of pollutants, noise levels and meteorological parameters and provide processed information to users. Such systems are able to transmit relevant information to wireless systems that is important

for assessing comfort and individual environmental risk. Such systems are reliable only in the immediate vicinity of contact meters.

At the same time, the question arises about the possibility of assessing the parameters of comfort and environmental safety in the widest possible class of territories where direct action parameters meters are not installed, but where environmental risks associated with environmental parameters can change by an order of magnitude compared to the observation point. This is typical for areas containing intense traffic flows. That is, a risk calculation model is needed not only at the observation point, but also in its surroundings. Accordingly, calculations of noise concentration and level in such areas are based on the intensity, structure and speed of traffic flows. For cities that have a developed network of external surveillance cameras for traffic flows, it is possible to assess the structure, speed and intensity of traffic flow based on the use of artificial intelligence technologies.

In addition, remote observations are also carried out using satellites, from which images can be used to estimate the size and canopy density of green areas inside cities, which are safe zones during thermal stress. Thus, non-contact remote sensing and AI can provide real-time, detailed spatial information about pollution levels and environmental and health risks based on indirect strategies.

## MATERIALS AND METHODS

The research methodology in this work is as follows. This paper discusses the methodology of the Internet service: for online calculations of noise levels and pollutant concentrations from intense traffic flows and microterritorial changes in temperature and wind speed in urban green areas with a closed canopy. For online calculations in real time, it is necessary that all calculated parameters are known or accessible through available Internet services. For the three selected types of environmental monitoring, as can be seen from Table 1, the list of parameters available through the services is significantly narrower than the entire set of calculated parameters. Environmental parameters for the online services were based on the ISO 37120-2020 Sustainable development of community. Indicators for city services and quality of life.

Table 1. Environmental quality parameters required for the online services

| Models | Environmental parameters and risks | Online options available on the Internet |
|---|---|---|
| Model for calculating noise levels from traffic flows | Roadside noise level, its speed, intensity and types of vehicles | Traffic flow speed according to online measurements using AI [1] |
| Gaussian model for calculating the dispersion of pollutants in atmospheric air | $N_{ox}$ CO, $SO_2$ concentration calculated based on traffic intensity and weather data | Traffic flow speed according to online measurements using AI [1]. Weather data |
| Model for calculating the mitigation of summer thermal stress by green areas | Risks of thermal (heat) stress | Satellite and aerial images of closed canopy green areas |

Special field studies were carried out. These studies made it possible to find an acceptable accuracy relationship between the parameters available via the Internet and the parameters necessary for calculations using the selected models.

This made it possible to create models for online calculations of noise levels, concentrations of pollutants from traffic flows and micro-territorial changes in temperature and wind speed, as well as tools to support processing and storage of information.

Let's consider the methodology for creating models for performing online calculations in real time using information available via the Internet. Online noise level calculations are performed for highways with heavy traffic.

For modern traffic flows in large Russian cities, the equivalent noise level at a distance of 7.5 m from the outer lane is calculated using the formula [2]:

$$L_{Aeq} = 9.5 * lgN_a + 12.94 * lgV + 6.98 * \lg(1 + S_{hv}) + 11.39 \quad (1)$$

$L_{Aeq}$- equivalent noise level

V – speed of traffic flow, km per/hour;

r – distance from the axis of movement of the vehicle to the calculated point, m,.

$N_a$ – intensity of traffic flow per hour,

$S_{hv}$ is the share of heavy trucks and buses in the traffic flow.

For streets with the most intense traffic flows, studies have been carried out showing the relationship between speed and road capacity. An example of such a study for a two-lane and one-lane road with one-way traffic is presented in Figures 1 and 2. A good approximation is the quadratic dependence of the intensity of traffic flow on its average speed [2].

$$N_a = a + b * V - c * V^2 \quad (2)$$

a , b, c – empirical parameters that ensure the conversion of the observed speed of traffic flow into its intensity. To assess the risk, you can select the parameters corresponding to the highest intensity at a given speed. The $S_{hv}$ parameter is usually known to researchers of traffic flows in each specific city for the main transport routes. Therefore, the goal of field research is to establish the relationship between traffic speed and noise. The calculations are only valid for dense flows, meaning that the noise and health risk calculations must be verified to ensure that the flow is dense before providing the user with a noise and health risk calculation. Otherwise, the risk calculation results will be significantly overestimated. As a result, a model was obtained for online calculation of the noise level from traffic flow from one single variable - traffic flow speed. At the same time, other variables such as the share of heavy vehicles and the number of lanes are considered a priori known.

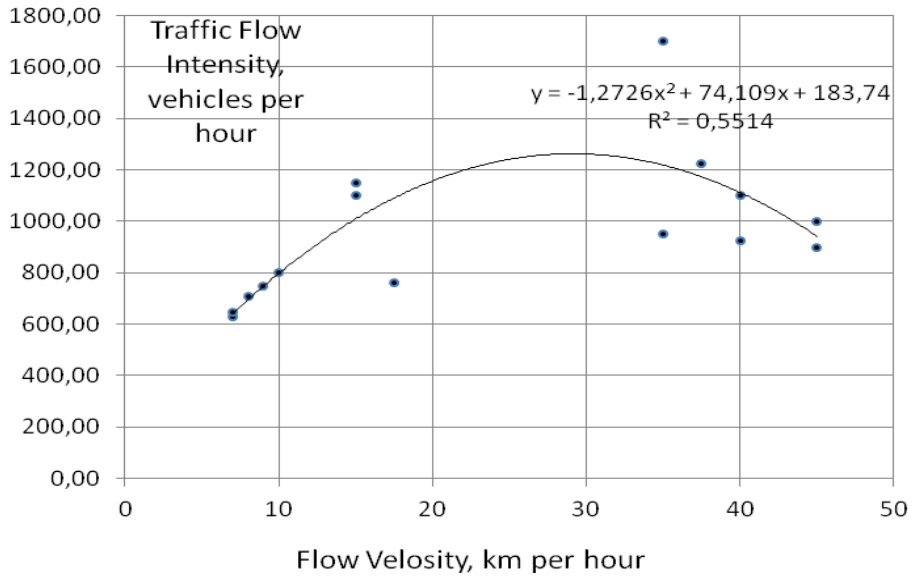


Figure 1. Traffic flow intensity for one lane [2]

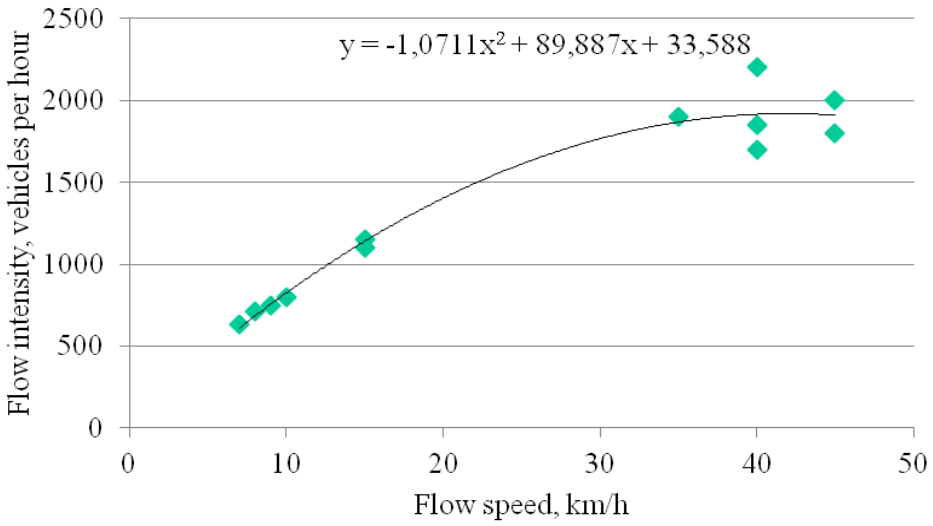


Figure 2. Traffic flow intensity for two lanes in one direction [2]

$$C = \frac{q}{\sqrt{2\pi} * \sigma_z * U * sin\varphi} + F; \quad (3)$$

Where

C – concentration of pollutants, g/m$^3$;

q – emissions of the pollutant per unit time per 1 m path;

$\sigma_z$ – dispersion of pollutants in atmospheric air, m;

U – wind speed, m/sec;

ϕ – the angle between the wind direction and the road, at an angle from 900 to 300 the wind speed should be multiplied by the sine of the angle, at an angle less than 300 - by a factor of 0.5;

F – background concentration level of the pollutant, g/m$^3$.

Emissions of the pollutant per unit time per 1 m path depends on intensity of traffic flow per hour $N_a$, traffic velocity V and type of engine. The most important is dependence of emission rate on traffic velocity as for the noise model: q($N_a$,V), see figure 3..

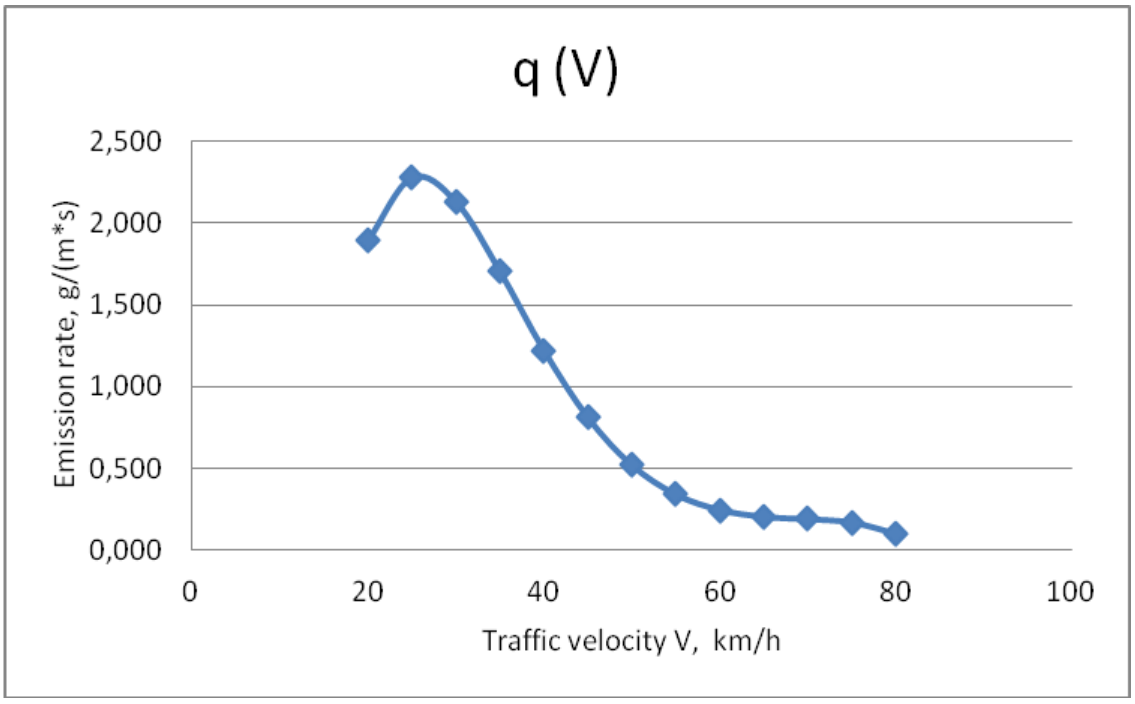


Figure 3. Change in traffic flow Emissions depending on its velocity

To increase the accuracy of calculations in this work Back Propagation methods of Artificial Neural Networks were used similar to [3]. The application of the algorithm is based on the following assumptions. Let the point of measurement of the concentration of the pollutant be located in the zone of influence of two roads and the background level. Emission is formed by sources - gasoline h1 and diesel engines h2. which cars and trucks are equipped with. The difference between the calculated and measured emissions is used in the error function to minimize it by refining the connection weights using the backpropagation method. Online calculation of emissions are based on traffic flow speed and weather data.

The online thermal stress risk assessment methodology is based on the identified ability of areas with a closed canopy of woody vegetation to maintain comfortable and safe conditions under thermal stress in summer. The study included the identification of microweather parameters that provide comfort during thermal stress. Based on the identified parameters, an online calculation of the perceived equivalent temperature is carried out.

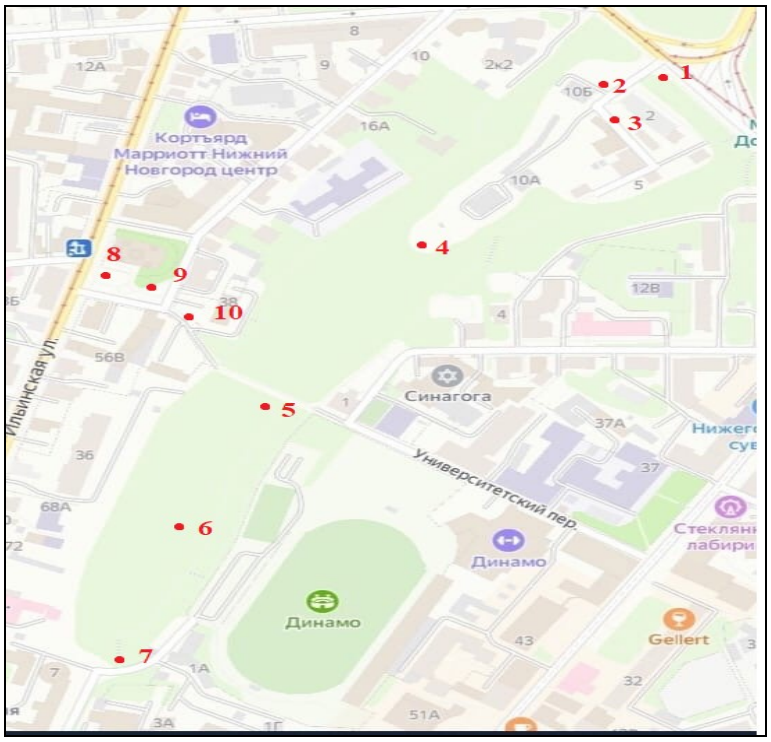


Figure 4. Location of ten meteorological observation points in the recreational area

Table 2. Results of calculating the coefficient of determination and Fisher's parameter for temperature, wind speed and the share of the area of green spaces with a closed canopy within a radius of 50 m from the measurement point

| Date of measurements | $R^2$ | F |
|---|---|---|
| 28.07.2022 | 0,7568 | 10,893 |
| 29.07.2022 | 0,7686 | 11,6275 |
| 30.07.2022 | 0,7945 | 13,5298 |
| 01.08.2022 | 0,7934 | 13,4422 |
| 02.08.2022 | 0,8293 | 17,0054 |
| 03.08.2022 | 0,6340 | 6,0635 |
| 04.08.2022 | 0,8121 | 15,1262 |

An important preliminary result is that there is a strong correlation between the proportion of an area with closed canopy and microweather characteristics, as seen in Table 2. The results of the study allow us to propose calculation formulas for extreme temperature T that creates the risk of additional mortality under conditions of thermal stress.

$$T = = 42,69 - 21,28 \cdot S - 12,24 \cdot U \quad (4)$$

Where S is the proportion of green spaces in the vicinity of an observation point with a radius of R=50 m.

## RESULTS

The result is a rationale for performing online calculations for environmental Internet services. Figure 5 shows examples of such online calculations for the level of air pollution in the vicinity of 4 streets.

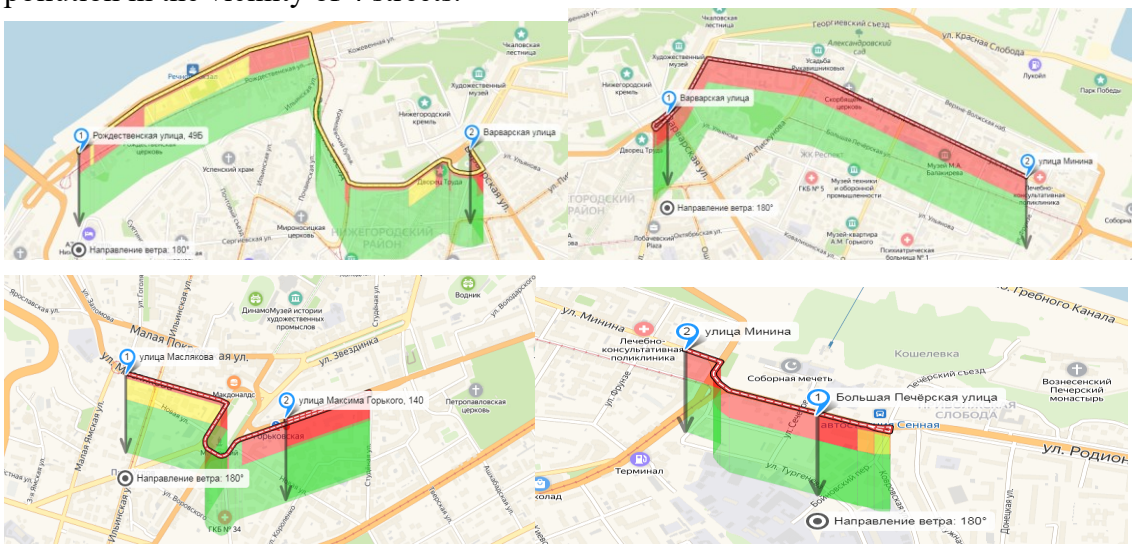


Figure 5. Calculation of the level of air pollution in the vicinity of 4 streets

## DISCUSSION

The obtained results allow online calculations of important environmental parameters with satisfactory accuracy. The results correspond to established scientific ideas and create an opportunity, important for practice, to make management decisions immediately

## CONCLUSION

This paper proposes a methodology for microterritorial online research on environmental safety and comfort for residential and recreational areas.

For this work, instruments were selected that form a measuring system for online monitoring of environmental comfort and safety. In practice, the methodology for measuring and processing environmental information was developed.

Studies of urban areas under thermal stress conditions have been carried out. Research has revealed significant microterritorial differences in environmental indicators that affect the risk of disease and thermal stress.

The concentrations of pollutants, noise and meteorological parameters obtained during measurements make it possible to provide initial data for online calculations of microterritorial characteristics of environmental safety of residential and recreational areas.

The results obtained are the basis for creating Internet resources for environmental monitoring in real time.

Based on the completed field studies and comparison of observation results with calculations, two models were proposed, including a model for online calculations of the concentration of pollutants in intensive traffic flows and assessment of the risk of immediate hazardous effects on public health; model for online calculations of the noise level created by intense traffic flows.[4]

Based on field studies of the microweather characteristics of green recreational areas, it was established that under conditions of thermal stress, the main role in reducing temperature and wind speed is played by the proportion of green spaces in areas, provided that their radius is at least 50 m.

The use of the proposed environmental monitoring models will ensure the functioning and design of the city in full compliance with the criteria of comfort and environmental safety, including real-time parameters

## REFERENCES

[1] Shepelev V, Slobodin I, Gritsenko A and Fadina O (2022) FORECASTING THE AMOUNT OF TRAFFIC-RELATED POLLUTANT EMISSIONS BY NEURAL NETWORKS. Front. Built Environ. 8:945615. doi: 10.3389/fbuil.2022.945615;

[2] Ivanov A.V, Platov A.Yu., Stepanov D.V., Ostanina I. M. (2018) ONLINE MONITORING OF URBAN ENVIRONMENT. 18th International Multidisciplinary Scientific GeoConference SGEM 2018. Conference proceedings. 2018. Volume 18 Issue 2.2, pp. 339-346..

[3] Novikova, S.V., NEURAL NETWORK SIMULATION FOR SOLVING THE MONITORING PROBLEMS UNDER CONDITIONS OF INCOMPLETE FUZZY INFORMATION (BY AN EXAMPLE OF ECOLOGICAL MONITORING), Doctoral (Tech.) Dissertation, Kazan: Kazan State Technical University, 2013, p. 258.

[4] Myagkov M.S., Gubernskiy Yu.D., Konova L.I., Lipkevich V.K. Gorod, architektura, chelovek I klimat (In Russian) Architektura C Publisher, 342 p. 2007, ISBN:978-5-9647-0113-2.

# SECTION

# GEODESY AND MINE SURVEYING

# A MYTH CONCERNING THE GEOMETRIC LEVELLING: CLOSING ERRORS AND LOOP CIRCUMFERENCES

**Dr. Vasil Cvetkov**[1]

[1] University of Architecture, Civil Engineering and Geodesy, **Bulgaria**

## ABSTRACT

The geometric levelling of the highest order has been the main method for many scientific and engineering tasks for more than 150 years. One of them is the monitoring of the recent vertical movements of the Earth's crust. In order to understand the low of accumulation of the discrepancies in levelling lines, many investigators have planned and performed various experiments and analysis through the years. As a result, the systematic effects of many sources of measurement errors have been studied, and partly or fully solved. However, the basic assumption about the relationship between the closing errors in levelling loops and the circumferences of the loops has hardly ever been the topic of wide discussions. It seems that this relationship is undoubted. The main objective of this article is to demonstrate that this popular belief about the accumulation of closing errors in the precise levelling is not valid regarding the data of the Third levelling of Bulgaria, the Second and the Third levelling of Finland. Using correlation and regression analysis we found that there is no statistically significant connection between closing errors and loop circumferences in the analyzed levelling networks. The correlation coefficients are below 0.35 considering each network, which means that the determination coefficients are up to 0.10. That is to say, the circumferences of the levelling loops cannot explain more than 10% of the variance of the closing errors. In addition, the p-values of the regression parameter $b$ in the equation $|W| = a + b.L^{0.5}$ are 0.104, 0.725 and 0.976, in the case of the Third levelling of Bulgaria, the Second and the Third levelling of Finland, respectively. Based on the above facts, we can conclude that some basic assumptions and methods regarding the processing of geometric levelling data should be an object of further modern consideration and revision.

**Keywords:** correlation, closing errors, geometric levelling, regression

## INTRODUCTION

The main purpose of precise levelling networks is to establish the height systems of the territories that they cover [3, 5, 7, 8, 9]. Simultaneously, the highest order geometric levelling networks are used for many different scientific investigations. One of them is the monitoring of the recent Earth's crust vertical movements and their velocities, which differ from each other in different areas [1, 3, 7, 9]. In some places the magnitude of the velocities is a few times greater than the accuracy of the precise levelling [3, 7], and there is no doubt about the plausibility of the conclusions concerning their speed and directions. Contrary, there are territories, where the magnitudes of the vertical velocities of the Earth's crust are equal or even below the accuracy of the precise levelling [1, 2].

Therefore, if we want to minimize the risk of making wrong conclusions regarding the nowadays-tectonic processes, we must process levelling data in the most appropriate way. We should have strict criteria regarding the assessment of the levelling accuracy. We have to use the relevant and reasonable weights in the adjustments of geometric levelling networks. We must develop statistically supported specifications about acceptance or rejection of the double-run measurements of the elevations in levelling lines [4, 8]. The solution of all these issues is unthinkable without clear understanding of the processes of forming of discrepancies and closing errors in the precise levelling line and loops.

However, in the estimation of the accuracy of the levelling results, there have always been difficulties arising from the large number of sources of levelling errors and from their specific characters [3]. As a result, during the last decades, several ways for estimating the accuracy have been presented [3, 8]. All of them are based on the classic assumption about the low of the error accumulation in the precise levelling, described perfectly by Kääriäinen [3, p.52], which supposes a relationship between the magnitude of the levelling errors and the length of the levelling route. That is to say, the bigger the levelling loop circumference, the greater its closing error.

The main objective of this article is to demonstrate that this popular belief about the accumulation of closing errors in the precise levelling is not valid regarding the data of the Third levelling of Bulgaria, the Second and the Third levelling of Finland. Consequently, the universality of the assumption about the relationship of the levelling accuracy and levelling distance must be revised.

## MATERIALS AND METHODS

In the current research we used the levelling data from the Third precise levelling of Bulgaria /1975-1984/ - Table 1, the Second precise levelling of Finland /1935-1955/ according to [3] and summarised by Table 2, and the Third precise levelling of Finland /1978-2006/ as given by [7] and recapitulated by Table 3.

**Table 1.** Absolute values of the closing errors $|W|$ and loop circumferences $L$ in the Third precise levelling network of Bulgaria /1975 – 1984/

| **Loop** | $\|W\|$ | $L$ | **Loop** | $\|W\|$ | $L$ | **Loop** | $\|W\|$ | $L$ |
|---|---|---|---|---|---|---|---|---|
| | *mm* | *km* | | *mm* | *km* | | *mm* | *km* |
| 1 | 9.58 | 361.05 | 9 | 43.59 | 480.63 | 17 | 35.91 | 472.14 |
| 2 | 15.23 | 229.96 | 10 | 15.16 | 414.20 | 18 | 7.30 | 437.74 |
| 3 | 41.31 | 315.06 | 11 | 29.95 | 439.94 | 19 | 37.84 | 450.38 |
| 4 | 24.38 | 359.07 | 12 | 20.42 | 391.62 | 20 | 40.08 | 450.90 |
| 5 | 10.82 | 451.84 | 13 | 42.64 | 392.27 | 21 | 23.04 | 494.79 |
| 6 | 19.60 | 366.52 | 14 | 0.71 | 307.69 | 22 | 5.46 | 499.56 |
| 7 | 9.04 | 372.90 | 15 | 5.32 | 298.72 | 23 | 5.63 | 75.92 |
| 8 | 24.70 | 250.40 | 16 | 26.09 | 412.71 | **Outer** | **2.85** | **2550.18** |

**Table 2.** Absolute values of the closing errors $|W|$ and loop circumferences $L$ in the Second precise levelling network of Finland /1935 – 1955/ [3, Table VI, Table IX].

| **Loop** | $\|W\|$ | $L$ | **Loop** | $\|W\|$ | $L$ | **Loop** | $\|W\|$ | $L$ |
|---|---|---|---|---|---|---|---|---|
| | *mm* | *km* | | *mm* | *km* | | *mm* | *km* |
| I | 7.18 | 239.02 | IX | 11.63 | 556.29 | XV | 11.20 | 551.15 |
| II | 0.06 | 428.87 | X | 5.53 | 545.30 | XVI | 5.62 | 662.12 |
| III | 8.94 | 369.79 | XI | 25.21 | 723.36 | XVII | 13.78 | 688.02 |
| VI | 20.06 | 413.61 | XII | 22.85 | 562.56 | XVIII | 20.61 | 324.29 |
| VII | 8.22 | 451.17 | XIII | 0.59 | 566.68 | **Outer** | **16.17** | **2890.46** |
| VIII | 6.05 | 709.25 | XIV | 17.66 | 588.17 | | | |

**Table 3.** Absolute values of the closing errors $|W|$ and loop circumferences $L$ in the Third precise levelling network of Finland /1978 – 2006 г./ [7, Fig. 6.2 and Appendix C].

| **Loop** | $\|W\|$ | $L$ | **Loop** | $\|W\|$ | $L$ | **Loop** | $\|W\|$ | $L$ |
|---|---|---|---|---|---|---|---|---|
| | *mm* | *km* | | *mm* | *km* | | *mm* | *km* |
| 1 | 14.62 | 164.18 | 11 | 19.67 | 305.51 | 21 | 7.54 | 453.13 |
| 2 | 5.73 | 158.76 | 12 | 1.90 | 443.27 | 22 | 1.17 | 699.68 |
| 3 | 19.87 | 372.66 | 13 | 6.04 | 282.10 | 23 | 17.35 | 711.08 |
| 4 | 13.89 | 245.59 | 14 | 27.12 | 504.15 | 24 | 4.71 | 335.64 |
| 5 | 4.51 | 425.06 | 15 | 17.51 | 509.08 | 25 | 25.11 | 319.39 |
| 6 | 3.17 | 571.21 | 16 | 22.51 | 566.41 | 26 | 10.54 | 395.29 |
| 7 | 0.56 | 493.64 | 17 | 19.27 | 563.38 | 27 | 43.19 | 400.33 |
| 8 | 17.55 | 556.56 | 18 | 28.49 | 602.26 | 28 | 20.57 | 519.94 |
| 9 | 14.87 | 414.90 | 19 | 4.73 | 503.58 | | | |
| 10 | 21.59 | 138.99 | 20 | 0.84 | 426.44 | | | |

In order to investigate the relationship between absolute values of the closing errors $|W|$ in loops, loop circumferences $L$, and the quantity $\sqrt{L}$ we determined Pearson's coefficients of correlation among $|W|$, $L$ and $\sqrt{L}$ by equation (1) [6].

$$\rho_{X,Y} = \frac{\sum_{i=1}^{n}(x_i-\bar{x})(y_i-\bar{y})}{\sqrt{\sum_{i=1}^{n}(x_i-\bar{x})^2}.\sqrt{\sum_{i=1}^{n}(y_i-\bar{y})^2}} \tag{1}$$

We also determined the statistical significance of the regression between the closing errors $|W|$ in loops and the square root of the loop circumferences $\sqrt{L}$ for the above-mentioned precise levelling networks, i.e. the model (2).

$$|W| = a + b.\sqrt{L} \tag{2}$$

It should be mentioned, that in our analysis we intentionally skipped the data concerning the outer loops in the networks.

## RESULTS

This section presents the results of our analyses. Table 4 contains the correlation coefficients of the pairs $|W| \leftrightarrow L$, $|W| \leftrightarrow \sqrt{L}$, $L \leftrightarrow \sqrt{L}$. Table 5 summarize the estimates of the model (2) and their statistical significance.

**Table 4.** Correlation coefficients among the absolute values of the closing errors $|W|$, loop circumferences $L$ and square root of $L$ in the analyzed precise levelling networks.

| Network | $\rho_{\|W\|,L}$ | $\rho_{\|W\|,\sqrt{L}}$ | $\rho_{L,\sqrt{L}}$ |
|---|---|---|---|
| | unitless | unitless | unitless |
| The Third Levelling of Bulgaria /1975-1984/ | 0.349 | 0.348 | 0.990 |
| The Second Levelling of Finland /1935-1955/ | 0.104 | 0.095 | 0.997 |
| The Third Levelling of Finland /1978-2006/ | -0.006 | -0.006 | 0.993 |

**Table 5.** Regression results concerning the relationship in the form $|W| = a + b.\sqrt{L}$.

| Network | Coefficients | St. Error | t Stat | P-value |
|---|---|---|---|---|
| | a(mm), b(mm/L$^{0.5}$) | a(mm), b(mm/L$^{0.5}$) | unitless | unitless |
| The Third Levelling of Bulgaria /1975-1984/ | a = -8.998 | 18.126 | -0.496 | 0.625 |
| | b = 1.583 | 0.931 | 1.701 | 0.104 |
| The Second Levelling of Finland /1935-1955/ | a = 6.430 | 14.487 | 0.444 | 0.663 |
| | b = 0.227 | 0.633 | 0.358 | 0.725 |
| The Third Levelling of Finland /1978-2006/ | a = 14.421 | 10.815 | 1.333 | 0.194 |
| | b = -0.016 | 0.521 | -0.031 | 0.976 |

According to Table 4, the correlation among quantity pairs $|W| \leftrightarrow L$ and $|W| \leftrightarrow \sqrt{L}$ is practically equal in the case of the analyses here levelling networks. Correlation coefficients are 0.35, 0.10 and -0.01 for the Third levelling of Bulgaria data, for the Second levelling of Finland data, and for the Third levelling of Finland data, respectively. According to Table 5, the regression coefficients $b$ are not significant at 95% level. Thus, at 95% significance level we can state that there is no statistical relationship between $|W|$ and $\sqrt{L}$. This conclusion is also valid for the relationship between $|W|$ and $L$.

## DISCUSSION

Are the presented results unexpected? In fact, they are not. According to [3], the errors in the precise levelling "are divided into two classes, accidental and systematic, which are assumed to be independent of each other. The accidental errors are caused by sources that are independent in all successive observations and obey the laws of Gauss. The systematic errors are due to causes acting in a similar manner on successive or adjacent levelling observations; these do not obey the laws of Gauss. They become accidental only for distances exceeding a certain limit Z of order of several tens of kilometres. The total error is the combined influence of both types of errors and is calculated for distances longer than the above limit as the quadratic sum of the accidental and systematic errors".

This Kääriäinen's thought implies that for distances exceeding a certain limit Z of several tens of kilometres the systematic effects of some factors vanished and / or some systematic effects neutralize others once. As a result, the accumulation of errors along

levelling routes longer than a hundred kilometres, such as the case of levelling loops in the precise levelling networks, has a stochastic nature. Consequently, the closing errors in the precise levelling loops, which are in fact true errors, has accidental nature and do not have relationships to factors similar to the loop circumferences $L$ or to the square root of the loop perimeters $\sqrt{L}$.

The results of our analysis fully support the above conclusion. The coefficient of determination is the proportion of the variation in the dependent variable Y that is predictable from the independent variable X. The coefficient of determination is equal to square of the coefficient of correlation [6]. Therefore, according to the results presented by Table 4, we can calculate that the coefficients of determination of the variation of the absolute values of the closing errors of the loops $|W|$ in the analysed here networks can be explained on 12.3%, 1.1% and 0.0% by the loop circumferences $L$ or their square root $\sqrt{L}$. The cited values of the determination coefficients are respectively for the Third levelling of Bulgaria, the Second levelling of Finland, and for the Third levelling of Finland.

Based on the discussed facts, one cannot take as a great surprise that the closing errors of the outer loops in the Third levelling of Bulgaria and the Second levelling of Finland are significantly less than the closing errors of some loops with shorter circumferences in the analysed networks. The circumferences of these loops are 2550.18 km and 2890.46 km, but their closing errors are 2.85 mm and 16.17 mm, respectively.

## CONCLUSION

In this article, we analysed the data of three national precise levelling campaigns, those of the Third levelling of Bulgaria /1975-1984/, the Second levelling of Finland /1935-1955/, and the Third levelling of Finland /1978-2006/. As one can see that the period, which covers both Finland's campaigns, is more than 70 years. During this time, the spirit levels were changed by automatic digital levels. Many systematic errors, which deteriorate the accuracy of the precise levelling observations, have been studied and appropriate corrections in measurement results were applied [3, 8]. Regardless of all these improvements in the levelling equipment and the methodology of performance of the observations there is something in common between the data of both levelling campaigns, i.e., the relationship between the loop circumferences and the loop closing errors. Despite the difference in climate and mountain conditions between Bulgaria and Finland, the conclusions about accumulations of the loop closing errors $|W|$ in respect to the loop circumferences $L$ or their square root $\sqrt{L}$ in both countries are identical. All these facts bring the additional weight to the conclusion that, the loop closing errors $|W|$ do not have to be described by the right proportion of $\sqrt{L}$. Consequently, the limits of the form (3) and a priori accuracy calculated by the formula (4)[3, 7, 8] should be revised.

$$W = \pm const.\sqrt{L} \tag{3}$$

$$m_w = \pm\sqrt{\frac{1}{n_w+1}.\left(\left[\frac{W^2}{L}\right]+\frac{W_e}{L_e}\right)}, \tag{4}$$

In equation (5) the following notation are applied:

$m_w$ – the mean standard error based on the closing errors in the loops;

$n_w$ – the number of the inner loops in the network;

$W_e$ – the closing error of the outer loop;

$L_e$ - the circumference of the outer loop.

Analyzing the standard error of the adjusted geopotential numbers of the nodal benchmarks in the Second levelling of Finland [3, Table VIII, p.88] it is obvious that their values do not correspond with the levelling accuracy based on formula (4), which was calculated to be 0.60 mgpu/$\sqrt{L}$. The same conclusion is also valid for the standard errors of the adjusted geopotential numbers of the nodal benchmarks in the Third levelling of Finland [7, Formula (6.18), Figure 6.3]. Therefore, the new criterion about the limits (3) and the assessment of the levelling accuracy should be created on basis of the available precise levelling data and modern stage of the statistics and computer technologies.

## REFERENCES

[1] Gospodinov S., Stereva K., Determining of areas on the territory of R Bulgaria with a low intensity of the recent vertical movements of the Earth`s crust, 20th International Scientific Multidisciplinary Conference on Earth and Planetary Sciences SGEM 2020, Albena, Bulgaria, 2020

[2] Gospodinov S., Peneva E., P. Penev, A specific approach to least squares adjustment of the state levelling network, 22nd International Multidisciplinary Scientific GeoConference SGEM 2022, Albena, Bulgaria, 2020, https://doi.org/10.5593/sgem2022/2.1/s09.20

[3] Kääriäinen E., The Second Levelling of Finland in 1935–1955, Publications of the Finnish Geodetic Institute No. 61, Helsinki, 1966

[4] Kunchev I., On standards and specifications for vertical control surveys, Annual of the University of Architecture, Civil Engineering and Geodesy – Sofia, Vol. 54, Issue 2, pp. 253 – 262, 2021, ISSN 1310-814X, ISSN 2534-9759 (on-line), in Bulgarian

[5] Peneva E., On the implementation of the European Vertical Reference System in Bulgaria, 21th International Multidisciplinary Scientific Geo Conference Surveying, Geology and Mining, Ecology and Management (SGEM 2021). Conference proceedings 2021, Albena, Bulgaria, 14 – 22 August, 2021, ISSN 1314-2704, doi.org/10.5593/sgem2021/2.1/s09.48

[6] Montgomery D., G. Runger, Applied Statistics and Probability for Engineers (6th ed.), Wiley, 2014, ISBN-13 9781118539712

[7] Saaranen V., Lehmuskoski P., Takalo M., P. Rouhiainen, The Third Precise Levelling of Finland. FGI Publications No. 161, Kirkkonummi, 2021, ISBN 978-951-48-0266-9 (print), ISSN 2342-7353 (online)

[8] Specifications for precise levelling I and II order, GUGK, 1980, Sofia, in Bulgarian

[9] Tsanovski Y., GNSS Measurements for the Needs of Precise Height Determinations in Bulgaria, Annual of the University of Architecture, Civil Engineering and Geodesy – Sofia, Vol. 54, Issue 2, pp. 211 –218, 2021, ISSN 1310-814X, ISSN 2534-9759 (on-line), in Bulgarian

# A SUSTAINABLE APPROACH TO GEOMATIC METHODS IN GULLY MONITORING AND ASSOCIATED NATURAL DISASTER PREVENTION

**Mircea Vasile Bondrea**[1]

**Virgil Mihai Rădulescu**[1]

**Sanda Marioara Naș**[1]

**Raluca Claudia Galgau**[1]

**Adrian Traian Rădulescu**[1]

[1]Technical University of Cluj Napoca, **Romania**

## ABSTRACT

This paper presents the monitoring of an eroding phenomenon (gully) near Ciurila, Cluj County, Romania, using UAV (Unmanned Aerial Vehicle) and GNSS (Global Navigation Satellite System) technologies. In this sense, the monitoring results through sustainable and non-invasive technologies are presented, following four cycles of observations, carried out between June 2019 and April 2021. The paper aims to present the advantages and limitations of such a study, as well as the importance of monitoring erosion phenomena (in this case, gullies) for the ecosystem, but also the nearby inhabitants. Software and technologies are used that allow the automatic calculation of the volume of the gully and the displacements between the different measurement cycles, which allows for obtaining objective conclusions and proposing further measures. The paper aims to present a complete cycle of interpretation of the results, from the point of view of the volume calculations and the differences between the measurement cycles. Cost-effective solutions are addressed and presented, to present a complete measurement-analysis-interpretation cycle that will contribute to the early identification of landslides that occur in gully areas. The chosen area is significant from the point of view of its proximity to Cluj Napoca, the second largest city in Romania, as well as its proximity to the inhabited area of Ciurila, which makes this area an area with potential danger for the living environment and safety citizens.

**Keywords:** UAS, Gullies, monitoring

## INTRODUCTION

The purpose of this article is to bring to attention the importance of monitoring a gully created in the aftermath of the erosion process, taking into consideration the risk that it presents to the nearby community, as well as the effect it has on agriculture in the area.

This gully caught our attention during a field visit, primarily due to its proximity to an inhabited area, but also due to the phenomenon of accelerated erosion that it manifests.

Accelerated erosion is defined as an increased rate of erosion above natural levels. This can be natural (for example, caused by hurricane damage) but is often caused directly or indirectly by human activities [1]. The landform that this study focuses on is a gully, the

largest landform created by erosion. The deep erosion process is due to the water that results from rain or snow melting. Furthermore, this study will also look at the surveying methods and the data processing and analysis. The United Nations Sustainable Development Goal No. 15 deals with life on land, with increased attention to the phenomena of erosion and desertification, so the authors wanted to choose some non-invasive and sustainable methods of surveying the details from the field.

Human beings are closely related to the natural ecological environment. With the development of the global economy, problems such as biodiversity reduction, aggravation of ecological disasters, and fragile ecological environment have become increasingly prominent [2]

## MATERIALS AND METHODS

The study area is in Romania, in Cluj County, near the village of Ciurila. Cluj County is situated in the north-western part of Romania, in the Hill Depression of Transylvania.

Going into further detail, the area of interest is located on the southern side of Feleacu Hill, in the Hășdate Depression **(Figure 1**). The studied gully spreads out over an 1170 square meters area, with the following linear dimensions: the valley floor is approximately 64 m long, the width ranging from 1 m at the top to 29 m at the knick point, and the height ranging from 0.2 m to 12 m, from initiation point to mouth. This study area has been chosen based on the next criteria: the gully should be active, there should exist accessibility up to the gully, and muster the necessary conditions for using a GNSS receiver and a drone. The area has been surveyed in a time range of almost two years (from June 2019 to April 2021). The gully has 3 big parts, as follows: the top of the gully (where the water trickles concentrate and facilitate the process of dislocation of materials), the guiding channel (the materials are transported through this channel, and where new materials are dislocated from the flanks of the gully, up to the mouth of the gully) and the alluvial cone (the place where the materials are deposited).

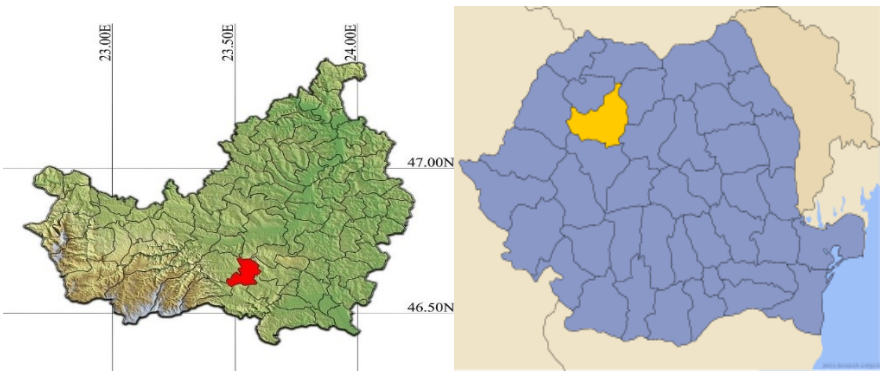


**Figure 1.** The Geographical position of the studied area within Cluj County, in Romania

The development of geomatics technologies now allows for the high-fidelity assessment of this aspect. These include Global Navigation Satellite System (GNSS) Total Stations + Levels precision, terrestrial and aerial photogrammetry, laser scanners with fixed stations, for each presenting technical data and products, analyzed sequentially and corroborated-complementary [3]. It has been decided that the surveying will be done using modern technologies, such as Global Navigation Satellite System (GNSS)

receivers and Unmanned Aerial Vehicles (UAV) – drones. It was decided that before carrying out the four measurement cycles, several six photogrammetric landmarks (GCP) would be established, the arrangement of which about the analyzed area can be seen in Figure 2.


**Figure 2.** The location of each GCP (Ground Control Point ) with red colour

The coordinates of the 6 landmarks were determined by GNSS (Global Satellite Navigation Satellite System) observations. The x and y coordinates of the points were determined in the National Stereo 70 Romania's Coordinate System, and the altimetric ones (z) in the National System "Black Sea 1975."

The figure below (Figure 3) shows the coordinates of the points, as well as the error (deviation) between the points determined by GNSS and the points subsequently resulting from the orthophoto plan generated from the images taken with the drone.

| Point no. | GNSS coordinates | | | UAV ortophotomap coordinates | | |
|---|---|---|---|---|---|---|
| | X (m) | Y (m) | Z (m) | X (m) | Y (m) | Z (m) |
| R7 | 572823,874 | 389177,235 | 631,416 | 572823,889 | 389177,229 | 631,396 |
| R8 | 572799,486 | 389160,146 | 633,272 | 572799,524 | 389160,153 | 633,261 |
| R9 | 572813,315 | 389029,754 | 632,647 | 572813,287 | 389029,725 | 632,656 |
| R10 | 572913,955 | 389072,022 | 614,608 | 572913,970 | 389072,068 | 614,661 |
| R11 | 572900,155 | 389094,105 | 619,694 | 572900,157 | 389094,106 | 619,718 |
| R12 | 572876,399 | 389118,232 | 624,487 | 572876,410 | 389118,237 | 624,502 |

| Point no. | ΔX (m) | ΔY (m) | ΔZ (m) |
|---|---|---|---|
| R7 | 0,015 | -0,006 | -0,020 |
| R8 | 0,038 | 0,007 | -0,011 |
| R9 | -0,028 | -0,029 | 0,009 |
| R10 | 0,015 | 0,046 | 0,053 |
| R11 | 0,002 | 0,001 | 0,024 |
| R12 | 0,011 | 0,005 | 0,015 |

**Figure 3.** The coordinates of the determined photogrammetric landmarks: at the bottom has presented the difference of coordinates between the determined GNSS points and those generated from the orthophotoplan obtained following the processing of the images taken by UAV. **The x and y coordinates of the points were determined in the National Stereo 70 Romania's Coordinate System, and the altimetric ones (z) in the National System "Black Sea 1975."**

We have calculated the volume that should have accumulated or been dug and compared it to the value obtained from the C0-C3 comparison.

The mean has been calculated with the formula:

$$V_{calculated} = \frac{V_{C1} \cdot \Delta t_1 + V_{C2} \cdot \Delta t_2 + V_{C3} \cdot \Delta t_3}{\Delta t_1 + \Delta t_2 + \Delta t_3}$$

The difference between volumes has been determined as:

$$\Delta V = V_{calculated} - V_{measured}$$

The erosion caused by water is the cause of many damaging events, such as loss of organic matter in the soil, degradation of soil structure, compaction of soil, reduced infiltration of water, reduced supply in the underground water, loss of the upper layer of soil, loss of nutritional substances from the soil, the creation of trickles that can lead to the apparition of gullies, uprooting plants and reducing soil productivity [4]. "Land degradation here primarily refers to the loss of life-supporting land resources through a mix of processes that include soil erosion, soil compaction, destruction of soil structure, loss of soil organic matter, loss of vegetation cover, desertification, salinization, and acidification" [5]. The quality of the soil suffers the most from erosion, with repercussions affecting the fauna and flora and, in the end, affecting the quality of human life. To better understand the term soil quality and the implications it has in this research, the term must be firstly defined: "The notion of "soil quality" (often known as "soil health") is the ability of soil to work as a "living system" since it plays an active role in shaping the interaction between the biotic component (such as animals and plants) and the abiotic component (e.g., light, rocks, water, and air) of ecosystems. Soil quality is intended as "the capacity of a soil to function, within land use and ecosystem boundaries, to sustain biological productivity, maintain environmental quality, and promote plant, animal, and human health". Preserving soil quality is therefore essential to guarantee the balance between human intervention and the resilience of natural systems. Soil conditions affect the overall functioning of the ecological infrastructure they belong to, food and hydrogeological safety, biodiversity protection, the effects of climate change, and trade deriving from ecosystem services" [6]. The study, prevention, and amelioration of soil erosion is an issue of sustainable development. Humans must protect the existing ecosystems, therefore making sure that the flora and fauna are not damaged or destroyed by erosive events, as well as paving the way for future generations so that they can continue living on our planet. It is already agreed by the research community that "sustainability" must be present in our studies, our policies, and our behavior as humans. "." Sustainability is essential for a straightforward reason: the quality of life and the Earth's ecosystems' prosperity cannot be maintained if it is not addressed." [7].

There are plenty of studies whose purpose is to monitor landslides and try to model their behavior, but there are only a few that do the same for gullies. A landslide and a gully have a lot of common characteristics, and some tell each other apart. The importance of monitoring such hazards is very well put in many research papers on landslides. "Geological disasters are responsible for the loss of human lives and for significant economic and financial damage every year. Considering that these disasters may occur anywhere - both in remote and/or in highly populated areas—and anytime, continuously monitoring areas known to be more prone to geohazards can help to determine preventive or alert actions to safeguard human life, property, and businesses" [8] We will try to conduct a comparison between the two hazards in an attempt to emphasize the importance of monitoring gullies and preventing further land degradation and economic losses. One of the key differences between a gully and a landslide is the trigger causing them. Landslides appear when the soil is replete with water and the

weight of the landmass is big enough that it can be moved by gravitational forces. Gullies, on the other hand, are the result of many trickles and streams of water carving the upper layers of the soil, detaching, and transporting sediments toward the alluvial cone. The semblance between landslides and gullies comes from their effect on the environment and the complexity of factors contributing to the evolution of these hazards. "Many factors affect landslides, such as topography, lithology, hydrology, rainfall, vegetation, and human activity. Such factors are known as causative or conditioning factors that have complex and nonlinear relationships" [9]. The same factors should be considered in the study of gullies.

The preliminary study of the area of interest has given us some insights into its topography and the causes that have led to the apparition and the expansion of the gully. The gully has emerged on a ground consisting of clay, sandy clay, and sand, dating from the Sarmatian Era. The soil in the area is brown eu-mesoblastic and brown luvic **(Figure 4)**. From a geomorphological point of view, the gully has appeared on a differential erosional depression with a hillocky aspect. It is located north of the Hăşdate Valley and the Ciurila Lake Complex. The vegetation is that of a hill and plateau meadow and the climate is continental temperate, with specific local phenomena, such as thermal inversion and the apparition of the föehn from the Apuseni Mountain. [10,11]

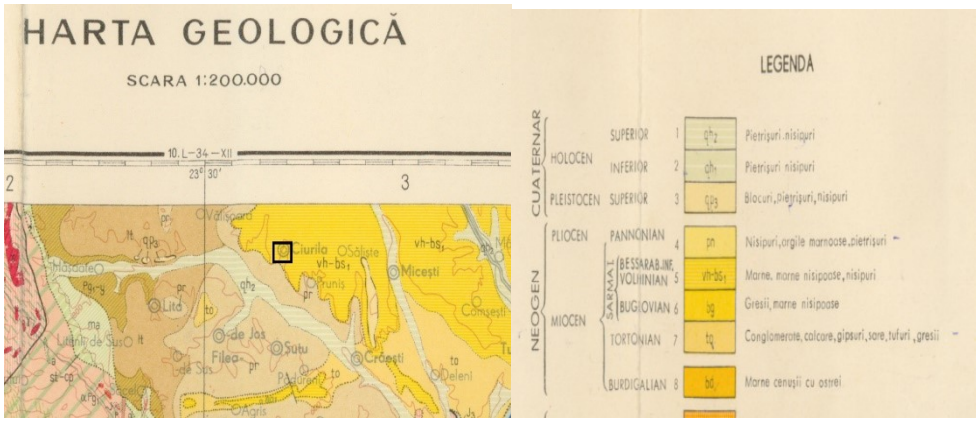


**Figure 4** Geological map of the area, with the studied area, highlighted, represented with yellow, which, according to the legend of the map, means an area with soils in the category of "sands, marly clays, gravels".

Since the object of this study is the monitoring of the erosion phenomenon, we have used recurrent surveys for data acquisition, specific to the land monitoring discipline.

**Table 2.** The programming of the surveys and drone flights.

| Name and code | Date | Instrument |
|---|---|---|
| Cycle 0 – C0 | 28.06.2019 | GNSS Receiver |
| Cycle 1 – C1 | 23.09.2019 | GNSS Receiver |
| Flight 1 – F1 | 18.10.2019 | UAV |
| Cycle 2 – C2 | 15.09.2020 | GNSS Receiver |
| Flight 2 – F2 | 15.09.2020 | UAV |
| Cycle 3 – C3 | 06.04.2021 | GNSS Receiver |

## RESULTS

The surveying methods used for data collection are modern topographical methods. These methods present many advantages compared to classical methods, in terms of time, economy, and precision. The methods used for monitoring our gully are the same that can be used for landslide monitoring, another similarity that can be associated with both landslides and gullies.

Two widely spread methods have been used for the survey: GNSS for surveying detailed points and photogrammetry for acquiring a larger set of data that complements the detailed points. Field surveys and visual interpretation of aerial photographs are the prevailing methods to map landslides. However, the mentioned approaches are limited because of the accessibility to remote areas for field surveys. Moreover, these approaches depend on the visual interpretation of expert experience and knowledge [12]

GNSS is used to define all the navigation systems that are based on satellites. Topographers use GNSS receivers to determine the coordinates of one or more points located on Earth's surface with precision, in each coordinate system. "Since 1990, global navigation satellite systems (GNSS) have been frequently used to monitor landslides, enabling researchers to determine landslide kinematics, by measuring displacements of a few centimeters working in differential mode. GNSS surveys are usually carried out with a given frequency (i.e., monthly, weekly) and results are discontinuous over time, and related to the cumulative movements of surface points" [13]. GNSS overviews are as a rule carried out with a given recurrence (i.e., month to month, week by week) and comes about are spasmodic over time and related to the total developments of surface points" [13]. GPS methods are broadly utilized in Romania for the observing of slope solidness and avalanche risks but inquire about appears a few confinements to utilizing this method. "Many conventional checking procedures, such as the Global Satellite Network (GPS) and leveling methods, are executed on possibly unsteady hillslopes to get surface misshapen, which can somewhat diminish financial losses and human casualties. However, limited ground monitoring equipment still hardly meets the demand of landslide warnings, especially in mountainous regions where numerous sudden landslides occur." [14]

Therefore, new methods need to be developed and used, methods that have fewer limitations and better efficacy. Airborne photogrammetry is such a method. Though photogrammetry has existed as a method for the past 150 years, only recently has it begun to be widely used in various fields. "Photogrammetry, as its name implies, is a three-dimensional coordinate measuring technique that uses photographs as the fundamental medium for metrology or measurement. The fundamental principle used in photogrammetry is triangulation. By taking photographs from at least two different locations, so-called 'lines of sight' can be developed from each camera to point on the object. These lines of sight, sometimes called rays owing to their optical nature, are mathematically intersected to produce the three-dimensional coordinates of the points of interest" [11]. With the apparition and development of UAVs and numerous cameras and sensors that can be attached to them and the accessible price of such technology, UAV photogrammetry has taken on a very large palette of topographical works, hazard monitoring being one of them. It has been used in plenty of studies on landslides, therefore it is worth using in the monitoring of a gully. "Airborne photogrammetry has also been used in subsidence and landslide studies to analyze individual ground

movements or wider regions. In these studies, digital terrain models (DTMs) or digital surface models (DSMs) are calculated using automatic correlation techniques" [15].

The GNSS receiver used was GeoMax Zenith10, accompanied by the Getac PS236 PDA. The drone used was the DJI Mavic 2 Enterprise, a UAV that has a photo-video camera and a built-in GNSS receiver.

The topographical method used for the ground survey was the section method. This method has been chosen after studying the landform in the land exploration phase. Because the gully has a transversal V-section, we have decided that we could recreate it best using multiple sections in key points. The key points have also been chosen during exploration. They were the points in the valley floor where we identified falls. To render the valley floor and its development, we have also surveyed points in the valley floor and later created its longitudinal section. The points chosen for both the transversal and the longitudinal sections are slope-changing points.

For processing the data obtained, multiple software has been used, such as AutoCAD 2021, TopoLT 14, Agisoft Metashape Professional 1.7.5, and Global Mapper 22. TopoLT 14 is a local (Romanian) extension to AutoCAD created for topographers that helps automatize some of the stages of survey data processing. AutoCAD 21 and TopoLT 14 have been used for processing the data collected by the GNSS receiver: inserting the points at the right coordinates in the national coordinate system (STEREO70), creating the 3D surface, and the contour lines, creating the outline of the gully and drawing the sections.

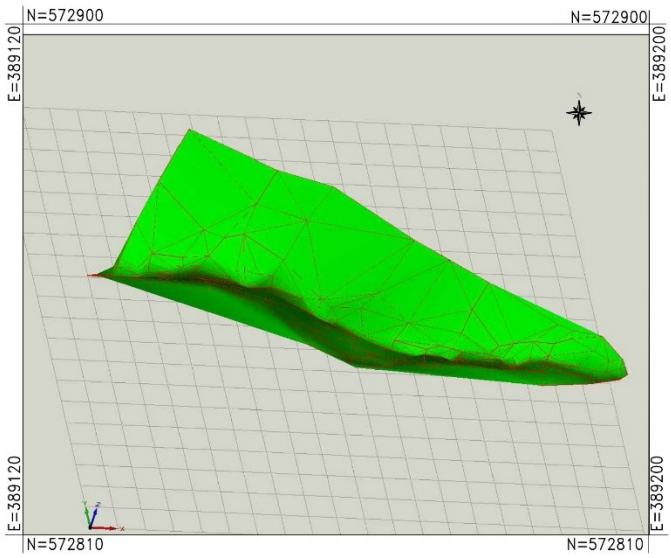


**Figure 5.** Georeferenced (Stereo70, Romanian Coordinate System) 3D Model obtained from GNSS survey.

Agisoft Metashape Professional 1.7.5. is the software that we used to process the images collected by the UAV, to create products that have been used in data analysis: the point cloud, the orthomosaic (Figure 6), the Digital Elevation Model (DEM) (Figure 7,8) and to export them in other formats. Global Mapper 22 has also been used for data analysis based on the orthomosaic and the DEM obtained in Agisoft Metashape Professional

1.7.5. We have created a watershed map to strengthen the conclusions derived from the mathematical analysis regarding the most affected erosion areas of the gully(Figure 12).

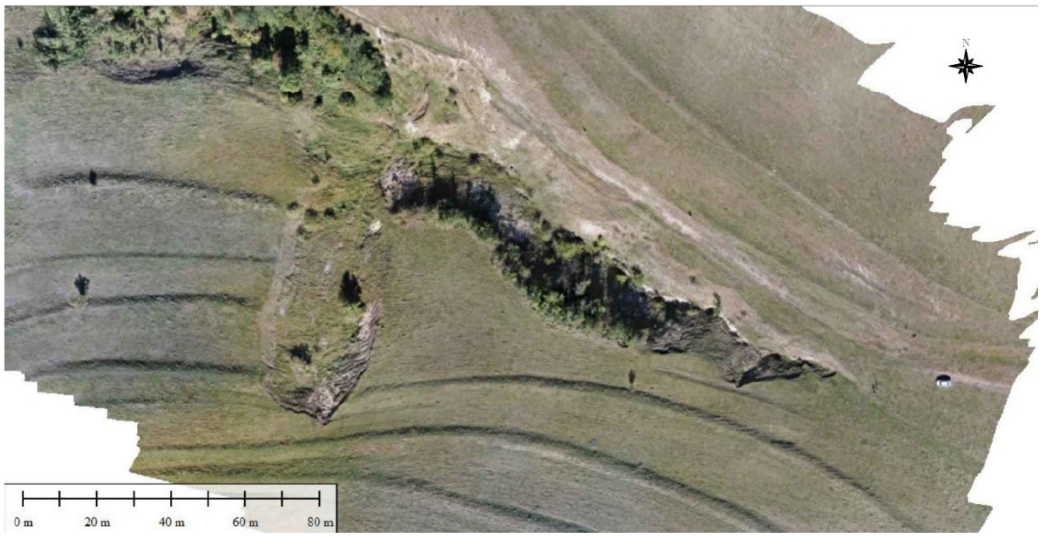


**Figure 6.** The orthophoto map (1:2000) resulted from the first drone flight above the surveyed area.

The mathematical analysis was done using Microsoft Excel, TopoLT 14 and the coordinate files obtained from the GNSS receiver, and the drone, and its purpose was to identify and quantify the relevant factors in the evolution of a gully. "Numerical modeling of slopes makes use of mathematical equations to solve the mechanical response of the unstable mass." [16]. To identify the parts of the gully where there have been significant clusters or deposed sediments of materials, by using Agisoft Metashape Professional 1.7.5. , our UAV photos and GCP (Ground Control Points) we generated the DEM (Digital Elevation Models) of the gully at each UAV flight. The resulting DEMs can be seen in Figure 7,8.

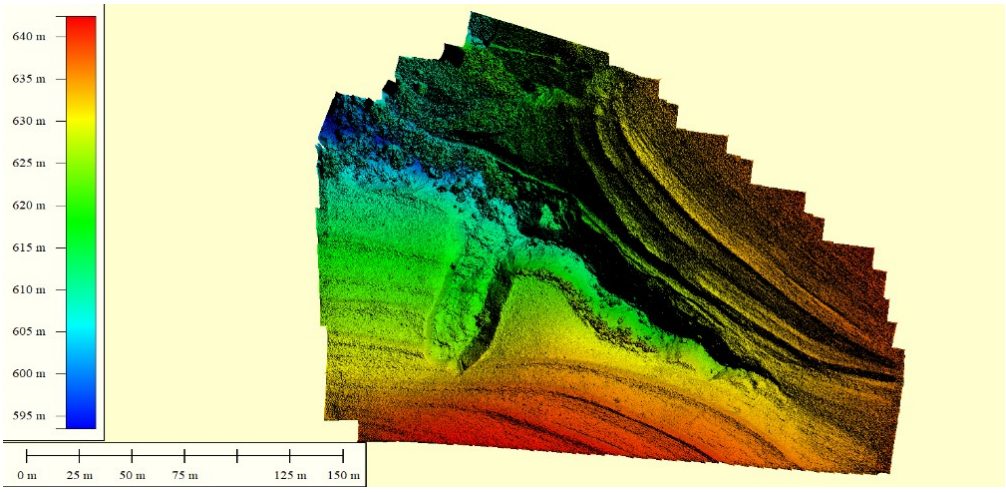


**Figure 7.** Digital Elevation Model generated after the first UAV flight.

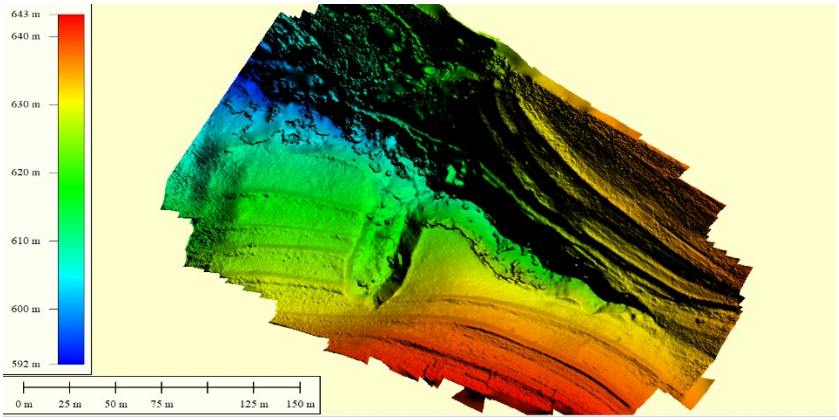


**Figure 8.** Digital Elevation Model generated after the second UAV flight.

We also calculated the slopes between our detail points and the average slope for each profile. The slope is the angle between the plane of the Earth's surface and the horizontal plane. The effects of gravity that determine the water flows and the materials removed vary depending on the slope (on higher slopes, the gravity and the speed of materials are more significant) [17].

The formulas used for calculation are the following:

$$p\% = {}^{\Delta H}/_{D} \cdot 100$$

$$p_m = \sum D \cdot p\% / \sum D$$

Where:

- p% - slope, in percentage
- ΔH – height difference between two consecutive points in the profile
- D – distance between two consecutive points in the profile
- $p_m$ – average slope

Using both the results from the mathematical calculations and the graphical results obtained from TopoLT and Agisoft Metashape Professional, we have done the following analyses: volume analyses, the correlation of volumes of materials and the quantity of precipitation, and the correlation of the watershed with the most active areas of the gully. The meteorological data used in this article has been downloaded from www.meteoblue.com. The data acquired from MeteoBlue is based on simulations and not on measurements because measured data could not be obtained for the desired period.

*3.1. Analysis of measured volumes*

We have started this analysis by considering the volumes as a linear function of time. We have analyzed the values obtained from consecutive cycles and the period between the two cycles considered and compared them to the values obtained from comparing the first and the last cycles (Figure 9,10).

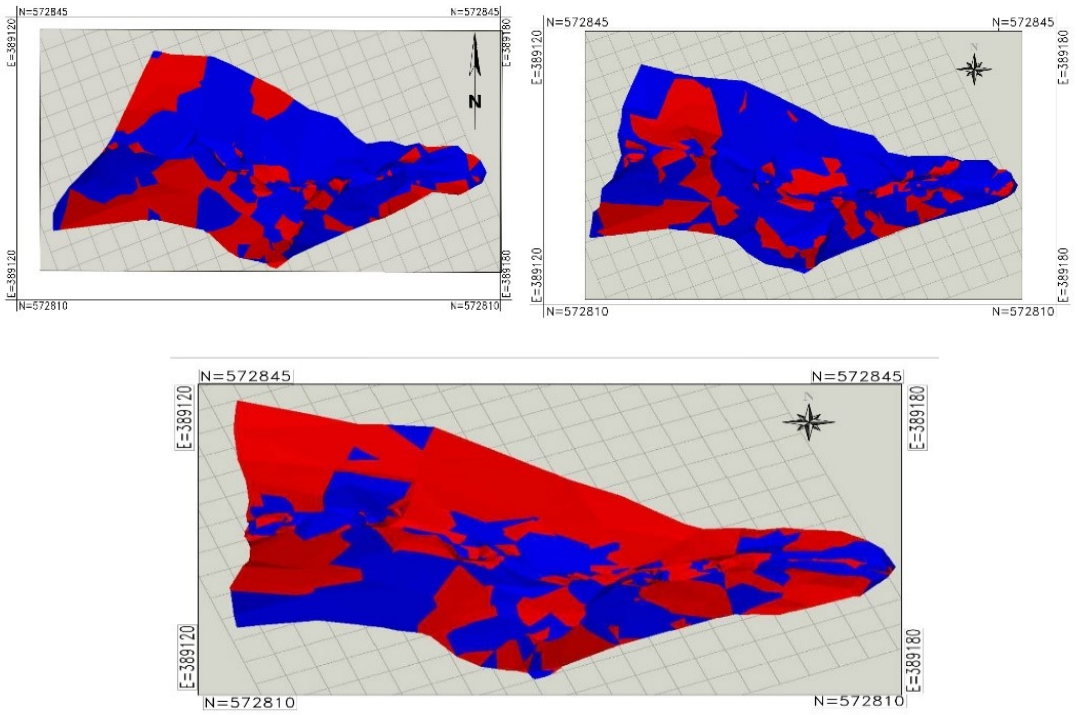


**Figure 9.** Volume comparisons between consecutive survey cycles: up left – comparison between C0 and C1; upright: comparison between C1 and C2; down – comparison between C2 and C3 (**red signifies sediment deposition and blue signifies loss**).

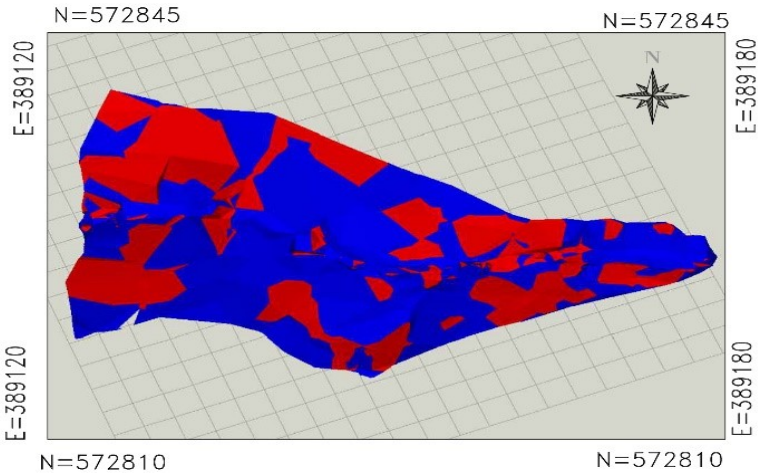


**Figure 10.** Volume comparisons between C0 and C3.

Between C0 and C1 we can identify the following regions where significant deposed sediments are located: the top of the gully and the middle of the north flank. On the opposite flank, an area of eroded sediments has been identified. Between C1 and C2, the most significant deposed sediments are identified on the south flank, while the north flank is characterized by generally eroded sediments. This changes between C2 and C3, where the north flank is characterized by deposed sediments, while on the south flank, the areas of deposed sediment and eroded sediment are opposed to the previous comparison, showing exactly how and where the materials have moved.

The guiding channel suffers the most radical changes between cycles, as it is continually modeled by the trickles of water and the materials transported. The valley floor is characterized by holes and falls, succeeded by clusters of materials. These changes can be best assessed by comparing the longitudinal profiles.

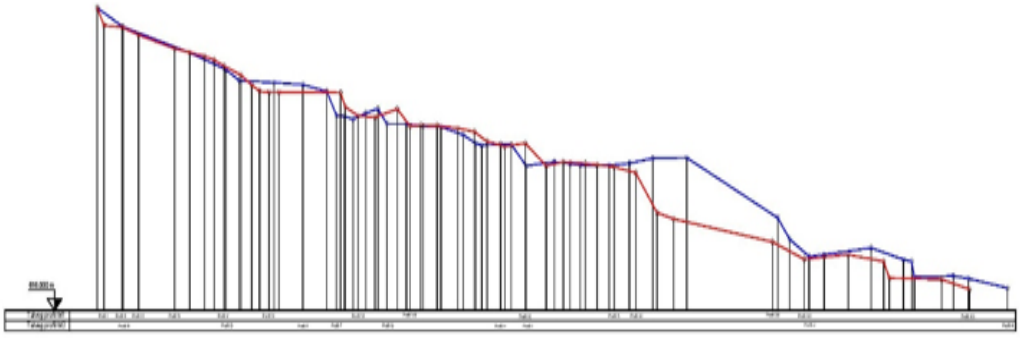

**Figure 11.** Comparison between the valley floor obtained from C0 (red) and C1 (blue).

The results shown in Figure 11 are based on the heights of points surveyed in C0 and C3, but after analyzing the results, they should also reflect the summing of height differences and volumes from all the surveying cycles. However, we have identified differences between the volumes obtained by summing the volumes obtained from every cycle and the volumes obtained from C0 and C3. These differences can be observed easily in Table 2.

**Table 2.** Volume comparisons.

| Comparison between | Cluster ($m^3$) | Deposed sediments ($m^3$) | Number of months between surveys |
|---|---|---|---|
| C0-C1 | 99.82 | -74.58 | 3 |
| C1-C2 | 61.63 | -139.46 | 12 |
| C2-C3 | 91.23 | -53.11 | 6 |
| Calculated volume | 75.54 | -105.52 | |
| C0-C3 (Measured volume) | 54.42 | -78.16 | |
| Difference | -21.12 | 27.36 | |

The differences between the calculated and the measured volumes could be explained by a multitude of factors, and we have considered the most suggestive of them depending on the type of volume. For the clusters, the negative difference is mostly owed to us not knowing the exact quantity of materials going from the gully to be deposited in the alluvial cone. That value cannot be precisely evaluated in this case because the alluvial cone serves two gullies. In the case of deposed sediments, the positive difference comes from the materials originating from outside of the gully that

are accumulated at a faster rate than the rate with which they can be dug. A significant number of sediments were redistributed within the gully itself.

*3.2. The watershed analysis*

Using the plans obtained from the drone flights, we have generated the watershed of the studied area (Figure 12).

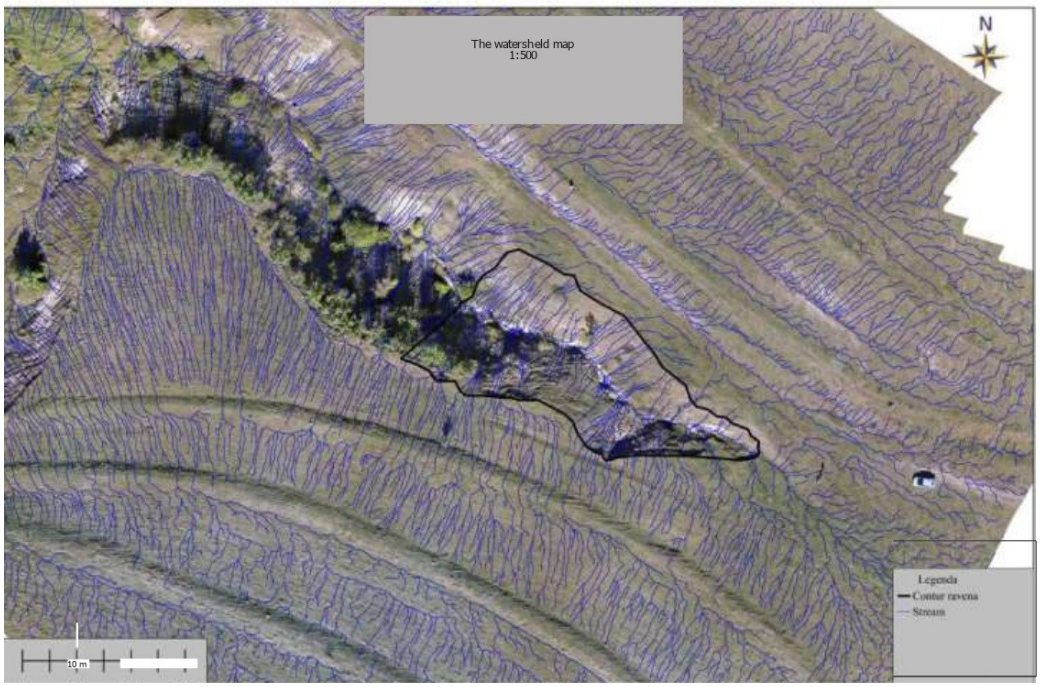


**Figure 12.** The watershed map. In thick black the analyzed contour of the ravine can be seen, in blue, it can be observed the watersheds.

The areas where the water channels are denser are the areas where the gully is most active, meaning that in those areas the clusters and the deposed sediments will be more prominent compared to other areas of the gully. As can be observed, a few trickles converge at the top of the gully, but on the left flank their density increases. Up to the middle of the left flank, these trickles reach a maximum density in an area that has already suffered major erosion (the gully has a v shape but goes outside of the V-shape in this massively eroded area). Furthermore, trickles are dense closer to the mouth of the gully, due to the very big slopes of the flanks in these areas (slopes of 80-85°). These areas can also be identified as the areas that change the most between cycle comparisons.

*3.3. The correlation between volumes of materials and the quantity of precipitation*

We have looked further into the matter and tried to correlate the measured volumes with the quantity of precipitation. We have considered precipitation as the most prominent factor in the expansion of the gully. The importance of rainfall in geological hazards has been previously emphasized in other research papers: “Rainfall usually increases the pressure heads in the slope and leads to a groundwater flow pattern change and a groundwater table rise” [16]. Therefore, we considered the quantity of materials dislocated as a direct result of the quantity of precipitation in a period. Based on the measured volumes and the monthly quantity of precipitation, we have determined a

mean value of materials clustered or dug for every l/m$^2$ of precipitation. The results of this analysis are presented in the following:

**Table 3.** Volume and precipitation correlation.

| | C0-C1 | C1-C2 | C2-C3 |
|---|---|---|---|
| Cluster volume (m$^3$) | 99.82 | 61.63 | 91.23 |
| Dug volume (m$^3$) | -74.58 | -139.46 | -53.11 |
| Time interval Δt (months) | 3 | 12 | 6 |
| Quantity of precipitation for period Δt (l/m$^2$) | 49.40 | 526.80 | 242.25 |
| Mean quantity of precipitation per month (l/m$^2$) | 16.47 | 43.90 | 40.38 |
| Monthly cluster volume for a mean quantity of precipitation (m$^3$) | 6.06 | 1.40 | 2.26 |
| Monthly deposed sediments volume for a mean quantity of precipitation (m$^3$) | -4.53 | -3.18 | -1.32 |

**Graph 1.** Volume and precipitation correlation

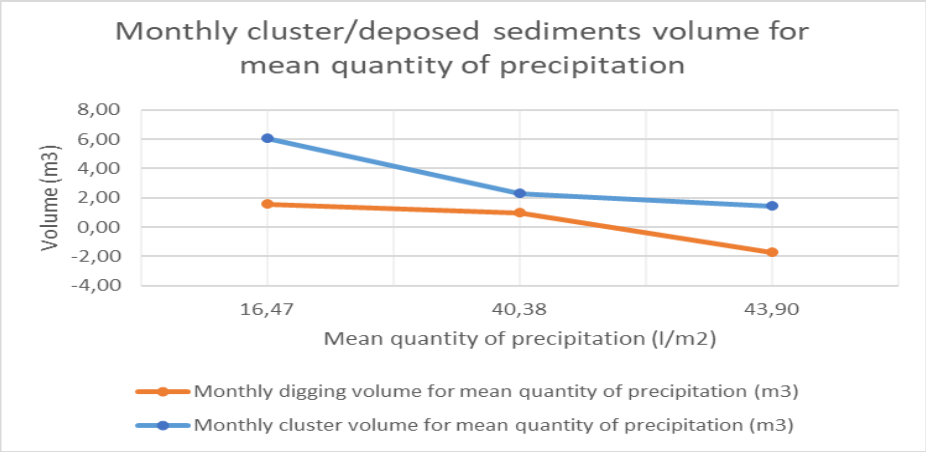


The hypothesis on which we started working was that there was a proportionality relation between the quantity of precipitation and the volumes (e.g. the bigger the quantity of precipitation, the bigger the deposed sediments and the smaller the cluster). However, this hypothesis has been proven wrong by the calculus and has left us to discuss the reasons behind this result and the impact the other factors have on the evolution of the gully. A significant number of sediments were redistributed within the gully itself.

## DISCUSSION

As the calculations have shown, modeling the gully based on two major factors can lead to results that show the evolutionary trend of the phenomenon of accelerated erosion. International research papers on soil erosion and subsidence monitoring can show us new methods that we can try to integrate into future studies of the erosion process. Different methods have been used in other research papers, as follows: Owing to the mechanism of landslides, understanding the major triggering factors and modeling their spatial probability have been challenging tasks, mainly researched through statistical and heuristic approaches [18]. These approaches are usually constructed using linear correction analysis between historical landslides and predisposing factors. [19].

Using different data acquisition methods can also improve the results of our study, to reduce the time spent in the field, without reducing the quality of the data. Traditional methods of gullies detection are commonly based on field surveys, in situ measurements, and visual analysis produced by an expert.To a certain degree, the results obtained are highly influenced by the knowledge and qualification of an expert. The adoption of remote sensing techniques for gullies detection has great advantages compared to field surveys. At the regional level, to solve problems associated with mudflow hazards, Earth Remote Sensing (ERS) data from satellites (multispectral and radar) are often used, the advantage of which is accessible to any territory, and the absence of the need for terrestrial field research [20]

There are also different analyses that we can perform and compare to our results. For example, we could use an old approach defined as “modern techniques encompassed morphometrical analysis of DEMs and interpretation of aerial photographs, orthoimages, and hillshade models in a GIS environment, along with analysis of terrain 3D models to extract virtual measurements and better observe the morphological features” [21].

The water trickles originate from outside of the gully and only converge in the gully, bringing along with them alluvial deposits from their course. That is how materials that are not original to the gully’s body end up being transported in the gully. The quantity of these materials cannot be precisely evaluated.

The quantity of precipitation alone cannot be correlated precisely with the dislocated and accumulated volumes. For example, knowing at what point the ground is saturated with water would prove very useful for further analysis. There are other unquantifiable factors related to precipitation that we consider factors in the behavior of the gully, such as the intensity and direction of precipitation. Other meteorological factors that are hard to quantify are the effect snow has on the terrain (the number of days in which there is snow, its mass, or how much of the snow infiltrates the ground and saturates it) and the freeze-unfreeze phenomenon, which results in rock disaggregation. Another possible factor can be the type of weather preceding the rains, as has been observed in a study in Northern Italy: “The erosive events characterized by low cumulated rainfall were always preceded by dry periods (at least a week). [22].

## CONCLUSIONS

A gully is a rapidly changing form of relief that undergoes drastic changes in a short period. This destructive nature of the form can prove to be a danger, both for the

agriculture in the neighboring area and for the village located a few hundred meters from the gully. A geological study of the area of interest can be recommended to increase the accuracy of this study and to identify solutions to improve the affected land. Having a total station, a GNSS system, and a UAV, we chose to use it to perform GNSS and UAV measurements. The reason was that the two types of equipment provided an accuracy close to the determination of the total station and we chose an accuracy obtained quickly, sufficient to study a phenomenon with such an accelerated development.

The field measurements took a short amount of time (a few hours for GPS and about 30 minutes for UAV), compared to the time we would have spent if we had to use a total station. The number of operators has also been reduced, from a minimum of 2 for the total station to one for both GPS and UAV. The post-processing time was also reduced, as we already had the GPS and UAV coordinates, while with a total station, we would have had to calculate the coordinates before entering them into the analysis. There was no need for static GNSS observation sessions or post-processing of points, as the accuracy obtained (2-3 cm) was sufficient to study a phenomenon with accelerated horizontal and vertical movements (of the order of meters/year).

We used the most modern methods available to us, and the results were satisfactory for the data we had available. Future studies will be performed by placing permanent sensors in key points of the gully, which can measure the movements in real-time. It is the idea that we intend to realize in a future study. Moreover, the monitoring of a gully is a long-term effort and can be done continuously, combining the methods already used with the newest ones, giving us perspectives on the accuracy of these. methods.

**Author Contributions:** All authors have contributed equally to the work.

**Funding:** This research benefited from funding from the TUCN Development Program

**Data Availability Statement:** The data presented in this study are available on request from the corresponding author.

**Conflicts of Interest:** The authors declare no conflict of interest.

## REFERENCES

[1] Park,C.,A Dictionary of Environment and Conservation (1 ed.), Oxford University Press, 2007, DOI: 10.1093/acref/9780198609957.001.0001

[2] Jin, X.; Wei, L.; Wang, Y.; Lu, Y. Construction of ecological security pattern based on the importance of ecosystem service functions and ecological sensitivity assessment: A case study in Fengxian County of Jiangsu Province, China. Environ. Dev. Sustain. 2021, 23, 563–590.

[3] Radulescu , V.M. ; Radulescu , G.M.T. ; Nas , S. ; Radulescu , A.T. ; Bondrea , M.V. ; Radulescu , C.M. , Synthetic Analysis Of Geoinformatics Technologies For Preservation Of Cultural Heritage, Methodological Approach , JOURNAL OF APPLIED ENGINEERING SCIENCES 2021 , DOI : 10.2478/jaes-2021-0005

[4] https://esdac.jrc.ec.europa.eu/projects/SOCO/FactSheets/RO%20Fact%20Sheet.pdf , (accessed on October 27th , 2021)

[5] Ewunetu, A.; Simane, B.; Teferi, E.; Zaitchik, B.F. Mapping and Quantifying Comprehensive Land Degradation Status Using Spatial Multicriteria Evaluation Technique in the Headwaters Area of Upper Blue Nile River. Sustainability 2021, 13, 2244. https://doi.org/10.3390/su13042244

[6] Nickayin, S.S.; Perrone, F.; Ermini, B.; Quaranta, G.; Salvia, R.; Gambella, F.; Egidi, G. Soil Quality and Peri-Urban Expansion of Cities: A Mediterranean Experience (Athens, Greece). Sustainability 2021, 13, 2042. https://doi.org/10.3390/su13042042

[7] Szabo, Z.K.; Szádoczki, Z.; Bozóki, S.; Stănciulescu, G.C.; Szabo, D. An Analytic Hierarchy Process Approach for Prioritisation of Strategic Objectives of Sustainable Development. Sustainability 2021, 13, 2254. https://doi.org/10.3390/su13042254

[8] Sousa, J.J.; Liu, G.; Fan, J.; Perski, Z.; Steger, S.; Bai, S.; Wei, L.; Salvi, S.; Wang, Q.; Tu, J.; Tong, L.; Mayrhofer, P.; Sonnenschein, R.; Liu, S.; Mao, Y.; Tolomei, C.; Bignami, C.; Atzori, S.; Pezzo, G.; Wu, L.; Yan, S.; Peres, E. Geohazards Monitoring and Assessment Using Multi-Source Earth Observation Techniques. Remote Sens. 2021, 13, 4269. https://doi.org/10.3390/rs13214269

[9] Pradhan, B.; Sameen, M.I.; Al-Najjar, H.A.H.; Sheng, D.; Alamri, A.M.; Park, H.-J. A Meta-Learning Approach of Optimisation for Spatial Prediction of Landslides. Remote Sens. 2021, 13, 4521. https://doi.org/10.3390/rs13224521

[10] Multiple aut., Geografia României I. Geografia fizică, Editura Academiei Republicii Socialiste România, București, 1983,113-114

[11] Multiple aut., Geografia României III. Carpații Românești și Depresiunea Transilvaniei, Editura Academiei Republicii Socialiste România, București, 1987, 57-58

[12] Shahabi, H.; Rahimzad, M.; Tavakkoli Piralilou, S.; Ghorbanzadeh, O.; Homayouni, S.; Blaschke, T.; Lim, S.; Ghamisi, P. Unsupervised Deep Learning for Landslide Detection from Multispectral Sentinel-2 Imagery. Remote Sens. 2021, 13, 4698. https://doi.org/10.3390/rs13224698

[13] Zárate, B.A.; El Hamdouni, R.; Fernández, T. GNSS and RPAS Integration Techniques for Studying Landslide Dynamics: Application to the Areas of Victoria and Colinas Lojanas, (Loja, Ecuador). Remote Sens. 2021, 13, 3496. https://doi.org/10.3390/rs13173496

[14] Yang, D.; Qiu, H.; Zhu, Y.; Liu, Z.; Pei, Y.; Ma, S.; Du, C.; Sun, H.; Liu, Y.; Cao, M. Landslide Characteristics and Evolution: What We Can Learn from Three Adjacent Landslides. Remote Sens. 2021, 13, 4579. https://doi.org/10.3390/rs13224579

[15] Josh Horswell, Encyclopedia of Forensic Sciences, Pages 368-371, Academic Press, 2013

[16] Necula, N.; Niculiță, M.; Fiaschi, S.; Genevois, R.; Riccardi, P.; Floris, M. Assessing Urban Landslide Dynamics through Multi-Temporal InSAR Techniques and Slope Numerical Modeling. Remote Sens. 2021, 13, 3862. https://doi.org/10.3390/rs13193862

[17] Ramos-Bernal, R.N.; Vázquez-Jiménez, R.; Cantú-Ramírez, C.A.; Alarcón-Paredes, A.; Alonso-Silverio, G.A.; G. Bruzón, A.; Arrogante-Funes, F.; Martín-González, F.; Novillo, C.J.; Arrogante-Funes, P. Evaluation of Conditioning Factors of

Slope Instability and Continuous Change Maps in the Generation of Landslide Inventory Maps Using Machine Learning (ML) Algorithms. Remote Sens. 2021, 13, 4515. https://doi.org/10.3390/rs13224515

[18] Dai, X.; Schneider-Muntau, B.; Fellin, W.; Franco, A.; Gems, B. Engineering-Geological Analysis of a Subaerial Landslide in Taan Fiord, Alaska. Remote Sens. 2021, 13, 4258. https://doi.org/10.3390/rs13214258

[19] Kavzoglu, T.; Teke, A.; Yilmaz, E.O. Shared Blocks-Based Ensemble Deep Learning for Shallow Landslide Susceptibility Mapping. Remote Sens. 2021, 13, 4776. https://doi.org/10.3390/rs13234776

[20] Gantimurova, S.; Parshin, A.; Erofeev, V. GIS-Based Landslide Susceptibility Mapping of the Circum-Baikal Railway in Russia Using UAV Data. Remote Sens. 2021, 13, 3629. https://doi.org/10.3390/rs13183629

[21] Gaidi, S.; Galve, J.P.; Melki, F.; Ruano, P.; Reyes-Carmona, C.; Marzougui, W.; Devoto, S.; Pérez-Peña, J.V.; Azañón, J.M.; Chouaieb, H.; Zargouni, F.; Booth-Rea, G. Analysis of the Geological Controls and Kinematics of the Chgega Landslide (Mateur, Tunisia) Exploiting Photogrammetry and InSAR Technologies. Remote Sens. 2021, 13, 4048. https://doi.org/10.3390/rs13204048

[22] Stanchi, S.; Zecca, O.; Hudek, C.; Pintaldi, E.; Viglietti, D.; D'Amico, M.E.; Colombo, N.; Goslino, D.; Letey, M.; Freppaz, M. Effect of Soil Management on Erosion in Mountain Vineyards (N-W Italy). Sustainability 2021, 13, 1991. https://doi.org/10.3390/su1304199

# ALGORITHM FOR THE TRANSFORMATION OF THE COORDINATES NEEDED TO SET OBJECTIVES EXTENDING OVER LARGE AREAS

**Lecturer Dr. Eng. Doina Vasilca**[1]

**Eng. Oana-Mihaela Biscoveanu**[1]

[1]Technical University of Civil Engineering Bucharest, **Romania**

## ABSTRACT

Constructions extending over large areas or distances raise problems regarding their setting out, because these elements are determined in the official projection of Romania, namely the 1970 Stereographic map projection. For the territory of our country, this produces distortions from -25 cm/km to approximately +64 cm/km in terms of distances and between -5 sq. m/ha and +12.76 sq. m/ha in terms of areas, depending on the distance from the projection pole and, implicitly, from the circle of zero distortions. For them to be applied on the ground, the coordinates should be calculated in a local projection plane where such distortions are minimal.

In the present work, double map projections were studied in which the surface of the reference ellipsoid was first represented on the surface of a sphere, after which the sphere was represented on the plane using conic, cylindrical, and azimuthal conformal oblique projections. The tangent/secant almucantar was chosen to pass through the centre of the area of interest. Through comparing the distortion values in the studied projections, we determined that the lowest values were obtained in the oblique conformal conic projection.

Furthermore, we proposed an algorithm for converting the coordinates of the points calculated in the official projection of Romania, according to the regulations in force, to the coordinates obtained from a local projection plane, which can then be transposed directly onto the ground.

**Keywords:** setting out large constructions**,** map projection distortions, local projection plane

## INTRODUCTION

According to the legislation in force, the geodetic, topographic, photogrammetric, and cartographic works necessary for the national economy of Romania are performed in the 1970 Stereographic map projection and altitude system, having the Black Sea as the reference plane. When representing the entire territory of Romania, this particular cartographic projection produces linear distortions between -25 cm/km, in the pole of the projection (the point of $\varphi$=46ºN latitude and $\lambda$=25ºE longitude, located approximately in the centre of the country) and +64 cm/km in the eastern extremity (Sulina) and the western extremity (Beba Veche) of the country. As for the area distortions, they fall between -499.937$m^2/km^2$ in the projection pole and +1300.42$m^2/km^2$ in the extreme points, respectively. Considering the above, for extensive works such as those in the field of road or railway constructions that span distances of hundreds of kilometres, these distortions

can reach the order of kilometres. Not only that, but their surface area is also affected by the above-mentioned distortions.

In order to reduce the distortions produced by the representation in the projection plane, the possibility of using local projection planes was studied.

For areas located at mid-latitudes, such as that of Romania, one can opt for oblique map projections. In these projections the surface of the Earth is approximated by the surface of a sphere. For the representation to be more accurate, the curvature of the Earth's surface must also be taken into account. This can be achieved with the help of double projections, meaning that firstly the surface of the ellipsoid is represented on the surface of a sphere, and then the surface of the sphere is represented on the plane. In the context of the present study, conformal map projections were used, since the surface of the ellipsoid was conformal when represented on the surface of the sphere and then the sphere was represented on the plane using a conformal oblique map projection. [1]

## MATERIALS AND METHODS

Various map projections were analysed from the point of view of the distortions produced by the representation in the projection plane, considering the location of the studied area on the ellipsoid. Conic, azimuthal, and oblique cylindrical projections were examined. The conformal, equivalent, equidistant representation on the meridians and parallels of the ellipsoid on the surface of a sphere was studied. Various railway/road sections located in various areas of the country were selected as case studies. For each of these, the position of the projection pole was determined so that the tangency/secant circle passes through three points on these sections. The distortions produced when representing in the selected map projections were afterwards calculated. For the evaluation of the total distortions, both the distortions produced when representing the ellipsoid on the sphere and the distortions produced when representing the sphere on the plane were taken into consideration. The distortions obtained were compared with those produced by the 1970 Stereographic map projection and the projection with the smallest distortions was ultimately chosen as the better alternative. Based on this result, an algorithm was developed for the transformation from the coordinates in the 1970 Stereographic map projection to the coordinates in the local plan of the selected map projection, which thus allows the setting out of objectives with minimum distortions on the ground.

## CASE STUDY

The 1970 Stereographic map projection is used with the Krasovsky (1940) ellipsoid. Therefore, in the present study the same ellipsoid was conformally represented on a sphere. Six railways sections were chosen from different areas of the country, each section being defined by three points as follows: București – Roșiorii de Vede - Craiova, Arad – Oradea – Satu Mare, Făurei – Bârlad – Iași, Ploiești – Focșani – Roman, Beclean – Miercurea Ciuc – Brașov and Deva – Câmpia Turzii – Dej. For each of these sections, the medium latitude, denoted by $\varphi_k$, was calculated as the average of the latitudes of the three points that define it. The radius of the sphere was determined by setting the condition that the parallel of latitude $\varphi_k$ is represented undistorted. Below are given the formulas for calculating the coordinates, $\varphi'$ and $\lambda'$, on the sphere and the distortions produced when representing the ellipsoid conformally on the sphere. [2]

$$\varphi' = \varphi - \left(\frac{e^2}{2} + \frac{5}{24}e^2 + \cdots\right)\sin 2\varphi + \left(\frac{5e^4}{48} + \cdots\right)\sin 4\varphi + \cdots$$

$$\lambda' = \lambda \tag{1}$$

$$R = a\left(1 - \frac{e^2}{2}\sin^2\varphi_k\right), \tag{2}$$

$$m = n = \frac{R}{a}\left(1 + \frac{e^2}{2}\sin^2\varphi\right),$$

$$p = m^2 \tag{3}$$

where: $m$ is the linear scale factor along meridians;

$n$ is the linear scale factor along parallels;

$p$ is the area scale factor.

For the inverse transformation the following formulas are applied:

$$\varphi = \varphi' + \left(\frac{e^2}{2} + \frac{5e^2}{24} + \cdots\right)\sin 2\varphi' + \left(\frac{7e^4}{48} + \cdots\right)\sin 4\varphi' + \cdots$$

$$\lambda = \lambda' \tag{4}$$

The pole coordinates are calculated according to the coordinates of three points ($\varphi'_1, \lambda'_1$), ($\varphi'_2, \lambda'_2$) și ($\varphi'_3, \lambda'_3$) located on a small circle with formulas [3]:

$$\lambda'_o = \frac{\lambda'_1 + \lambda'_2}{2} \arctan\left[\tan\left(\frac{\lambda'_2 - \lambda'_1}{2}\right)\tan\left(\frac{\alpha+\beta}{2}\right)\cot\left(\frac{\alpha-\beta}{2}\right)\right] \tag{5}$$

$$\varphi'_o = \arctan\left[\cot\left(45^o - \frac{\varphi'_1}{2}\right)\frac{\cos\left(\frac{\lambda'_o - \lambda'_1 + \alpha}{2}\right)}{\cos\left(\frac{\lambda'_o - \lambda'_1 - \alpha}{2}\right)}\right] + \arctan\left[\tan\left(45^o - \frac{\varphi'_1}{2}\right)\frac{\sin\left(\frac{\lambda'_o - \lambda'_1 - \alpha}{2}\right)}{\sin\left(\frac{\lambda'_o - \lambda'_1 + \alpha}{2}\right)}\right]$$

Where:

$$\alpha = \arctan\left[\cot\left(\frac{\lambda'_2 - \lambda'_1}{2}\right)\frac{\sin\left(\frac{\varphi'_1 - \varphi'_2}{2}\right)}{\cos\left(\frac{\varphi'_1 + \varphi'_2}{2}\right)}\right] - \arctan\left[\cot\left(\frac{\lambda'_3 - \lambda'_2}{2}\right)\frac{\sin\left(\frac{\varphi'_2 - \varphi'_3}{2}\right)}{\cos\left(\frac{\varphi'_2 + \varphi'_3}{2}\right)}\right] + \arctan\left[\cot\left(\frac{\lambda'_3 - \lambda'_1}{2}\right)\frac{\sin\left(\frac{\varphi'_1 - \varphi'_3}{2}\right)}{\cos\left(\frac{\varphi'_1 + \varphi'_3}{2}\right)}\right] \tag{6}$$

$$\beta = \arctan\left[\cot\left(\frac{\lambda'_2 - \lambda'_1}{2}\right)\frac{\sin\left(\frac{\varphi'_1 - \varphi'_2}{2}\right)}{\cos\left(\frac{\varphi'_1 + \varphi'_2}{2}\right)}\right] + \arctan\left[\cot\left(\frac{\lambda'_3 - \lambda'_2}{2}\right)\frac{\sin\left(\frac{\varphi'_2 - \varphi'_3}{2}\right)}{\cos\left(\frac{\varphi'_2 + \varphi'_3}{2}\right)}\right] - \arctan\left[\cot\left(\frac{\lambda'_3 - \lambda'_1}{2}\right)\frac{\sin\left(\frac{\varphi'_1 - \varphi'_3}{2}\right)}{\cos\left(\frac{\varphi'_1 + \varphi'_3}{2}\right)}\right]$$

For representing the sphere on a plane using an oblique map projection, we used spherical polar coordinates, the *A*-azimuth, and the *z*-zenith angular distance between the pole of the projection and the selected point on the surface of the sphere. These are calculated using the following formulas [2]:

$$\cos z = \sin\varphi' \sin\varphi'_o + \cos\varphi' \cos\varphi'_o \cos(\lambda' - \lambda'_o)$$

$$\tan A = \frac{\cos\varphi' \sin(\lambda' - \lambda'_o)}{\sin\varphi' \cos\varphi'_o - \cos\varphi' \sin\varphi'_o \cos(\lambda' - \lambda'_o)} \quad (7)$$

In order to obtain minimal distortions of the representation of the sphere in the plane, the oblique conic, oblique cylindrical and oblique azimuthal projections were studied. The relationships that can be used to determine the distortions in these map projections are:

For the oblique conic conformal map projection – in the case of the cone tangent to the sphere, the equations are:

$$\mu_1 = \mu_2 = \frac{\alpha k}{R \sin z}\tan^{\alpha}\left(\frac{z}{2}\right)$$

$$p = \mu_1^2 = \mu_2^2 \quad (8)$$

$$\omega = 0$$

Where: $\mu_1$ is the linear scale factor along verticals;

$\mu_2$ is the linear scale factor along almucantars;

$\omega$ is the maximum angular distortion.

In relations (8), $\alpha$ and $k$ are constants calculated based on the zenith angular distance, $z_k$, of the tangent circle.

$$\alpha = \cos z_k$$

$$k = R \tan z_k ctan^{\cos z_k}\left(\frac{z_k}{2}\right) \quad (9)$$

For the oblique azimuthal conformal map projection – in the case of the representation on a secant plane to the sphere:

$$\mu_1 = \mu_2 = cos^2\frac{z_k}{2} sec^2\frac{z}{2}$$

$$p = \mu_1^2 = \mu_2^2 \quad (10)$$

$$\omega = 0$$

For the oblique cylindrical conformal map projection – in the case of the secant cylinder to the sphere, with $z_k$ the zenith distance of the small secant circle:

$$\mu = \frac{\sin z_k}{\sin z}$$
$$p = \mu^2 \qquad (11)$$
$$\omega = 0$$

## RESULTS

For each section, we calculated the linear distortions, D[cm/km], and the area distortions, P[$m^2/km^2$], produced by the representation in the conic, azimuthal, and cylindrical map projections. The distortions were calculated in the interval $[z_k - 30', z_k + 30']$, which corresponds to a distance of approximately ± 55 km from the tangent circle whose zenith angular distance is $z_k$. The total linear distortions, $D_{total}$ [cm/km], and the total area distortions, $P_{total}$ [$m^2/km^2$], were also calculated, including the distortions produced by the conformal representation of the ellipsoid on the sphere.

**Table 1:** Extreme values of distortions obtained in the oblique conformal conic map projection

| Section | $D_{min\ total}$ [cm/km] | $D_{max\ total}$ [cm/km] | $P_{min\ total}$ [$m^2/km^2$] | $P_{max\ total}$ [$m^2/km^2$] |
|---|---|---|---|---|
| București – Roșiorii de Vede – Craiova | -1.64 | 7.54 | -32.71 | 150.89 |
| Arad – Oradea – Satu Mare | -4.86 | 10.38 | -97.30 | 207.55 |
| Făurei – Bârlad – Iași | -6.34 | 10.14 | -126.81 | 202.81 |
| Ploiești – Focșani – Roman | -6.00 | 10.98 | -119.97 | 219.60 |
| Beclean – Miercurea Ciuc – Brașov | -4.45 | 10.75 | -88.91 | 215.02 |
| Deva – Câmpia Turzii – Dej | -3.84 | 7.84 | -76.88 | 156.79 |

**Table 2:** Extreme values of distortions in the oblique conformal azimuthal map projection

| Section | $D_{min\ total}$ [cm/km] | $D_{max\ total}$ [cm/km] | $P_{min\ total}$ [$m^2/km^2$] | $P_{max\ total}$ [$m^2/km^2$] |
|---|---|---|---|---|
| București – Roșiorii de Vede – Craiova | -6.18 | 12.33 | -123.51 | 246.72 |
| Arad – Oradea – Satu Mare | -30.90 | 35.75 | -617.98 | 715.06 |
| Făurei – Bârlad – Iași | -28.64 | 33.87 | -572.64 | 677.59 |
| Ploiești – Focșani – Roman | -12.46 | 20.97 | -249.28 | 419.45 |
| Beclean – Miercurea Ciuc – Brașov | -8.66 | 17.04 | -173.20 | 340.88 |
| Deva – Câmpia Turzii – Dej | -6.52 | 13.96 | -130.43 | 279.14 |

**Table 3:** Extreme values of distortions in the oblique conformal cylindrical map projection

| Section | $D_{min\ total}$ [m/km] | $D_{max\ total}$ [m/km] | $P_{min\ total}$ [$ha/km^2$] | $P_{max\ total}$ [$ha/km^2$] |
|---|---|---|---|---|
| București – Roșiorii de Vede – Craiova | -277.54 | 623.90 | -47.81 | 163.70 |
| Arad – Oradea – Satu Mare | -123.08 | 163.34 | -23.10 | 35.33 |
| Făurei – Bârlad – Iași | -130.04 | 175.79 | -24.32 | 38.25 |
| Ploiești – Focșani – Roman | -247.83 | 491.41 | -43.42 | 122.43 |
| Beclean – Miercurea Ciuc – Brașov | -329.85 | 969.25 | -55.09 | 287.80 |
| Deva – Câmpia Turzii – Dej | -335.18 | 1016.69 | -55.80 | -55.80 |

Table 4 below contains an example of the calculations performed for the Beclean - Miercurea Ciuc - Brașov section in the oblique conformal conic map projection.

**Table 4:** Total linear distortions $D_{total}$ [cm/km] and total area distortions $P_{total}$ [$m^2/km^2$] for the Beclean – Miercurea Ciuc – Brașov section in the oblique conformal conic map projection. Tangent almucatar: $z_k$=1.0158°

| z | φ [°] | φ' [°] | z [°] | A [°] | $\mu_1=\mu_2$ | D[cm/km] | p | P[$m^2/km^2$] | $\mu_{total}$ | $D_{total}$ [cm/km] | $P_{total}$ | $P_{total}$ [$m^2/km^2$] |
|---|---|---|---|---|---|---|---|---|---|---|---|---|
| $z_k$-30' | 46.6819 | 46.4899 | 0.5158 | -7.7551 | 1.000048 | 4.82 | 1.000096 | 96.38 | 1.000065 | 6.46 | 1.000129 | 129.29 |
| | 46.2691 | 46.0769 | 0.5158 | 78.7699 | 1.000048 | 4.82 | 1.000096 | 96.38 | 1.000041 | 4.06 | 1.000081 | 81.21 |
| | 45.9138 | 45.7216 | 0.5158 | 119.6793 | 1.000048 | 4.82 | 1.000096 | 96.38 | 1.000020 | 1.99 | 1.000040 | 39.81 |
| $z_k$-10' | 47.0119 | 46.8201 | 0.8492 | -7.7551 | 1.000004 | 0.45 | 1.000009 | 8.99 | 1.000040 | 4.02 | 1.000080 | 80.31 |
| | 46.3300 | 46.1379 | 0.8492 | 78.7699 | 1.000004 | 0.45 | 1.000009 | 8.99 | 1.000000 | 0.05 | 1.000001 | 0.92 |
| | 45.7457 | 45.5535 | 0.8492 | 119.6793 | 1.000004 | 0.45 | 1.000009 | 8.99 | 0.999966 | -3.36 | 0.999933 | -67.17 |
| $z_k$-5' | 47.0944 | 46.9026 | 0.9325 | -7.7551 | 1.000001 | 0.11 | 1.000002 | 2.18 | 1.000042 | 4.15 | 1.000083 | 83.10 |
| | 46.3449 | 46.1528 | 0.9325 | 78.7699 | 1.000001 | 0.11 | 1.000002 | 2.18 | 0.999998 | -0.21 | 0.999996 | -4.15 |
| | 45.7035 | 45.5112 | 0.9325 | 119.6793 | 1.000001 | 0.11 | 1.000002 | 2.18 | 0.999961 | -3.95 | 0.999921 | -78.91 |
| $z_k$-2' | 47.1439 | 46.9522 | 0.9825 | -7.7551 | 1.000000 | 0.02 | 1.000000 | 0.34 | 1.000044 | 4.35 | 1.000087 | 87.02 |
| | 46.3538 | 46.1617 | 0.9825 | 78.7699 | 1.000000 | 0.02 | 1.000000 | 0.34 | 0.999998 | -0.25 | 0.999995 | -4.95 |
| | 45.6781 | 45.4858 | 0.9825 | 119.6793 | 1.000000 | 0.02 | 1.000000 | 0.34 | 0.999958 | -4.19 | 0.999916 | -83.70 |
| $z_k$-1' | 47.1604 | 46.9687 | 0.9992 | -7.7551 | 1.000000 | 0.00 | 1.000000 | 0.09 | 1.000044 | 4.43 | 1.000089 | 88.68 |
| | 46.3568 | 46.1647 | 0.9992 | 78.7699 | 1.000000 | 0.00 | 1.000000 | 0.09 | 0.999998 | -0.24 | 0.999995 | -4.86 |
| | 45.6696 | 45.4773 | 0.9992 | 119.6793 | 1.000000 | 0.00 | 1.000000 | 0.09 | 0.999958 | -4.25 | 0.999915 | -84.95 |
| $z_k$ | 47.1769 | 46.9852 | 1.0158 | -7.7551 | 1.000000 | 0.00 | 1.000000 | 0.00 | 1.000045 | 4.53 | 1.000091 | 90.51 |
| | 46.3597 | 46.1676 | 1.0158 | 78.7699 | 1.000000 | 0.00 | 1.000000 | 0.00 | 0.999998 | -0.23 | 0.999995 | -4.61 |
| | 45.6611 | 45.4689 | 1.0158 | 119.6793 | 1.000000 | 0.00 | 1.000000 | 0.00 | 0.999957 | -4.30 | 0.999914 | -86.02 |
| $z_k$+1' | 47.1934 | 47.0017 | 1.0325 | -7.7551 | 1.000000 | 0.00 | 1.000000 | 0.08 | 1.000046 | 4.63 | 1.000093 | 92.52 |
| | 46.3627 | 46.1706 | 1.0325 | 78.7699 | 1.000000 | 0.00 | 1.000000 | 0.08 | 0.999998 | -0.21 | 0.999996 | -4.18 |
| | 45.6526 | 45.4604 | 1.0325 | 119.6793 | 1.000000 | 0.00 | 1.000000 | 0.08 | 0.999957 | -4.35 | 0.999913 | -86.93 |
| $z_k$+2' | 47.2099 | 47.0182 | 1.0492 | -7.7551 | 1.000000 | 0.02 | 1.000000 | 0.33 | 1.000047 | 4.73 | 1.000095 | 94.69 |
| | 46.3656 | 46.1735 | 1.0492 | 78.7699 | 1.000000 | 0.02 | 1.000000 | 0.33 | 0.999998 | -0.18 | 0.999996 | -3.58 |
| | 45.6441 | 45.4519 | 1.0492 | 119.6793 | 1.000000 | 0.02 | 1.000000 | 0.33 | 0.999956 | -4.38 | 0.999912 | -87.66 |
| $z_k$+5' | 47.2594 | 47.0677 | 1.0992 | -7.7551 | 1.000001 | 0.10 | 1.000002 | 2.06 | 1.000051 | 5.11 | 1.000102 | 102.17 |
| | 46.3744 | 46.1823 | 1.0992 | 78.7699 | 1.000001 | 0.10 | 1.000002 | 2.06 | 1.000000 | -0.04 | 0.999999 | -0.83 |
| | 45.6187 | 45.4264 | 1.0992 | 119.6793 | 1.000001 | 0.10 | 1.000002 | 2.06 | 0.999956 | -4.45 | 0.999911 | -88.91 |
| $z_k$+10' | 47.3419 | 47.1503 | 1.1825 | -7.7551 | 1.000004 | 0.40 | 1.000008 | 8.05 | 1.000059 | 5.89 | 1.000118 | 117.75 |
| | 46.3890 | 46.1969 | 1.1825 | 78.7699 | 1.000004 | 0.40 | 1.000008 | 8.05 | 1.000003 | 0.34 | 1.000007 | 6.85 |
| | 45.5762 | 45.3839 | 1.1825 | 119.6793 | 1.000004 | 0.40 | 1.000008 | 8.05 | 0.999956 | -4.39 | 0.999912 | -87.88 |
| $z_k$+30' | 47.6719 | 47.4804 | 1.5158 | -7.7551 | 1.000033 | 3.35 | 1.000067 | 66.98 | 1.000108 | 10.75 | 1.000215 | 215.02 |
| | 46.4460 | 46.2539 | 1.5158 | 78.7699 | 1.000033 | 3.35 | 1.000067 | 66.98 | 1.000036 | 3.62 | 1.000072 | 72.43 |
| | 45.4051 | 45.2129 | 1.5158 | 119.6793 | 1.000033 | 3.35 | 1.000067 | 66.98 | 0.999976 | -2.44 | 0.999951 | -48.89 |

**Table 5:** Deformation in the 1970 Stereographic map projection in the cities that define the six analysed sections

| City | φ [° ' "] | λ [° ' "] | x [m] | y [m] | μ | D [cm/km] | p | P [m²/km²] |
|---|---|---|---|---|---|---|---|---|
| București | 44°26'48" | 26°04'26" | -172033.113 | 85478.163 | 0.999977 | -2.32 | 0.999954 | -46.446 |
| Roșiorii de Vede | 44°06'41" | 24°59'39" | -209856.815 | -467.011 | 1.000021 | 2.06 | 1.000041 | 41.287 |
| Craiova | 44°19'44" | 23°48'59" | -184997.232 | -94403.240 | 1.000015 | 1.51 | 1.000030 | 30.174 |
| Arad | 46°11'23" | 21°19'30" | 27638.201 | -283583.580 | 1.000249 | 24.89 | 1.000498 | 497.870 |
| Oradea | 47°04'12" | 21°56'09" | 123435.842 | -232677.494 | 1.000176 | 17.63 | 1.000353 | 352.706 |
| Satu Mare | 47°47'43" | 22°53'36" | 201667.679 | -157822.866 | 1.000153 | 15.30 | 1.000306 | 306.027 |
| Făurei | 45°04'57" | 27°16'29" | -99414.187 | 179054.340 | 1.000008 | 0.78 | 1.000016 | 15.520 |
| Bârlad | 46°12'55" | 27°40'23" | 27390.093 | 206190.979 | 1.000016 | 1.59 | 1.000032 | 31.760 |
| Iași | 47°09'57" | 27°34'12" | 132745.800 | 194813.938 | 1.000092 | 9.15 | 1.000183 | 183.055 |
| Ploiești | 44°53'60" | 26°00'00" | -121738.750 | 78971.643 | 0.999879 | -12.06 | 0.999759 | -241.181 |
| Focșani | 45°42'03" | 27°10'10" | -30949.494 | 168906.488 | 0.999931 | -6.88 | 0.999862 | -137.574 |
| Roman | 46°55'60" | 26°55'00" | 105497.543 | 145922.982 | 0.999949 | -5.07 | 0.999899 | -101.491 |
| Beclean | 47°10'37" | 24°10'55" | 131128.139 | -62003.764 | 0.999879 | -12.07 | 0.999759 | -241.399 |
| Miercurea Ciuc | 46°21'35" | 25°47'38" | 40281.024 | 61083.309 | 0.999783 | -21.71 | 0.999566 | -434.151 |
| Brașov | 45°39'40" | 25°36'49" | -37474.526 | 47810.700 | 0.999773 | -22.73 | 0.999545 | -454.593 |
| Deva | 45°53'04" | 22°54'36" | -10715.001 | -162187.448 | 0.999912 | -8.76 | 0.999825 | -175.275 |
| Câmpia Turzii | 46°32'50" | 23°52'47" | 61420.595 | -85901.306 | 0.999819 | -18.15 | 0.999637 | -362.906 |
| Dej | 47°08'29" | 23°53'40" | 127441.767 | -83849.272 | 0.999893 | -10.70 | 0.999786 | -213.956 |

## DISCUSSION

Analysing the results presented in Tables 1, 2, and 3 above for a strip of ±30' of $z_k$, though for all of the analysed sections a strip of z+11' was sufficient, the smallest distortions were obtained in the oblique conformal conic map projection. Consequently, it was selected as the local map projection for setting out construction projects extending over large distances or areas instead of the official projection of Romania. In the 1970 Stereographic map projection, for the sections analysed, depending on their position compared to the circle of zero distortions, the smallest values were obtained for the section București – Roșiorii de Vede – Craiova, namely linear distortions vary from -2.32 cm/km to +1.51 cm/km, and area distortions vary from -46.44 $m^2/km^2$ to +30.17$m^2/km^2$. On the other hand, the greatest distortions were obtained for the section Arad – Oradea – Satu Mare, ranging from +15.30 cm/km to +24.59 cm/km for the relative linear distortions and from +306.03 $m^2/km^2$ to +497.87$m^2/km^2$ for relative area distortions, respectively.

For the selected map projection, we propose the following algorithm for transforming the coordinates of the setting out points from the 1970 Stereographic map projection into the conformal oblique conic map projection:

- Transforming the rectangular 1970 Stereographic coordinates into geographic coordinates (φ, λ) on the 1940 Krasovsky ellipsoid;
- Representing the Krasovsky ellipsoid on a sphere in a conformal projection and calculating the geographic coordinates (φ', λ') using those on the ellipsoid, (φ, λ);

- Calculating the projection pole coordinates, noting that the tangent almucantar passes through the three chosen points on the section of interest;
- Transforming the coordinates, (φ', λ'), into polar spherical coordinates, (A, z);
- Calculating the polar plane coordinates (ρ, δ) as a function of (A, z);
- Calculating the rectangular coordinates (x, y) in the oblique conic map projection as a function of (ρ, δ).

## CONCLUSION

The setting out of objectives to be built in Romania requires the determination of plotting elements, either rectangular or polar coordinates, using the 1970 Stereographic projection plane, which is the official projection used in our country. While this projection is conformal, it generally distorts distances and areas, except for points located on the circle of zero distortions with a radius of 201.7 km and its centre at φ=46° and λ=25°. Therefore, when the perimeter due to be set out is located within the area of this circle, the distortions will be zero or comparable to the measurement errors, and so the exact coordinates calculated in the project can be set out on the ground. However, this particular scenario is very unlikely to be encountered in actual practice. To this end, when setting out the project on the ground, the distortions produced by the 1970 Stereographic map projection, which for the territory of Romania vary from -25 cm/km to approximately +64 cm/km in terms of distances and between -5 $m^2$/ha and +12.76 $m^2$/ha in terms of surface areas, must be taken into account. When setting out on the ground, if the area of interest has a large expanse, the curvature of the land must be considered. Therefore, a local projection plane must be found in which the deformations produced in the representation of the curved surface of the Earth are minimal. The present work proposes a unitary solution for determining plotting elements regardless of the application conditions on the ground (i.e. location of the objective on the territory of Romania in terms of geographical position), with the direct benefit of reducing the total cost of constructions spanning great distances or surface areas.

## ACKNOWLEDGEMENTS

This work was supported by a National Research Grants of the Technical University of Civil Engineering Bucharest UTCB, project number: $\mathrm{GNaC}_{2023}^{\mathrm{ARUT}} - \mathrm{UTCB} - 32$.

## REFERENCES

[1] Miljenko LAPAINE, Nedjeljko FRANČULA. Approximately Conformal, Equivalent and Equidistant Map Projections[J]. Journal of Geodesy and Geoinformation Science, 2022, 5(3): 33-40 doi: 10.11947/j.JGGS.2022.0304.

[2] Snyder, J. P., Map Projections – A Working Manual, United States Government Printing Office, Washington, 1987, pp. 15-31, ISBN 1839310219.

[3] Soloviev, M., D., Proiecții cartografice, Editura Militară MFA, București, 1955, pp. 93-95.

# APPLYING CORS NETWORKS FOR A FASTER AND MORE COST-EFFECTIVE APPROACH

**PhD Stanislav Genchev**[1]

[1] University of Architecture, Civil Engineering and Geodesy (UACEG), **Bulgaria**

## ABSTRACT

The issues related to the use of products generated from Continuously Operating Reference Station (CORS) for precise positioning are the main focus of the study. Geodetic measurements were conducted at a real site, and different types of data provided by commercial CORS networks were compared – Network Real Time Kinematic (Network RTK) via VRS, generated data for subsequent processing (Virtual Rinex), and raw data from a physical station. The current national regulations, as per [1], were adhered to, and the aim is to expand the methodology for applying a faster and more efficient approach to determining points in geodetic control networks, ensuring high reliability and accuracy through a comparative analysis.

The construction of geodetic control networks (GCN) and working geodetic bases (WGB) is an essential and integral part of designing and constructing any type of infrastructure projects. In geodetic practice, GNSS determinations are most commonly relied upon as a fast and effective method. For almost all applications, the points determined with GNSS are considered without errors, thus realizing the geodetic coordinate system for the project. With the development of technology and the construction of CORS networks, Network RTK has become the most commonly applied method due to the accessible and easy acquisition of the final result (coordinates of the determined points). However, its application often does not lead to reliable results. On the other hand, the Virtual Rinex product is not widely popular among the geodetic community, though it is not inferior in terms of cost-effectiveness. Some studies on its application have been published in [2], but its application is not embedded in any regulatory document in the Republic of Bulgaria.

**Keywords:** GNSS, CORS network, accuracy, methodology

## INTRODUCTION

In the territory of the Republic of Bulgaria, the Bulgarian Geodetic System (BGS2005) was introduced by a decree of the Council of Ministers [3]. This system represents (ETRS89, ETRF2000, ep. 2005, and DATUM GRS80). The index "2005" used in the name of the geodetic system refers to the year when the coordinates of the points from the State GPS network, which materialize the newly introduced reference system, were determined. The year of determination is not related to the epoch to which the coordinates of the points materializing the system are referred. The bearer of this coordinate system is the State GPS Network, supplemented by five commercial CORS networks, four of which have a certificate of conformity issued by the Geodesy, Cartography, and Cadastre Agency (GCCA) at the Ministry of Regional Development and Public Works (MRDPW).

This means that the coordinates of their physical stations, and the products they provide, can also be considered as carriers and disseminators of the introduced coordinate system.

Each commercial network provides several types of services for determining coordinates. The most used services are Real-time kinematic positioning (Network RTK) and Post-processing data (PPDATA). There are two more services, one of which is outdated and inapplicable for achieving accuracies greater than 10 cm – this is the VRS DGNSS (Virtual reference station Differential GNSS) service. There is a service similar to PPDATA, where points representing static measurements with customizable settings are software-generated. This service is called Virtual Rinex (VRinex), and its applicability for creating geodetic control networks is one of the main tasks of the study. It should be noted that in the context of the military conflict between Russia and Ukraine, as well as increased solar activity, real-time determinations are unreliable, and the only solution is to perform static measurements with subsequent processing, which should also be cost-effective.

For the purposes of the study, a GCN was chosen for railway construction due to the high required accuracy, recorded in [4] – no less than 10 mm in three-dimensional space. The layout of the developed control polygon according to the configuration of the commercial CORS network implies its division into two parts – points falling entirely within and outside the coverage of the CORS network.

The geodetic measurements carried out between June and September 2023 were performed in full compliance with the regulatory requirements in the Republic of Bulgaria. For the needs of statistical analysis, 53 points were measured under 3 determination scenarios.

## SCENARIOS

### I. Measuring points from the GCN by Network RTK service

Using Network RTK, measurements were performed with triple-frequency receivers. According to Instruction [1], points must be determined twice, with a minimum measurement duration of 30 seconds for each point. To increase the number of averages for the study's purposes, the points were determined for a minimum duration of 60 seconds, and during the measurement, the antennas were stabilized on tripods. The coordinate system in which the points were determined is BGS2005. The interval between the two measurements of the points was at least 10 minutes to change the measurement conditions.

### Result

1/ The measurement data is obtained directly without the need for subsequent processing. Each point has two measurements, and based on the similar accuracy assessment, the results are averaged equally. Permissible values that must be adhered to, depending on the declared accuracy of the applied method, are set as follows: the maximum difference between the two determinations in the horizontal position is 20 mm, and in the vertical position is 40 mm. For this purpose, the data is compared in the projection coordinate system (BGS2005 cadastral), and the transition is made using the officially accepted and operational BGSTrans 4.5, published on the GCCA website.

2/ For section 1, when the points fall within the CORS network configuration, the accuracies obtained for the horizontal and vertical positions are in the ranges of **5 - 12 mm** and **6 - 21 mm**, respectively. In the second section, the ranges are **8 - 18 mm** and **12 - 28 mm**.

3/ The measurement of all points was carried out within 2 days, with a working time of 2 hours per day by 4 teams..

## II. Determining points with the VRinex service

For the geodetic measurements, four phase triple-frequency GNSS receivers were used. The "leapfrog" (overlapping) method was applied, providing a continuous polygon of relative baseline vectors. The obtained vectors between the points will be calculated, and the polygon will be connected to BGS2005 by generating stations [7] using the VRinex service provided by the infrastructural network. The session length of the measurements was a minimum of 10 minutes. The recording interval used was 5 seconds with a height mask of 10°.

### Result

1/ The points are adjusted separately for each of the two sections. For the first section, three generated points were used as reference points, and for the second, only two. After adjusting the two networks, the points are obtained in the ETRS (European Terrestrial Reference System) 89 epoch 2005.0 coordinate system in the form of Cartesian coordinates XYZ.

2/ The accuracy with which the points were determined in the sections is as follows: for section 1, **2.5 – 7.1 mm** and **3.6 – 8.1 mm**, and for section 2, **2.0 – 5.2 mm** and **3.1 – 9.1 mm**. For transitioning to the BGS2005 Cadastral system, a transformation was made using the software provided by GCCA.

3/ The measurement of all points was carried out within 2 days, with a working day of 6 hours by 4 teams. Additionally, the network was processed with software within 2 days.

## III. Determining the points using classic static measurements.

For verifying the obtained results, classic static measurements were performed using eight phase dual-frequency receivers. The session length was a minimum of 45 minutes. Data was recorded every 5 seconds, and an angular mask of 10° was used to filter satellite signals. The network was connected to BGS2005 using raw data from physical permanent stations of the same commercial CORS network.

### Result

1/ The vectors were calculated with precise ephemerides [7] due to the long length of the determined vectors. The network adjustment was performed assuming that the coordinates of the physical stations were error-free.

2/ After adjusting the coordinates of the points, their accuracy for all sections and positions was under ±10 mm.

3/ The measurement of all points was carried out within 4 days, with a working day of 8 hours by 8 teams. Additionally, the network was processed with software within 2 days.

## Analysis of the Processed Results

A comparative analysis was conducted between classical static measurements and measurements using the VRinex and Network RTK services, based on the criteria described in [5]. Basic statistical methods were used to evaluate the series of values, and they were diligently checked for the presence of gross and systematic errors. The final results obtained were only affected by random errors, which is a prerequisite for correct conclusions.

When examining the differences in the horizontal and vertical positions, larger values were clearly identified in the vertical component (ellipsoidal heights), especially for the section outside the coverage of the infrastructural network, as shown in Figure 1. This fact necessitates the investigation of the obtained series according to the location of the points, specifically within and outside the coverage of the commercial CORS network, as visualized in Figure 2.

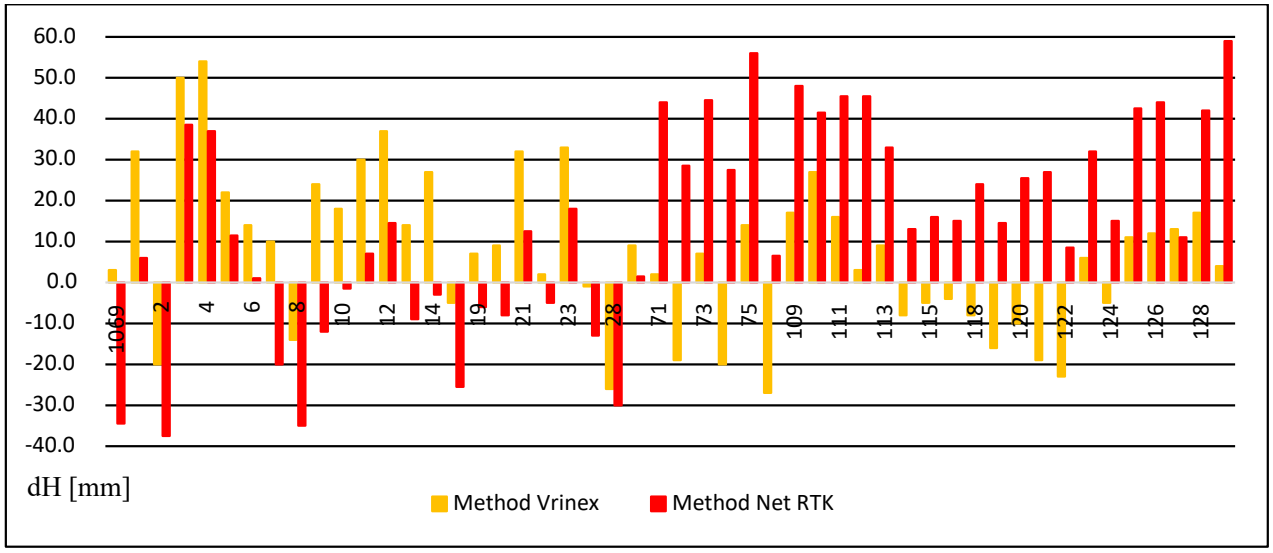


**Figure 1**. Differences of the VRinex and Net RTK Methods Compared to Classical Static Measurements in Vertical Position

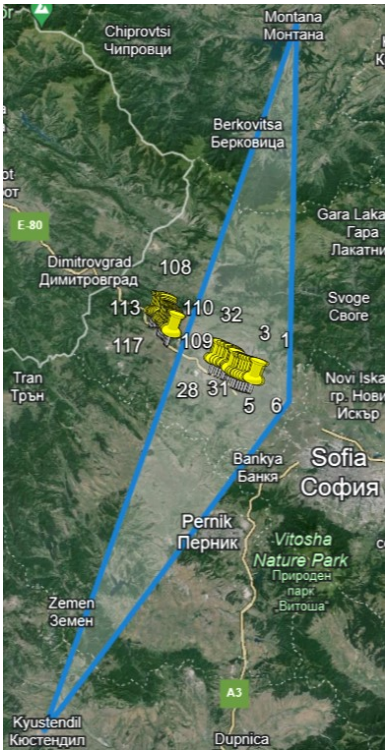


**Figure 2.** Visualization of Points Within and Outside the Network Coverage

Statistical processing was performed for all points and for points divided into the two distinct sections. The results for the mathematical approximation of the difference series are presented in Table 1, where it is clearly observed that the VRinex method performs twice as well as the NetRTK method on the whole network. If one looks more carefully at the results by site, it can be seen that in plan terms the results are similar, while in elevation terms the Network RTK method has underestimated accuracy.

**Table 1. Values of mathematical expection / Expected values**

| Method / Section | VRinex M(x) [mm] | | Net RTK M(x) [mm] | |
|---|---|---|---|---|
| | Horizontal | Vertical | Horizontal | Vertical |
| All points | 2.7 | 7.1 | 5.1 | 14.3 |
| Section I | 4.9 | -10.5 | 4.2 | 13.9 |
| Section II | 9.6 | -0.2 | 11.7 | 31.1 |

The values for the standard deviations are presented in Table 2, indicating the greater similarity of the results obtained from the VRinex method. This suggests that the VRinex method is fully applicable for precise determinations, adhering to a specific methodology for planning and implementing measurements [2]. It can be confidently asserted that the relative errors in the OGM fully satisfy the required accuracies in the implementation of most infrastructure projects, and the adherence to the current country CS is of negligible deviation.

**Table 2. Standard Deviation Values**

| Method / Section | VRinex σ(x) [mm] | | Net RTK σ(x) [mm] | |
|---|---|---|---|---|
| | Horizontal | Vertical | Horizontal | Vertical |
| All points | 19.3 | 20.1 | 19.5 | 29.1 |
| Section I | 20.1 | 16.6 | 22.0 | 20.6 |
| Section II | 14.5 | 14.3 | 13.6 | 15.1 |

Classical methods (geometric leveling) should be applied for the determination of the points in altitude in accordance with the regulatory requirements in the Republic of Bulgaria, and in the future, if a local geoid/quasigeoid model is determined for the country, the altitudes determined by GNSS can be transformed with the desired accuracy into the corresponding altitude system, and for this purpose it is necessary to remeasure the points that served to derive the model to verify the transformation.

To define such a model, the GNSS/levelling method is applied, and the accuracy of the model will depend on the density and accuracy of the source data, i.e. the data in the construction of the OGM (GNSS measurements and geometric levelling), tailored to the specifics described under [6].

## CONCLUSIONS

The utilization of products from infrastructure networks is an economically efficient approach, aiming for faster measurements with fewer instruments and fewer teams. However, achieving the desired accuracies in the determined coordinates requires careful consideration and the application of a clear methodology.

Two main rules should be followed:

- When using Network RTK, the determined points must be measured twice with a sufficient time interval between measurements. The final result should be obtained according to clear criteria;
- When using VRinex, the generated points serve as reference points. Therefore, it is mandatory to calculate the baseline vectors between them and determine the relative baseline vectors between the newly determined points.
- An analysis should be conducted regarding the location of the points relative to the coverage of the CORS network:
- Within the coverage of CORS network, both VRinex and Network RTK services provide satisfactory results when the specified rules are followed;
- For measurements located outside the range of the CORS network - the use of Network RTK does not give correct results, especially in altitude. When defining plan coordinates and with certain conventions, the VRinex service can be used.
- GNSS determination methods are constantly evolving, but each researcher should apply a methodology that ensures reliable, accurate and cost-effective results

**ACKNOWLEDGEMENTS**

I would like to thank the University of architecture, civil engineering and geodesy for the opportunity to perform this study.

**REFERENCES**

[1] Instruction No. RD-02-20-25 of September 20, 2011, for determining geodetic points using global navigation satellite systems, Ministry of Regional Development and Public Works, Bulgaria.

[2] Tsanovski, Yu., GNSS - Good Geodetic Practices, Monography, Paint Box Creative, 132 pages, 2023, ISBN: 978 619 92689-0-2

[3] Decree of the Council of Ministers No. 153 of 29 July 2010 and Regulation No. 2 of 30 July 2010 on the definition and maintenance of the Bulgarian Geodetic System 2005 (BGS2005).

[4] The Instruction for Shenazh and Reperazh from 2005.

[5] Kostadinov, K., Valchinov, V. Mathematical Processing of Geodetic Measurements, Sofia, 2012.

[6] Sl. Gospodinov, E. Peneva, P. Penev, T. Lambeva, Yu. Tsanovski, S. Dzhorova, G. Marinov. I. Radev, Contemporary Aspects of Geometric Leveling, Yearbook of UACEG Sofia 2016, Volume 49, Issue 4, pp. 9-23, ISSN 1310-814X, ISSN 2534-9759

[7] https://www.solitech.bg/bg/services/gnss-network-geonet - accessed on June 29, 2023.

# CALIBRATION OF MEASURING TAPES

**Dr. Pavol Kajánek,** [1]
**Dr. Richard Honti,** [1]
**prof. Dr. Alojz Kopáčik, PhD.**[1]
**Assoc. Prof. Dr. Ján Erdélyi.**[1]
**Assoc. Prof. Dr. Peter Kyrinovič.**[1]

[1] Slovak University of Technology, **Slovakia**

## ABSTRACT

Due to usage, handling, and improper storage, measuring tapes undergo changes in their condition over time. For this reason, regular inspection is necessary to ensure the desired quality of results, aiming to verify the accuracy of the tape and its usability in practice. During the calibration of measuring tapes, the position of the scale divisions on the tape is evaluated using a device known as a horizontal comparator. This device consists of a linear base on which a carriage with evaluating equipment, in our case a camera, is automatically moved. The position of the carriage movement is measured by laser interferometer. To eliminate the very laborious and time-consuming precise positioning of the camera over the division on the scale, the position of the division relative to the camera's projection centre is evaluated by processing the image of the calibrated tape. The article describes this novel solution and the device developed for this purpose. Using the developed comparator, calibration of tapes and other length measures, such as levelling staffs could be done. The entire calibration process is autonomous, thanks the user interface developed for the calibration process. Second part of the article focuses on the analysis of results and their comparison with another laboratory.

**Keywords:** measuring tape, calibration, comparator, interferometer, user interface.

## INTRODUCTION

During the calibration of measuring tapes, the actual, i.e., measured position of the division scale on the tape is compared with its nominal value. The actual position of the division scale is evaluated using a horizontal comparator, which facilitates the movement of the evaluated device (camera) over the scale of the calibrated tape and realise the nominal value along the calibrated scale. Generally, the comparator is unique equipment, based on the own knowledge and development of each institution [1 - 8]. A common feature of these solutions is the basic principle of the comparison, i.e., comparing the measured quantity (the actual position of the division of the calibrated scale) with their nominal value.

The precise positioning of the camera over the division scale of the calibrated measure (the tape) described in [4, 8 and 9] is very time-consuming and laborious. For this reason, the novel solution was developed, where the camera is approximately set above the evaluated division scale, and the distance between the main point of the image (camera centre) and the edge of the division scale is evaluated by processing the images made by the camera.

## METHODOLOGY

During the calibration the actual position of the division scale's centre of the calibrated tape is evaluated and compared with their nominal values to determine the corrections. The evaluating device with the camera (Fig. 1 – item 1) on a carriage (Fig. 1 – item 2) is moved over the scale (Fig. 1 – item 3) along a linear trajectory. The tape is fixed in a horizontal position on separate brackets during measurement, isolated from the comparator's structure. The imaging process is controlled by a Raspberry PI 3B microcontroller (Fig. 1 – item 4) powered by a 5V battery (Fig. 1 – item 5). The position of the camera is measured using a laser interferometer. For this reason, the end prism of the laser interferometer (Fig. 1 – item 6) is mounted on the carriage. The tilt of the carriage plate during their movement is monitored using a dual-axis Leica Nivel 220 inclination sensor (Fig. 1 – item 7). It is assumed, that the system placed on the carriage plate forms a single unit, i.e., the offsets between the system's components are without any changes.

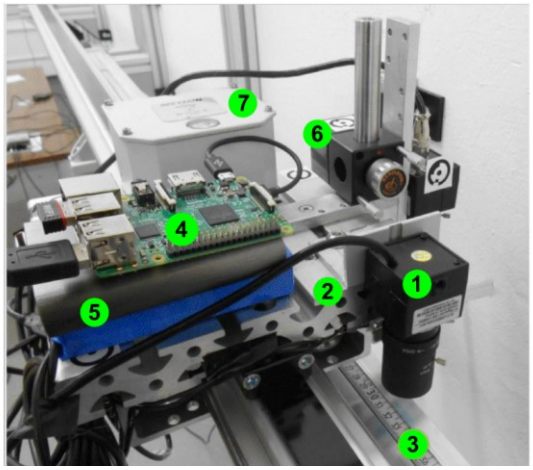


1 - camera for measuring tape
2 - carriage
3 - calibrated measuring tape
4 - Raspberry Pi 3B microcontroller
5 - battery 5V
6 - interferometer prism
7 - dual-axis Leica Nivel 220 inclination sensor

**Fig. 1** System for evaluating the position of the scale divisions on the calibrated tape

Before the calibration start, it is necessary to place the tape into the bracket and tension it with a force of 50 N, which is achieved by placing a 5 kg weight at the end of the calibrated section (Fig. 2 - Detail B). Since the range of the calibrated tapes, generally 30 m or 50 m, exceeds the measuring range of the comparator, which is 7.8 m, it is necessary to calibrate the tape in more sections. It was decided to use 5 m sections (Fig. 2 – blue dimension) whit 1 m overlap for each section. The decision was made based on a series of measurements, the geometry of the comparator's trajectory and the possibility of using a separately mounted brackets for placing the calibrated tape.

The zero point of measuring tapes (Fig. 2 – Detail A) is not fixed as in the case of other length-measures (e.g., levelling rods) and is often made from an unsuitable and thermally unstable material, which is different from the material used for producing measuring tapes. For this reason, the zero point and the beginning of the tape is not included to the calibration, which begins at the scale division 0.1 m.

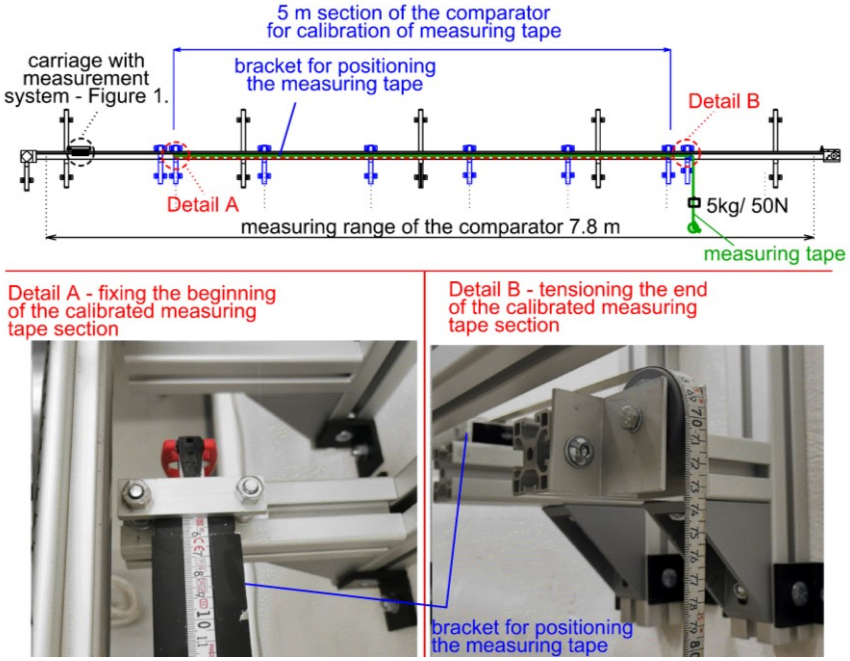


**Fig. 2** Placement and fixation of the measuring tape during the calibration

The bracket for placing the tape originally had an aluminium grey colour according to the material (aluminium) from which it was made. A series of measurements revealed problems with light reflections (glare) on the bracket, so it was decided to paint the bracket black, which prevented the occurrence of glare and improved the quality of the results.

The distance between the camera and the calibrated scale does not change significantly during calibration. The image in the camera's field of view was focused for this distance and then the camera lens was fixed to prevent any refocusing. For this focusing, a camera calibration was performed, based on which image idealization is carried out. During the calibration each section of the tape is fixed (Fig. 2) and automatically scanned in steps of 0.1 m. This step can be adjusted upon the client's request.

To avoid the incorrect identification of the division scale due to any damage or contamination of the calibrated scale, the approximate identification of division scales (Fig. 3.a) is made, using data from the laser interferometer. Precise subpixel evaluation of the division scale edge (Fig. 3.c) is carried out based on the evaluation of pixel intensity in a horizontal cross-section of the scale (Fig. 3.b – green line). Horizontal cross-sections are conducted over a length of 32 pixels, with the centre of the cross-section being in the approximate position of the division scale edge. The subpixel evaluation of the division scale edge is based on a threshold value for pixel intensity in the cross-section (Fig. 3.c). For determination of the threshold value, the average intensity value for the first and last 11 pixels of the cross-section is used from which the resultant threshold value is calculated as the average of these values. The edge of the division scale is then identified by interpolating the pixel intensities in the horizontal cross-section for the calculated threshold value. In this manner, the right and left edges of the division scale are evaluated in 100 horizontal cross-sections positioned one below the other. The final position of the division scale is determined as the centre between its right and left edges.

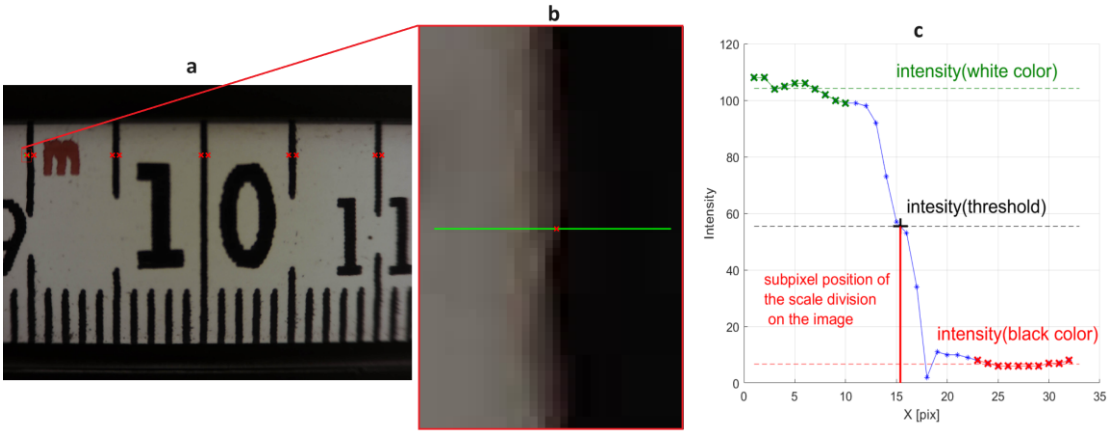


**Fig. 3** Subpixel evaluation of the edge of the tape scale division (a – image, b – detail on the section, c – the principle of subpixel evaluation of the division edge)

It's necessary to evaluate all 0.005 m division scales of the tape at the top and the bottom part of the scale (Fig. 4 – blue and orange points). Points belonging to the same division scale (top and bottom part of the scale) (Fig. 4 – magenta points) are approximated by a regression line (Fig. 4 – green lines). In the next step, a projective transformation is used to identify the mutual relationship between the plane of the tape and the plane of the camera's CCD sensor, thereby eliminating the non-uniform pixel size caused by the non-parallel alignment of these planes. Identical points (Fig. 4 - red points), located at the intersection of lines representing the centre of the division scale with the edge of the measuring tape (Fig. 4 – red lines), are used for calculating elements of the projective transformation. With the projective transformation, we bring the results (division scales identified from the image) into a common plane, where the measurement of the distance $d_{PM}$ between the main point of the image (Fig. 4 - blue cross) and the edge of the evaluated division scale takes place. This measurement occurs on the evaluated line (Fig. 4 - cyan line) running through the center between the top and bottom edges of the tape's margin. The final position of the division scales (Fig. 4 - yellow points) is defined as the intersection of the line running through the center of the division scale of the measuring tape with the evaluation line.

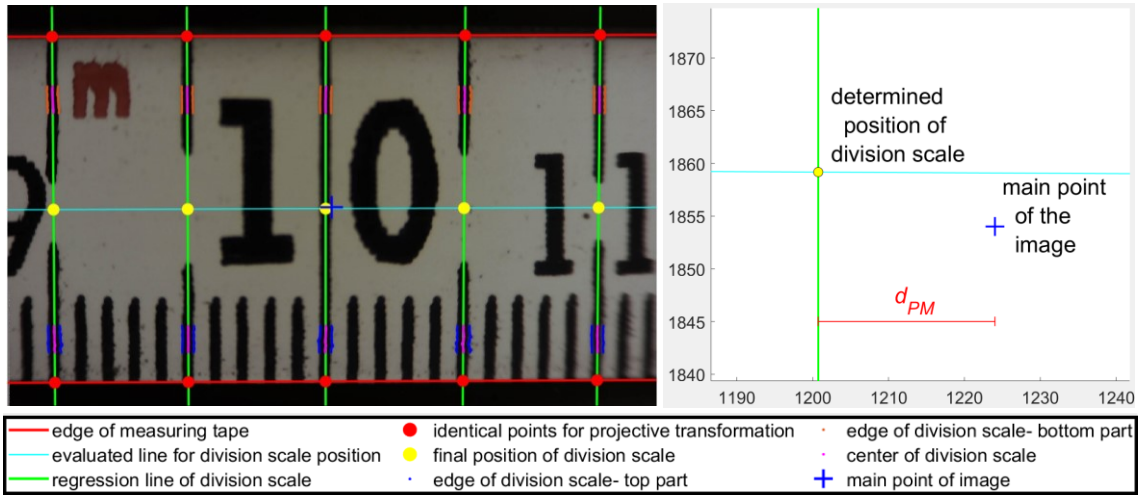


**Fig. 4** Evaluation of the precise position of the tape's divisions in the image

The final position of the division scale $l_M$ is determined based on the position of the camera's projection centre $l_P$ and the distance $d_{PM}$ between the main point of the image and the edge of the division scale (Fig. 4 – on the right side):

$$l_M = l_P + d_{PM} \tag{1}$$

Since we are calibrating measuring tapes of length 30 m or 50 m using a comparator which length is 7.8 m, the tapes must be calibrated in sections of five-meter longitude with a one-meter overlap. For this reason, in the calculation of the division scale position (2), the length corresponding to the currently calibrated section of the tape $k$ is added, and in the correction calculation (3), we must consider the average value of the corrections for the division scales in the overlapped section of the tape $l_O$.

$$l_M = l_P + d_{PM} + (k-1)\cdot 5 \tag{2}$$

The correction for a division scale $l_C$ is expressed as the difference between the measured position of the division scale $l_M$ and the nominal value of the division scale $l_N$ on the tape scale, with the addition of the average correction in the overlap section of the tape $l_O$:

$$l_C = l_M - l_N + l_O \tag{3}$$

The calculated corrections of the scale divisions are approximated by a regression line (Fig. 5).

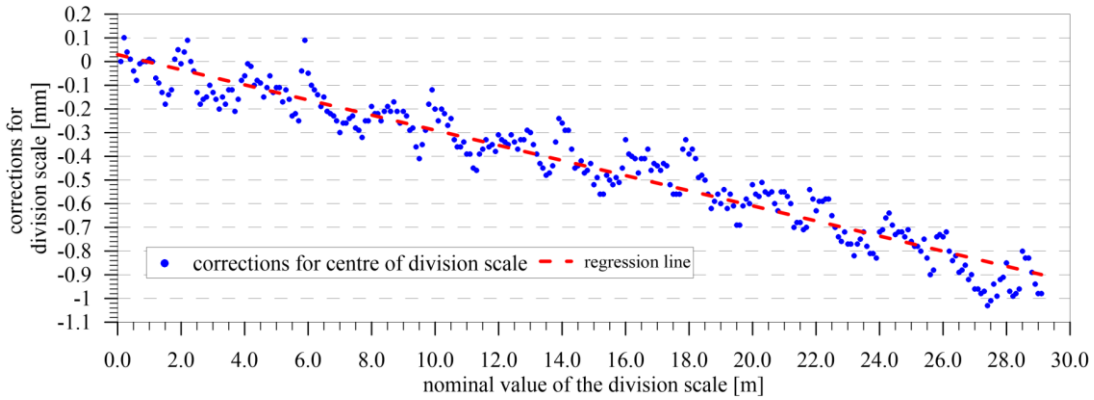


**Fig. 5** Corrections of the measuring tape's divisions approximated by regression line

For comparison of the achieved results of calibration, the available calibration certificate of the tape was used. The respective calibration from the available protocol was conducted on October 18, 2012, on a different type of comparator [4]. The current calibration was carried out on March 8, 2021. During this period the measuring tape was used only for special experts works and in a very limited mode (2-3 times per year). From the comparison of the division corrections (Fig. 6), we can primarily see the difference between the slopes of the regression lines, which may be related to the time interval between calibrations and the fact that the tape was used between calibrations.

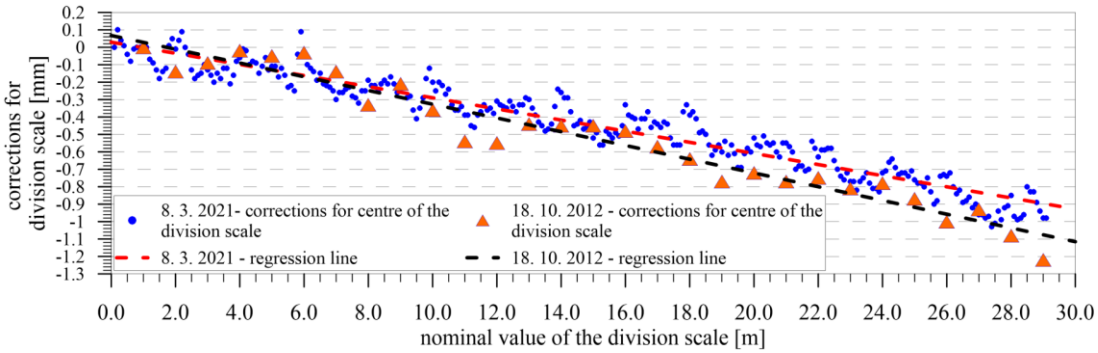


**Fig. 6** Comparison of results of two calibrations made by different calibration laboratories and after a time interval of 9 years between performed calibrations

## RESULTS

The calibration results of the measuring tape are delivered to the client in the form of a calibration certificate (Fig. 7), where corrections for the entire calibrated tape are presented in graphical form along with the regression line (Fig. 7.a), as well as in the form of numerically expressed corrections for individual divisions of the tape scale (Fig. 7.b). Based on this, the correction for a division is realized either by calculation through the regression line or directly by linear interpolation from the table of corrections.

**a**

**Calibration certificate no. 03/2021** Page 1/2

**Calibrated measurer (type, no.):**
30 m steel measuring tape on metal - plastic fork, no. 3-S12-3005 U-1
**Calibration range [m]:**
0.1 - 29.1
**Comparator:**
Horizontal comparator
**Contract:**
[redacted]
**Date:**
8.3.2021

**Laboratory of metrology of short lengths**
Slovak University of Technology in Bratislava
Faculty of Civil Engineering
Department of Surveying
Radlinského 11
810 05 Bratislava
[redacted]

**coefficient of expansion (standardized value for steel)**
$\alpha_{T_N} = 11\ ppm \cdot °C^{-1}$
**Position of the measuring tape during calibration:** horizontal

**Determinaion of scale factor:**

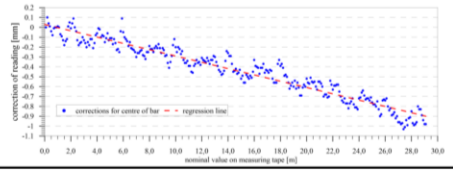


**Scale factor:** $m_0 = -0,03 \pm 0,0014\ ppm$ $T_0 = 19,8°C$

**Reading on the levelling staff after correction:**
$L = L' \cdot [1 + m_0 + \alpha_T \cdot (T - T_0) \cdot 10^{-6}]$

| | | | |
|---|---|---|---|
| $L'[m]$ | measured value | $m_0$ | scale factor |
| $T[°C]$ | temperature during measurement | $\alpha_T[ppm \cdot °C^{-1}]$ | coefficient of thermal expansion of steel |
| $T_0[°C]$ | temperature during calibration | | |

**Determination of scale factor:**

**1st measurement:**
scale factor:
-0.0250 ppm ± 0,001 ppm
Average temperature 20,2 °C
Average atmospheric pressure: 1016.4 hPa
Average deviation of measurement: ± 0.05 mm

**2nd measurement:**
scale factor:
-0.0388 ppm ± 0,001 ppm
Average temperature 19,4 °C
Average atmospheric pressure: 1016.0 hPa
Average deviation of measurement: ± 0.05 mm

**Average from both measurement:**
scale factor:
-0.032 ppm. ± 0,001 ppm
Average temperature 19,8 °C
Average atmospheric pressure: 1016.2 hPa
Average deviation of measurement: ± 0.05 mm

**b**

**Calibration certificate no. 03/2021** Page 2/2

**Leveling staff (type, no.):**
30 m steel measuring band on metal - plastic fork, no. 3-S12-3005 U-1
**Calibration range [m]:**
0.1-29.1
**Contract:**
[redacted]
**Date**
8.3.2021

**Corrections for the centre of the bar from the measuring tape [mm]:**

| m\dm | 0 | 1 | 2 | 3 | 4 | 5 | 6 | 7 | 8 | 9 |
|---|---|---|---|---|---|---|---|---|---|---|
| 0 | - | 0.00 | 0.10 | 0.04 | 0.01 | -0.04 | -0.08 | -0.01 | 0.00 | 0.00 |
| 1 | 0.01 | 0.00 | -0.07 | -0.09 | -0.13 | -0.18 | -0.14 | -0.12 | 0.01 | 0.05 |
| 2 | -0.01 | 0.04 | 0.09 | 0.00 | -0.04 | -0.13 | -0.18 | -0.16 | -0.15 | -0.10 |
| 3 | -0.13 | -0.16 | -0.20 | -0.15 | -0.18 | -0.12 | -0.12 | -0.21 | -0.16 | -0.08 |
| 4 | -0.06 | -0.01 | -0.02 | -0.10 | -0.08 | -0.09 | -0.15 | -0.11 | -0.06 | -0.13 |
| 5 | -0.11 | -0.11 | -0.17 | -0.12 | -0.16 | -0.23 | -0.22 | -0.25 | -0.04 | 0.09 |
| 6 | -0.05 | -0.10 | -0.12 | -0.14 | -0.19 | -0.15 | -0.21 | -0.22 | -0.23 | -0.25 |
| 7 | -0.30 | -0.26 | -0.26 | -0.24 | -0.23 | -0.28 | -0.29 | -0.32 | -0.25 | -0.25 |
| 8 | -0.19 | -0.22 | -0.22 | -0.25 | -0.21 | -0.19 | -0.21 | -0.17 | -0.21 | -0.26 |
| 9 | -0.21 | -0.23 | -0.29 | -0.28 | -0.36 | -0.41 | -0.35 | -0.29 | -0.18 | -0.12 |
| 10 | -0.20 | -0.25 | -0.20 | -0.22 | -0.27 | -0.24 | -0.33 | -0.36 | -0.36 | -0.34 |
| 11 | -0.39 | -0.39 | -0.45 | -0.46 | -0.39 | -0.37 | -0.33 | -0.36 | -0.35 | -0.38 |
| 12 | -0.31 | -0.33 | -0.34 | -0.35 | -0.31 | -0.34 | -0.37 | -0.33 | -0.33 | -0.29 |
| 13 | -0.30 | -0.35 | -0.39 | -0.43 | -0.45 | -0.48 | -0.47 | -0.44 | -0.34 | -0.24 |
| 14 | -0.26 | -0.29 | -0.29 | -0.37 | -0.45 | -0.44 | -0.42 | -0.47 | -0.46 | -0.43 |
| 15 | -0.52 | -0.49 | -0.56 | -0.56 | -0.48 | -0.50 | -0.52 | -0.49 | -0.51 | -0.45 |
| 16 | -0.33 | -0.39 | -0.40 | -0.41 | -0.47 | -0.41 | -0.41 | -0.37 | -0.46 | -0.43 |
| 17 | -0.44 | -0.46 | -0.43 | -0.44 | -0.52 | -0.56 | -0.56 | -0.56 | -0.37 | -0.33 |
| 18 | -0.39 | -0.37 | -0.41 | -0.49 | -0.48 | -0.50 | -0.56 | -0.62 | -0.59 | -0.56 |
| 19 | -0.60 | -0.54 | -0.62 | -0.56 | -0.61 | -0.69 | -0.69 | -0.61 | -0.58 | -0.60 |
| 20 | -0.52 | -0.56 | -0.57 | -0.51 | -0.55 | -0.56 | -0.55 | -0.60 | -0.63 | -0.55 |
| 21 | -0.55 | -0.57 | -0.60 | -0.70 | -0.68 | -0.68 | -0.71 | -0.70 | -0.54 | -0.58 |
| 22 | -0.63 | -0.59 | -0.59 | -0.58 | -0.58 | -0.65 | -0.70 | -0.74 | -0.76 | -0.72 |
| 23 | -0.77 | -0.77 | -0.82 | -0.77 | -0.75 | -0.72 | -0.78 | -0.81 | -0.81 | -0.83 |
| 24 | -0.72 | -0.71 | -0.66 | -0.64 | -0.69 | -0.73 | -0.72 | -0.72 | -0.74 | -0.71 |
| 25 | -0.76 | -0.78 | -0.78 | -0.80 | -0.75 | -0.83 | -0.90 | -0.88 | -0.74 | -0.73 |
| 26 | -0.74 | -0.72 | -0.80 | -0.84 | -0.82 | -0.89 | -0.88 | -0.86 | -0.92 | -0.90 |
| 27 | -0.96 | -0.96 | -0.98 | -0.97 | -1.03 | -1.01 | -0.94 | -0.99 | -0.92 | -0.91 |
| 28 | -0.85 | -0.97 | -0.99 | -0.98 | -0.96 | -0.80 | -0.83 | -0.83 | -0.89 | -0.94 |
| 29 | -0.98 | -0.98 | - | - | - | - | - | - | - | - |

*note: correction of the reading on the measuring tape can be realized in two ways, namely (1) using the relationship from the first page of this protocol or (2) adding a correction directly interpolated from the correction table mentioned above.*

Technical specialist: Ing. Pavol Kajánek, PhD. Bratislava, 8.3.2021
Laboratory director: doc. Ing. Ján Erdélyi, PhD. Institute director: prof. Ing. Alojz Kopáčik, PhD.

**Fig. 7** Calibration certificate for the measuring tape: a – graphical representation of corrections and the regression line, b – numerical expression of corrections

The software used for managing the calibration process includes a graphical user interface (Fig. 8), which facilitates working with the comparator during the tape

calibration and displays partial calibration results in quasi-real time (approximately 7 seconds of processing for each new position/image).

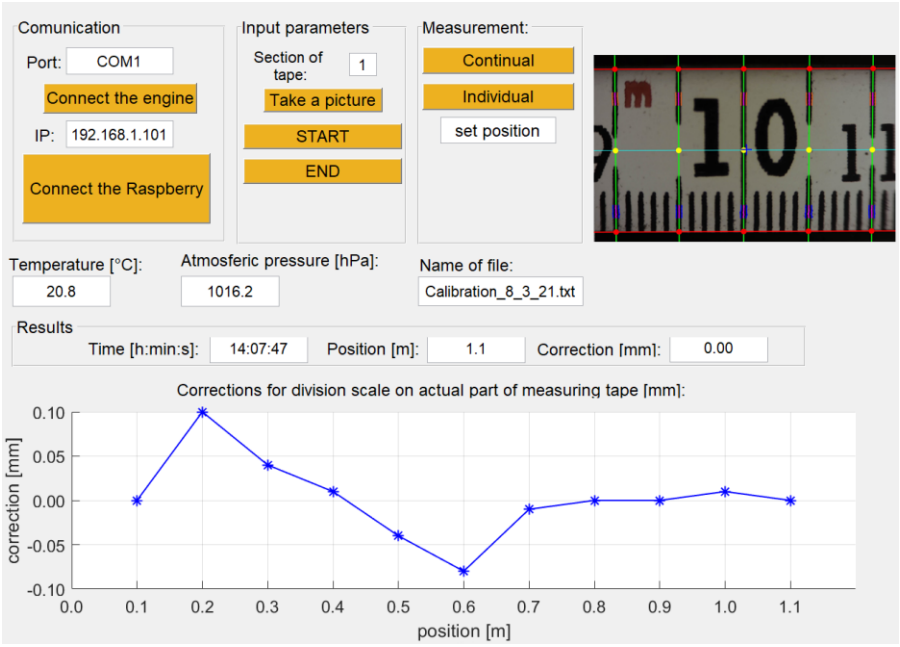


**Fig. 8** Graphical user interface

## DISCUSSION

Based on the analysis of system performance the internal precision of determination of the division position could be stated, that the accuracy of interferometric measured values is at level of $(0.5\times10^{-6}\times L[m])$ mm, where $L$ is the measured length in meters.

The accuracy of the values determined using image processing, including the corrections (offset, inclination, etc.) could be given by 0.005 mm. According to the final precision of the position of the division scale will be 0.006 mm. This precision also indicates the accuracy of the corrections, determined as the difference between the determined position and the nominal position of the division at the calibrated scale, which will be given by 0.01 mm. This value represents the expanded measurement uncertainty determined based on the accuracy of the evaluation of the division scale correction and an expansion factor of 2.

## CONCLUSION

Measuring tapes, like other geodetic measuring instruments, are subject to regular checks to verify the quality of the measuring device to achieve the required accuracy in measurements. For this purpose, a comparator was developed and tested in the Laboratory of Levelling Systems and Length Measures. The laboratory belongs to the Calibration Centre for Geodesy in Slovakia. Its role is to realise the standard for the calibration of short linear measures.

During calibration, the actual position of the scale divisions on the measuring tape is evaluated based on interferometric measurement and image processing of the calibrated tape's scale. Interferometric measurement is used to measure the change in position of the camera's projection centre. During calibration, the camera is not precisely positioned over the edge of the scale division, but the distance from the edge of the evaluated

division to the main point of the image is evaluated. The result of the calibration are corrections of the divisions, which are determined as the difference between the nominal value of the scale division and its actual measured value evaluated on the comparator. This process is fully automated from the moment the calibrated tape is placed and fixed on the comparator. The accuracy of the determination of corrections is 0.01 mm.
To verify the results, a comparison of calibration results with results of another calibration laboratory, based on an available calibration certificate, was carried out. These express the correctness of the result achieved. To increase the reliability of calibration results is planned to carry out a set of comparative calibrations in the future.

## ACKNOWLEDGEMENTS

This publication was created with the support of the Scientific Grant Agency of the Ministry of Education, Science, Research, Development and Youth of the Slovak Republic and the Slovak Academy of Sciences for the project No VEGA-1/0272/22.

This work was supported by the Slovak Research and Development Agency under the Contract No APVV-18-0247.

## REFERENCES

[1] Wang P., Zhao H., Ren G. Development and Application of Standard Device for Calibrating Steel Measuring Tape Based on Machine Vision, Applied Science, vol. 12, p. 7262, 2022. doi: https://doi.org/10.3390/app12147262
[2] Chen S., Qian X., Zhou M. Research of Automation Steel Tape Measurement System Based on PLC and Computer Vision Technology, 2009 WRI World Congress on Software Engineering, Xiamen, China, 2009, pp. 251-255, doi: https://doi.org/10.1109/WCSE.2009.15.
[3] Kang S. Y. Distributed multi-channel computer vision measurement system, Optical Technology, vol. 27, No. 4, pp. 344-345, 2001.
[4] Kuchtová M., Mitáš J. Metrological Support of Lengths at the Department of Theoretical Geodesy of SUT in Bratislava, Proceedings of the Seminar "Metrology in Geodesy". Bratislava, Slovak Republic, 2001, pp. 137-142.
[5] Yandayan T., Ozgur B. A motorized 5 m tape comparator for traceable measurements of tapes and rules, Measurement, vol. 49, pp. 113-125, 2014. doi: https://doi.org/10.1016/j.measurement.2013.11.040
[6] Haitjema H. Calibration of Displacement Laser Interferometer Systems for Industrial Metrology. Sensors. vol. 19, p. 4100, 2019. doi: https://doi.org/10.3390/s19194100
[7] Kim J. W. et al. A 50 m laser interferometer for automatic calibration of surveying tapes using wireless communication. Measurement Science and Technology, vol. 19. p. 17003, 2007. doi: https://doi.org/10.1088/0957-0233/19/1/017003
[8] Judson, L. V. Calibration of line standards of length and measuring tapes at the National Bureau of Standards. 1960.
[9] OCTAGON Precision (2018), OCTAGON Measuring Scale & Tape Calibration System Model MSTC-1000 comparator. Available on April 15, 2024. Available at: https://www.scicron.co.th/octagon-measuring-scale-tape-calibration-system-mstc-1000.html?___store=thai&___from_store=default

# EXPERT EVIDENCE AND INVENTORY OF CADASTRAL MAP DERIVATIVES

**Assoc. Prof. Ľubica Hudecová, MSc., PhD.** [1]

**Peter Kyseľ, MSc., PhD.**[2]

**Natália Faboková, BSc.**[1]

[1] Slovak University of Technology in Bratislava, Faculty of Civil Engineering, Department of Surveying, **Slovakia**
[2] Research Institute of Geodesy and Cartography in Bratislava, **Slovakia**

## ABSTRACT

Land administration system in Slovakia is a large system. Many incomplete data and errors have been incorporated into its content since 1850. Most problems in the field of land administration system are solved by judicial proceedings, in which the expert testimony is required to reach the conclusion. The gathering of data about a particular land parcel consists of investigation of documents and maps. The investigation of map documents is very important for the whole process. The derivatives of these maps are stored in archives, cadastral offices, and other institutions. The availability of map sheets is also complicated by the fact, that not all of them have been digitized. An application has been created by the authors of this paper, by which the map sheets can be accessed. Projective photogrammetry method and Structure-from-Motion method were used to fill in the map sheets inventory. These methods provide a good readability of the map sheets, so they could be used by the experts. The application enables the ordering of the map sheets by the name of the map sheet, by the actual or historical name of the location and by the location of the physical map sheet storage. The contents of the inventory can be extended gradually with the digitized map sheets. This application providing the access to the map sheets inventory reflects the experts' requirements, who point out on the great time requirements of their activities in the field of the land administration systems for a long time. The solution proposed in this paper on a small group of map sheets could serve as an example for the facilitation of access to the map sheets from the whole territory of Slovakia for the experts.

**Keywords:** map sheets, geodesy and cartography court experts, land administration system, application

## INTRODUCTION

The need for expert work is a necessity in most court proceedings. Ensuring the performance of expert work in all fields is a society-wide requirement and it is generally expected that it will be implemented at the highest possible quality level. The conclusions presented by the expert during proceedings before the court represent the result of an exact and independent assessment of the facts related to the proceedings [1]. The expert thus represents the highest level of knowledge and quality in the given field in the court proceedings. These expectations of the society are represented in the proceedings by the logical and legal claim of both parties to exercise the right at the legislative, technical, and ethical level. In the field of geodesy and cartography, more than 90% of resolved

cases concern the land administration system (LAS) – the real estate cadastre. The reasons are given by its historical development [2]. LAS represents an extensive work that has been under development for several decades. It includes the content of older records, which it followed up on. These were based on different legislative and technical regulations, therefore the procedures for recording land and its identifying features, as well as ownership rights and their limitations, were different. Along with its content, its shortcomings, inaccuracies, and errors have been transferred to today's LAS documentation. On the other hand, older written records and maps are still important today. They fill in the "blanks" in missing or incomplete LAS data and they help to resolve disputes. They are used by experts when preparing expert testimonials. The professional nature of expert work depends on the legal nature of the filing (lawsuit) and on the requirements set by the court for their processing. Submitted proposals from the field of cadastre are generally oriented to [3], [4]:

- determining the ownership boundary of the property,
- determining the ownership right to the real estate,
- resolving disputes in neighborly relations,
- location of the building according to the construction procedure,
- construction implementation according to the project documentation,
- restoration of the legal status in the field.

Searching for data about land parcel is represented by an examination of documentation and maps, based on which the land parcel, its identifying features, ownership rights and their restrictions were originally recorded in LAS. All available older documents are examined to reconstruct the procedure of registration of rights to the real estate, the accuracy and completeness land parcel boundaries, and to exclude possible errors. Deeds proving ownership and other rights are examined, the boundary of the original land parcel is identified in older graphic documents, which can be derivatives of original maps, surveying sketches or allotment plans (Fig. 1).

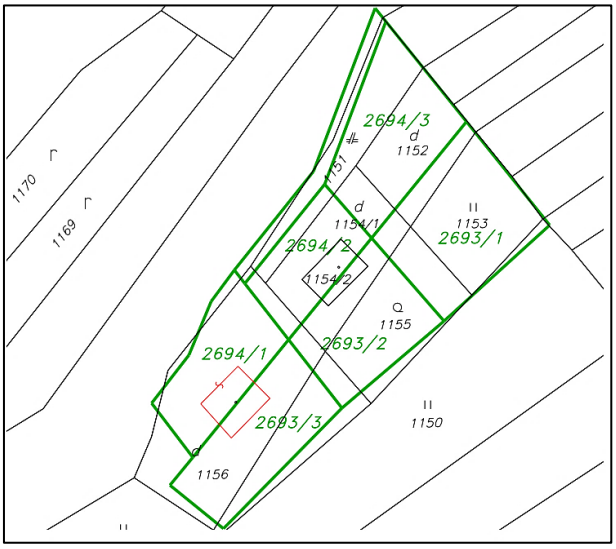


**Fig. 1:** Usage of the original map derivative for the creation of the graphical document for an expert testimony.

The variety and time-consuming nature of LAS expert work requires good organization of the work to minimize costs to the expert. It is not always sufficient to search information about the land in the documents available at the cadastral office; the expert must visit several institutions that manage archival documents. The Law on Experts [1] allows an expert to claim compensation only for out-of-pocket expenses, which are to be reasonable and expedient.

The idea to create an inventory of map sheet derivatives as well as an application allowing access to map sheets for geodesy and cartography court experts, reflects the requirements of practice [3] as well as experience from abroad [4], [5].

Currently, only a part of the cadastral map derivatives is digitized in Slovakia. The Central Archive of Geodesy and Cartography in Bratislava digitized analogue maps using scanning technology between 2013 and 2019. Metadata records have been processed for these raster maps [6]. However, there are no electronic services for the usage of these maps. In this paper, a fast and accessible way of digitizing map sheets for populating the "Inventory of cadastral map derivatives" is presented and the metadata content is proposed to provide easy searching of maps for geodesy and cartography court experts. The functionality of the proposed application assumes that the map sheets will be catalogued after digitization so that they can be searched according to different criteria, e.g.:

- a title (a numeric, alphabetic, or combined designation given in marginal information that reflects the location in the layout of map sheets) within a particular map collection,
- the name of the location that the map sheet depicts according to both the now standardized geographical names and the original historical geographical names (possibly also in other languages),
- the location (place of physical storage of the specific map sheet - cadastral office, archive, other).

## MATERIALS AND METHODS

The materials used for the creation of the "Inventory of cadastral map derivatives" were 40 analogue map sheets obtained from district cadastral offices and from the Central Archive of Geodesy and Cartography in Bratislava. The contents of the inventory will be extended gradually with the digitizing of the map sheets.

Map scanning is generally perceived as a secondary form of digitization. In the department of Geodesy and Cartography in Slovakia, the scanning process is regulated by a technical regulation, according to which the accuracy of map scanning is given by a mean coordinate error $m_{xy} \leq 0.10$ mm, and the scanning density from 400 to 600 dpi [7]. Scanners used for scanning of the cadastral maps must have a quality certificate, which must be updated annually.

Photogrammetric methods, namely the Structure-from-Motion (SfM) method and the projective photogrammetry method, were used to create the “Inventory of cadastral map derivatives”. A NIKON D850, a digital single-eye reflex camera, was used to take images of the map sheets. The camera has a 35.9 mm × 23.9 mm FX, CMOS image sensor. Two

lenses with different focal lengths (35 mm and 20 mm) were used in the imaging. Since a scanning sensitivity of at least 400 dpi is prescribed for scanning map sheets [7], the scanning distance of the camera was adjusted accordingly. For the focal length of f = 35 mm, the scanning distance was approximately 50 cm and for a focal length of f = 20 mm approximately 30 cm.

SfM processing in Agisoft Metashape software allows reconstruction of scenes based on the camera movement relative to the object. Agisoft Metashape is a software for photogrammetric processing of digital images and creation of 3D data based on them. The software must identify the tie points in all the images in which they are located in order for the software to reconstruct a scene. This task is performed by the interest operators. Once these have been obtained, it moves on to so-called feature matching, i.e. matching based on features or surfaces. In this process, the points or areas that have been determined by the algorithms as interest operators, are matched on individual frames. In the case of points, these are most often edges or patches. For surfaces, not only the points are used, but also their surroundings are considered, and in some cases the whole window is used. Cross-correlation is used to find these pairs in the images. One feature is taken as a sample - reference - and the features in the search window are compared with it. The search window is applied on the reference one and the correlation coefficient r is calculated for each position by successive scrolling (always by 1 pixel).

Processing by the projective photogrammetry method in PhotoModeler software uses the central projection. The central projection generally expresses the relationship of the position of center of projection between the reference and image coordinate systems. It is a projective relationship that is given by the collinearity equations. Accuracy is closely related to the geometric distortion that is caused by lens distortion. To obtain the most optimal results, the relations must be solved with the coordinates corrected for lens distortion. As for the reference accuracy, it depends on four basic parameters, namely the scale number of the image, the size of the image element, the accuracy of the measurement of the image element, and the rotation of the image with respect to the observed plane. In order to achieve constant accuracy over the entire image area, it is ideal to take the images so with minimal tilt. Another variable to be considered is the effect of object roughness. If the object is not planar but differs from the ideal case, a radial shift occurs in the image. This displacement subsequently affects the position of the points in the reference system. This method is used especially for redrawing planar facades for photo plans or for determining plane deformations. Its main advantage is simplicity, but also high accuracy. The method can be performed without the use of control points (CP), but in such case it is necessary to introduce some other conditions. Like any method, it has its drawbacks. The main weakness is the strong emphasis on application to planar objects only. For optimal results, it is necessary to use non-tilted images. The minimum requirements for the method include the existence of at least one image, the use of at least 4 CPs (optimally 5 CPs) or the use of 6 conditions, a planar object, and optimally a correction for distortion.

The application to make the "Inventory of cadastral map derivatives" available to geodesy and cartography court experts was developed based on a software solution, the Python programming language and the Visual Studio Code programming environment were used. Several libraries were used to ensure the creation of a suitable user interface.

## RESULTS

The results of the photogrammetric methods in terms of the quality of map sheet imaging do not reach the accuracy of a large-area scanner, but they are sufficient for the purpose of creating the "Inventory of cadastral map derivatives". It can be stated that each processing procedure has advantages and disadvantages.

The first method – the use of SfM, had the longest scanning time. A larger number of images were taken for the reconstruction of one map sheet. It should also be mentioned that an individual approach was needed for each map sheet. If there was sparse or bland artwork on a map sheet, this significantly increased the processing time. This method also required a significantly larger amount of memory space on the digital workstation. However, the great advantage is that a very high-resolution raster can be produced if required. Scanning and using the projective photogrammetry method in PhotoModeler software was significantly faster despite the camera calibration. The procedure was relatively simple and straightforward. The disadvantage was the not quite perfect redrawing of parts of the frames of the map sheet after processing if they were folded.

The fact that the original map sheet had many derivatives during the period of its use, the information about the creation of the map (map campaign), the updating of the map and its renewal is very important for the expert activity. The scope of the proposed metadata record items of cadastral map derivatives is shown in (Tab. 1).

**Tab. 1:** Characteristics of cadastral map derivatives - metadata record items and selected codelist values.

| Information | Predefined codelist values |
|---|---|
| map designation | - |
| form | original, copy |
| scale | decadic, non-decadic, without scale |
| mapping campaign | Hungarian coordinate systems (1851-1930), concretual maps (1851-1875), The A Manual (1930-1950), substitute maps (1956-1960), Technical-Economical Mapping (1961-1980), Base Map (since 1981), without mathematic base |
| year of creation | - |
| mapping method (availability of coordinates) | graphical (without coordinates), geodetic (with coordinates), geodetic (without coordinates), photogrammetric (without coordinates), photogrammetric (with coordinates), combined, other |
| usage of the map at the time of its creation | Stable Land Cadastre, Czechoslovak Land Cadastre, Land Registry Book, Uniform Land Registry, Land Registry, Cadastre of Real Estate |
| language | Slovak, German, Slovak with Hungarian transcription, Hungarian, Russian, Latin |
| map renewal | connection of map sheets, erasure of ownership boundaries outside built-up areas, decadization, mass updating of map, without renewal |
| year of the state of the drawing | - |
| availability | central archive of Geodetic and Cartographic Institute, cadastral office, district archive, other |

For each map sheet, the content of a metadata record of the imaging procedure and basic processing characteristics was designed. (Tab. 2).

**Tab. 2:** Imaging - metadata record items and selected codelist values.

| Metadata record item | Predefined codelist values |
|---|---|
| map designation | - |
| color of the original map | color, colorized, black and white with color updates, black and white with color labeling, reduced map |
| preservation | good, moderate damage, damaged |
| specifics of the map | torn-up margins, missing part of the sheet, unreadable part of the sheet, other |
| quality of paper | rough paper, rough paper with canvas, ordinary paper, thin paper, cardboard, foil, tracing paper, other |
| whiteness | not yellowed, slightly yellowed, stained, yellowed |
| imaging method | - |
| map sheet dimensions | - |

The application for making the inventory available to geodesy and cartography court experts was created on the basis of a software solution. It is functional, physically fully portable, and distributable. It allows the display of basic cadastral map derivative data. The viewed map sheet can be zoomed in such a way that the details - parcel numbers, symbols, parcel boundaries and marginal map sheet information - are readable. Work is underway to improve the user interface and search functionality according to all the proposed criteria (Fig. 2).

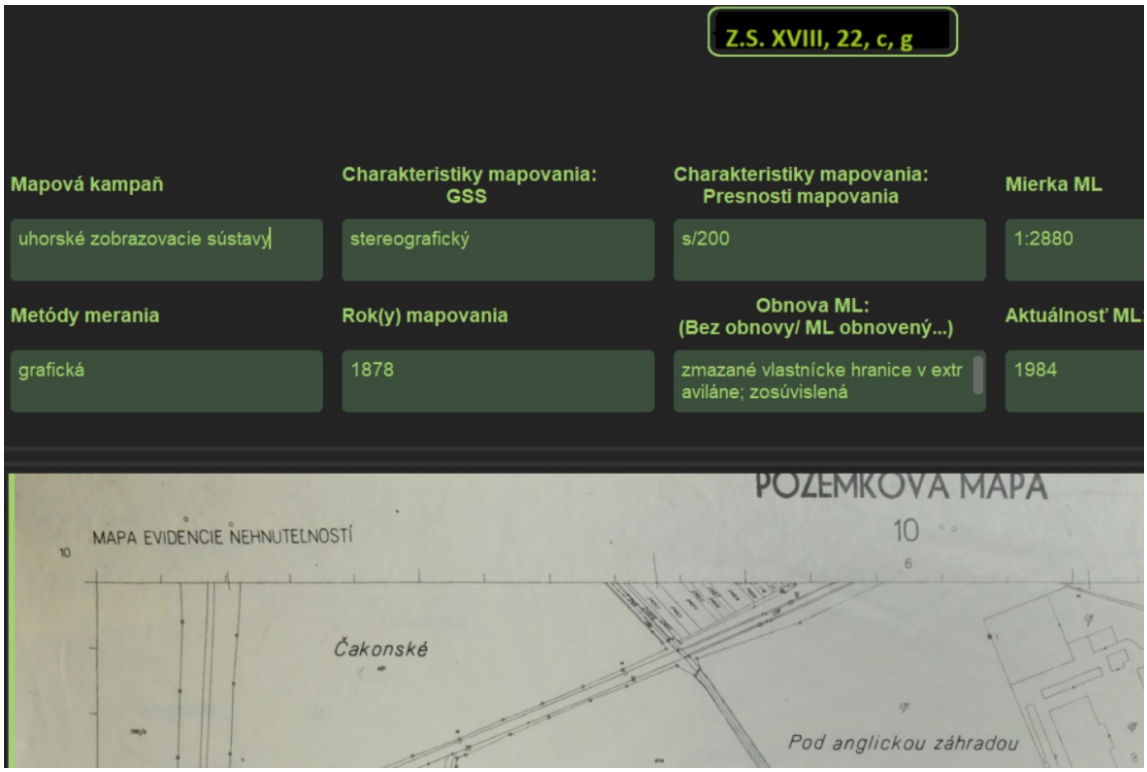


**Fig. 2.** User interface of the application for making the map inventory available to geodesy and cartography court experts.

## DISCUSSION

The aim of the paper was to highlight the needs of geodesy and cartography court experts. Graphical documents (cadastral map derivatives) needed for expert testimony are nowadays obtained from several institutions. There is no inventory of them and many of them are still not in digital form. Two digitization methods were tested on a sample of 40 analogue map sheets. Court expert uses all available cadastral map derivatives in his work, on which he analyzes the geometric characteristics of specific land parcels - shape and dimension of the depicted objects. The achieved results in terms of the quality of imaging are sufficient for the needs of court testimony. To creating the "Inventory of cadastral map derivatives" it is recommended to use the projective photogrammetry method in the PhotoModeler software. It is more efficient, the imaging was done quickly, the processing process did not occupy a large amount of computer memory and, moreover, the processing can be done in one software with a relatively simple procedure.

However, it is worth thinking about improving the results when using photogrammetric methods. The reduction in the readability of the images was caused by:

- the map sheets were not loaded (e.g. with transparent material) when the image was taken; if the map sheets had significant folds in the middle part or at the corners, this caused complications in the processing, in addition to a reduction in image quality,
- the map sheets were not properly illuminated during imaging; this caused glare when using the flash on the camera or reflections from the surrounding environment.

## CONCLUSION

The displaying of the land parcels in the older graphic documents are not sufficiently accessible to surveyors today. The idea of creating the inventory of cadastral map derivatives and making it available to geodesy and cartography court experts in a simple way is a respond to the requirements of practice. For the proposed “Inventory of cadastral map derivatives” to fulfil its purpose, it must make all cadastral map derivatives available to the experts. Those that exist today only in analogue form must be digitized. The creation of a reliable application for geodesy and cartography court experts also implies the completion of metadata records on the process of digitization of the map sheets, on the basic characteristics of the processing, on the characteristics of the derivatives and on their availability.

The paper contains recommended procedures for creating the “Inventory of cadastral map derivatives”, as well as an outline of a solution for creating an application for geodesy and cartography court experts. A part of the future nationwide solution may be a database based on queries through a user interface, e.g. on the SQL query language or linking the data with the graphical part, similarly as it currently works in the Map Client ZBGIS® application, whose administrator is the Geodetic and Cartographic Institute Bratislava [8]. Court expert would mark the territory of interest on the map of and based on this, a list of cadastral maps derivatives that exist in this territory would be generated and following information would be provided: year of the map creation, mapping campaign, where (in which archive) and how (online or physically) they are available. The solution could make use of the ZBGIS® Map Client application, which allows to retrieve the map sheet layout of some mapping campaigns by demarcation of a location in the map (Fig. 3).

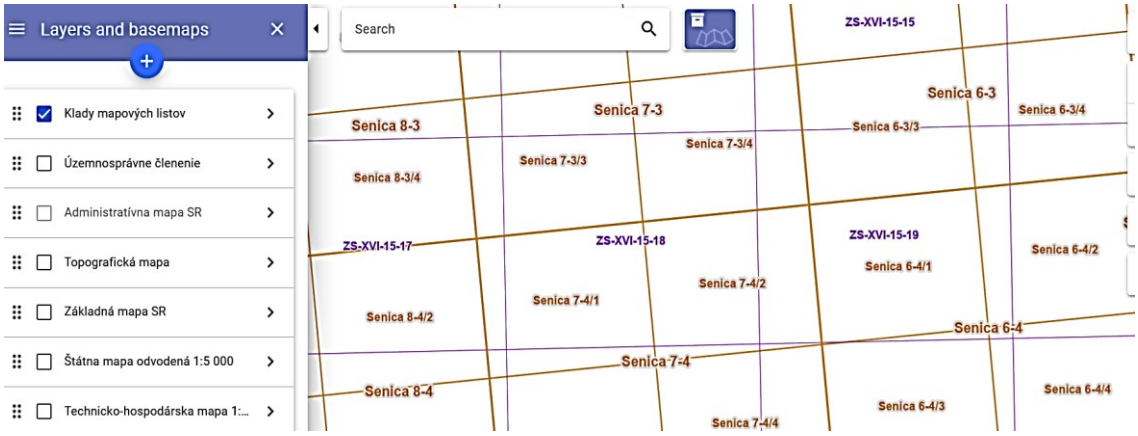


**Fig. 3.** Archive theme - ZBGIS® Map Client (Source: ZBGIS® Map Client).

## ACKNOWLEDGEMENTS

This work was supported by the Ministry of Education of the Slovak Republic and the Slovak Academy of Science [grant number KEGA 001STU-4/2023].

## REFERENCES

[1] Act No. 382/2004 Coll. on experts, interpreters and translators and on amendments to certain laws.

[2] Gašincová, S., Gašinec, J., Hudecová, Ľ., Černota, P., Staňková, H., Analysis of the Usability of the Maps from the Former Cadastre of Lands in Terms of Parcels Area Registered in the Cadastral Documentation, Inzynieria Mineralna, Poland, no. 2, pp 191-200, 2018. ISSN 1640-4920. DOI: 10.29227/IM-2018-02-24.

[3] Horňanský, I., A positive Step Towards Optimizing the Expert Activity of Geodesy, Cartography and Real Estate Cadastre, Geodetický a kartografický obzor, Czech-Slovak, vol. 65 (107)/issue 7, pp 157-160, 2019. ISSN 1805-7446.

[4] Hanus, P., Pęska-Siwik, A., Szewczyk, R., Spatial analysis of the accuracy of the cadastral parcel boundaries. Computers and Electronics in Agriculture, Netherlands, vol.144, pp 9–15, 2018. DOI: https://doi.org/10.1016/j.compag.2017.11.031.

[5] Roić, M., Križanović, J., Pivac, D., An Approach to Resolve Inconsistencies of Data in the Cadastre. Land, Switzerland, vol. 10 (1), pp 1-20, 2021.

DOI: 10.3390/land10010070.

[6] Kmeťková, R, Pechová, P., Digitization of cadastral maps of the Slovak Republic and the creation of their metadata, Cartographic letters, Slovakia, vol. 21 (2), pp 11-23, 2013. ISSN 1336-5274.

[7] Instruction for the scanning and transformation of cadastral maps no. P-1588/2002. Geodesy, Cartography and Cadastre Authority of the Slovak Republic, 2002.

Available at: https://www.skgeodesy.sk/sk/ugkk/technicke-predpisy-ine-akty-riadenia/

[8] Geoportal. “Concretual maps.” [online]. Updated:05.12.2023 [cit. 2024-01-12].

https://www.geoportal.sk/sk/archiv/komasacne-mapy/konkretualne-mapy.html

# FINAL QUALITY EVALUATION OF THE KINEMATIC MODEL OF THE EARTH'S CRUST HEIGHT MOVEMENT ON THE CROATIAN TERRITORY

**Blaženka Bukač**[1],
**Assoc. Prof. Ivan Razumović**[1],
**Prof. Nevio Rožić**[1]
[1] University of Zagreb – Faculty of Geodesy, **Croatia**

## ABSTRACT

The paper presents a quality evaluation of the kinematic model concerning the relative height movement of the Earth's crust that refers to the territory of the Republic of Croatia. This kinematic model enables determination of vertical displacements and movement speeds of discrete points on the Earth's crust. So far, the quality of the model has been rated only for certain parts of the Croatian territory, but this paper shows the results of the model's quality evaluation for the entire territory of the Republic of Croatia. The model's quality is evaluated using the geometric levelling measurements of the 2nd order state network by applying the indirect quality assessment method. The criteria for measurement accuracy are determined at both the *a priori* and the *a posteriori* level and are expressed with reference probable errors. In the first case, the quality assessment is based on the levelling loop misclosures before network adjustment using the original and reduced measurements, and in the second case, on the network adjustment results using the original and the reduced measurements. The results indicate quite a successful elimination of the systematic effect of the relative height movements of the crust from the levelling measurements of the 2nd order network, leading to the final conclusion that the height movement kinematic model for the entire Croatian territory can be reliably used for the determination of regional relative height changes due to vertical crustal movements with the centimetre level of accuracy.

**Keywords:** kinematic model, height displacement, vertical crustal movements, quality evaluation, Croatia

## INTRODUCTION

Changes in the shape of the Earth are the result of various dynamic processes in the Earth's system as a whole [1]. Monitoring and modelling these changes over a determined period enable quantification of displacements in a certain area, which represents a starting point for an interdisciplinary interpretation of the processes that led to them. An adequate basis for monitoring the changes on the Earth's surface are the permanently stabilised geodetic points with the coordinates referring to the chosen reference coordinate system, especially if there is repeated data for the same area over a longer period of time.

Focusing only on the height component, a height movement kinematic model of the Earth's crust for the Republic of Croatia has been created and is presented in [2]. The data basis for the kinematic model creation consists of a benchmark data set that is the result of continuous levelling works that had been being carried out during over more than a century and include three basic geometric levelling networks of the 1st order [3]. These are the Austrian Precise Levelling Network – APN (1874 – 1909), the First High

Accuracy Levelling Network – INVT (1946 – 1963) and the Second High Accuracy Levelling Network – IINVT (1970 – 1973) of the former Yugoslavia. An overview of the levelling data origin on the Croatian territory, the methods of their analysis and computational processing, the procedure of the vertical displacement determination as well as the methodology of height displacements grid model creation, are presented in detail in [4]. Height displacement grid models served as a basis for the creation of the height movement kinematic model whose purpose is to mathematically define the movements of the Earth's crust in the area of interest. It can be used to solve various professional and scientific tasks in geodesy as well as related geosciences. So far, two kinematic models have been created, a more complex one in the form of a uniformly accelerated/decelerated motion and a simpler one in the form of a uniform motion. The key information that determines the suitability of the kinematic model's usage for a specific purpose is the evaluation of its quality through the aspects of internal and external accuracy. Internal accuracy assessment of the kinematic model of uniformly accelerated/decelerated motion is available in [2], and results indicate a reliable centimetre level of accuracy. In the absence of a suitable set of independent reference (control) data for direct quality evaluation, external accuracy assessment was performed using an indirect method. Results of all external quality analyses of the kinematic model performed so far, in accordance with the methodology presented in [5], for certain parts of Croatia, are published in [6]. However, until this moment, the quality of the kinematic model has not been finally rated for the entire Croatian territory. That is why the previously performed analyses documented in [6] can be supplemented by including the levelling data for the remaining parts of the Republic of Croatia.

The Croatian height reference system for the epoch 1971 (HVRS71), in addition to the 1st order levelling network (IINVT), also consists of lower-order levelling networks. Because of that, the data basis for quality assessment comprises geometric levelling measurements from the 2nd order state network (precise levelling network – PN). Given that the measurements of the 1st and the 2nd order levelling networks were performed in significantly different epochs, it can be claimed that the same benchmarks in different epochs of field survey had different height positions due to the Earth's crust height movements. It should be noted that the time of the IINVT network realisation as a frame of the height reference system HVRS71 is very short and it is considered that potential changes in benchmarks' height positions that might have occurred during the survey are negligible. Therefore, the indirect method of external accuracy assessment of the kinematic model is based on the comparison between the accuracy of the original 2nd order levelling measurements from the epoch of field survey and the accuracy of those same measurements but reduced to the epoch of national height reference system realisation (IINVT network). Since there is an adequate time lapse between these epochs, the reduction of original measurements can be considered their correction for the systematic effect of the Earth's crust relative height movement. Consequently, it is assumed that the reduction of the measurements would result in an increase in measurement quality. Ultimately, the assessment of the kinematic model's external accuracy can be indisputable and very satisfactory if it can be used for the reduction of the measurements from the original survey epoch to any alternative epoch. This paper provides a final quality assessment of the Earth's crust height movement kinematic model for the entire Croatian territory.

## HEIGHT MOVEMENT KINEMATIC MODEL

The kinematic model of uniformly accelerated/decelerated motion of the Earth's crust, described in detail in [2], covers the territory of the Republic of Croatia, as well as of the neighbouring countries, Slovenia and Bosnia and Herzegovina. According to the period when the measurements of levelling networks APN, INVT and IINVT were carried out, the kinematic model can be used reliably for the time interval between 1874 and 1973. The kinematic model is available for download online [7]. It is created in the form of a grid model and enables the prediction of kinematic parameters of vertical motion; a point's relative height in the initial epoch $t_o = 1874.0$ which refers to the year when the survey of the APN network started, the point's vertical movement speed in the initial epoch and constant acceleration; for any point on the Earth's surface with known ellipsoidal position (Bessel ellipsoid) within the scope of the model. Determination of kinematic parameters using the grid model can serve to determine the relative height displacements for any epoch with respect to the initial epoch as well as to determine the point's current movement speeds in a certain epoch. Also, it is possible to determine height displacement of the same benchmark between two different arbitrary epochs. If two benchmarks connected with a measured height difference are observed, the kinematic model allows the calculation of the reduction (correction) of the measured height difference for the effect of the Earth's crust height movement.

## DATA AND QUALITY DETERMINATION METHODOLOGY

Since a data set independent from the kinematic model that would serve to directly assess the quality of the kinematic model is not available, an indirect method was applied. It implies the comparison between the accuracy indicators of the original levelling measurements of the precise level (2nd order) and those same measurements but reduced by the systematic influence of the Earth's crust height movement. Namely, by applying the created kinematic model, the reduction of the levelling measurements from the survey epoch to the mean epoch of the IINVT network survey (1971.1) i.e., to the epoch of the Croatian height reference system (HVRS71) realisation, is sustainable. According to the availability of the original and reduced measurements, levelling loop misclosures with the original and reduced measurements can be determined. Theoretically, misclosures should reflect only random effects, however, they usually contain systematic effects as well. Reducing the measurements results in the removal of the systematic effects that are related to the benchmarks' height displacements. Moreover, in the next step, independent processing (adjustment) of the levelling network with the original and reduced measurements is tenable. In both cases, reference probable errors of the original and reduced measurements (from the levelling loop misclosures and from the network adjustment) can be determined and compared. It can be expected that the reduction of the benchmarks' height displacement from the original measurements will result in better quality of the reduced measurements, from which a conclusion regarding the quality of the kinematic model can be indirectly derived. Quality assessment has been previously analysed only for some parts of the Republic of Croatia in [5], [6] and [8].

Quality assessment of the kinematic model encompasses nine levelling figures of the IINVT network (1st order) that cover the territory of the Republic of Croatia. The levelling figures are the following: I, III, IV, V, VI, VIII, IX, XII and XIV. Also, it should be noted that some levelling figures are only partially located on the Croatian territory. In accordance with the hierarchical principle, levelling data belonging to the 2nd order network that is the basis for the kinematic model's indirect quality assessment rely on the 1st order levelling network and jointly close a certain number of loops.

The configuration of the 2nd order levelling network in figures I, III, VI, IX and XII of the IINVT is shown in Figure 1. Figures I, III, IX and XII have previously been part of quality assessment performed in [6] where they are described in detail. Figures III and V (see also Figure 2) of the IINVT have been previously included in quality assessment of the kinematic model in [5] as a part of the initial testing of the kinematic model shortly after its creation, and have been selected due to their specific, yet mutually heterogeneous relief and topographic characteristics, as well as the fact that the data for these parts was available at that moment. Hence, relief characteristics of the areas selected for levelling line routes also affect the level of the systematic influence and should be taken into account when interpreting the results. Namely, figure III of the IINVT extends to the lowland area (Figure 1), while figure V of the IINVT is in the mountainous area (Figure 2). Figure VI of the IINVT represents a new data set that has not yet been included in the analysis and assessment of the kinematic model's accuracy. It consists of 8 levelling lines of the IINVT and 20 levelling lines of the 2nd order, forming 7 loops, out of which loop III is partially located on the territory of Bosnia and Herzegovina. Measurements of the 2nd order network in this area have been carried out from 1949 to 1962, which is, compared to the measurements in figure I of the IINVT, for about 20 years longer.

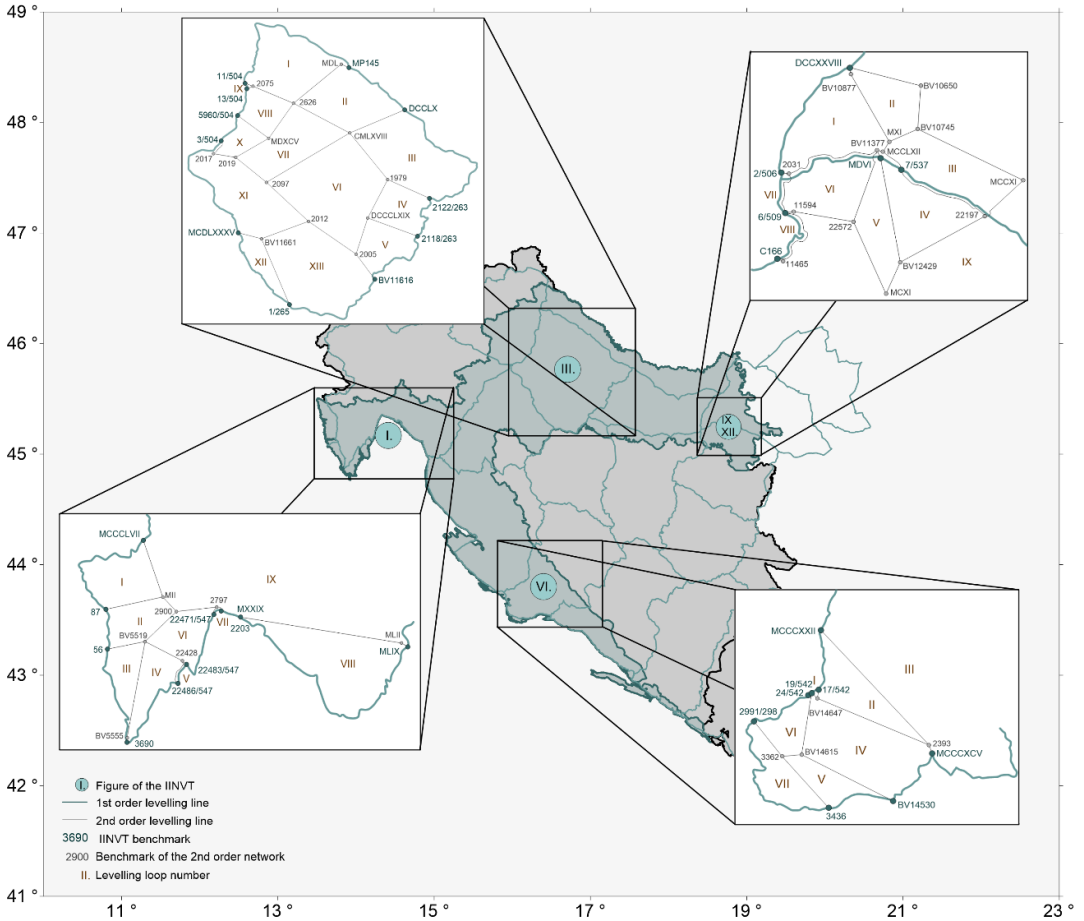


**Figure 1.** The configuration of the 2nd order network in the figures I, III, VI, IX and XII of the IINVT

The configuration of the 2nd order levelling network in figures IV, V, VIII and XIV of the IINVT is shown in Figure 2. Thereat, figures IV and VIII have been part of quality assessment described in [6]. Figure XIV of the IINVT includes 3 levelling lines of the 1st

order and 6 levelling lines of the 2nd order that jointly form 3 loops. In terms of quantitative data coverage, this is the figure with the smallest number of levelling measurements which have been carried out between 1949 and 1955. Also, figure XIV has not yet been included in the assessment of the quality of the kinematic model and therefore presents a new data set.

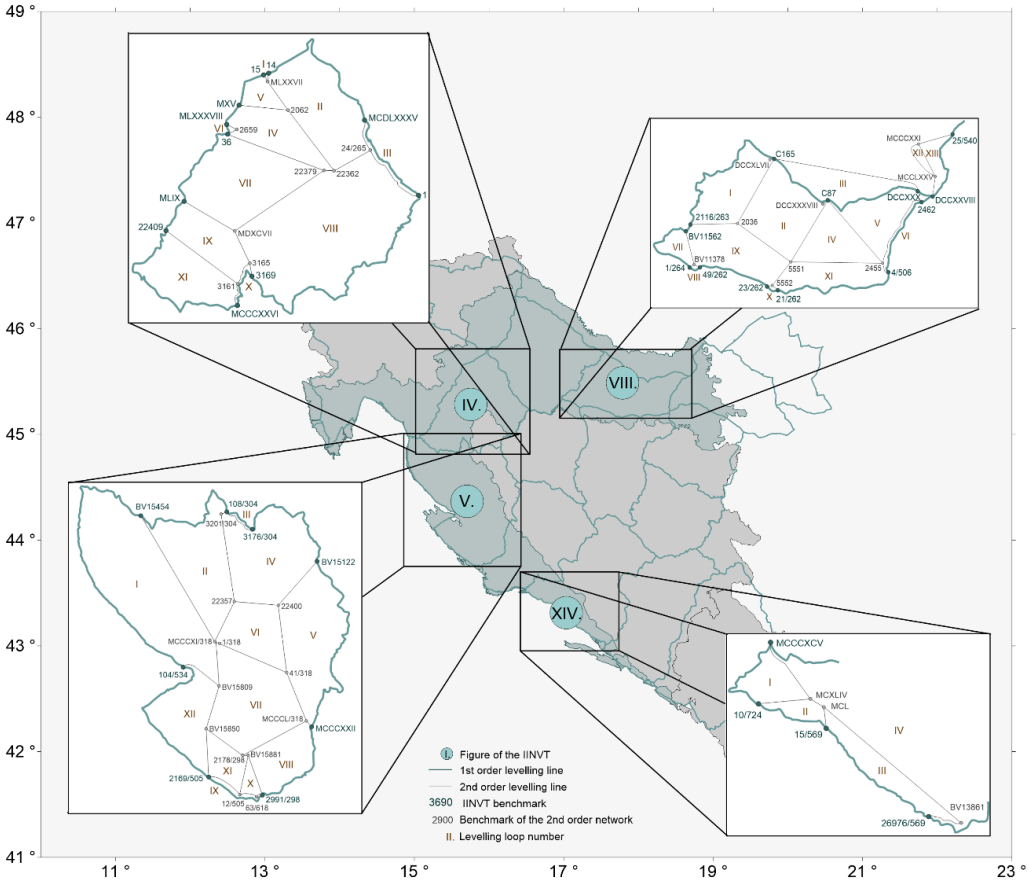


**Figure 2.** The configuration of the 2nd order levelling network in the figures IV, V, VIII and XIV of the IINVT

## QUALITY ASSESSMENT

*A priori* measurement accuracy is determined before network adjustment based on the network levelling loop misclosures with the original $\Delta h$ and reduced $\Delta h_r$ measurements. At the same time, each figure is observed as a separate element, although in reality they form a geometrically firm structure. *A priori* reference probable error of the original measurements $u_F$ is calculated from the levelling loop misclosures $W$ using the original measurements $\Delta h$, where the lengths of individual loops $F$ are introduced as weights according to the expression in [9]. Reference probable error of the reduced measurements is also calculated using the previously mentioned expression, however, in that case, the levelling loop misclosures $W_r$ calculated with the reduced measurements $\Delta h_r$ are used. *A posteriori* measurement accuracy criterion refers to the network adjustment, first with the original measurements and then with reduced measurements, where the entire network is considered as a whole. The adjustment was performed by applying the parametric adjustment and the least squares method, while the measurement weights were defined as reciprocal values of levelling line lengths [10]. Here, measurements of the 2nd order

network are relied on the adjusted values of the IINVT network. *A posteriori* reference probable error $u_\gamma$ is calculated separately for the original and reduced measurements [5]. In a theoretical sense, the values of *a priori* and *a posteriori* reference probable errors should be consistent if the measurements contain only random errors. In the case of eliminating the systematic influence of the benchmarks' height movement, accuracy criteria of the reduced measurements should be of a higher quality if the kinematic model is of sufficient quality to calculate the reduced measurements.

## RESULTS

Accuracy assessment results of the original and reduced measurements that form the basis for the conclusion regarding the quality of the kinematic model, are presented below. Namely, table 1 contains levelling loop misclosures with the original and reduced measurements. Their comparison shows that out of the total of 78 figures, loop misclosure values with the original measurements by reduction were noticeably reduced in 47 cases, while in 2 cases the values remained the same. A slight increase in loop misclosure values of less than 1.5 mm is observed in 9 cases, while in 20 cases the increase in values is more significant. The consistency of the loop misclosure sign is noted, except in 5 figures where there was a change. Also, there is a balanced relationship between the number of positive and negative loop misclosure values. Where the positional distribution of the loops that record increase of misclosure values after reducing is observed, it is evident that these loops are relatively evenly distributed over the entire Croatian area.

**Table 1.** Loop misclosures calculated with the original $W$ and reduced measurements $W_r$

| Loop | F [km] | W [mm] | $W_r$ [mm] |
|---|---|---|---|
| Figure I | | | |
| I | 135.26 | 32.5 | 4.1 |
| II | 109.55 | 14.7 | 6.7 |
| III | 120.43 | 25.6 | 9.8 |
| IV | 136.87 | 24.1 | 44.4 |
| V | 26.82 | -32.6 | -30.6 |
| VI | 119.38 | -11.1 | -10.1 |
| VII | 11.89 | -3.5 | -4.4 |
| VIII | 254.14 | -65.4 | -18.6 |
| IX | 681.05 | 15.7 | -1.4 |
| Figure III | | | |
| I | 150.25 | 2.2 | 6.8 |
| II | 127.06 | 13.6 | 2.4 |
| III | 175.50 | -9.4 | -7.3 |
| IV | 115.73 | -6.2 | -7.5 |
| V | 108.73 | 45.1 | 29.6 |
| VI | 200.89 | 39.2 | 38.7 |
| VII | 143.06 | 14.1 | 13.9 |
| VIII | 87.97 | 59.6 | 64.6 |
| IX | 5.96 | -13.9 | -13.6 |
| X | 66.09 | -64.8 | -59.0 |
| XI | 161.84 | -13.2 | -10.4 |
| XII | 99.98 | -28.0 | -3.3 |
| XIII | 166.77 | -38.3 | -54.9 |
| Figure IV | | | |
| I | 4.09 | 4.0 | 2.0 |
| II | 186.69 | -7.1 | 12.2 |
| III | 99.98 | 28.0 | 4.9 |
| IV | 147.84 | 9.0 | -7.5 |

| Loop | F [km] | W [mm] | $W_r$ [mm] |
|---|---|---|---|
| Figure IV | | | |
| V | 66.00 | -6.6 | -2.9 |
| VI | 9.53 | 15.2 | 13.9 |
| VII | 198.13 | -32.6 | -32.7 |
| VIII | 291.27 | 21.7 | 18.3 |
| IX | 145.91 | 17.4 | 15.0 |
| X | 49.23 | 10.6 | 3.2 |
| XI | 172.26 | -59.6 | -26.4 |
| Figure V | | | |
| I | 312.24 | -24.6 | -14.0 |
| II | 238.99 | -39.4 | -73.1 |
| III | 43.36 | 3.6 | -3.4 |
| IV | 214.62 | 48.2 | 43.7 |
| V | 243.99 | 5.4 | 42.9 |
| VI | 147.62 | 2.4 | 3.0 |
| VII | 204.83 | -67.0 | -67.7 |
| VIII | 128.24 | 57.8 | 57.7 |
| IX | 70.82 | -21.5 | -12.7 |
| X | 77.23 | 22.0 | 22.0 |
| XI | 144.23 | -18.1 | -18.0 |
| XII | 220.81 | 31.2 | 19.6 |
| Figure VI | | | |
| I | 9.53 | -1.6 | -1.9 |
| II | 144.13 | 0.5 | 13.4 |
| III | 482.45 | 42.7 | 25.8 |
| IV | 167.87 | -31.8 | -33.5 |
| V | 111.45 | 7.1 | 18.5 |
| VI | 154.08 | 4.2 | 0.0 |
| VII | 91.04 | -21.1 | -22.4 |

| Loop | F [km] | W [mm] | $W_r$ [mm] |
|---|---|---|---|
| Figure VIII | | | |
| I | 165.87 | -10.6 | -15.2 |
| II | 179.08 | 48.0 | 37.3 |
| III | 167.07 | 22.5 | 26.3 |
| IV | 156.50 | -6.8 | -7.1 |
| V | 137.53 | -40.1 | -34.3 |
| VI | 67.01 | -7.6 | -17.8 |
| VII | 65.88 | -24.1 | -18.0 |
| VIII | 11.85 | 1.1 | -1.0 |
| IX | 150.05 | 33.1 | 49.8 |
| X | 13.30 | -0.9 | 3.5 |
| XI | 157.65 | 7.9 | 2.7 |
| XII | 51.26 | -15.9 | -15.9 |
| XIII | 96.73 | 23.0 | 16.3 |
| Figures IX and XII | | | |
| I | 127.78 | 0.6 | 15.6 |
| II | 85.89 | -24.0 | -23.2 |
| III | 116.60 | 2.6 | 2.9 |
| IV | 119.24 | 1.7 | 1.6 |
| V | 111.64 | -14.5 | -14.4 |
| VI | 105.06 | 7.0 | 6.8 |
| VII | 30.90 | 3.0 | 7.4 |
| VIII | 48.66 | -8.1 | -2.3 |
| IX | 807.33 | 31.7 | 5.6 |
| Figure XIV | | | |
| I | 608.82 | -21.6 | -11.7 |
| II | 190.98 | -5.5 | -18.5 |
| III | 92.47 | 19.4 | 22.6 |
| IV | 117.62 | 7.7 | 7.6 |

The results presented in table 2 contain values of *a priori* $u_F$ and *a posteriori* $u_\gamma$ reference probable errors of the original and reduced measurements. Decreased values of both reference probable errors for reduced measurements can be observed in 5 out of 8 figures of the IINVT compared to reference probable error for original measurements. This indicates accuracy increase of the reduced measurements. In figure VIII, an increase in the *a posteriori* reference probable error is noticed, while *a priori* value retained the same value. However, in figures V and XIV, the values of both reference probable errors increased, but these values are moderate, from 0.1 mm to 0.3 mm.

**Table 2.** *A priori* and *a posteriori* reference probable errors for original and reduced measurements

| Indicator | Δh | Δh$_r$ |
|---|---|---|
| Figure I | | |
| $u_F$ [mm/km] | 1.5 | 1.0 |
| $u_\gamma$ [mm/km] | 3.1 | 2.2 |
| Figure III | | |
| $u_F$ [mm/km] | 2.0 | 1.9 |
| $u_\gamma$ [mm/km] | 3.4 | 3.1 |
| Figure IV | | |
| $u_F$ [mm/km] | 1.5 | 0.9 |
| $u_\gamma$ [mm/km] | 2.6 | 1.7 |

| Indicator | Δh | Δh$_r$ |
|---|---|---|
| Figure V | | |
| $u_F$ [mm/km] | 1.8 | 2.0 |
| $u_\gamma$ [mm/km] | 2.3 | 2.6 |
| Figure VI | | |
| $u_F$ [mm/km] | 1.1 | 1.0 |
| $u_\gamma$ [mm/km] | 2.1 | 1.8 |
| Figure VIII | | |
| $u_F$ [mm/km] | 1.5 | 1.5 |
| $u_\gamma$ [mm/km] | 2.2 | 2.4 |

| Indicator | Δh | Δh$_r$ |
|---|---|---|
| Figures IX and XII | | |
| $u_F$ [mm/km] | 0.7 | 0.6 |
| $u_\gamma$ [mm/km] | 1.0 | 0.9 |
| Figure XIV | | |
| $u_F$ [mm/km] | 0.6 | 0.7 |
| $u_\gamma$ [mm/km] | 1.5 | 1.7 |
| Average | | |
| $u_F$ [mm/km] | 1.4 | 1.2 |
| $u_\gamma$ [mm/km] | 2.3 | 2.0 |

Increase in the reference probable error values after the reduction and elimination of the systematic influence of height movement (figures V and XIV) is probably the result of a disturbance in the level of mutual compensation of different systematic measurement errors, especially taking into account the relief characteristics of areas where these figures are located. Specifically, these are mountainous parts of the Republic of Croatia, which are, generally, the most unsuitable places for the application of the geometric levelling method. It is possible to assume that the kinematic model may not be of sufficient quality for the successful reduction of measurements, i.e., the full elimination of the systematic effect of height movement. However, the average values of reference probable errors calculated with the data that comprises all figures indicate higher measurement reduction quality and consequently, better elimination of systematic influence. The average decrease in the reference probable error values after reducing the measurements is 0.2 mm for the *a priori* criterion and 0.3 mm for the *a posteriori* criterion, indicating an increase in measurement accuracy. Also, the obtained results indicate an appropriate level of accuracy, which in the case of *a priori* and *a posteriori* accuracy is mostly in accordance with the pre-declared measurement accuracy standard for levelling lines of the 2$^{nd}$ order network which equals ±2 mm/km for the influence of random errors.

Generally speaking, the quality of the kinematic model depends primarily on the quality of the levelling data that is the basis for the creation of the relative height displacement model. Moreover, it depends on the methodology applied in the creation of the relative height displacement model, and finally on the methodology used in the creation of the kinematic model. The quality of the levelling data is a reflection of the quality of the benchmark's stabilisation and their preservation over time, the availability of data for the same benchmarks in several different epochs and a more or less favourable positional distribution. Considering that this analysis includes data of satisfactory measurement accuracy (2$^{nd}$ order) with adequate quality of the benchmarks' stabilization that neutralizes their own vertical motion, it can be determined that the detected displacements of the same benchmarks in different epochs are primarily the consequence of the Earth's crust movement.

## CONCLUSION

In continuation of the results of previous external quality assessments of the height movement kinematic model, published in [5], [6] and [8] this paper presents the results of the final quality assessment on the territory of the Republic of Croatia, which completes the insight into the quality level of the kinematic model. Application of the indirect quality assessment procedure confirmed that the kinematic model in the Republic of Croatia is relatively suitable for reducing the measurements from the original survey epoch to another alternative epoch. Moreover, it enables the removal of systematic influences of the Earth's crust vertical movements from levelling measurements, and it can be used to determine regional changes in the relative height relationships of discrete points on the Earth's crust during the period from 1874 to1973 at the reliable centimetre level.

## REFERENCES

[1] Plag, H. P., Altamimi, Z., Bettadpur, S., Beutler, G., Beyerle, G., Cazenave, A., Crossley, D., Donnellan, R., Forsberg, R., Gross, R., Hinderer, J., Komjathy, A., Ma, C., Mannucci, A.J., Noll, C., Nothnangel, A., Pavlis, E.C., Pearlman, M., Poli, P., Schreiber, U., Senior, K., Woodworth, P.L., Zerbini, S. and Zuffada, C. (2009). The goals, achievements, and tools of modern geodesy. In *Global Geodetic Observing System: Meeting the Requirements of a Global Society on a Changing Planet in 2020*, 15-88. Springer Berlin Heidelberg.

[2] Rožić, N. (2015). Kinematic models of recent motion of the Earth's crust on the territory of Croatia, Slovenia and Bosnia and Herzegovina:(in Croatian). *Geofizika*, *32*(2), 209-236.

[3] Rožić, N. (2001). Fundamental levelling networks and height datums at the territory of the Republic of Croatia. *Acta geodaetica et geophysica hungarica*, *36*(2), 231-243.

[4] Rožić, N., Razumović, I., and Nazifovski, I. (2011). Modelling of the recent crustal movements at the territory of Croatia, Slovenia and Bosnia and Herzegovina. *Geofizika*, *28*(1), 183-213.

[5] Rožić, N. (2017). Quality evaluation of height movement kinematic model of the Earth's crust on the Croatian territory. Geofizika, 34(1), 67-92.

[6] Radanović, M., Rožić, N., and Razumović, I. (2019). Quality Evaluation of the Earth's Crust Height Movement Kinematic Model in the Northern Part of the Republic of Croatia. In *IOP Conference Series: Earth and Environmental Science*, 221(1), 1-10. IOP Publishing.

[7] Rožić, N. (2016). Recent crustal movements kinematic model. http://www2.geof.unizg.hr/~nrozic/RCM/

[8] Radanović, M., and Rožić, N. (2018). Ispitivanje kvalitete kinematičkog modela recentnih relativnih visinskih gibanja Zemljine kore na teritoriju poluotoka Istre. [Quality assessment of the kinematic model of the Earth's crust relative height movements on the territory of the peninsula Istra]. [In Croatian]. *Geodetski list*, *72*(2), 75-92.

[9] Braaten, N. F., Dore, P., Kukkamäki, T. J., Rune, J., and Vignal, J. (1950). Note sur l'évaluation de la précision d'un nivellement. *Bulletin Géodésique*, *18*, 494-548.

[10] Ghilani, D. C., and Wolf, P. R. (2006). Adjustment Computations. Spatial Data Analysis, John Wiley & Sons. Inc, Hoboken, New Jersey, SUA.

# LINE DISCREPANCIES AS WEIGHTS IN THE ADJUSTMENT OF PRECISE LEVELLING NETWORKS

**Dr. Vasil Cvetkov**[1]

[1] University of Architecture, Civil Engineering and Geodesy, **Bulgaria**

## ABSTRACT

Precise levelling networks play an important role in the research of many scientific processes, e.g. the recent crustal movements, the change of ocean and sea levels, geoid or quasi-geoid, etc. Their appropriate adjustment goes through the choice of suitable weights, which have physical common sense and minimize the standard errors of the adjusted heights. The conventional weights are supposed to be inversely proportional to the length of levelling lines, due to the assumption that the accumulation of errors in the geometric levelling is proportional to the square root of the distance between benchmarks. On the other hand, it is a well-known fact that the more accurate random observations are, the less is their spread around the quantity expectation. Thus, the absolute values of the discrepancies in the lines in levelling networks seem reasonable and natural candidates of weights. In order to check the "supremacy" of the conventional weights in the geometric levelling, we adjusted the Third Levelling network of Finland in two variants. In the first variant, we used the traditional weights inversely proportional to the length of the levelling lines. In the second variant, we used weights inversely proportional to the absolute values of the discrepancies in the lines. The t-Test Paired Samples for means applied with the means of the sample of the standard errors yielded by both variants revealed that the second variant produced statistically significant better results at significance level greater than 99 %.

**Keywords:** adjustment weights, precise levelling networks, reference height systems

## INTRODUCTION

Precise levelling has been the basic method for monitoring the recent vertical movements of the Earth's crust [3, 4, 10], evaluation of geoid and quasi-geoid models [7], verification and validation of vertical measurements by Global Navigation Satellite Systems /GNSS/ [10], determining the slope and the level of the oceans and sees [1], etc., for a long time. Despite the high accuracy of the method, there are some questions about geometric levelling results that have not been fully explained yet. For example, there are evidences about some systematic slopes of many precise national levelling networks [1]. Analysing the velocities of the recent vertical movements of the Earth's crust in Bulgaria [3, 4], we can see that the researchers of both teams obtained different results, not only in the magnitudes of the velocities, but also in their directions.

In our opinion, based on the publication [2], one potential reason for the mentioned facts is the use of the weights into adjustment of the precise levelling networks that are a function of the length of levelling lines. According to [2], the classical assumption about the relationship between the accumulations of the differences $|D|$ in double-measured elevations between terminal benchmarks in levelling lines and a square root of the length of the lines $\sqrt{L}$ [5, 8, 9] must be revised, due to the presence of heteroscedasticity [6], when we try to explain $|D|$ by $\sqrt{L}$ or $L$. In agreement with the conclusions in the study [2], we present by Figure 1 the residuals of the regression equation (1) based on the data from the Third Levelling of Finland /1978-2006/ [8].

$$|D| = a + b.\sqrt{L} + c.L \tag{1}$$

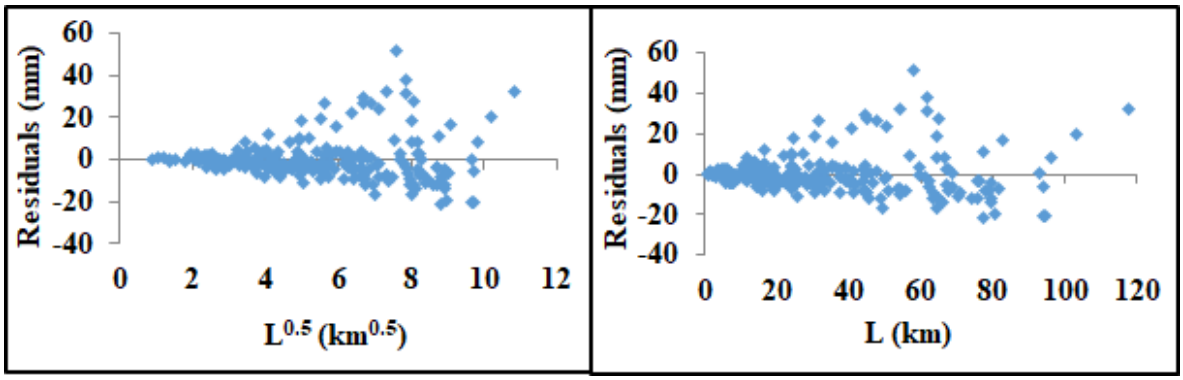


**Figure 1.** The residuals of the regression equation $|D| = a + b.\sqrt{L} + c.L$ regarding the independent variables $\sqrt{L}$ /in the left chart/ and $L$ /in the right chart/, based on the levelling data, collected in the Third Levelling of Finland campaign [8].

Let us look at equation (4), which gives the standard error $m_i$ of the adjusted height / geopotential number of a random nodal benchmark $i$ in a precise levelling network.

$$m_i = (n-k)^{-0.5}.[(-A.(A^TPA)^{-1}.A^TPf + f)^T.P.(-A.(A^TPA)^{-1}.A^TPf + f).Q_{ii}]^{0.5} \tag{2}$$

In equation (2), the follow notation are applied:

$n$ – The number of levelling lines;

$k$ – The number of the nodal benchmarks, whose heights / geopotential numbers we determine by the adjustment;

$A$ – The information matrix. This matrix presents the configuration of the levelling network;

$P$ – The matrix of the weights;

$f$ – The vector matrix of the free terms;

$Q_{ii}$ – The $i^{th}$ member in the main diagonal of the covariance matrix $Q_{(k,k)} = (A^TPA)^{-1}$.

According to equation (2), the standard error of the adjusted height / geopotential number of each nodal benchmark is a function of the configuration of the network, the applied weight model and the accuracy of the observations, presented by the matrixes *A, P* and *f*. Thus, the appropriate choice of weights is very important concerning the minimization of the standard errors (2). Consequently, in accordance with Figure 1, it seems reasonable to adjust a precise levelling network with different types of weights from the widely used classical ones (3) [8, 9].

$$w = 1/L \tag{3}$$

It is a known fact that the more accurate observations of a measured quantity are less spread around the true value of the quantity than the less accurate observations of the same quantity. In the precise levelling, we have only two measurements of each elevation in a levelling network. Therefore, the weights (4) based on the differences $|D|$ in double-measured elevations between terminal benchmarks in levelling lines seem a relevant surrogate of the classical weights (3).

$$w = 1/|D| \tag{4}$$

The main objective of the current study is to demonstrate that the weights (3) are not always the best ones concerning adjustments of the precise levelling networks. In addition, we aim to show that the automatic choice of the weights (3) is likely to be the reason for the appearance of a systematic slope of some precise levelling networks.

## MATERIALS AND METHODS

In the current research we used the levelling data from the Third precise levelling of Finland /1978-2006/ as given by [6]. The scheme of the network is given by Figure 2.2 in the study of Saaranen et al. [6]. We adjusted this precise levelling network as a free network by parametric least-squares method. As a datum point in our adjustments, we used the benchmark 2183 in Kauklahti. The network was adjusted twice in two variants. In the first variant, we used the classical weights (3). In the second variant, we adjusted the network by the use of the weights, given by equation (4).

In order to compare the accuracy of both variants, we used Paired t-test for means. The initial data in this two-sample test were the samples of the standard errors of the adjusted geopotential numbers of the nodal benchmark in the network. Our choice of the test was motivated by the prescriptions given by [6], regarding the choice of hypothesis testing procedure for comparison of two samples, namely:

- Generally, the parametric tests are more powerful than their non-parametric equivalents, when the distributions of the compared samples are moderately large; say the number of observations $n > 40$ or 50.
- If the experimental units are relatively heterogeneous (large differences in the standard deviations of both samples) and there is a large positive correlation within pairs, the paired experiment should be used. Typically, this case occurs when the experimental units are the same for both treatments.

The next step in our research was to compare the differences between the values of the adjusted geopotential numbers of the identical benchmarks in both adjustment variants. Due to the appearance of a systematic trend of these differences in regards of the

remoteness from the datum point in Kauklahti, we estimated the slope of the fitting regression line.

## RESULTS

This section presents the results of our analyses. Table 1 contains information about the remoteness of each nodal benchmark in the analysed networks from the datum points and its standard errors, obtained by both adjustments of the network with weights (3) and (4), respectively.

**Table 1.** Correlation coefficients among the absolute values of the closing errors $|W|$, loop circumferences $L$ and square root of $L$ in the analyzed precise levelling networks.

| Benchmark | km from Kauklahti | $p=L^{-1}$ | $p=\|D\|^{-1}$ | Benchmark | km from Kauklahti | $p=L^{-1}$ | $p=\|D\|^{-1}$ |
|---|---|---|---|---|---|---|---|
| Oulunkyla | 25.1 | 4.2 | 2.2 | Toivala | 512.1 | 11.7 | 10.7 |
| Ojakkala | 44.1 | 4.7 | 4.8 | Haapajarvi | 544.5 | 11.8 | 11.9 |
| Karjaa | 60.7 | 5.4 | 4.4 | Joensuu | 586.5 | 12.5 | 8.9 |
| Hyvinkaa | 85.4 | 5.5 | 4.8 | Iisalmi | 589.2 | 12.2 | 11.4 |
| Riihimaki | 98.9 | 6.1 | 5.5 | Ylivieska | 609.1 | 12.3 | 11.4 |
| Kyminlinna | 158.1 | 8.7 | 7.3 | Lieksa | 691.6 | 13.6 | 11.0 |
| Lahti | 163.7 | 8.1 | 7.4 | Vaala | 694.9 | 13.1 | 12.4 |
| Turku | 178.8 | 8.7 | 5.0 | Kontiomaki | 702.8 | 12.8 | 11.3 |
| Toijala | 180.4 | 8.3 | 5.4 | Ammansaari | 786.5 | 14.0 | 12.2 |
| Kouvola | 222.4 | 8.6 | 7.3 | Kempele | 788.1 | 13.5 | 11.5 |
| Tampere | 230.1 | 9.1 | 6.7 | Oulu | 799.5 | 13.7 | 12.2 |
| Lielahti | 238.5 | 9.3 | 6.8 | Laurila | 913.4 | 16.0 | 13.8 |
| Eurajoki | 297.7 | 10.0 | 8.2 | Kuusamo | 959.8 | 15.4 | 12.7 |
| Simola | 303.4 | 9.9 | 8.4 | Aavasaksa | 1011.7 | 17.1 | 16.6 |
| Parkano | 310.5 | 9.8 | 6.9 | Rovaniemi | 1022.2 | 16.7 | 15.5 |
| Peipohja | 331.1 | 10.1 | 7.7 | Sinetta | 1045.3 | 16.9 | 16.0 |
| Vaajakoski | 337.8 | 9.7 | 7.9 | Kemijarvi | 1108.3 | 16.7 | 12.9 |
| Iyvaskyla | 342.7 | 9.7 | 7.9 | Lohiniva | 1122.3 | 17.6 | 16.1 |
| Haapamaki | 344.6 | 9.8 | 7.2 | Kolari | 1144.1 | 17.9 | 16.3 |
| Ruosniemi | 355.6 | 10.2 | 8.7 | Kittila | 1181.5 | 17.9 | 17.7 |
| Noormarkku | 363.8 | 10.2 | 8.1 | Sirkka | 1205.5 | 18.2 | 18.3 |
| Seinajoki | 392.2 | 10.4 | 8.9 | Sodankyla | 1226.1 | 18.0 | 19.1 |
| Pieksamaki | 408.9 | 10.2 | 8.1 | Muonio | 1234.1 | 18.6 | 17.1 |
| Lapua | 424.6 | 10.9 | 8.9 | Ivalo | 1391.3 | 19.9 | 27.2 |
| Sarkisalmi | 427.2 | 11.4 | 8.9 | Inari | 1436.3 | 20.0 | 26.1 |
| Viitasaari | 452.4 | 11.3 | 8.8 | | | | |

Table 2 gives comparison between the samples of standard errors, yielded by both variants. Figure 2 illustrates the trend of the differences between the adjusted geopotential numbers of the nodal benchmarks in the Third Levelling of Finland, derived

by the weights $p=L^{-1}$ and the weights $p=|D|^{-1}$ from one hand and the remoteness of the benchmarks from the datum point.

**Table 2.** t-Test: Paired Two Sample for Means results, based on the samples of standard errors of the adjusted geopotential numbers, produced by the weights $p=L^{-1}$ and $p=|D|^{-1}$.

| ***Description*** | $p=L^{-1}$ | $p=\|D\|^{-1}$ |
|---|---|---|
| Mean | 12.13 | 10.83 |
| Median | 11.35 | 8.89 |
| Variance | 16.76 | 26.72 |
| Observations | 51 | 51 |
| Pearson Correlation | 0.94 | |
| t Stat | 4.82 | |
| P(T<=t) two-tail | 1.39E-05 | |
| t Critical two-tail | 2.01 | |

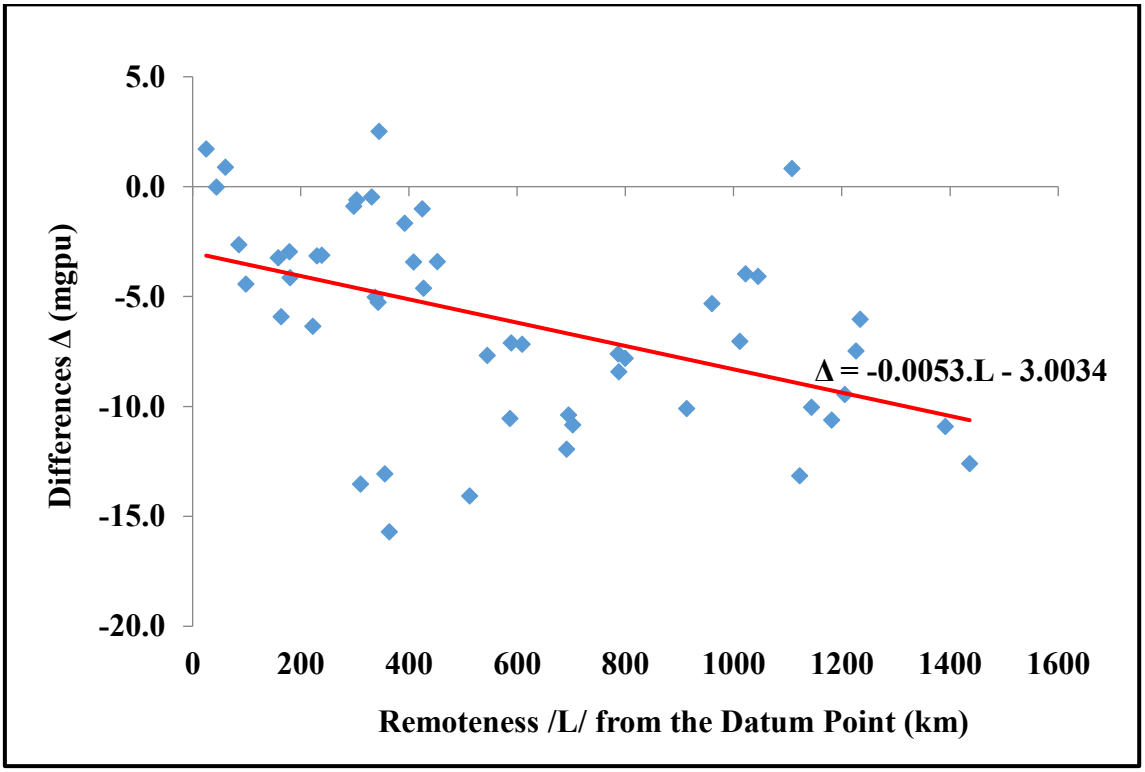


**Figure 2.** The trend of the differences between the adjusted geopotential numbers of the nodal benchmarks in the Third Levelling of Finland, derived by the weights $p=L^{-1}$ and the weights $p=|D|^{-1}$ from one hand and the remoteness of the benchmarks from the datum point.

According to Table 1 and Table 2, the weights (4) lead to significantly less standard errors of the adjusted geopotential numbers of the nodal benchmarks in comparison to the similar standard errors, but produced by the weights (3). The regression of the differences between the adjusted geopotential numbers by both type of weights concerning the remoteness from the datum point was also found to be statistically significant. The estimated regression p-Value is equal to 0.00057.

## DISCUSSION

The main objective of the current study was to demonstrate that the weights (3) are not always the best ones concerning adjustments of the precise levelling networks. Looking at Table 1, one can count that the use of weights (4) leads to minimization in the standard errors of 45 out of 51 nodal benchmarks in comparison to the standard error of the identical benchmarks, but yielded by the adjustment with weights (3). As a result, the mean of the standard errors based on the adjustment with weights (4) is 12% less than the mean of the sample of the standard errors based on the adjustment with weights (3). According to the results presented by Table 2, the null hypothesis that the means of both samples are equal was rejected at a significance level higher than 99 %.

Comparing the medians of both standard error samples, we can calculate that improve of the accuracy in the adjustment with weights (4) is even more representative in comparison to the accuracy of the adjusted geopotential numbers of the nodal benchmarks, but obtained by the classical weights (3). The median of the sample of the standard errors produced by the use of weights (4) is 28% less than the median of the sample of the standard errors, but derived by the weights (3).

Are these results unexpected? Of course not. There is another publication [2], where the "supremacy and universality" of the classical weights (3) is also revealed.

Additional aim of the current research was to point at a possible reason for appearance of a systematic slope of some precise levelling networks [1]. According to Figure 2, the weights (3) produced physically greater values of the adjusted geopotential numbers than the weights (4). It was also found that there is a statistically significant trend / at a level higher than 99% / in the increase of the differences between the adjusted geopotential numbers of the nodal benchmarks obtained by weights (3) and (4) in regards to the remoteness from the datum point. Assuming that the variant of the adjustment with weights (4) is significantly more accurate, based on the results given by Table 1 and Table 2, we can conclude that the classical weights (3) have led to a systematic downward slope of the analysed network in the south-north direction. Thus, we indirectly showed a possible reason for inclination of some precise levelling networks.

## CONCLUSION

In this article, we demonstrate that the classical approach of the adjustment of the highest order levelling networks [8, 9] by the use of the weights (3) is not always the best variant of the adjustment of this type of levelling networks. It is likely that there are other better solutions, which we may miss, if we assume that the classical variant of the adjustment of levelling networks is universal and its relevance is unquestionable. In fact, this is hardly ever true.

Since the information matrix $A$ in equation (2) is inherited before the adjustment of the network, we can optimize the standard errors of the adjusted quantities by some manipulation as:

- Minimize the impact on the network configuration by using different types of weights. The elevations between nodal benchmarks in a levelling network are different, which supposes unequal weighting concerning the vertical component of the network configuration. In addition, the nodal benchmarks are not homogeneously distributed through the area. As a result, the length of levelling

lines are not equal, which supposes unequal weighting regarding the horizontal component of the network configuration. Thus, it is reasonable for some iterative procedures, e.g., Inverse Distance Weighting or /and Inverse Absolute Height Weighting [2], to be applied in order to optimize the influence of the network configuration on the final accuracy.

- Because the average of two observations is quite unstable, the initial data should be selected from both measurements of the line elevations and their means in such manner, which minimizes the closing errors in levelling loops.

Minimizing the standard errors of the adjusted heights / geopotential numbers by the above prescriptions will result in yielding of more accurate heights / geopotential differences between levelling benchmarks. Consequently, we will be able to perform more relevant conclusions about the velocities of the recent vertical movements of the Earth's crust, the ocean and sea levels and their slopes, validation of gravity models, verification of GNSS vertical measurements, etc.

## REFERENCES

[1] Afrasteh Y., Slobbe D.C., Sacher M. et al., (2023), Realizing the European Vertical Reference System using model-based hydrodynamic leveling data. J Geod 97, 86. https://doi.org/10.1007/s00190-023-01778-2

[2] Cvetkov V., Two adjustments of the second levelling of Finland by using nonconventional weights, Journal of Geodetic Science, vol. 13, no. 1, 2023, https://doi.org/10.1515/jogs-2022-0148

[3] Gospodinov S., Peneva E., P. Penev, A specific approach to least squares adjustment of the state levelling network, 22nd International Multidisciplinary Scientific GeoConference SGEM 2022, Albena, Bulgaria, 2020, https://doi.org/10.5593/sgem2022/2.1/s09.20

[4] Kanev D., Mladenovski M., The recent vertical movements of the Earth's crust in Bulgaria, Publications of Bulgarian Cartographic Association, Vol. IX, pp. 17-26, 1969, in Bulgarian

[5] Kunchev I., On standards and specifications for vertical control surveys, Annual of the University of Architecture, Civil Engineering and Geodesy – Sofia, Vol. 54, Issue 2, pp. 253 – 262, 2021, ISSN 1310-814X, ISSN 2534-9759 (on-line), in Bulgarian

[6] Montgomery D., G. Runger, (2014), Applied Statistics and Probability for Engineers (6th ed.), Wiley, ISBN-13 9781118539712

[7] Peneva E., I. Georgiev, 2010, Evaluation of the Quasigeoid Models EGG97 and EGG07 with GPS/levelling Data for the Territory of Bulgaria, In IAG Book series "Gravity, Geoid and Earth Observation", International Association of Geodesy Symposia 135, Mertikas (ed.), Springer-Verlag Berlin Heidelberg, p. 303-307, ISBN 978-3-642-10633-0, https://doi.org/10.1007/978-3-642-10634-7_39 .

[8] Saaranen V., Lehmuskoski P., Takalo M., P. Rouhiainen, The Third Precise Levelling of Finland. FGI Publications No. 161, Kirkkonummi, 2021, ISBN 978-951-48-0266-9 (print), ISSN 2342-7353 (online)

[9] Specifications for precise levelling I and II order, GUGK, 1980, Sofia, in Bulgarian

[10] Tsanovski Y., GNSS Measurements for the Needs of Precise Height Determinations in Bulgaria, Annual of the University of Architecture, Civil Engineering and Geodesy – Sofia, Vol. 54, Issue 2, pp. 211 –218, 2021, ISSN 1310-814X, ISSN 2534-9759 (on-line), in Bulgarian

# MONITORING THE SPATIOTEMPORAL DEFORMATION DISTRIBUTION IN SALT MINES

**Jakub Pietras**[1]

**Damian Kurdek**[2]

**Agnieszka Malinowska**[3]

[1]The Research and Development Center for Mining of Chemical Raw Materials CHEMKOP Ltd., Krakow, **Poland**
[2]"KŁODAWA" Salt Mine S.A. Aleja 1000-lecia, 62-650 Kłodawa, **Poland**
[3]AGH University of Science and Technology, Al. A. Mickiewicza 30, 30-052 Krakow, **Poland**

## ABSTRACT

Underground mining operation in salt deposits requires special control over rock mass stability. Changes in stress within the rock mass cause gradual convergence of underground workings. A slow convergence process with a complex spatiotemporal distribution requires the measurements with high accuracy, which is carry out on a well-planned spatial distribution of observation network.

The aim of the study was to present the procedure of designing and implementing observations of convergence in salt caverns within a salt dome deposit in Kłodawa salt mine in Poland. The studies focused on identifying the most important factors that should be considered when establishing new observation networks to assess the stability of salt rock mass. The algorithm was developed based on experiences is measurements conducted over a period of 50 years in one section of the Kłodawa mine. The most significant components of spatio-temporal deformation process in 3D space were presented. Measured convergence in relation to the salt dome geometry, geological and mining condition were taken into account to design a new network in another part of salt dome. Presented experiences may originate as a premise for designing a new observation network in other salt mines where extraction is planned with the chamber and pillar method.

**Keywords:** salt dome deposit, deformation monitoring, convergence, rock masses, stability

## INTRODUCTION

The exploitation of salt deposits constitutes a significant branch of the mining industry in Poland and worldwide. Besides providing a mineral resource, these deposits may have strategic importance as gas deposit storage. In general, salt extraction is carried out using either the room-and-pillar method or by leaching salt caverns. Both methods disrupt the natural equilibrium of the rock mass. Therefore, continuous monitoring of deformations in the rock mass and the surface is crucial [1-3]. Surface measurements mainly include leveling, GNSS, and INSAR [4-6], but also UAV-based measurements [7]. Underground measurements are often based on leveling, laser scanning [8-10], probe measurements [11], and measurements of length changes (convergence and linear deformations) [12-16]. These measurements need to be meticulously designed due to

the very slow process of closure in empty spaces within the rock mass, necessitating highly accurate measurements. Measurement in salt domes also requires a well-distributed measurement network. The obtained measurements provide information on the deformation process over time and are critical for assessing the stability of the rock mass or any instability.

This study collected experiences from measurements conducted over the past 44 years at the Kłodawa rock salt mine. Based on the mining, geological, and hydrogeological characteristics of the rock mass, the key elements to be considered in designing deformation monitoring in salt caverns and pillars were identified. Guidelines and recommendations for designing convergence measurement networks were developed based on measurements in the rock salt field no. 2 (Fig. 1). The presented approach is supported by convergence measurement results in the field no. 2 and could be a basis for convergence measurements in other salt fields and deposits. Using these guidelines, a new convergence measurement network was designed for another salt field no. 1.

## STUDY SITE

The potash and magnesium salt deposits in Greater Poland and Kuyavia constitute the largest rock salt complex in Poland [17]. The Kłodawa salt mine, operating in this salt dome, is the country's most significant salt producer. As a result of extraction using the room-and-pillar method since the 1950s, there is now an underground void complex reaching up to 23 million m³. The research was conducted in two fields, 1 and 2, which have been mined using the room-and-pillar method for the last 50 years (Figure 1) [18].

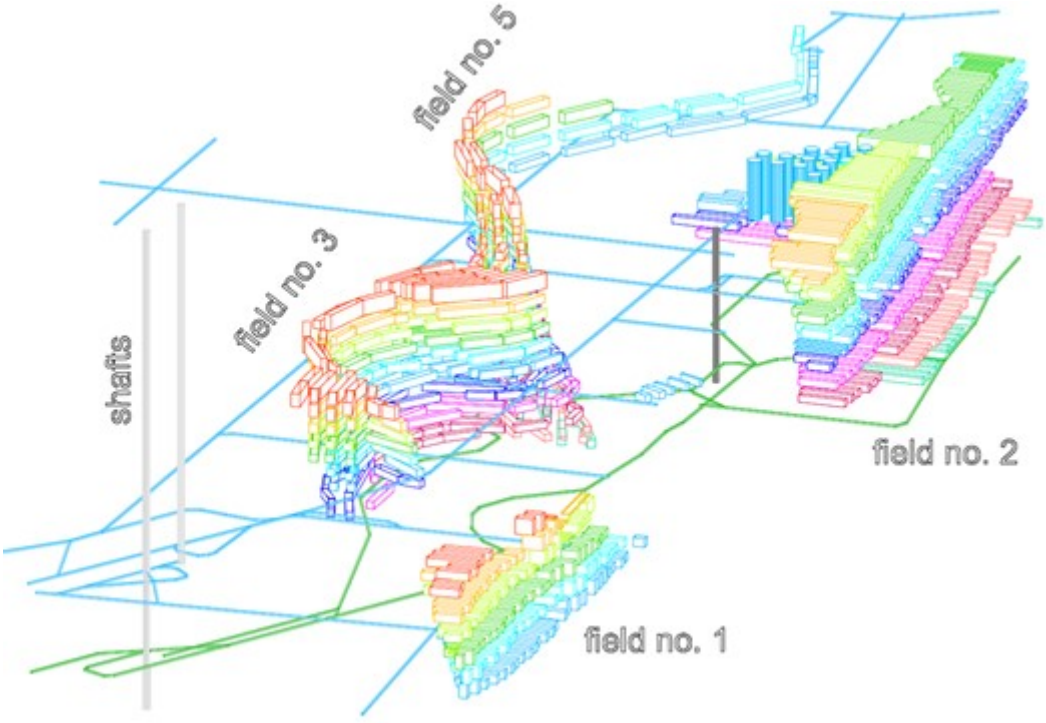


**Figure 1.** Underground mine workings in Kłodawa" salt mine. Mined out cavern geometry in filed no. 2, and filed no. 1 [12]

## RESEARCH METHODOLOGY

Based on experiences from research and measurements conducted in the test field 2, factors that significantly influence the reliability of measurements were selected. These factors include measurement technology, mining-geological conditions, and hydrogeological conditions (Figure 2).

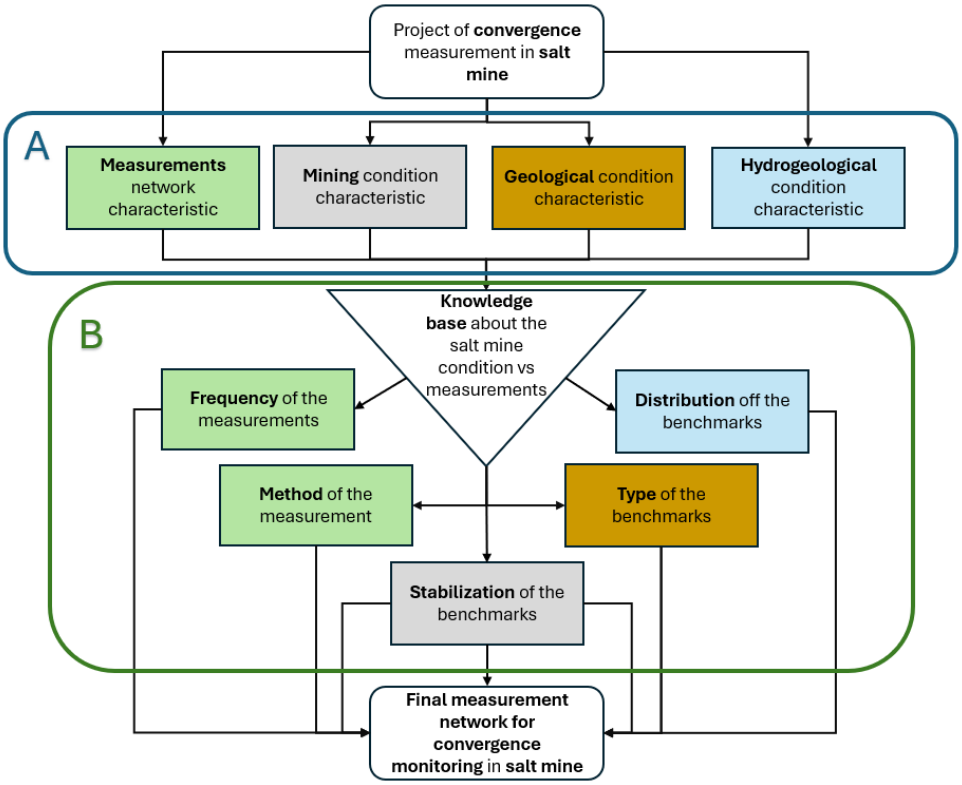


**Figure 2.** Scheme of the work flow

### Premises and guidelines from measurements carried out in the field no. 2

The first stage of the research was analyzing the convergence measurement results from field 2 over the past 44 years. Over the years, the post-exploitation deformation monitoring network in the room-and-pillar system in field 2 was progressively expanded. Currently, it covers three main areas: the field center, its zone under the protective shelf, and the southeastern part of the field (Figure 3) [12, 13]. The reason of installation of measurement points varied for each described area:

- Measurement bases were centrally located in field 2 to record the most dynamic convergence values (Ks-11, Figure 3).
- Vertical convergence measurement points located under the protective shelf were particularly important. The observations support an early warning system against water hazards in that area (Ks1, Ks7, Ks18, Ks29, Ks36, Figure 3) [19, 20].
- Peripheral convergence measurement bases in the southeastern part of the field were installed to water phenomena and the heterogeneous geology of the rock mass deformation analysis (Ks1h-f, Figure 3).

- Chambers located in the central part of the field (KS-21) were base of information about deformation due to the different extraction direction in this area (Ks21, Figure 3).

Based on that network the observations brought a novel knowledge about the deformation process in that study site. Analyzing the vertical convergence rates in relation to the depth and the age of the workings following observation has been done. In the central part of the field, in the KS-11 and KS-21 profiles, a clear increase in vertical convergence rate with depth is visible (Figure 3). This is due to both the depth of the chambers in the rock mass and their age. Chambers located at lower levels are younger, and the convergence phenomenon is most intense immediately after extraction is completed. Over time, it stabilizes but do not stop. The convergence velocity is table in time and the values depends on the age and depth of the workings. That tendency is true for the central part of mine workings. Whereas, in the southeastern peripheral part of field 2, the convergence rate is not related to depth (Ks1h-f, Figure 3). Under the protective shelf in field 2, small vertical displacement rates were observed, likely due to the different locations of individual chambers within the field structure and their varying heights (Ks1, Ks7, Ks18, Ks29, Ks36, Figure 3).

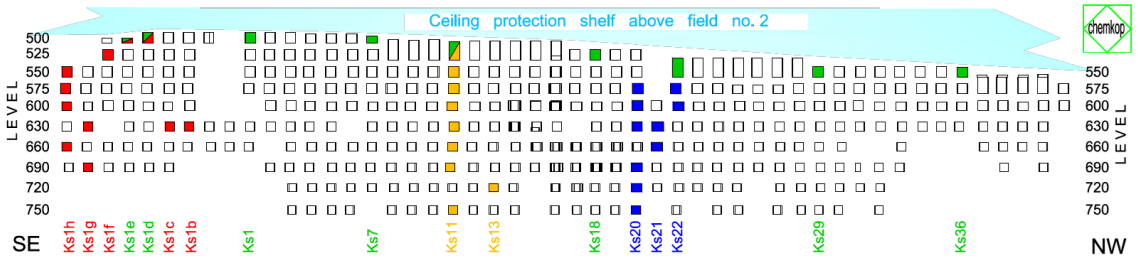


a)

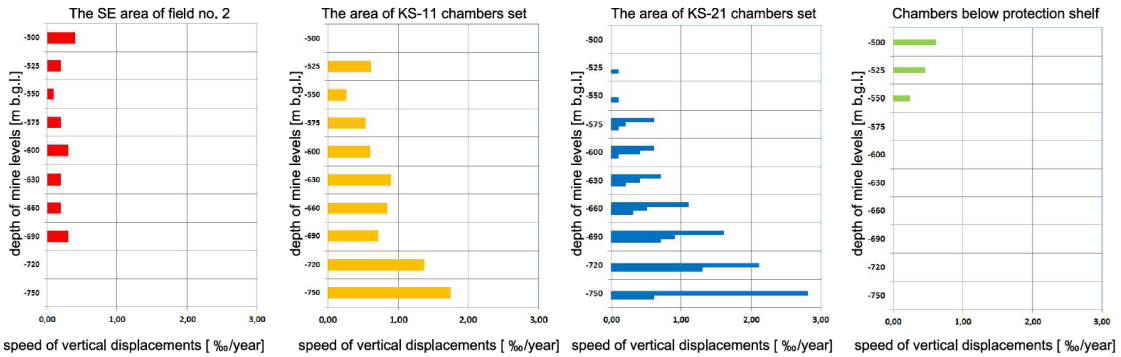


b)

**Figure 3.** Central zone of the field marked in yellow and blue, peripheral zone marked in red, zone under the protective shelf marked in green, a). Vertical displacement rates as a function of depth, divided into central zone (yellow and blue), peripheral zone (red), and zone under the protective shelf (green), b) [12].

For the KS-21 area the more detailed spatial distribution of convergence was presented due to the installation of more measurement bases in that area (Figure 4). The main conclusion from the observation is a very high variability of vertical convergence rate at different levels and depths. The convergence is lower at higher levels (from -0.2

‰/year) and it increase to -2.7 ‰/year in the bottom of mined out part of the deposit. Moreover, the convergence rates are significantly lower in the deposit's boundary zones. That evidence was supported by observations in other areas in the field 2.

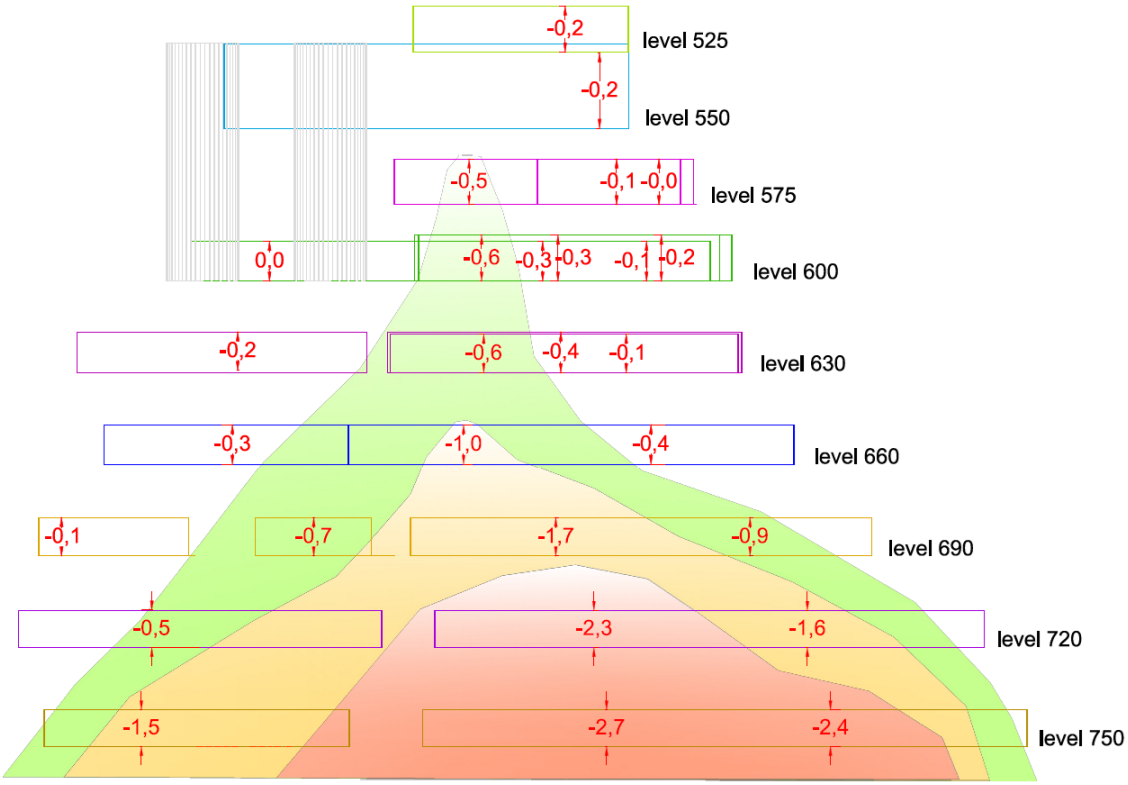


**Figure 4.** Variability of the relative vertical convergence rate of caverns in the area of the KS-21 ( field no. 2) in the 2022-2023 measurement cycle [‰/year].

Furthermore, based on the post-exploitation deformation rates in the Kłodawa salt dome, the optimal measurement interval was determined. For convergence measurements in the central part of field 2, it is one year. For its upper and peripheral, southeastern parts, it is 1-2 years. Spatial network measurement under the protective shelf should be conducted no more frequently than every 2 years. Based on the experiences gained over many years of measurements in field 2 presented above the guidelines for the measurements in other areas were established.

**Designed Measurements network in field no. 1**

The network in field no. 1 had to cover the smaller area of underground workings. That is why, the convergence measurements initially were planned in two chamber profiles. The first chamber profile was located in the central part of the exploitation field, where chambers have the greatest length and volume (Ks-2, Ks-3, Figure 5). It was assumed that the measurements carried out in that area will allow recording the maximum convergence values in field 1. The second chamber profile was located in the southeastern, peripheral part of the exploitation field. In that area the smallest post-exploitation deformations in the entire complex were expected to be recorded.

The distribution of the measurement stations in every chamber was similar to the solution applied in the field 2. The convergence was measured in vertical, horizontal, and diagonal directions (scheme of base location, Figure 5 right bottom). The

measurement applied in mining site ensures an accuracy of 1 mm per every base line. Due to the short length of the chambers in field 1 (compared to field 2), it was decided to install one measurement station in each selected chamber.

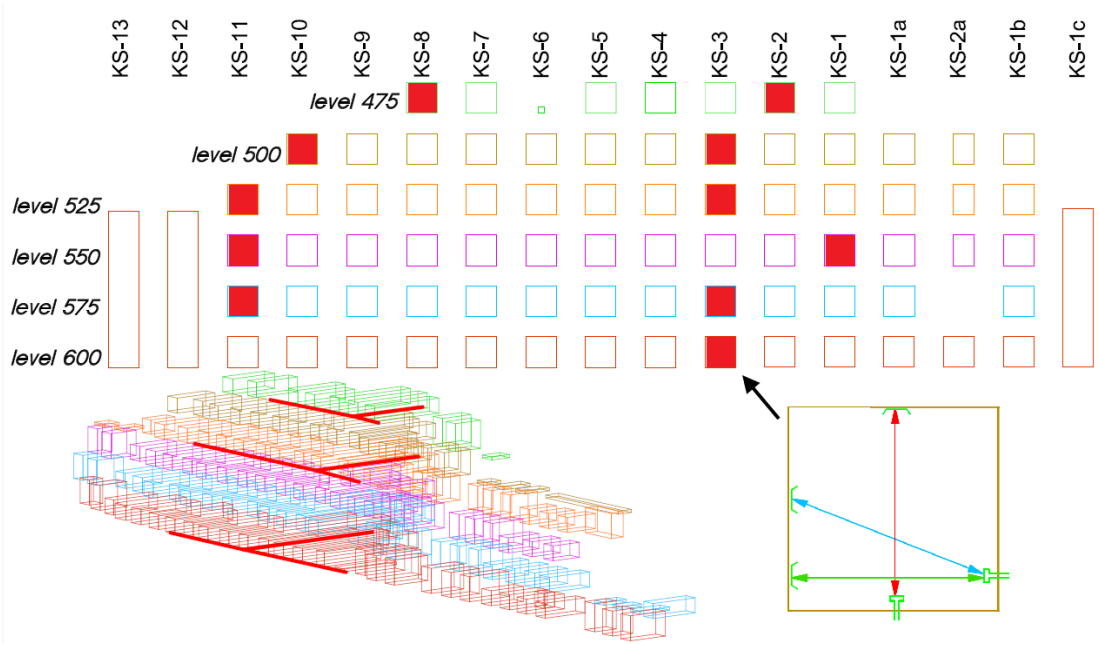


**Figure 5.** The location of the new measurement network in the field no. 1 with the scheme of the benchmarks location in cavern for the convergence measurements

The placement in two areas of the field in a vertical arrangement at all depths will provide an image of the convergence of individual exploitation chambers over time. Additionally, it will be possible to analyze the growth of the chamber closure phenomenon with depth in each chamber profile. Comparing convergence results recorded in the two chamber profiles will allow for analyzing the distribution of global deformations within exploitation field 1.

## RESULTS AND CONLUSIONS

Based on many years of convergence measurements in field 2, guidelines were developed for installing new measurement networks in the room-and-pillar salt extraction system. Measurement stations should be installed first in places with existing or potential hazards. In salt mines, these are areas where water hazards have been observed and areas with heterogeneous rock mass. In the case of measurements in a hazardous area, it is recommended to measure convergence in the entire chamber profile, from the deepest to the shallowest chamber. This allows recording stress depending on depth and identifying any increase in deformation rate. Significant deformation increases may indicate a loss of stability in a part of the rock mass. Measurements should also cover workings under the protective shelf and near the edge pillar. In such areas, measurement stations should be installed in a dispersed system, enabling comprehensive measurements for these zones.

The highest convergence rates occur in the central parts of exploitation areas, while the lowest are at the edges. It is advisable to place measurement stations in regions with varying deformation dynamics, allowing for the recording of both local deformations

(convergence of individual exploitation chambers) and analyses of chamber closure growth with depth within each chamber profile. Comparing convergence results enables the analysis of spatial deformation distribution within the exploitation area. The measurement network should also be gradually expanded with mining progress. Installing stations immediately after completing a chamber is beneficial, allowing the initial, intense deformation process to be recorded. The deformation will stabilize over time at a level characteristic of the depth of the working. These guidelines should allow for ongoing monitoring of deformations resulting from the convergence of salt chambers, ensuring safety, not only for underground workings, but also for the terrain surface.

## ACKNOWLEDGEMENTS

This research was funded by the AGH University of Science and Technology, Faculty of Geo-Data Science, Geodesy, and Environmental Engineering [grant number 16.16.150.545].

## REFERENCE

[1] Bieniasz J., Wojnar, W., Zarys historii pomiarów i wybrane wyniki obserwacji zjawiska konwergencji wyrobisk w pokładowych złożach soli, Gospodarka Surowcami Mineralnymi, Poland, vol. 23, pp 133-142, 2007.

[2] Hejmanowski R., Malinowska A A., Land subsidence inversion method application for salt mining-induced rock mass movement, Gospodarka Surowcami Mineralnymi, Poland, vol. 33/issue 3, pp 179-200, 2017, http://doi.org/10.1515/gospo-2017-0034

[3] Maj A., Florkowska L., Obserwacja oddziaływania wyrobisk na powierzchnię terenu w warunkach kopalń soli, Prace Instytutu Mechaniki Górotworu PAN, Poland, vol. 15, pp 107-113, 2013.

[4] Piątkowska A., Surała M., Perski Z., Graniczny M., Application of the SAR interferometric methods to identify the mobility of the area above the salt diapir in Inowrocław and the regional salt structures in central Poland, Geology, Geophysics and Environment, Poland, vol. 38, pp 209-220, 2012, http://doi.org/10.7494/geol.2012.38.2.209

[5] KIM T. T. H., TRAN H. H., BUI K. L., LIPECKI T., Mining-induced Land Subsidence Detected by Sentinel-1 SAR Images: An Example from the Historical Tadeusz Kościuszko Salt Mine at Wapno, Greater Poland Voivodeship, Poland, Journal of the Polish Mineral Engineering Society, Poland, Vol.1, pp 42-52, 2021, http://doi.org/10.29227/IM-2021-02-04

[6] Witkowski W. T., Łukosz M., Guzy A., Hejmanowski R., Estimation of Mining-Induced Horizontal Strain Tensor of Land Surface Applying InSAR, Minerals, Poland, vol. 11, pp 788, 2021, http://doi.org/10.3390/min11070788.

[7] Bhardwaj A., Sam L., Martín-Torres F. J., Zorzano M., Luque J., UAV Imaging of a Martian Brine Analogue Environment in a Fluvio-Aeolian Setting, Remote Sensing., vol. 11, 2019, http://doi.org/10.3390/rs11182104

[8] Ochałek, A., Lipecki, T, Jaśkowski W., Analysis of convergence and deformation measurements based on classical and geodetic surveys and Terrestrial Laser Scanning in

"Wieliczka" Salt Mine, 18th International Multidisciplinary Scientific GeoConference, Bulgaria, vol. 18, pp 583-590, 2018, http://doi.org/10.5593/sgem2018/2.2/S09.073.

[9] Szafarczyk A., Gawałkiewicz R., Defining the Cubature Changes of Historic St. Kinga Chamber in Bochnia Salt Mine, Using Laser Scanning Technology, Poland, vol. 35, E3S Web of Conferences 35 POL-VIET 2017, pp 04006, 2018, https://doi.org/10.1051/e3sconf/20183504006

[10] Lipecki T., Jaśkowski W., Gruszczyński W., Inventory of the geometric condition of inanimate nature reserve Crystal Caves in "Wieliczka" Salt Mine, Acta Geod Geophys, Poland, vol. 51, pp 257–272, 2016, https://doi.org/10.1007/s40328-015-0125-5

[11] Szczerbowski Z., Niedbalski Z., Jóźwik M., Migdas T., Kawalec A., Orzeł K., Zastosowanie elektronicznych pomiarów odkształceń górotworu na przykładzie wyrobiska KS Bochnia, Poland, Przegląd Górniczy, pp 19-26, 2020.

[12] Bieniasz J., Pietras J., Deformacje górotworu wywołane eksploatacją pola nr 2 w Kopalni Soli „Kłodawa" S.A., Poland, Przegląd Solny, vol. 14, pp 15-20, 2018.

[13] Bieniasz J., Pietras J., Marcola-Sadowska J., Kurdek D., Zmienność zjawiska zaciskania wyrobisk komorowych w przestrzeni pola nr 2 w Kopalni Soli „Kłodawa", Przegląd Solny, Poland, vol. 16, pp 20-28, 2021.

[14] Kurdek D., Pomiary konwergencji wyrobisk chodnikowych w Kopalni Soli „Kłodawa" S.A., Przegląd Solny, Poland, vol. 15, pp 56-61, 2020.

[15] MAJ A., Konwergencja w warunkach nieregularnie rozproszonych wyrobisk, na przykładzie kopalni Wieliczka., Prace Instytutu Mechaniki Górotworu PAN, Poland, vol. 13, pp 121-130, 2011.

[16] Świerczyńska E. J., Kurdek D., Jankowska I., Accuracy of the application of mobile technologies for measurements made in headings of the Kłodawa Salt Mine, Reports on Geodesy, Poland, vol. 117, pp 55-68., 2024, https://doi.org/10.2478/rgg-2024-0007.

[17] Czapowski G., Geologia permskich struktur i złóż solnych w Polsce - aktualny stan wiedzy i perspektywy zagospodarowania, Przegląd Geologiczny, Poland, vol. 54, pp 301-302, 2006.

[18] Cała M., Tajduś A., Andrusikiewicz W., Kowalski M., Kolano M, Stopkowicz A, Cyran A., Jakóbczyk J., Long term analysis of deformations in salt mines: Kłodawa salt mine case study, central Poland, Archives of Mining Sciences, Poland, vol. 62, pp 565-577, 2017, https://doi.org/10.1515/amsc-2017-0041.

[19] Kortas G., Maj A., Okoliczności i skutki katastrofalnego wdarcia wód do kopalni soli w Wapnie. Uwagi do wydarzeń z sierpnia 1977 r., Poland, Przegląd Solny, vol. 10, 2014.

[20] Poborska-Młynarska K., Katastrofy wodne w górnictwie solnym na świecie - przyczyny, sposoby zwalczania, skutki, Poland, Przegląd Solny, vol. 10, 2014.

# OPTIMIZED SOLUTION IN ENTERING ZERO-POINT DRIFT CORRECTIONS IN RESULTS FROM RELATIVE GRAVITY MEASUREMENTS

**PhD Eng. Severina Djorova**[1]

[1] University of Architecture, Civil Engineering and Geodesy, Faculty of Geodesy, Sofia, **Bulgaria**

## ABSTRACT

The study of a gravimetric network is closely connected with determining the value of the drift on the gravimeter scale (zero-point drift; drift). The realization of a great number of over-measured quantities makes preliminary processing of gravity measurements a hard, slow, and delicate process. The main purpose of this research is to investigate a method that would simplify the overall technology of gravimetric measurement and post-processing of the results obtained. A modification of the commonly adopted adjustment approach is offered, where the velocity of the zero-point drift is introduced as an additional unknown quantity in the parametric adjustment. The options for optimization of the complete program of measuring and processing a gravimetric network are described. The advantages of the applied method are explained. It is shown that this is a more reliable and rational way to process gravimetric measurements. The analysis is supported by an example from a specific and real object. Conclusions and recommendations follow.

**Keywords:** gravimetric network, drift of the zero-point, parametric adjustment, gravity corrections

## INTRODUCTION

The process of adjustment and studying a gravimetric network requires determination of the drift of the used gravimeter. The necessity of repeated and consecutive observations of one and the same gravimetric station over a certain period of time additionally complicates the process of measuring and processing of the obtained data.

This article compares the results of an applied method for optimized solution in drift calculation as well as the options for significant facilitation of the overall technology of measuring and subsequent processing of results from relative gravity measurements. Real data, collected from a specific site, is used for the study.

All postulates and their related analyses are realized given the assumption that the zero-point drift of the instrument is exclusively linear. This means that the time for measuring each gravimetric unit must be appropriately selected depending on the specifics of the particular gravimeter. The advantages of the offered approach for calculation over the commonly used methods for processing results from relative gravity measurements are substantiated.

## MATERIALS AND METHODS

It is chosen to be calculated linear gravimeter drift because of difference method of measurement (Fig. 1). One connection is formed from three measurements, that's why for time of this measurement linear drift is calculated (according to [8]). The value is determined from double measurements in every gravity connection (gravimetric point 1). Value of linear drift for middle point (gravimetric point 2) is calculated upon time of measurements.

For computation of the drift (U) is used empirical formula [4, 7]:

$$U = c\left(\frac{O_1^{''} - O_1'}{t_1'' - t_1'}\right) \quad (1)$$

where: c - constant of the instrument, which transforms the reading into mGal. For gravimeters with automatic adjustment, the value of the constant is eliminated from the formula; $O_1', O_1^{''}$- repeated readings, placed in station 1; $t_1', t_1^{''}$– time of readings $O_1', O_1^{''}$.

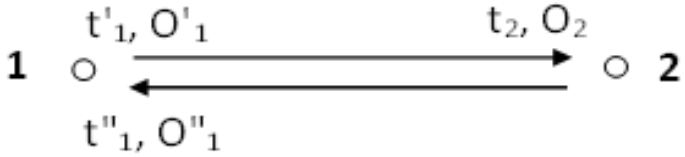


**Fig.1**. Linear drift calculation for connection (gravity difference in acceleration)

The other model for applying of drift correction is to take all data measurements in each gravimetric day and to model square gravimeter drift which should be applied for every measurement. This square drift will be formed actually from linear drift in connections in same gravimetric day.

After application of drift correction in every gravity reading is calculated gravity difference in acceleration for two points:

$$O_1^{\text{corrected}} = O_1'' - U, \quad (2)$$

$$O_2^{\text{corrected}} = O_2 - U(t_2 - t_1'). \quad (3)$$

For the purposes of determining the mean gravity value of the drift ($\overline{U}$), the following equation is used:

$$\overline{U} = \frac{\sum_{i=1}^{n} U_i P_i}{\sum_{i=1}^{n} P_i} \quad (4)$$

The weight ($P_i$ of the i-measurement) is calculated under the following formula [1]:

$$P_i = \frac{\text{const.}}{m_i{}^2} \quad (5)$$

In the stations where repeated measurements are made, Root Mean Square (RMS) of the i-measurement $m_i$ is calculated under the next formula [1]:

$$m_i^2 = m'^2_i + m''^2_i \quad (6)$$

Weight is inversely proportional to the time interval between the moment of measurement in the station ($t_i$) and a particular initial moment ($t_0$):

$$P'_i = \frac{1}{t'_i - t_0} \quad \text{and} \quad P''_i = \frac{1}{t''_i - t_0}, \tag{7}$$

where: $t'_i, t''_i$ – time of first and second readings in station i.

For the time of the first measurement of the first station, coinciding with the initial moment ($t_0 \equiv t'_1$), weight equals one. The following expression is used as a final expression of the weight of the i-measurement:

$$P = \frac{P' P''}{P' + P''} \tag{8}$$

Since more than two reports can be made at each station, the introduction of an arithmetic mean reading $\overline{O_i}$ is necessary:

$$\overline{O_i} = \frac{1}{n} \sum_{i=1}^{n} O_i, \tag{9}$$

where: n – number of readings in each station.

The residuals ($v_i$) are solved for by using the next formula:

$$v_i = O_i - \overline{O_i} \tag{10}$$

In such case, the average error value of a quantity, measured multiple times, may be recorded as follows [1]:

$$m = \pm \sqrt{\frac{\sum(vv)}{n-1}} \tag{11}$$

If the number of readings in each gravimetric station is greater, readings $O_i$, as designated in formulas (1), (2), and (3), are replaced with their arithmetic mean values $\overline{O_i}$, as calculated under formula (9).

## RESULTS

For the purposes of the study, real data from the measurement of the gravimetric network of the Republic of North Macedonia is used.

There are two models which are used to calculate mean reading from every session of measurements (6 time cycle measurements) in each station. Gravity readings with their standard deviations (SD) were obtained from file with measurements. The two used models are: Arithmetical mean model (AMM) of six readings and arithmetical mean standard deviations of the readings; Mean proportional model (MPM) of six readings and mean proportional standard deviations of the readings.

In these calculations is presented estimation of accuracy. Measurements which not satisfied adopted criteria are eliminated.

Formulas used for calculations:

- Arithmetical mean model (AMM):

$$O_{AM} = \frac{1}{6}(O_1 + O_2 + O_3 + O_4 + O_5 + O_6) \quad (12)$$

$$m_{AM} = \frac{1}{6}(m_1 + m_2 + m_3 + m_4 + m_5 + m_6), \quad (13)$$

where: $O_{AM}$ - arithmetical mean reading, $m_{AM}$ - arithmetical mean of SD.

- Mean proportional model (MPM):

$$P_i = \frac{(\Sigma {m_i}^2/6)}{{m_i}^2} \quad (14)$$

$$M_{MP} = \Sigma\left[\left(\frac{P_i}{\Sigma P}\right)^2 * {m_i}^2\right] \quad (15)$$

$$O_{i_{MP}} = \frac{\Sigma P_i O_i}{\Sigma P_i}, \quad (16)$$

where: $M_{MP}$ – average error of mean proportional, $O_{iMP}$ – mean proportional reading.

Since the realized measurements refer to a longer period of time, they are grouped in several weeks. The purpose of such grouping is differentiation of periods, during which a linear motion of the gravimeter drift may be identified. Thus, the values of the zero-point drift for each particular week ($U_1, U_2, U_3, U_4$) are calculated in advance. Table 1 shows the results of the drift calculation for gravimeters Scintrex CG3 and CG5.

**Table 1** Preliminary calculated value of the drift for each week

| Week | Final value of the drift [mGal/h] | | | |
|---|---|---|---|---|
| | **Gravimeter CG3 AMM** | **Gravimeter CG3 MPM** | **Gravimeter CG5 AMM** | **Gravimeter CG5 MPM** |
| First week | 0.0031 | 0.0029 | -0.0037 | -0.0037 |
| Second week | 0.0005 | 0.0005 | -0.0048 | -0.0047 |
| Third week | 0.0026 | 0.0024 | 0.0016 | 0.0018 |
| Fourth week | -0.0008 | -0.0008 | -0.0008 | -0.0008 |

Two way of adjustments have been applied: a standard adjustment – commonly used in practice, comprising calculation of a linear drift for each gravimetric connection separately; and an adjustment, where the zero-point drift is introduced using four components, identified with four additional unknown quantities (one for each week). The results of two adjustment approaches are compared only for mean proportional reading for gravimeter Scintrex CG5 - Table 2.

**Table 2** Comparative table showing the value of the zero-point change of the instrument for each week, Root Mean Square (RMS) of unknown parameters and Root Mean Square of unit weight (μ)

| Compared values | $U_1$ [mGal/h] | $mU_1$ [mGal] | $U_2$ [mGal/h] | $mU_2$ [mGal] | $U_3$ [mGal/h] | $mU_3$ [mGal] | $U_4$ [mGal/h] | $mU_4$ [mGal] | μ [mGal] |
|---|---|---|---|---|---|---|---|---|---|
| Standard method of adjustment, usually applied in practice | -0.0037 | - | -0.0047 | - | 0.0018 | - | -0.0008 | - | 18.871 |
| Optimized adjustment approach, where the drift is identified with four additional unknown quantities | -0.0043 | 0.0028 | -0.0041 | 0.0015 | 0.0012 | 0.0018 | -0.0008 | 0.0030 | 8.433 |

## DISCUSSION

The obtained results and the presented comparisons prove the degree of correctness of the proposed adjustment approach.

The comparisons show that the values for the drift for each week, obtained under the two approaches, differ with 0.001 [mGal/h]. RMS of unit weight (μ) is two times less in the second adjustment approach. Accuracy depends primarily on the precision with which the measurements are made and the accuracy of the source data used.

After adjustment RMS of unknown parameters also obtained (mU), while the standard approach of processing and adjusting does not give the value of this estimation.

## CONCLUSION

In conclusion of the conducted research, it can be said that equating by introducing the zero drift as four additional unknowns (one for each week) is a reliable way to process the results of relative gravimetric measurements.

For the purposes of accuracy and considering the results of conducted studies, it is worth mentioning that the optimized adjustment approach is applicable only in certain cases, provided that the zero-point of the instrument keeps its linear drift nature over the whole period of measuring or for several specifically differentiated sub-periods!

Therefore, it is advisable that before starting the actual gravity measurements and during the measurements, the motion of the gravimeter is tested for identifying its nature.

Based on the comparisons several basic advantages of the offered optimized solution for drift calculation, comprising its introduction as an additional unknown quantity in the parametric adjustment, may be identified:

- It is not imperative to follow a particular measuring scheme.

- Options for significant facilitation of the complete technology of measuring and processing gravimetric measurements are created.
- There is no longer any need to calculate in advance the velocity of the drift of the instrument.
- The research done leads to optimization of the measurement plan with correct accuracy assessment. They are a prerequisite and for reliable derivation of a local geoid/ quasigeoid model [2, 5] (with an accuracy of less than 3mm, which is more than 5 times higher accuracy than previously achieved [3]), and bearing in mind that reliable and accurate results are required for levelling, GNSS and gravimetric measurements accompanying the performance of precise geometric levelling [6].

## REFERENCES

[1] Atanasov, S.N., Theory of mathematical processing of geodetic measurements, State Publishing House "Technique", 1988

[2] Cvetkov V., Adjustment of the highest order geometric levelling networks, Monography, Sofia, 2024, ISBN 978-619-92816-0-4

[3] Cvetkov V., On initial data in adjustments of the geometric levelling networks (on the mean of paired observations), Journal of Geodetic Science, vol. 14, no. 1, 2024, pp. 20220170, https://doi.org/10.1515/jogs-2022-0170

[4] Ogorodova, L.V., Shimbirev, B., Yuzefovich, A., Gravimetry, Moscow, "Nedra", 1983

[5] Peneva, E., On the implementation of the European Vertical Reference System in Bulgaria, 21th International Multidisciplinary Scientific Geo Conference Surveying, Geology and Mining, Ecology and Management (SGEM 2021). Conference proceedings 2021, Albena, Bulgaria, 14 – 22 August, 2021, ISSN 1314-2704, doi.org/10.5593/sgem2021/2.1/s09.48

[6] Tsanovski, Y., GNSS Measurements for the Needs of Precise Height Determinations in Bulgaria, Annual of the University of Architecture, Civil Engineering and Geodesy – Sofia, Vol. 54, 2021, Issue 2, pp. 211 –217, ISSN 1310-814X, ISSN 2534-9759

[7] Veselov, K.E., Gravimetric Survey, Moscow "Nedra", 1986

[8] Valev, G., Gospodinov, S., Adjustment of geodynamic networks by introducing the velocities of geodetic points as additional unknowns, Annual of the VIAS, Volume III, Geodesy and Land Management, Volume XXXIII, 1987-88

# THE POSSIBILITIES OF USING THE HANDHELD SCANNER FOR THE REAL ESTATE CADASTRE

**Ing. Petr Jadviščok, Ph.D.**[1]

**Ing. Tereza Jadviščoková**[1]

**Ing. Rostislav Dandoš, Ph.D.**[1]

**Ing. Jiří Plesník, Ph.D.**[1]

[1] VSB - Technical University of Ostrava, **Czech Republic**

## ABSTRACT

Mobile handheld laser scanning is already an established technology in today's surveying practice. Mobile handheld scanners are mostly used for surveying and 3D rendering of indoor spaces. However, the subject of this paper will be the area of real estate cadastre. The aim of this paper is to verify the capabilities of mobile handheld laser scanning technology for cadastre of real estate purposes. The paper will focus specifically on surveying activities related to the production of a survey sketch for designation of the building on the cadastral map. The real accuracy of the survey and the efficiency of the measurement will be analysed. Factors that may negatively affect the resulting accuracy and usability will also be evaluated. The aim will be to verify and analyse the situation on concrete data obtained in a real terrain during practical measurements. The experimental measurements will be carried out on an atypical building. The results obtained with the Leica BLK2GO will be compared with the results of combined GNSS and terrestrial surveying using a total station. For measurement work in the cadastre of real estate in the Czech Republic it is necessary to use the binding coordinate reference system S-JTSK. The issue of transformation to the binding reference system will also be part of the paper.

**Keywords:** cadastre of real estate, handheld laser scanner, GNSS, building, cadastral map.

## INTRODUCTION

The aim of the paper will be to verify and analyze situation on concrete data obtained in a real environment during practical measurements. A model situation will be established in the implementation of contracts from surveying practice. The evaluation of accuracy will be done primarily by comparing the results of manual laser scanning with terrestrial surveying using a total station. In surveying practice, a very wide range of buildings are encountered when surveying objects. Buildings differ in shape and size of the object but also in the complexity of the building design. In cadastral practice, there is an inconsistent approach to surveying and subsequent representation of buildings in cadastral maps for more complex objects. Although the procedures and principles for surveying and depicting buildings are generally known among the professional public, the reality is often different in practice.

When taking a closer look at the actual shape of the building in the field and its representation on the cadastral map, there can be significant inconsistency. It always depends on the approach of the particular surveyor who carries out the measurements in the field and subsequently prepares the geometric plan. From this point of view, terrestrial laser scanning technology could be a significant asset as it can produce a very detailed 3D image of reality. [1]

## REALIZATION OF EXPERIMENTAL MEASUREMENT

The test object was the Geological Pavilion of Prof. Pošepný situated in the premises of VŠB-TUO. When selecting a building for the experimental measurements, it was important to choose an object that would represent a certain group of buildings in geodetic practice. The aim was to select an atypical building, with the walls of the building overlapping the terrain. Such buildings are encountered more and more often. Thus, the Geology Pavilion building, with its shape, number of points and complexity of plan, offered itself as a suitable building for testing. The test object is shown in Figure 1 below.

**Figure 1:** Test object - Geological Pavilion of Prof. Pošepný

According to the valid regulations in the area of the cadastre, the change to be measured must be linked to the binding coordinate system S-JTSK (Datum of Uniform Trigonometric Cadastral Network) without exception. Therefore, for each measurement for the purposes of the land registry, it is necessary to carry out activities related to connecting the site to the binding S-JTSK reference system. [2]

The application of measurement work with handheld or static scanners is not usually associated with referencing to a binding coordinate system. In most cases, we make do with the results in the local coordinate system of the scanner. However, if we were to consider the possibilities of using this technology for cadastral purposes, the reliable connection of the resulting point cloud would be one of the core tasks of the whole workflow. [2]

Based on the above, a workflow for the field measurement work was proposed. The workflow was chosen in such a way that its widespread implementation could be considered regardless of the specifics of the site of interest. Other requirements for the workflow include simplicity and clarity for any surveyor with previous experience in land registration.

As part of the Geology Pavilion test measurements, the paper was extended to test a pair of ground control point types. Black and white ground control points, designated as Type B, and red and white Type A ground control points were acquired. An example of the ground control points is shown in Figure 2.

**Figure 2:** Type of ground control points

The ground control points were evenly spaced in the vicinity of the object according to the general geometric principles in geodesy. The coordinates of the individual points were determined twice independently by GNSS technology using the RTK method. The GNSS equipment chosen for the measurements was a Leica GS18 T receiver and a Leica CS20 controller.

A Leica BLK2GO handheld laser scanner was chosen for scanning. The handheld scanner is controlled via the iPhone mobile device in the BLK2GO Live app. Before the actual scanning, the scanner is calibrated in the calibration pad. After calibration, the instrument starts scanning. When scanning, it is necessary to hold the scanner overhead and then walk around each object. The scanning time is directly dependent on the size of the object, the complexity of the object and the walking speed. In the case of this object, the scan time was between 2 and 3 minutes. It should be noted that in processing the results so far, it was found that there was no need to purposely slow down the walking. This time is incomparable to the time of a classical terrestrial measurement, where for this more complex object it was necessary to select 5 stations and the whole measurement process, including connection to the binding reference system S-JTSK, amounted to two hours. [3]

The 30 x 30 cm checkerboard ground control points are commonly used in aerial photogrammetry in the application of unmanned aerial vehicle technology and as ground control points in terrestrial laser scanning. Ground control points points are made of hardened plastic in black and white. As it is necessary to stabilize the points so that the same position of the control target is ensured throughout the measurement period, partial adjustment and addition of the purchased ground control points was started. The lower part of the threading point was supplemented with a cylinder-shaped preparation into which a threaded hole was made. A steel mandrel is screwed into this

hole, which will enable a reliable and stable securing of the ground control point in the field during the entire scanning period, including its subsequent targeting by the GNSS-RTK receiver. The fixtures used to anchor the insertion points to the terrain were designed and manufactured on a 3D printer directly at the Department of Geodesy and Mining Surveying in Ostrava. An example of the solution can be seen in Figure 3.

**Figure 3:** Ground control points – technical solution and GNSS measurements

When working with the scanner, it is necessary to adapt the scanning trajectory to the object to be scanned, taking into account the theoretical range of the handheld scanner. According to the technical parameters and based on personal experience with the Leica BLK2GO handheld scanner we can state that the real reliable usable range of the handheld scanner is around 30 meters. These facts must be taken into account not only in the scanning process, but especially in the activities related to the placement of the ground control points. [3]

It is therefore highly desirable to carefully consider the positions and placement of the ground control points not only in relation to the object to be measured but also to the planned scanning route. The scanning must be done in such a way that the resulting point cloud contains the measured object including all the ground control points. Working with a handheld scanner can be seen in Figure 4.


**Figure 4:** Scanning process in the field with handheld laser scanner the Leica BLK2GO

Figure 5 shows the number and location of the auxiliary points of the measurement network from which the reference terrestrial orientation was carried out using the polar method, which documents the time-consuming nature of the classical procedure. Furthermore, the approximate trajectory using a handheld scanner and the spatial relationship between the chosen scan trajectory, the ground control points and the object of measurement are indicated.

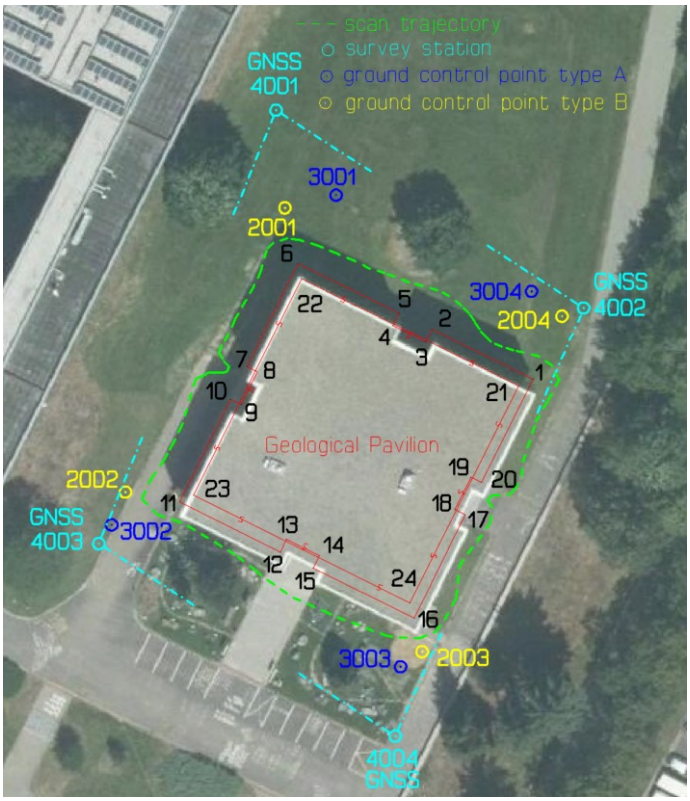


**Figure 5:** Situational plan

The tested objects were also targeted by commonly established procedures in the field of real estate cadastre. Individual breaking points on the perimeter of the building were focused using the polar method. The terrestrial survey served as a reference measurement for subsequent evaluation and analysis of the accuracy of the procedures used.

## PROCESSING OF MEASURED DATA

A key step towards the successful use of the measured data for cadastral purposes will be the georeferencing of the 3D point cloud into the S-JTSK binding reference system. If this computational step could not be implemented for some reason, it would completely prevent the use of this measurement for the purpose of making a geometric plan. The transformation of the 3D point cloud is carried out by means of ground control points located e.g. by GNSS technology. The processing of the measured data including the transformation was performed with the Leica Cyclone REGISTER 360 software. After successful transformation of the 3D point cloud, the coordinates from the 3D point cloud were offset in Leica Infinity. [3] An example of measured data processing is shown in the figure 6.

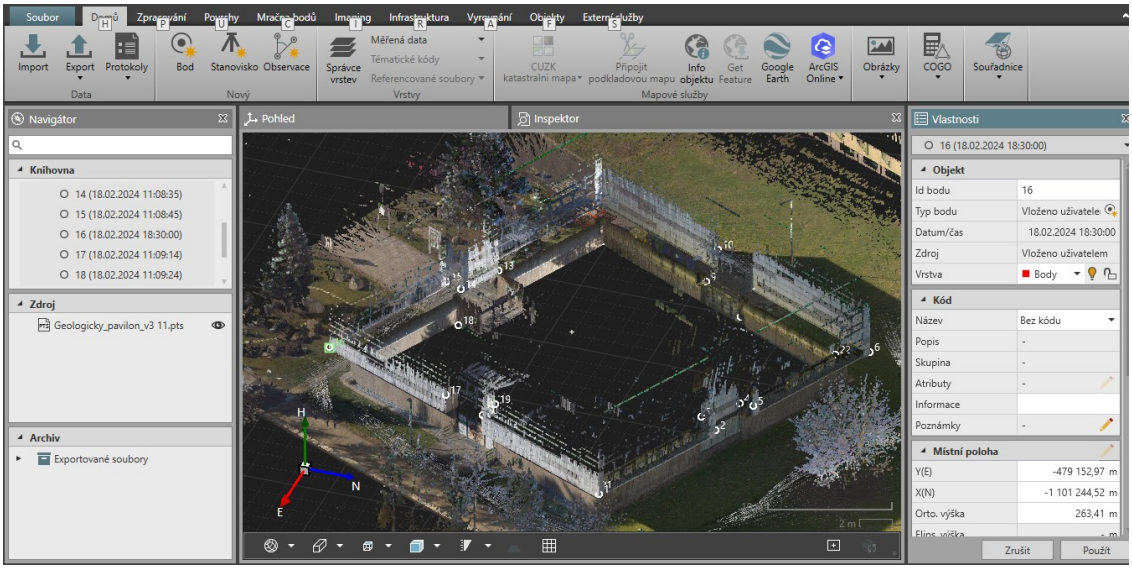


**Figure 6:** Point cloud in Leica Infinity

## RESULTS

The results of the experimental measurements are summarized in Table 1 below. A total of 24 points were tested, with the majority of points consisting of atypical building overhangs above the ground. Terrestrial surveying was carried out from four sites, with the time required for terrestrial surveying being approximately 2 hours of measurement time. Regarding the scanning time, it can be said that in the case of the handheld scanner, the scanning was carried out in two minutes, with more than 10 million points evaluated, and the scanning path length reached 160 m. The georeferencing into the binding reference system was successful, the 3D transformation accuracy was favourable, the spatial mean transformation error reached 0.025 cm.

To compare the coordinates of the selection of detailed points, the coordinate differences are calculated, where $y_m$ and $x_m$ are the resulting coordinates of the detailed point determined by the terrestrial polar method and $y_k$, $x_k$ are the coordinates of the same point as the results of the above-described procedure of determining these points by 3D laser scanning technology. The mean sampling coordinate error $m_{xy}$ is calculated as the quadratic mean of the mean coordinate errors mx, my, which are determined from the following formulas. [3]

$$m_x = \sqrt{\frac{1}{k.N}\sum_{i=1}^{n}\Delta x_i^2}\,; \quad m_y = \sqrt{\frac{1}{k.N}\sum_{i=1}^{n}\Delta y_i^2}\,; \quad m_{xy} = \sqrt{\frac{m_x^2 + m_y^2}{2}}$$

In relation is N equal to the number of points in the selection and k is equal to 2 if the control determination has the same accuracy as the position measurement, or is equal to if the control measurement has a higher accuracy. $\Delta y = y_m - y_k$ and $\Delta x = x_m - x_k$ are the deviations, the coordinate differences between the terrestrially determined coordinates and the coordinates that were determined by laser scanning technology. The sampling mean coordinate error reached $m_{xy}$ = 0.046 m in the case of handheld scanner measurements.

**Table 1:** Results achieved BLK2GO handheld scanner

| Test object - Geological Pavilion of Prof. Pošepný | | | | | | | |
|---|---|---|---|---|---|---|---|
| Point number | Leica BLK2GO | | Leica TS16 | | Differences [m] | | |
| | Y [m] | X [m] | Y [m] | X [m] | Δy | Δx | Δp |
| 1 | 479137,49 | 1101213,29 | 479137,50 | 1101213,26 | 0,01 | -0,03 | 0,03 |
| 2 | 479150,70 | 1101206,75 | 479150,70 | 1101206,71 | 0,00 | -0,04 | 0,04 |
| 3 | 479151,50 | 1101208,38 | 479151,48 | 1101208,36 | -0,02 | -0,02 | 0,03 |
| 4 | 479155,77 | 1101206,27 | 479155,80 | 1101206,23 | 0,03 | -0,04 | 0,05 |
| 5 | 479154,96 | 1101204,66 | 479154,99 | 1101204,61 | 0,03 | -0,05 | 0,06 |
| 6 | 479168,20 | 1101198,17 | 479168,16 | 1101198,11 | -0,04 | -0,06 | 0,07 |
| 7 | 479174,74 | 1101211,59 | 479174,85 | 1101211,58 | 0,11 | -0,01 | 0,11 |
| 8 | 479173,44 | 1101212,25 | 479173,46 | 1101212,28 | 0,02 | 0,03 | 0,04 |
| 9 | 479175,42 | 1101216,47 | 479175,55 | 1101216,51 | 0,13 | 0,04 | 0,14 |
| 10 | 479176,87 | 1101215,79 | 479177,00 | 1101215,84 | 0,13 | 0,05 | 0,14 |
| 11 | 479183,63 | 1101229,29 | 479183,64 | 1101229,31 | 0,01 | 0,02 | 0,02 |
| 12 | 479170,40 | 1101235,88 | 479170,44 | 1101235,87 | 0,04 | -0,01 | 0,04 |
| 13 | 479169,63 | 1101234,24 | 479169,69 | 1101234,25 | 0,06 | 0,01 | 0,07 |
| 14 | 479165,37 | 1101236,35 | 479165,37 | 1101236,36 | 0,00 | 0,01 | 0,01 |
| 15 | 479166,17 | 1101238,00 | 479166,20 | 1101238,00 | 0,03 | 0,00 | 0,03 |
| 16 | 479152,97 | 1101244,52 | 479153,01 | 1101244,51 | 0,04 | -0,01 | 0,05 |
| 17 | 479146,28 | 1101231,03 | 479146,32 | 1101231,02 | 0,04 | -0,01 | 0,05 |
| 18 | 479147,69 | 1101230,32 | 479147,70 | 1101230,31 | 0,01 | -0,01 | 0,01 |
| 19 | 479145,57 | 1101226,05 | 479145,62 | 1101226,08 | 0,05 | 0,03 | 0,06 |
| 20 | 479144,14 | 1101226,75 | 479144,19 | 1101226,75 | 0,05 | 0,00 | 0,05 |
| 21 | 479139,38 | 1101214,14 | 479139,37 | 1101214,11 | -0,01 | -0,03 | 0,03 |
| 22 | 479167,73 | 1101200,17 | 479167,69 | 1101200,10 | -0,04 | -0,07 | 0,08 |
| 23 | 479181,76 | 1101228,43 | 479181,84 | 1101228,49 | 0,08 | 0,06 | 0,10 |
| 24 | 479153,47 | 1101242,55 | 479153,51 | 1101242,53 | 0,04 | -0,02 | 0,05 |

## DISCUSSION

The red and white ground control points are also reliably identifiable in point clouds despite their smaller size (20 x 20 cm), but the checkerboard targets in black and white are clearly more impressive in point clouds. Here, the resulting contrast is quite unambiguous and the marking of such an insertion point is more reliable and simpler. Even so, some experience is necessary when working with point clouds.

Another important factor that can to some extent influence the resulting quality of the georeferencing into a binding coordinate system and consequently the whole measurement result is the shadows of the building. When carrying out the measurement work, it is advisable to take into account the current lighting conditions and the orientation of the sunlight or cast shadows of the building. It is advisable to place the aiming points on the illuminated part of the terrain. If they were signalled at locations where shadow falls, these points would be more difficult to identify. Ultimately, this could have a negative impact on the resulting accuracy of the transformation. Especially when using a handheld scanner, where the point cloud does not exhibit the same quality as a static scanner. Also shows a higher level of noise in the trajectory of the moving scanner due to the movement of the meter. Therefore, it is desirable to choose the

position for the ground control points appropriately and to adjust the trajectory of the handheld scanner so that the ground control points are not overwhelmed by unwanted noise.

## CONCLUSION

There were a total of 24 detailed points on the Geology Pavilion test object. The results of the deviations obtained using the manual scanning with the Leica BLK2GO are favourable for land registry purposes. Points 7, 9, 10 and 23 show the lowest accuracy. The most susceptible parts of the tested objects are the inner corners of the building, with shorter dimensions of the masonry plan. In the case of the Geology Pavilion, other factors were also negatively affected. In particular, a technical element in the form of an exit evacuation ladder, installed directly on the building to be surveyed. Already when viewing the point cloud, the situation in the vicinity of detail point 9 was negatively affected by the presence of the exit ladder and the position of the point was not as clear as it was for detail points in other parts of the building.

In the case of 3D laser scanning, it is important to determine the scanning direction relative to the object being measured and the current illumination of the object. Before the actual measurement, a thorough reconnaissance should be carried out. Based on a well performed reconnaissance of the building, we will get an overview of which parts of the building will need to be measured with increased care, critical areas, where there are potential obstacles, how complex the building layout is, in which direction the building casts a shadow, etc. If we do not carry out these activities and start scanning immediately, we are unable to take these facts and circumstances into account when scanning. Very often, this thoughtless and incorrect scanning procedure will then have a negative impact on the final accuracy and quality of the overall work. The precision achieved is undoubtedly satisfactory for land registry purposes. In the Czech Republic, the required accuracy is characterised by a primary mean coordinate error of 0.14 m. The limit is the error twice the primary error.

## ACKNOWLEDGEMENTS

This contribution was created with the financial support of project SP2024/027: Possibilities of using UAV mapping means in the field of reclamation and smoothing of mining activity.

## REFERENCES

[1] MUDIČKA, Štefan a KAPICA, Roman. Digital Heritage, the Possibilities of Information Visualisation through Extended Reality Tools. Online. Heritage. 2023, Vol. 6, issue. 1, p. 112-131. ISSN 2571-9408.

[2] Staňková, H.; Černota, P. A principle of forming and developing geodetic bases in the Czech Republic. Geodesy and Cartography 2010, 36(3), 103-112. DOI: 10.3846/gc.2010.17

[3] MUDIČKA, Štefan a KAPICA, Roman. Application of handheld scanner in documentation of historical buildings. Online. 19th International Multidisciplinary Scientific Geoconference, SGEM 2019, Vol. 19, issue. 2.2, p. 39 - 46. ISSN 13142704.

# SECTION PHOTOGRAMMETRY AND REMOTE SENSING

# ASSESSMENT OF THE RESULTS FROM THE MATTERPORT SYSTEM USING A 360-DEGREE CAMERA

**Dr. Richard Honti**[1]

**Assoc. Prof. Dr. Ján Erdélyi**[1]

**Assoc. Prof. Dr. Tomáš Funtík**[2]

[1] Department of Surveying, Faculty of Civil Engineering, Slovak University of Technology in Bratislava, **Slovakia**
[2] Department of Building Technology, Faculty of Civil Engineering, Slovak University of Technology in Bratislava, **Slovakia**

## ABSTRACT

Accurate 3D data from indoor environments play a crucial role in construction, indoor navigation, real estate management, and many more applications. Mobile scanning systems, including simultaneous localization and mapping (SLAM) and mobile devices equipped with LIDAR (Light Detection And Ranging) and modern techniques like Matterport, provide efficient means to create virtual models of measured objects (and even generate point clouds). However, it is essential to note that the quality of these methods often needs to improve compared to the accuracy achieved by terrestrial laser scanning (TLS). Therefore, assessing results obtained from these systems is essential for utilizing them for 3D data capture. This paper evaluates the Matterport system using a 360-degree camera (Ricoh Theta Z1). The evaluation compares it to survey-grade Terrestrial Laser Scanning point clouds obtained from four distinct test sites, each with varying properties such as size, complexity, and noise levels. The analysis highlights both technical and practical strengths and weaknesses.

**Keywords:** 3D Capture, SLAM, 360-degree photogrammetry, TLS, Matterport

## INTRODUCTION

The architecture and construction industry is constantly evolving. The need for efficient and innovative technologies and solutions drives it. The need for accurate documentation of building structures is well justified, as these data can be used as the basis for decisions, structural analysis, the creation of accurate 3D models (such as Building Information Models (BIM)), and so on. Significant progress in the digitization of the construction industry is being made through innovative data capture techniques and the development of information technologies. This makes it possible to automate (to some extent) all the processes involved in building.

However, conventional field measurements can be laborious, time-consuming, and inefficient for larger and more complex buildings or objects, requiring a significant number of measurements. Therefore, these methods do not primarily meet the requirements for automating digitisation processes in the construction industry. Over the last decade, however, the development of surveying and mapping technologies has

greatly improved 3D data capture methods. The need for 3D surveying and accurate 3D information continues to grow in all areas, including the digitization or 3D modeling of the built environment [1], [2], BIM models (with the Scan-to-BIM methodology) [3], [4], geometric verification with the Scan-vs-BIM methodology [5], [6], geological surveys, reverse engineering, documentation, and preservation of cultural heritage [7], and more. 3D visualization offers a better understanding and more opportunities for different types of analysis [8].

To capture and digitize the geometry of real-world objects, several 3D data capture techniques can be used. The most common methods are terrestrial laser scanning (TLS), close-range (or 360°) photogrammetry, SLAM (Simultaneous Localisation And Mapping) enabled handheld scanning systems and mobile LIDAR-equipped devices. Compared to other techniques, terrestrial laser scanners produce point clouds with high accuracy and relatively low noise. Data collection can take longer and requires careful planning. In contrast, SLAM-capable mobile laser scanners (MLSs), methods such as Matterport, or mobile devices with LIDAR sensors offer the possibility to measure the geometry of the object more quickly and effectively, but achieving some level of accuracy in the final model can be difficult and complex.

This paper assesses the capability and usability of the Matterport models captured with a 360-degree camera. For the assessment, the control point approach is applied. The control point approach involves manually choosing two control points in specific characteristic areas of an object, such as corner points on building structures or openings. Next, the Euclidean distances between these points are calculated and compared with the reference point clouds. For the evaluation of the resulting models generated by Matterport, the reference data were acquired using terrestrial laser scanning. Terrestrial laser scanning systems are non-contact measurement techniques for determining 3D coordinates of points on the surface of an object with survey-grade accuracy by emitting laser pulses toward the object. The space polar method is the basic operating principle of most laser scanners. Based on the measured horizontal and vertical angles and the measured length, the 3D position of each point is determined [9].

## MATTERPORT

Matterport is a commercial indoor mapping system that was selected for evaluation because it offers an interesting solution for indoor mapping at a low cost. Matterport's camera system offers an efficient alternative to traditional terrestrial laser scanning. Unlike TLS, which requires complex field survey planning, Matterport's approach can be faster and more straightforward at the price of lower accuracy and reliability. Matterport captures real-world objects using its camera system. The system collects two types of data [10]:

- **Images** – used for visualizing the measured object
- **Depth maps** are used to estimate the distance between the acquisition sensor position and the measured object surface.

Using the acquired data, Matterport generates a digital photogrammetric model of the surveyed space. For the 3D model generation, Matterport employs its artificial intelligence called Cortex AI. This deep-learning neural network can create 3D data from various capture devices, including LIDAR cameras, 360-degree cameras, and smartphones [11].

The entire measurement process is managed through the Matterport mobile application. After capturing the images, they are uploaded to the Matterport cloud for processing, creating a 3D photogrammetric virtual model. Various sensors can be used for data capturing, from smartphones to 360-degree cameras, to Matterport's cameras, such as the Matterport Pro2 and Matterport Pro3 LIDAR cameras, and laser scanners, such as the Leica BLK360.

**Matterport system with a 360-degree camera to capture**

In this paper, a readily available and affordable 360-degree camera, the Ricoh Theta Z1 (Figure 1), is used for capturing, the manufacturer's flagship model recommended by Matterport itself for the highest quality 360° capture. The Ricoh Theta camera series uses two CMOS sensors equipped with wide-angle lenses to capture both hemispheres of the environment. The images from these sensors have a small area of overlap, which is then stitched together to create a seamless panoramic picture. The ability to capture images in RAW format with minimal post-processing is an outstanding feature of the Z1 [12]. The camera has a 1.0-inch (25.4 mm) back-illuminated CMOS sensor with approximately 23 effective megapixels (6720x3360). It supports RAW format with a resolution of 7296 × 3648 pixels and JPEG format with a resolution of 6720 × 3360 pixels. The camera has a 1" (25.4 mm) OLED information display with a resolution of 128 × 36 pixels. The dimensions of the camera are 48mm (W) x 132.5mm (H) x 29.7mm (D), and its weight is approximately 182g, making it a very compact camera.

**Figure 1:** The 360-degree camera Ricoh Theta Z1

## THE SELECTED BUILDING SPACES FOR EVALUATION

Four building spaces in the building of the Faculty of Civil Engineering at the Slovak University of Technology in Bratislava were selected for the evaluation of the Matterport models captured with a 360-degree camera. These spaces differ in shape, size, complexity, geometric arrangement, and density of objects.

A Trimble TX5 3D laser scanner was used to capture the reference data, with a ranging error of ±2 mm at a 25-meter distance with an operational range of 0.6 meters to 120 meters. The scanning resolution in all four building scenes was set at 7.7 millimeters at a 10-meter distance. In each case, the distance between the scanner and the object measured was below 15 m. The distance between the individual scanning positions ranged from 5 to 7 m. Scan registration was carried out based on the overlapping areas between the point clouds from several scanning positions in the Leica Cyclone (Version 2023.1.0) software.

The first test scene for evaluation is an oblong room with a repeating geometric structure, serving as a **Laboratory of Surveying** (Figure 2 - left). The laboratory's dimensions are approximately 29.5 meters (D) x 9.8 meters (W) x 3.6 meters (H). As for the second

building space, a **long hallway** (Figure 2 - right) was selected, also featuring a repeating geometric structure. This hallway measures 2.2 meters (D) x 3.2 meters (W) x 3.6 meters (H) and has windows along one side.

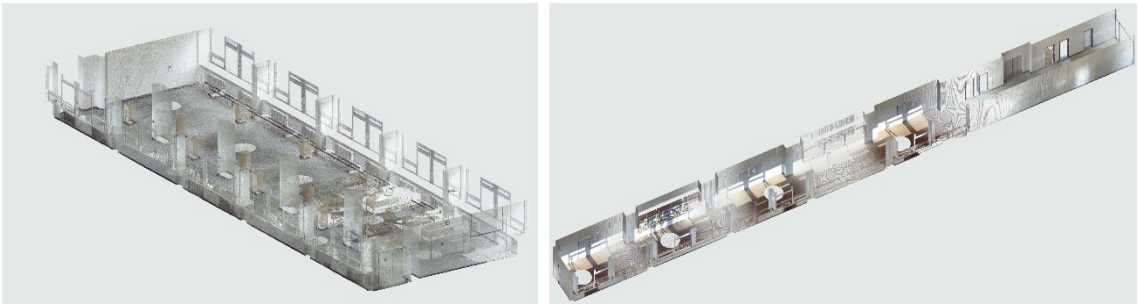

**Figure 2:** The point cloud from TLS of the first building space (left) and the second building space (right) for evaluation

The third building space for evaluation, depicted on the left side of Figure 3, is a rectangular **auditorium** featuring a stepped structure with desks and dimensions of 14.2 meters depth, 11.8 meters width, and a height that ranges from 4.0 to 7.0 meters. The fourth test scene, depicted on the right side of Figure 3, is **an office** with smaller dimensions. This office is furnished with various items and has a window at one end. Its dimensions are 6.9 meters (depth) x 2.5 meters (width) x 3.6 meters (height).

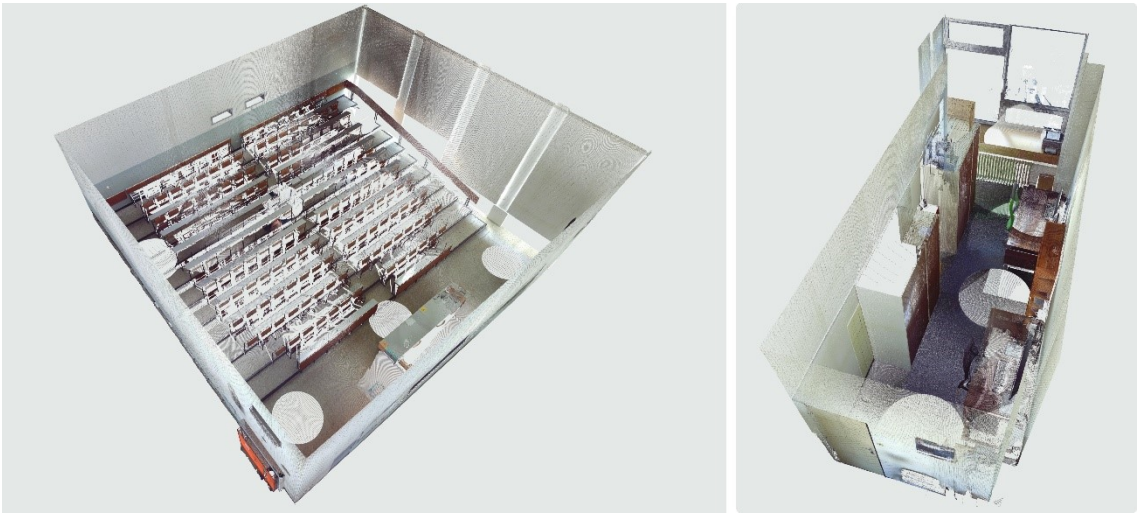

**Figure 3:** The point cloud from TLS of the third (left) and the fourth (right) evaluated building space

The process of capturing the building spaces was repeated with varying distances between camera positions. First, the distance between the camera positions was approximately 5 m, then 3 m, and finally 1.5 m. In the case of the third building space (Auditorium), the capturing was done with 5 m and 3 m distances between the camera positions. Table 1 presents a comparison of the fundamental capturing parameters for the Matterport system and the TLS. The table includes the number of instrument positions (pos.) and the time required for capturing (time).

**Table 1:** Comparison of the capturing details

| | **Matterport** | | | | | | **TLS (reference)** | |
|---|---|---|---|---|---|---|---|---|
| | **5 m** | | **3 m** | | **1.5 m** | | | |
| | pos. | time | pos. | time | pos. | time | pos. | time |
| **Laboratory of Surveying** | 23 | 12 min | 43 | 22 min | 92 | 35 min | 11 | 40 min |
| **Long Hallway** | 12 | 6 min | 18 | 8 min | 32 | 13 min | 6 | 25 min |
| **Auditorium** | 28 | 12 min | 60 | 25 min | - | - | 20 | 60 min |
| **Small Office** | 2 | 1 min | 4 | 1 min | 8 | 3 min | 4 | 10 min |

## RESULTS

The resulting models captured with the Matterport system were evaluated using the control point approach, which involved a comparison with data from survey-grade TLS. This method entailed identifying several control point pairs across various corners within the building interiors, such as the edges of the structure and window frames. The Euclidean distances between these points were calculated. These spatial measurements were initially taken from the reference point cloud captured by TLS. Before determining the dimensions in the reference point clouds, the selected corner points were modeled as intersections between three perpendicular planes near the chosen corners to ensure the highest possible measurement accuracies. For each four building space, at least ten control point pairs were selected from various locations within the scene. These represented various objects, including different sizes, shapes, orientations, colors, and materials. Moreover, a metric called the Root Mean Square (RMS) was defined to compare the Euclidean distances.

$$RMS = \sqrt{\frac{\sum_{i=1}^{n} \Delta^2}{n}}, \tag{1}$$

Where the Δ represents the variance in the measured dimensions between the TLS point cloud and from the Matterport system, while "n" represents the number of the dimensions used for the assessment.

The acquisition process resulted in 11 photogrammetric virtual models; for three building spaces (Laboratory of Surveying, Long Hallway, Small Office), three different models were generated, corresponding to the distances between the camera positions of 5 meters, 3 meters, and 1.5 meters. In the case of the Auditorium, the result was two models taken with a distance of 5 meters and 3 meters between the camera positions.

**Table 2:** Assessment of the results for the Matterport models

| | Distance between positions | Differences from → to [mm] | RMS [mm] |
|---|---|---|---|
| **Laboratory of Surveying** | 1.5 m | -137 → 278 | **187** |
| | 3 m | -157 → 358 | **221** |
| | 5 m | -187 → 413 | **230** |
| **Long Hallway** | 1.5 m | -8 → 77 | **41** |
| | 3 m | -125 → 159 | **89** |
| | 5 m | -145 → 189 | **94** |
| **Auditorium** | 3 m | -92 → 131 | **64** |
| | 5 m | -132 → 211 | **99** |
| **Small Office** | 1.5 m | 8 → 220 | **116** |
| | 3 m | -76 → 247 | **110** |
| | 5 m | 28 → 306 | **171** |

Table 2 provides a comparative analysis for all four building spaces evaluated. The middle column shows the range of differences in measured dimensions between the TLS and Matterport models, along with the RMS differences for each test scene. The average RMS for the various distances between camera positions are as follows: a **115 mm** RMS for the models captured at 1.5 m distance, a **121 mm** RMS for the models captured at 3 m distance, and a **149 mm** RMS for the 5 m distance between camera positions.
In particular, the models from the Laboratory of Surveying achieved the worst results, possibly due to the space's dimensions, variety, and complexity.

Regarding the Matterport system, which employs a 360-degree camera for the measurement, the performance is significantly influenced by the camera orientation at the time of data acquisition.

## CONCLUSION

Matterport represents an innovative and low-cost method for effectively capturing the interiors of buildings. It's crucial to understand the system's limitations and verify its accuracy for the digitalization process of building elements.

The paper presents a comparative analysis of the Matterport system using a 360-degree camera for capturing building spaces. Four different building spaces were selected for the assessment, varying in size, complexity, shape, and geometric structure. In addition, the measurement for each space was repeated with different distances between the camera positions (5 m, 3 m, and 1.5 m) to determine the dependence of the accuracy of the obtained photogrammetric virtual models on this variable.

The evaluation utilized the control point approach, wherein each space with at least ten dimensions from the Matterport models was compared against the reference models, which were the point clouds captured with the survey-grade TLS. The differences for the measured dimensions varied from 8 to 413 mm in absolute values, with an average RMS error of 130 mm across all spaces. The values of the measured dimensions in the Matterport models are significantly dependent on the number of images covering the area of the measured object.

The assessment confirms the presumption that TLS-generated point clouds have higher geometric accuracy. However, in some cases, TLS surveys can be more demanding in terms of planning and time investment. The insights and findings of this research can guide the choice of the most appropriate system for specific documentation needs.

## ACKNOWLEDGEMENTS

This work was supported by the Slovak Research and Development Agency under the Contract no. APVV-18-0247.
This publication was created with the support of the Scientific Grant Agency of the Ministry of Education, science, research and sport of the Slovak Republic and the Slovak Academy of Sciences for the project VEGA-1/0272/22.

## REFERENCES

[1] C. Dold and C. Brenner, "Automatic matching of terrestrial scan data as a basis for the generation of detailed 3D city models," *Int. Arch. Photogramm. Remote Sens.*, vol. 35, no. Part B3, pp. 1091–1096, 2004.
[2] Ľ. Kovanič, M. Štroner, P. Blistan, R. Urban, and R. Boczek, "Combined ground-based and UAS SfM-MVS approach for determination of geometric parameters of the large-scale industrial facility – Case study," *Measurement*, vol. 216, p. 112994, Jul. 2023, doi: 10.1016/j.measurement.2023.112994.
[3] M. Kellner, B. Stahl, and A. Reiterer, "Reconstructing Geometrical Models of Indoor Environments Based on Point Clouds," *Remote Sens.*, vol. 15, no. 18, p. 4421, Sep. 2023, doi: 10.3390/rs15184421.
[4] M. Jarząbek-Rychard and H.-G. Maas, "Modeling of 3D geometry uncertainty in Scan-to-BIM automatic indoor reconstruction," *Autom. Constr.*, vol. 154, p. 105002, Oct. 2023, doi: 10.1016/j.autcon.2023.105002.
[5] F. Bosché, M. Ahmed, Y. Turkan, C. T. Haas, and R. Haas, "The value of integrating Scan-to-BIM and Scan-vs-BIM techniques for construction monitoring using laser scanning and BIM: The case of cylindrical MEP components," *Autom. Constr.*, vol. 49, pp. 201–213, Jan. 2015, doi: 10.1016/j.autcon.2014.05.014.
[6] J. Erdélyi, R. Honti, T. Funtík, P. Mayer, and A. Madiev, "Verification of Building Structures Using Point Clouds and Building Information Models," *Buildings*, vol. 12, no. 12, p. 2218, Dec. 2022, doi: 10.3390/buildings12122218.
[7] K. Pavelka Jr. and J. Pacina, "Using of modern technologies for visualization of cultural heritage," *Civ. Eng. J.*, vol. 32, no. 4, Art. no. 4, Dec. 2023, doi: 10.14311/CEJ.2023.04.0041.
[8] N. A. B. Hariffin, M. H. B. Razali, L. C. Luh, S. A. Sulaiman, and M. B. M. Hashim, "The Suitability of Matterport for Building Parcel Dimension Survey," in *2023 IEEE 13th International Conference on System Engineering and Technology (ICSET)*, Shah Alam, Malaysia: IEEE, Oct. 2023, pp. 239–244. doi: 10.1109/ICSET59111.2023.10295134.
[9] G. Vosselman and H.-G. Maas, *Airborne and Terrestrial Laser Scanning.* 2010.
[10] "How Matterport Works | Matterport," How Matterport Works | Matterport. Accessed: Feb. 09, 2024. [Online]. Available: https://matterport.com/how-it-works
[11] "Cortex AI | Matterport." Accessed: Feb. 09, 2024. [Online]. Available: https://matterport.com/cortex-ai

[12] I. MacPherson, R. F. Murray, M. S. Brown, R. F. Murray, and M. S. Brown, "A 360° Omnidirectional Photometer using a Ricoh Theta Z1," *Color Imaging Conf.*, vol. 30, pp. 124–128, Nov. 2022, doi: 10.2352/CIC.2022.30.1.23.

# COASTAL DUNES UNDER THREAT OF DESTRUCTION: NECESSITIES CONSERVATION AND INCLUSION INTO THE CADASTRAL MAPS AND REGISTRIES OF THE BULGARIAN BLACK SEA COAST

**PhD Bogdan Prodanov**[1]

**PhD Radoslava Bekova**[1]

[1]Institute of Oceanology – Bulgarian Academy of Sciences, **Bulgaria**

## ABSTRACT

The coastal beach-dune systems along the Bulgarian coast are of significant ecological import, necessitating rigorous monitoring and management. Oversight and dune management inaccuracies have been recurrently identified, particularly within the Bulgarian Black Sea coast cadastral registers. This research highlights discrepancies in depositional areas, such as Asparuhovo-Varna, Byala, Burgas-South, and Poda beach-dune systems. The coastal dunes within these regions have been systematically documented through detailed geomorphological surveys. The results accentuate the urgent necessity for precise documentation and integration of these dune formations into the Specialized Cadastral Maps and Registers. Such measures are imperative to ensure the effective conservation and sustainable management of these critical coastal resources. In conclusion, the comprehensive documentation of the presented examples of coastal dune landforms with a total area of approximately 250 200 $m^2$ in the Specialized Cadastral Registers represents a pivotal step towards ensuring the effective conservation and sustainable management of these ecologically significant habitats. Through collaborative efforts and informed governance, it is possible to strike a delicate balance between preserving natural heritage and fulfilling human needs, thereby securing the long-term viability of coastal ecosystems along the Bulgarian coast.

**Keywords:** sand dunes, coastal dune landforms, geomorphological survey, cadastral maps and registries, Bulgarian Black Sea Coast

## INTRODUCTION

Coastal dunes are prevalent sandy features found along ocean, sea, and other water body shores worldwide. They result from geomorphological settings, waves, currents, sediment, and psammophilous vegetation interactions. Coastal dune landforms (CDL) mainly formed during the Holocene and modern eras, primarily from sand supplied from the sea floor and alongshore sources like cliffs or bluffs composed of soft sandstone or glacial drift deposits [1]. Beaches, as highly dynamic components of coastal systems, serve as exposed sediment sources. Luijendijk et al. (2018) [2] found that 24% of the world's sandy beaches are persistently eroding, while 27% are accreting. CDLs, often adjacent to sandy beaches, result from wind-driven sand deposition in the landward section. CDLs vary widely in size and shape, ranging from small forms on rocky embayments to large features extending tens of kilometers alongshore [3]. Initially, sediments transported from the backshore are trapped by vegetation, forming foredune ridges parallel to the shoreline [3]. CDLs serve as sinks in

coastal sediment budgets, mainly comprising fine sand with characteristics similar to beach sands [3].

The evolution of CDLs is closely linked to vegetation, which reduces wind speed and facilitates sediment deposition [3]. They offer significant environmental and landscape value and act as natural coastal defenses, protecting landward territories [3]. Geomorphologically, dunes are classified into primary (foredunes and embryonic dunes) and secondary dunes, each with distinct characteristics modified by different processes [3]. Primary dunes, crucial coastal forms, are closely tied to nearshore processes on the fronting beach. Dunes exhibit various morphologies, including foredunes, parabolic dunes, blowouts, transgressive sheets, and dune fields, associated with ridges, mounds, terraces, and swales formed by different geomorphological processes [4].

This study aims to map four specific dune sites currently absent from cadastral records. These areas are deemed vulnerable due to their lack of legal protection until they are duly registered within the cadastral maps and registries. Given the intricate nature of coastal sectors and the delicate ecosystems present in dune habitats, mapping efforts necessitate high-accuracy unmanned aerial systems (UAS). The urgency of this endeavor lies in the imminent threat these zones face in the absence of legal recognition and protection outside of the areas under the Habitat Directive. Furthermore, these areas remain susceptible to various forms of exploitation and degradation without inclusion in cadastral records. Therefore, timely mapping and subsequent registration are imperative to ensure their preservation and sustainable management.

## STUDY AREA

***Bulgarian Black Sea Beach-Dune Systems*** are crucial recreational resources along the Bulgarian Black Sea Coast (BBSC), mainly prevalent in the southern region [5]. The sand beaches constitute 131 km, representing approximately 25% of the shoreline length of 518.7 km [6]. Coastal dune systems, on the other hand, encompass 14% of the Bulgarian shoreline, totaling 73 km in length [6]. These dune systems cover a total area of 988.21 hectares (9.8 $km^2$) along the BBSC, and they have been delineated into 46 distinct beach-dune systems [6]. These systems are closely linked to estuaries, lagoons, and other coastal features, exhibiting intense spatio-temporal variations due to morphodynamic processes and anthropogenic activities [5],[6],[7].

Through UAS mapping, DSM-based morphometric analysis, sediment sampling, visual recognition, and plant reconnaissance, 46 beach-dune systems were identified, covering 14% of the shoreline (73 km) and totaling 988 ha (0.0089% of Bulgaria) [6]. The dunes were classified into primary and secondary types based on their relationship with local morphology, aeolian and morphodynamic processes, and vegetation density. Primary dunes, comprising embryonic and foredunes, are closest to the shoreline, experiencing significant wave effects [6]. Secondary dunes, formed due to coastal progradation, are further inland and include various landforms such as blowouts, dune fields, parabolic dunes, transgressive dunes, mature foredune ridges, and cliff-top dunes. These secondary dunes cover 676.3 ha, constituting 68% of the total dune area [6]. Over the years, various studies have also enriched the knowledge about the dunes on the BBSC in a geological-geomorphological [8],[9],[10],[11],[12] and ecological aspect [13],[14],[15],[16],[17],[18],[19],[20].

## DATA AND METHODS

The methodology [6],[21] of the study combines various techniques, such as spatio-temporal GIS-aided analysis of archival data, drone mapping, sedimentological analysis, and visual observations, integrated into a GIS environment to identify and classify dune landforms. The steps involved follow the following sequence:

Inventory Data Source. Archive of IO-BAS. In the late 1970s, IO-BAS conducted pioneering scientific studies on the BBSC, mapping beach-dune systems through in-situ campaigns. Unfortunately, these studies remained confidential during Bulgaria's socialist era, with only beach and dune locations accessible in the IO-BAS archives. Since 1991, systematic studies of the Bulgarian coast have resumed, with detailed records available [22].

Cadastral-Administrative Information System (CAIS) [23] of the Republic of Bulgaria. CAIS includes a webGIS-based information system containing thematic geospatial data, including coastal features such as beaches, dunes, estuaries, and wetlands, mandated by the Black Sea Coast Spatial Development Act (BSCSDA) [24]. However, the CAIS thematic module does not accurately represent these coastal features' current locations and boundaries due to various factors such as data update challenges, cadastral parcel-based delineation, and discrepancies in coastal classifications.

Methods include UAS Mapping and Field Surveys [6]. Unmanned aerial systems (UAS), commonly known as drones, have become a prevalent method for conducting global photogrammetric surveys of beach-dune systems. Drones offer an efficient and cost-effective means for environmental monitoring, habitat mapping, and analysis of geomorphic processes. Scientific UAS surveys in Bulgaria have focused on generating georeferenced data using Structure-from-Motion (SfM) techniques for various purposes, including geomorphological mapping, landslide processes, and geoarchaeological mapping [6]. Since 2018, IO-BAS has employed drones such as Phantom 4 Pro, Phantom 4 RTK, and WingtraOne to survey the Bulgarian coast. These surveys have covered over 97% of the coastline, excluding restricted areas. Geodetic GNSS surveys were conducted to physically trace dune landforms in wooded areas and establish ground control points (GCPs) to enhance the accuracy of photogrammetric measurements. Additionally, photo verification of landforms and vegetation within beach-dune systems was conducted at numerous locations.

Flight data collected by drones were processed using specialized photogrammetric software like Agisoft Metashape, Pix4D, and Global Mapper. Digital Surface Models (DSMs) derived from this data were georeferenced to the Baltic Height System and integrated into a coherent geodatabase with WGS 1984/UTM zone 35N as a spatial reference.

Identification and Classification of Coastal Dune Landforms. To minimize anthropogenic influence, coastal dune landforms (CDLs) were identified and classified through geomorphological field surveys conducted systematically during non-tourist seasons. Spatial distribution analysis relied on morphometric analysis of Digital Surface Models (DSMs), visual examination of Orthophotos (OMs) or 3D photorealistic models, and on-site verification. CDLs were categorized into primary (embryonic and foredunes) and secondary (blowouts, transgressive, parabolic, cliff-top, perched) or fixed versus mobile dunes, crucial for studying land-sea interactions and coastal resources [6].

## RESULTS

The comprehensive analysis conducted on the dune systems along the Bulgarian coastline, as presented in the report, sheds light on a pressing issue of environmental conservation. Despite the efforts of Prodanov et al. (2023) [6] to provide extensive data on these dunes, a significant portion remains unrecorded in the cadastral registers. This regulatory gap leaves these dune areas vulnerable, lacking the legal protection the BSCSDA provides [24]. Addressing this discrepancy is paramount to ensure the preservation of these ecologically significant landscapes for future generations.

### *Coastal dunes at Asparuhovo, Varna Coast*

The embankment and I-shaped groin of the navigation canal delimit the northern dune system (Fig. 1). Over time, this dune area has been transformed into an unauthorized parking zone during the summer months, exerting significant anthropogenic pressure on a substantial portion of the dunes. In contrast, within the confines of Asparuhovo Park, observations reveal sandy patches beneath the vegetative cover, showcasing ancient dune landforms as documented in various historical sources, exemplified by Peychev and Peev (2006) [25]. The conversion of these dune fields, lacking registration in the cadastral records, into sites for camping and unauthorized parking is of concern. The total dune area was assessed at 96 100 $m^2$.

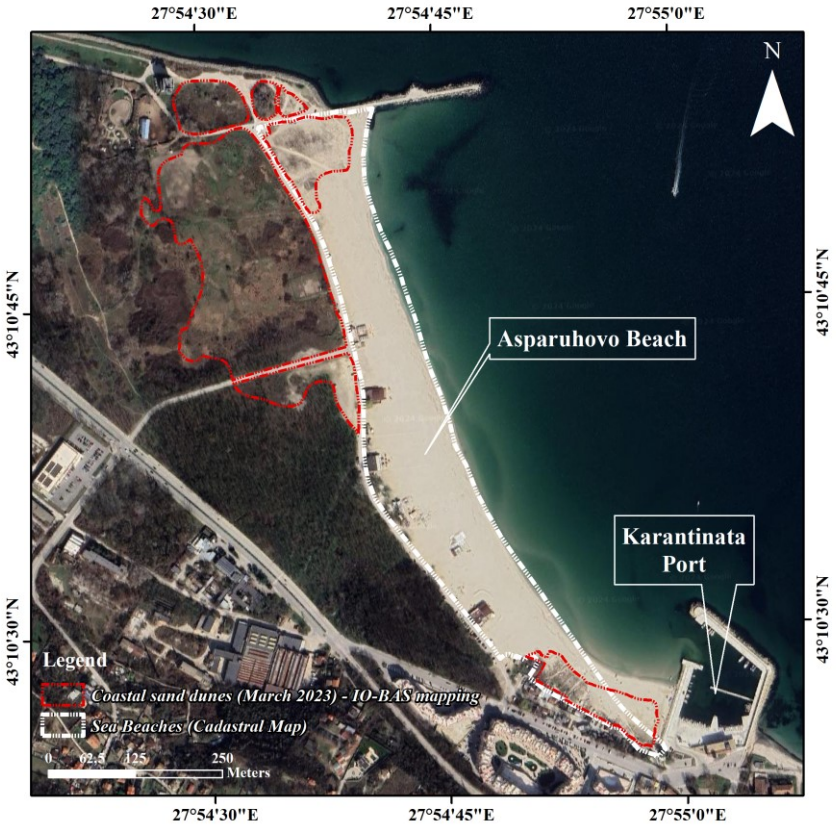


**Fig. 1.** Spatial distribution of unregistered dunes in Cadastral Map of the "Asparuhovo" Beach, Bulgarian Black Sea Coast.

Conversely, the southern sector has recently formed within the last four years and urgently requires protection from the transportation of fishing boats through the dunes.

This emergent sector is susceptible to disturbances due to its nascent state, necessitating immediate measures to mitigate potential environmental impacts and preserve its ecological integrity. Furthermore, a comprehensive scientific analysis of sediment dynamics, vegetation composition, and anthropogenic pressures across all sectors is imperative to formulate effective management strategies for the sustainable conservation of the Asparuhovo Beach coastal dune system.

***Coastal Dunes at the Byala Port***

The coastal dune system with an area of 7 630 $m^2$ within the “Byala Chajka 1” beach near the Port of "Byala" has undergone formation within the last decade (Fig. 2). After the quay wall construction, a zone of wave shadow emerged in the rear area of the port aquatory. Over the years, the dunes have stabilized in geomorphological terms and continue to develop and become covered with vegetation. As of April 2024, the dunes are absent from the cadastral registers, posing an obstacle to their conservation efforts. Furthermore, the Municipality of Byala plans to expand the fishing harbor, inevitably destroying the dune habitats. Given the ecological significance of these dunes and their role in shoreline stabilization and biodiversity conservation, it is imperative to reassess development plans and implement measures to mitigate the adverse impacts on this fragile coastal ecosystem.


**Fig. 2.** Spatial distribution of unregistered dunes in Cadastral Map of the “Byala Chajka 1” beach, Bulgarian Black Sea Coast.

### *Coastal Dunes at the Southern Burgas coastal sector*

The mapping of these dunes proves exceptionally challenging due to the extensive anthropogenic alteration of the terrain over the past 70 years. Significant portions of the expansive coastal dune systems have been encroached upon by the development of infrastructure, including segments of the Burgas Port, residential complexes in the Pobeda Quarter (Fig. 3), and the Burgas Shipyard [5]. Approximately a century ago, the coastal zone comprised a sandy shoreline with dunes separating the Burgas Lake, playing a role as barrier dunes.

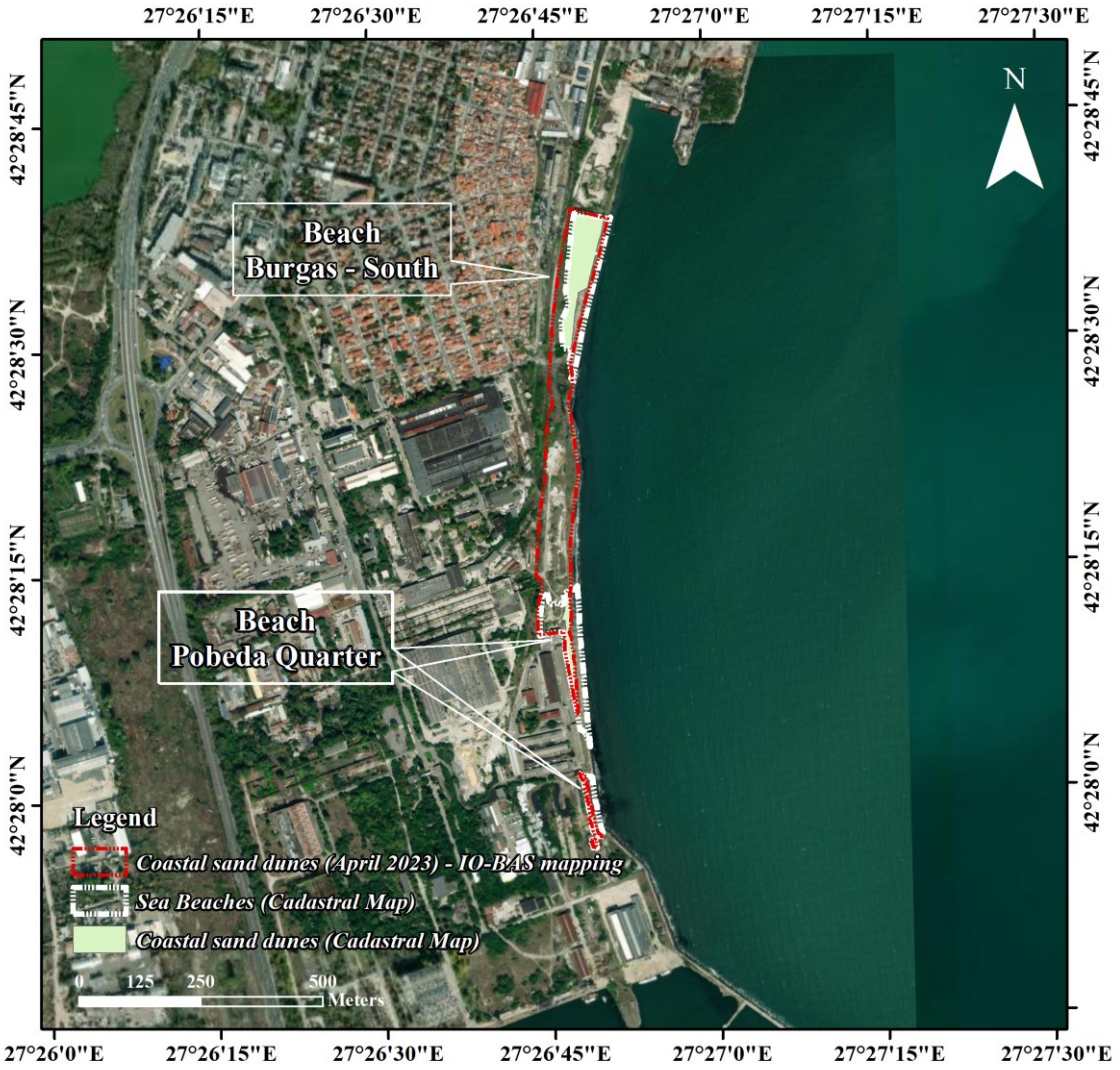


**Fig. 3.** Spatial distribution of unregistered dunes in Cadastral Map of the Burgas coastal sector, Bulgarian Black Sea Coast.

As of 2023, only a small area of these dunes, measuring a mere 56 599 $m^2$, remains preserved. Over 90% of their original area has undergone substantial modification, with instances of sand extraction and their conversion into refuse sites being documented. Despite their stabilization over time, these dunes are being subjected to gradual degradation due to the absence of protective designations in cadastral records.

From a scientific point of view, this situation underscores the intricate interplay between natural geomorphological processes and human intervention, with profound implications for coastal management and environmental conservation. The loss of these dune formations not only diminishes the aesthetic and ecological value of the coastal landscape but also disrupts crucial ecosystem functions such as sediment stabilization, biodiversity support, and coastal resilience against erosion and storm surges.

***Coastal Dunes at Poda-Burgas***

The coastal dune system of Poda falls within the confines of the Poda Protected Area and is situated between the Burgas Shipyard and the mouth of the Uzungeren Lakes (Fig. 4). These dunes have been stabilized. They are exceptionally well-preserved, with minimal construction activities occurring within the protected area. However, the road network constructed along the shoreline has caused damage to the surface layer of the dune habitat. Nevertheless, the sparse anthropogenic activities allow for preserving these dunes in good status.


**Fig. 4.** Spatial distribution of unregistered dunes in Cadastral Map of the Poda - Burgas coastal sector, Bulgarian Black Sea Coast

In 2023, sandy dunes were identified beyond the boundaries of the Poda Protected Area. These dunes are located in the vicinity of the Burgas Shipyard and remain unaffected by construction activities. The total area covered by these dunes is estimated to be 89 935 $m^2$.

From a conservation perspective, the presence of the Poda Protected Area plays a crucial role in safeguarding the integrity of these coastal dunes. However, the identification of additional dunes outside the protected area highlights the need for expanded conservation efforts and the implementation of measures to mitigate potential threats from future development activities. Furthermore, continued monitoring and management of the road network adjacent to the dune habitat are essential to minimize further degradation and ensure the long-term preservation of this valuable coastal ecosystem.

## DISCUSSION

The mapping and analysis of coastal dune systems along the Bulgarian Black Sea Coast (BBSC) provide crucial insights into these coastal features' geomorphological and ecological dynamics. Unmanned Aerial Systems (UAS) application for detailed photogrammetric surveys, combined with GIS-based analysis and sedimentological studies, has enabled a comprehensive delineation and classification of the dune systems. This study marks the first time these dunes have been systematically mapped, revealing their extensive distribution and highlighting the pressing need for conservation.

The identification and classification of 46 distinct beach-dune systems, covering approximately 14% of the Bulgarian coastline and totaling 988 hectares, underscore the significant presence of these geomorphological formations. These dunes were categorized into primary and secondary types based on their proximity to the shoreline, morphology, and vegetative cover. Primary dunes, including embryonic and foredunes, are directly influenced by wave action, while secondary dunes, such as blowouts, parabolic, and transgressive dunes, are located further inland and result from coastal progradation.

The comprehensive data collection and analysis revealed several key findings. The extensive mapping effort has uncovered that many dune areas remain unregistered in the cadastral records, leaving them vulnerable to anthropogenic pressures. This regulatory gap is particularly evident in areas such as the Asparuhovo dunes at Varna Coast and the Byala Port dunes, where significant portions of the dune systems are at risk due to unauthorized activities and planned developments. The Asparuhovo dunes, for instance, have been transformed into an unauthorized parking zone, while the Byala Port dunes face threats from the proposed expansion of the fishing harbor.

Moreover, the study highlights the dynamic nature of these dune systems, which are subject to continuous changes due to natural processes and human interventions. The Southern Burgas coastal sector exemplifies this dynamic interplay, where extensive anthropogenic alteration over the past century has led to the degradation and loss of significant dune areas. Despite these challenges, the presence of protected areas like the Poda Protected Area offers some hope for the preservation of these critical habitats.

The findings of this study emphasize the urgent need for enhanced regulatory measures and conservation strategies to protect the coastal dune systems of the BBSC. The integration of UAS mapping and GIS-based analysis provides a robust framework for

ongoing monitoring and management, ensuring the sustainable conservation of these ecologically and geomorphologically valuable landscapes. Identifying unregistered dunes and documenting their current state serve as a critical step toward raising awareness and driving policy changes to safeguard these coastal ecosystems for future generations.

## CONCLUSION

The research presented in this study underscores the critical importance of proactive measures by state authorities to conserve and protect coastal dune ecosystems. The data in Table 1 represent only a fraction of the inaccuracies and improperly reflected the spatial distribution of dunes. The presented scientific research can serve as a basis for the Ministry of Environment and Water to map these dune systems according to best methodological practices [6],[21].

**Table 1.** A List of coastal dune areas needs integration into the Cadastral maps and registries

| **Beach (Black Sea coastal area [23])** | | **Total area** | **Sediment Type** | **Survey data** | **Methodology** |
|---|---|---|---|---|---|
| **Number** | **Name** | **m²** | | | |
| 10135.PL.45 | Asparuhovo | 96 100 | Fine sand | March 2023 | [6],[21] |
| 07598.PL.389 | Byala Chaika 1 | 7 630 | Fine sand | February 2023 | [6],[21] |
| 07079.PL.22 | Burgas - South | 57 048 | Medium to Fine sand | April 2023 | [6],[21] |
| 07079.PL.319 | Pobeda | | | | |
| 07079.PL.23 | Burgas - Poda | 86 703 | Medium to Fine sand | April 2023 | [6],[21] |

Bulgaria's regulatory framework for dune protection is limited to the Law on the Development of the Black Sea Coast, which falls short of addressing the specific conservation needs of these fragile habitats. Moreover, the sporadic mapping of dune habitats, occurring only once every decade, exacerbates the challenge of accurately monitoring and managing these dynamic environments. As of 2024, a concerning 5% of Bulgaria's dune area remains under constant anthropogenic pressure, threatening the integrity of these ecosystems.

Addressing these shortcomings requires urgent action. Firstly, the Ministry of Environment and Water must update the mapping of dune systems using state-of-the-art methodologies and technologies. This would provide a more accurate representation of the spatial distribution of dunes and facilitate targeted conservation efforts. The findings of this research can serve as a valuable foundation for such mapping endeavors, offering insights into the characteristics and dynamics of dune habitats.

Furthermore, integrating unmanned aerial photogrammetric surveys is highlighted as a crucial tool for enhancing our understanding of dune geomorphology and vegetation patterns. Using advanced remote sensing techniques, researchers can gather high-resolution data essential for effective management and conservation planning.

In addition to mapping and monitoring efforts, comprehensive scientific analyses of the impacts of anthropogenic activities on dune ecosystems are clearly needed. Habitat fragmentation, soil erosion, and biodiversity loss are among these habitats' critical threats, necessitating interdisciplinary research to assess their ecological health and inform conservation strategies. Collaboration between environmental scientists, policymakers, and local communities is essential for developing holistic management approaches that balance conservation objectives with socio-economic development priorities.

In conclusion, safeguarding Bulgaria's coastal dunes requires concerted action at policy and implementation levels. By strengthening regulatory frameworks, updating mapping methodologies, leveraging advanced technologies, and fostering interdisciplinary collaborations, we can work towards ensuring the long-term sustainability of these invaluable ecosystems. Failure to act decisively risks irreversible damage to coastal dunes' ecological integrity and biodiversity, with far-reaching consequences for both present and future generations.

## ACKNOWLEDGEMENTS

The presented surveys discussed herein were supported financially by the project "*Raising Public Awareness, mapping, and Reducing Anthropogenic Litter for the Protection of the Bulgarian Black Sea Beaches and Dunes*" and "*Citizen Science for Reducing Anthropogenic Litter on the Seabed, Beaches, and Dunes along the Bulgarian Black Sea Coast*" part of the scientific research program of the DER TOURISTIK FOUNDATION, Germany

## REFERENCES

[1] Huggett, R., Coastal landscape. In: Fundamentals of Geomorphology, Londen, Routledge, pp.41, 2016. https://doi.org/10.4324/9781315674179

[2] Luijendijk, A., Hagenaars, G., Ranasinghe, R., Baart, F., Donchyts, G., Aarninkhof, S., The State of theWorld's Beaches, Scientific reports, 8(1), 6641, 2018.

[3] Davidson-Arnott, R., An Introduction to Coastal Processes and Geomorphology, Cambridge University Press, New York, pp.442, 2009.

[4] Bird, E., Coastal geomorphology: an introduction (second edition). John Wiley & Sons Ltd, The Atrium, Southern Gate, Chichester, pp.411, 2008.

[5] Popov, Vl., Mishev, K., Geomorphology of the Bulgarian Black Sea coast and shelf, Academic Press of the Bulgarian Academy of Sciences, Sofia, pp.268, 1974.

[6] Prodanov, B., Dimitrov, L., Kotsev, L., Bekova, R., Lambev, T., Spatial distribution of sand dunes along the Bulgarian Black Sea Coast: Inventory, UAS mapping, and new discoveries. In: Black Sea ecosystem in the spotlight, Nature Conservation, 54, 81-120, 2023.

[7] Stancheva, M., Ratas, U., Orviku, K., Palazov, A., Rivis, R., Kont, A., Peychev, V., Tõnisson, H., Stanchev, H., Sand dune destruction due to increased human impacts along the Bulgarian Black Sea and Estonian Baltic Sea Coasts. Journal of Coastal Research, pp.324–328, 2011.

[8] Baltakova, A., Coastal foredune enlargement–a sign of sea-level change? An example from the Kavatsite beach-dune system. Review of the Bulgarian Geological Society, 84 (3), pp.329-332. 2023.

[9] Petrov, G., The dunes along the Bulgarian Black Sea Coast. Geol. Miner. Resour. J. 2013, 3–4, 15–22, 2013.

[10] Valchev, B., Arkutino Sand Dunes - the pearl amongst the geological phenomena in Ropotamo Reserve. Proc. of National Conference with international participation “GEOSCIENCES 2014”, 125-126, 2014.

[11] Valchev, B., Sand dunes along the Bulgarian Black Sea Coast south of the town of Burgas-statute and geoconservation value. Review of the Bulgarian Geological Society, 76(1): 89 – 111, 2015.

[12] Sinnyovsky, D., Sinnyovska, D., The sands in camping South between Kiten and Lozenest – dunes or beech sands. National Conference with international participation “GEOSCIENCES 2016”, 179 – 180, 2016.

[13] Gussev, Ch., Tsonev, R., Natural habitats of European importance in the Strandja Protected Area. Directorate of Nature Park "Strandja" Malko Tarnovo, p.304, 2014.

[14] Marcenò et al., 2018; Marcenò, C., Guarino, R., Loidi, J., Herrera, M., Isermann, M., Knollová, I., Tichý, L., Tzonev, R.T., Acosta, A.T.R., FitzPatrick, Ú. Et al., Classification of European and Mediterranean coastal dune vegetation. Appl. Veg. Sci. 21(3), 533–559, 2018.

[15] Tashev, A.N., Vitkova, A.A. and Alexandrova, A.V., Floristic composition and current state of non-forest natural habitats in Natura 2000 protected sites “Kamchia”(BG0000116) and “Shkorpilovtsi Beach”(BG0000100). Acta Zoologica Bulgarica, pp.75-80, 2018.

[16] Bertacchi, A., Marius, F., Similarities and differences in dune habitats between Tuscan and Dobrogean Coasts (North-western Italy versus Romania & Northern Bulgaria). Contributii Botanice, 54, pp.133-148, 2019.

[17] Dimitrov, D., Vutov, V., 2019. Biodiversity of plants and natural habitats in the vicinities of Arapya Bay, Ropotamo Natural Reserve, Alepu Beach, Sinemorets and Silistar cape (Bulgarian Southern Black Sea Coast). Trakia Journal of Sciences, 17(4), p.359, 2019.

[18] Valcheva, M., Sopotlieva, D., Apostolova, I., 2020. Current state and historical notes on sand dune flora of the Bulgarian Black Sea Coast. Flora, 267, 151594, 2019.

[19] Valcheva, M., Sopotlieva, D., Meshinev, T., Apostolova, I., 2019. Is penetration of non-psammophytes an underestimated threat to sand dunes? – a case study from the Western Pontic coast. J. Coast. Conserv. 23, 271–281, 2020.

[20] Valcheva, M.; Sopotlieva, D., Apostolova, I., Tsvetkova, N., 2021. Vegetation Characteristics and Recent Successional Trends of Sand Dune Habitats at the Bulgarian Black Sea Coast. Coasts, 1, 1-24. 2021.

[21] Prodanov, B., Valcheva, M., Gussev, Ch., Sopotlieva, D., Methodology for mapping, determining boundaries, and the type of sand dunes, in accordance with Article 11, Paragraph 2 of Regulation No. 1 of September 16, 2008, for the creation and maintenance of specialized maps and registers of objects under Article 6, Paragraphs 4 and 5 of the Black Sea Coast Planning Act. Ministry of Environment and Water, p.30., 2008.

[22] Passports of the Bulgarian Beaches, Sciences found of Institute of Oceanology - Bulgarian Academy of Sciences, 1994.

[23] Cadastral-Administrative Information System (CAIS) – GCCA, Portal for electronic administrative services, Module. Black Sea coastal area – Geodesy, cartography and cadaster agency, https://kais.cadastre.bg/bg/Map

[24] Black Sea Coast Spatial Development Act of the Republic of Bulgaria, 2008, https://lex.bg/laws/ldoc/2135555697.

[25] Peychev, V., Peev, Pr., Evolution of the Bulgarian Black Sea coast after the Early Holocene. Slavena, Varna, pp.123, 2006.

# LAND COVER DEGRADATION CHALLENGES IN UKRAINE: NATURAL DRIVERS AND PROCESSES

**PhD. Lesya Yelistratova**[1]

**PhD. Alexander Apostolov**[1]

**PhD. Artur Khodorovskyi**[1]

**Maksym Tymchyshyn**[1]

[1] State Institution "Scientific Centre for Aerospace Research of the Earth of the Institute of Geological Sciences of the National Academy of Sciences of Ukraine", **Ukraine**

## ABSTRACT

Land cover degradation poses global challenges, both economically and scientifically, with significant implications for Ukraine's sustainable development. Understanding the need for effective strategies to prevent soil degradation, address degraded lands, and reduce associated risks is crucial at both global and regional scales. Early identification and degradation monitoring require establishing natural predictors (drivers) to preserve ecosystems and biodiversity for future sustainable development.

An objective assessment of land cover degradation and its predictors involves integrating remote sensing data across diverse regions and socioeconomic conditions. Research has identified land cover degradation types in Ukraine's territory and the natural drivers triggering this process using remote sensing data.
Identifying natural drivers and processes encompasses various aspects, including driving forces (sub-drivers), factors, causes contributing to the degradation, and the degradation processes affecting Ukraine's soil cover. These aspects are integrated into a comprehensive graphic model, illustrating the sequence of driver influences on land cover degradation. Examples of land cover degradation in Ukraine detected through the developed conceptual framework, are provided. The proposed approach explores scenarios for future degradation processes, consequences, and adaptation pathways.

**Keywords:** land cover degradation, drivers (predictors), ecosystems, remote sensing data, Ukraine

## INTRODUCTION

Population growth and environmental changes caused by stressful influences such as climate change and ecosystem stability disruption further reduce the land's ability to sustainably respond to natural or human pressures. In recent years, many reports have been published on the results of studies on land degradation, which, for example, say that more than 10 million hectares of arable land worldwide are degraded every year [1]. The impacts of land degradation are unevenly distributed across the entire population and primarily affect the vulnerable which depend on land for their livelihood. There are also research papers in the scientific world that consider the phenomenon of land degradation [2-9].

The problem of land degradation is actually for the territory of Ukraine. It is one of the most serious challenges for the sustainable development of the country, which entails

significant environmental and socio-economic problems. The most large-scale degradation processes are water and wind erosion of soils (about 57% of the country's territory), land flooding (approximately 12%), acidification (almost 18%), salinization, and solonetzization of soils (more than 6%). According to various criteria, about 20% of Ukrainian lands are polluted. About 23 thousand cases of landslides are recorded annually. As a result of abrasion, up to 60% of the coast of the Azov and Black Seas and 41% of the coastline of the Dnieper reservoirs are being destroyed. More than 150 thousand hectares of land have been disturbed as a result of mining and other activities. The number of underground and surface karst manifestations is about 27 thousand. As a result of land degradation during 1986-2010, the humus content decreased by 0.22% and is 3.14%. During this period, the loss of humus in the arable layer was 5500 kilograms per hectare. Every year, with the harvest of agricultural crops, 77-135 kilograms of nutrients (nitrogen, phosphorus, potassium) are irretrievably alienated from each hectare. The problems of land degradation are exacerbated due to the rapid pace of climate change, which is accompanied by an increase in average annual temperatures, the frequency and intensity of extreme weather events, including droughts, covering every two to three years from 10 to 30% of the country's territory, and once every 10 – 12 years - from 50 to 70% of its total area. Land degradation also leads to loss of biodiversity, deterioration or disappearance of water bodies, aggravation of problems of water supply for the population and sectors of the economy, and, as a result, deterioration of people's living conditions. The poverty rate of the population in rural areas, traditionally more dependent on the state of use and protection of land and other natural resources, over the past 10 years has been 2-11% higher than the national average, which leads to excessive exploitation of natural resources, their further depletion and degradation [10].

First of all, to identify degradation and further monitor the process of land degradation, it is of great importance to establish their predictors (drivers). The driver is the driving force of change, where all factors directly or indirectly entail changes in nature. In general, we can distinguish between natural processes and processes caused by human activities.

A deep, operational, and objective assessment of land degradation can be carried out by integrating remote sensing data covering large areas at the level of regions, and countries with different physical and geographical conditions and different socio-economic status.

**The purpose of this research** is to develop methodological approaches to determine the degradation of land cover inherent in the territory of Ukraine and its natural drivers using satellite data.

## MATERIALS AND METHODS

As a study, we chose a test site for the territory of Kryvyi Rih – a city with powerful industrial potential and modern environmental problems and its surroundings, which are undergoing degradation processes caused by both natural components and human economic activities. The selection of such a territory is important for solving the problem of separating the natural component of the degradation process of the land cover. Coordinates of the test site: north latitude (47°27′13.76" N – 48°20′54.99" N) and east longitude (32°55′56.57" E – 34°14′40.60" E).

For the quantitative assessment of the process of degradation of the earth's surface according to DEM (digital elevation model) data obtained from the Shuttle satellite, taking into account the methodology [11], potentially erosive areas were calculated in the study area. To identify the natural factor of desertification according to the method [12], aridity indices were calculated for two periods: 2000–2004 and 2018–2022. To determine degradation processes caused by changes in biodiversity, the NDVI index (https://ladsweb.modaps.eosdis.nasa.gov/) was used for comparison between 2000 and 2022. 240 MODIS products were used in the study, their processing was carried out in the Erdas Imagine program.

## RESULTS

The developed methodological approaches for determining the influence of natural drivers on the land cover of Ukraine using satellite information are presented as a graphical model of the flowchart for studying the influence of natural drivers on land cover degradation in Fig. 1.

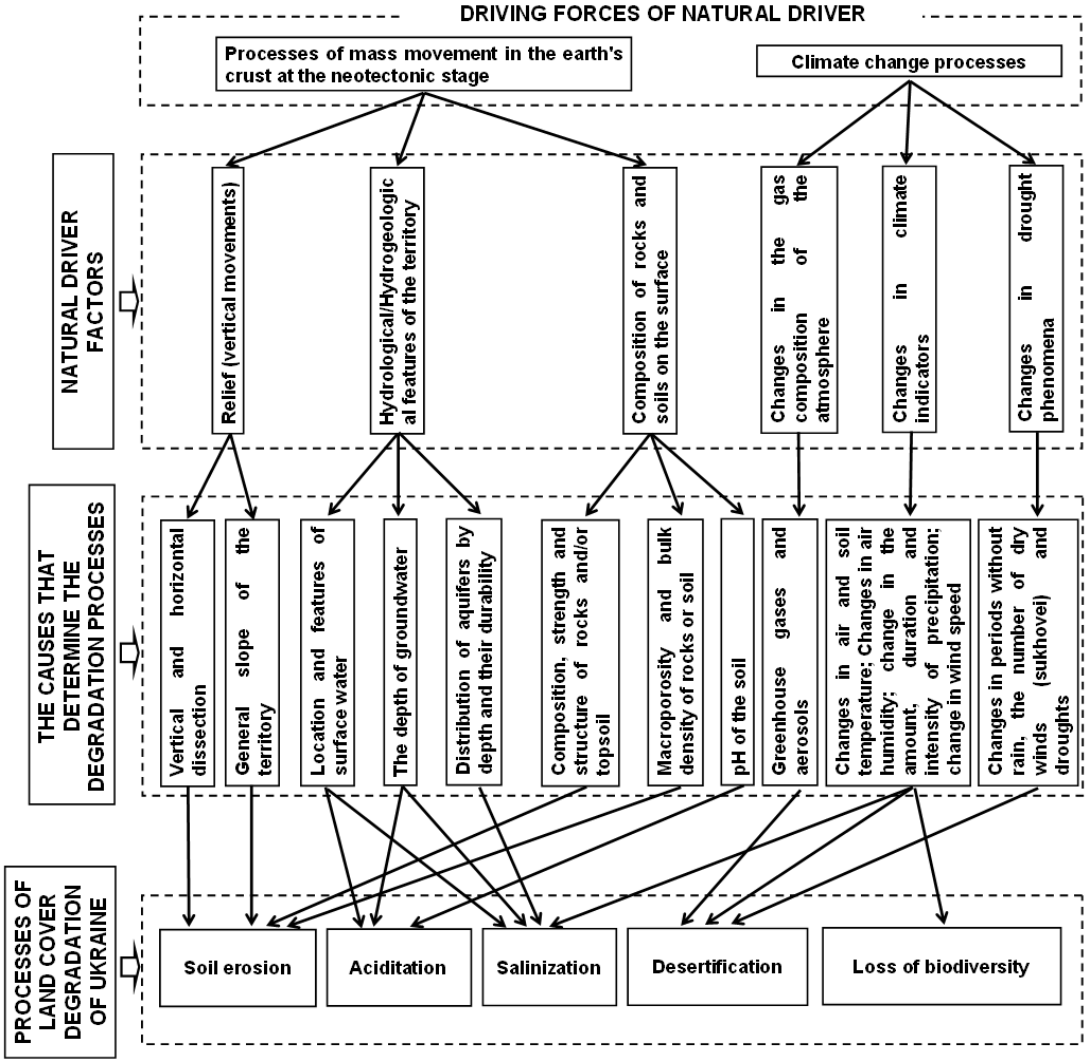


**Figure 1** – Graphical model of the flowchart for studying the influence of natural drivers on land cover degradation

There are many factors and processes of land cover degradation, and they interact in different ways. The most important natural driving forces are caused by a range of factors from very short and intense events to slow depletion on a century-scale of land cover. These are several aspects (namely, identification of driving forces, driver factors, and causes–that determine the process of degradation, and directly the processes of degradation of the land cover of Ukraine). These aspects are combined into a general concept, which displays the sequence of implementation of the influence of natural drivers on land cover degradation (fig. 1).

For approbation, the proposed methodical approaches to the research area, some examples of the influence of natural drivers on land cover degradation (soil erosion, desertification, loss of biodiversity) were calculated as shown in Fig. 2.

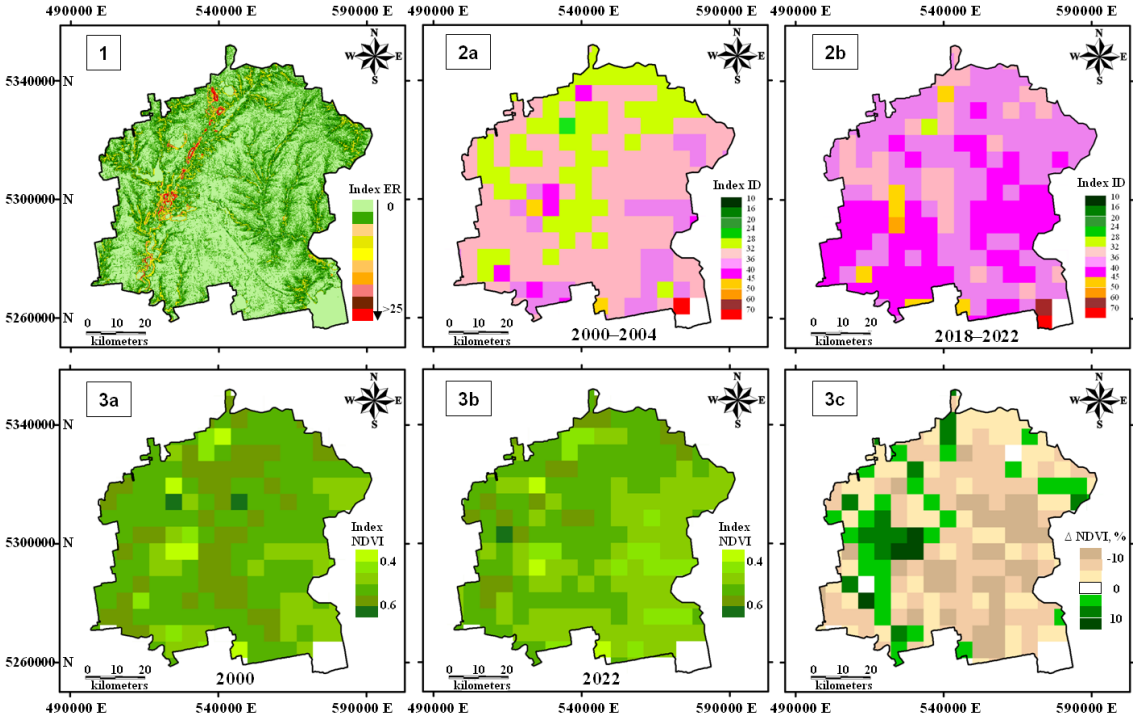


**Figure 2** – Examples of land cover degradation caused by natural factors: 1- assessment of the degree of erosion danger according to the ER index; 2- assessment of the degree of desertification of the territory according to the ID index; 3- assessment of the deterioration of the state of vegetation according to the NDVI index

## DISCUSSION

Ukraine is known for its fertile arable lands, which are the main natural resource of the country. But during the 20th century, the land cover of Ukraine changed as a result of human activity. Long-term changes in landscape complexes took place, and their significant transformation led to their degradation. In this context, identifying and distinguishing the role of the influence of natural drivers on land cover degradation, especially in anthropogenically loaded territories, is an extremely important task, because the rapid change of drivers can lead to non-linear changes that will be difficult, if not impossible, to predict and stop.

A variety of natural factors of land cover degradation in most cases are interconnected and interdependent. They can be combined into two groups, which differ in the source

of the forces that cause them. The first group includes factors that are closely related to the nature of the formation and development of the day surface, which are caused by neotectonic movements in the bowels of the Earth. The second group includes factors that are associated with weather and climatic conditions.

The first group of factors, their origin and development is determined by neotectonic movements of the earth's surface, the source of forces of which is the constant movement of matter in the bowels of the Earth. Neotectonic displacements of matter lead to a change in the relief of the day surface, to an increase in the absolute marks of the relief, which is accompanied by the movement of matter on the Earth's surface. These processes cover rather large territories. As a result, not only the height marks of the relief can change, but also the direction of the general slope of the territory, and the angle of inclination. But more importantly, an increase in marks of relief can increase the rate of linear and areal erosion. In addition, a change in the elevation marks of the relief affects the change in the level of groundwater occurrence, the direction of their overflows, the occurrence of areas of flooding or drainage, etc.

The rate of change in relief marks varies widely and is closely related to the nature of the geological structure of the study area. They are maximum in geosynclinal areas and much smaller on platforms. But even within these regional structures, the rates of vertical displacements of the earth's surface are very variable and depend on the features of their deep structure and the geological structures that compose them. They are always higher within anticlinal structures of different scale levels than in synclinal structures of the same level. Intrusive massifs of different compositions are characterized by rather high rates of vertical movements. Fault zones, and especially fault crossing nodes, are characterized by high rates of vertical movements and significant variability, both along strike and cross strike. At the same time, along faults of different orientations, the intensity of displacements is different and depends on the nature of the deformations.

The morphology of the relief was formed under the influence of both endogenous and exogenous processes and therefore contains important information about the features of the manifestation of these processes in the study area. Such general characteristics of the relief as plains, mountains, depressions, plateaus, rises, valleys, etc. are insufficient to solve most natural resource and environmental problems. More detailed, and most importantly quantitative, characteristics of the relief morphology are needed. To analyze the morphology of the relief and its variability at different scale levels, such well-known quantitative morphometric indicators as the vertical and horizontal dissection of the modern relief can be used, which makes it possible to obtain information about the relief in quantitative form. As is known, vertical dissection allows us to assess the energy of modern erosion processes, and horizontal dissection evaluates the erosional dissection of the territory. The combined use of these two indicators makes it possible to assess the intensity of the movement of surface waters and the movement of sediments carried by them.

Land degradation processes can also begin with changes in the hydrogeological system. Decreasing water table: This usually occurs when aboveground extraction exceeds the natural recharge capacity of the water table.

The entry of fine sediment into the streams of rivers, streams. Under these conditions, both terrestrial and shallow subsurface flows rapidly increase with precipitation. Thus

creating high peak velocities in the very streams that cause channel erosion. It should be noted that changes in precipitation patterns increase the risk of land degradation.

Soil condition is one of the best indicators of land degradation. The composition of rocks and soils on the day surface leads primarily to soil erosion. Soil erosion is a serious, long-term, almost irreversible degradation of land because in most cases the rate of soil formation is very low. Each of the listed factors of the natural driver of land degradation has its own causes, which are shown in Figure 1.

The second group of factors is caused by the processes that cause climate change. Climate change is already contributing to land degradation and will become an increasingly important driver of it during the 21st century. There is a strong interaction between climate variability, especially medium-term climate variability, and the anthropogenic component, which affects the process of land degradation. As for the estimates of the influence of natural factors on the climate, they have a large degree of scientific uncertainty. Such factors are solar activity, which determines the influx of electromagnetic radiation, and charged particles, as well as volcanic activity, which determines aerosol pollution of the atmosphere, the so-called "small" climate-forming forces. , assessments of their role in climate change are not generally accepted and are the subject of discussion. In this case, it is necessary to consider the possible mechanisms of the impact of solar activity on the climate, which will be determined due to changes in the properties of the atmosphere. If the solar constant changes due to the ultraviolet part of electromagnetic radiation, then the real mechanism may be the mechanism associated with radiation-chemical processes and, first of all, with a change in the ozone content in the atmosphere [13-14].

Since the pre-industrial period (1850-1900), the observed mean land surface air temperature has significantly increased compared with the global mean surface (land and ocean) air temperature (GMSAT). From 1850-1900 to 2006-2015 global average land surface temperature increased by 1.53°C (very likely range 1.38°C to 1.68°C) while GMSAT increased by 0.87°C (likely range 0.75°C to 0.99°C) [15]. Long-term air temperature variation over Ukraine repeats the global one. Regional air temperature has risen by 1.2°C over the past 30 years [12]. The warming has led to an increase in the frequency, intensity, and duration of thermal phenomena, including heat waves, changes in rainless periods, and an increase in the number of hot winds and droughts in most regions of the land, including Ukraine. Climate change can exacerbate land degradation processes, including through an increase or decrease in other climatic indicators, in particular changes in the amount and intensity of precipitation. As warming increases, climate zones are projected to shift further poleward at mid and high latitudes (high confidence) [15]. In Ukraine, this process is already underway and affects the degradation of the land cover, since some ecosystems cannot adapt so quickly to new climatic and natural conditions [11].

The above-listed natural drivers, their factors, and the causes that determine the processes of degradation have direct consequences for the natural environment of Ukraine. As shown by a quantitative assessment of the degree of erosion danger of the territory under the index (erosion index) ER, potentially dangerous areas constitute 13.24% of the entire test site, which is 754 $km^2$. Considering the anthropogenic load of this territory, this further reduces the ability of the land to respond sustainably to natural

environmental changes caused by stress impacts and disturbances in the stability of ecosystems (Fig. 2.1).

One of the stressful natural impacts is climate change, which in Ukraine is manifested by a regional increase in temperature and an intensification of the drying process. An assessment of the process of drying of the territory according to the index of drought index (ID) for two periods 2000 – 2004 and 2018 – 2022 is given (Fig. 2.2a and Fig. 2.2b). A strong increase in the ID drought index of up to 40% was established in comparison with the period 2000–2004 for an area of 4026 km2 at the local level. For Ukraine as a whole, changes in the process of dryness for the worse amounted to 70%. It should be noted that the study deals with only one negative climate process. Overall, climate change in Ukraine may trigger and worsen the effects of land degradation and reduce the viability of some options for preventing, reducing, and reversing land degradation. Note that land degradation itself is the main cause of climate change. Considering the so-called closedness of this process, in both cases feedback connections may be activated that could lead to irreversible negative consequences for the ecosystems of Ukraine.

It is known that land degradation is widespread, increasing, and occurring in all types of vegetation cover [10]. An assessment of the degradation process caused by the loss of biodiversity was shown using the example of the deterioration of vegetation according to the NDVI index for 2000 (Fig. 2.3a) and 2022 (Fig. 2.3b). In 2022, the state of vegetation according to the NDVI index worsened compared to 2000 and decreased by 26.8%. The total area of vegetation deterioration was 4394 $km^2$, which occupies 77% of the entire area of the study territory (Fig. 2.3c).

As the above discussion showed, which is based only on quantitative estimates calculated at the local level and highlighting only the natural component using the proposed methodology, the territory of Ukraine is characterized by degradation processes. If we consider the spread of these approaches throughout Ukraine, land degradation is a serious environmental problem, which in the future can lead to economic and social negative consequences.

## CONCLUSION

The application of remote sensing methods provides new insights into the research of land cover degradation. Thematic maps obtained as a result of processing multispectral images allowed us to assess the state and trends of land cover degradation (soil erosion, desertification, salinization, loss of biodiversity), which occurs due to natural drivers.

It should be noted that in Ukraine, as well as throughout the world, the dynamics of land change, climate, and biodiversity are closely interconnected. To solve these complex problems, the proposed methodological approaches to determining the influence of natural drivers on land degradation can be used for the best possible use of Ukraine's natural resources, as well as the assessment of ecosystem services. This method of determining the influence of natural drivers on the land cover of Ukraine based on the analysis of data from remote monitoring of the Earth allows us to detect degradation processes at an early stage and to obtain quantitative estimates of this process through the further application of relevant indices.

## ACKNOWLEDGEMENTS

This project has received funding from the European Union's Framework Programme for Research and Innovation Horizon Europe – the Framework Programme for Research and Innovation (2021-2027), Grant Agreement No. ID 101086250.

## REFERENCES

[1] ELD Initiative (2019). ELD Campus. Module: Land degradation versus sustainable land management. 32 p. Available from www.eld-initiative.org

[2] Barger, N., Gardner, T. A., Sankaran, M. Meyfroidt, P. (2018). Direct and indirect drivers of land degradation and restoration. 198 p.314 http://hdl.handle.net/2078.1/207386

[3] Berdimbetov T, Ma Z-G, Shelton S, Ilyas S and Nietullaeva S (2021). Identifying Land Degradation and its Driving Factors in the Aral Sea Basin From 1982 to 2015. Front. Earth Sci. 9:690000. doi: 10.3389/feart.2021.690000

[4] Douglas, I. (2006). The local drivers of land degradation in south-East Asia. Geographical Research, 44(2): 123–134. doi:10.1111/j.1745-5871.2006.00373.x.

[5] Jiang, L., Jiapaer, G., Bao, A., Li, Y., Guo, H., Zheng, G., Chen, T., De Maeyer, P. (2019). Assessing land degradation and quantifying its drivers in the Amudarya River delta. Ecological Indicators, 107, 105595. doi:10.1016/j.ecolind.2019.105595

[6] Karimian, H., Zou W, Chen Y, Xia J, Wang Z (2022). Landscape Ecological Risk Assessment and driving factor analysis in Dongjiang River Watershed, Chemosphere, 307, p. 135835. doi:10.1016/j.chemosphere.2022.135835.

[7] Mirzabaev A., Nkonya E., Goedecke J, Johnson T, Anderson W (2015). Global drivers of land degradation and improvement. Economics of Land Degradation and Improvement – A Global Assessment for Sustainable Development, pp. 167–195. doi:10.1007/978-3-319-19168-3_7.

[8] Perović, V., Kadovi´, R., Đurđevi´, V., Dragana Pavlovi´, D., Pavlovi´, M., Cakmak, D., Mitrovi´, M. (2021). Major drivers of land degradation risk in western Serbia: Current trends and future scenarios, Ecological Indicators, 123, 107377, p.1-14. doi:10.1016/j.ecolind.2021.107377.

[9] Turrini, Tabea; Knop, Eva (2015). A landscape ecology approach identifies important drivers of urban biodiversity. Global Change Biology, 21(4), 1652–1667. doi:10.1111/gcb.12825

[10] Concept of combating land degradation and desertification, dated October 22, 2014 № 1024-p. Available from https://zakon.rada.gov.ua/laws/show/1024-2014-%D1%80#Text

[11] Apostolov A. A., Yelistratova L. A., Romanciuc I. F., Zakharchuk I. (2021). Identifying potential landslide areas by employing the erosion relief index and meteorological criteria in Ukraine. Rev. Roum. Géogr./Rom. Journ. Geogr., 65(2), p. 125–141

[12] Lyalko, V.I., Apostolov, A.A., Elistratova, L.A., Romanciuc, I.F., Zakharchuk, I.V. (2023). Desertification Intensity Assessment Within the Ukraine Ecosystems Under the Conditions of Climate Change on the Basis of Remote Sensing Data. In: Pande, C.B., Moharir, K.N., Singh, S.K., Pham, Q.B., Elbeltagi, A. (eds) Climate Change Impacts on Natural Resources, Ecosystems and Agricultural Systems. Springer Climate. Springer, Cham. pp. 29-47. https://doi.org/10.1007/978-3-031-19059-9_2

[13] Loginov V.F. Forecast of changes in the natural environment of Belarus for 2010-2020. Minsk “Minsktipproekt”, 2004. 180 p.
[14] Loginov V.F. Causes and consequences of climate change. Minsk «Navuka i technika». 1992. 320 p.
[15] Climate Change and Land/Intergovernmental Panel on Climate Change, 2020. Electronic versions of this Summary for Policymakers are available on the IPCC website at: www.ipcc.ch

# REMOTE SENSING AND DEEP LEARNING INTEGRATION FOR SPATIAL INTELLIGENCE

**Ventsislav Polimenov**
**Krassimira Ivanova**
Institute of Mathematics and Informatics, Bulgarian Academy of Sciences, **Bulgaria**

## ABSTRACT

This review article provides an overview of the combination of remote sensing with deep learning techniques in the last ten years. It specifically examines the emerging patterns and applications in both fields, highlighting their combined use in processing remote sensing data. It focuses on how these techniques have brought about significant changes in environmental monitoring, urban planning, agricultural management, security, and change detection. The article discusses various satellite probes, detailing their specific capabilities, technological attributes, and suitability for diverse observational tasks. Also, it stops attention on multispectral fusion techniques aimed to integrate data from multiple spectral bands or sensors to enhance the overall quality of remote sensing imagery. Additionally, it provides an overview of potential neural network architectures, highlighting the necessity for innovative algorithms that can effectively manage the growing amount and diversity of remote sensing datasets. The discussion revolves around the authors' aspirations for future research, employing advanced deep learning models for understanding complex spatial and spectral patterns.

**Keywords**: Remote Sensing, Deep Learning, Artificial Intelligence, Image Processing, Image Fusion

## INTRODUCTION

The rapid development of technology especially in the last decade has led to a huge leap in the advancement of remote sensing technologies and their use in various disciplines including environmental monitoring, agriculture, urban planning, and disaster management. Technological innovations in the field of satellites and drones, as well as significant improvements in sensors for capturing various terrestrial features, have democratised access to remote sensing data and created the possibility of using the collected data to conduct intelligent analyses that support informed decision-making. Collaborative efforts between academia, industry, governments, and international organizations have led to a growing development of innovation in remote sensing technologies, resulting in improved spatial resolution, temporal coverage, and data processing techniques. Of great importance in this process is the integration of remote sensing with the disciplines related to the analysis of large volumes of data and artificial intelligence (in particular, deep learning), which has created new opportunities for extracting meaningful insights from huge and complex data sets.

The increased interest in remote sensing as well as the integration of this area with the capabilities of artificial intelligence techniques is also evidenced by the increasing number of articles indexed in Scopus. Figure 1 shows this trend based on the number of publications over the last ten years filtering in keywords by (1) "remote sensing" and (2)

"remote sensing" in combination with ("artificial intelligence" OR "machine learning" OR "deep learning" OR "neural networks"). The number of publications for 2024 is approximated based on the first quarter of the year when this research is done. Figure 2 shows that generally the research is focused on proposing new or enhancing existing mathematical algorithms (about a quarter of research is in the area "Computer Science and Mathematics"), engineering (16%), as well as applying such techniques to support the research in Earth and Planetary Sciences, Astronomy, Environment, and Agricultural and Biological Sciences.

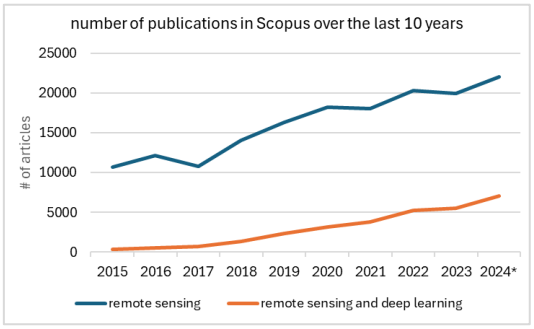


**Figure 1:** Number of publications in Scopus over the last ten years filtering in keywords by (1) "remote sensing" and (2) "remote sensing" in combination with ("artificial intelligence" OR "machine learning" OR "deep learning" OR "neural networks"). The number of publications for 2024 is approximated based on the first quarter of the year.

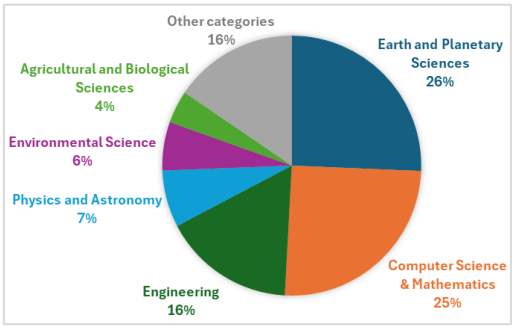


**Figure 2**: Publications in Scopus over the last ten years filtering in keywords by "remote sensing" in combination with ("artificial intelligence" OR "machine learning" OR "deep learning" OR "neural networks") grouped by subject areas (some publications are classified in more than one area).

Due to the high interest over the last few years in this area, we are going to review the current state-of-the-art methods and methodologies to apply deep learning models to remote sensing data. Furthermore, we will identify gaps and misconceptions in the current understanding and applications of these satellite technologies. Additionally, we will outline potential solutions and improvements to enhance accuracy and efficiency.
In Chapter 2 we describe the current trends in Remote Sensing and Deep Learning as well as the combination of both fields. In Chapter 3 we discuss the benefits and optimisation strategies. And finally, we conclude with future directions and final remarks.

## CURRENT TRENDS IN REMOTE SENSING AND DEEP LEARNING

The questions that we posed in this study can be summarised as follows:
1) what are the current trends in remote sensing and respective needs;
2) what is the current state of deep learning algorithms directly related to those needs;
3) how effective is deep learning in remote sensing.
In the next subsections we will try to answer these questions.

### 2.1. Trends in Remote Sensing

Remote sensing satellite missions are essential for land conservation and global sustainability by providing crucial data through multispectral imaging. Such images

depict spectral signatures that represent distinct land cover features throughout the electromagnetic spectrum [10]. The increase in worldwide open data satellite missions has significantly expanded the use of remote land observation, leading to widespread accessibility to satellite imagery [2].

In remote sensing, the main types of images used are [17]:

– Panchromatic images (PAN) record data in a spectral band covering the visible spectrum and near-infrared region. These images are high-resolution single-channel grayscale and allow visual analysis of the Earth's surface.
– Multispectral images (MS) record data in multiple spectral bands in the electromagnetic spectrum. Multispectral imagery is commonly used in applications such as land cover classification, agricultural monitoring, and environmental analysis.

Furthermore, a crucial attribute is the radiometric resolution. The sensitivity of the sensors is defined as their ability to detect small variations in energy levels. This sensitivity is typically measured in bits, which enables a more precise distinction between similar, although not identical, targets.

PAN images can provide high spatial resolution but are composed of only one band. The MS images possess several spectral bands and contain an array of spectral information, but the spatial details are inferior to the details in the PAN images. On the other side, freely available satellite imagery generally has lower spatial resolution compared to commercial satellites, which can make extensive analysis more challenging.

During the last few decades, the availability of high spatial, temporal, spectral, and radiometric resolution imagery from low-orbiting small satellites has greatly improved, widening the remote sensing applications further with better precision and accuracy. Especially, satellites such as GeoEye, IKONOS, KOMPSAT-3, Landsat 8, Pleiades 1A, Pleiades 1B, QuickBird, Sentinel 2, and WorldView-3 have been effectively utilised in many agricultural applications [16]. These applications encompass but are not restricted to the retrieval of vegetation indices [12], the estimation of plant height [15], evapotranspiration [11], leaf/canopy chlorophyll content [6], and yield [7].

The diversity in spatial and temporal resolutions, spectral characteristics (Table 1 and Figure 3), and the varying shapes of output images from different satellite probes complicate the application of deep learning algorithms to remote sensing imagery. These variances need the creation of versatile, adaptable models that can effectively handle datasets with varying quality and dimensions.

**Table 1**: Spatial and temporal resolution and spectral differences between different satellite probes [10][17]

| Satellite | Spatial resolution PAN (m) | Spatial resolution MS (m) | Spectral bands (#) | Temporal resolution (days) | Radiometric resolution (bits) | Swath width (km) | Wavelength range (nm) |
|---|---|---|---|---|---|---|---|
| GeoEye-1 | 0.41 | 1.65 | 4 | 1 – 3 | 11 | 15.2 | 250 – 800 |
| IKONOS | 0.82 | 3.2 | 4 | 1 – 3 | 11 | 11.3 | 445 – 853 |
| KOMPSAT-3 | 0.7 | 2.8 | 5 | 1 | 14 | 15 | 450 – 900 |
| Landsat 8 | 15 | 30 | 11 | 16 | 16 | 185 | 433 – 12500 |
| Pleiades 1A, 1B | 0.5 | 2 | 4 | 1 | 12 | 20 | 430 – 950 |
| QuickBird | 0.65 | 2.62 | 4 | 1 – 3.5 | 11 | 16.5 | 450 – 900 |
| Sentinel 2 | 10 | 20 | 13 | 2 – 3 | 12 | 290 | 442 – 2186 |
| WorldView-2 | 0.46 | 1.84 | 8 | 1.1 | 11 | 16.4 | 400 – 1040 |
| WorldView-3 | 0.31 | 1.24 | 28 | 1 | 11 | 13.1 | 397 – 2373 |

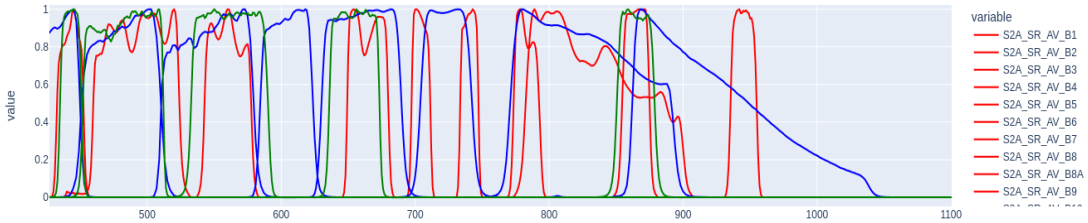


**Figure 3:** Differences between spectral bands of WorldView-3 (blue), Landsat 8 (green) and Sentinel 2 (red).

Regardless of the constant increase in the quality of multispectral imaging sensors, there is always a need for improving the spatial resolution of multispectral bands – a process called pansharpening. There are different image fusion methods used for pansharpening – some of them based on classical data mining methods, such as component substitution and multiresolution analysis, as well as the new deep learning techniques, which can generally be classified into three main groups – source image concatenation (the neural network directly combines MS and PAN images into one), feature concatenation (firstly as preprocessing step two different sub-networks filtered some redundant information and this way avoid spatial and spectral distortions in the fused image), and feature fusion (aimed to merge the complementary information of MS and PAN images in the feature domain by different fusion rules) [17]. For example, in [9] authors introduced a novel approach for applying image fusion across different satellite probes. They took advantage of the relationship between Land surface temperature and spectral indices to downscale the data from 1000 to 10 and 30 m resolutions.

### 2.2. Deep Learning

Recently, with the successful applications of deep learning in the field of computer vision, there has been a significant increase in research that invents or improves such methods in tasks involving the use of remote sensing data. According to [8] the following deep learning techniques and combinations of them are most frequently used in remote sensing applications:

- Convolutional Neural Network (CNN) is used as a basis of most models. CNN is designed to learn spatial hierarchies of features automatically and adaptively from input data. CNNs are successfully used for various tasks such as classification, object detection, and feature extraction. Wildly used varieties of CNN are FCN (where fully connected layers are replaced by convolutional layers allowing to preserve of spatial information across layers and this way very appropriate for tasks involving pixel-wise predictions), U-net (the most widely utilized model, which uses skip connections for facilitating the fusion of low-level and high-level features), and SegNet (which utilizes the max-pooling indices obtained during the downsampling in the encoder phase to perform efficient upsampling in the decoder phase) [8].
- Attention Mechanism is another prevalent technique, inspired by the idea of selective focus in human perception and cognition. It allows the model to dynamically focus on different parts of the input data, giving greater weight to certain features based on their applicability to the task at hand. Such mechanisms show better performance and interpretability against other models, especially in tasks involving sequential or structured data.

- Multi-Scale Strategy refers to the use of procedures that examine and interpret data at several levels or resolutions to encompass a broad spectrum of characteristics, ranging from fine details to more general patterns. By using multi-scale representations, models can enhance their ability to generalize across a wide range of input data sizes and forms, resulting in improved accuracy and robustness. Such models are very convenient for detecting objects, for instance – vehicles [5].
- Transformer was originally applied in the field of natural language processing but has been adapted to handle spatial data by transforming the images into non-overlapping patch sequences and has demonstrated remarkable performance in remote sensing tasks like classification, semantic segmentation, and change detection [8].
- Generative Adversarial Network (GAN) is a relatively new paradigm, that has gained a lot of popularity recently. GANs generate new synthetic data that resembles real data by pitting two neural networks (Generator and Discriminator) against each other. The generator tries to capture the true distribution of the data to generate new samples. On the other hand, the discriminator tries to distinguish the real from the generated samples as accurately as possible. In remote sensing, GANs are used for data augmentation, pansharpening, super-resolution, cloud removal, etc. [3]

Regardless of the improvements that each of the above mechanism provides, the classical application of neural networks assumes the presence of a vast amount of training data. For this reason, the transfer-learning methods have recently come into force. In transfer learning a pre-existing model created for one generic activity is used as a base for a model designed for a specific purpose. The use of it in remote sensing is particularly valuable because of the extensive variety and quantity of data, frequently accompanied by a lack of labelled samples for certain tasks [5]. Transfer learning, through the utilisation of pre-trained models on larger datasets, enables improved generalisation, reduces the requirement for substantial processing resources, and decreases the training time. This makes it highly efficient for remote sensing applications.

### 2.3. Remote Sensing and Deep Learning

Deep learning techniques have found wide application in remote sensing due to their ability to extract complex patterns and features from satellite or aerial imagery [1]. As the main tasks in which deep learning is used in remote sensing, we can single out:

- Classification: Categorising images into predefined categories, such as land cover types. Such applications are very useful in land use planning, environmental monitoring, and disaster management.
- Regression: Applying statistical methods to model and assess the relationships between spectral data captured by various sensors and the actual conditions on the ground. This could be fundamental for tasks such as predicting crop yields, which is a complex but crucial activity for managing agricultural lands effectively. The success of these predictions depends on multiple factors, including climate, weather conditions, soil properties, fertilizer usage, and the types of seeds used.
- Segmentation: Identifying objects or regions in the image to delineate buildings, water surfaces, agricultural fields, etc. In this case, each pixel of the image is assigned a class label (semantic segmentation [13]) or an object label (instance segmentation [14]).
- Change detection: Analysis of multiple images of the same location to identify ongoing changes such as urban growth, deforestation, change of riverbeds, etc. This type of task is particularly important for monitoring environmental trends.

Deep learning techniques are also extremely useful as elements in the preprocessing step of more complex tasks, such as:

- Enhancing the spatial resolution and improving the visual quality of remote sensing images (so-called techniques for super-resolution).
- Integrating information from different remote sensing modalities (so-called data fusion techniques).
- Extracting valuable insights and meaningful features from remote sensing images. Such tasks include using classification, anomaly detection, and feature extraction techniques.

## DISCUSSIONS

The application of deep learning in remote sensing also encounters some specific obstacles and limitations [4], some of which are:

- Cost and accessibility – The high cost and limited accessibility of high-resolution satellite imagery pose significant challenges, especially for small-scale projects or researchers with limited funding. High-resolution images, which provide detailed information crucial for precise analysis, are typically more expensive because of the advanced technology required to capture them. Additionally, the best quality imagery is often controlled by private companies or governments, which can restrict access based on commercial interests or security concerns. This can inhibit the ability of researchers and organizations to conduct timely and effective environmental monitoring, urban planning, and disaster response initiatives.
- Data variability, volume, and management – The collection of remote sensing data under diverse environmental and temporal conditions leads to significant variability in the data, which presents challenges for deep learning models especially in regard of consistency. Variability can affect various aspects such as lighting, shadows, and atmospheric conditions, thus causing significant changes in data representation and making the task of consistency challenging. In addition, the large amount of data generated by remote sensing technologies requires the need of robust data management systems to store, process, and retrieve data effectively. This adds complexity to both operational logistics and computational processing.
- Model adaptability – Developing deep learning models that can effectively process and analyse data across multiple dimensions – spatial, spectral, and temporal is a difficult task. Each dimension adds complexity: spatial analysis must account for variations in scale and perspective, spectral analysis requires decoding information across different wavelengths (which may indicate vegetation types, water bodies, etc.), and temporal analysis tracks changes over time, adding dynamic behaviour to the model. The integration and simultaneous analysis of these dimensions require sophisticated algorithmic strategies and substantial computational resources, often challenging the limits of current technologies and methodologies.
- Transferability – Transferability is a significant challenge in remote sensing models, where a model trained on data from one geographic area or under specific conditions might fail to generalise to other areas or different environmental conditions. This constraint frequently arises due to the presence of various land cover types, atmospheric conditions, and seasonal fluctuations that are not accounted for in the training dataset. Thus, to improve the capacity of a model, it is necessary to train it

extensively on a wide range of datasets or use sophisticated methods such as domain adaptation, which would allow models to perform effectively in multiple domains.

## CONCLUSION AND FUTURE DIRECTIONS

Our research presents an examination of the latest advancements in both remote sensing and deep learning as applied to image processing. We highlighted several critical limitations that need addressing to advance further. In addition, we have identified crucial areas that require more investigation and advancement to improve the capabilities and potential uses of these technologies in the future.

Developing a unified neural network capable of processing multispectral images across varying spatial resolutions and spectral characteristics would represent a significant advancement in remote sensing technology. Such a network would need to robustly handle the details and complexities of different image types, allowing for more flexible and comprehensive analysis. This would involve advanced techniques in image processing and neural network design, leveraging architectures that can dynamically adjust to the input image characteristics.

Furthermore, our research highlighted the significant differences in spectral bands across various satellite probes and their sensors. Moving forward, we anticipate conducting follow-up research aimed at developing methods to normalize these spectral variations, facilitating the creation of a unified analytical framework for multispectral image processing.

Advanced pansharpening algorithms are also increasingly necessary to enhance the accuracy and effectiveness of image fusion, improving both spatial and spectral quality. The development of these techniques requires the improvement of algorithms to successfully combine high-resolution spatial information with broad spectrum data, resulting in clearer and more detailed representations of targeted areas.

## ACKNOWLEDGEMENTS

The research is partially supported by “NGIC – National Geoinformation Center for monitoring, assessment and prediction of natural and anthropogenic risks and disasters” under the Program “National Roadmap for Scientific Infrastructure 2017–2023”, financed by the Bulgarian Ministry of Education and Science.

## REFERENCES

[1] Adegun A., S. Viriri, and J.-R. Tapamo. Review of deep learning methods for remote sensing satellite images classification: experimental survey and comparative analysis. Journal of Big Data, vol. 10, p. 93, Jun 2023.

[2] Agutu N., J. Awange, A. Zerihun, C. Ndehedehe, M. Kuhn, and Y. Fukuda. Assessing multi-satellite remote sensing, reanalysis, and land surface models’ products in characterizing agricultural drought in East Africa. Remote Sensing of Environment, vol. 194, pp. 287–302, 2017.

[3] Dash A., J. Ye, G. Wang. A review of generative adversarial networks (gans) and its applications in a wide variety of disciplines: from medical to remote sensing. IEEE Access, 12, pp. 18330–18357, art. no. 3346273, 2024.

[4] Han W., X. Zhang, Y. Wang, L. Wang, X. Huang, J. Li, S. Wang, W. Chen, X. Li, R. Feng, R. Fan, X. Zhang, and Y. Wang. A survey of machine learning and deep learning in remote sensing of geological environment: Challenges, advances, and

opportunities. ISPRS Journal of Photogrammetry and Remote Sensing, vol. 202, pp. 87–113, 2023.
[5] Hosseiny B., M. Mahdianpari, M. Hemati, A. Radman, F. Mohammadimanesh, and J. Chanussot. Beyond supervised learning in remote sensing: a systematic review of deep learning approaches. IEEE Journal of Selected Topics in Applied Earth Observations and Remote Sensing, 17, pp. 1035–1052, 2024.
[6] Houborg R., M. McCabe, A. Cescatti, F. Gao, M. Schull, and A. Gitelson. Joint leaf chlorophyll content and leaf area index retrieval from landsat data using a regularized model inversion system (regflec). Remote Sensing of Environment, vol. 159, pp. 203–221, 2015.
[7] Lai Y., M. Pringle, P. Kopittke, N. Menzies, T. Orton, and Y. Dang. An empirical model for prediction of wheat yield, using time-integrated landsat ndvi. International Journal of Applied Earth Observation and Geoinformation, vol. 72, pp. 99–108, 2018.
[8] Lv J., Q. Shen, M. Lv, Y. Li, L. Shi, and P. Zhang. Deep learning-based semantic segmentation of remote sensing images: a review. Frontiers in Ecology and Evolution, 11, art. no. 1201125, 2023.
[9] Mokhtari A., H. Noory, F. Pourshakouri, P. Haghighatmehr, Y. Afrasiabian, M. Razavi, F. Fereydooni, and A. Sadeghi Naeni. Calculating potential evapotranspiration and single crop coefficient based on energy balance equation using landsat 8 and sentinel-2. ISPRS Journal of Photogrammetry and Remote Sensing, vol. 154, pp. 231–245, 2019.
[10] Radočaj D., J. Obhođaš, M. Jurišić, and M. Gašparović. Global open data remote sensing satellite missions for land monitoring and conservation: A review. Land, vol. 9, no. 11, 2020.
[11] Reyes-Gonzalez A., J. Kjaersgaard, T. Trooien, C. Hay, and L. Ahiablame. Estimation of crop evapotranspiration using satellite remote sensing-based vegetation index. Advances in Meteorology, vol. 2018, p. 4525021, Feb 2018.
[12] Tattaris M., M. Reynolds, and S. Chapman. A direct comparison of remote sensing approaches for high-throughput phenotyping in plant breeding. Frontiers in Plant Science, vol. 7, 08 2016.
[13] Wang L., C. Zhang, R. Li, C. Duan, X. Meng, and P. M. Atkinson. Scale-aware neural network for semantic segmentation of multi-resolution remote sensing images. Remote Sensing, vol. 13, no. 24, 2021.
[14] Xu Z., T. Wang, A.K. Skidmore, and R. Lamprey. A review of deep learning techniques for detecting animals in aerial and satellite images. International Journal of Applied Earth Observation and Geoinformation, vol. 128, art. no. 103732, 2024.
[15] Yang Z., Y. Shao, K. Li, Q. Liu, L. Liu, and B. Brisco. An improved scheme for rice phenology estimation based on time-series multispectral hj-1a/b and polarimetric radarsat-2 data. Remote Sensing of Environment, vol. 195, pp. 184–201, 2017.
[16] Zhang C., A. Marzougui, and S. Sankaran. High-resolution satellite imagery applications in crop phenotyping: An overview. Computers and Electronics in Agriculture, vol. 175, p. 105584, 2020.
[17] Zhang, K., F. Zhang, W. Wan, H. Yu, J. Sun, J. Del Ser, E. Elyan, and A. Hussain. Panchromatic and multispectral image fusion for remote sensing and earth observation: Concepts, taxonomy, literature review, evaluation methodologies and challenges ahead. Information Fusion, 93, pp. 227-242, 2023.

# REMOTE SENSING, GEOPHYSICAL AND GEOLOGICAL SURVEYS IN THE BULGARIAN BLACK SEA SECTOR: REVIEW OF AVAILABLE DATA AND ADVANCEMENTS

**PhD Martin Ivanov**[1]

[1]Institute of Oceanology – Bulgarian Academy of Sciences, **Bulgaria**

## ABSTRACT

This study presents an review of the geophysical and geological data available for the Bulgarian Black Sea shelf, highlighting the methodologies employed for data storage and their effectiveness. Such data are crucial for understanding the shelf's historical dynamics and ongoing changes, serving as a foundation for various scientific investigations. Through an analysis of geological, morphological, geophysical, and geochronological data, we trace the evolution of the shelf's structure and movements, delineating its key characteristics and trends. The research, inquiries, and interpretations conducted over the years have yielded significant hypotheses and conclusions, setting the stage for future multidisciplinary studies. Technological advancements in data collection and processing have continually enhanced the depth, accuracy, and scope of the information gathered, underpinning the importance of these studies for the scientific community's efforts in diverse exploratory missions. This article details the data sourced from the Institute of Oceanology (BAS) and the Centre for Underwater Archaeology (CUA-Sozopol), emphasizing the use of primary geophysical techniques such as single and multibeam echo sounders, unmanned aerial vehicles, side-scan sonar, sub-bottom profilers, LIDAR, and localized electrical and magnetic surveys.

**Keywords:** seabed surveys, remote sensing, digital terrain model, shelf, Bulgarian Black Sea

## INTRODUCTION

In contemporary times, there is an increasing reliance on non-destructive integrated geophysical prospecting techniques for studying marine environments. To meet the goals of such research endeavors and enhance the quantity and quality of collected data, a synergistic approach combines various non-destructive geophysical methods for detailed remote sensing. Given the diverse objectives of marine surveys, encompassing geological, exploratory, engineering, and archaeological investigations, meticulous attention is devoted to ensuring high precision and optimal spacing of survey track lines, thereby facilitating the acquisition of reliable information about the surveyed areas' characteristics. The methodology utilized is based on a suite of geophysical remote sensing techniques. Acknowledging the inherent limitations of individual geophysical prospecting methods, a comprehensive array of acoustic, magnetic, and electric remote-sensing equipment is utilized to achieve the surveys' objectives. Illustrated examples of the obtained results are provided in the subsequent discussion. Due to the unique nature of these research endeavors, a thorough review of prior data is conducted to enable a meaningful comparison between terrestrial and corresponding marine sections.

The review aims to provide a succinct overview of the application of marine geophysical methods and remote sensing technologies for geological, geomorphological, archaeological, and geochronological investigations of the Bulgarian shelf, alongside supplementary information aimed at enriching and establishing connections with marine records.

## REMOTE SENSING FOR SEABED MAPPING

Recent advancements in technology for seabed surveying have opened unprecedented opportunities for in-depth mapping of the Bulgarian Black Sea shelf. This development is especially significant in light of Bulgaria's accession to the European Union, where adherence to stringent environmentally-focused EU Directives plays a pivotal role. Such directives emphasize the critical need for comprehensive exploration and understanding of this marine region. Historically, the pioneering research endeavors in this area during the latter half of the 20th century were predominantly led by the Institute of Oceanology - BAS, in close collaboration with Soviet scientists [1]. These foundational efforts set the stage for today's advanced exploration methodologies, which promise to unveil new insights and enhance our stewardship of the marine environment.

***Echo Sounding mapping***. The evolution of sonar technology, initially propelled by its strategic wartime applications during World War II, has transformed the exploration of ocean floors into a detailed and feasible endeavor. In subsequent decades, geophysical acoustic and imaging techniques have experienced significant advancements, evolving into sophisticated and multifaceted tools [1]. In contemporary practice, the seabed mapping of the Bulgarian Black Sea shelf and adjacent coastal zones leverages various remote sensing methods. Techniques such as multi-beam and single-beam echo sounding, sub-bottom profiling, and magnetic and electric surveying are complemented by advanced LiDAR scanning and UAV photogrammetry. These methods, which draw parallels with satellite-based observation systems, have been specifically adapted to address the intricacies of the marine environment [2],[3].

Since 2007, significant strides have been made in the exploration of the Bulgarian Black Sea shelf through the collection and analysis of extensive Multibeam bathymetric data and side-scan sonar imaging. These innovative techniques have facilitated the identification of various seabed formations and the mapping of different substrates, covering an area of approximately 5700 km². This represents a substantial, albeit partial, survey of less than 17% of the Bulgarian Exclusive Economic Zone (EEZ) in the Black Sea (Fig. 1). Despite the seemingly limited scope, these efforts are pivotal, laying the foundational groundwork for a more comprehensive understanding of the seabed morphology across the Bulgarian shelf and coastal zones [3],[4].

The integration of diverse data sets, including bathymetric readings, side-scan sonar mosaics, and geological information, has significantly advanced the geomorphological mapping efforts in key areas such as Varna Bay [5], Avren coastal zone [6] and Strandzha coastal zone [7],[8], alongside substrate and habitat mapping endeavors along the Southern Bulgarian coastal zone [2],[7],[9],[10],[11]. The application of side-scan sonar technology is particularly noteworthy for its critical role in these efforts. This technology excels in imaging the seabed, enabling the detailed visualization and identification of various features and potential points of interest across expansive areas [10],[11]. Its capacity to provide high-resolution imagery is instrumental in delineating

complex seabed features, identifying potential archaeological sites, assessing habitats, and supporting environmental monitoring and conservation initiatives [12],[13],[14].

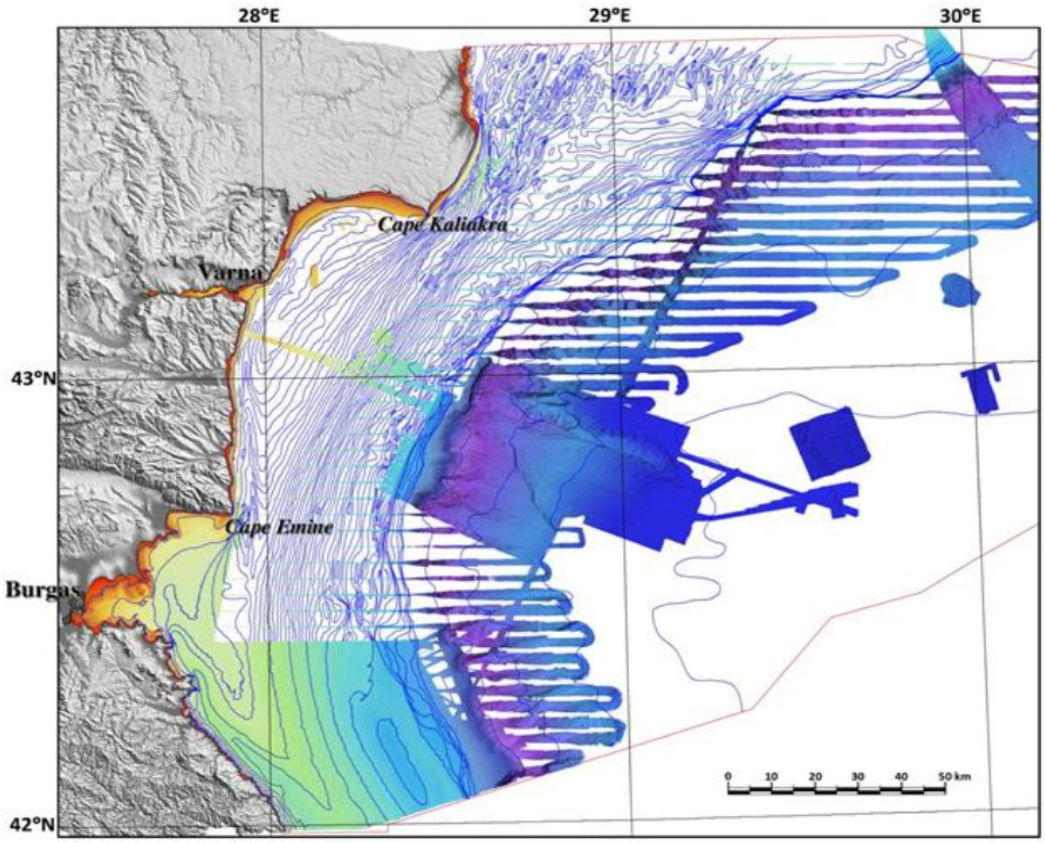


**Fig. 1.** Available DTM of the surveyed area with MBES and SBES and digitized water lines in the Bulgarian EEZ of the Black Sea (after Prof. L. Dimitrov [3],[4]).

***LiDAR scanning***. The first Lidar scanning in the Black Sea was conducted as part of the CUA's project. Blom Aerofilms Ltd scanned an area of 100 km$^2$, including both land and water, along the Southern Bulgarian Black Sea Coast - Fig. 2. The maximum measured depth was about 22 m. The collected data were used for creating a precise DTM with pixels of 1m² for the ground and 5 m² for the seabed. It was the base of the spatial analyses for the predictive modeling of Late Chalcolithic and Early Bronze Age settlements [14].

***UAS for seabed mapping***. In parallel, the swift advancement of drone technology, or unmanned aerial vehicles/systems (UAVs/UAS), has revolutionized remote sensing and photogrammetry, particularly in coastal environments [15],[16],[17]. Drones facilitate the acquisition of high-resolution digital surface models and orthomosaics, proving indispensable for identifying landforms, mapping landscapes, and conducting shallow bathymetry along the Bulgarian Black Sea Coast [18],[19],[20] (Fig. 2). Establishing an initial UAV geodatabase, encompassing over a third of the coastline, is a significant milestone providing a robust foundation for ongoing and future environmental monitoring and assessment endeavors [21],[22],[23],[24].

The utility of UAV-based photomapping is vividly demonstrated in the context of coastal change assessments, such as those conducted in the Bay of Chernomorets, where

recent port construction activities have altered the natural landscape. Despite the evident advantages of drone photomapping, the absence of a systematic, annual shoreline monitoring program constrains our ability to fully understand and mitigate the impacts of human activities on these dynamic coastal systems. Nevertheless, the strategic deployment of UAVs offers a promising avenue for acquiring essential geodata that can inform various coastal management decisions, including survey planning, erosion mitigation, and sediment management strategies [21].

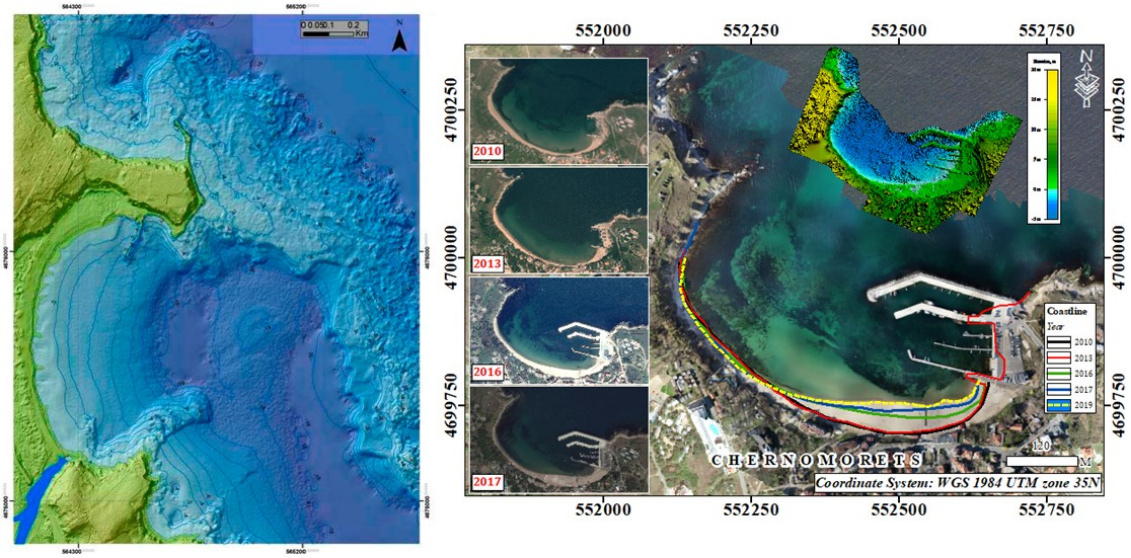


**Fig. 2.** Example of part of LiDAR-based Digital terrain model along the Southern Bulgarian coast (Port of Kiten), on the left side [14]; Example of high-resolution Orthophoto and DSM derivation from UAV photogrammetry data showing the shoreline change of the port of Chernomorets [21], on the right side.

## REVIEW OF AVAILABLE SEABED DATA FOR THE BULGARIAN BLACK SEA COASTAL ZONE AND SHELF

***Geophysical data***. Sub-bottom profiling and magnetic and electric surveying techniques significantly deepen our insight into the obscured seabed features and geological structures, offering perspectives unattainable through conventional surface scanning methods [10]. Additionally, the adoption of LiDAR scanning within the Centre for Underwater Archaeology (CUA) project marks a critical leap forward, enabling the precise delineation of both terrestrial and marine landscapes (Fig. 3; Fig. 4). This technological advancement is crucial for predictive modeling and the exploration of ancient settlements along the Southern Bulgarian Black Sea Coast, shedding light on historical shoreline dynamics and settlement patterns [14],[17],[18].

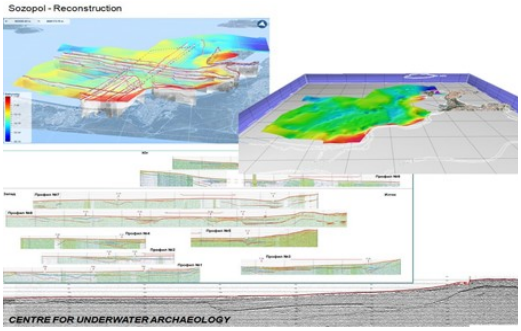


**Fig. 3.** Reconstruction of Sozopol Bay paleo relief based on data obtained with a sub-bottom profiler [10].

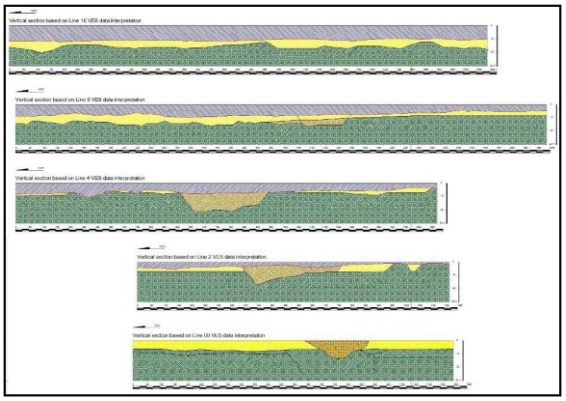

**Fig. 4.** Example of determination of geological composition of the Pasha Dere coastal sector from electrical resistivity data [10].

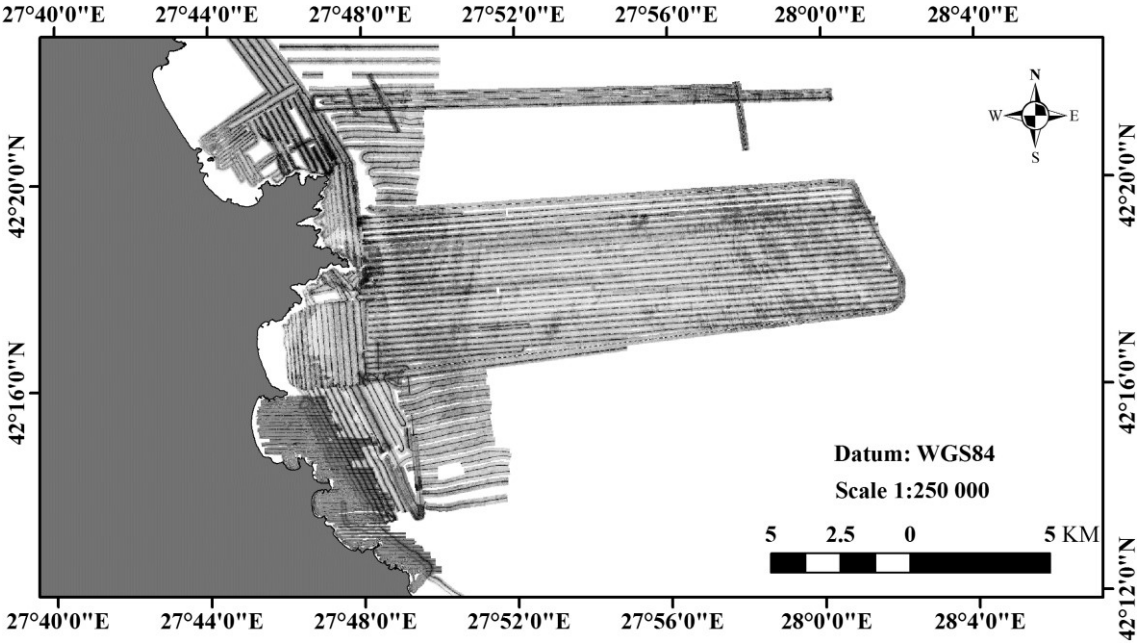


**Fig. 5.** Side-scan sonar mosaic of the southern part of the coastal zone in front of Strandzha Coast by Project "COCONET" [7].

***Geological Maps.*** Unlike bathymetric surveys, substrate mapping offers significantly broader coverage. By 2024, various substrate maps ranging from 1:20,000 to 1:50,000 had been successfully compiled at a large to medium scale. Figures 6, 7, and 8 showcase the most detailed sediment maps along the southern coastline. These maps integrate all presented remote sensing and geophysical methods supported by underwater verification [2],[7].

The production of these geological maps represents a significant advancement in our understanding of seafloor composition and structure. By combining remote sensing data with ground-truthing techniques, researchers have created comprehensive maps that provide insights into the distribution of sediment types, geological formations, and potential hazards.

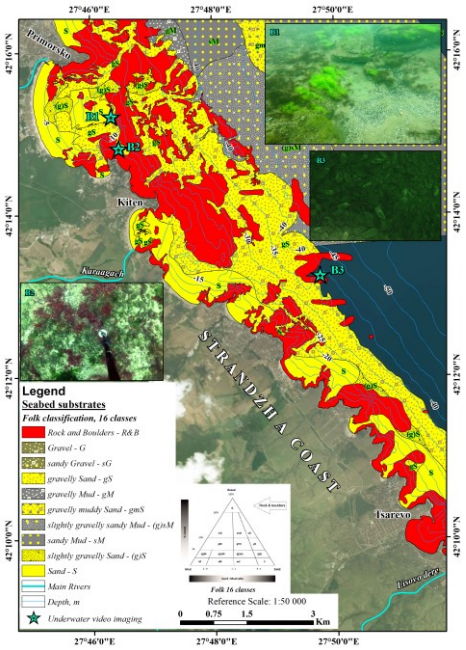


**Fig. 6.** Seabed substrate map of the coastal zone between Primorsko and Tsarevo [2].

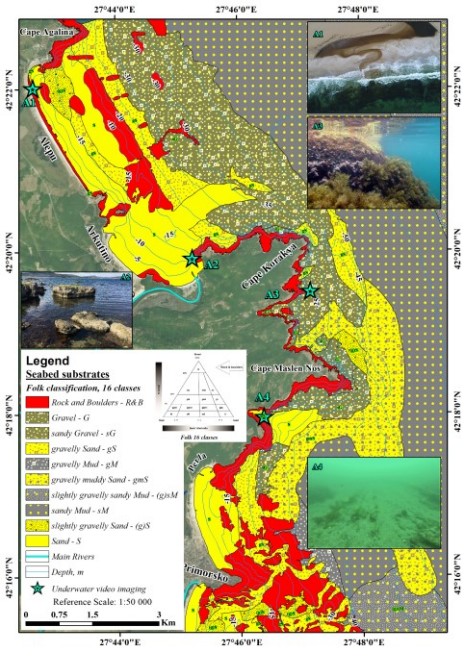


**Fig. 7.** Seabed substrate map of the coastal zone between Cape Agalina and town of Primorsko [2].

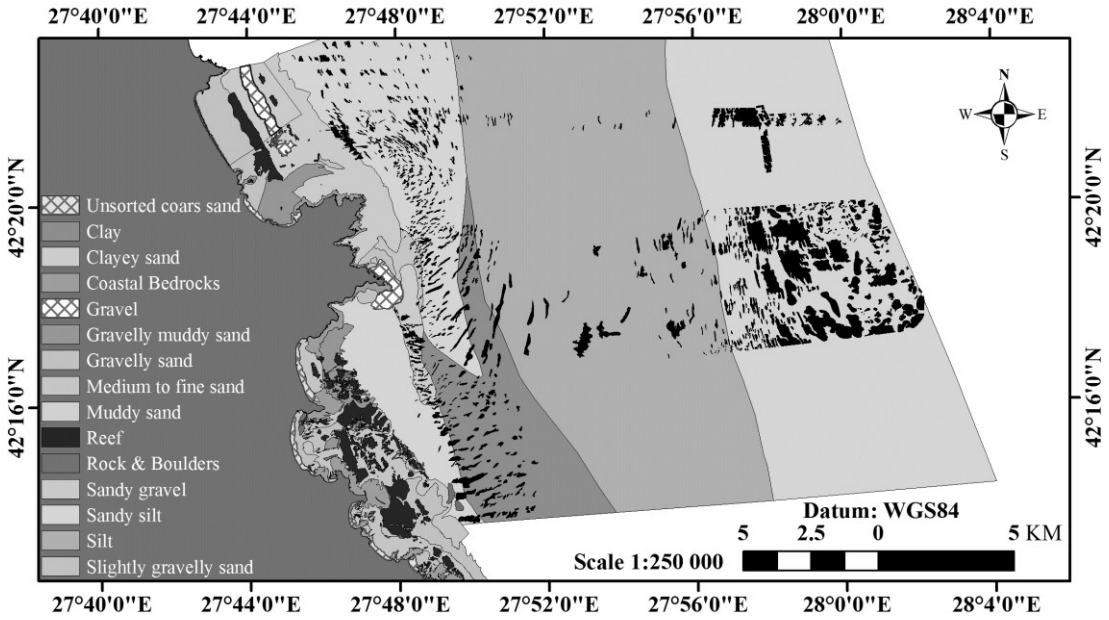


**Fig. 8.** Seabed substrate map of the southern part of the coastal zone in front of Strandzha Coast by Project "COCONET" [7].

In 2023, a landmark achievement in marine research was realized with the creation of the most intricate sediment map ever produced for Burgas Bay (Fig. 9). This milestone served as the cornerstone for a thorough classification of the seabed, shedding light on the region's complex underwater landscape. Researchers meticulously surveyed and analyzed sedimentary compositions using state-of-the-art technology and methodologies, unveiling a wealth of information about the underwater environment.

The typologies established in this study represent a significant step forward in aligning with the rigorous standards set forth by the Water Framework Directive. By adhering to these guidelines, the classification system accurately reflects the natural variability inherent in the hydromorphological regime of Burgas Bay (Fig. 9).

Furthermore, the classification system developed in this study provides invaluable insights into the ecological health and functioning of the marine ecosystem within Burgas Bay. Researchers can better understand sediment transport dynamics, habitat suitability, and potential ecological risks by discerning the distinct sedimentary patterns and compositions.

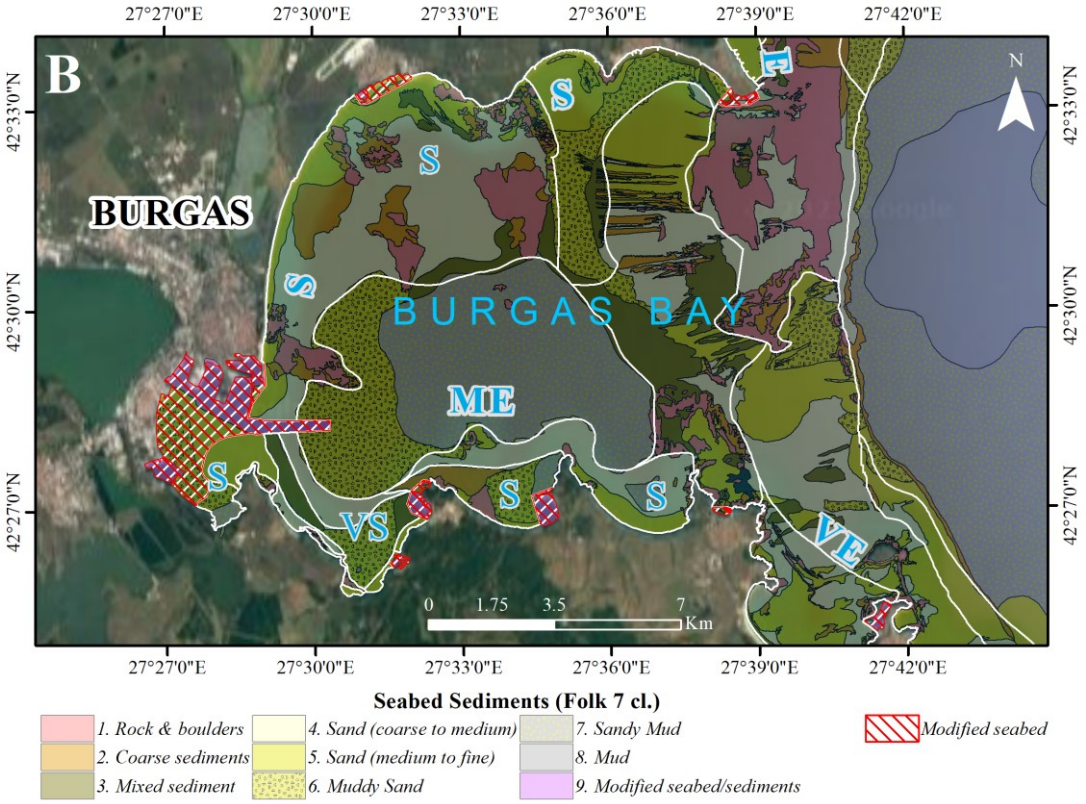


**Fig. 9.** Superimposition of detailed sediment map and wave exposure indications as a basis for the discretization of areas of type-specific hydromorphological conditions in the Burgas Bay [25]

***Geomorphological maps***. Studying shallow coastal bedforms in dynamic environments offers critical insights into the nuanced interplay among climatic forces, wave dynamics, riverine inputs, tidal movements, sea-level changes, and the underlying coastal geology. A multidisciplinary approach has been adopted to unravel this complexity, leveraging an array of advanced survey techniques. The utilization of multi-beam sonar systems, single-beam echo sounders, orthophoto imaging, and seafloor sediment sampling has been pivotal in compiling a comprehensive geo-database. This rich repository of data underpins the creation of an intricate seafloor geomorphological map of Varna Bay (Fig. 11) and Avren Coast (Fig. 10), which not only categorizes distinct subzones influenced by local hydrodynamic conditions but also identifies and classifies specific bedforms according to their origins [5],[6].

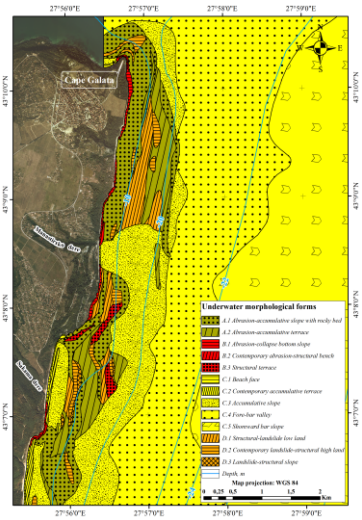


**Fig. 10.** Map of identified seabed geomorphological forms along the Avren Plateau coastal sector [6]

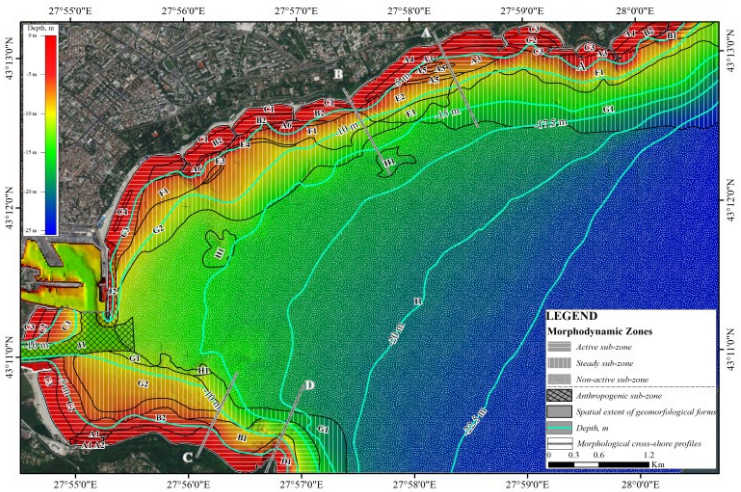


**Fig. 11.** Map of identified seabed geomorphological forms along the Avren Plateau coastal sector [5]

Establishing a regular, comprehensive monitoring framework would enhance our understanding of coastal dynamics and facilitate timely identification and management of vulnerabilities, contributing to more resilient and sustainable coastal ecosystems.

## CONCLUSION

This review presents the rich tapestry of geophysical and geological data pertinent to the Bulgarian Black Sea shelf, aiming to acquaint various institutions, organizations, and individuals with the invaluable records and insights accrued. This review presents the rich tapestry of geophysical and geological data pertinent to the Bulgarian Black Sea shelf, aiming to acquaint various institutions, organizations, and individuals with the invaluable records and insights accrued. The available data represents a substantial, albeit partial, survey of less than 17% of the Bulgarian Exclusive Economic Zone (EEZ) in the Black Sea.

This comprehensive data set is pivotal for advancing the geological understanding of the Bulgarian continental shelf but also serves as a foundational resource poised to address multifaceted future challenges encompassing engineering, environmental, and geological queries, as well as aiding in the meticulous planning of various coastal activities.

The existing data compilation, characterized by its diversity and depth, holds the potential to catalyze advancements across diverse disciplines. It can be employed directly to inform end-product studies or as a critical auxiliary tool to enhance the interpretation of other research findings. Numerous issues spanning geological exploration, engineering, and archaeological prospecting have been effectively addressed by applying these data records. It is evident that possessing a comprehensive and detailed dataset underpins the efficacy of future research endeavors, significantly mitigating the costs, risks, and uncertainties associated with these ventures.

To maximize the utility and impact of these data sets, stakeholders must engage in continuous data sharing and collaborative research. Maintaining and updating the

database will also ensure its relevance and applicability in addressing emerging challenges and leveraging opportunities along the Bulgarian Black Sea coast. Ultimately, this knowledge repository is a cornerstone upon which sustainable development, informed decision-making, and proactive problem-solving can be built, marking a significant stride toward a well-understood and meticulously managed marine environment.

## ACKNOWLEDGEMENTS

The study was performed within the project “Coastal HYdro-Morphological Regime changes in the mAn-modified environment – CHYMERA” contract № КП-06-Н54/8/01.12.2021 funded by the Bulgarian National Science Fund under the Ministry of Education and Science of the Republic of Bulgaria.

## REFERENCES

[1] Geological and Geophysical Studies of the Bulgarian Black Sea Zone, Bulgaria, 317, 1980 (in Russian).

[2] Dimitrov, L., Prodanov, B., Doncheva, V., Berov, D., Trifonova, E., Seabed mapping of the Bulgarian coastal zone between Sozopol and Tsarevo (Southern Bulgarian Black Sea). Comptes rendus de l’Academie Bulgarie des Sciences, 72(5), pp 634-640, 2019.

[3] Report Analysis and Interpretation of Data on the Ecological State of Marine Waters - 2021, Agreement No. D-31-6/12.04.2021 between the Ministry of Environment and Waters and the Institute of Oceanology - BAS, Varna, for the fulfillment of obligations to monitor the Black Sea based on Art. 171, para. 2, Item 3 of the Water Act, 2022.

[4] European Marine Observation and Data Network (EMODnet), https://emodnet.ec.europa.eu/geoviewer

[5] Prodanov, B., Keremedchiev, St., Dimitrov, L., Andreeva, N., Seabed Morphology of the Varna Bay coastal zone, Bulgarian Black Sea. Comptes rendus de l’Academie Bulgarie des Sciences, 72(8), pp 1078-1085, 2019. https://doi.org/10.7546/CRABS.2019.08.10;

[6] Prodanov, B., Dimitrov, L., Andreeva, N., Keremedchiev, St., Geomorphological setting of the coastal zone between cape Galata and cape Paletsa, Bulgaria Black Sea. Comptes rendus de l’Academie Bulgarie des Sciences, 70(8), pp 1137-1142, 2017.

[7] Todorova, V., Dimitrov, L., Doncheva, V., Trifonova, E., Prodanov, B., Benthic Habitat Mapping in the Bulgarian Black Sea. Proceedings of 12th International Conference on the Mediterranean Coastal Environment (MEDCOAST 2015), V.1, Varna, pp 251-262, 2015.

[8] Prodanov, B., Dimitrov, L., Morphology of the Strandzha Coastal zone, Southern Bulgarian Black Sea Coast. Proc. of 20th International Multidisciplinary Scientific GeoConference SGEM 2020, 20, 2.2, pp. 186-196, 2020. http://doi.org/10.5593/sgem2020/1.1/s01.024;

[9] Bekova, R., Raikova-Petrova, G., Prodanov, B., Maturity, Sex Ratio and Spawning Time of Liza aurata Risso, 1810 and Liza saliens Risso, 1810 (Mugilidae) from the Bulgarian Black Sea Coast. Comptes rendus de l'Academie Bulgarie des Sciences, 72(7), pp.916-923, 2019. http://doi.org/10.7546/CRABS.2019.07.09;

[10] Velkovsky, K., Marine Remote Sensing Archaeological Surveys along the Southern Bulgarian Black Sea Coast (2013 – 2021). Bulletin of the Burgas Museum, vol.VIII, part I, ISSN 2815-4010, 2022.

[11] Lambev, T., Prodanov, B., Digital terrain model of the seafloor of South Bulgarian Black Sea Coast. 10th Congress of the Balkan Geophysical Society (BGS2019), European Association of Geoscientists & Engineers, vol.1, pp 1-6, 2019.

[12] Lambev, T., Prodanov, B., Dimitrov, L., Kotsev, I., Digital terrain model of the Varna and Beloslav Lakes (North Bulgaria Black Sea Coast). Proc. SPIE 11524, Eighth International Conference on Remote Sensing and Geoinformation of the Environment (RSCy2020), 1152422, 2020. https://doi.org/10.1117/12.2571104;

[13] Lambev, T., Prodanov, B., Dimitrov, L., Kotsev, I., Digital bathymetric model of the Broad Burgas Bay (Bulgarian Black Sea), Proc. SPIE 11524, Eighth International Conference on Remote Sensing and Geoinformation of the Environment (RSCy2020), 1152421, 2020. https://doi.org/10.1117/12.2571101;

[14] Prahov, N., Archaeological predictive model for late chalcolithic and early bronze age coastal settlements along the Southern Bulgarian Black Sea coast, International conference "Where are the sites?", Bulgaria, vol. 1/issue 6, pp 119-127, 2013.

[15] Kotsev, I., Prodanov, B., Lambev, T., Bekova, R., UAS-based mapping of depositional landforms along the North Bulgarian Black Sea coast in support of nature conservation. In: Proc. SPIE 11524, Eighth International Conference on Remote Sensing and Geoinformation of the Environment (RSCy2020), 1152426, 2020. https://doi.org/10.1117/12.2571907;

[16] Prodanov, B., Lambev, T., Bekova, R., Kotsev, I., Applying Unmanned Aerial Vehicles for high-resolution geomorphological mapping of the Ahtopol coastal sector (Bulgarian Black Sea coast). Proceedings of International Multidisciplinary Scientific GeoConference: SGEM, 19(2.2), pp 465-472, 2019.

[17] Prahov, N., Prodanov, B., Dimitrov, K., Dimitrov, L., Velkovsky, K., Application of Aerial Photogrammetry in the Studies of Underwater Archaeological Heritage of Nesebar. Proc. of 20th International Multidisciplinary Scientific GeoConference SGEM 2020, 2.2, 2020, ISBN:978-619-7603-07-1, ISSN:1314-2704, pp. 175-182, 2020. http://doi.org/10.5593/sgem2020/2.2/s10.021;

[18] Prahov, N., Prodanov, B., Dimitrov, K., Velkovsky, K., The negative impact of human activities on underwater cultural heritage: Case studies from the Bulgarian Black Sea Littoral. Proceedings of 21st International Multidisciplinary Scientific GeoConference SGEM 2021, Vol.21, Book 2.1, pp. 743-751, 2021. https://doi.org/10.5593/sgem2021/2.1/s11.89;

[19] Prodanov, B., Dimitrov, L., Lambev, T., Mapping of coastal and submarine morphological landforms using Unmanned Aerial Systems and Echo-sounding data, Case study: Bulgarian Black Sea coastal sector between cape Sivriburun and cape

Kaliakra, In: 21st International Multidisciplinary Scientific GeoConference SGEM 2021, Vol. 21, Book 2.1, pp. 717-725, 2021. https://doi.org/10.5593/sgem2021/2.1/s11.86;

[20] Prodanov, B., Kotsev, I., Bekova, R., Dimitrov, L., Lambev, T., UAS photogrammetry as an effective tool for high-resolution mapping of depositional landforms and monitoring geomorphic change. Case Study: Kamchia-Shkorpilovtsi beach, Bulgarian Black Sea Coast, In: 21st International Multidisciplinary Scientific GeoConference SGEM 2021, Vol. 21, Book 2.1, pp. 623-634, https://doi.org/10.5593/sgem2021/2.1/s10.75;

[21] Prodanov, B., Kotsev, I., Lambev, T., Bekova, R., Unmanned Aerial Vehicles for surveying the Bulgarian Black Sea Coast. Comptes rendus de l'Academie Bulgarie des Sciences, 73(5), pp 666-672, 2020. http://doi.org/10.7546/CRABS.2020.05.09;

[22] Prodanov, B., Kotsev, I., Lambev, T., Dimitrov, L., 3D high-resolution mapping and identification of coastal landforms using Unmanned Aerial Vehicles, case study: Shabla Municipality coastal sector, Bulgaria. In: Proc. SPIE 11524, Eighth International Conference on Remote Sensing and Geoinformation of the Environment (RSCy2020), 115242D, 2020. https://doi.org/10.1117/12.2571059;

[23] Prodanov, B., Kotsev, I., Lambev, T., Dimitrov, L., Bekova, R., Dechev, D., Drone-based geomorphological and landscape mapping of Bolata Cove, Bulgarian coast, Sustainable Development and Innovations in Marine Technologies, Georgiev & Guedes Soares (Eds.). Taylor & Francis Group, London, pp 592-598, 2019. http://dx.doi.org/10.1201/9780367810085-78;

[24] Prodanov, B., Bekova, R., Kotsev, I., Vachkova, V. 2021. Habitat Lost: Analysis of the eutrophication magnitude at a protected coastal lake in Bulgaria using satellite and drone imagery. In: Proceedings of 21th International Multidisciplinary Scientific GeoConference Surveying, Geology and Mining, Ecology and Management – SGEM 2021, Vol. 21, Book 5.1, pp. 253-260, https://doi.org/10.5593/sgem2021/5.1/s20.032;

[25] Valchev, N., Prodanov, B., Dimitrov, L., Andreeva, N., Lambev, T., Eftimova, P., Identification of Type-Specific Reference Hydromorphological Conditions of Bulgarian Coastal Waters in Support of Marine Environmental Management. In: 23rd SGEM International Multidisciplinary Scientific GeoConference Proceedings 2023, Water Resources. Forest, Marine and Ocean Ecosystems, Vol 23, Issue 3.1, 2023.

# SATELLITE MONITORING OF ANTHROPOGENIC PROCESSES AND FACTORS OF LAND DEGRADATION IN UKRAINE

**PhD. Lesya Yelistratova**[1]
**PhD. Alexander Apostolov**[1]
**PhD. Artur Hodorovsky**[1]
**PhD. Olha Tomchenko**[1]
**Maksym Tymchyshyn**[1]
[1] State Institution "Scientific Centre for Aerospace Research of the Earth of the Institute of Geological Sciences of the National Academy of Sciences of Ukraine", **Ukraine**

## ABSTRACT

The relevance of the research lies in the fact that the well-being of the Ukrainian nation, present and future generations, largely depends on the preservation of existing ecosystems, their support, and the enhancement of their quality and biodiversity. Particular attention should be paid to the problem of land cover degradation. Land cover currently holds a unique status regarding food security and is a dominant source for renewing crucial biospheric functions, ensuring the diversity of living organisms.

The anthropogenic and technological pressure on Ukraine's environment (land cover) exceeds several times the corresponding indicators in developed countries. A remote sensing data methodology was proposed to assess the impact of human, technical activities (anthropogenic predictor) on land cover degradation.

As a result of the research, the obtained data allowed for the assessment of Ukraine's land cover status and revealed the degree of its degradation caused by the influence of anthropogenic factors, namely, irrational agricultural practices, non-efficient long-term exploitation of mineral deposits, ineffective urban infrastructure design, irrational practices in forestry and park management, the influence of reservoirs, forest, and steppe fires, as well as military activities.

**Keywords:** land cover degradation, degradation factors, anthropogenic influence, site, remote sensing data.

## INTRODUCTION

All human life ultimately depends on the earth. The earth provides people with the means to live, and from the very beginning, it became a source of important resources. But in the modern world, the earth is no longer able to cope with the pressure of human activity on its limited resources, and leads to land degradation. The geographic scale of degradation processes covers all terrestrial regions and biomes of the world, with the exception of only the continent of Antarctica. This covers the full range of human-modified systems, including, but not limited to, drylands, agricultural and agroforestry systems, forests, and associated water systems. This includes wetlands and aquifer systems, including saline systems as well as areas of swamps, peat bogs, natural or artificial reservoirs, permanent or temporary, with static or flowing and fresh water, etc [1-5].

https://doi.org/10.5593/sgem2024/2.1/s10.35

An actual problem is land degradation in the territory of Ukraine, in particular, caused by human activity. Identification of areas subject to degradation and factors that have the greatest negative impact on the country's land cover is one of the important tasks.

The development of information technologies, the emergence of high- and ultra-high-resolution satellite images, the development of methods, and improvements in models of geodetic equipment have led to qualitative changes in methods for assessing land cover degradation. In this regard, recently remote sensing methods and geographic information technologies have become the leading methods for assessing land cover degradation.

**The purpose of this research** is to identify, assess, and analyze the anthropogenic component (human technical activities) of the process of land cover degradation in Ukraine using remote sensing materials.

## MATERIALS AND METHODS

The proposed algorithm for estimating the anthropogenic load on the land cover of Ukraine using satellite information. The work algorithm consists of the following stages: 1) obtaining remote zoning data of the Earth for the study area; 2) initial processing of satellite survey data using the Erdas Imagine program; 3) selection of the territory of Ukraine by vector layer from the vector map "Ukraine 500" and selection of the studied area territory according to the set contour using the Subset function of the Erdas Imagine program; 4) calculation, if necessary, of spectral index values and their differences using the Model Marker function of the Erdas Imagine program; 5) creating a GIS project in the ArcGIS program and presenting all input and calculation data; 6) creation of the original image using the Layout function of the ArcGIS program with the addition of geographic coordinates, scale, and legend.

In the research process, remote sensing data from Landsat 5/9 and WorldView-2 satellites was used. To determine changes in the study area, data for a 30-year period were compared. The results of the research were displayed in the program for working with geospatial data, ArcGIS. Direct processing of remote sensing data was carried out using the program Erdas Imagine.

Quantitative and qualitative calculations were carried out on the example of the territory of the test site, which is characterized by constant industrial development (fig. 1).

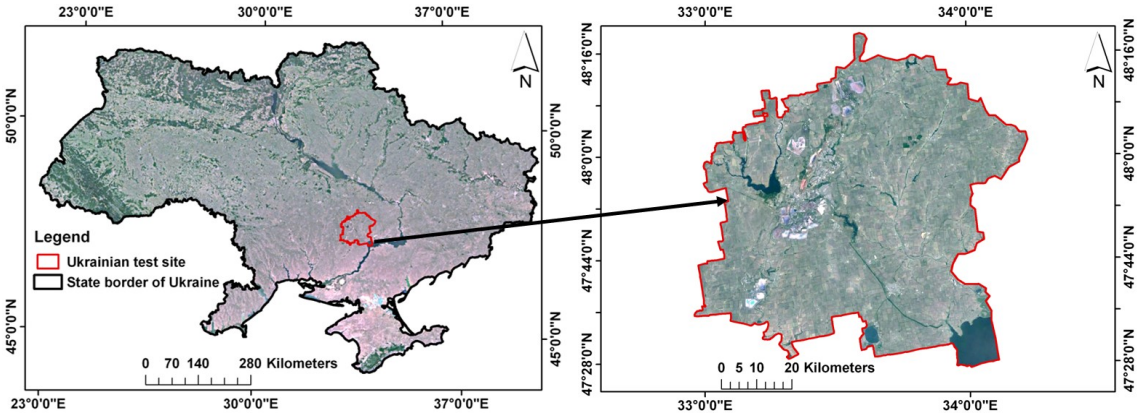


**Figure 1** – Space image of the test site and its location within Ukraine.

## RESULTS

Since land degradation is a complex interconnected natural-anthropogenic phenomenon, an approach to identifying and understanding anthropogenic processes must take into account the driving forces and factors underlying the anthropogenic component of degradation. Based on information, bibliography, and analytical and detailed analysis, Figure 2 shows the main existing factors of anthropogenic pressure on the natural environment of Ukraine.

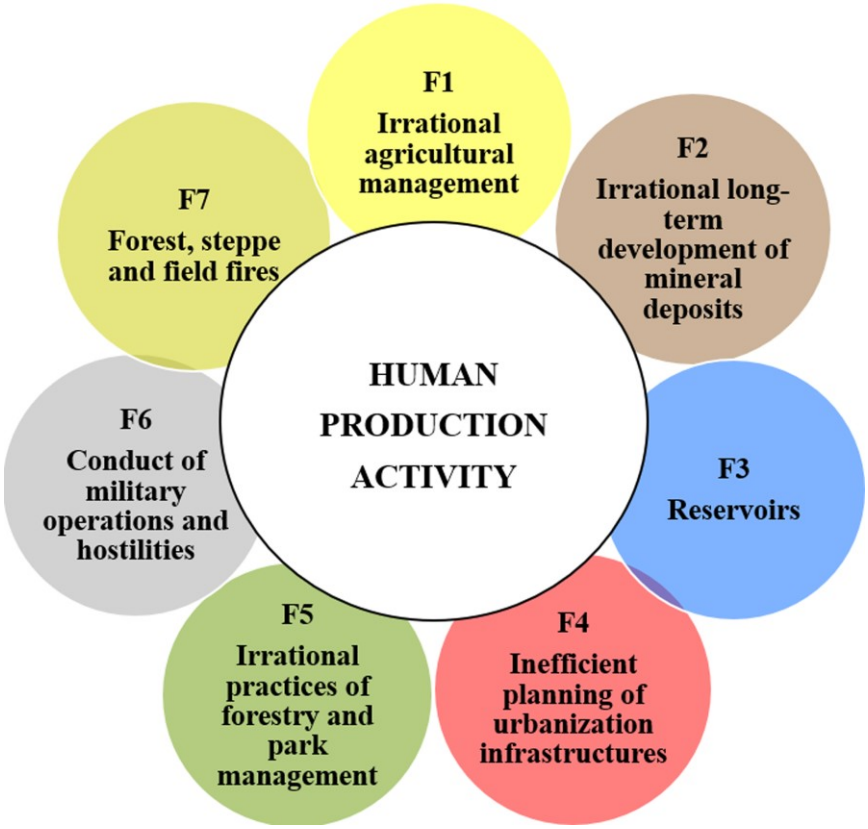


**Figure 2** – Main anthropogenic factors influencing the degradation of land cover in Ukraine

In Ukraine, the factors of land cover degradation based on anthropogenic load are provoked by the following conditions, which give rise to causes of degradation, and the very processes of land cover degradation in Ukraine are shown in Figure 3.

https://doi.org/10.5593/sgem2024/2.1/s10.35

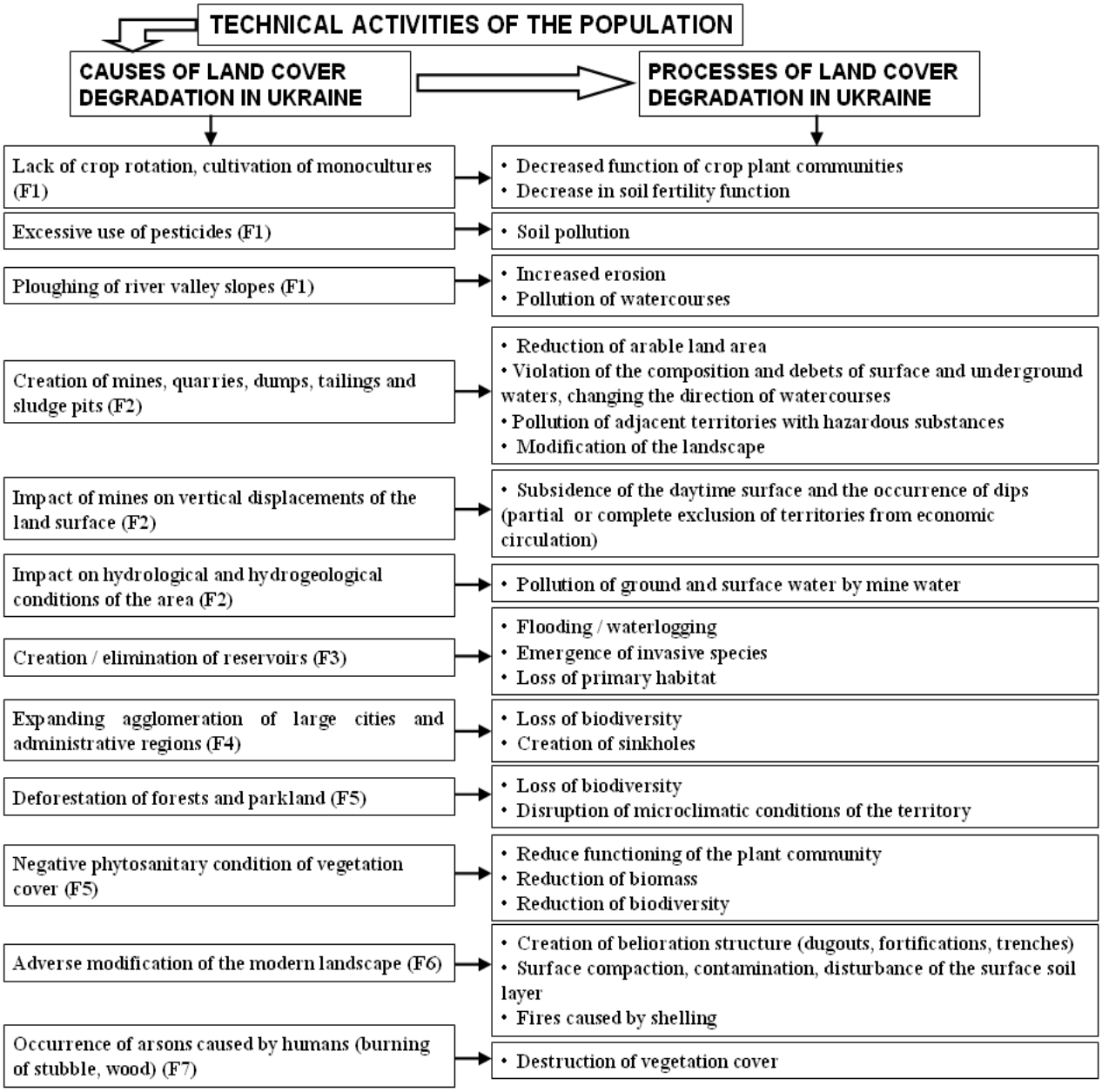


**Figure 3** – Graphical model of the studying human technical activity (anthropogenic predictor) on land cover degradation in Ukraine

These are the following conditions: a way of life with an unbalanced level of consumption and production in a combined economy (in Ukraine, a mixed type of economy with income below the average, including the fact that full-scale military actions and her condition worsen), which also aggravates this condition [6-7]; unstable levels of expansion of agriculture, extraction of natural resources and minerals; urbanization; growing demand for food, feed, fuel, and raw materials, which increases the load on land resources; and competition for natural resources.

Based on the information provided (Fig. 2, 3), the impact of human technical activities on the land cover degradation processes of the Ukrainian was assessed using the following quantitative and qualitative examples (Fig. 4-5).

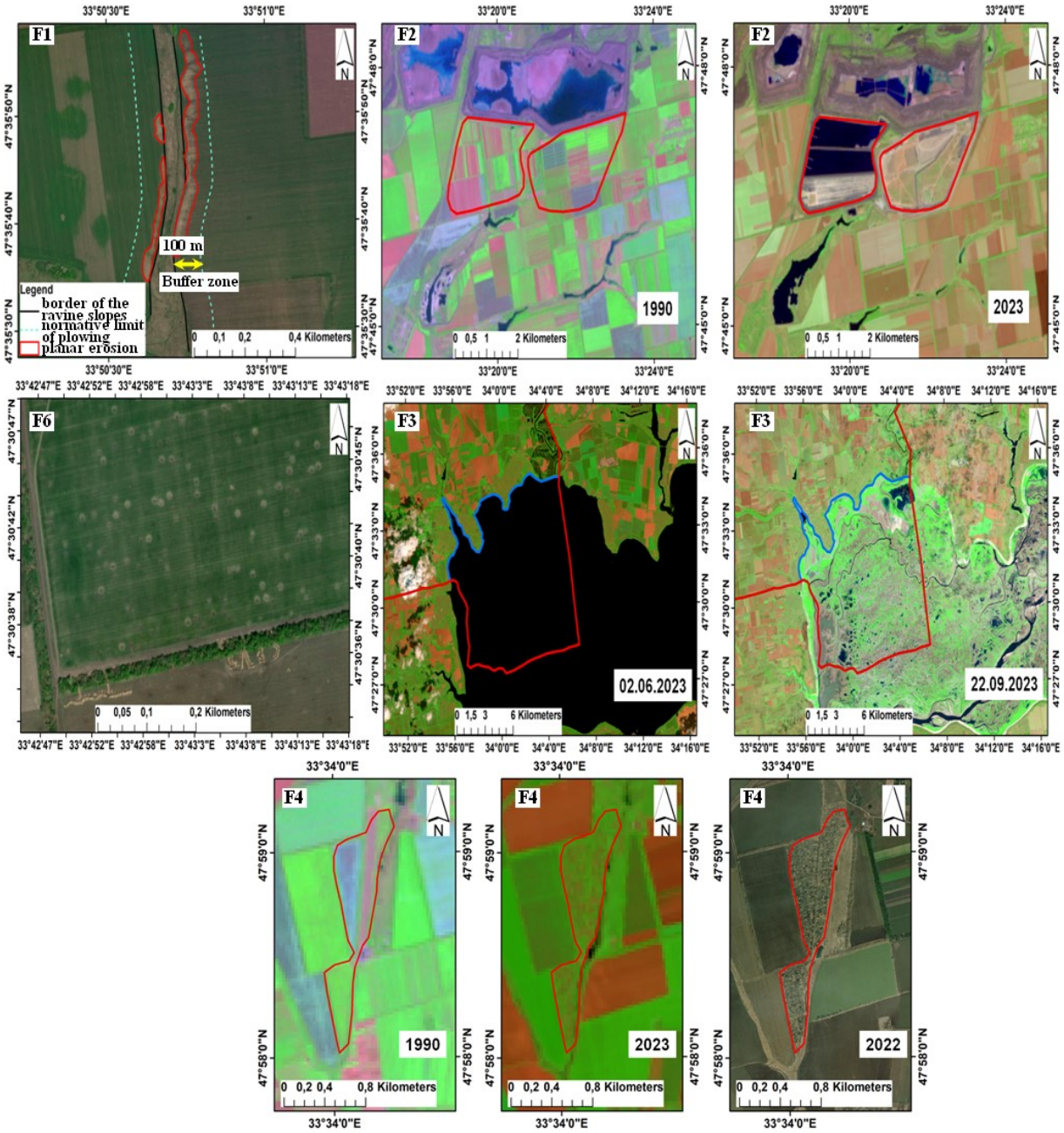


**Figure 4** – Examples of land cover degradation processes in Ukraine: F1 – planar erosion caused by slope plowing; F2 – impact of long-term development of mineral deposits on land cover degradation. The *red color* shows the change in territory due to anthropogenic influence; F3 – impact of the liquidation of the Kakhov reservoir on the degradation of the land cover. The boundary of the test site is shown in *red*, and the boundary of the water table is shown in *blue*; F4 – expanding the agglomeration of the city of Kryvyi Rih due to agricultural landscapes. The *red color* is the border of the fragment of territory where changes in the land cover took place; F6 – disturbance of the surface layer of the soil as a result of shelling and the creation of belioration structures (trenches and dugouts).

https://doi.org/10.5593/sgem2024/2.1/s10.35

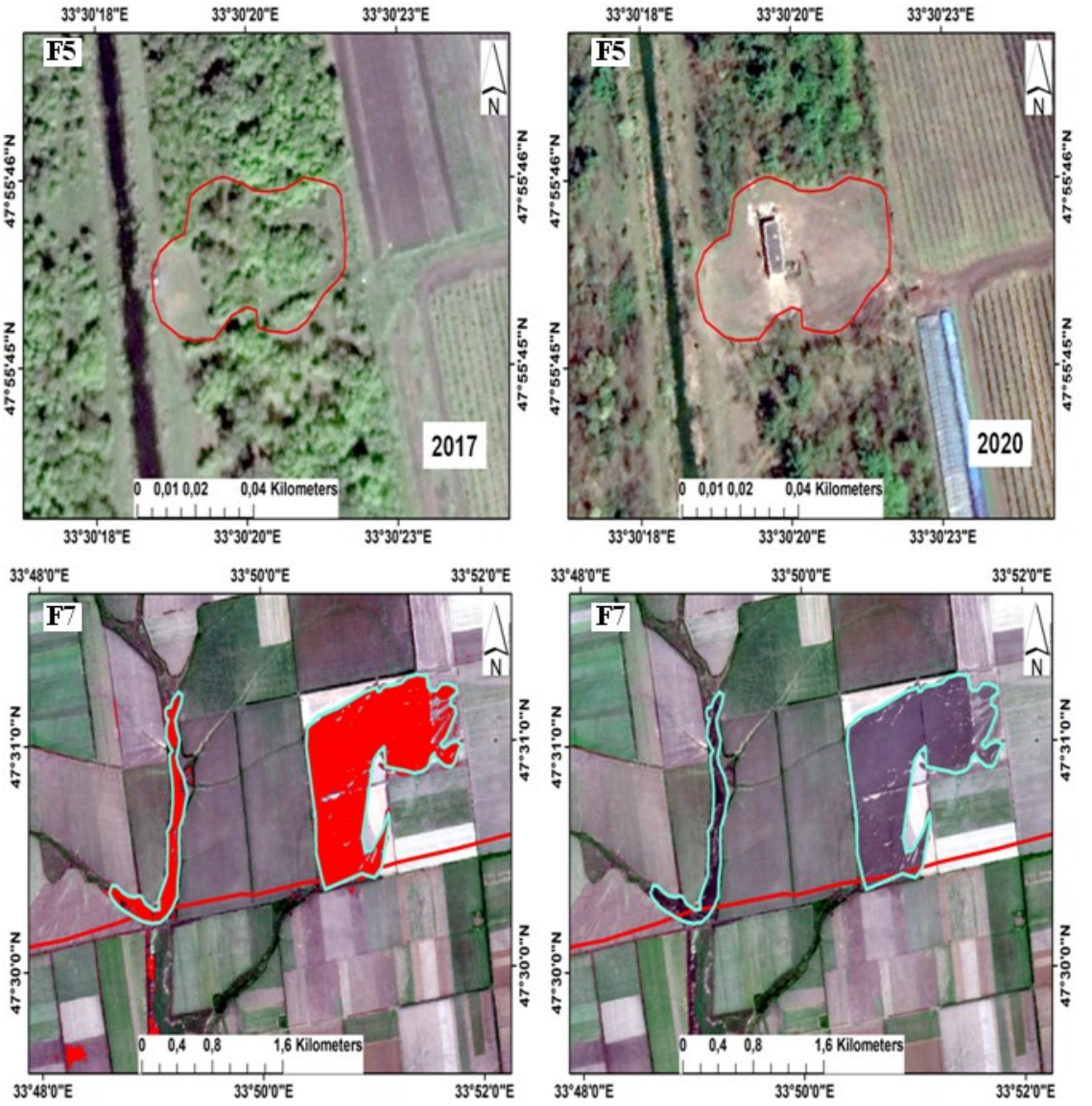


**Figure 5** – Examples of land cover degradation processes in Ukraine: F5 – irrational forestry practice – deforestation within the forest strip on the territory. The *red color* is the boundaries of the territory change fragment; F7 – stubble burning in the territory according to data from the Sentinel-2 satellite for August 2022. The *blue line* is the contour of the burned area.

## DISCUSSION

Human technical activity is now the most important force influencing the degradation of ecosystems in all major biomes in Ukraine. Long-term factors of land degradation continue to grow in most of Ukraine. Recent large-scale drivers of change, such as regional climate change and war, are further exacerbating their impact. Now the population of the country is in a qualitatively different and new world (compared to what it was only a few decades ago), and the totality of those factors shown in Fig. 2 creates significant problems for mitigating further land degradation in Ukraine. There are no regions in Ukraine that are currently free from any form of human influence.

In Ukraine, as a result of the long-term dominance of resource- and energy-intensive technologies, the unbalanced structure of the land fund, and the unsparing use of land,

significant development has resulted in degradation processes (erosion), especially on agricultural lands.

Figure 4.F1 shows an example of the impact of irrational agricultural management on the degradation of the land cover, namely the development of erosion processes. Based on the data [8], the consequences of erosion processes due to non-compliance with existing requirements are shown regarding the limits of establishing buffer protection zones. Figure 4.F2 shows the negative anthropogenic influence of the long-term development of mineral deposits, namely the change of agricultural land (1990, data from the Landsat 5 satellite) with anthropogenically modified landscapes, namely mud collectors and abandoned lands (2023, data from the Landsat 9 satellite). The total area of changes in the given fragment is 8.156 $km^2$. The paper [9] shows that the loss of agricultural land with an area of 13 ha is estimated at the monetary equivalent of 6.5 million dollars USA.

An example of a technogenic, ecological, and social disaster is the destruction of the Kakhovskaya HPP, which became a real disaster for a huge region in the lower reaches of the Dnieper up to its confluence with the Black Sea. This caused casualties among the local population in the flooded area, the death of domestic and wild animals, changes in natural and cultural landscapes, damage to buildings and infrastructure, and deterioration of water quality. The impact of the liquidation of reservoirs on the degradation of the land cover of the Ukrainian test site is shown in Fig. 4.F3. The water surface area of the Kakhov reservoir within the Ukrainian test site as of June 2, 2023, was 140 $km^2$, taking into account the average depth of the reservoir of 8.4 m [10], and the total volume was ~ 1.2 $km^3$. As a result of the explosion of the Kakhovskaya HPP dam on June 6, 2023, there is no permanent water mirror in the study area.

The expansion of agglomeration of cities, and irrational construction within agglomerations also leads to degradation consequences of the land cover, namely, loss of primary habitat, loss of biodiversity, etc. Figure 4.F4 shows an example of the expansion of the agglomeration of the city of Kryvyi Rih over 30 years using data from Landsat 5/9 and WorldView – 2 satellites. The lost area of agricultural landscapes due to construction is 0.57 $km^2$.

The conduct of hostilities on the territory of Ukraine leads to catastrophic consequences for the natural environment. An example of the negative modification of the agricultural landscape from the conduct of active hostilities during the war in Ukraine is shown in Figure 4.F6. The eco-destructive nature of the war consists not only in the direct extremely negative environmental consequences of the war but also in the long-term consequences of a collateral nature.

Irrational forestry practices are the cause of land cover degradation. Figure 5.F5 shows an example of deforestation, the indicated deforestation occupies 2027 $m^2$. The territory of the test site is located in the Steppe zone of Ukraine and is forest-deficient.

The destruction of vegetation due to fires caused by the human factor is shown in Figure 5.F7. For reference: when burning straw and harvest residues in conditions of low soil moisture, not only plant organic matter is burned, but also humus - the most fertile surface layer of the soil, as a result of which its microbiological activity decreases. This is considered an extreme degree of degradation.

https://doi.org/10.5593/sgem2024/2.1/s10.35

Therefore, the given quantitative and qualitative assessments of the specified degradation processes show that the territory of Ukraine falls under anthropogenic factors of the load on the natural environment.

## CONCLUSION

The cause-and-effect relationships of the process of land cover degradation under the influence of anthropogenic load have been established. The driving force behind these changes is human technical activity. On the basis of the conducted research, seven main complexes of various conditions (factors) that affect the process of degradation of the land cover have been determined. From the identified factors, the causes that generate degradation processes were singled out.

The obtained quantitative and qualitative assessments confirm and emphasize the level of anthropogenic load from technical activities (anthropogenic factor) on the natural environment of Ukraine. The interrelationship of intensive development in agriculture, mining, construction, and other human activities caused a high level of degradation within the studied territory.

The proposed methodical approaches, with the use of remote methods, make it possible to obtain and understand the long-term processes of the degradation of the land cover of Ukraine with the isolation of the anthropogenic component of influence on this process. Also, this approach can be used in further research for a differentiated approach to achieve the balanced potential of the economic complex of Ukraine, especially during the period of the country's military reconstruction.

## ACKNOWLEDGEMENTS

This project has received funding from the European Union’s Framework Programme for Research and Innovation Horizon Europe – the Framework Programme for Research and Innovation (2021-2027), Grant Agreement No. ID 101086250.

## REFERENCES

[1] Economics of Land Degradation and Improvement – A Global Assessment for Sustainable Development (2016). Ephraim Nkonya, Alisher Mirzabaev, Joachim von Braun (Eds). Springer Cham. 686 p. DOI: https://doi.org/10.1007/978-3-319-19168-3. Softcover ISBN: 978-3-319-36426-1

[2] ELD Initiative. (2015). The value of land: Prosperous lands and positive rewards through sustainable land management. 165 p. Available from www.eld-initiative.org. ISBN: 978-92-808-6061-0

[3] FAO and ITPS. (2015). Status of the World’s Soil Resources (SWSR) – Main Report. Food and Agriculture Organization of the United Nations and Intergovernmental Technical Panel on Soils, Rome, Italy. 607 p. ISBN: 978-92-5-109004-6

[4] IPBES. (2018). Summary for policymakers of the assessment report on land degradation and restoration of the Intergovernmental Science-Policy Platform on Biodiversity and Ecosystem Services. R. Scholes, L. Montanarella, A. Brainich, N. Barger, B. ten Brink, M. Cantele, B. Erasmus, J. Fisher, T. Gardner, T. G. Holland, F. Kohler, J. S. Kotiaho, G. Von Maltitz, G. Nangendo, R. Pandit, J. Parrotta, M. D. Potts,

S. Prince, M. Sankaran and L. Willemen (eds.). IPBES secretariat, Bonn, Germany. 44 p.

[5] IPCC (Intergovernmental Panel on Climate Change). (2019). IPCC Special Report on Climate Change, Desertification, Land Degradation, Sustainable Land Management, Food Security, and Greenhouse gas fluxes in Terrestrial Ecosystems: Summary for Policymakers. 42 p.

[6] Yelistratova L., Apostolov A., Lyalko V., Tomchenko O., Khyzhniak A., Hodorovsky A. (2022). The results of socio-ecological monitoring during military operations in Ukraine using satellite information. *Rev. Roum. Géogr./Rom. Journ. Geogr.*, 66(2), 117–136.

[7] Ievsiukov T. O., Martyn A., Elistratova L., Apostolov A., Kostyuchenko Yu. V. and Yuschenko M. (2018) An Investigation of the Impact of the Military Crisis in Ukraine on Agricultural Production and Land Resources in Crisis Territories: Approaches, Algorithms, and Methods. *in: Agricultural Production: Management, Opportunities and Challenges*, ed. by Sarah Waechter, Nova Science Publishers, USA, pp. 21-86. ISBN: 978-1-53613-719-4

[8] Water Code of Ukraine. (1995). Code dated 06.06.1995 No. 213/95-VR. https://zakon.rada.gov.ua/laws/card/213/95-%D0%B2%D1%80

[9] Starodubtsev V., Haychenko V., Ladyka M. (2023). The destruction of the Kakhovskaya HPP is a man-made, ecological and social disaster. National University of Bioresources and Nature Management of Ukraine. http://nubip.edu.ua/node/129547

[10] Svetlichny A.A. (2008). Studies of water erosion of soils and modern problems of erosion. Visnyk of Odesa National University. Geography and Geology. 13(6), 171.

https://doi.org/10.5593/sgem2024/2.1/s10.35

# UPDATING OF THE CADASTRAL MAP USING UNMANNED AERIAL VEHICLES IN SLOVAKIA

**Peter Kyseľ, MSc., PhD.**[1]

**Assoc. prof. Ľubica Hudecová, MSc., PhD.**[2]

**Hana Vesteg, BSc.**[2]

[1] Research Institute of Geodesy and Cartography in Bratislava, **Slovakia**
[2] Slovak University of Technology in Bratislava, Faculty of Civil Engineering, Department of Land Surveying, **Slovakia**

## ABSTRACT

A functioning land management is one of the key attributes of the successful management of a country. The cadastre of the real estate is one of the most important land management systems. However, for the successful management of land, the cadastre needs to be filled with complete and high-quality data. In Slovak Republic, the problem of the quality of cadastral data have been a long-discussed topic. One of the biggest quality issues of the cadastre is its map collection. Some of the maps in the cadastral map collection can originate up to the second half of the 19th century. The renewal of these maps is necessary to ensure the recording of real estates of a high quality. Besides the renewal of the cadastral maps, they also need to be constantly updated with new data. One of the main sources for the updating of cadastral maps is a measurement of a land surveyor. In Slovakia, the classical land surveying measurement methods are mainly used for the cadastral surveys nowadays, such as the GNSS-RTK method or polar method using a total station. However, the modern measurement methods, such as the photogrammetry using unmanned aerial vehicles (UAV photogrammetry), are getting into the routine land surveying practice, so their precision has to be tested. The main aim of this paper is to present the results of a cadastral survey of a small countryside land parcel using a DJI Phantom 4 RTK drone, which would then serve as a base for the cadastral map updating. The precision and effectiveness of this method would be compared to the classical measurement methods. The precision would be evaluated according to the now-effective Slovak cadastral regulations. Various approaches to the image processing and the measurement on the resulting products have also been tested.

**Keywords:** cadastre of real estate, unmanned aerial vehicle, photogrammetry, measurement

## INTRODUCTION

The cadastre of the real estate is one of the key components of the land management system in Slovakia. It includes positional and geometrical definition of real estates, as well as the ownership and other rights to these real estates. There is a great quantity of data in the cadastre originating in various periods, which means that their quality varies. The map collection is one of the most important parts of the cadastre. The biggest problem of the cadastral map collection is the inaccuracy of cadastral maps. Many of

these maps were originally created in the 19th century and they do not meet today's requirements for the precision and level of detail. Moreover, the newer maps include some errors, which decrease their precision. A complex renewal of the whole cadastral map collection is needed. Besides this complex renewal, it is also necessary to constantly update these maps. In the present, only classical land surveying methods are used for the measurements in the cadastre, mostly the GNSS-RTK method and the polar method using a total station. However, in recent years, there has been a new trend in the land surveying measurement – the photogrammetry using the images from unmanned aerial vehicles (UAV photogrammetry).

The topic of the use of photogrammetry in the cadastral surveys has been long known not only in foreign publications [1] [2] [3] but also in Slovakia [4]. The focus was mainly on the classical aerial photogrammetry but also on the cadastral surveys using ortho-rectified images or high-resolution satellite imagery. However, in recent years the focus has shifted in particular to the methods using the unmanned aerial vehicles (UAVs). The topic of using UAVs for cadastral surveys has been well analysed in several other countries, using UAV-derived orthomosaic [5], [6], stereo mapping on UAV imagery [7] and even an automatic extraction of cadastral boundaries from the products of UAV photogrammetry [8]. In the neighbouring Czech Republic, the accuracy analysis of the UAV photogrammetry and UAV laser scanning for cadastral purposes was carried out recently [9]. The results of the UAV photogrammetry can be used not only for cadastral surveys, but also for other purposes [10]. Moreover, the authors have carried out an analysis of the accuracy and efficiency of the UAV photogrammetry in a cadastral survey of a fishpond [11]. However, in Slovakia the UAV photogrammetry is not commonly used for updating cadastral maps and there are no official regulations concerning the use of this method for cadastral purposes.

The main aim of this paper is to analyse the accuracy and effectiveness of the UAV photogrammetry for the purpose of updating the cadastral map. The first part describes the process of planning and carrying out the UAV flight and the processing of the data as well as the process of precision evaluation in the Slovak cadastre. In the second half of the paper, the results of the UAV survey are described, and the overall precision and effectiveness of the method is assessed. This paper can serve as a basis not only for further research but also for creation of official regulations regarding the use of the UAV photogrammetry in cadastral surveys in Slovakia.

## MATERIALS AND METHODS

At the beginning, it was necessary to choose an area for testing the UAV photogrammetry for the updating measurement. The chosen area is located in the cadastral unit of Šoporňa in the Galanta district. This cadastral unit is approximately 50 km away from the capital city of Bratislava. The surveyed area is a typical Slovak countryside landscape, which includes family houses and gardens (Fig. 1). The update of the cadastral map involves a measurement of an older family house, which has been renovated recently and changed its shape during the renovation, and a new smaller building, which serves as a gardening tools storage. Besides the buildings, the surrounding land parcel and its close surroundings were also surveyed to provide a link between the new measurement and the currently valid cadastral map. The area of the surveyed location is approximately 12,000 square meters.

**Fig. 1:** Overview of a testing area (*source: Mapový klient ZBGIS [26-03-2024]).*

The images were shot with a DJI Phantom 4 RTK drone. It is equipped with 1" CMOS sensor with 20-megapixel resolution and mechanical shutter, which prevents the blur on images caused by the movement of the drone. This drone is also mounted with a GNSS module, which can utilize the real time kinematic measurement method (RTK). During our flight, the GNSS receiver was connected to the SKPOS national GNSS permanent network, which can provide coordinates in the national Unified Trigonometric Cadastral network (UTCN) coordinate system with high precision up to 1 cm using the RTK method. Its takeoff weight is 1391 g, which is ideal for work in the built-up areas.

Besides the GNSS-RTK measurement in the drone GNSS receiver, a set of 6 ground control points (GCPs) was determined. These GCPs were determined using a FOIF Geo Mini 10 GNSS receiver. The measurement was also connected to the SKPOS permanent GNSS network and the coordinates were determined in the UTCN coordinate system. The GCPs were evenly distributed over the surveyed area, their configuration is on Fig. 2, left. The GCPs were marked by blue crosses on the ground, which were made using a spray (Fig. 2, right).

The imaging flight was conducted using a combination of nadir and oblique imagery. The nadir imagery phase was planned with a planning application and the flight was conducted in an automatic mode. The height of the flight was set to 35 m, which resulted in the ground sampling distance (GSD) with approximately 1 cm value, and the speed was set to 2.7 m per second. The height and speed of flight in the oblique phase was set to the identical values but the UAV was piloted manually in this phase. The 70-80 % overlap between the images was also planned.


**Fig. 2:** Configuration (left) and marking (right) of GCPs.

The data were processed in the 3DSurvey photogrammetry processing software using a standard Structure-from-Motion practice. Besides the image processing tools it also includes the X-ray function, which provides an orthoimage of a point cloud, where the walls of the buildings are visible, and the CAD mode for the vectorization of point cloud and 3D model. The images were processed in three different scenarios according to the way of orientation of the images. In the first scenario, only the telemetry data were used for the orientation. In the second scenario, the telemetry data were combined with the GCP data. The last scenario utilized only the GCP data for the orientation of the images. After the orientation, computation of the dense point cloud, full 3D mesh and the orthomosaic, the X-ray orthomosaic was also computed and combined with the classical orthomosaic. This combined orthomosaic served as a primary source for the determination of coordinates of detailed points, which would be part of the update of the cadastral map. The precision of the point coordinates determined based on the UAV photogrammetry outputs was evaluated according to the Slovak cadastral regulations [12] by comparing the coordinates obtained by the UAV photogrammetry with the coordinates determined by a different measurement method. In this case, the coordinates of the points were measured using a combination of the GNSS-RTK and polar method and then compared to the coordinates from all of the image processing scenarios. For the new points, which would be included in the update, their mean coordinate error $m_{xy}$ should not exceed the value of 0.08 m. In practice it means that the positional deviation of coordinates between two different measurement methods should not exceed the value of 0.14 m. The efficiency of the UAV photogrammetry method was also evaluated by comparison of the time needed for the field work and office work between the UAV photogrammetry and the classical land surveying methods.

## RESULTS

The UAV flight with the DJI Phantom 4 RTK drone was conducted in the cadastral unit of Šoporňa in February 2024. The parameters of the flight were planned in advance using a flight planning application and for the nadir phase the UAV was flying autonomously monitored by a professional UAV pilot. In the oblique phase the UAV was piloted manually according to the planned flight parameters. Altogether, approximately 330 nadir and oblique images were taken. The whole UAV flight lasted approximately 10 minutes. Besides the UAV flight, the GCPs were also measured using a FOIF Geo Mini 10 GNSS receiver. The GCPs were determined using the RTK measurement method with the connection to the SKPOS national permanent GNSS

network. The determination of GCPs also took approximately 10 minutes, so the whole field work did not last more than 20 minutes.

The images were processed using the 3DSurvey photogrammetric software. The software adopts the standard Structure-from-Motion workflow. Three different scenarios were employed for the image processing based on the use of the flight telemetry and GCPs. The images were oriented either using only the flight telemetry (scenario no. 1), a combination of the flight telemetry and GCPs (scenario no. 2), or only with the GCPs (scenario no. 3). The coordinates of the cameras and the GCPs in the UTCN coordinate system were obtained using a transformation service provided by the authority for geodesy and cartography in Slovakia. In the scenario no. 1, the value of the maximum error in the camera position was 0.08 m. In the scenarios no. 2 and 3 the maximum error in the GCP position was 0.05 m. In all further steps of the processing, identical parameters were used for all the scenarios. After the bundle adjustment (global mode, 40,000 detected features, normal feature level detection) and the orientation, the dense point cloud (high level), the full 3D mesh (medium level, Fig. 3), and the orthomosaic (top-down, 2 cm/px resolution) were calculated. The X-ray image of the point cloud (60 % color transparency, 2 cm/px resolution) was also calculated and merged with the classical orthomosaic. The whole image processing took approximately 90 minutes.

**Fig. 3:** Full 3D mesh.

The second step of the data processing was the determination of points, which would be used for updating the cadastral map and assessing their precision. There were 15 points determined using the orthomosaic merged with the X-ray image of the point cloud in the CAD mode of the 3DSurvey software (Fig. 4). The same points were also determined using the classical land surveying methods – the GNSS-RTK method combined with the polar method. The equipment used was the FOIF Geo Mini 10 GNSS receiver and the Topcon GPT-7005 total station. This classical land surveying measurement in the field took approximately 1 hour. The positions determined based on the photogrammetric outputs and the land surveying measurement were compared and the positional deviations were calculated on each point. From these positional deviations, their average value, maximum value and root mean square error (RMSE) were determined for the assessment of the precision (Tab. 1).

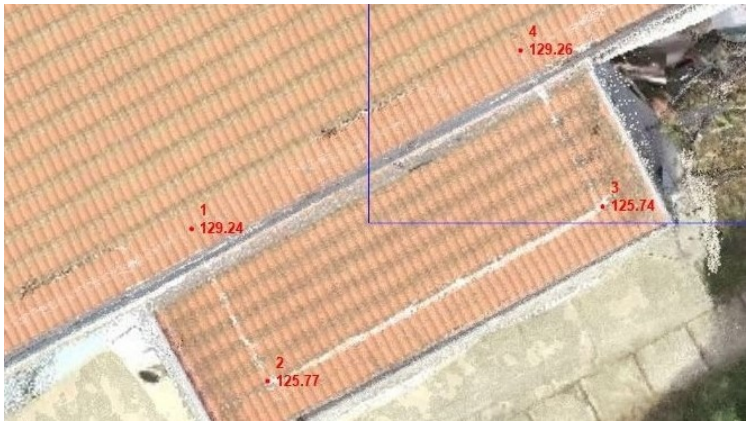


**Fig. 4:** Determination of points on the X-ray orthomosaic.

**Tab. 1:** Precision assessment of the UAV photogrammetry measurements

| scenario | No. 1 (telemetry only) | No. 2 (telemetry + GCPs) | No. 3 (GCPs only) |
|---|---|---|---|
| average positional deviation [m] | 0.03 | 0.04 | 0.03 |
| maximum positional deviation [m] | 0.07 | 0.09 | 0.09 |
| RMSE [m] | 0.039 | 0.042 | 0.036 |

## DISCUSSION

The main aim of the article was to assess the precision of the UAV photogrammetry for the purposes of updating the cadastral map. The precision of this method was assessed by way of comparison of the position of 15 check points, which would be part of the update, determined based on the photogrammetric products with the position determined using the classical land surveying methods (the GNSS-RTK and polar method), which are currently the main methods for the cadastral map updating. The results of the comparison (Tab. 1) show that the maximum value of positional deviation between the two different measurement methods was 0.09 m. This means that the precision of points according to Slovak legislation [12] was respected in all the check points. The average and RMSE values also show that most of the positional deviations were well below the maximum value. The overall results are very satisfying, and the UAV photogrammetry proved to be precise enough for the purposes of updating the cadastral map. All three scenarios of image processing also provided similar results. This means that for small areas, such as the testing area used in this paper, using only the telemetry data for the image orientation is sufficient to get data, which would be precise enough for the purposes of the cadastral map updating. However, it should be still recommended to use the GCPs as an additional verification of the precision, mainly for greater areas.

The second aim of the paper was to assess the effectiveness of the UAV photogrammetry for the purposes of updating of cadastral map. When using the UAV photogrammetry, the field work lasted up to 20 minutes and the image processing took approximately 90 minutes. The measurement of the points on the X-ray orthomosaic was very quick and took no more than 5 minutes. The overall time for the UAV

photogrammetry was 2 hours at most. The classical land surveying measurement with the GNSS receiver and total station took approximately 1 hour. In this case, the overall time needed for the classical measurement was shorter than the time needed for the UAV photogrammetry. From this amount of time, the image processing in the photogrammetric software took the longest. However, in the scenarios no. 2 and no. 3, the measurement of GCPs was the only step that had to be done manually, while the other steps were done automatically. In the scenario no. 1, where only the telemetry data was used for the image orientation, the whole process was fully automated using the batch processing tool. The image processing does not need to be monitored, so other activities can be done during this time. On the contrary, the time amount needed for the field work was vastly reduced with the UAV photogrammetry. Thus, it can be said that the effectiveness of the UAV photogrammetry is similar to or higher than that of the classical land surveying measurement. The additional benefit of the UAV photogrammetry is that it provides not only coordinates of the measured points but also other products, such as the point cloud, detailed 3D model of the area (Fig. 3), digital surface model or high-resolution orthomosaic, which can be used by many other professionals. However, testing of the precision and effectiveness of the UAV photogrammetry in the cadastral surveys of greater areas will be subject to further research.

## CONCLUSION

A functional land management system is one of the basic prerequisites for an effective administration of a country. The cadastral data need to have high quality and have to be up to date. This means that the cadastral maps also have to be constantly updated. In the present, only classical land surveying methods are used for the cadastral map updating in Slovakia. The UAV photogrammetry is not commonly used for cadastral surveys and only a few studies have focused on its use for this purpose in Slovakia. This paper deals with the assessment of precision and effectiveness of a cadastral map updating using the UAV photogrammetry. The update involved a registration of one new building and one older structure which has changed its shape. The verification of surrounding land parcel boundaries and nearby points is also part of the update. The field work was performed in February 2024 in the cadastral unit of Šoporňa in the western part of Slovakia using a DJI Phantom 4 RTK drone. For the precision assessment, coordinates of 15 check points were determined based on the photogrammetric products in three scenarios of image processing and compared to the coordinates determined by classical land surveying methods. The precision proved to be sufficient for the cadastral purposes in all the scenarios. The aim of the paper was also to assess the effectiveness of this method. The time needed for the field work and the processing of data obtained through the UAV photogrammetry was approximately twice as long as the time needed for the classical survey. However, the image processing in the photogrammetric software, which is a highly automated process, took most of the time, so it can be said that the overall effectiveness of the UAV photogrammetry is comparable to the classical surveys and can increase with the increase of the surveyed area. Another benefit of the UAV photogrammetry is that it provides not only the point coordinates, but also other products such as point clouds, 3D models or orthomosaics. Testing of this method in various conditions and greater areas will be subject to further research in Slovakia in the future.

**ACKNOWLEDGEMENTS**

This work was supported by the Ministry of Education of the Slovak Republic and the Slovak Academy of Science [grant number KEGA 001STU-4/2023].

**REFERENCES**

[1] Demir, O., Uzun, B., Çete, M., Turkish cadastral system, Survey Review, Vol. 40(307), pp. 54–66, 2008. DOI: http://dx.doi.org/10.1179/003962608X253484.
[2] Alkan, M., Solak, Y., An investigation of 1:5000 scale photogrammetric data for cadastral mapping uses: A case study of Kastamonu-Taskopru, African Journal of Agricultural Research, Vol. 5(18), pp. 2576–2588, 2010. ISSN 1991-637X.
[3] Ali, Z., Tuladhar, A. M., Zevenbergen, J. A., An integrated approach for updating cadastral maps in Pakistan using satellite remote sensing data, International Journal of Applied Earth Observation and Geoinformation, Vol. 18, pp. 386–398, 2013. DOI: http://dx.doi.org/10.1016/j.jag.2012.03.008.
[4] Horňanský, I., Ondrejička, E., Šuppová, I., Obnova mapového fondu od roku 1964 po súčasnosť, Zborník prednášok z 11. medzinárodnej konferencie o katastri nehnuteľností, pp. 18–35, Častá-Papiernička, 2014.
[5] Rijsdijk, M., et al., Unmanned Aerial Systems in the Process of Juridical Verification of Cadastral Border, ISPRS - International Archives of the photogrammetry, Remote Sensing and Spatial Information Sciences. Vol. XL-1/W2. pp. 325–331, 2013. DOI: http://dx.doi.org/10.5194/isprsarchives-XL-1-W2-325-2013.
[6] Sung, S. M. and Lee, J. O., Accuracy of Parcel Boundary Demarcation in Agricultural Area Using UAV-Photogrammetry, Journal of the Korean Society of Surveying, Geodesy, Photogrammetry and Cartography, Vol. 34(1), pp. 53–62, 2016. DOI: http://dx.doi.org/10.7848/ksgpc.2016.34.1.53.
[7] Chio, S., Chiang, Ch., Feasibility Study Using UAV Aerial Photogrammetry for a Boundary Verification Survey of a Digitalized Cadastral Area in an Urban City of Taiwan, Remote Sensing, Vol. 12, pp. 1682, 2020. DOI: http://dx.doi.org/10.3390/rs12101682.
[8] Crommelinck, S., et al., Interactive Cadastral Boundary Delineation from UAV Data, ISPRS Annals of the Photogrammetry, Remote Sensing and Spatial Information Sciences, Volume IV-2, pp. 81–88, Riva del Garda, Italy, 2018. DOI: http://dx.doi.org/10.5194/isprs-annals-IV-2-81-2018.
[9] Šafář, V., et al., The Use of UAV in Cadastral Mapping of Czech Republic. ISPRS International Journal of Geo-Information, Vol. 10, pp. 380, 2021. DOI: http://dx.doi.org/10.3390/ijgi10060380.
[10] Klapa, P., Mitka, B., Zygmunt, M., Integration of TLS and UAV data for the generation of a three-dimensional basemap, Geodesy and Cartography, Vol. 71(2), 2022. DOI:dx.doi.org/10.24425/agg.2022.141301.
[11] Kyseľ, P., Hudecová, Ľ., Cadastral Survey of a Fishpond Using UAV Photogrammetry, FIG e-Working Week 2021: technical programme and proceedings. Netherlands, 2021. ISBN 978-87-92853-65-3.
[12] Decree No. 461/2009 Coll. of the Office of Geodesy, Cartography and Cadastre of the Slovak Republic, implementing the Act No. 162/1995 Coll. on the real estate cadastre and the entries of ownership and other rights to the real estate (the cadastre act).

# SECTION

# CARTOGRAPHY AND GIS

# GEOSTATISTICAL MODELLING OF URBAN HEAT ISLAND EFFECT: ANALYSING THE RELATIONSHIP BETWEEN LAND USE PATTERNS AND LAND SURFACE TEMPERATURE IN LAGOS, NIGERIA

**Okeke Onyedikachi J**[1]
**Adurogangan Saheed O.**[2]
**Adedoyin Samuel J.**[2]
**Abiala F. Olufisayo**[2]
**Isaac Adedamola F.**[3]
[1]Department of Mathematics Statistics, University of New Mexico, Albuquerque **New Mexico, USA**
[2]Department of Remote Sensing and GIS, Federal University of Technology Akure, **Ondo State, Nigeria**
[3]Department of Teacher Preparation, Administration, and Leadership, New Mexico State University, Las Cruces, **New Mexico, USA**

## ABSTRACT

Rapid urbanization across Lagos, Nigeria has driven extensive land cover modifications with significant climatic impacts. This study analyzed interlinkages between land use land cover (LULC) transformations and land surface temperature (LST) shifts in the intensely developing Lagos suburb of Ikorodu from 1991-2021 utilizing robust geospatial techniques. Multi-spectral Landsat 5, 7 and 8 data enabled reliable LULC classification into five covers using a Random Forest algorithm. Subsetting the Ikorodu area facilitated localized change analyses across 1991, 2001, 2011 and 2021. LULC changes significantly impacted regional microclimates by altering surface energy budgets. Replacing vegetation with constructed materials increased LSTs while diminishing humidity via lower transpiration. Quantifying alteration magnitudes and spatial patterns provided crucial historical perspectives on urban expansion and climatic changes. Over 30 years, built-up area rose from 14% to 65% while vegetation declined from 52% to 9%, with LST increasing from 23.13°C to 27.21°C. Statistical analyses indicated LST strongly, and positively correlated with a Built-Up Index. Cooling prevailed on semi-rural peripheries with more intact vegetation. This research demonstrates and models LULC-LST interlinkages over years of swift development around Lagos, delivering a framework for crafting sustainable growth policies and balancing modernization goals with ecological stability. Explicit urban heat island effect mitigation strategies combining infrastructural adaptations and green space retention are recommended to promote regional climate resilience.

**Keywords:** Land Use Land Cover (LULC), Land Surface Temperature (LST), Urban growth, Spatial Statistics, Geographic Information System.

## INTRODUCTION

Global urbanization has driven extensive land use and land cover (LULC) modifications, with major implications for local climates. Specifically, the proliferation of artificial impervious surfaces coupled with declining vegetation enhances the phenomenon of urban heat islands (UHIs) [1]. Rapid and vast urban growth in Lagos, Nigeria has rendered understanding associated thermal shifts critical. This research examined the interrelationship between LULC transformations and land surface temperatures (LSTs) in the severely urbanizing area of Ikorodu over 30 years utilizing a robust geographic information system and remote sensing methodologies. LULC dynamics significantly impact regional microclimates by influencing surface energy budgets. Replacing natural covers with constructed materials alters heat storage and radiation properties, typically elevating LSTs [2]. Relatedly, diminishing vegetation decreases transpiration and humidity, further escalating warming [3]. Lagos has exhibited extreme growth and environmental degradation. Ikorodu specifically has undergone extensive development and population surges, with inevitable thermal repercussions [4]. While prior analyses have modelled Nigerian LULC-LST interlinkages [5], finer-resolution Ikorodu focus has been lacking. This research addressed these knowledge gaps. Multispectral Landsat 5, 7, and 8 data enabled reliable LULC classification into key covers [6]. Extracting LSTs from thermal bands facilitated examining LULC ties [7]. Subletting Ikorodu enabled localized change analyses across 1991, 2001, 2011 and 2021. Quantifying alteration magnitudes and spatial patterns offered crucial historical perspectives. Statistical tests evaluated variable correlations and UHI presence. Findings illuminated LULC transitions potentially driving climatic shifts in Ikorodu specifically. Recommendations target urban designers and policymakers for crafting suitable growth strategies balancing modernization and environmental protection. This project delivered a replicable framework and actionable intelligence for sustaining safer, sustainable Lagos expansion.

## MATERIALS AND METHOD

### 2.1 Study area description

Ikorodu is a city and Local Government Area situated in Lagos State, Nigeria along the Lagos Lagoon. Encompassing a total land area of 345 km2, it is bounded by geographic coordinates $6^{0}31'30"N$, $6^{0}42'30"N$, and longitudes $3^{0}25'30"E$ and $3^{0}42'30"E$ (Figure 1.1). The city experiences a tropical climate with average temperatures around 26°C, a distinct wet season from April to October and a pronounced dry season from November to March [9]. As Lagos State's largest local government jurisdiction and second most populous city, Ikorodu

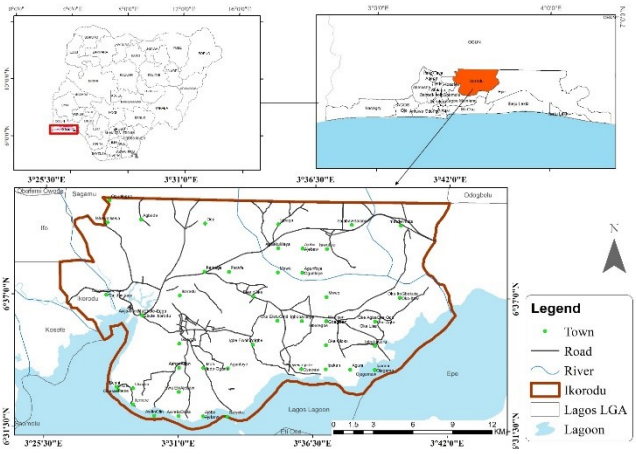


*Figure 1: The Study Area Map showing Ikorodu, Towns, Roads, and Rivers, Lagos state, Nigeria.*

houses over one million residents as of 2022, reflecting massive growth at 5.26% annually per World Population Review projections [10]. Located approximately 36 kilometres northeast of the Lagos central business district and 26 kilometres from the state capital Ikeja, Ikorodu spans 18 kilometres east to west paralleling the Lagos Lagoon shoreline. Along with most of the Lagos State, the Local Government Area occupies relatively flat low-lying terrain with gently undulating features. The climate mirrors broader Nigeria conditions given its tropical position, marked by distinct wet versus dry seasonal phases [9].

### 2.2 Data and Method

This study leveraged three key software platforms for conducting the geospatial and satellite imagery analysis: ArcGIS Pro, Google Earth Engine, and GeoDa. ArcGIS Pro facilitated two and three-dimensional data visualization, mapping, editing, and spatial analysis. Google Earth Engine provided a robust cloud-based system for accessing multi-petabyte global satellite datasets spanning decades and enabled complex pixel-level computations required for tracking earth surface changes over time. GeoDa supplied critical capabilities for spatial regression modelling, clustering analysis, and autocorrelation assessments essential for relating land characteristics to temperature shifts.

**Table 1: Data sets**

| s/n | Data | Variables | Year | Source | Format |
|---|---|---|---|---|---|
| 1 | Landsat 5,7 & 8 satellite Images | Landuse/cover Classification | 1991,2001,2011,2021 | Google Earth Engine https://earthengine.google.com/ | Raster |
| 2 | Administrative boundaries | Lagos State and Local Government Area boundary | recent | GRID3 https://grid3.gov.ng | Shapefiles |
| 2 | Open Street Map (OSM) | Landuse type & Rivers | recent | OpenStreetMap https://download.geofabrik.de/africa/nigeria.html | Shapefiles |

Together these technologies enabled comprehensive geographic information system processing, land cover classification, land surface temperature derivations, and statistical modelling suited for evaluating the intricate relationships between urban expansion and climatic impacts in the intensely developing Lagos region using publicly available historical earth observation sources. the methodology for a land use/land cover (LULC) change analysis using satellite imagery from 1991-2021.

## Random Forest

Supervised classification using a Random Forest algorithm [11] was implemented to classify imagery into five classes. The Random Forest (RF) algorithm was used for land use/land cover (LULC) classification in this study. The prediction equation for RF is given below:

$$y(x) = mode_{b=1}^{B}[T_b(x)]$$

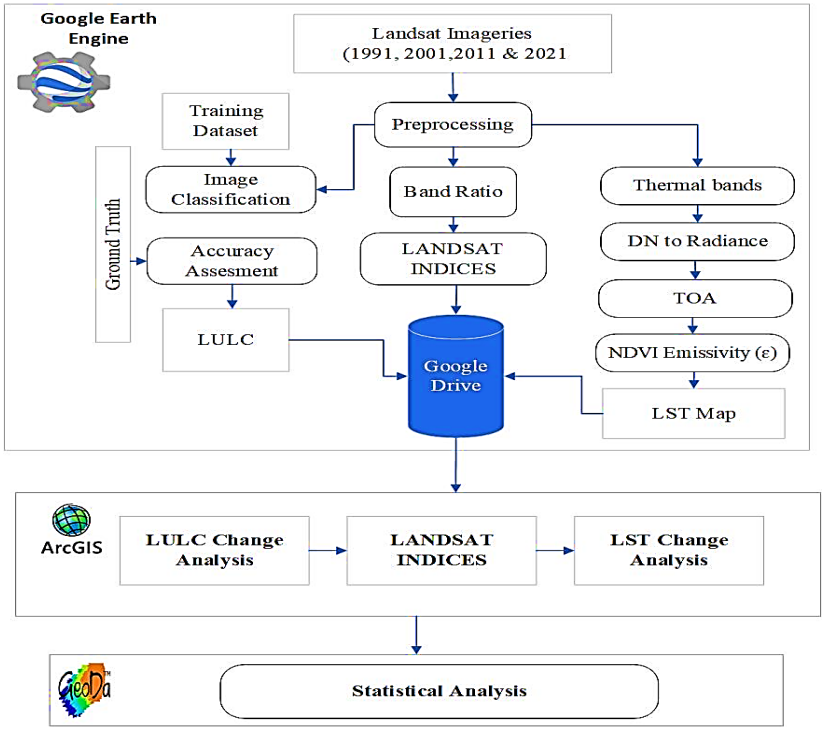


*Figure 2: Analysis Flowchart*

$y(x)$ is the predicted LULC class for a pixel $x$, the number of decision trees in the RF model is $B$ and $T_b(x)$ is the prediction from the bth decision tree for input x mode is used to select the majority voted class. which is the value that appears most frequently in the set of predictions from all decision trees. The RF algorithm has numerous implementations of classification and regression trees (CART) as base learners [11]. The training data with labels was used to build these CART models. During prediction, the input pixel x is fed to each of the B decision trees, and a LULC class is predicted by each tree. The RF algorithm then takes the mode or majority vote of all the B trees to assign the final label to that pixel. This ensemble method leverages multiple deep CART models to improve classification accuracy.

Accuracy assessment was performed by comparing classified pixels to reference data [12]. Overall accuracy ranged from 92-97% across years. The Kappa coefficient,

measuring agreement between classification and validation data indicated moderate to strong agreement [12].

**Normalized Indices**

The Normalized Difference Vegetation Index (NDVI) uses the near-infrared NIR and Red bands to observe vegetation greenness globally.

$$NDVI = \frac{NIR - RED}{NIR + RED}$$

It ranges from -1 to 1, with higher positive values indicating healthier, denser vegetation [13]. The Normalized Difference Built-up Index (NDBI) characterizes land development and urbanization using SWIR and NIR bands.

$$NDBI = \frac{SWIR - NIR}{SWIR + NIR}$$

Higher positive NDBI values indicate built-up areas, while negative values indicate water bodies [14]. The Normalized Difference Water Index (NDWI) The Normalized Difference Water Index (NDWI) enhances water-related features in landscapes using NIR and SWIR bands.

$$NDWI = \frac{NIR - SWIR}{NIR + SWIR}$$

It efficiently extracts water information in most cases [13].

**Conversion of DN values to Radiance Sets**

The equations using Landsat bands and metadata are applied to convert DN values to spectral radiance and eventually at-sensor brightness temperature for land surface temperature (LST) corrected for spectral emissivity is computed as follows LST = $\frac{T_B}{\left(1+\left(\lambda\frac{T_B}{\rho}\right)+\ln\varepsilon\right)}$ retrieval. While $L\lambda = \frac{L_{max}\lambda - L_{min}\lambda}{Q_{cal.Max} - Q_{cal.Min}} * (Q_{cal} - Q_{cal.Min}) + L_{min}\lambda$, $L\lambda$ is the spectral radiance, $Q_{cal}$ the quantized calibrated pixel value in DN, $L_{min}\lambda$ a radiance scaled to $Q_{cal.Min}$ while $L_{max}\lambda$ is a radiance scaled to $Q_{cal.Max}$ and for Landsat OLI-TIRS, DN values were converted to Radiance using the equation below, making use of the rescaling factors provided in the metadata file [15]. $L\lambda = ML * Qcal + AL$, where $L\lambda$ = TOA Reflectance, $L\lambda$ = Reflectance additive scaling factor for the band, Qcal = L1 pixel value in DN, $L\lambda$ = Band-specific multiplicative rescaling factor from the metadata. The spectral Radiance that was obtained from converting DN values was further converted to at-sensor brightness temperature using $TB = \frac{K^2}{In(\frac{K_1}{L_\lambda}+1)}$ TB represents the brightness temperature, measured in Kelvin, K is a constant value associated with the thermal band, ln denotes the natural ($In$) logarithm function, $K_1$ is a band-specific thermal conversion constant obtained from metadata, where x is the thermal band number, and Lλ represents Top of Atmosphere (TOA) reflectance, which is the ratio of observed radiance to the radiance from a perfect reflector in remote sensing [15][16].

**Determination of Surface Emissivity**

Determination of Surface Emissivity The NDVI threshold method determines surface emissivity using NDVI to calculate the proportion of vegetation ($Pv$) using the equation $Pv = \left(\frac{\text{NDVI}-\text{NDVI}_{\text{min}}}{\text{NDVI}_{\text{max}}-\text{NDVI}_{\text{min}}}\right)^2$ [12].Now that the NDVI and $Pv$ have been calculated, the Surface Emissivity ε can now be determined using the equation $\varepsilon = 0.004 * Pv + 0.986$ which ε is the Surface Emissivity and 0.986 the Correction value of the equation.

**Change Detection**

For the Change Detection LULC change detection compares classified maps from different years to analyze changes over time using the rate of change formula.

$$R(\%) = \frac{(A_2 - A_1)}{(t_2 - t_1)} * 100$$

$R(\%)$ Represents the percentage change, where $R$ is the symbol for the percentage change. The formula calculates the percentage change between two values ($A_1$ and $A_2$) over a specified time interval ($t_1$ to $t_2$). The numerator ($A_1$ and $A_2$) represents the absolute change in the variable, and the denominator ($t_2 - t_1$). $A_1$ ) normalizes this change relative to the initial value.

LULC changes were detected by comparing classified maps of an area from 1991-2021 at 10-year intervals. The rate of change for each LULC class was calculated using a formula that quantifies the proportional area change normalized by the time difference. This yields either a positive or negative rate, indicating if the coverage of a particular LULC type increased or decreased [17].

**RESULT**

The analysis revealed significant 1991-2021 land use change in Ikorodu LGA (fig .3), with loss of natural vegetation and expansion of urban areas [8]. Key drivers are urbanization, population growth, and economic development. Such changes degrade habitats, increase disasters like flooding, and alter local climate [9].

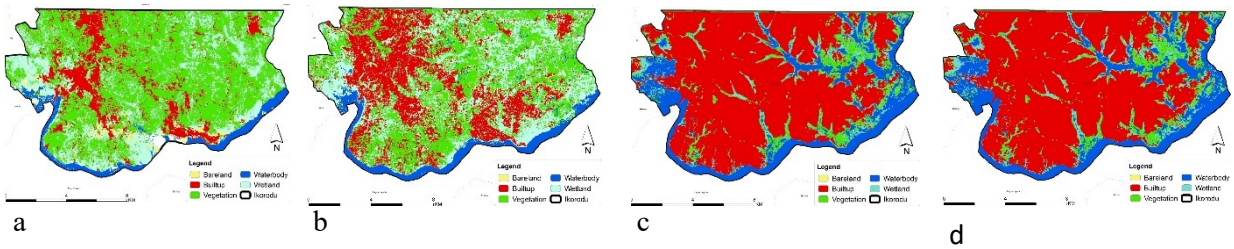


*Figure 3: Map showing Landuse/cover of Ikorodu in a)1991, b)2001, c)2011 & d)2021.*

The observed LST trends (fig. 4i) rising for built-up areas while decreasing for vegetation match prior evidence [18]. Factors impacted by urbanization like moisture and air temperature influence land surface temperature. Vegetation decline (falling NDVI) and urban growth (fig. 4ii) over 30 years drove LST increases. Aligning with wider trends, maximum temperatures rose 0.15°C annually [9].

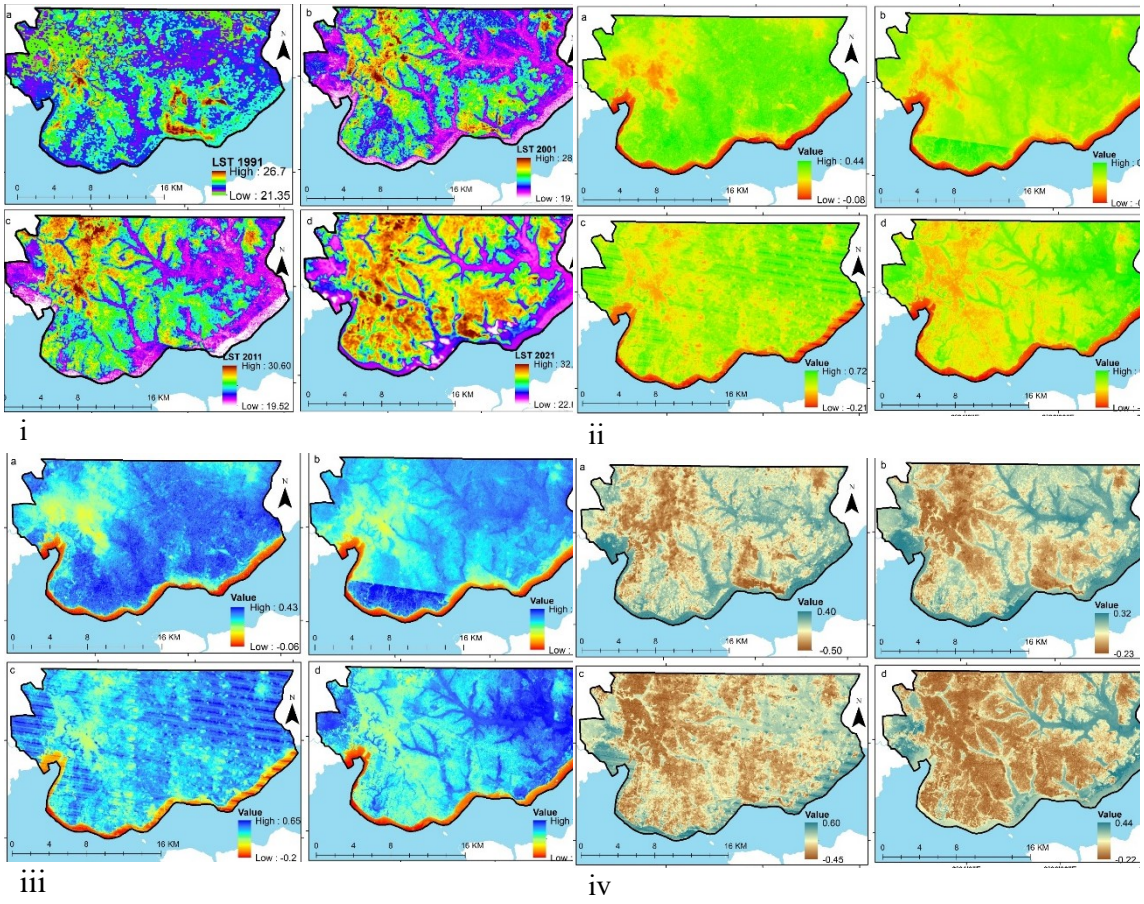


*Figure 4: (i) LST Map, a) 1991, b) 2001, c) 2011, d) 2021. (ii) NDVI Map of a) 1991, b) 2001, c) 2011, d) 2021. (iii) NDWI Map of a) 1991, b) 2001, c) 2011, d) 2021. (iv) NDBI Map of a) 1991, b) 2001, c) 2011, d) 2021.*

Mirroring the proliferation of impervious surfaces that trap solar heat, LST heat zones shifted to higher temperatures as urban lands expanded [19]. Vegetation's evaporative cooling and lower thermal inertia decrease LST amplitude compared to the built environment. Strategies like green roofs, cooler neighbourhood microclimates, and low-energy buildings can mitigate the urban heat island effect towards sustainable development [20].

**Table 2: Analysis of variance result**

| Source | DF | Sum of squares | Mean squares | F | Pr > F |
|---|---|---|---|---|---|
| **Model** | 1 | 9.131 | 9.131 | 7.743 | **0.006** |
| **Error** | 389 | 458.697 | 1.179 | | |
| **Corrected Total** | 390 | 467.828 | | | |
| ***Computed against model Y=Mean(Y)*** | | | | | |

**Table 3: Model parameters**

| Source | Value | Standard error | t | Pr > \|t\| | Lower bound (95%) | Upper bound (95%) |
|---|---|---|---|---|---|---|
| **Intercept** | 20.638 | 0.898 | 22.976 | **< 0.0001** | 18.872 | 22.404 |
| **25.152356** | 0.092 | 0.033 | 2.783 | **0.006** | 0.027 | 0.156 |

Tables 2 & 3 show results from a statistical model analyzing the relationship between land surface temperature (LST) and an independent variable over 30 years in Ikorodu. With 389 degrees of freedom, the model is significant (p=0.006) in explaining variation in LST, the dependent variable. The model parameter estimates indicate a positive relationship between LST and the predictor variable, with a slope coefficient of 0.092 9 (fig.5). This means that on average, a 1 unit increase in the independent variable is associated with a 0.092 unit rise in LST. The t-test shows this effect is unlikely due to chance (p=0.006).

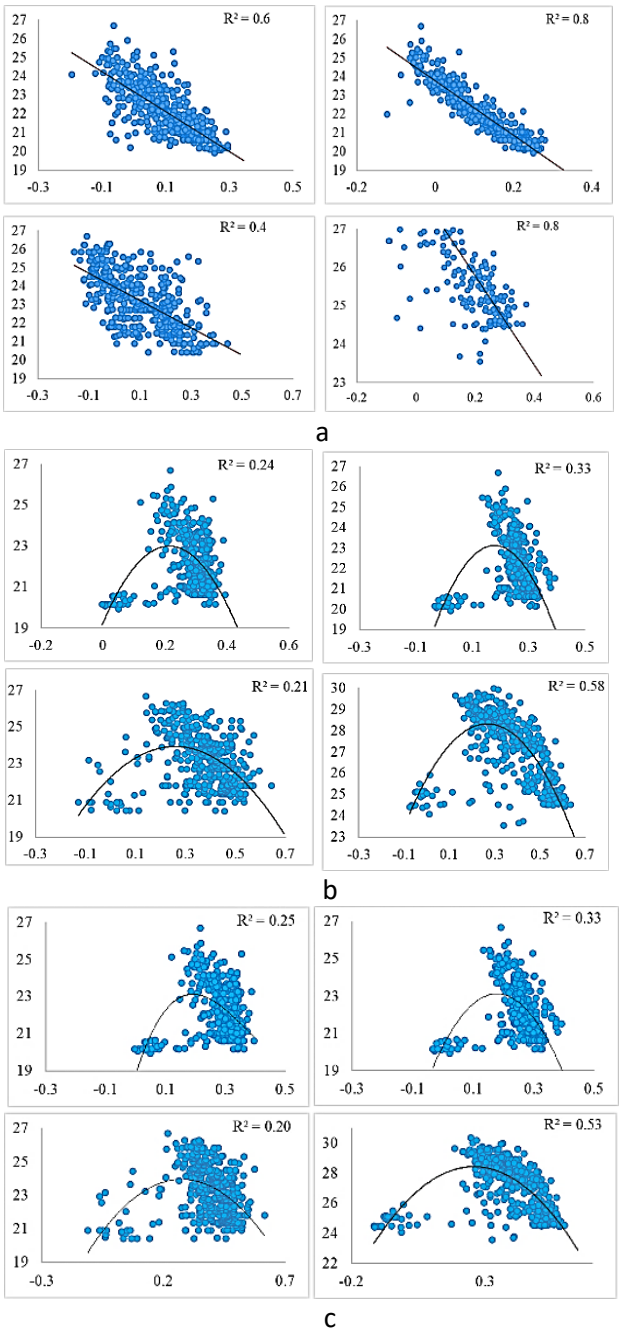


*Figure 5: (a) Correlation between LST and NDBI in 1991, 2001, 2011, and 2021, (b) Correlation between LST and NDVI in 1991, 2001, 2011, and 2021, (c) Correlation between LST and NDWI in 1991, 2001, 2011, and 2021*

Urban expansion and vegetation loss explain the rise in LST since human-made infrastructure stores and emits more heat than natural ecosystems [21]. Cooler temperatures prevailed on the semi-rural fringes where vegetation remained intact [19]. This spatiotemporal analysis quantified built land's influence on LST over three decades of rapid development in Lagos State, Nigeria. Urban planners should consider "cool city" interventions like reflective building materials, green spaces, revegetation programs, and infrastructure to boost ventilation and shading [14]. These counter the heat-trapping effects of dense construction and land cover change. Zoning policies could concentrate mid-rise eco-buildings downtown while preserving agricultural greenbelts [8].

## CONCLUSION

Urban expansion's impact on land surface temperature (LST) also has public health implications due to heat-related illnesses [18]. As Lagos rapidly develops, explicit urban heat island policies could promote sustainability and climate resilience. Integrating engineering and ecological strategies may optimally tackle extreme heat [16][20]. This study revealed Ikorodu's high urbanization rate, occupying 65% of land by 2021 versus 14% in 1991. Deforestation and loss of open spaces accompanied this, causing mean LST to rise from 23.13°C (1991) to 27.21°C (2021). Temperature will likely continue increasing under business-as-usual urban growth. Expanding the statewide tree planting initiative to Ikorodu could create cool zones benefiting the quality of life [17]. Future research should explore LST's socioeconomic impacts and model the statistical relationship between LST and urbanization in greater depth [18]. As Lagos develops, evidence-based urban planning and policymaking can balance economic growth with ecologically sustainable climate resilience.

## REFERENCES

[1] Stewart, I. D., & Oke, T. R. (2012). Local climate zones for urban temperature studies. Bulletin of the American Meteorological Society, 93(12), 1879-1900. https://doi.org/10.1175/BAMS-D-11-00019.1

[2] Voogt, J. A., & Oke, T. R. (2003). Thermal remote sensing of urban climates. Remote sensing of environment, 86(3), 370-384. https://doi.org/10.1016/S0034-4257(03)00079-8

[3] Ramachandra, T. V., Bharath, H. A., & Durgappa, D. S. (2012). Insights into urban dynamics through landscape spatial pattern analysis. International Journal of Applied Earth Observation and Geoinformation, 18, 329-343. https://doi.org/10.1016/j.jag.2012.03.005

[3] Oyinloye, M. A., & Adesina, F. A. (2011). Urbanization: Challenges in Modern Africa. Asian Economic and Financial Review, 1(1), 1.

[5] Adeyeri, O. E., Akinsanola, A. A., Ishola, K. A., Arason, T., & Ebhuoma, E. E. (2017). Assessing the relationship between land surface temperature and land use land cover of Lagos Nigeria. Journal of Applied Geography, 86, 177-193. https://doi.org/10.1016/j.jag.2017.01.020

[6] Jensen, J. R., & Cowen, D. C. (1999). Remote sensing of urban/suburban infrastructure and socio-economic attributes. Photogrammetric engineering and remote sensing, 65(5), 611-622. https://doi.org/10.14358/PERS.65.5.611

[7] Chander, G., Markham, B. L., & Helder, D. L. (2009). Summary of current radiometric calibration coefficients for Landsat MSS, TM, ETM+, and EO-1 ALI sensors. Remote sensing of environment, 113(5), 893-903. https://doi.org/10.1016/j.rse.2009.01.007

[8] Adeoye, N. O., Adeyemo, A. B., & Oladapo, O. D. (2018). Spatio-temporal dynamics of urban expansion in Lagos state. Journal of Sustainable Development Studies, 12(1), 1-23.

[9] Akinsanola, A. A., & Ogunjobi, K. O. (2014). Analysis of rainfall and temperature variability over Nigeria. Global Journal of Human-Social Science Research.

[10] World Population Review. (2022). Ikorodu, Nigeria Population 2022. World Population Review. https://worldpopulationreview.com/world-cities/ikorodu-population

[11]Breiman, L. (2001). Random forests. Machine learning, 45(1), 5-32. https://doi.org/10.1023/A:1010933404324

[12] Landis, J. R., & Koch, G. G. (1977). The measurement of observer agreement for categorical data. biometrics, 159-174. https://doi.org/10.2307/2529310

[13]Rouse, J. W., Haas, R. H., Schell, J. A., & Deering, D. W. (1974). Monitoring vegetation systems in the Great Plains with ERTS. NASA special publication, 351, 309.

[14] Zha, Y., Gao, J., & Ni, S. (2003). Use of normalized difference built-up index in automatically mapping urban areas from TM imagery. International Journal of Remote Sensing, 24(3), 583-594. https://doi.org/10.1080/01431160304987

[15] USGS (2016). Landsat 8 (L8) Data Users Handbook. Department of the Interior U.S. Geological Survey. https://www.usgs.gov/centers/eros/landsat-8-l8-data-users-handbook

[16] Markham, B. L., & Barker, J. L. (1986). Landsat MSS and TM post-calibration dynamic ranges, exoatmospheric reflectances and at-satellite temperatures. EOSAT Landsat technical notes, 1(1), 3-8.

[17] Ayanlade, A. (2017). Assessing influences of city growth dynamics on urban heat island phenomena. Climate, 5(4), 79. https://doi.org/10.3390/cli5040079

[18] Ullah, S., You, Z. J., Ullah, W., Zhang, H., & Wang, T. (2019). Factors influencing surface urban heat islands in South Asia. Science of the Total Environment, 658, 1346-1356. https://doi.org/10.1016/j.scitotenv.2018.12.206

[19] Gui, X., Wang, L., Yao, R., & Yu, D. (2019). Investigating the urbanization process and its impact on vegetation change and urban heat island in Wuhan, China. *Environmental Science and Pollution Research, 26*(30), 30808–30825. https://doi.org/10.1007/s11356-019-05725-x

[20] Deilami, K., Kamruzzaman, M., & Liu, Y. (2018). Urban heat island effect: A systematic review of spatio-temporal factors, data, methods, and mitigation measures. International journal of applied earth observation and geoinformation, 67, 30-42. https://doi.org/10.1016/j.jag.2017.12.009

[21]Asaeda, T., Ca, V. T., & Wake, A. (2016). Heat storage of pavement and its effect on the lower atmosphere. Atmospheric Environment, 128, 413-427. https://doi.org/10.1016/j.atmosenv.2015.10.037

# TOPOGRAPHIC STUDY NECESSARY FOR THE UPDATE OF THE CARTOGRAPHIC BASE NECESSARY FOR THE EXECUTION OF THE FOREST MANAGEMENT IN THE LOCATION OF DRINOVA, ROMANIA

**Assoc. Prof. Ph. D. Bârliba Luminita Livia**[1]
**Assoc. Prof. Ph. D. Bârliba C.**[1]
**Assoc. Prof. Ph. D. Eles G.**[2]
**Assoc. Prof. Ph. D. Loredana Copacean**[1]
**Bârliba C. Florin**[3]
[1] University of Life Sciences "King Michael I" from Timisoara, **România**
[2] Politehnica University of Timisoara, **România**
[3] Authorized Individual, Timisoara, **România**

## ABSTRACT

The Lugoj Forest Administration is a subunit of the Timiș Forestry Directorate and is located in the western part of Romania in the hilly area of Timiș County. It has as its object of activity the application of the Romsilva strategy for the forests received under administration, the conservation and sustainable development of the publicly owned forest fund of the state, the management of the hunting and fishing funds assigned according to the law, the harvesting and valorization of specific forest products according to the legal provisions in conditions of efficiency economic, also exercising public service duties with specific forestry.[1]

The management of forests represents the set of concerns and measures aimed at ensuring the bringing and keeping of forests in an appropriate state from the point of view of the ecological, economic and social functions that they perform.

The inventory and record activity of the forest fund is based on topographical measurement works, pedological maps and parcel descriptions showing all the factors on which the production and optimal utilization of forest products depends.

The aim of the paper was to update the cartographic base of the forestry fund of the Lugoj Forest Ring Road, of which only one production unit is presented, because the documentation is very extensive. [2] [3]

A GPS was used for the topographic surveys of the boundaries of the forest bodies using the static method and the Stop & Go kinematic method, and the Autodesk AutoCAD - Raster Design package was used to process and draw up the cartographic documentation in order to create the thematic digital maps.

**Keywords:** topographic study, cartographic base, cadastral plan.

## INTRODUCTION

The total area of the forest fund managed by the Timiş Forest Directorate through the six forestry enclaves is 77,515 ha, which represents about 11% of the area of Timiş county, respectively 2.4% of the area of state forests managed by RNP-Romsilva. [4]

By species group, the area of the state-owned forest fund is distributed as follows: 6.0% softwood, 33.6% beech, 37.7% oak, 19.4% various hard species and 3.3% various soft species. (Figure 1.)

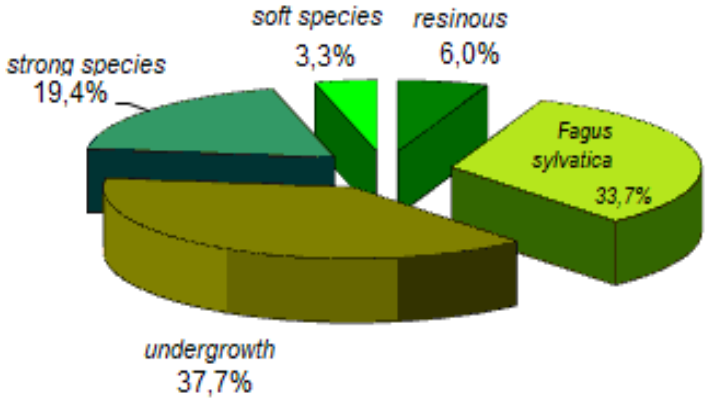


**Figure 1. The Forest Fund of Timiș County** [5]

The Lugoj Forest Administration is a subunit of the Timiș Forestry Directorate within the National Forestry Authority - Romsilva.

The publicly owned forest fund of the state with an area of 12185.39 ha administered by the Lugoj Forestry includes the publicly owned forests of the state located in the west of the country, within the boundaries of Timiș counties (in proportion to 99.7%), Arad (in proportion to 0, 2%) and Caraș-Severin (in proportion to 0.1%), in the southeastern part of Timiş county, respectively in the meadow, the plain and the low hills on the slopes of the Bega river but also the left slope of the Timiş river. [8] [9]

Considering an administrative point of view, the area of the bypass is located in Timiș County, on the UAT radius: Lugoj, Coșteiu, Bethausen, Bârna, Traian Vuia, Fârdea, Nădrag, Găvojdia, Știuca, Victor Vlad Delamarina, Darova, Ohaba Lungă, Mănăștiur, Bara, Făget, in Arad County on the UAT radius: Bata, Birchiș, Ususău and in Caraș-Severin County on the UAT radius: Fârliug, Copăcele. [11]

The Lugoj Forest Administration is divided into 6 production units (U.P. I, II, III, IV, V, VI) with access to the national roads DN6 (E70) Caransebeș - Lugoj - Timișoara, DN68A (E673) Ilia - Făget - Lugoj and DN58A Lugoj - Fârliug - Soceni.

Consequently, the production units have a pronounced administrative character. If within a production unit established in this way there are trees to which a management regime different from the common regime is to be applied, for most of the trees in the respective unit, those can constitute production sub-units. Production units are quite homogeneous in terms of natural production conditions and can have the same destination, they form, in their entirety, the object of a layout. [6]

The production unit III Drinova is topographically located in the area of the middle and low hills of Lugoj municipality (Figure 2.).

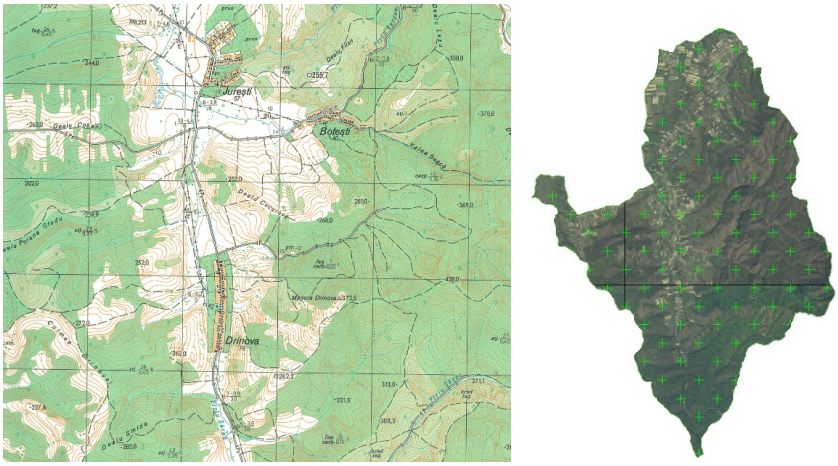


**Figure 2. The forest fund of the Drinova Production Unit, Timiș County**

The total area of the production unit is 3156.85 ha and is divided into 141 plots and 391 sub-plots and is part of four administrative-territorial units, these being Bârna, Fârdea, Lugoj and Nădrag. [7]

For the determination of the surfaces and the production unit maps, returned aerial photogrammetric plans with contour lines at a scale of 1:5000 was used for the entire area of 3156.58 ha, corrected with recent orthophoto plans and measurements made with GPS technology. [10]

## MATERIAL AND METHOD

In order to prepare the conditions of a forest management, the following steps are necessary: the creation of a topographical plan for each forestry management unit, which contains details related to exploitation needs; the division of the total area of the forestry management unit into homogenous parcels from an economic-forestry point of view; description of the plots obtained.

The way a forest is organized depends on the circumstances in which it is located: natural, economic, social. The prior information about them constitutes the first step in the forest development action and is achieved through a general recognition (of the situation). For this purpose, the landscaper first orients himself on maps, by photograms and various other sources of information. Then, also on maps or topographical plans, he projects the expected solutions for the organization (planning) of the forest and figures the way and manner of development in time and space of the works planned for this purpose.

For the execution of the topographic surveys, a GARMIN type GPS equipment was used (Figure 3.), used to identify the limits for the entire surface, respectively a GPS South V82 (Figure 4.). with the radio antenna to determine the limits, where they were not clear, respectively checking all the limit posts.

The methods used to carry out the work are GPS and AutoCad. To perform the GPS measurements, the following operations were carried out: planning and designing the static and kinematic measurements, performing and processing the measurements. The fundamental condition that had to be respected in the case of measurements consisted in

the permanent reception of the signals emitted by at least four satellites, both during the stationing and in the time intervals in which the movement from one station to another is made.


**Figure 3. GPS GARMIN**

**Figure 4.GPS SOUTH S82**

AutoCad was used to process the data collected from the field, but especially AutoCad Raster Design. The cartographic base used for the current layout consists of topographic plans at a scale of 1:5000. To determine the surfaces, measurements were carried out with GPS technology, and when drawing up and updating the maps within the layout, they were overlaid with satellite images of the orthophotoplan type recently made, namely in 2018, made available by O.C.P.I. Timis.

## RESULTS AND DISCUSSION

To carry out the measurements carried out in the field, the following aspects were taken into account:

- Establishing methods of working in the field in order to make topographic measurements more efficient with high precision results;

- Establishing the equipment used;

- Choosing an optimal period for measurements;

- Identification of the boundaries, parcel and sub-parcel boundaries, borders and the production unit limit;

- Processing data collected from the field.

Plot boundaries are mostly natural, with obvious landforms such as water or, in the case of isolated plots, the edge of the forest.

The boundaries of the state-owned forest fund are marked with signs specific to each forest body, applied to the boundary trees and at the same time through the posts. Within the territorial limits of the parcel unit under study, the state-owned forest fund is adjacent to the forest fund owned by legal entities, natural persons, with pastures and hayfields owned by local residents of the neighboring villages.

Borders are represented by boundaries, being materialized by parcel boundary, parcel unit or detour signs (Figure 5.).

**Figure 5. Forest marking**
**for a plot** **for sub-plot**

Following the measurements made on the parcel boundaries located in the land and their processing on basic topographic plans, it was found that, in some situations, the boundary existing in the land does not coincide with the one on the development plan. Due to this fact, it was necessary to create new plans based on real bases existing in the field and determined geodetically.

The bollards are made of reinforced concrete, they have the number written in red paint on a white background, being also materialized on the nearest tree.

Figure 6 shows a concrete bollard, respectively their location plan.

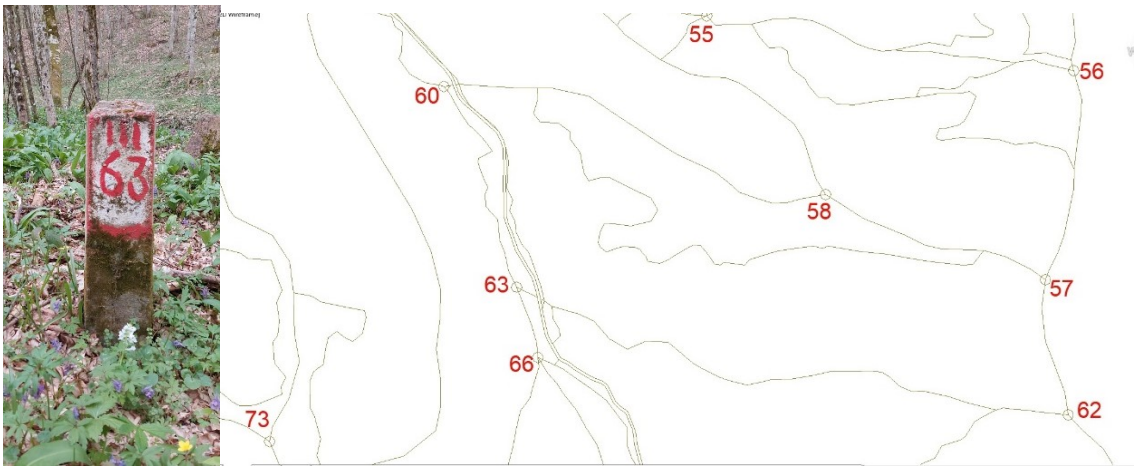


**Figure 6. Concrete landmark and their location plan**

There are 320 landmarks in the public forest fund of the state.

Of the 320 terminals, 42 are new, and in order to identify the new ones, they are marked (figure 7). The landmarks are placed in the field by the staff of the Lugoj forestry bypass, according to the landscaping map. Their location plan was made using AutoCAD after the stations were downloaded.

Also in the data processing stage, the coordinates obtained after downloading the GPS station were imported into AutoCAD and the data processing for each individual forest body was carried out, establishing their limits and surfaces. It should be noted that for the Drinova production unit, a number of 10 compact forest bodies delimited by exploitation roads were established from a topographical point of view (Figure 7.).

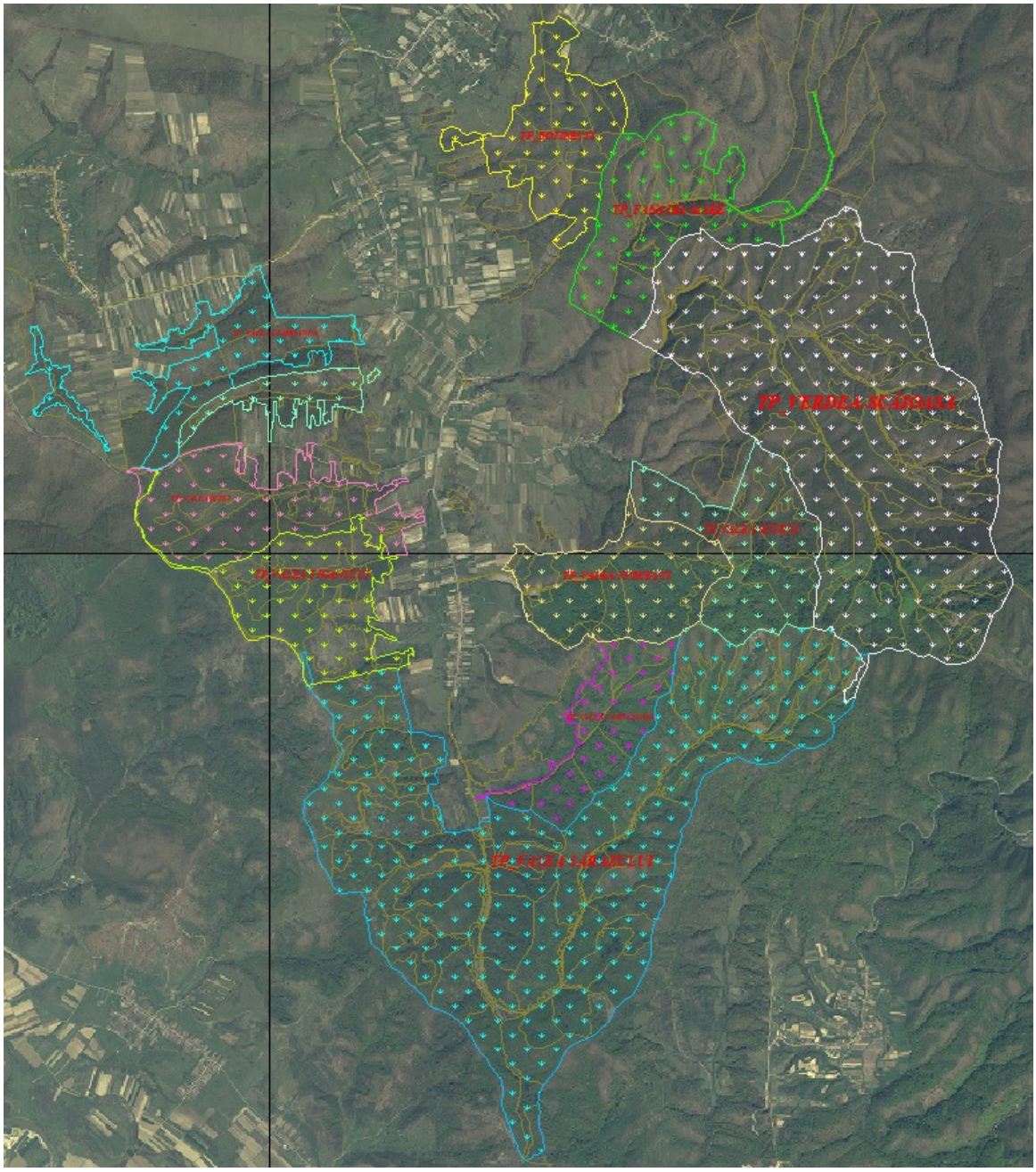

**Figure 7. General plan of forest corps**

For the accessibility and transport needs of the III Drinova production unit, in addition to the existing exploitation roads, which mostly satisfy the travel needs, new forest roads were established that complete the infrastructure of the development (Figure 8.).

**Figure 8. New forest road**

Within the production unit III Drinova there are 4 buildings for the accommodation of forestry personnel and workers, respectively a canton: the Săraz forestry canton and 3 cottages (Figure 9.).

**Figure 9. Săraz forestry canton**

## CONCLUSIONS

Determining the non-correspondence of the parcel boundaries materialized in the land with the existing boundary on the development plan drawn up by topographical measurements carried out on the parcel boundaries;

Through the current arrangement, the functional continuity of the forests within the Lugoj Forest Ring Road was achieved in full accordance with the new social-economic objectives existing within its radius;

The difficulty of the measurements consisted in the lack of GPS signal in some places, in semi-open areas such as clearings and exploitation (forestry) roads;

Taking the measurements was also more difficult due to the rugged terrain with steep slopes.

## ACKNOWLEDGEMENTS

” This paper is published from the own research funds of the University of Life Sciences "King Mihai I” from Timisoara”

## REFERENCES

[1]. Badea G., *Măsurători Terestre-fundamente,* Volumul II, *Cadastru*, Editura Matrix Rom, Bucureşti, 2002;

[2]. Bârliba Luminita Livia, Bârliba C., Eles G., Chiscop N., *Implementarea Cadastrului Forestier prin Aplicarea Legii Proprietății în vederea înregistrării unei parcele forestiere*, Editura Formec, Timișoara 2010;

[3]. Boş N., *Cadastru general*, pp.1-37, Editura All Beck, Bucureşti, 2003;

[4]. Costea C., *Organizarea si planificarea producției forestiere*, 2015;

[5]. Giurcă, A., Dima, D. P. *The Plan B for Romania’s Forests and Society* [online] Brașov, Editura Universității Transilvania, 2022;

[6]. Oncea Cristina, *Ghidul de aplicare a bunelor practici agricole in silvicultura,* Editura cadrelor didactice, 2013;

[7]. Popescu A. C., Popescu G., *Îndrumător pentru elaborarea unui proiect de cadastru*, Editura Eurobit, Timișoara, 2016;

[8]. Rucăreanu N., *Amenajarea pădurilor*, Editura Aldus Bucureşti, 2007;

[9]. *** - Lege nr. 46 din 19 martie 2008 - Codul silvic, Republicată în Monitorul Oficial nr. 238 din 27 martie 2008;

[10]. *** - Lege nr. 133 din 8 iunie 2015 pentru modificarea şi completarea Legii nr. 46/2008 - Codul silvic, Publicat în Monitorul Oficial nr. 411 din 10 iunie 2015;

[11]. *** - Amenajament silvic Ocolul Silvic Lugoj, 2021.